Cranfield University

Heinz Joachim Kohn

Controllability of Road Vehicles at the Limits of Tyre Adhesion

School of Mechanical Engineering

Ph. D. Thesis

Cranfield University

School of Mechanical Engineering

Ph. D. Thesis

Academic Year 1997 - 98

Heinz Joachim Kohn

Controllability of Road Vehicles at the Limits of Tyre Adhesion

Supervisor Professor R.S. Sharp

July 1998

This thesis is submitted in fulfilment of the requirements for the Degree of Doctor of Philosophy.

Acknowledgements

The author wishes to thank all those who contributed to the research on the 'Controllability of Road Vehicles at the Limits of Tyre Adhesion' which provided the material of this thesis. I should like to thank Prof. RS Sharp from Cranfield University, Dr A.R. Williams from at Dunlop Tyres Limited and Dr R.A. Williams from Jaguar Cars Limited for their encouragement, ideas and criticism provided throughout the project. My thanks also go to my former colleagues at Dunlop Tyres Limited, especially to Paul Stephens, with whom I enjoyed sharing the research work, to M.J. Beeson for assisting the editorial process, Mr J. Pennells for his efforts on running the Inertia Rig, and to the test drivers Mr E. Dorman and Ellis Hadley.

Abstract

The research project 'Controllability of Road Vehicles at the Limits of Tyre Adhesion' (CROVLA) was established to investigate how tyre and chassis properties contribute to the handling characteristics and stability of vehicles operating at or near to the limit condition. The project involved the Department of Transport, SP Tyres UK Limited, Jaguar Cars and Cranfield University.

An extensive proving ground test program of typical limit handling tests provided characteristic driver input and vehicle response data for a variety of vehicle configurations. The test data analysis was based on the concept of correlation. Cross-correlation coefficients and average response time delays were obtained for various pairs of quantities, namely steering angle and torque for the input and yaw rate and lateral acceleration for the response. The predictability of the vehicle response was evaluated by the rate by which the correlation coefficients change with severity.

Analogous to the proving ground work, vehicle dynamics simulations were carried out. Two programs were employed to study the steady state performance and the transient limit handling behaviour.

The 'Steady State Cornering Model' was used to confirm some basic suspension design rules established for optimising the lateral adhesion of a suspension design. The importance of controlling camber and vehicle jacking by an appropriate suspension design was identified.

A detailed vehicle model was built-up using the simulation code AUTOSIM. After validating the model against proving ground data, some parametric studies were conducted to quantify the effects of suspension and tyre properties on the transient limit response behaviour.

Proving ground and simulation results suggest that response time lags and cross-correlation coefficients in combination with other handling parameters can be used as objective quality measures. The results quantified to what extent tyre and chassis modifications change the limit handling behaviour.

Contents

list of symbols

position vectors [m]:

$\vec{r}_f^{\,CoG}$	: vector from ground to centre of gravity of vehicle body
$\vec{r}_i^{\,CP}$	: vector from ground to contact point of wheel i
$\vec{r}_i^{\,W}$	: vector from ground to centre of gravity of wheel i

forces [N] and moments [Nm]:

$F_{f,i}^{S}$	: spring force i
$F_{f,i}^{y}$	: side force acting at contact point of wheel i
ΔF_y^-	: side force loss due to camber
ΔF_y^+	: side force gain due to camber
$F_{f,i}^{z}$	: vertical force acting at contact point of wheel i
$F_{z,r}$	: rear axle load
$F_{Z,stat}$	: static wheel load
ΔF_Z	: change of wheel load due to lateral load transfer
T	: vehicle body torque
M^{HW}, M_{SW}	: hand wheel torque
M_i^{AL}	: aligning torque acting on wheel i

coordinates and displacements [m]:

∂y_0	: virtual lateral displacement whole front end
$y_{f,i}^{w}$	: lateral position of contact point i
∂z_0	: virtual vertical displacement whole front end
∂z_f^B	: virtual vertical displacement sprung mass
z_f^B	: vertical vehicle body displacement
$z_{f,i}^{W}$	: vertical wheel travel measured at contact point i
$\Delta l_{f,i}$	: spring deflection of spring i

angles [rad]:

$\alpha_{i\,r}$	: slip angle at front wheel i
β	: vehicle slip angle
$\gamma_{f,i}$	: camber angle of front wheel i
γ_{out}	: camber angle of outside wheel when cornering
γ_{in}	: camber angle of inside wheel when cornering

γ^{RH} : camber angle at right hand side

γ^{LH} : camber angle at left hand side

$\delta_{i\,r}$: total steering angle at front wheel i

δ_i^{KP} : steering angle at wheel i due to column rotation

$\Delta\delta_i$: roll steer angle at wheel i

$\delta_{0,i}$: static toe in

δ^{LC} : angle at lower end of steering column

δ_{SW} : hand wheel angle

μ_0 : friction coefficient in 'Magic Formula'

$\partial\varphi_0$: virtual roll displacement of whole car

φ_f : front body roll angle

$\partial\varphi_f^B$: virtual roll displacement of sprung mass

ψ : vehicle yaw angle

velocities and other time derivatives:

$a_y, \ddot{y}$: lateral acceleration [m/sec^2]

v : forward speed of vehicle [m/s]

$v_{x,i}^W$: forward velocity of wheel i [m/s]

$v_{y,i}^W$: lateral velocity of wheel i [m/s]

$\dot{\beta}$: vehicle slip acceleration [sec^{-1}]

$\dot{\psi}$: vehicle yaw rate [sec^{-1}]

limit handling assessment parameters:

$c(\tau)$: correlation coefficient [/]

f_0 , f_1 : frequency of 1. harmonic of 'lane change sweep' steering input [Hz]

f_2 : twice the frequency of 1. harmonic of 'lane change sweep' steering input [Hz]

T : record length of a signal [sec]

v_0 : initial velocity for 'lane change sweep' manoeuvre [m/sec]

v_{max} : maximum velocity for 'lane change sweep' manoeuvre [m/sec]

f_2 : twice the frequency of 1. harmonic of 'lane change sweep' steering input [Hz]

$x(t)$: input signal for correlation

$y(t)$: output signal for correlation

λ_0 : wavelength 'lane change sweep' manoeuvre [m]

$\sigma_{\dot{\delta}}$: standard deviation of hand wheel angle velocity [rad/sec]

$\sigma_{\dot{\delta},\beta}$: standard deviation of hand wheel angle activity for controlling side slip motion of vehicle [rad/sec]

$\sigma_{\ddot{\psi}}$: standard deviation of yaw rate [rad/sec]

$\sigma_{\ddot{y}}$: standard deviation of lateral acceleration [m/sec^2]

δ_1 : amplitude of 1. harmonic of 'lane change sweep' steering input

δ_2 : amplitude of 2. harmonic of 'lane change sweep' steering input

τ : time shift increment between two signals [sec]

capital letters:

$G^r_{\delta_{SW}}$: yaw rate gain [sec^{-1}]

K : driver steering gain [rad/m]

T_P : driver preview time [sec]

T_W : half track width [m]

UG : understeering gradient [rad sec^2/m]

Greek letters:

υ_f : eigenfrequency of undamped vehicle model [rad/sec]

σ_f : damping coefficient of vehicle model [sec^{-1}]

ρ : turning radius [m]

τ : time shift increment [sec]

τ_{PV} : driver preview time [sec]

constants:

a, l_f : horizontal distance from front axle to CoG of vehicle [m]

b, l_r : horizontal distance from rear axle to CoG of vehicle [m]

$a_{i,1}$: first order kinematic steering coefficient for wheel i [/]

$a_{i,2}$: 2. order kinematic steering coefficient for wheel i [rad^{-1}]

$c_{C,i,1}$: first order camber coefficient for wheel i [rad/m]

$c_{C,i,2}$: 2. order camber coefficient for wheel i [rad/m^2]

$c_{L,i,1}$: first order spring length coefficient for wheel i [/]

$c_{L,i,2}$: 2. order spring length coefficient for wheel i [m^{-1}]

c_{comp} : composite steering column stiffness [Nm/rad]

c_{RH} : lateral stiffness btw. rack housing and chassis [N/m]

c_{TB} : steering column torsion bar stiffness [Nm/rad]

$c_{Y,i,1}$: first order scrub coefficient for wheel i [/]

$c_{Y,i,2}$: 2. order scrub coefficient for wheel i [m^{-1}]

$c_{\alpha,f}$: front cornering stiffness [Nm/rad]

$c_{\alpha,r}$: rear cornering stiffness [Nm/rad]

c_{φ}^{C} : steering column torsional stiffness [Nm/rad]

$c_{\varphi,f}^{RB}$: anti roll bar torsional stiffness front [Nm/rad]

$c_{\delta,i,1}$: first order roll steer coefficient for wheel i [rad/m]

$c_{\delta,i,2}$: 2. order roll steer coefficient for wheel i [rad/m^2]

h_f : height of vehicle body centre of gravity [m]

i_L, r_c : steering ratio hand wheel/ road wheel [/]

J_Z : yaw inertia of whole vehicle [kg m^2]

$K_{f,i}$: suspension spring stiffness for wheel i [N/m]

$K_{f,i}^{BS}$: suspension bump stop coefficient for wheel i [N/m^4]

l : wheelbase [m]

m : mass of whole vehicle [kg]

m_f^B : sprung mass front [kg]

$m_{f,i}^W$: unsprung mass front [kg]

r_r : ratio btw. rack displacement and road wheel angle [m/rad]

$R_{f,i}$: static rolling radius of front tyre [m]

s : Laplace operator [rad/sec]

T_e : effective yaw rate time constant [sec]

t_f : half track width front [m]

t_r : half track width rear [m]

$t_{\dot{\psi}}$: approximation of yaw rate response time [sec]

$\Delta l_{f,0}^{BS}$: spring deflection at bump stop engagement

1 Introduction

The limit of tyre adhesion is of great concern in road vehicle dynamics, since it defines the state of minimal directional control, leaving the driver with the smallest margin for error to avoid accident damage and injury. The research project 'Controllability of Road Vehicles at the Limits of Tyre Adhesion' (CROVLA) was established in order to investigate the factors contributing to the handling characteristics and stability of vehicles operating at or near to the limit condition. The project involved the Department of Transport, SP Tyres UK Limited, Jaguar Cars and Cranfield University.

The limit of tyre adhesion is reached if the tyres cannot provide the horizontal forces necessary to maintain or change course. High speed cornering, braking or accelerating in turns, avoidance manoeuvres as well as driving on wet or icy roads are conditions for which the tyres operate at their peak performances, and for which the vehicle's response becomes either very sensitive or indifferent to any disturbances. These conditions require a driver control activity considerably different from that exerted during normal driving conditions.

The behaviour of a vehicle encountering severe driving conditions is determined by its chassis layout, the operating conditions of its tyres, the surface properties of the road and the driver's control inputs. The interaction between driver, vehicle and tyres was analysed to obtain a better understanding of which response characteristics constitute a user friendly limit handling and how it can be achieved from the tyre and chassis design point of view.

The project work involved the development of suitable tyre and vehicle models. The theoretical work was accompanied by extensive tyre rig testing and a comprehensive proving ground vehicle handling test program. The thesis summarises the work completed on matters concerning vehicle modelling and testing, while a summary of the findings regarding tyre testing and modelling can be found in /1.0.1/.

1.1 Relevance of limit handling with respect to road safety

The response behaviour of vehicles is regarded as one factor responsible for accidents. Other factors are seen in the fitness and skill of drivers and the environment, such as the road layout, surface condition and street lighting. However, it has not been established yet to what extent vehicle handling characteristics contribute to the number of accidents, let alone which objective handling properties are most related to road safety. The Casualty Report /1.1.1/ about road accidents in Great Britain breaks down accident rates in terms of road and driver characteristics, which does not allow conclusions to be drawn as to what extent the vehicle behaviour was a contributing factor. The figures for accidents involving skidding vehicles suggest that the loss of control due to saturating guidance forces is a feature of about 15% of all car accidents.

Accidents in which the car skidded cause disproportionately more casualties compared to those for which this loss of control feature was not reported.

1.2 Vehicle and tyre behaviour at high slip rates

The large number of research papers dealing with Anti-locking Brake Systems (ABS) and with active chassis control systems, such as Four Wheel Steering (4WS) /1.2.1-4/ and Vehicle Dynamics Control (VDC) /1.2.5/, indicate the interest of the automotive industry and their suppliers in the stability of vehicles operating near the road-tyre friction limit. While 4WS systems aim to improve the handling for all conditions, the others only intervene if a potentially dangerous driving state is recognised. An imminent spin is compensated by controlling the drive torque and by distributing brake torques of different magnitudes to the four wheels. As for passive chassis designs, the development of these active chassis control systems requires accurate tyre data in order to evaluate the system performance as well as to eliminate potential failure modes. The efforts made by the TIME project /1.2.6/ and by the TYDEX workgroup /1.2.7/ indicate the need for standardised tyre testing methods and corresponding tyre data interfaces providing realistic tyre data, which can be exchanged between vehicle manufacturers and their suppliers using a common format.

1.3 Matching tyres to vehicles - state of art

Tyres are matched to the vehicle design undergoing an iterative homologation process. During the homologation a tyre supplier submits various tyre design evolutions to the vehicle manufacturer. The evaluation of the handling performance is mainly based on subjective appraisals by professional test drivers obtained from a proving ground test program. The proving ground testing may be conducted without establishing any objective performance or quality measures, except recordings of lap times and maximum speeds for a given test manoeuvre.

The tests often reveal that small tyre design changes, whose effects are hardly recognisable from laboratory tyre force and moment characteristics, lead to noticeable changes in the response behaviour of the vehicle.

During the homologation process both the vehicle and the tyre design are subject to a continuous, but not necessarily mutually coordinated, development, which makes it difficult for the tyre designer to tune the product to the vehicle for which the final specification is not fully available. Establishing an acceptable compromise between comfort and handling, which are only two criteria to be met among many others, follows mainly an empirical approach which has evolved from previous development programs. In addition, laboratory tyre test data is consulted to address the comments made by the test drivers on the comfort and handling properties.

So far, only predictive engineering tools of limited capability are available for tyre designers to investigate the effects of a design change or the performance of a prototype tyre in its natural environment, i.e. the vehicle for which it is designed. It has yet to be demonstrated that such simulation facilities provide an advantage in the development process, actually leading to information which enables the designer to introduce modifications improving the vehicle handling without incurring significant drawbacks in terms of comfort, rolling resistance and noise generation. A beneficial use of vehicle dynamics simulation tools would require updated vehicle data to be obtained from the customer or established from rig testing.

1.4 Objectives of research

The CROVLA research program was set up with the objective of providing a better understanding of the response behaviour of road vehicles encountering the adhesion limit between tyre and road as well as of the impact of such driving conditions on the controllability by typical drivers. It is known that the control of a vehicle operating near the friction limit is more demanding, which is reflected by the disproportionately high number of accidents occurring in wet or icy road conditions. The drivers involved either failed to recognise a potential limit manoeuvre or lost control of the vehicle when having to cope with a response behaviour to which they were not accustomed by previous experience. Hence, the research work addressed the interrelated effects of various suspension and tyre properties on the generation of guidance forces as well as the question of which vehicle response behaviour is desirable for assisting the driver in maintaining or regaining control over the direction of travel. The findings of this research in conjunction with tools and methods for analysing these areas may then be employed by tyre and suspension engineers to improve their respective designs, ideally in a concurrent process.

Considerable research has been carried out in the past to establish objective handling parameter defining a desirable handling response. Correlating vehicle handling properties with subjective ratings has led to some criteria, by which the handling quality can be assessed for normal driving conditions. However, relatively little is known of which response properties establish a controllable limit behaviour.

In order to obtain more insight into the relation between vehicle response and controllability, a comprehensive proving ground test program was conducted which involved tyre-vehicle combinations yielding very different handling characteristics. The vehicle response and the driver's control inputs were recorded. The data analysis in combination with test driver comments led to the identification of some criteria for evaluating the limit handling quality.

Individual effects of tyre and chassis properties on the limit handling behaviour were further quantified by a series of vehicle dynamics simulations. In the absence of rules for matching a tyre design to a chassis, the modelling approach allows a

comparatively quick and cheap way of analysing the influence of the various components whose interrelation determines whether the vehicle performs in a user friendly fashion.

The modelling work included the development of a 'Magic Formula' based representation of the tyre forces and moments, which interfaces not only with the vehicle dynamics models built up during the project but also with the Tyre Property Prediction software (TPP), a program developed in-house by SP Tyres UK for predicting tyre characteristics from the design and materials data of a prototype design.

The relatively simple formalism of the 'Magic Formula' tyre model represents generic tyre properties, such as cornering stiffness, camber thrust, peak friction and the roll-off behaviour of the transition between adhesion and sliding dominated contact. This tyre model can be regarded as a standard routine employed for vehicle handling analysis. The sophisticated TPP program provides the link between tyre construction and material properties on the one hand and those generic force and moment characteristics on the other.

A fairly detailed vehicle handling model, which incorporated the 'Magic Formula' tyre representation, was developed and validated against proving ground data obtained for a range of manoeuvres, covering conditions from low severity up to limit driving, so that these predictive tools can be used with some confidence for tyre and chassis development purposes. However, it has yet to be established to what extent the findings and deliverables of the project contribute to a more efficient collaboration between tyre and chassis designer on the component matching problem.

Unfortunately, some limit handling aspects were only partly addressed by the project work. The project plan was envisaged to include studies into the effects of varying vertical loads as well as those of combined longitudinal and lateral slip on the behavioural properties of tyres and vehicles. These are the topics requiring further work.

2 Literature survey

A literature survey was carried out focusing on published work related to the limit handling of road vehicles and its mathematical modelling. Research papers were studied dealing with tyre testing and modelling aspects, vehicle modelling, proving ground test methods, human factors involved in the control of road vehicles. A number of papers were found on vehicle and tyre design, road surface and the driver's sensation of vehicle response. The on-line catalogue of MIRA with its keyword search facility was a great help to find a large number of publications relevant for the project. More than a hundred papers were found for keyword entries like 'tyre', 'adhesion', 'modelling', 'simulation' and others. After reading their abstracts several were ordered from MIRA or borrowed from Cranfield University Library. Hardly any papers were found explicitly dealing with the limit behaviour or with the road-tyre-suspension matching problem. But the large number of publications presented in the past on the development of Four Wheel Steering systems (4WS), active chassis control and anti-locking brake systems clearly show the significance of and the interest in improving the vehicle handling behaviour with regard to a better and safer handling.

Some papers were found dealing with the important issue of the correlation between measurable vehicle handling characteristics and the subjective perception of the driver. These were clearly of interest for our purposes and are discussed in more detail further on. Other publications inspired some ideas about devising proving ground handling tests suitable for evaluating the handling quality.

During the development of a new car, experimental as well as computer aided or numerical methods are used in order to find a satisfactory compromise between handling and comfort. Numerical methods can be employed early in the design process helping to find a better understanding of the problems involved, which leads to more precise prototype configurations, fewer iterations and experiments necessary.

For the simulation of vehicle handling and comfort these methods are widely used, which is reflected by the large amount of publications dealing with the development of more powerful software packages /2.0.1, 2.0.2/ on the one hand and their application on the other. Furthermore, the demand for faster and more accurate analysis tools has encouraged theoretical work on the mathematical description of complex vehicle components such as tyres and suspension elements. The software tools available can be divided in single and multi purpose codes. For the former the model structure is predefined restricting the inclusion of model details, while the latter known as multi-body system (MBS) programs enable unlimited extensions and a continuous model development.

Detailed models obviously need a fairly large number of input data describing the inertia, stiffness and damping properties as well as the geometry of the model and its elements, which has reinforced the development and use of more sophisticated test rigs /2.0.3, 2.0.4/ and parameter estimation techniques /2.0.5, 2.0.6/. Accurate

parameter determination is of great concern in order to accomplish a consistent model description and an appropriate prediction capability.

Results of vehicle dynamics simulations are physical quantities, from which gradients, gains and response times are derived, which are considered as 'objective' parameters for the handling evaluation. These have to be correlated with the subjective sensation of the driver or to a statistical representative of the potential customer group. Experimental work has been carried out to establish relations between the 'objective' response, as measured or calculated, and the actual 'feel' of the driver. This work also led to the standardisation of certain test procedures by which different vehicle designs are assessed and compared more objectively.

After indicating the basic subjects of interest with regard to the vehicle and its handling, some information is given about the research carried out into the tyre-road interface, concentrating on its impact on vehicle dynamics simulation.

In the tyre industry, numerical analysis methods are applied for studies into tread pattern optimisation for improving wet grip, tread noise formation, heat generation, and stress concentration, whereas tyre models for vehicle dynamics have been developed mainly by universities according to the increasing interest of the automotive industry.

Over the years various tyre models have been proposed focusing on different aspects of the rolling contact problem and with varying accuracy and computational performance. Many of those described in the literature are developed for the use of vehicle handling simulation with minimal computational effort. In the literature we find empirical as well as physically founded approaches to reproduce tyre behaviour.

More advanced models cover a frequency range well above say 5 Hz, enabling the simulation of non-stationary rolling contact problems, for which tyre vibrations and the tyre's ability to envelop obstacles to a certain extent become important features. These models are very complex and need considerable CPU time for the road contact problem, let alone the whole road-tyre-vehicle simulation. For the time being, their use in vehicle dynamics is restricted to research studies /2.0.7-2.0.9/.

2.1 Statistics about accidents involving loss of vehicle control

As pointed out in the introduction, the Casualty Report /1.1.1/ about road accidents in Great Britain breaks down accident rates in terms of road and driver characteristics, which does not allow conclusions to be drawn as to what extent the vehicle behaviour was a contributing factor. According to /1.1.1, table 23/ cars were involved in 205 177 accidents causing 1749 driver and occupant fatalities and 763 pedestrian deaths. The numbers of these road users seriously injured are about 12 times as high. The figures for accidents involving skidding vehicles /1.1.1, table 43/ suggest that the loss of

control due to saturating guidance forces is a feature of about 15% of all car accidents. Accidents in which the vehicles skidded cause disproportionately more casualties compared to those for which this loss of control feature was not reported. For the year 1990 /2.1.1/, those 15 percent of all accidents in which at least one vehicle skidded were responsible for 41% of all vehicle user deaths and for 30 percent of serious injuries. The accident and casualty rates involving skidded cars increase with vehicle speed /2.1.1, table 6e/. Accidents in which vehicles skidded are more likely to happen on non built-up roads for vehicle speeds beyond 40 mph.

Accident Researchers were approached in order to obtain more information about extent and nature of accidents, for which skidding or loss of control was an observed feature. Dr. J. Broughton from TRL could not recommend references giving information about research on the causes of skidding and spinning out accidents. He pointed out, that usually police reports do not contain a reconstruction of the manoeuvre leading to the accident. Those records state driver age, sex and condition, which is used for major research on drunk driving.

From Mr. Cuerdon, a member of the Accident Research Centre of Birmingham University, four papers were obtained, in which statistics are quoted about the number and location of accidents involving skidding and /or road departure. Two of them /2.1.2, 2.1.3/ deal with several aspects of single-vehicle accidents and discuss measures for improving road design in the USA. The other two papers come from authors of TRRL and investigate the effect of variations in road surface friction on the number of skidding accidents.

Location and frequency of accidents

The references /2.1.2/ and /2.1.3/ from 1979 and 1982 respectively, describe the extent and nature of single-vehicle accidents in the USA, for which the vehicle left the road ('run off the road accidents'). They discuss several measures concerning road design such as road marking, barrier construction and the layout of ditches and embankments, which have helped to reduce fatalities and injuries.

The following facts are reported:

- 40 % of fatal accidents occurred off the road width (USA, 1980, /2.1.3/])
- for approximately 40% of fatal accidents (1981, /2.1.3/]) the vehicle overturned (all other accidents listed there concern impacts with road side objects, e.g. tree, pole, embankment)

The influence of road geometry was analysed by a study of 8000 accident reports compiled by specially trained police officers over a one year long period.

The findings include:

- 44% of the accidents analysed occurred on curves (1975-1976, /2.1.2/), indicating a higher accident rate for these sites than for tangent sections

- more run-off the road accidents occur on left-hand curves (27% :17%) suggesting that outside lane gives room for recovery for failures in approaching a right-hand curve

- 3/4 of accidents featured departures to the outside of a curve

- smaller departure angles (13°) are stated for right-hand than for left-hand curves (20°),

- proportion of departures to the outside increases with curvature

- downgrades are reported to constitute another accident-prone road site (63% higher accident rate than on upgrades)

The authors note, that driver condition and behaviour are more important factors determining the extent of injury severity than road condition and design. Furthermore, lower injury rates were established for snow covered roads and sharper curves, which is explained by the lower speed associated with these conditions, and the possibly increased precaution taken by the driver.

Effect of road friction on accident frequency

The other two papers /2.1.4, 2.1.5/ deal with the influence of road surface friction on skidding accident rate for wet and dry conditions. Skidding resistance is related to accident frequency in order to establish skidding resistance levels minimising accidents in relation to costs for road maintenance. The benefit of increased surface friction for a reduction in accident rate is quantified by an example calculation.

The road surface friction varies considerably over a year. It is higher during the winter months and lowest for July/ August. The road friction is quantified by the 'Sideways Force Coefficient (SFC)', which is the ratio of lateral to normal force as measured by TRRL test equipment. Recommended levels vary dependent on road speed and site between 0.3 and 0.75 for wet roads /2.1.4/].

Those seasonal friction changes were used to correlate surface friction to skidding accident rate. Records of injury accidents in the UK for the period 1979-1982 were analysed. The number of wet skidding accidents as a percentage of all accidents is about 26% and almost double as high as the number of dry road skidding accidents (14%, /2.1.5, p.2, table 1/). The amount of wet road skidding accidents as a percentage

of all wet road accidents varies between 23% and 44% with road speed, road class, region and vehicle weight. The findings are summarised as follows:

- month-to-month wet friction changes correlate well with skidding accident rates

- wet skidding rate higher on higher speed roads

- it is believed that results apply to dry road conditions to a lesser extent, namely that an increase of dry road skidding resistance is less effective in reducing accident rates than an increase of wet road skidding resistance

As an example it is shown that a hypothetical increase of surface friction of 20% would reduce the wet road skidding rate by 13% (/2.1.5/, p.10, table 9).

Summary

The first two papers summarised /2.1.2, 2.1.3/ provide some evidence for the assumption, that guiding a vehicle on curves and downgrades, for which non steady state control action may be required (braking & steering), is more difficult. They quantify the extent of accidents as a consequence of loss of control. The authors state that driver behaviour and condition is more influential on injury severity than road design, which raises the question, how and to what extent vehicle handling qualities may improve driving capability and thus reducing accident rate and severity.

In /2.1.5/ data is presented quantifying the amount of skidding accidents. It is shown that the skidding accident rate corresponds clearly to road surface friction, and that traffic and light conditions are less significant.

The values of the SFC given in /2.1.4/ for wet roads can be useful for adjusting tyre model parameters for handling simulations on wet roads, after corrections are made regarding the TRRL test equipment used.

2.2 Simulation tools in vehicle handling dynamics

In the introduction, it was distinguished between single and multi purpose simulation tools. The former comprises vehicle models with a predefined structure with a limited number of degrees of freedom (DoF). The input data describing the suspension characteristics consist of composite or lumped parameters by which either global properties of an actual design or a generic type of suspension can be represented. Their application may be restricted to certain driving manoeuvres.

Examples of this category of simulation codes are VDANL /2.2.1/, FRESH and the 'Steady State Cornering Model' presented further on.

These models can be build up in a rather short period of time requiring only a limited number of input parameters. Parameter studies can be carried out with regard to those composite suspension characteristics, e.g. roll stiffness and compliance steer, independently from a specific design. This approach makes it easier to analyse and compare changes in the vehicle and suspension layout.

Multi Body System (MBS) codes are software tools of the second group allowing continuous model development, which may lead to models with more than 50 DoF and a variety of non-linear elements. Their open structure enables to include additional model elements such as tyres, driver models, power steering systems and traction controllers. Usually, these programs are applied for detailed studies into the effects of rather subtle design alterations and especially for investigations of manoeuvres in which nonlinearities play a significant role.

For the CROVLA project both types of simulation tools are available. The 'Steady State Cornering Model', discussed in chapter 3, allows conducting basic studies into the suspension-tyre interface, while the MBS code AUTOSIM /2.2.2/ was preferred to the more common ADAMS software /2.2.3/ for the development of general vehicle models, which include many non-linear components considered to have a significant effect on the transient vehicle behaviour.

AUTOSIM, a fairly recent development which can be implemented on a PC, provides a symbolic representation of a model in the form of a Fortran code, whereas ADAMS computes the equations of motion numerically.

The advantage of the former approach is that it allows developing and describing models and its elements separately from any input data sets defining the actual geometry and physical properties. Models can be exchanged easily between the parties involved in the project on the basis of a neutral interface provided by the Fortran code.

AUTOSIM
symbolic representation of model Fortran code gives neutral interface
implemented on PC
available at Cranfield University

ADAMS
numerical representation of model
workstation based
available at SPUK, Jaguar
expertise available
highly developed pre- and post processing facilities

ADAMS models have to be defined by the declaration of specific input data and the program does not account for a separation between model build up and data input preparation. The features of both MBS codes are summarised in the tables above.

2.3 Standardised vehicle handling tests and subjective handling evaluation

2.3.1 Introduction

Limit situations, like all other driving manoeuvres, have to be recognised and controlled by the driver. The vehicle has to provide fast and predictable response to the driver's steering and throttle adjustments to allow for an adaptive controlling process for different driving and road conditions. From that point of view, the driver's sensation of the vehicle's limit behaviour, the subjective judgement of the vehicle response as well as the control activity have to be seen as an important aspects of the project.

Although considerable research has been carried out on the correlation between subjective judgement on the one hand and vehicle response on the other, it has not led to well-defined guidelines separating well handling and poor handling vehicles. In these studies outdoor as well as driving simulator tests of several open and closed loop manoeuvres with a number of test drivers were conducted /2.3.1, 2.3.5-7, 2.3.11/. Some characteristic vehicle response quantities were found, which proved to correlate with the driver's perception. The knowledge obtained by these investigations has led to the definition of so called 'objective' handling parameters associated with those tests. Although absolute levels for these handling parameters have not been specified, guidelines and rules of thumb are known characterising the quality of the handling. On the other hand the relationship between these 'objective' handling parameters and accident avoidance has still to be established, presuming that there is one.

The handling tests include:

- steady state cornering test (constant radius test)
- lateral transient response test /2.3.3/
  (comprising ramp steer, sinusoidal and random steering input)
- braking in a turn (open or closed loop test)
- lane change manoeuvres
- rough road cornering

The objective handling parameters associated with the steady state cornering test refer to the understeer/ oversteer characteristics and steering sensitivity of the vehicle. Several other parameters relate to the vehicle slip angle, which is seen as a relevant quantity for the driver's perception of the handling.

Apart from this test all other test procedures listed above are transient open or closed loop manoeuvres. From the lateral transient test for example time lags, response times (for lateral acceleration, vehicle slip angle and yaw rate), overshoot gains and several gain factors can be derived as well as parameters belonging to the frequency domain analysis (frequency response of lateral acceleration, yaw rate, phase angles between

response and steering wheel activity). For the braking in a turn test, parameters are established describing the course maintaining quality of the vehicle.

The analysis and evaluation of vehicle handling cannot be reduced to pure exercises in investigating the effects of certain vehicle design parameters on the directional response. A thorough study involves also the driver's control action, his/her perception and assessment of the vehicle responses to intended inputs as well as external disturbances. The complex control interactions have to be addressed together with the prevailing environmental conditions in order to obtain a complete picture of the man-vehicle system.

While vehicle response characteristics can be expressed in meaningful physical quantities, such as gains, time lags and certain gradients, the driver's control strategy, his/her sensitivity to the experienced vehicle motion and the criteria used for assessing the handling are not fully understood. The capability of any driver to preview events, monitor the vehicle reaction and changing driving conditions, e.g. given by wind gusts or a varying road surface properties, and to compensate undesired reactions is difficult to quantify, and it is even harder to establish those criteria on which the subjective appraisal relies and how these are related to the vehicle design.

From the vehicle engineer's point of view, it is desirable to find objective measures characterising the quality of vehicle performance, which are reflected by subjective judgements. Some research in that direction was carried out, especially during the 70's and early 80's. The results of that research and associated problems on correlating vehicle response parameters against subjective assessment are summarised here.

The task of improving handling is not exclusively directed towards increasing preventive safety, which is often associated with the maximum cornering performance, but also to provide an easy control for normal driving conditions and according to Sano /2.3.4/ to introduce so called 'fun to drive' qualities dependent on the customer group. In his report, Bergmann /2.3.5/ concludes, that ease of control during severe, not necessarily limit manoeuvring is the most important handling quality rather than the maximum cornering capability of a given design. He analysed data, which suggest that the vast majority of drivers utilise the cornering capabilities of a vehicle only marginally (48%) and prefer braking to steering control for emergency situations, because it requires less skill and effort. Although the vehicle design contributes most significantly to the overall handling performance for limit conditions, he believes that less severe tests are suitable to establish ease of control measures representing the driver's workload.

Jaksch /2.3.6/ and Weir /2.3.7/ report on successful correlation exercises for less severe manoeuvres (avoidance and lane change driving tasks), for which the lateral acceleration (latac) of 5 m/sec^2 was not exceeded. For their studies randomly selected as well as expert drivers were used as evaluators, respectively.

A different approach is proposed by Belsdorf et al. /2.3.8/. They recommend limit task performance tests, which are said to provide better discrimination between evaluated vehicles. It can be objected that expert drivers can detect very subtle differences of the car's behaviour and provide appraisals of higher resolution. Furthermore, results of limit task performance tests will be affected by the skill and experience of the evaluators, questioning their objectivity and reproducibility.

Sano presents in his paper a list of characteristics, which are reported to relate to preventive safety. They are in order of their importance:

1) vehicle response to steering input — Table 2.3-1
2) braking in a turn
3) straight-line braking performance
4) vehicle steady state cornering performance
5) visibility
6) rollover immunity
7) crosswind immunity
8) steering returnability (free control characteristics)

which confirms Bergmann's assumption, that easy steering and combined steering and braking control are the most desired properties for emergency situations.

The following paragraphs discuss how the term 'ease of control' and related subjective ratings were correlated against 'objective' vehicle response signals and thus translated into physical parameters. For that, driving tests were specified, which excite the main directional vehicle modes and represent driving manoeuvres encountered on roads. Some of the tests proposed in the literature are discussed in section 2.3.3. Results of successful correlation experiments are given next. Some reported problems in devising suitable handling tests are summarised in section 2.3.5. But firstly, the most relevant parameters used in vehicle dynamics are compiled, which may help to interpret the experimental results.

2.3.2 Vehicle dynamics parameters

Many vehicle dynamics parameters are derived from the well known 'bicycle' model /2.3.2/, which describes the yaw and lateral motion of a vehicle. For linear tyre and steering properties and for constant speed manoeuvres analytical solutions can be found relating the yaw and lateral motion to the steering angle input.

For steady state cornering, an understeering gradient UG is commonly used to define the behaviour of the vehicle. It is dependent on the vertical load distribution and on the cornering coefficients of the tyres, and is computed as follows:

$$UG = m \cdot \frac{c_{\alpha,r} \cdot b - c_{\alpha,f} \cdot a}{c_{\alpha,r} \cdot c_{\alpha,f} \cdot (a+b)} \qquad (2.3.2.1)$$

m = mass of vehicle

$c_{\alpha,r}$ = cornering stiffness of rear axle

$c_{\alpha,f}$ = cornering stiffness of front axle

a = distance from front axle to centre of gravity of the vehicle

b = distance from rear axle to centre of gravity of the vehicle

Note that the cornering stiffness is composed of lateral tyre, suspension and steering system stiffness.

The understeering gradient UG can also be expressed by the so called characteristic velocity v_{CH}, for which an understeering car (UG>0) reaches its maximum yaw rate gain:

$$UG = \frac{(a+b)}{v_{CH}^2} \qquad (2.3.2.2)$$

with

$$v_{CH}^2 = \frac{c_{\alpha,r} \cdot c_{\alpha,f} \cdot (a+b)^2 a}{m \cdot (c_{\alpha,r} \cdot b - c_{\alpha,f} \cdot a)} \qquad (2.3.2.3)$$

The steady state yaw rate gain $G_{\delta_{SW}}^{r}$ represents the directional response $\dot{\psi}$ to the steering wheel angle δ_{SW}. It increases for an understeering vehicle with forward velocity v until its peak value is reached at a speed equal to the characteristic velocity v_{CH}. The following relation applies in which i_L gives the steering ratio between the hand wheel and the road wheels.

$$G_{\delta_{SW}}^{r}(s=0) = \frac{1}{i_L \cdot (a+b)} \cdot \frac{v}{1 + \frac{UG}{(a+b)} \cdot v^2}$$

or with (2.3.2.2)

$$G_{\delta_{SW}}^{r}(s=0) = \frac{1}{i_L \cdot (a+b)} \cdot \frac{v}{1 + \left(\frac{v}{v_{CH}}\right)^2} \qquad (2.3.2.4)$$

Another important steady state parameter is the vehicle side slip angle β, for the linear system determined by:

$$\beta = \beta_0 - \frac{F_{z,r}/g}{c_{\alpha,r}} \cdot a_y, \text{ where}$$

β_0 = constant dependent on turning radius

$F_{z,r}$ = rear axle load

a_y = lateral acceleration

Apart from these static parameters, a few quantities referring to the vehicle dynamics are compiled, which play their role in the control task the driver has to perform in the closed loop. The eigenvalues of the 'bicycle' model are determined by the following quantities, leading to the damping factor and eigenfrequency for the standard case of conjugate complex values.

$$2 \cdot \sigma_f = \frac{J_Z \cdot (c_{\alpha,r} + c_{\alpha,f}) + m \cdot (c_{\alpha,r} \cdot b^2 + c_{\alpha,f} \cdot a^2)}{J_Z \cdot m \cdot \mathrm{v}} \qquad (2.3.2.5a)$$

$$\upsilon_f^2 = \frac{c_{\alpha,r} \cdot c_{\alpha,f} \cdot (a+b)^2 + m \cdot v^2 (c_{\alpha,r} \cdot b - c_{\alpha,f} \cdot a)}{J_Z \cdot m \cdot \mathrm{v}^2}, \text{ where} \qquad (2.3.2.5b)$$

J_Z denotes the yaw inertia.

Again, we notice the velocity dependence of the vehicle's dynamic behaviour. For the transient analysis of the vehicle, parameters are used, which represent response gains and time or phase lags with respect to the steering wheel input.

The most important ones are the yaw rate transfer function and the yaw rate response time $t_{\dot{\psi}}$, which represent the rate and the rapidity of the vehicle's directional reaction to a steering input. They are given by:

$$G^r_{\delta_{SW}}(s) = \frac{\dot{\psi}}{\delta_{SW}}(s) = G^r_{\delta_{SW}}(s=0) \cdot \frac{1 + \frac{m \cdot \mathrm{v} \cdot a}{c_{\alpha,r} \cdot (a+b)} s}{1 + \frac{2\sigma_f}{\upsilon_f^2} s + \frac{1}{\upsilon_f^2} s^2}, \qquad (2.3.2.6)$$

and

$$t_{\dot{\psi}} \approx \frac{\pi}{2} \cdot \sqrt{\frac{J_Z \cdot m}{c_{\alpha,f} \cdot c_{\alpha,r} \cdot (a+b)}} \cdot UG^{-1} \qquad (2.3.2.7)$$

The Laplace operator in (2.3.2.6) is denoted by s.

Presuming an understeering vehicle, $t_{\dot{\psi}}$ gives the time elapsed until the first yaw velocity peak occurs after the steering wheel angle reaches a steady state. The vehicle reacts strongly and quickly to the steering input for a high steady state yaw rate gain and for a low response time $t_{\dot{\psi}}$, which can be accomplished with high understeer gradients UG. On the other hand low values of UG indicate a less stable system, which can be deduced from (2.3.2-5a, b).

2.3.3 Closed loop handling tests

The difficulty in correlating subjective assessment of vehicle handling characteristics against physical quantities or measured response data lies in the complex cross-coupling of the subsystems driver, vehicle and environment, forming a closed loop.

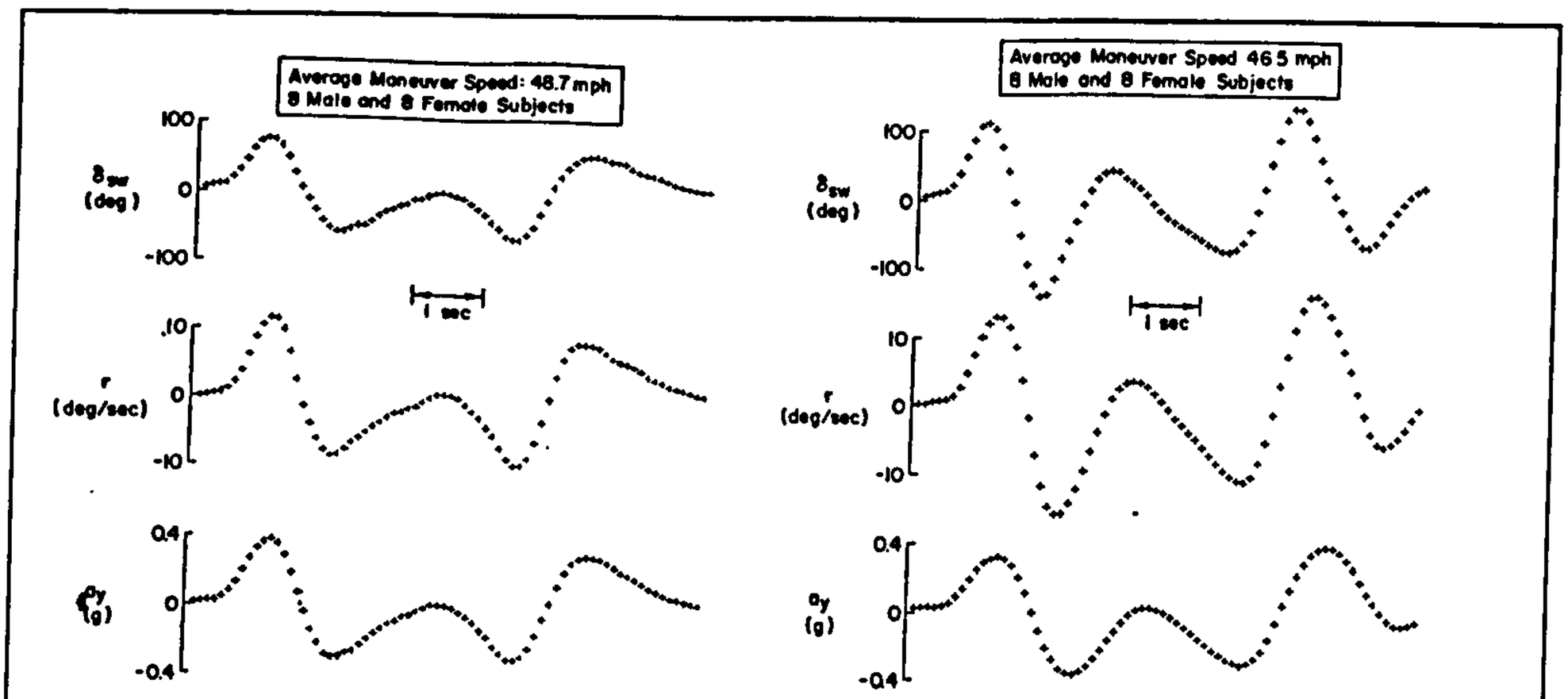

Fig. 11 – Ensemble average time histories for 50 mph double lane change maneuver, STI configuration D ($T_e \triangleq 0.15$)

Fig. 12 – Ensemble average time histories for 50 mph double lane change maneuver, STI configuration B ($T_e \triangleq 0.46$)

Fig. 2.3-1 ensemble time histories for a lane change manoeuvre /2.3.7/

In order to decouple these components, Bergmann suggested in /2.3.5/ a procedure of three open loop tests and three others conducted in the closed loop. The open loop driving manoeuvres are conducted to collect characteristic vehicle response data unaffected by driver skill or control strategy, whereas the closed loop tests were designed for obtaining subjective appraisal data, which is assumed to correspond to the 'ease of control' experienced by the evaluators. He argues that objective handling properties cannot be deduced from measurements of closed loop tests, since the data will be filtered according to the driver's compensating effort, hiding inherent shortcomings of the vehicle. On the other hand closed loop driving tasks are seen as the only means to obtain subjective judgements reflecting the physical and mental workload of the evaluators. According to /2.3.5/ they are not suitable to provide an ease of control measure, if only absolute performance levels are established such as maximal lateral acceleration, maximum speed achieved for a lane change or success rate of maintaining course for an avoidance task. These quantities rather indicate the skill of the driver than the effort required. A similar approach was followed by Crolla et al. for their study /2.3.11/. There, subjective ratings were correlated with time and frequency domain metrics, such as response times and sensitivities, response gains and phase lags, which were obtained from standard open loop tests.

Weir /2.3.7/ suggests that ensemble time histories of the control input, given in fig. 2.3-1, give more information about the task difficulty, revealing the complexity of the

input signals by the number of peaks and by the order of discontinuity recorded for the control input. Fig. 2.3-1 shows the input and response signatures for two different vehicles performing a lane change at 50 mph. For the more responsive car, smoother input and response time histories were obtained.

Linke /2.3.1/ follows the same strategy as Bergmann and adds driving simulator studies to his investigation, whereas Jaksch /2.3.6/ conducted and analysed only closed loop lane change manoeuvres. He measured 'objective parameters' such as root mean squares for the side slip angle β, steering wheel velocity $\dot{\delta}_{SW}$ and the yaw rate response time $t_{\dot{\psi}}$ from the data recorded and correlated them against driver ratings.

Corresponding to table 2.3-1, the discussion of suitable closed loop handling tests begins with the lane change manoeuvre, by which the transient steering characteristics of the driver-vehicle system are assessed. The dynamics of the lane change are similar to those for an accident avoidance manoeuvre. Derivatives of the lane change found in the literature are the sudden lane change and the double lane change /2.3.4/. The lane change was selected by Bergmann /2.3.5/, Weir /2.3.7/ and Jaksch /2.3.6/ for their correlation exercises. The keywords below indicate the procedures and test conditions.

<u>lane change test</u>

Bergmann /2.3.5/ : single lane change, const. speed of 96 kph
various levels of severity up to limit performance tested

Weir /2.3.7/ : double lane change tests were analysed, const. speed of 80 kph
latac ≤0.5 g

Jaksch /2.3.6/ : single lane change tests were analysed,
const. speed of 40 and 80 kph
latac ≤0.4 g

Another test, referring to the transient steering control, concerns the cornering on rough road experiment, for which the vehicle initially negotiates a turn of constant radius until it encounters a single bump or a grid of rubber slabs. Bergmann recommends single bump tests, if it is desired that wheel hop resonance effects do not dominate results of tests at a particular velocity.

<u>rough road cornering</u>

Bergmann /2.3.5/ : single bump test, constant speed of 48 kph,
steady state latac=0.5g

Belsdorf /2.3.8/ : grid of rubber slabs; up to max. achievable latac
(limit performance test)

The effect of deceleration on the directional stability of a cornering vehicle is analysed by the 'braking in a turn' test.

braking in a turn

Bergmann /2.3.5/ : cornering with initial speed of 88 kph, latac=0.5g
succession of tests with progressive brake application until front or rear wheels locked

Belsdorf /2.3.8/ : test to obtain minimal stopping distance within path constraints (limit performance test)

All of these tests can be used for the assessment of the ease of control quality as well as for establishing limit handling conditions. Measurements for limit task performance tests result in maximal achievable speed for the lane change, maximal lateral acceleration for the rough road test and shortest stopping distance for the braking in a turn test.

2.3.4 Objective handling parameters

Different measures for the ease of control were proposed by the authors referenced. Bergmann extracted the values of these objective parameters from open loop tests similar in their dynamics to their closed loop counterparts. The open loop test conditions and those objective parameters correlating well with driver opinion are given below.

Corresponding open loop test for the lane change are:

Bergmann /2.3.5/ : reverse steer ramp against stops while cornering on constant radius,
constant speed of 96 kph, various levels of severity

Ervin /2.3.9/ : sine steer, constant speed of 45, 60 mph

Bergmann introduced the following ease of control parameter, the normalised angular side slip acceleration:

$$C_\beta = \frac{v \cdot \ddot{\beta}}{\dot{a}_y}, \text{ with} \qquad (2.3.4.1)$$

$\ddot{\beta}$ = vehicle side slip angle acceleration

$\dot{a}_y$ = time derivative of lateral acceleration

This ratio addresses the observed sensitivity of drivers to changes in side slip. A large peak value of the parameter (2.3.4.1) established by the reverse ramp steer test is said to be desirable, representing a short exposure time to side slip.

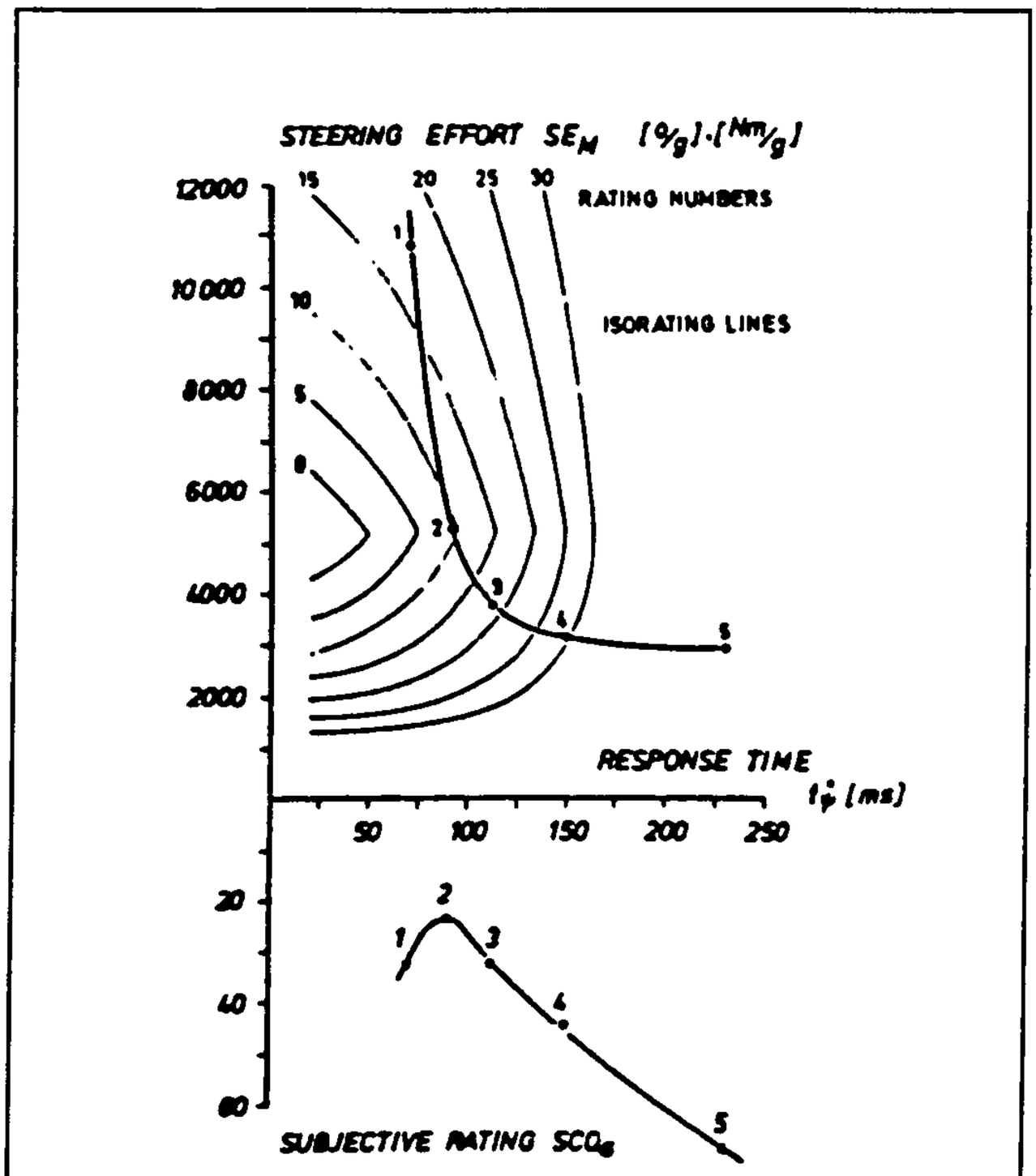

Fig. 2.3-2 Steering effort vs. yaw response time for different subjective ratings /2.3.6/

Jaksch /2.3.6/ developed a performance index, the steering control quality, which consists of a weighted sum of physical steering and mental steering effort. The former is given by the product of the measured steering wheel and hand wheel torque sensitivities. The mental effort is assumed to be linearly dependent on the yaw rate response time $t_{\dot{\psi}}$. Fig. 2.3-2 shows the physical steering effort SE_M against the mental workload given by $t_{\dot{\psi}}$. Rating lines with low values indicate 'easy to drive' qualities.

Weir /2.3.7/ used the steady state yaw gain and an 'equivalent yaw response time' as measures for driver strain, which will be discussed later.

The fixed control rough road cornering test can be conducted as its closed loop counterpart, except for the compensation of the path deviation. An objective criterion is seen in :

$$C_r = \frac{\dot{\psi}_{max} - \dot{\psi}_{min}}{\dot{\psi}_0} \text{ , with} \qquad (2.3.4.2)$$

$\dot{\psi}_{max}$ = max. vehicle yaw velocity after hitting bump

$\dot{\psi}_{min}$ = min. vehicle yaw velocity after hitting bump

$\dot{\psi}_0$ = vehicle steady state yaw velocity

giving the relative error in yaw velocity presuming that a change in vehicle attitude is not desired.

Ervin et al. suggest measuring peak side slip angle velocity and the curvature ratio motivated by the notion that large changes of the vehicle side slip angle and large deviations from the original path given by R are not desired. He says that large angles β may disorient the driver and expose the vehicle with a larger projection area on the road.

The fixed control test for braking in a turn can again be processed as described for the closed loop procedure, except the steering activity.

braking in a turn (open loop)

Bergmann /2.3.5/ : cornering with initial speed of 48 kph, latac=0.3g
succession of tests with progressive brake application
until front or rear wheels locked

Ervin /2.3.9/ : cornering with initial speed of 64 kph, latac=0.3g
brake application as above

Bergmann defines the 'normalised understeer gradient', $\Delta\delta_u$, as a representative performance index. It is computed according to:

$$\Delta\delta_u = \frac{l}{\ddot{x}}\left(\frac{\dot{\psi}}{v} - \frac{\dot{\psi}_0}{v_0}\right), \text{ with} \qquad (2.3.4.3)$$

$\dot{\psi}$ = peak vehicle yaw velocity

$\dot{\psi}_0$ = vehicle steady state yaw velocity before brake application

v = forward velocity corresponding to $\dot{\psi}$

v_0 = velocity before brake application

$\ddot{x}$ = vehicle deceleration

l = wheelbase

The index gives the change of directional response due to change in velocity as well as path curvature. The speed reduction results in a decrease of lateral acceleration forcing the vehicle onto a smaller radius, while the reduction in tyre side force capability has the opposite effect for an understeering vehicle, partly cancelling the former tendency. Ervin suggests the same parameters for this test as those used for the rough road cornering evaluation.

summary

The procedures of major handling tests and some objective parameters suggested in the literature have been described. The closed loop tests are seen as the only means for subjective evaluation studies. Their open loop counterparts allow the measurement of

vehicle response parameters. Another category of closed loop tests are task performance experiments revealing the limit performance of driver and vehicle. Other tests not mentioned here, since they do not reflect the dynamics of manoeuvres to be investigated in this project or are similar to those discussed, include surprise avoidance manoeuvres /2.3.8/, straight line braking, roll over test /2.3.9/, J-turns and slalom tests.

Following the description of the handling tests, some results of successful correlation exercises carried out by Bergmann /2.3.5/, Weir /2.3.7/ and Jaksch /2.3.6/ are discussed. For the lane change manoeuvre, the three authors report good correlation between their performance indices and the corresponding subjective appraisals.

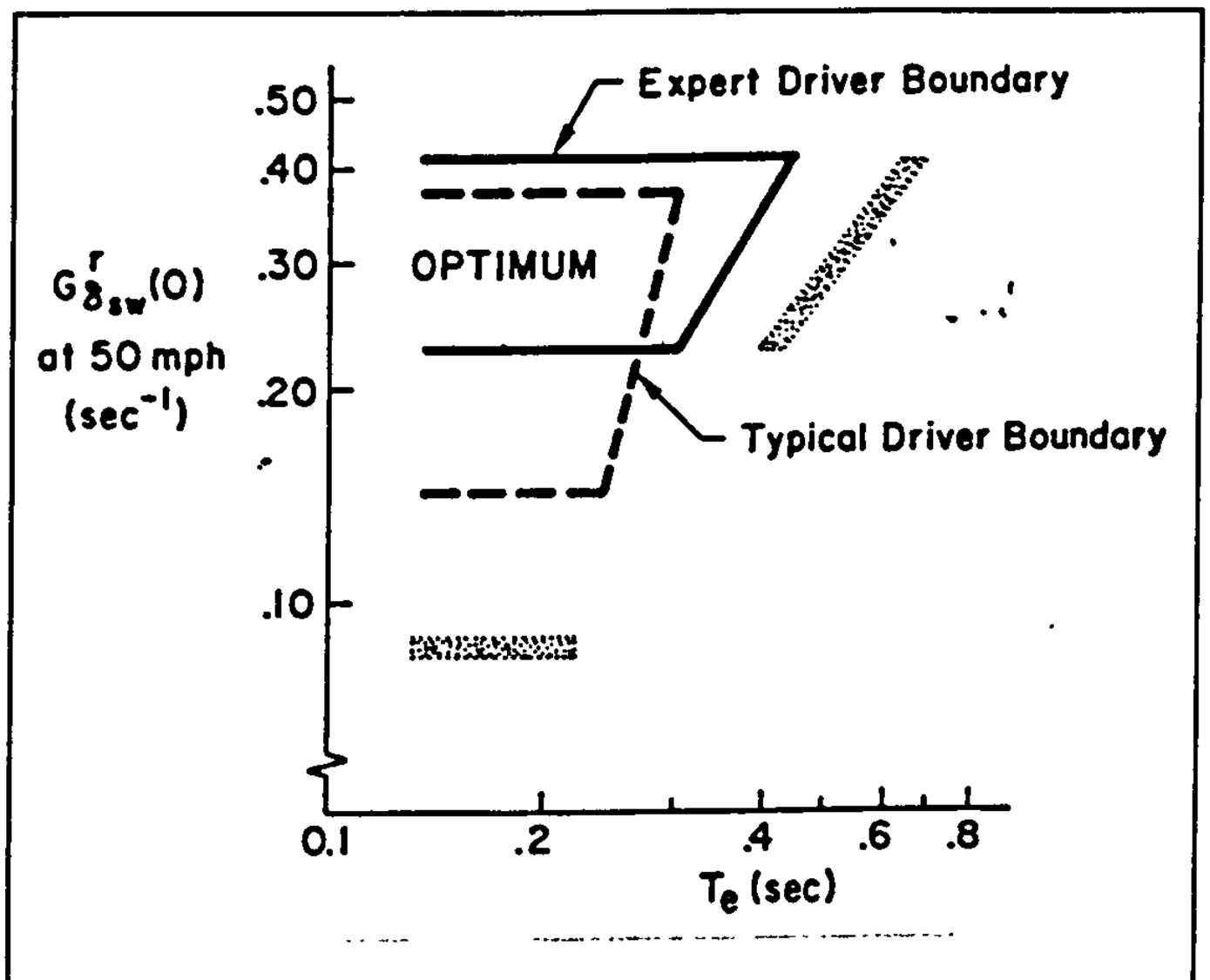

Fig. 2.3-3 Yaw rate gain vs. effective time constant /2.3.7/

According to Bergmann a high value of the normalised angular side slip acceleration (2.3.4-1), indicating an increased rapidity of directional response, is favoured by the evaluators.

The objective response parameters proposed by Weir and Jaksch are related to the steering inputs and the lag between steering wheel input and the yaw rate response.

Weir summarises his findings in the plot shown by fig. 2.3-3, where the optimal regions for the two parameters, the steady state yaw rate gain and the so called effective time constant for the directional mode, are given for expert as well as for typical drivers.

The effective time constant T_e refers to a transfer function introduced by Weir as follows:

$$\frac{r}{\delta_{SW}} = G^r_{\delta_{sw}}(s=0)\frac{1}{T_e s+1}$$

which simplifies the true yaw rate transfer function of the 'bicycle' model as given by (2.3.2.6) considerably. The value of T_e can easily be established by a frequency response test. It is the inverse value of the frequency for which a phase angle of 45

deg is recorded. Mitschke /2.3.10/ writes that the simplified relation is only valid for low velocities.

The performance plot in fig. 2.3-3 suggests that typical drivers accept a wider range of steady state yaw rate gains and at the same time prefer a more responsive car associated with lower T_e levels. The expert drivers favour less understeering vehicles indicated by the higher horizontal levels. They seem to be more prepared to handle less responsive vehicles.

Jaksch presents his results in a similar plot (fig. 2.3-4) showing an optimal area for physical steering effort and yaw rate response time. The steering effort is calculated from the product of the steering wheel angle and steering wheel torque sensitivities according to:

$$SE_M = \left(\frac{d\delta_{SW}}{da_y}\right)\left(\frac{dM_{SW}}{da_y}\right), \text{ with}$$

$\left(\frac{d\delta_{SW}}{da_y}\right)$ = steering wheel angle sensitivity with respect to latac

$\left(\frac{dM_{SW}}{da_y}\right)$ = steering wheel torque sensitivity with respect to latac

He found that driver judgement of the steering control quality is much more sensitive to the time lag $t_{\dot{\psi}}$ than to the physical effort given by SE_M. Furthermore, his results given in fig. 2.3-2 suggest that there is a lower limit for the yaw rate response time. He found that, for very strong understeering vehicles, the steering effort SE_M increases, worsening the subjective ratings. This result might be due to the test conditions. Only one vehicle type was used, whose handling properties were varied by different settings of tyre pressures. Therefore, the only degrees of freedom for that experiment are the cornering stiffnesses of the tyres, front and rear, and their relaxation lengths, which might limit the validity of the results given in fig. 2.3-2 to a smaller bandwidth.

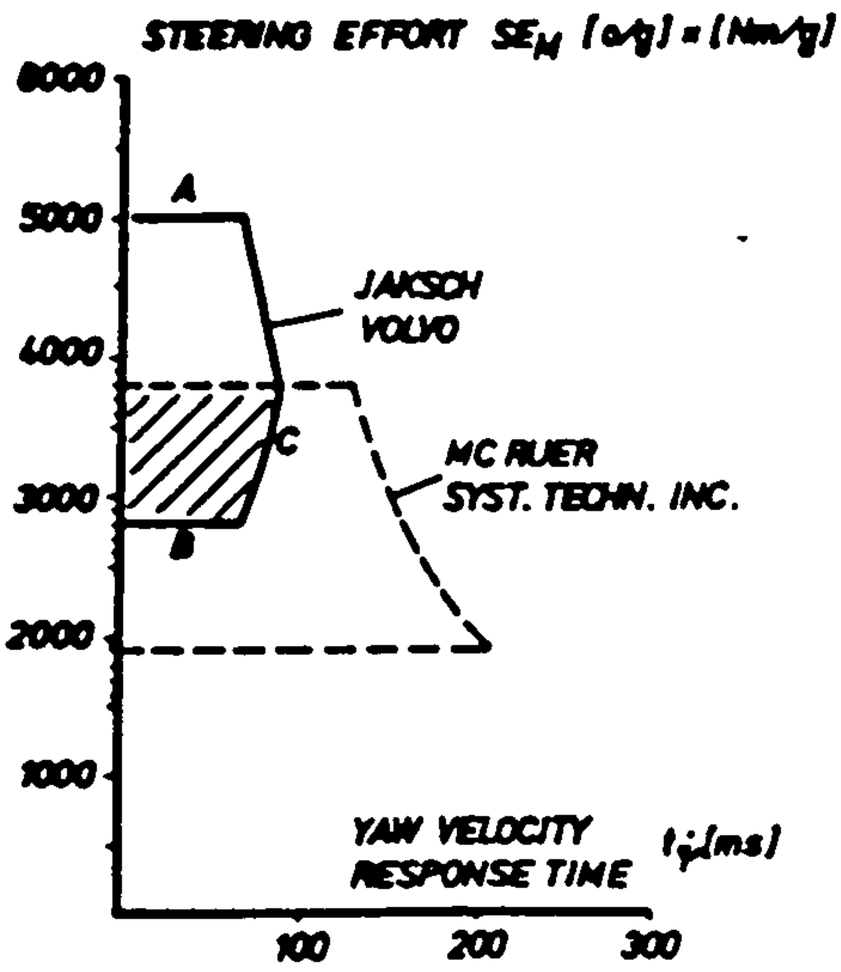

Fig. 2.3-4 Steering effort vs. yaw rate response time /2.3.6/

For the rough road and braking in a turn tests, Bergmann reports a good correlation of his performance criteria. Vehicles exhibiting low yaw rate velocity increments as defined in (2.3.4-2) achieved a better rating, while lower values of normalised understeer angle increments (2.3.4-3) corresponded with the evaluators preference.

For the limit task performance tests conceived by Belsdorf et al. /2.3.8/ excellent repeatability and discrimination between the tested vehicles is reported.

2.3.5 Problems

Some of the authors comment on the problems encountered in designing a feasible experiment. For the subjective appraisal, the number of test drivers as well as the skill level required has to be selected. For limit task performance tests, researchers rely on expert drivers, whereas for ease of control assessments, both expert and typical drivers were used. A required minimal number of evaluators necessary for a valid correlation could not be found in the literature cited. Bergmann conducted his tests with 20 drivers, while Jaksch had 40 available.

According to Bergmann, proven methods to measure the evaluator's perception and rating ability are not available. In order to account for individual preferences he developed a screening technique, which quantifies each evaluator's rating variance with respect to the consensus judgement.

Another source of experiment noise is tyre wear, which can seriously affect the validity and repeatability of results, especially if repeated test runs are conducted. The problem is reported in /2.3.9/.

2.3.6 Summary

Some research papers dealing with the relation of vehicle response and driver perception and judgement have been discussed, and differences in the approach to the subject by the referenced authors summarised. There are strong indications, that handling or control quality cannot be assessed by the limit performance alone. Good controllability for less severe manoeuvres has to be established as a priority.

Different parameters characterising the ease of control were proposed by several authors and others might be found to correlate with driver opinion equally well. It remains to be investigated, whether some of the given objective parameters are related to each other or whether they are functionally dependent on others.

The last section dealt with some problems, which were addressed by the researchers. The choice of drivers and the effects of tyre wear on the results indicate the difficulty in designing representative experiments.

2.4 Tyre models

This section gives a brief survey about tyre models, their constraints and application in vehicle handling analysis. Corresponding to the partly conflicting requirements to be met by the tyre-vehicle coupling and to the complexity of the rolling contact problem, different modelling approaches can be found in the literature. An introductory example is given to illustrate the main phenomena determining the tyre's performance.

A perfect compromise for the tyre-vehicle interface provides precise and safe handling, comfortable ride and low noise levels for varying road surface conditions. These three features are usually treated as separate problems and are distinguished by frequency domains. For the vehicle's handling and ride comfort analysis, the tyre's ability to provide horizontal guidance forces and vertical flexibility are the only important matters, whereas inertia effects of the tyre can be neglected. The dominant effects to be considered are the elastic deformation of the tyre's contact patch and the friction provided by the material combination in contact, which can be represented by a spring model. Tyre models for that type of simulation have to approximate the contact forces as accurately and to be as computationally inexpensive as possible.

For studies concerning comfort characteristics at higher frequencies, known as harshness and noise, the structural properties, e.g. mass and stiffness distribution, the tyre's damping and the kinematic conditions prevailing in the contact region have to be considered.

Before we continue with the discussion of tyre models developed for the use in vehicle handling analysis, it has to be pointed out that according to /2.4.1/ good handling and comfort are two contrasting demands to be met by the tyre design. Both are mainly determined by the choice of tread compound, reinforcing materials, belt and casing materials and structure. At the present time the best match is concluded from the appraisal of experienced test drivers after a long and costly trial and error process involving vehicle and tyre engineers.

2.4.1 Tyre models for vehicle handling analysis

The handling of road vehicles, especially their response to and controllability for severe manoeuvres, depend much on the performance of its tyres, and the quality of results obtained from vehicle handling simulations will rely on the accuracy achieved in modelling the tyre's behaviour throughout its operating range. Although only three quantities, the longitudinal and lateral force, which provide the directional control, as well as the aligning torque, which contributes to the steering feel, have to be considered, their mathematical description remains a difficult task corresponding to the complex nature of the rolling contact problem on the one hand and the anisotropic tyre structure and non-linear, viscoelastic rubber properties on the other.

The mechanism by which the tyre generates shear stresses in its contact region, resulting in the three quantities, is illustrated by a simple spring model shown in fig. 2.4-1. The flexibility of the pneumatic tyre allows the rubber elements travelling through the contact area to deflect longitudinally and laterally, so that shear stresses between road and rubber are generated up to a certain friction dependent level. The deflection of the contact patch is caused by different velocities or directions of travel, both known as slip, between road and the rubber elements entering this region.

Fig 2.4-1 shows how those tread elements are distorted away from their original path, tangential to the circumference of the wheel, on to a new trajectory given by the velocity vector of the wheel hub. For small slip angles the elements are able to follow the trajectory established and thus compensate any velocity difference.

The shear stresses generated are proportional to the deflection, which is reflected by the linear branches of the side force-slip angle α curves in fig. 2.4-2. The maximal shear stress to be transmitted is limited by the friction available from the material combination. After reaching the maximal shear stress, the elements cannot longer adhere to the ground and begin to slide towards the trailing edge of the contact region. This partly sliding condition is illustrated by condition 2 and 3 in fig. 2.4-1. It corresponds to the transition from the linear branch to the peak value of the side force-slip curves.

The full sliding condition is determined by the friction only, which itself is dependent on temperature, pressure distribution and sliding velocity. The influence of the friction coefficient and the contact shape on the peak lateral force can be seen by taking the ratio of peak value and applied vertical load from fig. 2.4-2 .

After this introductory example indicating the different phenomena taking place in the contact area and their contributions to the shape of the force-slip curves, we proceed in giving some aspects of their mathematical modelling. Firstly, the different approaches found in the literature are worked out, before one model is discussed in more detail.

A comparison of the various tyre models developed for vehicle handling analysis and their theoretical background can be found in /2.4.3/. They are divided into three categories according to the theoretical approach. The first two include physically founded models, which are based on a theoretical representation of the rolling contact mechanism. The horizontal tyre forces and the moments are calculated from the deflection of a finite contact area for given or assumed elastic and frictional properties, pressure distribution and slip conditions of that region. The first category includes those models, which have to compute their output variables, e.g. the longitudinal and lateral force as well as the aligning torque on-line according to the values of the variable passed from the vehicle simulation algorithm, whereas those of the second category provide these instantly without any additional computation. Examples of these models can be found in /2.4.4, 2.4.5/.

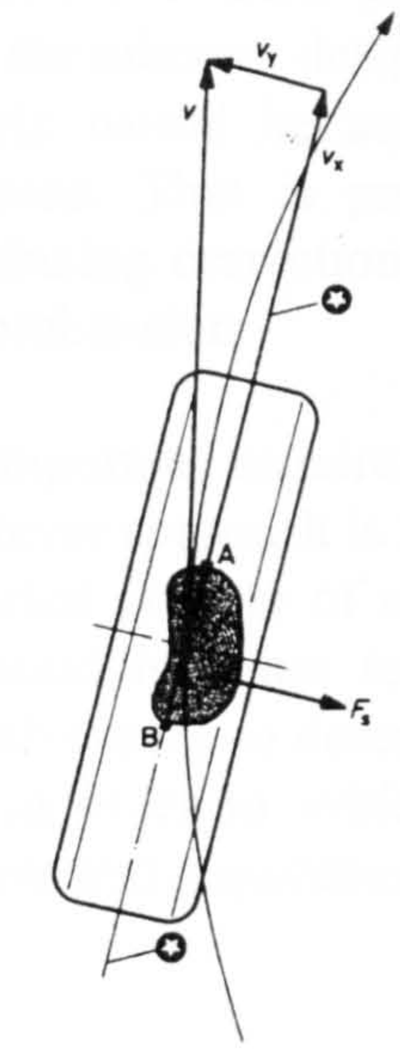

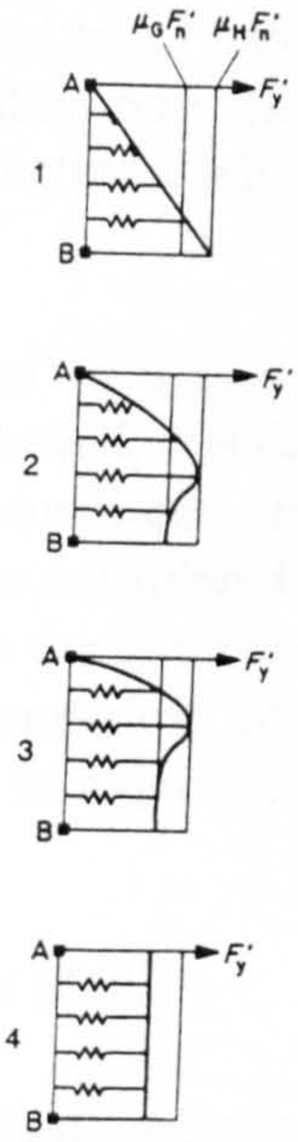

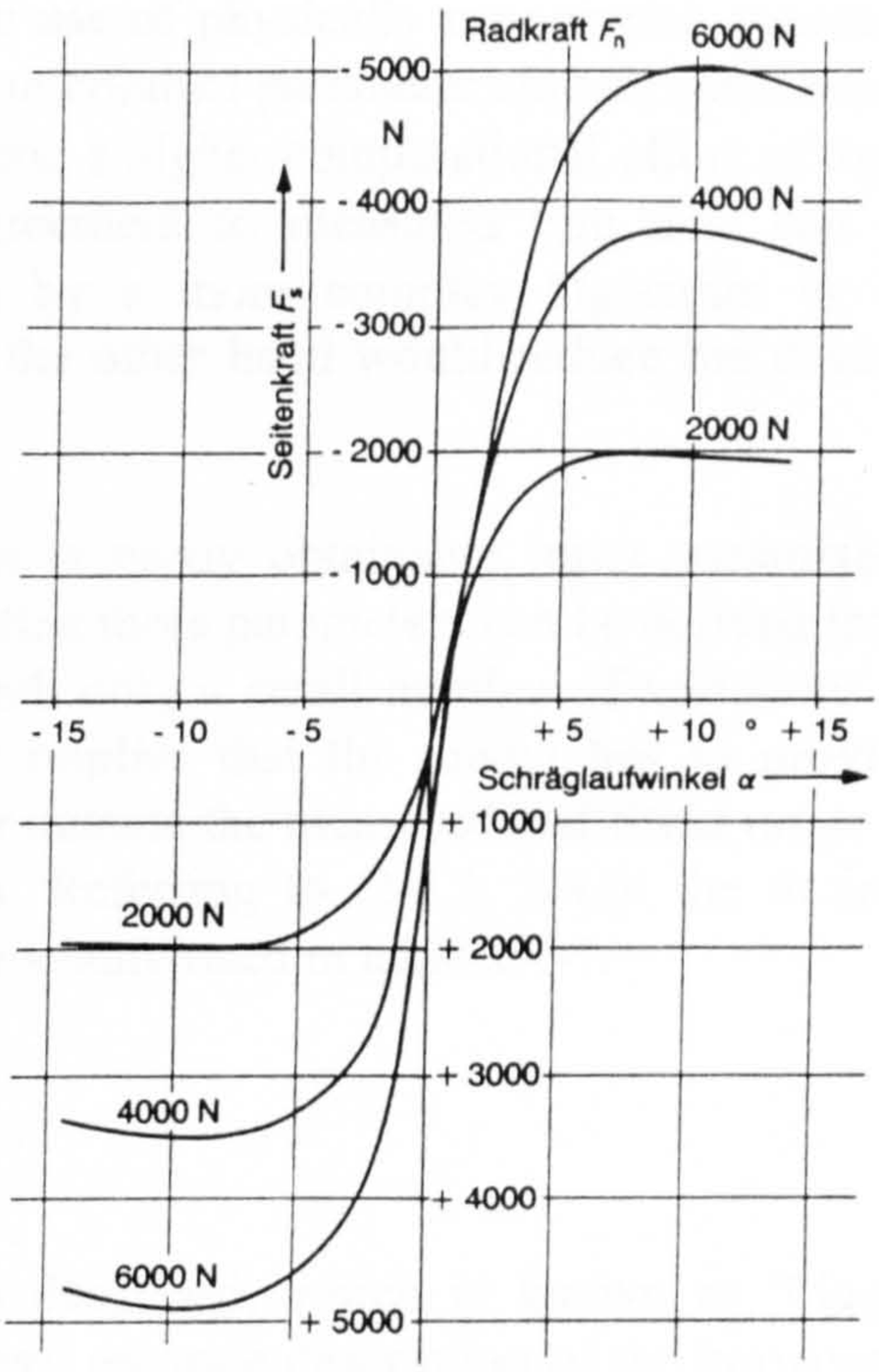

Fig. 2.4-1 shear stress generation /2.4.2/ *Fig. 2.4-2 side force - slip curve 2.4.2/*

Algorithms approximating the tyre behaviour by fitting functions or look-up tables to measured data belong to the third group of 'empirical' models. The functions used comprise polynomials, the exponential function as well as the transcendental 'Magic Formula' by which an almost perfect match to the experimental data can be achieved. On the other hand, high resolution necessitates the introduction of a very high number of parameters compared to the physically founded models, which are often difficult to associate with the actual tyre geometry and its structural properties.

The models of the first and second categories are the most satisfying in terms of enhancing understanding of the contact region mechanics. Their physical foundation allows both tyre and vehicle engineer to interpret the parameters used as structural and material quantities, which enables an easier identification

criteria for tyre models
accurate agreement with measured data
number of tests and test conditions necessary
theoretical limits of model application
computational speed
meaningful model description/ parameter identification
consistent parameter variation (ideal tyre)
numerical stability

Table 2.4-1 tyre model criteria

of their influences on vehicle handling. The use of physically meaningful quantities for the model description makes it possible to conduct parameter studies consistently with the inherent design constraints. Therefore, a higher computational effort of these models would be acceptable, if better agreement to measured tyre data can be achieved. That is probably only possible by a more complex algorithm or by introducing correction functions, which on the other hand would reduce the desired comprehension.

An important requirement to a tyre model is easily obtainable input parameters. Whatever approach is followed, it is desired that these parameters can be derived from a limited number of measurements, for which only a small number of variations of test conditions has to be considered. That implies that the model has to provide smooth curves to describe the tyre behaviour outside the measured and fitted range as well in order to avoid numerical problems. Referring to /2.4.3, 2.4.6/ the desired features and requirements of a tyre model are summarised in table 2.4-1.

2.4.2 Magic Formula Tyre Model

In this section an empirical tyre model is described, which is known as 'Magic Formula' /2.4.6, 2.4.7, 2.4.8/. It provides a very accurate description of the horizontal forces and the aligning moment for the steady state behaviour and has been further developed since it was presented in 1987. In this paper a model suitable only for the approximation of the tyre's steady state behaviour is presented, which, in the mean time, was further developed to include transient effects as well.

pure slip

The main feature of the model is a transcendental formula by which the lateral and the braking or the driving force as well as the aligning torque are determined. The argument is the corresponding slip quantity corrected by an offset representing tyre imperfections. The four parameters used in the formula depict physically meaningful quantities and will be discussed for the side force-slip angle curve shown in (Fig. 2.4-3) for a constant vertical load F_z.

The sine reflects the anti-symmetric shape of all three quantities for positive and negative slip values. The offsets S_V and S_H account for a vertical or horizontal shift existing in the real tyre data due to ply steer or conicity. The extent or wave length used of a pure sine function is controlled by the shape factor C, which accounts for the very different shapes of the lateral and longitudinal force as well as the aligning torque for the sliding dominated region.

Parameter D defines the maximal side force available for a given load F_z. The product BCD determines the slope of the curves for zero slip and is for this example equivalent to the cornering stiffness. Parameter E adjusts the curvature near the peak

describing the transition from the adhesion dominated to the sliding dominated part of the side force curve. It also determines the slip value for the maximum force.

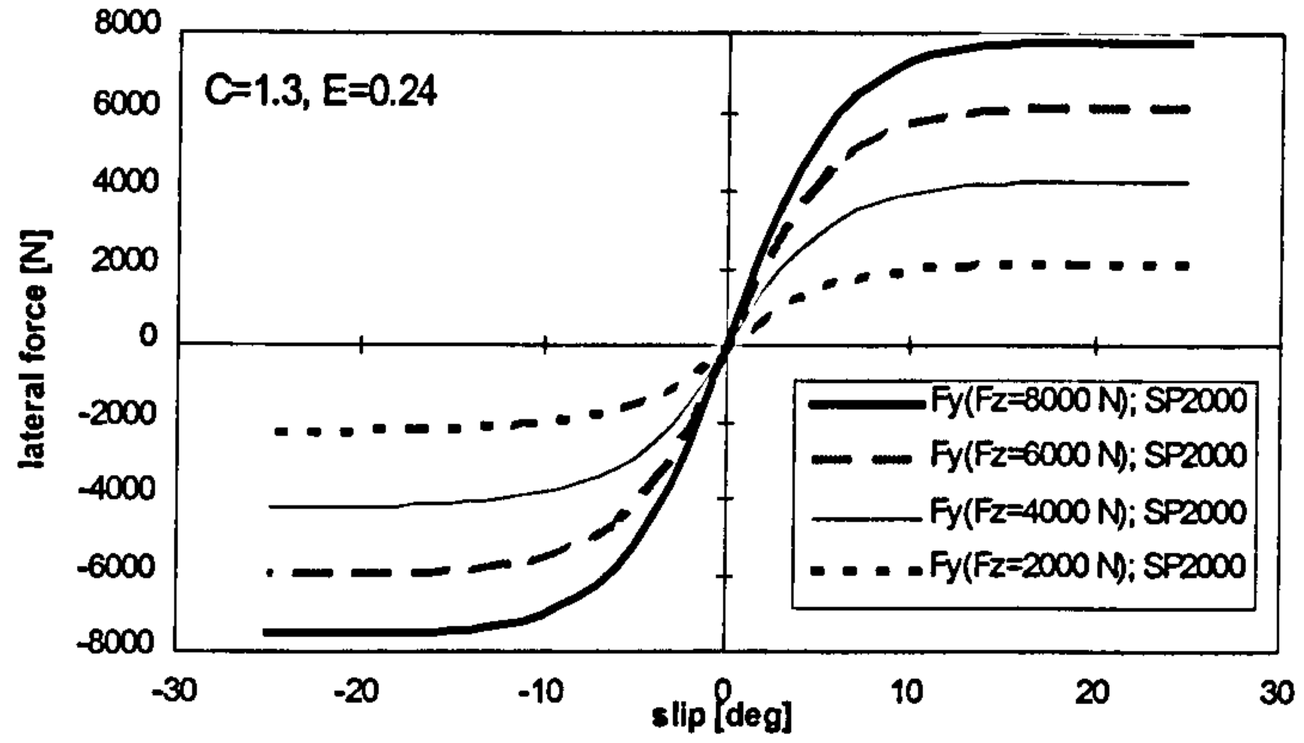

$$F_y = D \cdot \sin\{C \cdot \arctan\{(Bx - E \cdot (Bx - \arctan((Bx))\}\}$$

$$D = \left[(a_1 F_z + a_2) \cdot (1 - a_{15}\gamma^2)\right] \cdot F_z$$

$$BCD = a_3 \cdot \sin\left\{2 \cdot \arctan\left\{F_z / a_4\right\}\right\} \cdot (1 - a_5 \cdot |\gamma|)$$

$$E = (a_6 F_z + a_7) \cdot \left[1 - (a_{16}\gamma + a_{17}) \cdot \mathrm{sgn}(\alpha + S_{hy})\right]$$

$$S_{vy} = a_8 \cdot F_z + a_9 + a_{10} \cdot \gamma$$

$$S_{hy} = a_{11} \cdot F_z + a_{12} + (a_{13} \cdot F_z^2 + a_{14} \cdot F_z) \cdot \gamma$$

Fig. 2.4-3 characteristic parameters of the 'Magic Formula'

The only constant of the four parameters is the shape factor, whereas the other three are dependent on the vertical load F_z and the camber angle γ, which is expressed by polynomials of up to the second order. Referring to the version given in /2.4.7/, 15 polynomial coefficients for the side force, 13 for the longitudinal force and 20 for the aligning torque have to be determined from the measured data in order to obtain a complete model description for pure slip conditions. Suggestions for conducting the necessary tyre tests and a discussion of problems concerning the fitting of the coefficients can be found in /2.4.9, 2.4.10/.

combined slip

For pure slip conditions, either laterally or longitudinally, the three quantities are determined separately from each other. Each quantity is determined by an independent set of coefficients defining its characteristic parameters B, C, D and E. For combined slip the interactions of lateral and longitudinal force and their influence on the aligning torque has to be considered. This is done by introducing composite or 'normalised' slip quantities, so that these combined slip conditions can be described by the same formula, using the parameters already determined for pure slip conditions.

Replacing the pure lateral and longitudinal slips by their 'normalised' slip quantities follows the notion of an anisotropic contact area distorted in both horizontal directions by a resultant shear force acting in the direction given by a resultant slip angle. The

computation of this resultant slip angle, by which the shear force can be resolved in its two components again, includes the effects of a torsionally compliant belt.

The sequence of computation for combined slip conditions is preserved, but ten new coefficients are introduced, which have to be determined by the corresponding test, increasing the experimental effort considerable.

<u>transient tyre behaviour</u>

Further work has been carried out to include the transient tyre characteristics into the model as well /2.4.11, 2.4.12/. For non steady state manoeuvres, e.g. travelling on uneven roads, time varying steering input or throttle application, the tyre response is delayed. The forces and the aligning moment lag behind their corresponding slip quantity. For the side force this effect is represented by the relaxation time or length, which gives a measure of the distance the wheel has to travel until the equivalent steady state value is reached after a sudden steering wheel input has been applied.

For driving manoeuvres on undulated road surfaces which give rise to vertical load variations two effects influence the side force generation. The variation in load leads to a so called 'static loss', which can be explained by the degressive relation between side force and vertical load. This loss is increased due to the dependency of the relaxation length on the vertical load illustrated by fig. 2.4-4. Parameter R gives the amplitude ratio for the vertical excitation. Experimental and theoretical studies /2.4.12/ indicate that the relaxation length is also a function of the slip angle. In the latter paper a model is presented, which allows incorporating these transient effects for wave lengths greater than two meters into the 'Magic Formula' formalism without having to introduce new coefficients. It gives satisfactory agreement to the experimental data for the pure slip conditions.

The 'Magic Formula' model satisfies most of the requirements listed in table 2.4-1. Its ability to approximate measured data accurately for pure and combined slip has been demonstrated and the formula can be used for the transient tyre behaviour as well. Computational speed and smoothness of the curves reproduced outside the measured range is given.

The model is easy to use in vehicle dynamics simulations once the parameters have been established. The three relevant quantities, the horizontal forces and the aligning torque are described by the same formula, differing only by the values of the four parameters B, C, D and E each. These parameters represent the tyre behaviour throughout its operating range in a physically meaningful fashion but their determination involves the calculation of many coefficients.

The idea of a continuous contact area, which is deformed by the shear stresses according to the resultant slip, implies that the horizontal forces and the aligning torque are not decoupled quantities as suggested by the formula. For instance, some coefficients defining the side force curve influence the shape of the aligning torque curve to a certain extent as well. This was addressed by recent modifications to the 'Magic Formula' /2.4.13/ The new 'Magic Formula' expresses the aligning torque as a product of the side force and the pneumatic trail. Further modifications to the 'Magic Formula' involved the introduction of shape functions which are applied to the pure slip tyre force characteristics for representing the influence of a combined slip condition. Replacing the semi-physically based model of the combined slip condition with an empirical approach followed the ideas published in /2.4.14/ and improved the quality of fit between measured and model data /2.4.15/.

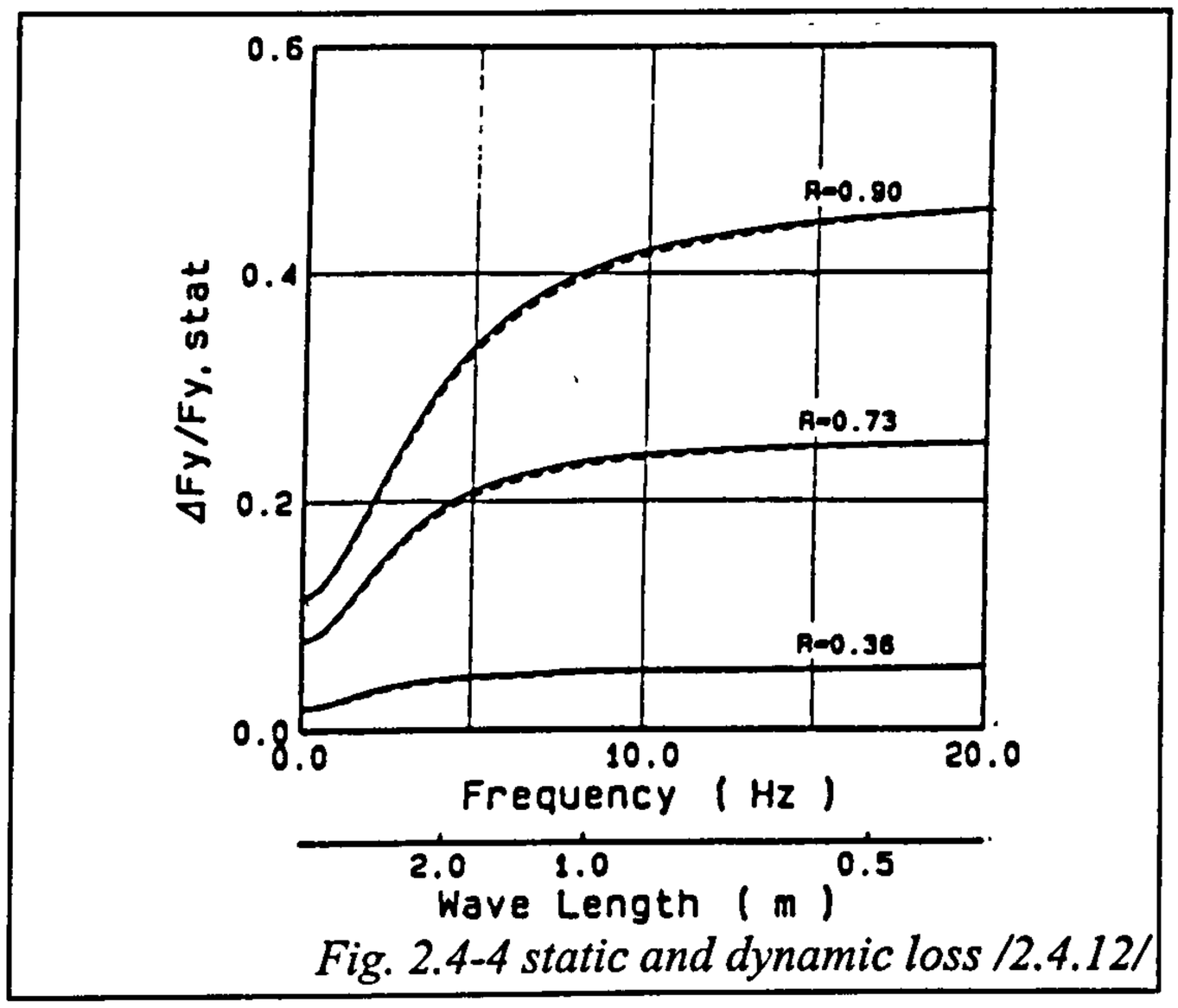

Fig. 2.4-4 static and dynamic loss /2.4.12/

2.5 Driver modelling

Vehicle models of varying complexity are available and frequently used for simulations of fixed control manoeuvres, for which driver inputs are defined in advance. Corresponding to the increased research into the relationship between subjective driver judgement of handling characteristics and objective vehicle response, it is desirable to include a driver model into the simulation, which approximates the control behaviour realistically. This would allow simulation of closed loop manoeuvres, comparable with those performed in real life situations and on test tracks. From the computed time histories performance indices could be determined, not only representing the directional response characteristics of the vehicle, but also the workload of the driver. These performance criteria might then be compared with the data made available by correlation exercises, discussed in section 2.3, in order to evaluate the ease of control.

It is accepted that the development of a realistic driver model remains very difficult and that a model, which can be used with confidence for all sorts of driving tasks is not yet available. Little is known about the structure of the probably complex control

pattern drivers rely on, their sensation of vehicle motions, the processing of incoming signals and how these are translated into corresponding control inputs and their recognition of risk thresholds.

Drivers control their vehicle subconsciously with little effort, for normal conditions. Given practice, they are also capable of performing more challenging manoeuvres, for which the vehicle behaves nonlinearily, demanding an increasing mental and possibly physical effort.

Driver models dealt with in the literature are approximated by linear controllers. Models differ in the number of input quantities considered, which lead to the two output signals steering wheel angle and throttle/brake position. Most of the driver models surveyed in /2.5.1/ take only future or actual path deviation into consideration. Other possible signals perceived by the driver, which influence the control strategy may comprise the following variables:

- hand wheel torque
- lateral acceleration (latac), vehicle side slip angle, roll angle and derivatives
- tyre squeal
- previewed path curvature / estimated future latac

A low steering resistance can indicate tyre saturation due to low friction or high cornering speed. From the experienced vehicle response, the driver might establish a personal risk threshold according to which the brake or throttle application is triggered. The previewed path curvature provides information about the severity of the forthcoming driving task.

Linear models have the advantage that they can be used for analysing the stability of the closed loop driver-vehicle system /2.5.2/. Their application makes sense, as long as low severity driving conditions are investigated, but may be unreasonable for limit manoeuvre simulations. On the other hand, their use may be justified by the assumption that a typical driver maintains a linear control pattern even for emergency manoeuvres and cannot adapt in time to meet the control demands.

Some characteristic parameters used for the linear modelling shall be summarised next, beginning with those associated with the steering control.

steering control parameters

Steering control consists of two major concurrent actions, the preview and regulation task. Scanning the environment the driver estimates the future path deviation, which provides the signal according to which the steering wheel is adjusted in advance, in order to compensate for the known response lag of the vehicle. The input may not lead to the desired directional attitude, forcing the driver to correct the steering until the vehicle follows the desired path.

The preview time T_P is one of the most important driver parameters. Multiplied with the velocity it gives the distance the driver looks forward to establish the new course. That notion implies that a driver focuses on only one point per time increment rather than scanning a finite range. The preview time is treated as a constant and determines to a great extent the stability of the closed loop system. Mitschke /2.5.3/ shows, for the case of a J-turn (entry of a turn), how this parameter is related to the vehicle design. He gives the following relationship, which is consistent with experimental results referenced in his book:

$$T_P \approx \frac{\sqrt{2}}{v_f}, \text{ or } T_P \approx \frac{2\sigma_f}{v_f^2}$$

This relationship indicates, that drivers adapt their control to vehicle properties as defined in section 2.3.2. Jaksch used a driver model /2.3.6/ with a preview time equivalent to the yaw rate response time as defined in (2.3.2.7). For other models, the preview time is adjusted to emulate the steering characteristics of a test driver or to achieve a certain tracking performance /2.5.4-5/.

Other driver characteristics are given by:

T_C: correction time; used for improving tracking performance /2.5.1/
T_d: delay time constant; representing the driver's input delay until he reacts to the incoming signal, independent of vehicle design /2.5.1/
T_I: lag time constant; representing the time needed to adjust steering to intended level signal, dependent on driver skill and vehicle design /2.5.1/

Another parameter dependent on driver experience as well as vehicle design is the steering angle gain, denoting the weighing factor between steering wheel angle and path deviation or possibly other relevant input signals. This parameter can be determined experimentally or by applying optimal control theory as demonstrated in /2.5.1/.

Optimal control theory is also used for the development of more complex driver models, which consider more than one incoming signal. The application of the theory yields to the minimisation of a performance index containing several weighted criteria, such as square path error, heading angle error and the physical steering effort. Furthermore, the theory allows the determination of certain driver constants. Another approach is pursued by MacAdam /2.5.6/. He proposed a neural network based driver representation. This driver model has to undergo a learning period in which it establishes suitable weights for previewed multi-point path deviations, before it emulates the steering characteristics of a real driver, as measured on a proving ground or established by a driving simulator.

throttle control

An example of a throttle control strategy is given in /2.5.1/. It is presumed that drivers apply throttle or brake according to the expected lateral acceleration. Deceleration is initiated, if a permissible lateral acceleration predetermined by the driver's experience is exceeded.

Summary

For studies of the driver-vehicle limit behaviour, it would be very helpful to have a driver model available, which simulates concurrent braking/throttle and steering control. There are strong indications that the vehicle handling is sensitive especially to this control activity, which is associated with the more complex tyre slip conditions.

2.6 Conclusions

The literature survey summarised some of the research activities on vehicle handling aspects. Some accident statistics were presented indicating a more qualitative relation between vehicle handling characteristics and road safety. From the accident data available, quantitative conclusions cannot be drawn as to what extent individual handling properties were contributing factors.

The extensive research on active chassis control systems indicates the efforts made on improving the driver's control. The development of some of these designs /1.2.4, 1.2.5/ is based on the notion that typical drivers have limited control skills obtained exclusively from low severity manoeuvering well within the limit of tyre-road adhesion. These chassis control systems, featuring either 4WS or brake and drive torque control, are designed to emulate the linear steady state behaviour to which the driver is accustomed, when a limit condition is encountered. The idea is to maintain a fairly linear relationship between the lateral response of the car and the steering input by the driver, involving low response delays. This certainly increases the linear performance bandwidth of the vehicle which has to be regarded as beneficial. However, it can be argued that the driver requires a degree of warning before the vehicle is about to approach its performance limit (or that of the driver). It is desirable that the vehicle response provides cues indicating to what extent the vehicle has approached its limit and by which rate the controllability decreases with severity. Some accident data from the USA /2.6.1/ indicate that the benefits of ABS seemed to have been partly compensated by a higher risk taking of drivers. It seems that an enlarged performance envelope has to be accompanied by some in-built warning features.

Some research has contributed to the knowledge of which characteristics constitute a desirable handling behaviour. Some results of correlation exercises were summarised, in which objective handling parameters were related to driver ratings. The findings

indicate that a fast vehicle response involving little vehicle side slip are beneficial attributes. Most of the this work addressed the linear vehicle behaviour prevalent for low severity manoeuvres. However, it seems that relatively little is known about which handling properties establish a beneficial, driver-friendly response behaviour for the transition from normal to limit driving, and especially about how tyres and suspensions have to be matched to achieve this goal. Nevertheless, the literature provided some useful information on how proving ground tests should be conducted to obtain informative data for handling evaluation.

It is accepted that modelling allows a cheap as well as informative analysis of the various design aspects involved in the design process of tyres and vehicles. For vehicle dynamics simulations, tyre models are usually used in a black box mode. They are embedded in vehicle dynamics codes, simulating the force and moment characteristics corresponding to the experimental data usually obtained from a drum or Flat Trac test rig. There are a few problems associated with this approach which require further investigation. The characteristics obtained from rig testing are influenced to some extent by the drum curvature, the increasing tyre wear during a test and by temperature effects. These factors are most influential for the high slip angle data. The measured characteristics may therefore reflect the tyre behaviour on the road imperfectly /2.6.2-3/.

3 Modelling facilities

This chapter gives an account of the modelling facilities employed for the research project. It consists of sections providing details about the vehicle and tyre modelling approach adopted.

The first two sections, 3.1 and 3.2, describe the two vehicle simulation codes used for carrying out studies of the tyre-suspension interface problem for limit conditions. The 'Steady State Cornering Model' was used to investigate and quantify effects of suspension and tyre properties on the steady state cornering performance of vehicles. A comprehensive documentation is found in section 3.1.

The following section 3.2 gives an introduction of the multi-body simulation package AUTOSIM, which was employed to develop a vehicle model for analysing the transient handling behaviour. The introduction is followed by an account of some modelling details including those not considered in the 'Steady State Cornering Model'. For both models a 'Magic Formula' based representation of the tyre forces and moments is used.

The determination of the parameters defining the 'Magic Formula' from tyre force and moment test data was a significant part of the project work. A summary of this work is found in the project report /1.0.1/.

Furthermore, in /1.0.1/ some information is given on SP Tyres' in-house developed tyre model TPP. The model predicts the force and moment characteristics for a tyre design. It can be used as an alternative to a force and moment test carried out on a rig for providing the data from which 'Magic Formula' parameters can be extracted.

3.1 Steady State Cornering Model

In this section the work on a program for the computation of the steady state road vehicle cornering behaviour is described. The importance of the constant radius test will be discussed briefly before the equations and assumptions on which the program is based are explained. After that a few plots are presented to demonstrate how the program's output helps to identify those parameters involved in determining the limit cornering behaviour.

3.1.1 The Steady State Cornering Test for Road Vehicles

The steady state cornering test is an important and widely used manoeuvre together with other standardised test procedures to analyse vehicle handling. In this experiment the car is driven around a circle of constant radius with a constant velocity and hand wheel angle. The lateral acceleration of the vehicle and possibly yaw velocity (yaw rate) and vehicle side slip as well as hand wheel angle and torque are recorded for a representative period of time before the velocity is increased to a slightly higher level for the next measurement until the limit of adhesion is reached. From the data recorded or in the case of a numerical simulation from those calculated, a 'handling diagram' (fig. 3.1-3) can be produced, showing the hand wheel angle against the lateral acceleration. This graph reveals the change in cornering behaviour of a vehicle, especially for its approach to the limit of adhesion. Steady state cornering is distinguished by the slopes of the shown curve. An increasing hand wheel angle with a rise in cornering speed is known as 'understeer', whereas a downwards inclined tangent indicates 'oversteer'. For the latter condition the driver has to turn the steering wheel in the opposite direction in order to balance the car.

An understeering vehicle remains in a stable condition, since a disturbance of the steady state initiated by a wind gust, a road irregularity or a driver input puts the vehicle onto a wider radius, therefore reducing its lateral acceleration. After a transient period the car reaches a new steady state condition. The reason for this is that the resultant force produced by the front tyres saturates first, giving the rear end a higher lateral resistance than the front end. An oversteering vehicle becomes unstable for a certain velocity depending on the actual slopes of the side force-slip angle (fig. 2.4-2) relation, which theoretically causes a self excited rotational motion (spin out).

The handling diagram can be divided into a linear region (up to 0.4 g), where the tyres operate at low slip angles and where load transfer from the inside wheels to the outside wheels is not an important feature, and into a second one, for which much increased understeer or a change towards oversteer occurs. The curved part reflects the non-linear tyre behaviour represented by high slip angles and large load differences between inside and outside wheel. The kinematic constraints of the

suspension may impose different slip and camber angles at the wheels of each axle, which influence the curvature as well, especially at the limit.

Since the driver cannot directly assess the degree of tyre saturation, the vehicle design has to provide the necessary signals for sensing the limit of adhesion. The most important ones are the steering feel at high lateral acceleration and the vehicle slip angle, though less obvious .

3.1.2 Numerical Simulation of Steady State Cornering

A detailed study into the parameters, which influence the shape of the handling diagram can only be done numerically, since the sheer number of those and their combinations are too high to be analysed in an experiment. Numeric experiments need not allow for either variances in driver or tyre performance and weather conditions. They give repeatability by definition, but rely very much on a thorough model description.

The model described here incorporates a precise description of the suspension and steering system as well as an advanced tyre model, in order to predict the cornering capability at higher lateral acceleration more accurately. The model was developed by Sharp /3.1.1/ and has been extended by certain features to be explained in this section. The equations on which the model is based are discussed and some program output is presented.

The simplest representation of road vehicle handling is given by the so-called 'bicycle model', which has two degrees of freedom (DoF) defining the yaw and slip motion. It is extensively discussed in /3.1.2/ and /3.1.3/ and widely used in the literature. The model does not account for vehicle roll and load transfer from the inside to the outside wheels, which are considered in the 'Segel model' /3.1.3/.

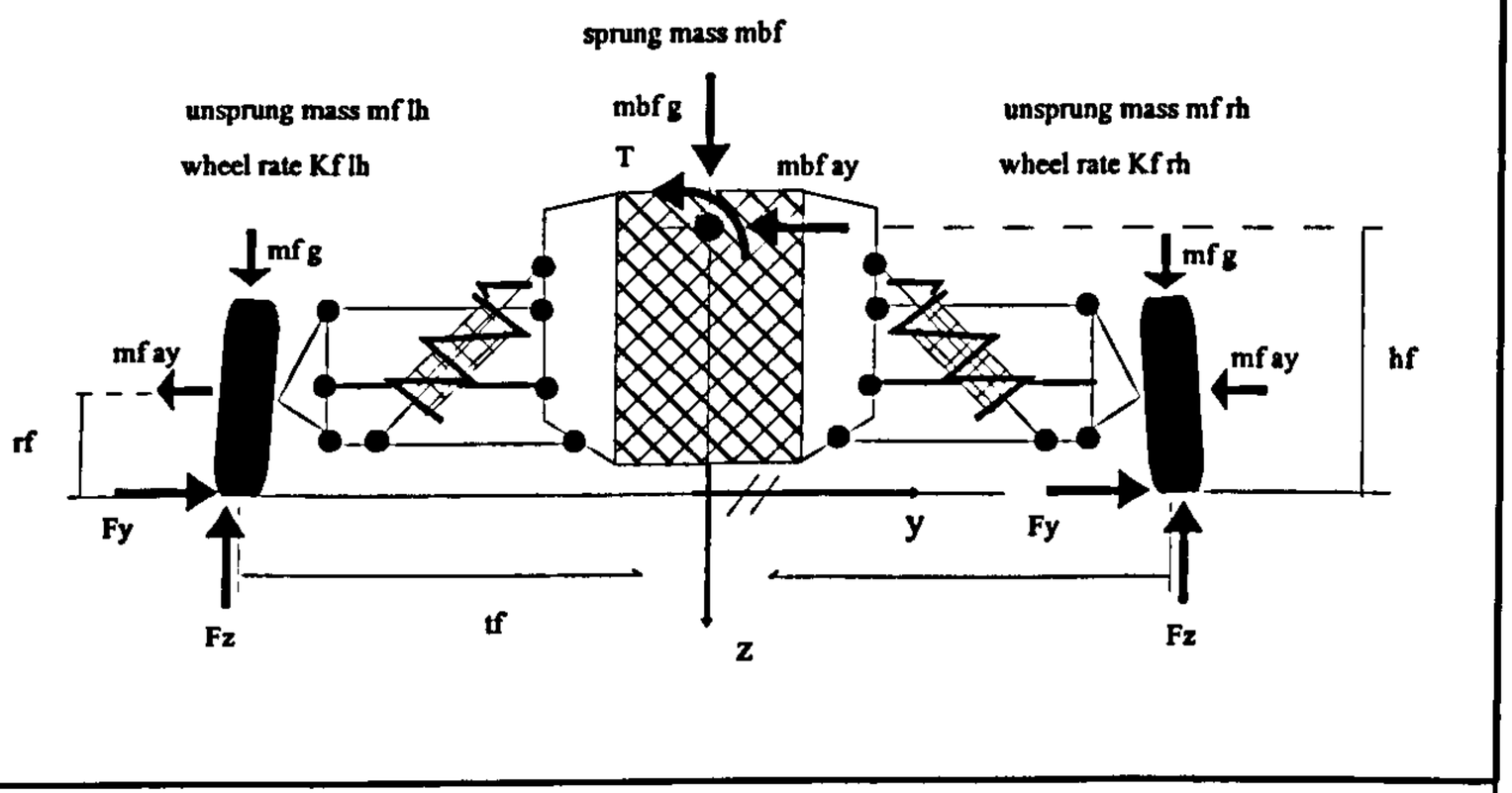

Fig. 3.1-1 front suspension model

The models mentioned above can be used for the dynamic handling analysis as well, whereas the current version of the 'Sharp model' allows only the steady state computation. Front and rear end of the vehicle are treated almost independently. For each front and rear end two DoF are introduced defining the vertical and roll motion of the sprung mass, which are equivalent to heave, roll and pitch of the whole car. It is assumed that the wheels remain in contact with the road surface, by which the vertical motion of the unsprung masses can be expressed in terms of body heave z and roll φ. Their lateral motion in y-direction relative to the body is predefined as a suspension property dependent on the wheel travel. Figure 3.1-1 shows the forces acting on the sprung and unsprung masses for a right hand turn. The inertia forces in the lateral and vertical direction are kept in equilibrium by the forces acting at the contact points of the tyres. The torque T accounts for the flexibility of the chassis, allowing different roll angles front and rear. The spring forces and possibly an anti roll bar resist the heave and roll motion. Apart from the two DoF both vertical and lateral forces as well as the slip angles α have to be determined giving a total number of eight unknowns for each end. The equations for the vertical forces and for the displacements heave z and roll φ are derived by applying the principle of d'Alembert. They are discussed in following section. Each lateral tyre force is dependent on the slip angle α, camber γ and the vertical load F_Z. Their relation is described by the 'Magic Tyre Formula'. The kinematic constraint implies that the vehicle turns on a constant radius and leads to the additional equations for the slip angles, which are explained in section 3.1.4. The kinematic properties of suspension and steering, e.g. camber and track change as well as roll steer, are predefined as known quantities dependent only on the wheel travel.

3.1.3 Equations for body heave and roll

The equations are written down only for the front end of the vehicle indicating the respective parameters by a subscript 'f'. The computation for the other is done in the same fashion. Those equations for the heave and roll motion, as well as those additional two for the vertical forces, are obtained by using d'Alembert's principle. For that the virtual work done by each force acting on the vehicle for a small displacement has to be calculated. Those small or virtual displacements are derived from the geometry shown in fig. 3.1-1. The vector from a coordinate system that is located at ground level, and which we will denote by the superscript '(0)', to the centre of gravity (CoG) of the sprung mass $m_{b,f}$ is:

$$\vec{r}_f^{\,CoG} = \begin{Bmatrix} 0 \\ (-h_f + z_f^B) \end{Bmatrix}^{(0)}, \text{ where } z_f^B \tag{3.1.1}$$

is the vertical displacement of the sprung mass with respect to the ground.

For each vector to the contact point we write:

$$\vec{r}_i^{CP} = \vec{r}^{CoG} + \begin{Bmatrix} y_{f,i}^W \cdot \cos\varphi_f - (h_f + z_{f,i}^W) \cdot \sin\varphi_f \\ y_{f,i}^W \cdot \sin\varphi_f + (h_f + z_{f,i}^W) \cdot \cos\varphi_f \end{Bmatrix}^{(0)}, \text{ where } y_{f,i}^W \text{ and } z_{f,i}^W$$

denote the lateral distance from the body CoG to the contact point and the vertical displacement of each wheel i, i=1,2 respectively. The inertia forces of the unsprung mass act at:

$$\vec{r}_i^W = \vec{r}_i^{CP} + \begin{Bmatrix} r_{f,i} \cdot \sin\gamma_{f,i} \cdot \cos\varphi_f + r_f \cdot \cos\gamma_{f,i} \cdot \sin\varphi_f \\ r_{f,i} \cdot \sin\gamma_{f,i} \cdot \sin\varphi_f - r_f \cdot \cos\gamma_{f,i} \cdot \cos\varphi_f \end{Bmatrix}^{(0)},$$

where $r_{f,i}$ is the rolling radius of each wheel i.

For small roll angles φ_f and φ_r ($\sin\varphi \sim \varphi$, $\cos\varphi \sim 1$) and neglecting terms of second order those vectors become:

$$\vec{r}_i^{CP} = \vec{r}^{CoG} + \begin{Bmatrix} y_{f,i}^W - (h_f + z_{f,i}^W) \cdot \varphi_f \\ y_{f,i}^W \cdot \varphi_f + (h_f + z_{f,i}^W) \end{Bmatrix}^{(0)} \text{ and} \qquad (3.1.2)$$

$$\vec{r}_i^W = \vec{r}_i^{CP} + R_{f,i} \cdot \begin{Bmatrix} \sin\gamma_{f,i} + \varphi_f \cdot \cos\gamma_{f,i} \\ \varphi_f \cdot \sin\gamma_{f,i} - \cos\gamma_{f,i} \end{Bmatrix}^{(0)}. \qquad (3.1.3)$$

The kinematic constraints, that the wheels maintain road contact, are expressed by the relations:

$$z_{f,i}^W = -z_f^B - y_{f,i}^W \cdot \phi_f, \qquad (3.1.4)$$

which means that the relative wheel travel between unsprung and sprung mass $z_{f,i}^W$ is composed of the chassis heave z_f^B and a component due to roll, which is proportional to half the track width $y_{f,i}^W$. This gives introduced in (3.1.2)

$$\vec{r}_i^{CP} = \begin{Bmatrix} y_{f,i}^W + (-h_f + z_f^B) \cdot \varphi_f \\ 0 \end{Bmatrix}^{(0)}. \qquad (3.1.5)$$

From (3.1.1), (3.1.3) and (3.1.5) the respective virtual displacements are computed:

$$\delta\vec{r}_f^{CoG} = \frac{\partial\vec{r}_f^{CoG}}{\partial z_{f,i}^B}\delta z_{f,i}^B + \frac{\partial\vec{r}_f^{CoG}}{\partial\varphi_{f,i}^B}\delta\varphi_{f,i}^B = \begin{Bmatrix} 0 \\ \delta z_f^B \end{Bmatrix}^{(0)} \qquad (3.1.6)$$

$$\delta\vec{r}_i^{CP} = \delta\vec{r}^{CoG} + \left\{\begin{matrix} \frac{\partial y_{f,i}^W}{\partial z_{f,i}^B} + \varphi_f \\ 0 \end{matrix}\right\}^{(0)} \delta z_{f,i}^B + \left\{\begin{matrix} \frac{\partial y_{f,i}^W}{\partial \varphi_{f,i}^B} + (-h_f + z_f^B) \\ 0 \end{matrix}\right\}^{(0)} \delta\varphi_f \qquad (3.1.7)$$

$$\delta\vec{r}_i^W = \delta\vec{r}_i^{CP} + r_{f,i} \cdot \frac{\partial \gamma_{f,i}}{\partial z_f^B} \cdot \left\{\begin{matrix} -\varphi_f \cdot \sin\gamma_{f,i} + \cos\gamma_{f,i} \\ \varphi_f \cdot \cos\gamma_{f,i} + \sin\gamma_{f,i} \end{matrix}\right\}^{(0)} \delta z_f^B +$$

$$\left[\frac{\partial \gamma_{f,i}}{\partial z_f^B} \cdot \left\{\begin{matrix} -\varphi_f \cdot \sin\gamma_{f,i} + \cos\gamma_{f,i} \\ \varphi_f \cdot \cos\gamma_{f,i} + \sin\gamma_{f,i} \end{matrix}\right\}^{(0)} + \left\{\begin{matrix} \cos\gamma_{f,i} \\ \sin\gamma_{f,i} \end{matrix}\right\}^{(0)}\right] \cdot r_{f,i}\delta\varphi_f \qquad (3.1.7)$$

Applying d'Alembert's principle we write

$$\sum_{i=1}^{2}\left(\frac{\partial \Delta l_{f,i}}{\partial z_f^B} \cdot F_{f,i}^S \cdot \delta z_f^B + \frac{\partial \Delta l_{f,i}}{\partial \varphi_{f,i}} \cdot F_{f,i}^S \cdot \delta\varphi_{f,i}\right) + \sum_{i=1}^{2}\left(c_{\varphi,f}^{RB} \cdot \varphi_{f,i} \cdot \delta\varphi_{f,i}\right)$$

$$= (\delta\vec{r}_f^{CoG}, \begin{pmatrix} m_f^B \cdot \frac{\mathrm{v}^2}{\rho} \\ m_f^B \cdot \mathrm{g} \end{pmatrix}) + \sum_{i=1}^{2}(\delta\vec{r}_{f,i}^{CP}, \begin{pmatrix} F_{f,i}^y \\ F_{f,i}^z \end{pmatrix}) + \sum_{i=1}^{2}(\delta\vec{r}_{f,i}^W, \begin{pmatrix} m_{f,i}^W \cdot \frac{\mathrm{v}^2}{\rho} \\ m_{f,i}^W \cdot \mathrm{g} \end{pmatrix}) \qquad (3.1.8)$$

where the expression on the left hand side gives the internal work done by the spring forces $F_{f,i}^S$, and the roll bar moment given by $c_{\varphi,f}^{RB} \cdot \varphi_{f,i}$, while the scalar products on the right hand side give the virtual work done by the applied forces to the sprung and unsprung masses. The spring force $F_{f,i}^S$ is proportional to the spring deflection, which itself is a function of the wheel travel $z_{f,i}^W$ defined by (3.1.4). For the two independent virtual displacements we obtain the equilibrium equations for the heave and roll motion:

$$\delta z_f^B \{\sum_{i=1}^{2}(F_{f,i}^S \frac{\partial \Delta l_{f,i}}{\partial z_f^B}) - m_f^B \mathrm{g}$$

$$-\sum_{i=1}^{2} m_{f,i}^W \cdot \mathrm{g} \cdot R_{f,i} \cdot \frac{\partial \gamma_{f,i}}{\partial z_f^B} \cdot (\varphi_f \cdot \cos\gamma_{f,i} + \sin\gamma_{f,i})$$

$$-\sum_{i=1}^{2} F_{f,i}^y (\frac{\partial y_{f,i}^{CP}}{\delta z_f^B} + \varphi_{f,i}^B) \qquad (3.1.9)$$

$$+\sum_{i=1}^{2} m_{f,i}^W \cdot \frac{\mathrm{v}^2}{\rho} \cdot [\frac{\partial \gamma_{f,i}^{CP}}{\delta z_f^B} + \varphi_{f,i}^B + R_{f,i} \cdot \frac{\partial \gamma_{f,i}}{\partial z_f^B} \cdot (-\varphi_f \cdot \sin\gamma_{f,i} + \cos\gamma_{f,i})]\} = 0$$

and

$$\delta\varphi_f^B \{\sum_{i=1}^{2}(F_{f,i}^S \frac{\partial \Delta l_{f,i}}{\partial \varphi_f^B}) + c_{\varphi,f}^{RB} \cdot \varphi_f^B + \mathrm{T}$$

$$-\sum_{i=1}^{2} m_{f,i}^W \cdot \mathrm{g} \cdot r_{f,i} \cdot [\frac{\partial \gamma_{f,i}}{\partial \varphi_f^B}(\varphi_f \cdot \cos\gamma_{f,i} + \sin\gamma_{f,i}) + \sin\gamma_{f,i}]$$

$$-\sum_{i=1}^{2} F_{f,i}^y \cdot [\frac{\partial y_{f,i}^{CP}}{\delta \varphi_f^B} - (h_f - z_f^B)] \qquad (3.1.10)$$

$$+\sum_{i=1}^{2} m_{f,i}^W \cdot \frac{\mathrm{v}^2}{\rho} \cdot [\frac{\partial y_{f,i}^{CP}}{\delta \varphi_f^B} - (h_f - z_f^B)]$$

$$+\sum_{i=1}^{2} m_{f,i}^W \cdot \frac{\mathrm{v}^2}{\rho} \cdot r_{f,i} [\frac{\partial \gamma_{f,i}}{\partial z_f^B}(-\varphi_f \cdot \sin\gamma_{f,i} + \cos\gamma_{f,i}) + \cos\gamma_{f,i}]\} = 0$$

By relaxing the system from its vertical constraints two more equations are derived for the determination of the vertical tyre forces. The first one is obtained by moving the whole front end of the vehicle vertically:

$$\delta z_0 \{-m_f^B \mathrm{g} - \sum_{i=1}^{2} m_{f,i}^W \mathrm{g} + \sum_{i=1}^{2} F_{f,i}^Z\} = 0 \qquad (3.1.11)$$

The second equation describes the equilibrium for a small roll displacement of the whole system:

$$\partial\varphi_0 \{-m_{f,i}^W \cdot \frac{\mathrm{v}^2}{\rho} \cdot (h_f - z_f^B) - T$$

$$+\sum_{i=1}^{2} m_{f,i}^W \cdot \mathrm{g} \cdot r_{f,i} \cdot (\varphi_f \cdot \cos\gamma_{f,i} + \sin\gamma_{f,i})$$

$$+\sum_{i=1}^{2} m_{f,i}^W \cdot g \cdot [y_{f,i}^{CP} - (h_f - z_f^B) \cdot \varphi_f] \qquad (3.1.12)$$

$$-\sum_{i=1}^{2} F_{f,i}^Z [y_{f,i}^{CP} + (h_f - z_f^B) \cdot \varphi_f]$$

$$-\sum_{i=1}^{2} m_{f,i}^W \cdot \frac{\mathrm{v}^2}{\rho} r_{f,i} \cdot (-\varphi_f \cdot \sin\gamma_{f,i} + \cos\gamma_{f,i})\} = 0$$

After having derived the equations for the two DoF's as well as two for the vertical forces at the front end of the car, equations relating the lateral tyre forces and the slip angles have to be established. The 'Magic Tyre Formula' provides two equations for the four unknowns $F_{f,i}^Y$ and α_i, i=1,2. A third one can easily written down as follows:

$$\partial y_0 \{\frac{\mathrm{v}}{\rho}(-m_f^B - \sum_{i=1}^{2} m_{f,i}^W) + \sum_{i=1}^{2} F_{f,i}^Y\} = 0 \qquad (3.1.13)$$

by which lateral forces are summed leaving one more equation to be found.

3.1.4 Kinematics of steady state cornering

In order to obtain a complete set of equations for the two slip angles at the left and right hand side, a kinematic constraint has to be imposed, relating the two variables. In the first version of the model these were set to be equal, which is true for large cornering radii and a steering system which positions the wheels at both ends parallel to each other. For a more general approach a simple steering model has been incorporated, allowing the analysis of effects due to steering column elasticity, roll steer and non-parallel steering. The slip angles are defined by the velocity computed for each wheel. Referring to fig. 3.1-2 we write for the front:

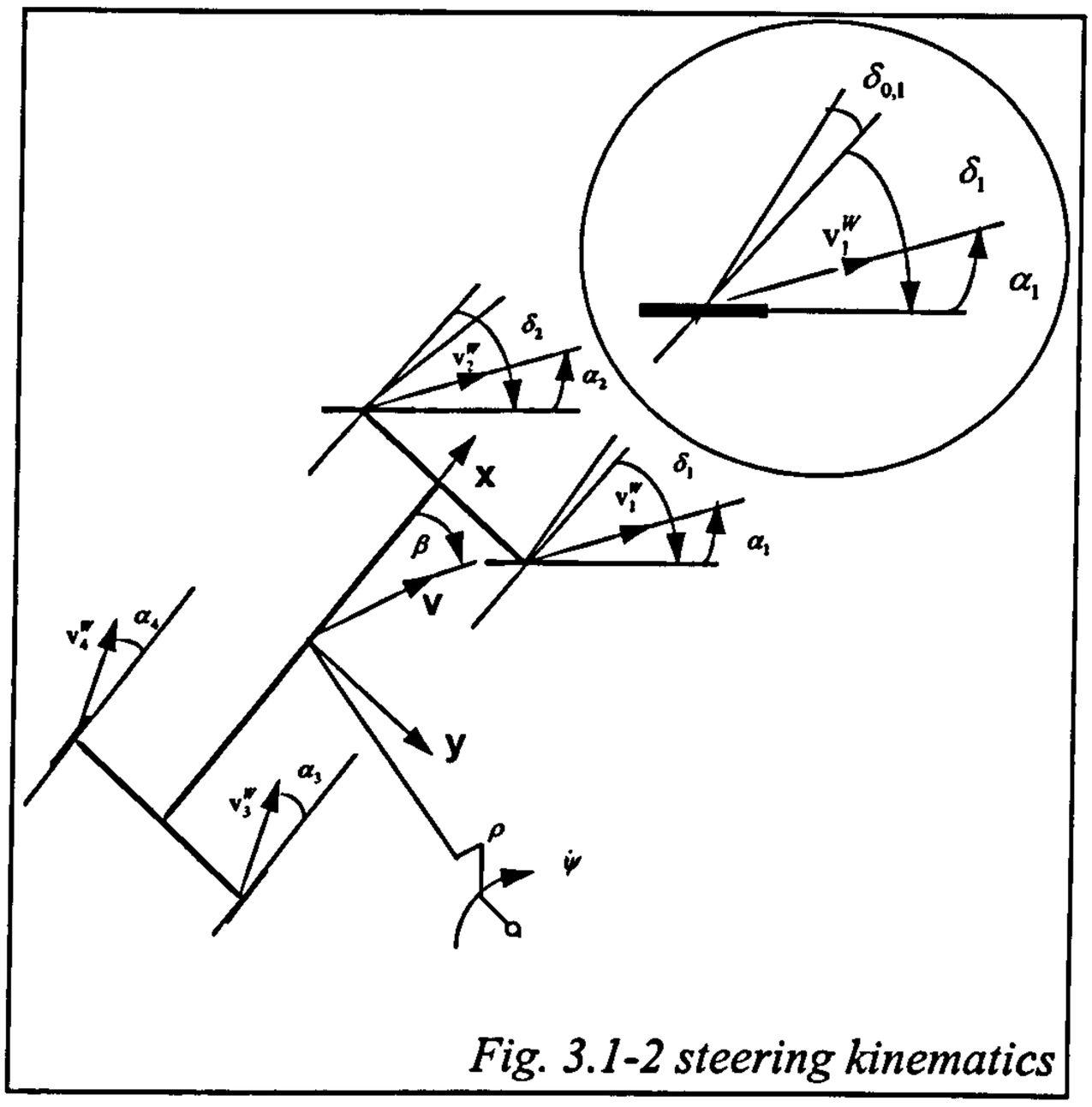

Fig. 3.1-2 steering kinematics

$$\tan(\delta_i - \alpha_i) = \frac{v_{y,i}^W}{v_{x,i}^W}, \text{ with} \qquad (3.1.14,15)$$

$$v_{x,i}^W = v \cdot \cos\beta - \dot{\psi} \cdot y_{f,i}^{CP}, \text{ and } v_{y,i}^W = v \cdot \sin\beta + \dot{\psi} \cdot l_f$$

for i=1, 2 and

$$\tan(\delta_i - \alpha_i) = \frac{v_{y,i}^W}{v_{x,i}^W}, \text{ with} \qquad (3.1.16,17)$$

$$v_{x,i}^W = v \cdot \cos\beta - \dot{\psi} \cdot y_{r,j}^{CP}, \text{ and } v_{y,i}^W = v \cdot \sin\beta - \dot{\psi} \cdot l_r$$

i=3, 4 for the rear, where v is the velocity of the vehicle, β the vehicle slip angle and $\dot{\psi}$ the yaw rate. The latter is for a steady state identical to v/ρ, where ρ is the cornering radius. The variables $v_{x,i}^W$ and $v_{y,i}^W$ are the longitudinal and lateral velocities at the contact point with respect to the coordinate system shown in fig. 3.1-2 The parameters l_f and l_r denote the longitudinal distance from the vehicle's CoG to the front and rear axle. The equations (3.1.14-17) indicate that front and rear end are no

longer independent from each other because of the common dependency of the slip angles α_i at the wheels on the variable β.

Each steering angle δ_i is composed by the static toe angle $\delta_{i,0}$, the angle δ_i^{KP} at the kingpin, which is established by the steering column rotation δ^{LC}, and an angle $\Delta\delta_i$ due to roll steer:

$$\delta_i = \delta_i^{KP}(\delta^{LC}) + \Delta\delta_i + \delta_{0,i} \qquad (3.1.18\text{-}21)$$

The roll steer characteristics are given as a polynomial with the wheel travel as the independent variable and with $c_{\delta,i,j}$ j=1, 2 as coefficients. For the front end

$$\Delta\delta_i(z_f^B, \varphi_f^B) = c_{\delta,i,1} \cdot (z_f^B \pm t_f \cdot \varphi_f^B) + c_{\delta,i,2} \cdot (z_f^B \pm t_f \cdot \varphi_f^B)^2 \qquad (3.1.22\text{-}23)$$

and for the rear

$$\Delta\delta_i(z_r^B, \varphi_r^B) = c_{\delta,i,1} \cdot (z_r^B \pm t_r \cdot \varphi_r^B) + c_{\delta,i,2} \cdot (z_r^B \pm t_r \cdot \varphi_r^B)^2 \qquad (3.1.24\text{-}25)$$

holds. Finally, a steering ratio is introduced, which provides the functional dependency between δ_i^{KP}, the angle prevalent at the kingpin, and δ^{LC} defining the column rotation:

$$\delta_i^{KP}(\delta^{LC}) = a_{i,1} \cdot \delta^{LC} + a_{i,2} \cdot \delta^{LC^2} \qquad (3.1.26\text{-}29)$$

Again, a second order polynomial is used, for which the first parameter $a_{i,1}$ represents the linear ratio, whereas the second one allows introducing non-parallel steering characteristics. Note that this relation refers to the front as well as to the rear wheels, so that the rear wheels can be steered relative to the front wheels according to the function $\delta_i^{KP}(\delta_i^{LC})$.

Equations (3.1.9-13) applied for both front and rear end give a total of 10. These added to the equations (3.1.14-17) and those four, provided by the 'Magic Tyre Formula' for the lateral forces, constitute a complete set to calculate the 18 unknown variables z_f^B, φ_f^B, $F_{f,i}^Z$, $F_{f,i}^Y$, z_r^B, φ_r^B, $F_{r,i}^Z$ $F_{r,i}^Y$ and α_i, i=1,2 as well as β and δ^{LC}. Compared to the set of only 16 unknowns for which differences in the slip angles at each end are neglected the two variables β and δ^{LC} are augmented to the system of equations. From the equations (3.1.10), (3.1.12) and (3.1.14-17) we see that the interaction between front and rear end is determined by the chassis torque T and vehicle's slip angle β only.

3.1.5 Suspension kinematics

In the equations presented so far some expressions occur, which represent the kinematic and stiffness properties of the suspension. All of those are functions of the vertical wheel travel and are defined by fitting a polynomial up to the second order to the real suspension data. The following equations refer to the front of the car again. The suspension characteristics modelled comprise the camber angle $\gamma_{f,i}$, the track change $y_{f,i}^{CP}$ and the spring deflection $\Delta l_{f,i}$. They have to be provided as a second order polynomial according to:

$$\gamma_{f,i}(z_f^B, \varphi_f^B) = \gamma_{f,0,i} + c_{C,i,1} \cdot (z_f^B \pm t_f \cdot \varphi_f^B) + c_{C,i,2} \cdot (z_f^B \pm t_f \cdot \varphi_f^B)^2 \quad (3.1.30\text{-}31)$$

$$y_{f,i}(z_f^B, \varphi_f^B) = \pm t_f + c_{Y,i,1} \cdot (z_f^B \pm t_f \cdot \varphi_f^B) + c_{Y,i,2} \cdot (z_f^B \pm t_f \cdot \varphi_f^B)^2 \quad (3.1.32\text{-}33)$$

$$\Delta l_{f,i}(z_f^B, \varphi_f^B) = c_{L,i,1} \cdot (z_f^B \pm t_f \cdot \varphi_f^B) + c_{L,i,2} \cdot (z_f^B \pm t_f \cdot \varphi_f^B)^2 \quad (3.1.34\text{-}35)$$

Parameter t_f denotes the nominal half track change. The spring forces are given by:

$$F_{f,i}^S(\Delta l_{f,i}) = F_{f,0,i}^S + \mathrm{K}_{f,i} \cdot \Delta l_{f,i} \quad (3.1.36\text{-}37)$$

where $\mathrm{K}_{f,i}$ denotes the linear spring stiffness and $F_{f,0,i}^S$ the preload. According to (3.1.34-35) the spring deflection $\Delta l_{f,i}$ is a quadratic function of the wheel travel, so that a non-linear spring rate with respect to the wheel travel can be introduced.

The coefficients of the polynomials, together with those of the 'Magic Tyre Formula', are the main part of the model's input data. For a real suspension the parameters given in (3.1.30-37) are not independent of each other, so that a consistent representation can only be achieved by either a good measurements or by a preliminary kinematic analysis.

3.1.6 Numerical computation

Although there are only 18 DoF present in the model, the program solves for 42 variables. The equations (3.1.9-13), (3.1.14-17), (3.1.30-37) and the expressions for the derivatives of (3.1.30-35) are included into the system of algebraic equations solved by a Newton-Raphson algorithm. These 42 equations obtained for front and rear end are much simpler than the those for the smaller system, where all dependent variables had to be substituted by the DoF, and allow a much easier computation of the Jacobian. Furthermore, extensions to the model are easier to incorporate.

3.1.7 Steering model

As mentioned in the introduction of this chapter, hand wheel angle and hand wheel torque are important parameters for the driver's perception of the handling performance. The change in hand wheel angle for an increasing lateral acceleration is largely dependent on the vehicle mass distribution as well as suspension and tyre properties. A further factor affecting the shape of the handling diagram, not yet considered, is the compliance in the steering system resulting from the column twist and from the elastic deformations of the bushings, which connect the different suspension parts to the body and to the wheel hub. Only the former effect is accounted for in the model.

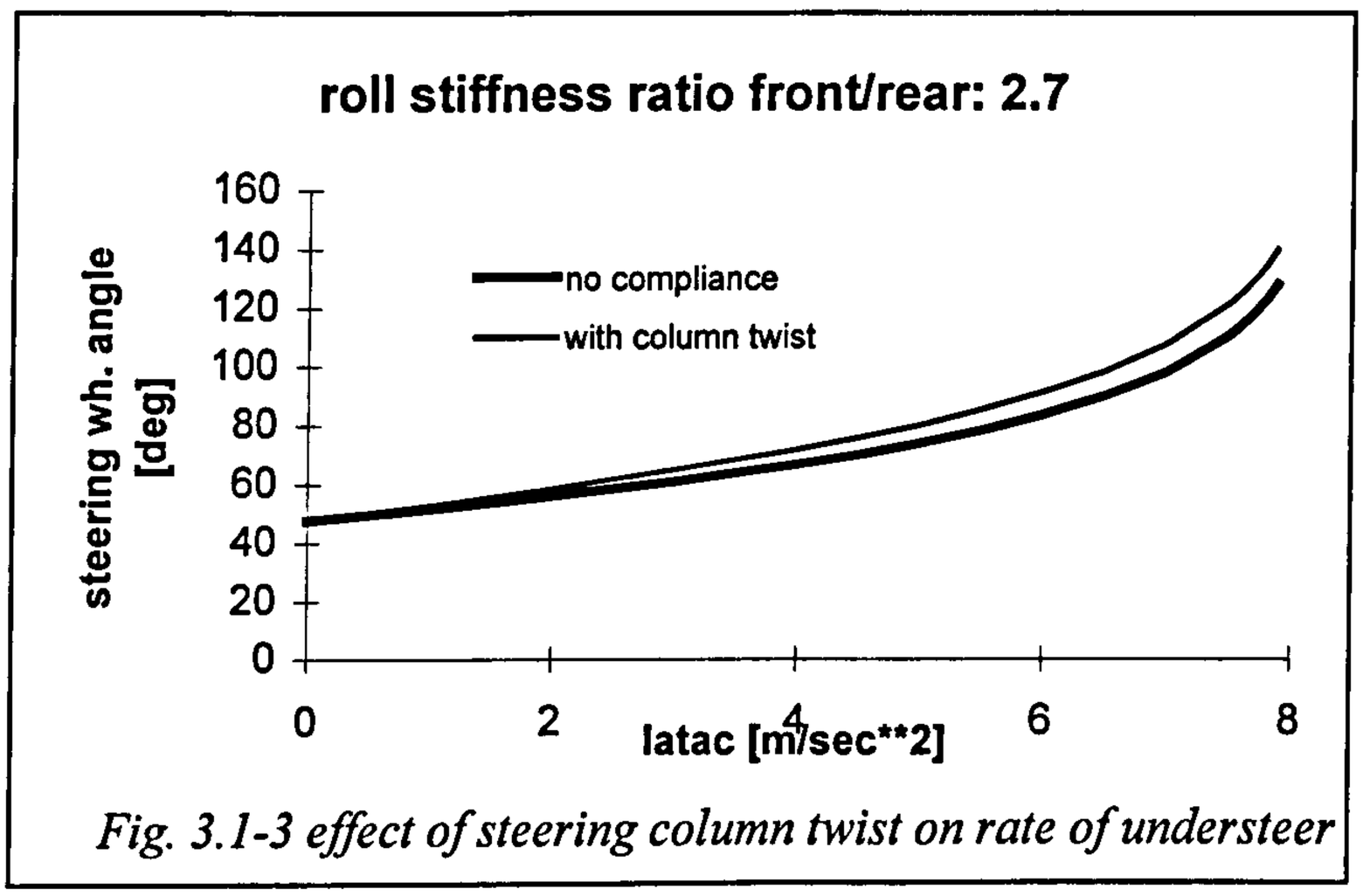

Fig. 3.1-3 effect of steering column twist on rate of understeer

The presence of column twist means that the driver has to adjust a rather higher hand wheel angle δ^{HW} than for a rigid steering system, while angles and torques present at each wheel remain the same. We introduce the column stiffness c_φ^C to account for the column compliance leading to a difference in δ^{HW} and δ^{LC}. Applying the principle of virtual work again, we calculate the steering wheel angle from the work done by the aligning torques M_i^{AL} and by the column spring c_φ^C. The aligning torques are given by the 'Magic Tyre Formula' and can be computed off-line.

$$\sum_{i=1}^{2} M_i^{AL} \frac{\partial \delta_i}{\partial \delta^{LC}} = c_\varphi^C \cdot (\delta^{LC} - \delta^{HW}) \qquad (3.1.38)$$

Using (3.1.18-19) and (3.1.22-23), we write for the hand wheel angle:

$$\delta^{HW} = \delta^{LC} + \frac{1}{c_\varphi^C} \cdot \sum_{i=1}^{2} M_i^{AL} (a_{i,1} + 2 \cdot a_{i,2} \cdot \delta^{LC}) \qquad (3.1.39)$$

The hand wheel torque is easily computed by:

$$M^{HW} = -c_\varphi^C \cdot (\delta^{LC} - \delta^{HW}) \qquad (3.1.40)$$

Fig. 3.1-3 shows the influence of the column elasticity on the handling diagram.

3.1.8 Bump and rebound stop model

For cornering manoeuvres with high lateral acceleration, one or more wheels may run into their bump or rebound stop, preventing them to hit the wheel arches. The wheel travel in bump and rebound direction is limited by rubber elements, which almost prevent any further relative motion between wheel and vehicle body after their engagement. Restricting the wheel travel also limits the camber and track changes, which are described as polynomials of the former, and changes the roll stiffness distribution in favour of the end, where one of these rubber springs compresses first.

Neglecting these elements in the simulation would lead to unrealistic high wheel displacements and corresponding camber and track changes for high lateral accelerations. After conducting some simulations it became apparent that the camber angles influence the side force distribution of the vehicle considerably, and thus the limit handling behaviour.

The following bump stop force relation is introduced:

$$F_{f,i}^{BS}(\Delta l_{f,i}) = \mathrm{K}_{f,i}^{BS} \cdot (\Delta l_{f,i} - \Delta l_{f,0}^{BS})^4 \qquad (3.1.41)$$

This relation provides a smooth transition from the nominal spring behaviour given by (3.1.36, 37) to the spring characteristics, established by suspension spring and bump stop acting in parallel. The shape of the transition is controlled by parameter $\mathrm{K}_{f,i}^{BS}$, while the threshold value for the bump stop engagement is specified by the spring deflection constant $\Delta l_{f,0}^{BS}$. The bump stop force increases with the forth power of the normalised spring deflection as given by (3.1.41). A similar relation is introduced for the rebound stops.

3.1.9 Application and limits of the model

The application of the steady state cornering model is best presented by examples. Fig. 3.1-4 shows the plot of a handling diagram for a heavy saloon car, for which the static toe-in angles have been varied for the front and rear wheels respectively. The curve in the middle refers to zero toe-in all around. The curve above represents the same car with one degree toe out at the front and one degree toe in at the rear, whereas the lower one has been produced for a car with the opposite setting. There is not much difference for low lateral acceleration up to 2 m/sec^2, for which hardly any load transfer occurs. The side forces are determined by the slip angles only in a linear fashion, so that toe-in/ toe-out effects cancel each other out at each axle. As soon as load transfer becomes significant, the three curves differ from each other in a

progressive way. Toe in at the front allows the heavier loaded tyre to produce the same side force, travelling with a smaller slip angle compared to the reference curve in the middle of the plot, and thus giving less understeer. The opposite effect dominates the upper curve representing a more understeering vehicle. The steering wheel angle for the limit state is almost double the one of the configuration discussed before. On the other hand the car provides a smoother behaviour for the transition from the linear to the limit region.

Other simulation results can be found in chapter 8 dealing with the tyre-suspension interface.

This section ends with some notes about the assumptions made as well as the limits of the steady state cornering model. The first simplification implies that roll angles remain small, so that certain parts of the equations derived in section 3.1.3 could be linearised. This assumption is sensible, since roll angles remain usually below 10 deg.

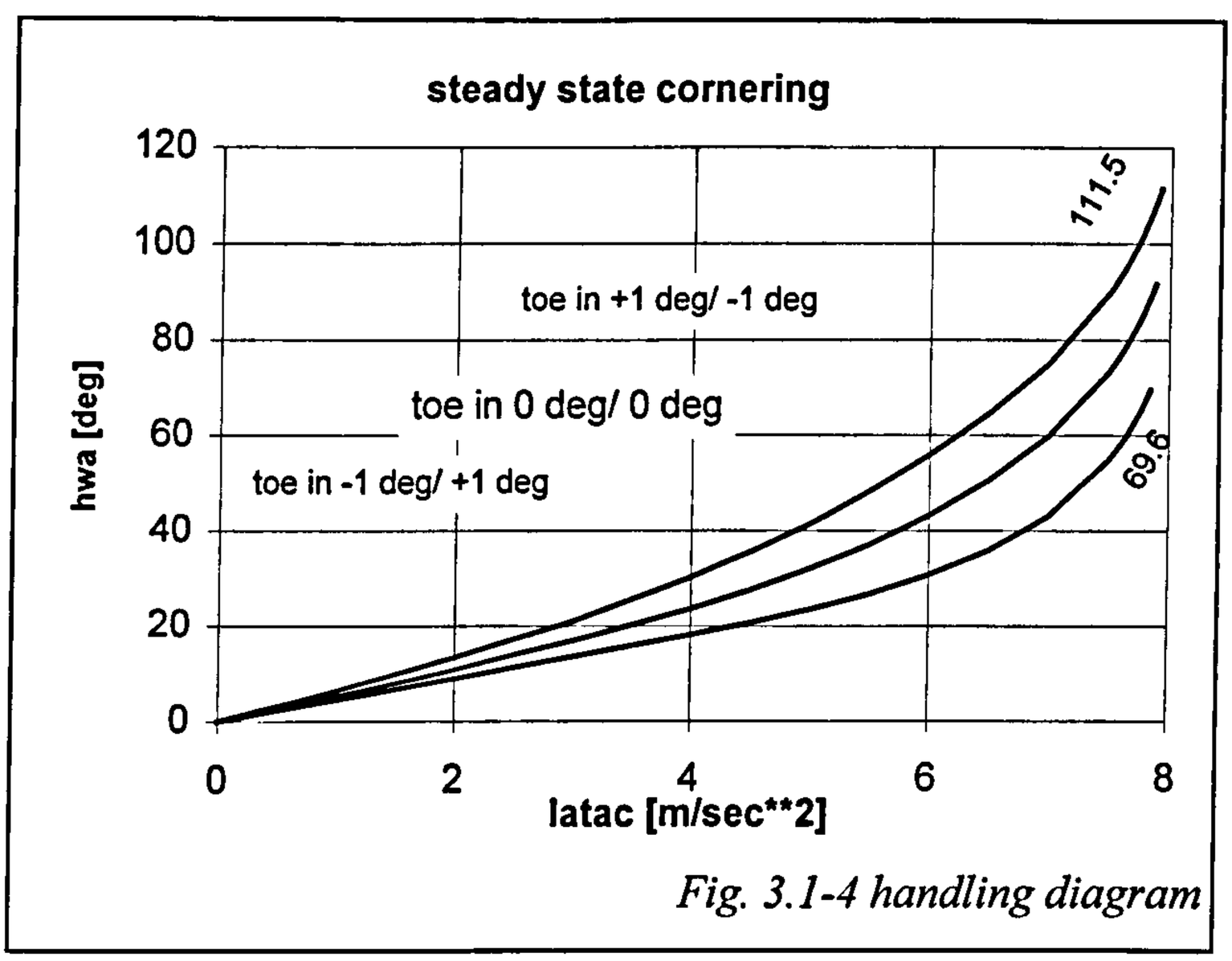

Fig. 3.1-4 handling diagram

The suspensions of the model are not truly independent according to the assumption that the wheels stay in contact to the road all the time. A cornering car with one of its inside wheels off the ground, for instance, is not accounted for. Furthermore, the tyre deflection is not considered in the equations defining the kinematics and the equilibrium of the system. Only the roll angle is adjusted according to the tyre squash. These issues have to be considered for the limit handling analysis of vehicles featuring a suspension spring stiffness of the same order as that of the tyre.

Driving and aerodynamic forces as well cornering drag are not included in the model. Especially, the driving forces can affect considerably the handling for low friction levels. Elastic deformations of the suspension due to the horizontal guidance forces are not considered either. But, these effects are of smaller interest and can be investigated by more powerful programs available.

3.1.10 Summary of steady state model description

A program for the computation of steady state cornering behaviour of a road vehicle has been developed. Due to the accurate description of the suspension system, it allows a fairly accurate prediction, especially of the non-linear part of a handling diagram showing the relation of hand wheel angle and lateral acceleration ('latac'), where the lateral acceleration exceeds 0.4 g.

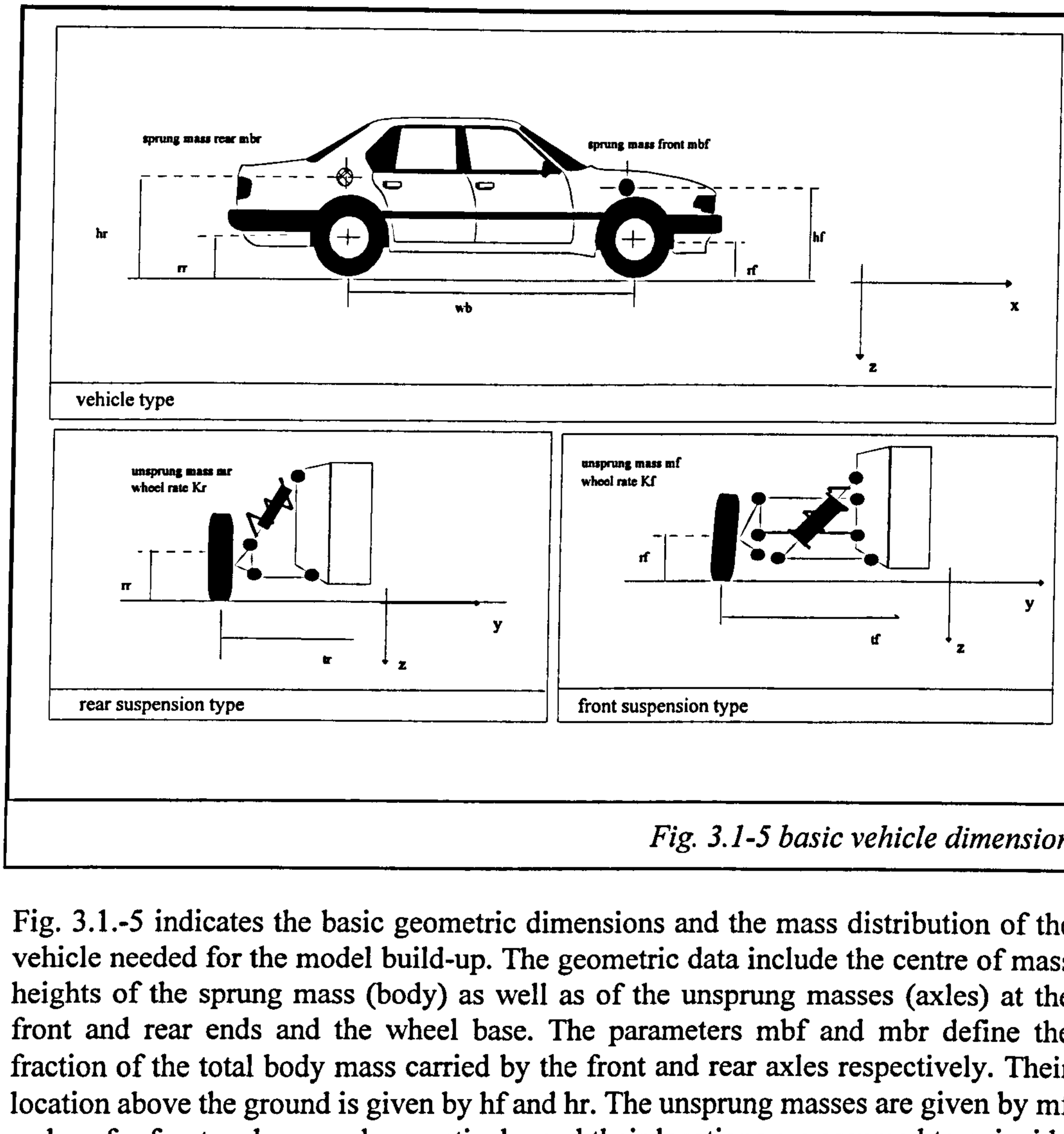

Fig. 3.1-5 basic vehicle dimensions

Fig. 3.1.-5 indicates the basic geometric dimensions and the mass distribution of the vehicle needed for the model build-up. The geometric data include the centre of mass heights of the sprung mass (body) as well as of the unsprung masses (axles) at the front and rear ends and the wheel base. The parameters mbf and mbr define the fraction of the total body mass carried by the front and rear axles respectively. Their location above the ground is given by hf and hr. The unsprung masses are given by mf and mr for front and rear end respectively, and their locations are assumed to coincide with half of the track width tf or tr in the longitudinal, and with the rolling radius rf or rr in the vertical direction.

The suspension data necessary for a complete model description are shown as plots, referring to the suspension type employed for the front and rear end of the vehicle (fig. 3.1-6, 3.1-7). Except the steering ratio, all kinematic and mechanical characteristics are dependent on the wheel travel[1] and are approximated by second order polynomials order (parabolic), which should give a good fit to the real data. Note that the camber angle is given here relative to the vehicle.

The body spring force is modelled as a function of the actual spring deflection, which again is a function of the wheel travel. Note that the force given in the plots, referring to fig. 3.1-6 and fig. 3.1-7, is the total force acting along the spring rather than its vertical component. These spring characteristics could be derived also from a graph of the measured wheel rate against the wheel travel.

Additional to the functions of camber, track change, roll steer and the spring force, the kinematic steering angles at the wheels have to be known as a function of the hand wheel or better lower steering column rotation, since the latter is not affected by column twist. For the model, the kinematics of the ideally rigid steering system have to be defined, given by the plot showing the steering angles for the front suspension (fig. 3.1-6), which do not include any compliance or static toe. The only compliance accounted for in the model of the steering system stems from a linear elastic column spring connecting steering wheel and lower column end.

A few more parameters complete the model description, which are:

- anti roll bar stiffness front and rear given in [Nm/rad]; not the stiffness of the actual bar against a torsional moment is meant here, but its contribution to the overall rigid body roll stiffness.
- chassis torsional stiffness [Nm/rad]; this parameter defines the structural stiffness of the body against twist (in vehicle dynamics this parameter is assumed to be infinite giving both front and rear end of the car equal roll angles)
- static toe in front and rear [rad]
- steering column stiffness [Nm/rad]; parameter introduces compliance due to column elasticity, which leads to larger hand wheel angles compared to a rigid steering system
- mechanical trail [m]; a positive value increases the steering effort

In the appendix A1 a data deck comprising all model parameters and their brief description can be found as well as a list of symbols used in this chapter.

[1] wheel travel is understood as the vertical travel of the contact point of the wheel

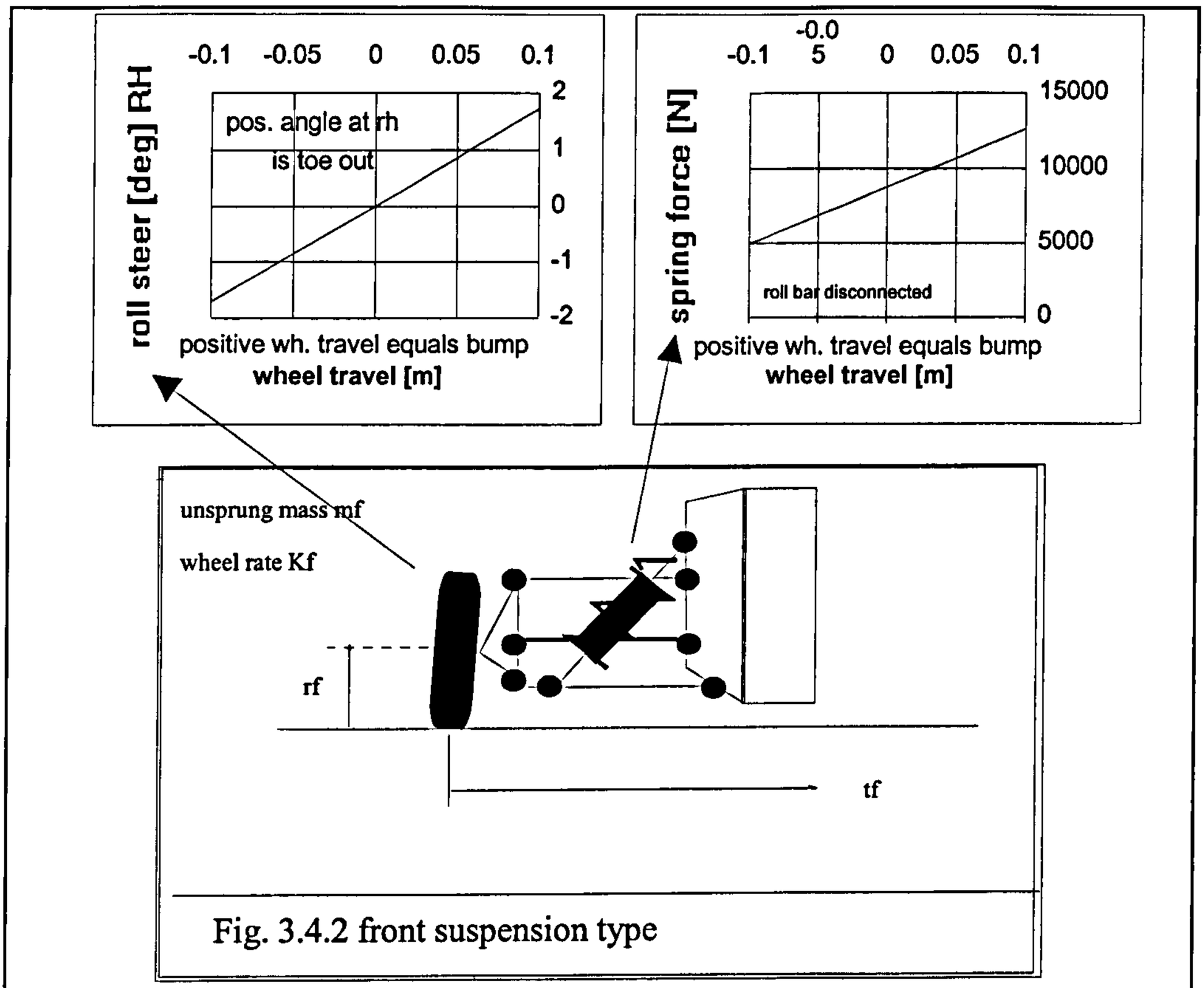

Fig. 3.4.2 front suspension type

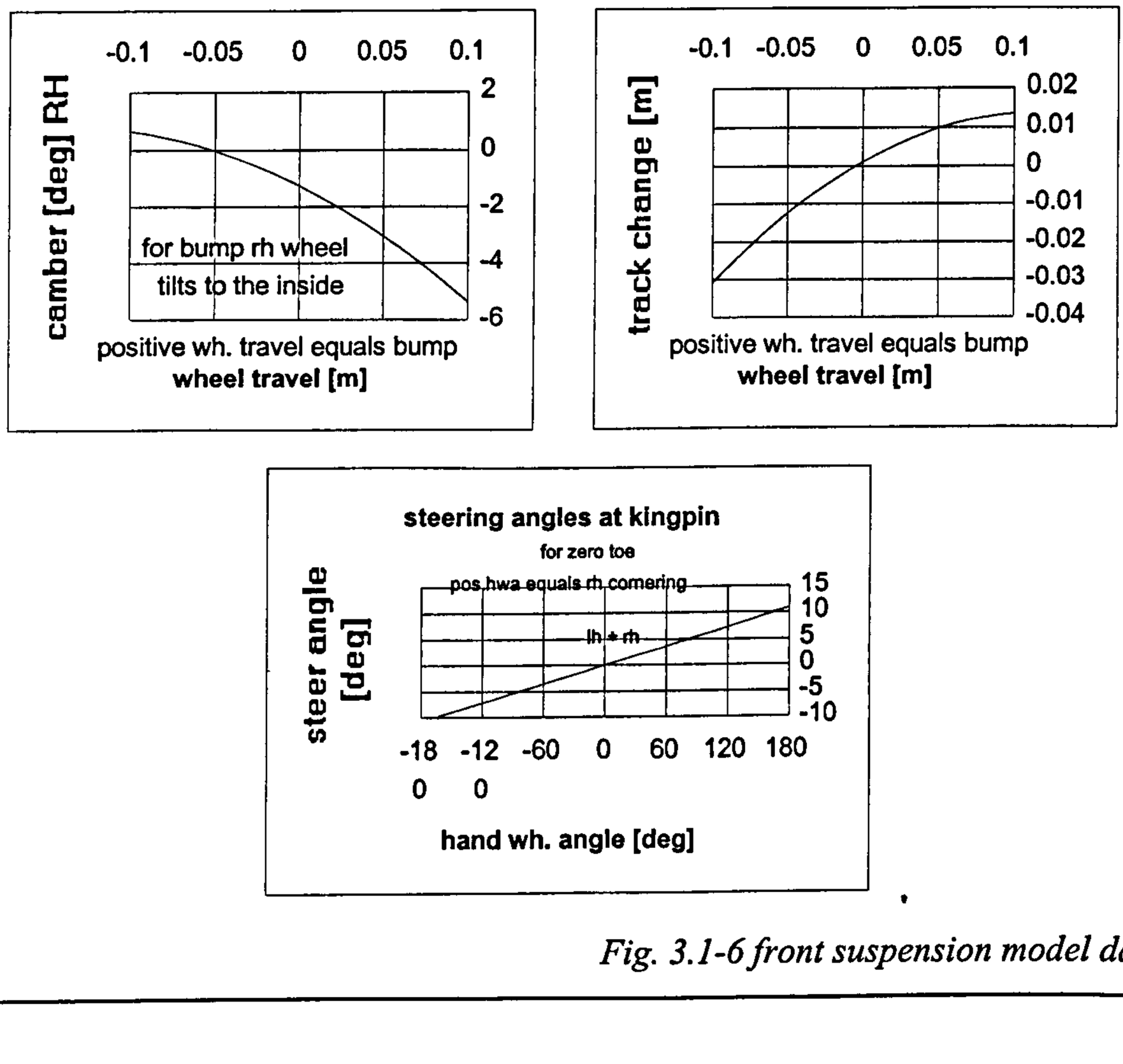

Fig. 3.1-6 front suspension model data

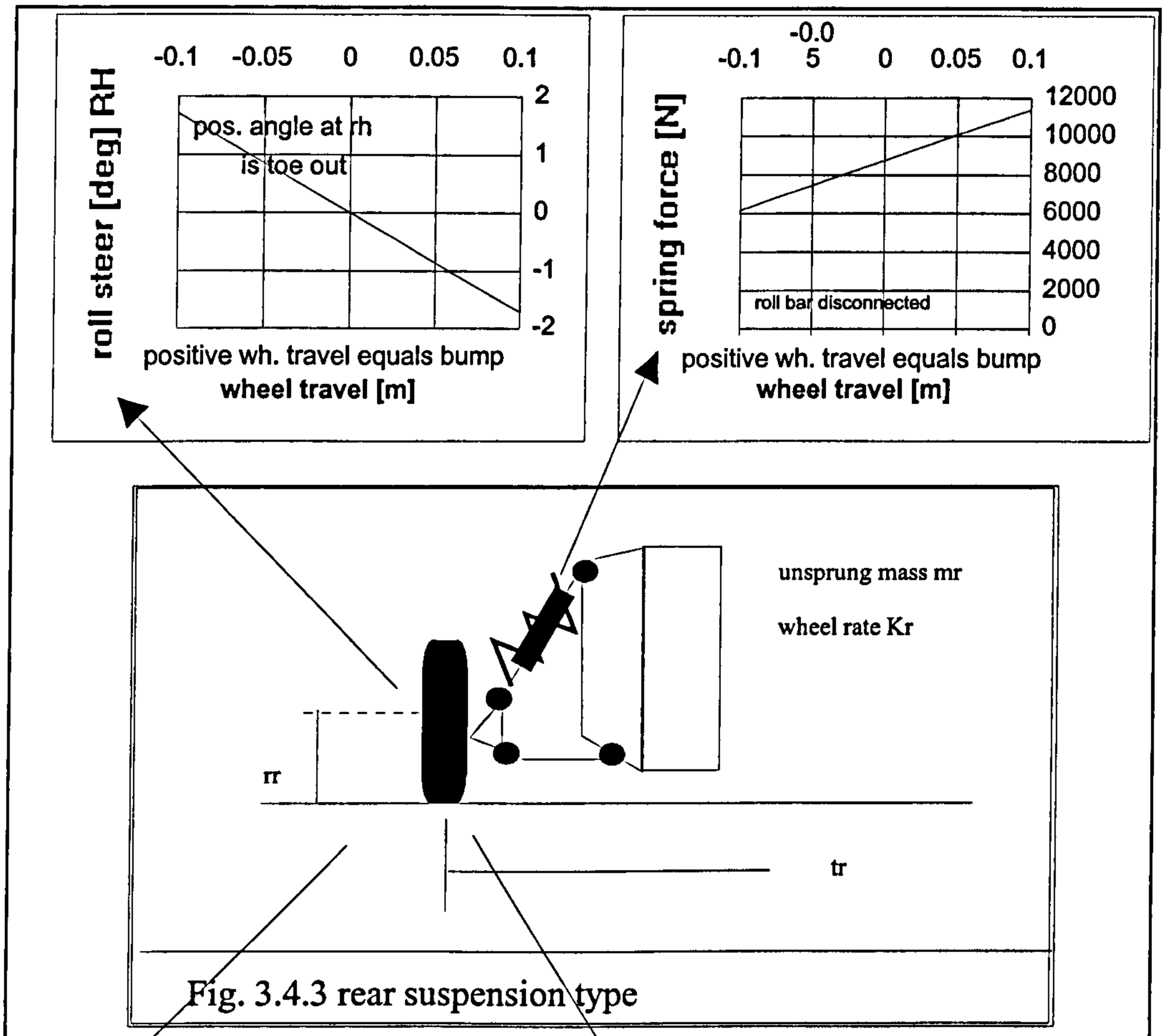

Fig. 3.4.3 rear suspension type

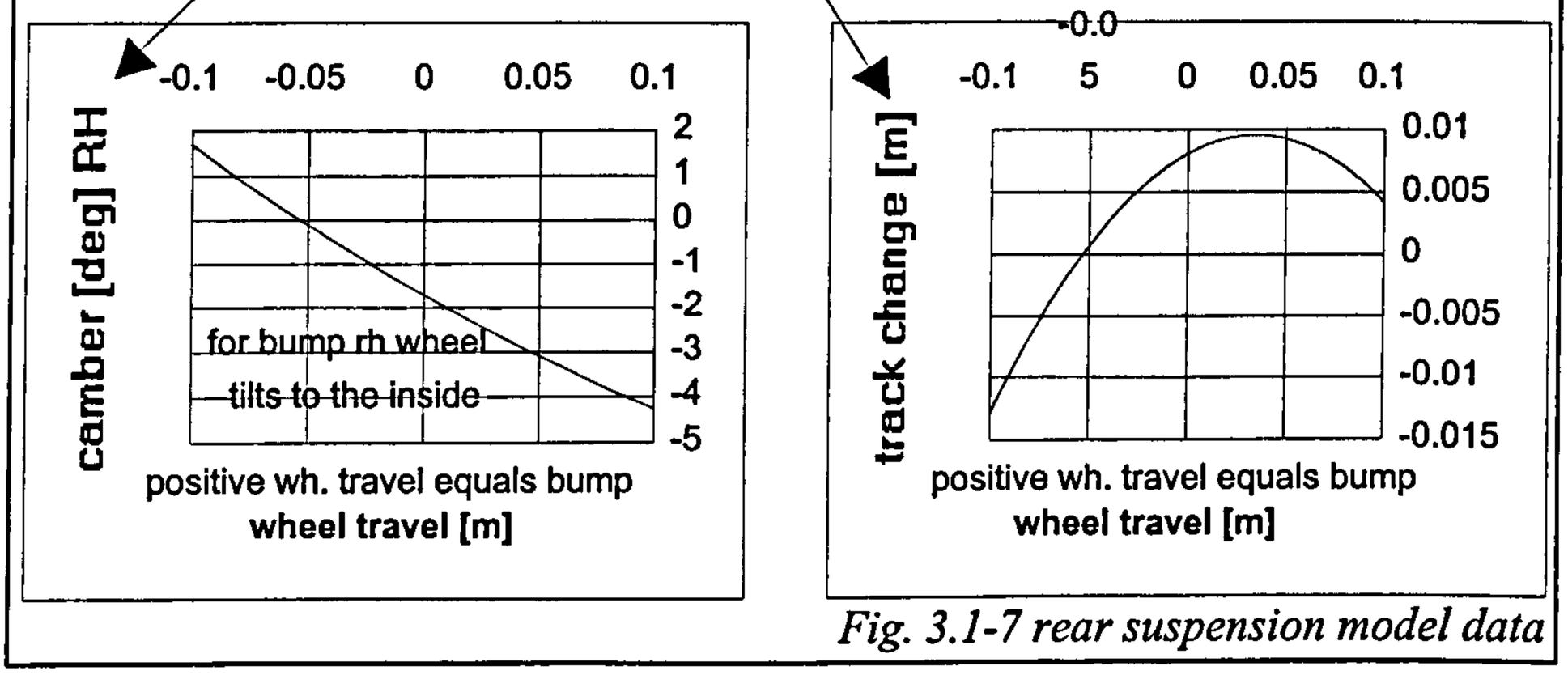

Fig. 3.1-7 rear suspension model data

3.2 Vehicle modelling with AUTOSIM

This section describes the vehicle modelling approach adopted for simulating transient manoeuvres, such as lane changes. Vehicle models for these purposes were developed with the commercially available software tool AUTOSIM /2.2.2/. The mathematical representation of a vehicle, as established by the AUTOSIM model, is very similar to that adopted for the 'Steady State Cornering Model'. Therefore, only a brief account of its structure is given. However, some vehicle components, such as the steering system, were modelled with greater detail, and are discussed in more depth. The modelling with AUTOSIM is illustrated using some excerpts from the vehicle model.

The AUTOSIM package is based on a language that enables its users to define any mechanical structure composed of interfacing rigid bodies entirely by symbolic expressions as opposed to numerical input data. Symbols rather than figures are used to describe the topology of the model and the properties of its various elements.

In the 'Steady State Cornering Model' the multi-body representation of a vehicle consists of a few rigid components representing the sprung mass, the four unsprung masses and possibly elements describing parts of the steering and suspension systems. Some of these components are connected to others either by certain types of joints, defining the relative degrees of freedom (DoF) between two rigid bodies, or by spring and damper elements, establishing a force or moment action. Definitions of the external forces and moments acting on the rigid bodies complete the model.

Essentially, the vehicle model is composed of various statements, which define the inertia properties of each rigid body, the location and type of each joint, the stiffness and damping properties of elastic elements and the magnitudes and points of action of external forces and moments. Unlike other multi-body simulation codes, such as ADAMS, the AUTOSIM user defines the model by symbols representing the geometric and physical properties mentioned above. This avoids having to deal with numerical data for defining coordinates of characteristic points, the mass and inertia of a rigid body and force and moment magnitudes during the model development.

After the model has been defined, AUTOSIM derives a set of differential and algebraic equations describing the system dynamics and constraints symbolically. This has the advantage that this generic model applies to any set of system properties chosen for a dynamic or kinematic analysis. Codes, deriving the equations of motion numerically in the form of system matrices, represent only one model variant corresponding to a set of specific properties. This necessitates the derivation of these matrices for each alteration of the parameter set prior to a simulation.

AUTOSIM can write the differential and algebraic equations of a rigid body system into a text file. However, this facility is rarely used for rather complex models, involving many DoF and non-linearities. The content of these equations would be too complicated to be understood or verified by the user.

After having established the equations for the system dynamics and constraints, AUTOSIM creates a corresponding code, either in Fortran, C or in a MATLAB compatible language, which can be used for simulating the system. This program is a stand-alone facility allowing simulation independently from the AUTOSIM package. Again, this differs from the approach adopted by ADAMS, in which problem definition, simulation and post-processing are carried out by the same package.

AUTOSIM generates a code designed to allow fast computation of time domain simulations. While processing the equations of motion and those for the constraints, it establishes the minimum number of DoF present in the system. Constraints, as introduced by joints, are used to eliminate the corresponding degrees of freedom between two bodies, so that the least number of equations for describing the system is derived. These equations are of a more complex nature than those derived by some other multi-body simulation codes, which add the equations for the constraints to those of the system dynamics. The latter approach leads to a larger number of less coupled equations.

3.2.1 Structure of AUTOSIM vehicle handling model

The AUTOSIM model consists of the same basic components as used for the 'Steady State Cornering Model' described in section 3.1. A brief account is given of the model structure, before some more detailed information is given in section 3.2.2 on the steering model employed.

<u>rigid body degrees of freedom</u>

The sprung mass is represented by a single rigid body having six DoF for three translations and rotations. The unsprung masses represented by four further rigid bodies are attached to the chassis body by joints enabling each wheel to travel vertically, scrub laterally, camber and steer.

<u>suspension characteristics</u>

Suspension characteristics, such as track and camber change, spring deflection and bump steer, are described using the same derivative approach as for the 'Steady State Cornering Model'. The equations relating these characteristics to the wheel travel are introduced as constraints, allowing AUTOSIM to eliminate the corresponding DoF. For the AUTOSIM model, however, suspension derivatives for the lateral scrub refer to the motion of the wheel centre rather than to its contact point with the road, as was the case for the 'Steady State Cornering Model'.

suspension springs and tyre forces and moments

The definitions for the spring, bump and rebound forces are identical to those given for the 'Steady State Cornering Model'. The same tyre model based on the 'Magic Formula' is employed. Tyre forces act through the wheel centre. However, additional moments are introduced to account for the moment arm provided by the distance between the wheel centre and the contact point of the tyre.

The 'Magic Formula' for combined longitudinal and lateral slip was coded, but not used in the simulations presented in chapter 12.

parameters for non-steady state simulations

The AUTOSIM model was developed for simulating the dynamics of a vehicle performing transient manoeuvres. Therefore, damping and inertia properties had to be included. Suspension damper forces were introduced acting in parallel with the spring forces. Different damper characteristics for the front and rear ends can be defined in the input data file. A non-linear characteristic between damper force and wheel travel velocity can be introduced by a spline representation.

control of vehicle speed

The forward speed of the vehicle model is controlled in either an open or closed loop. For the former mode of simulation the time history of the forward velocity, measured at the centre of gravity, has to be specified. In the closed loop mode the speed is adjusted to specified target values by a throttle controller, which demands an increase or decrease of engine torque to be transmitted through the differential into the driven wheels, corresponding to the speed error established. For the latter mode of simulation a representation of the longitudinal forces is required, which interact with the driving torque. The throttle control model includes a simple representation of a differential. However, for the simulation results presented in chapter 12, the open loop speed control was used.

3.2.2 Steering system

In comparison to the 'Steady State Cornering Model' the steering system was modelled with considerably greater detail. The steering system represented by the AUTOSIM model includes power assistance and a

figure 3.2.2-1 steering model

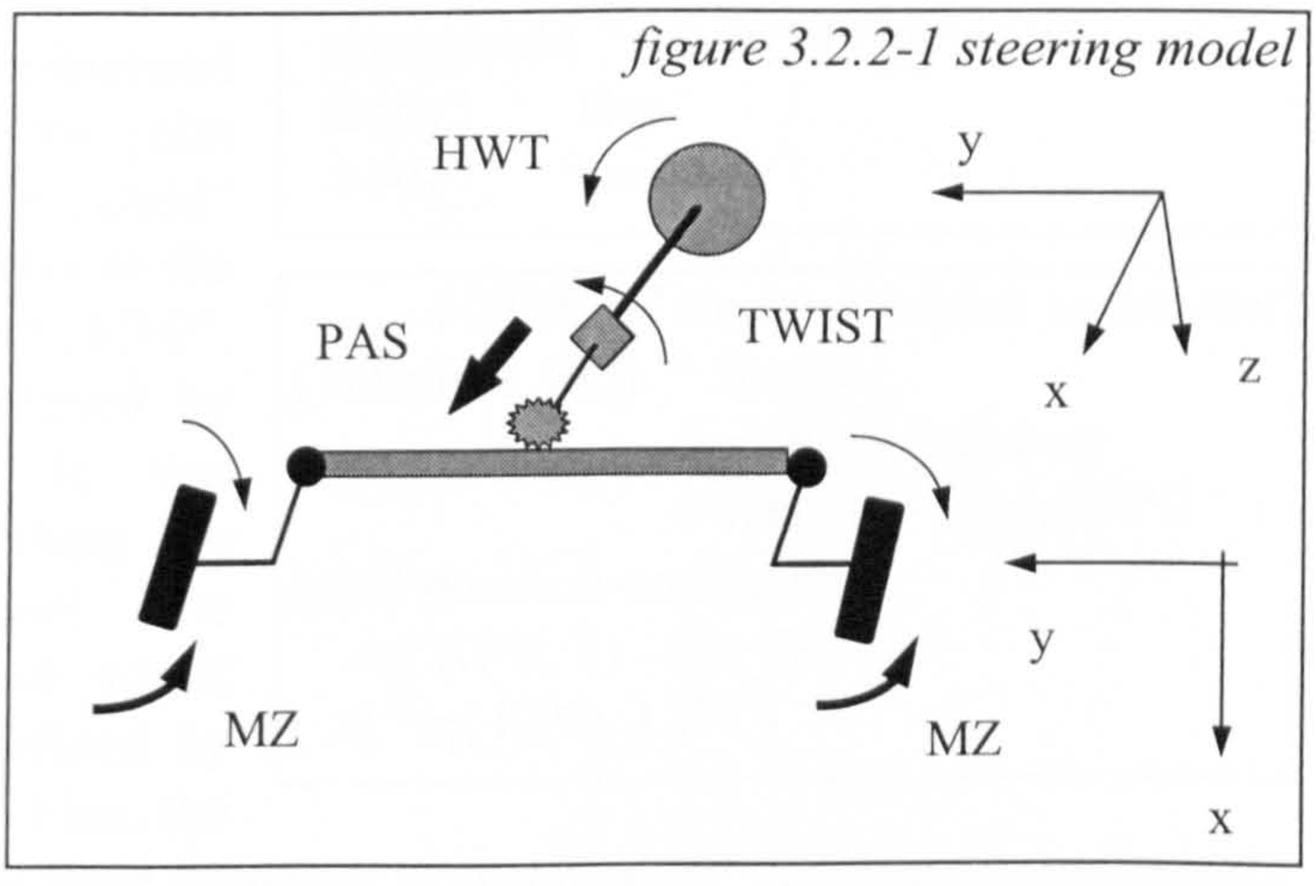

compliant steering rack. This model is discussed in more depth using some excerpts of the corresponding AUTOSIM file. Fig. 3.2.2-1 illustrates the steering model consisting of two rigid bodies. The first represents the hand wheel and the other the lower steering column. The steering rack is not included as a further rigid body. Only its ratio of translating a column rotation into a road wheel steering motion is considered. The curved arrows in the illustration indicate the steering torque exerted by the driver, the column twist and the aligning moments acting about each kingpin against the steering motion of the road wheels. The thick arrow indicates the hydraulic power assistance torque provided. The corresponding AUTOSIM statements are given below. The first frame contains the „add-body“ statement defining the hand wheel. This rigid body is referenced by the symbol „Hw“. Its properties are defined by symbols following a colon.

The first statement underneath the „add-body“ command defines the reference or „parent“ body for the hand wheel. The degrees of freedom of the hand wheel body are defined relative to the chassis body, referenced by „Mb“. The location of the joint between the „parent“ and the „child“ body is given by the coordinates of the point referenced by the symbol „Mb0“. Relative translations are assigned by the „translate“ statement. In this example none („NIL“) of these are defined for the hand wheel. The rotational DoF of the hand wheel relative to the chassis are defined by the four following properties. First, the number of rotational DoF and their sequence is specified by the „body-rotation-axis“

AUTOSIM steering model: hand wheel

```
( add-body Hw
        :parent Mb
        :mass  0
        :name          "hand wheel"
        :inertia-matrix ( Ihw 0 0 )
        :joint-coordinates Mb0
        :cm-coordinates   Mb0
        :translate        NIL
        :body-rotation-axes  x
        :parent-rotation-axis x
        :reference-axis      y
        :no-rotation              NIL     )
```

AUTOSIM steering model: column

```
( add-body Lcol
        :parent Mb
        :mass  0
        :name       "lower steering column"
        :inertia-matrix 0
        :joint-coordinates Mb0
        :cm-coordinates   Mb0
        :translate              NIL
        :body-rotation-axes     x
        :parent-rotation-axis   x
        :reference-axis         y
        :no-rotation            NIL       )
```

AUTOSIM steering model: torsion bar

```
( add-moment TBc
  :name      "column torsion bar moment"
  :direction  [Hwx]
  :magnitude  " - c_stcol * @twist"
  :body1      Hw
  :body2      Lcol )
```

AUTOSIM steering model: constraint

```
( setsym s_fRH  "  toefRH
                 + scfRH1 * @steer
                 + scfRH2 * @steer**2 " )
( add-position-constraint
  " rq( KPfr, 1) - @s_fRH "
  :q "rq( KPfr, 1 )"   )
```

property. For the hand wheel only one („x“) out of three (x, y, z) rotations is permitted. The axis of rotation is given by the following statement, which aligns the axis of the hand wheel rotation with the forward direction („x“) of the vehicle. In order to provide a proper initial configuration a second unit vector is required for the hand wheel body in addition to the one defining its axis of rotation. The „reference-axis“ property provides this information. It aligns the second unit vector of the hand wheel body with the lateral („y“) direction of the chassis body. The last statement is simply a flag for allowing a rotational DoF between „parent“ and „child“ body.

The other statements found in the „add-body“ command refer to the mass and inertia properties of the rigid body. The hand wheel is assumed to be massless. The elements of its inertia matrix are defined by symbols. In this example only one parameter is declared („Ihw“), which represents the inertia with respect to the axis of rotation. The location of the centre of gravity is specified by the „cm-coordinates“ property. It coincides with a point already defined on the parent body „Mb“, represented by symbol „Mb0“.

The steering column is defined in a similar fashion, as can be seen from the „add-body“ statement given in the second frame. This body has neither mass nor inertia associated with it. It is connected to the steering wheel by a torsional spring, representing a torsion bar. The corresponding „add-moment“ command is given in the third frame. It establishes that the torque transmitted between the hand wheel and the column is proportional to the column twist, as represented by the symbol „@twist“ in the statement defining the magnitude of the moment.

The fourth frame contains two statements by which the road wheel steer angle is related to the column rotation. The first statement introduces a symbol for the road steer angle on the right hand side („s_fRH“). The road steer angle is composed of the static toe angle and the angle established by the rack displacement. The contribution of the latter is expressed as a proportion of the column rotation „@steer“. The non-linear steering ratio between the road wheel angle and the column rotation is defined by the two coefficients „scfRH1“ and „scfRH2“. The second command defines the constraint established by the steering rack and the steering arms. AUTOSIM interprets the „add-position-constraint“ command to mean that the expression given in quotes is zero. For this example it means that the steering DoF of the road wheel, denoted by „rq(Kpfr, 1)“, is equal to the expression represented by the symbol „@s_fRH“. A corresponding constraint is introduced for the road wheel steer angle velocity.

AUTOSIM steering model: PA torque

```
( add-moment PAS
  :name       "power steering assistance torque"
  :direction  [Lcolx]
  :magnitude  " boost(@valve) * Area * abs(drdlc) "
  :body1      Lcol
  :body2      Mb )
```

The fifth frame contains another „add-moment“ command by which the power assistance is modelled. The assisting torque acts between the column („Lcol“) and the chassis body („Mb“). Its magnitude depends on the twist angle of the torsion bar, which controls the amount of hydraulic fluid going through the valves into the rack housing. The pressure, supporting the rack in steering the road wheels, is given as a non-linear spline function of the valve opening („@valve“), which corresponds to a proportion of the column twist. The assisting torque is given by the product of the supplied pressure, the rack area and a geometric constant („drdlc“), the latter defining the ratio of the rack travel to the column rotation. The last two parameters may be set to one in the input data file if the user prefers to specify the relationship between the assisting torque and the corresponding column twist. An example of an input file can be found in appendix B1.

steering rack compliance

In addition to the power assistance, a simple representation of the steering rack compliance was introduced. The compliance results from the elastic bushes by which the rack housing is mounted to the chassis. The flexibility of the rack housing establishes the same compliance steer angles at the inside and outside wheels, whereas compliant wishbone or McPhearson strut mountings would give different angles at the two sides, depending on the magnitude of the traction and cornering forces.

For the AUTOSIM model only a compliant rack was considered. Assuming that the compliance of the rack and the elasticity of the torsion bar can be considered as two torsional springs put in line, their composite effect can be represented by a single spring element. The stiffness for the column, denoted by „c_stcol“ in the third frame is in fact the composite stiffness of the steering rack and the torsion bar. The composite stiffness of the column is smaller than its nominal value. It can be computed according to:

$$c_{comp} = \left(\frac{1}{r_c \cdot c_{TB}} + \frac{r_c}{r_r^2 \cdot c_{RH}} \right)^{-1}, \text{ where} \qquad (3.2.2.1)$$

c_{TB} denotes the torsion bar stiffness in [Nm],

c_{RH} denotes the lateral stiffness of the rack housing in [N / m],

r_c denotes the steering ratio between column rotation and road wheel angle in [rad / rad] and r_r denotes the ratio between rack housing displacement and corresponding road wheel angle in [m / rad]

Consequently, the twist angle of the column is larger compared to a model with two separate springs representing the two compliant components. It is composed of an angle equivalent to the displacement of the rack housing and of a component due to the nominal compliance of the column, established by an elastic torsion bar.

However, for the power steering model it is necessary to distinguish between the column twist due to the torsion bar and that due to the compliant rack. Only the former is relevant for establishing the assisting pressure. The model distinguishes between column twist („@twist") and valve opening („@valve"). The latter is a proportion of the former, established by the ratio of the composite column stiffness c_{comp} [1] and the nominal torsion bar stiffness c_{TB}.

caster, kingpin inclination and ground offset

The steering system representation of the AUTOSIM model includes caster and kingpin inclination angles as well as an offset between the kingpin and the wheel centre. The position and orientation of the kingpin are defined relative to the corresponding wheel by four parameters. The first two specify the forward and lateral coordinates of the point where the kingpin axis intersects the road. The other two specify the caster and the kingpin inclination angle.

3.2.3 Driver model

In order to carry out simulations of closed loop path tracking manoeuvres, a simple driver model was developed. Such a model simulates the steering wheel input of a real driver when driving through a given course, such as a lane change.

As mentioned in the introduction to chapter 9, the steering activity can be regarded as being composed of two parts. The first part represents the preview based steering wheel input, and the second part refers to the steering adjustments made by the driver to compensate for deviations from the given course and for undesired attitude angles.

For the simple driver model presented here, only the first part of the steering input of a real driver is considered. Fig. 3.2.3-1 illustrates a vehicle tracking a given course indicated by the curved arrow. The rate by which the course changes with distance is denoted by the path angle φ. The broken line describes the vehicle's actual direction of travel, which differs from its yaw attitude ψ by the slip angle β. The driver looks ahead by a preview distance of $v \cdot \tau_{pv}$ to establish the future position of the vehicle relative to the course. The vehicle forward speed is denoted by v, and τ_{pv} represents the preview time.

As can be seen from the illustration, the vehicle drifts off the straight ahead heading direction by a rate of $v \cdot \beta$. In addition, the path error, measured by the distance between the vehicle's horizontal heading direction, given by a dotted line, and the desired course, increases by a rate of $v \cdot (\varphi - \psi)$.

---

[1] The composite stiffness is equivalent to the column spring stiffness c_{φ}^{C} used for the 'Steady State Cornering Model'

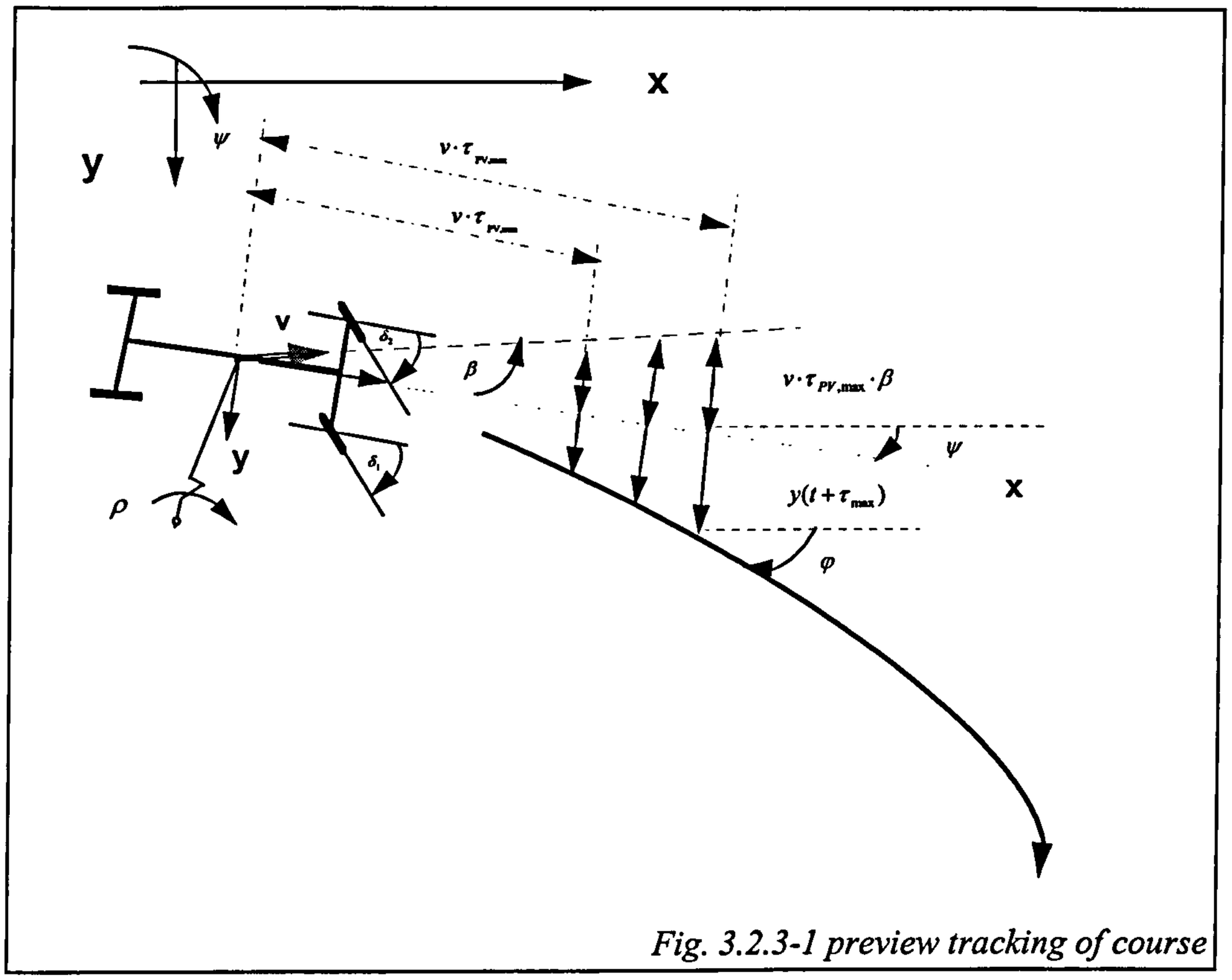

Fig. 3.2.3-1 preview tracking of course

For the driver model it is assumed that a driver establishes a preview error $y(t+\tau_{PV})$ composed of these two components. This preview error is then weighted by a gain to obtain a corresponding steering angle. The relationship between preview error and steering wheel angle reads:

$$\delta_{HW} = \underbrace{r_C}_{\text{steering ratio}} \cdot \underbrace{K}_{\text{gain}} \cdot \underbrace{\left\{ y(t+\tau_{PV}) - v \cdot \tau_{PV} \cdot \beta \right\}}_{\text{effective preview error}} \qquad (3.2.3.1)$$

This relation considers only a single preview error, established at a distance $v \cdot \tau_{PV}$ away from the actual position of the vehicle. The gain K can be established for the simple case of tracking a constant radius. For steady state cornering it can be expressed by:

$$K = \left\{ \frac{1}{\left(\dot{\psi}/\delta\right)_{st.st.}} \right\} \cdot \frac{2}{v \cdot \tau_{PV}^{\,2}} \qquad (3.2.3.2)$$

The ratio found in the parenthesis denotes the steady state yaw rate gain with respect to the road wheel steer angle.

In order to establish a more realistic representation, a weighted mean of the preview errors, established within a preview window, is computed according to:

$$\delta_{HW} = \underbrace{r_C}_{\text{steering ratio}} \cdot \frac{1}{\tau_{PV,\max} - \tau_{PV,\min}} \cdot \int_{\tau_{PV,\min}}^{\tau_{PV,\max}} \underbrace{K(v,\tau_{PV})}_{\text{gain}} \cdot \underbrace{\{y(t+\tau_{PV}) - v \cdot \tau_{PV} \cdot \beta\} d\tau_{PV}}_{\text{effective preview error}} \tag{3.2.3.3}$$

Fig. 3.2.3-2 Gain K vs. preview time; vehicle data taken from /2.5.4/

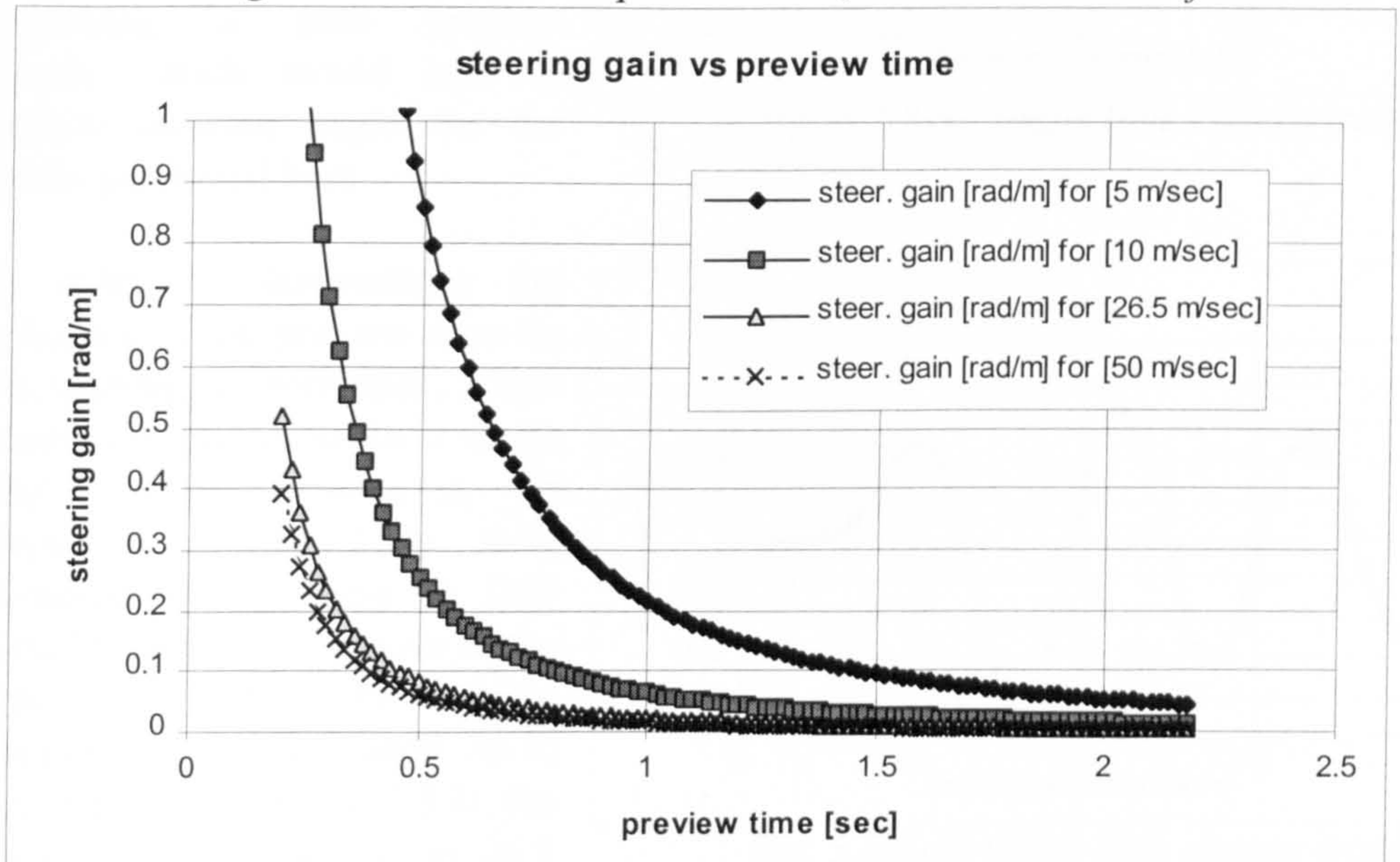

The gain K is now a function of the preview time τ_{PV}. Path errors in the proximity of the vehicle are weighted more than those far away. As can be seen from (3.2.3.2) the weight would become infinite for a preview distance of zero. The relationship between the gain K and the preview time τ_{PV} is illustrated by fig. 3.2.3-2. For a simulation the integral is replaced by a sum over a finite number of preview points.

The driver model given by (3.2.3.2) is defined by three parameters. The preview window, as illustrated in fig. 3.2.3-1, and the yaw rate gain found in (3.2.3.2) can be adjusted to tune the tracking performance. In an iterative process these parameters are readjusted to correspond to the vehicle's response characteristics. A high gain K in combination with short preview times improves the tracking performance, but involves a more oscillatory vehicle response. The opposite case provides more damping to the system, but lacks in tracking the given course accurately.

The driver model presented here appears to be similar to the multi-point preview model proposed by MacAdam /2.5.4/. Both models represent a proportional controller defined by a gain, which is a function of the preview distance, and a maximum preview time. However, there is a fundamental difference, in that the gain used in the

former model accounts for the dynamic response characteristics of the vehicle, whereas only the vehicle's steady state properties are considered for the gain K given by (3.2.3.3). In MacAdam's model, the preview errors are weighted and integrated for a preview window beginning at zero preview length, which would lead to infinite steering angle for the model presented here.

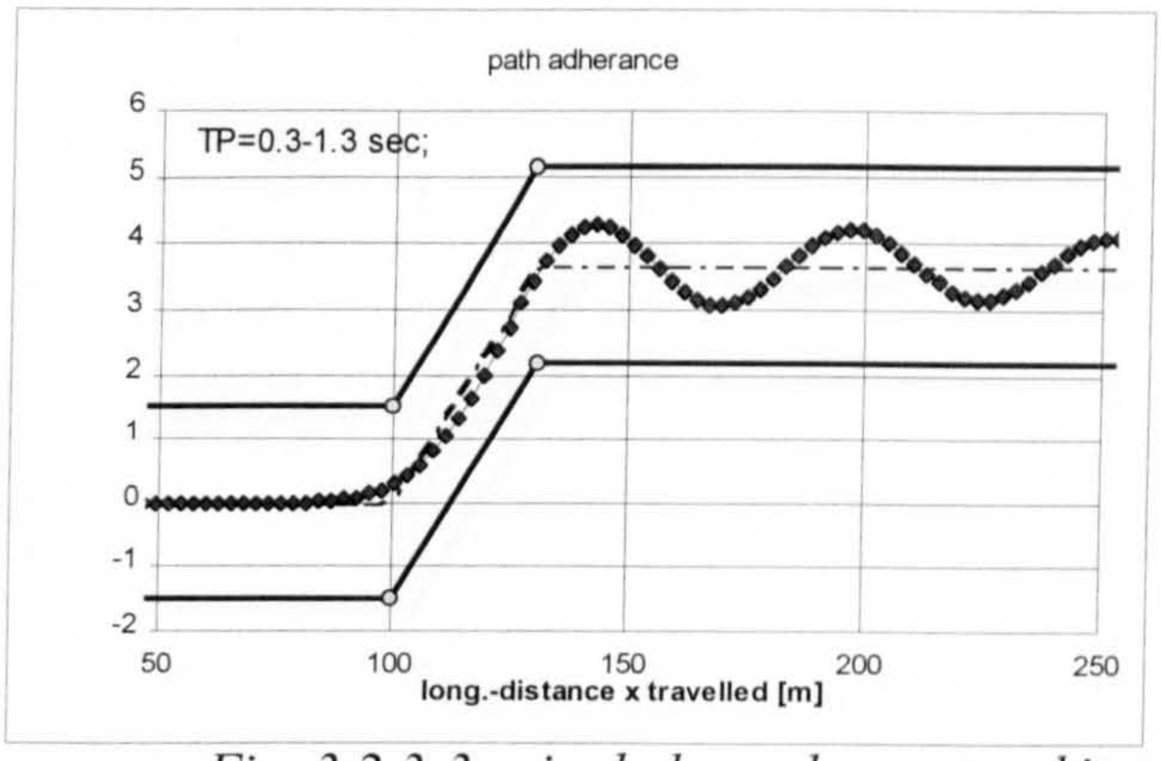

Fig. 3.2.3-3a single lane change tracking

In order to demonstrate the influence of the preview time on the tracking performance, a few results are presented for a single lane change manoeuvre, as found in /2.5.4/. They were obtained for a linear 2 DoF vehicle model, also known as the 'bicycle model'. The vehicle data used in /2.5.4/ is used. As in the examples given in /2.5.4/, the forward speed was set to 26.8 m/sec. The results shown in the figures 3.2.3.3a, b refer to a preview window between 0.3 and 1.3 seconds, which is equivalent to a preview interval ranging from 8 m to 35 m ahead of the vehicle. Preview errors were computed for ten points within this window and weighted according to (3.2.3.3). The target course indicated by a broken line was specified by a spline.

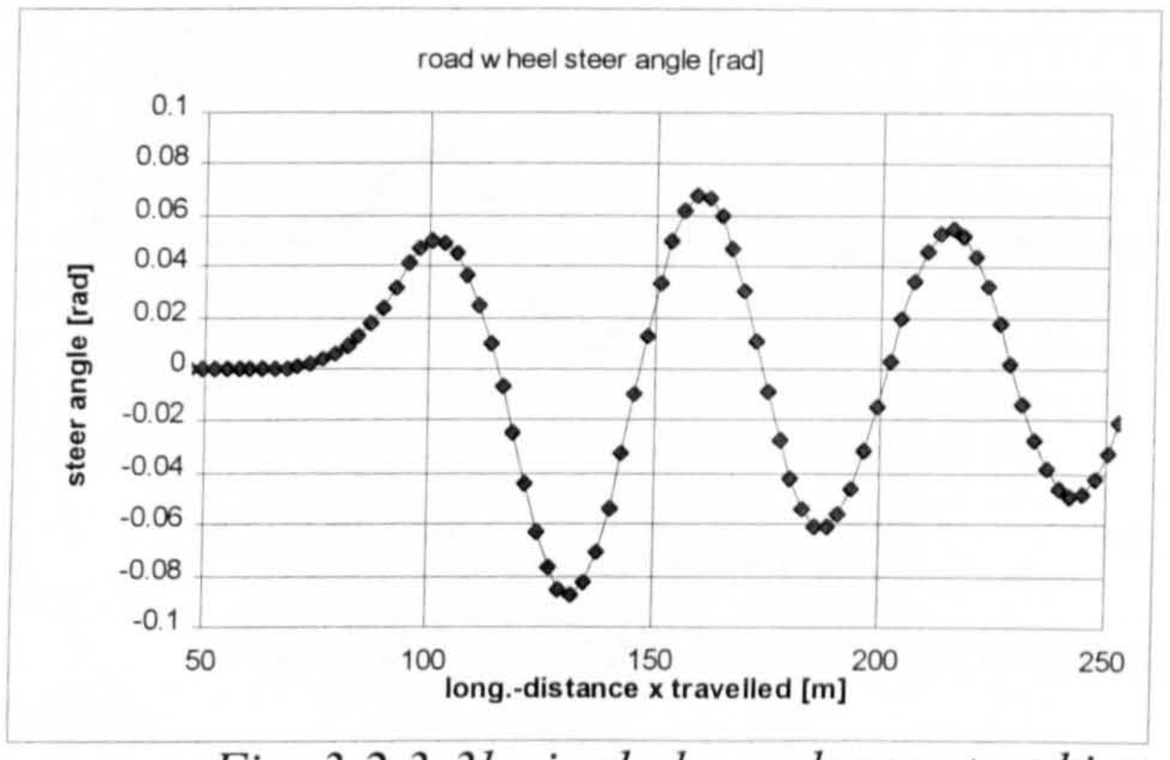

Fig. 3.2.3-3b single lane change tracking

Fig. 3.2.3-3a illustrates the motion of the vehicle's centre of gravity through the lane change. The vehicle follows the target course, given by a broken line, very well for the initial part of the manoeuvre, before it starts to oscillate strongly from the entry to the new lane onwards. The oscillations about the target line decay very slowly. The corresponding road[2] wheel steer angle is shown below.

Changing the minimum preview time from 0.3 to 0.6 results in a much smoother vehicle behaviour, as can be seen from figures 3.2.3-4a, b. Although the vehicle maintains the target line less well for the middle section of the manoeuvre, it enters the offset lane with a much smaller overshoot. The following oscillations are well damped. The corresponding road wheel angle is shown below. The amplitudes are

[2] the road wheel steer angle is shown rather than the hand wheel angle to allow comparison with MacAdam's results found in /2.5.4/.

much smaller than those given in fig. 3.2.3-3b and a steady state is reached much more quickly.

The driver model coped well with manoeuvres of low or medium severity. It was tested in combination with a linear vehicle model for single and double lane changes. However, when it was introduced to the non-linear AUTOSIM vehicle model, it became apparent that it cannot represent a real driver in a limit driving situation. Some further information is given in chapter 12.1.

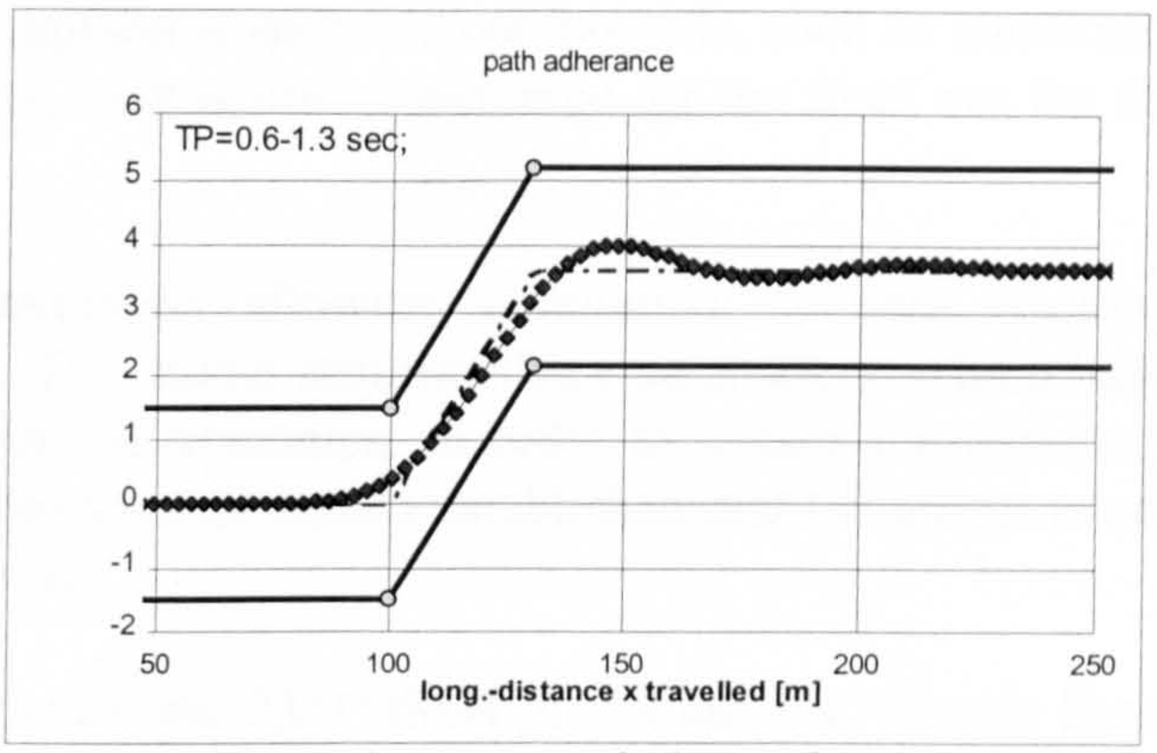

Fig. 3.2.3-4a single lane change tracking

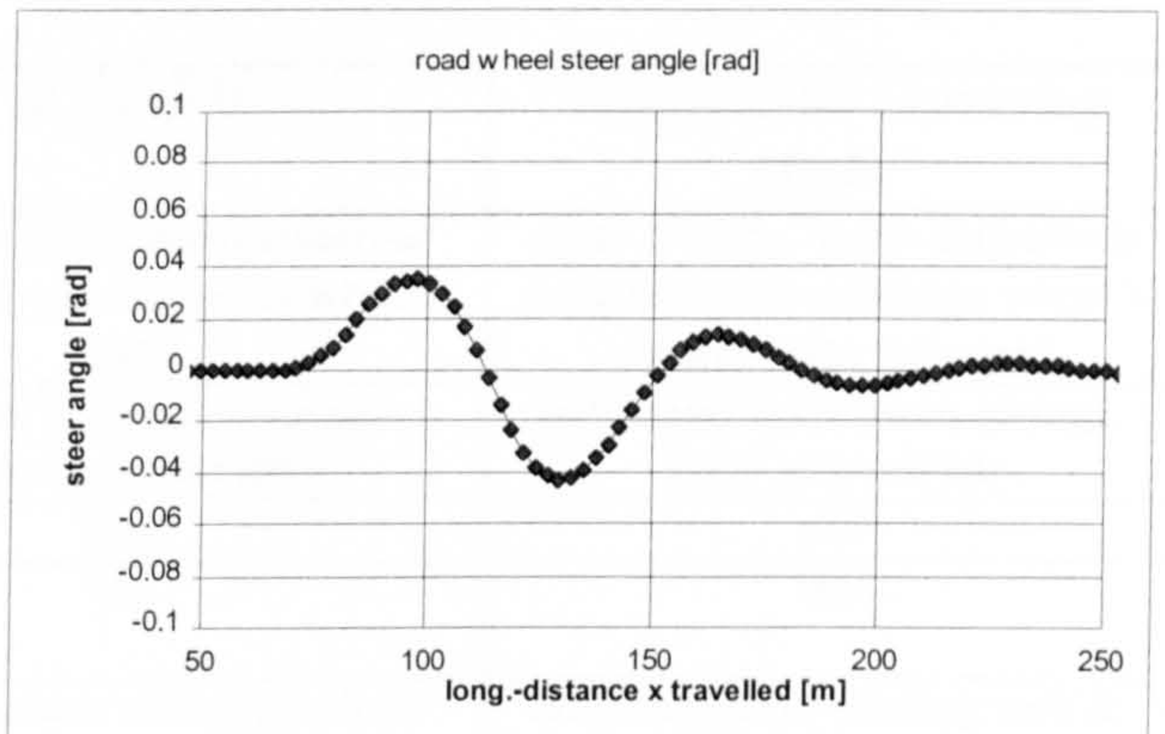

Fig. 3.2.3-4b single lane change tracking

3.2.4 Summary of AUTOSIM modelling

The physical representation of a vehicle as modelled with AUTOSIM follows the concept adopted for the 'Steady State Cornering Model' to a great extent. Sprung and unsprung masses are defined as rigid bodies. Camber, scrub and bump steer characteristics are introduced by suspension derivatives. The same description for the suspension springs and for bump and rebound stops is used.

However, the AUTOSIM model is designed for vehicle dynamics simulations, for which additional parameters, such as inertia properties and damper characteristics, are required. The latter are specified by a spline relating the damper force to the wheel travel velocity. The AUTOSIM model comprises a more detailed steering system, which includes geometric properties, such as caster and ground offset, and power assistance. A compliant steering rack can be considered too by representing the compliance of the rack and the steering column as a single torsional spring with a composite stiffness.

As for the 'Steady State Cornering Model', tyre forces and moments are described by the 'Magic Formula'. The AUTOSIM model was not tested for or validated against manoeuvres involving combined longitudinal and lateral slip.

Camber or steer changes due to compliant suspension components, such as elastically mounted wishbones or trailing arms, were neither considered for the front nor for the rear axles.

A simple driver model was developed allowing simulation of path tracking manoeuvres, such as lane changes. The model requires three parameters, which have to be matched iteratively to the vehicle dynamics, in order to obtain a satisfactory tracking performance. However, experimental results established that the model is not suitable for severe driving manoeuvres.

The differences and similarities between the AUTOSIM model and the 'Steady State Cornering Model' are summarised in table 3.2.4-1.

property	*AUTOSIM*	*'Steady State Cornering Model'*
suspension derivatives	up to 3. order; scrub derivatives are given with respect to wheel centre	up to 2. order, scrub derivatives are given with respect to wheel's contact point with road
suspension springs	non-linear suspension springs, linear anti-roll bar	non-linear suspension springs, linear anti-roll bar
bump & rebound stops	yes	yes
caster/ kingpin inclination/ ground offset	yes	no
suspension compliance characteristics	only compliant steering rack & column considered	only compliant steering rack & column considered
tyre properties	'Magic Formula', 1991 version[3]; code for 1996 version[4] also available	'Magic Formula', 1991 version[3] for lateral slip and camber only
power steering	yes, spline approximation of assisting torque given as a function of torsion bar twist	no
damper	non-linear damper characteristics modelled by a spline	not applicable
forward speed control	open loop or by throttle controller; throttle controller requires models of differential and traction forces	not applicable
steering control	open loop or by driver model	not applicable

Table 3.2.4-1 details for the AUTOSIM and 'Steady State Cornering Model' models

[3] The 1991 version is published in /2.4.7/.
[4] The 1996 version is found in /2.4.13/.

4 Inertia Rig

The first section of this chapter describes the SPUK's Vehicle Inertia Rig. This test facility was used during the project for providing estimates of some vehicle parameters, which were required for subsequent vehicle dynamics simulations. The description of the SPUK Vehicle Inertia Rig includes some comments on vehicle rig testing and parameter identification in order to point out the differences, regarding instrumentation and estimation method employed for this rig, in comparison to others.

The project work devoted to the development of the rig is summarized in section 4.2. After that some details are discussed regarding the approach employed to estimate vehicle properties from the rig measurements. The Inertia Rig test schedule is given in section 4.3, while a discussion of the test results and conclusions from the development work can be found in chapter 5.

At the beginning of the project, it was suggested to utilise the Inertia Rig to obtain some vehicle parameters, which then could be used as input data for the vehicle simulation to follow. Although the rig was not an issue of the original project plan, it was decided to allow for some project work to be spent on the development and use of this facility. A better understanding of the rig's potential and the prospect of having a fully working development tool available to SPUK and its customers were seen as benefits.

The rig was recommissioned in 1989. However, it was not in operation for some time, since parts of the soft- and hardware equipment became obsolete and were not updated due to a lack of resources at the time.

It was decided to carry out the necessary work to make the rig fully operational again. Furthermore, it was agreed to research how the test procedure can be made more efficient and to establish which additional equipment may have to be employed to obtain more accurate data and potentially further vehicle and tyre properties.

In order to provide some support for carrying out these tasks, an MSc project was set up to conduct a theoretical study of suitable rig testing and parameter identification methods. J.D. Rayner from Cranfield University completed his thesis on the 'Investigation of Vehicle Parameters using the SP Tyres Vehicle Inertia Rig' in August 1995. His work provided the foundation for further development of the test procedure, data analysis and the parameter identification techniques, which were finally implemented.

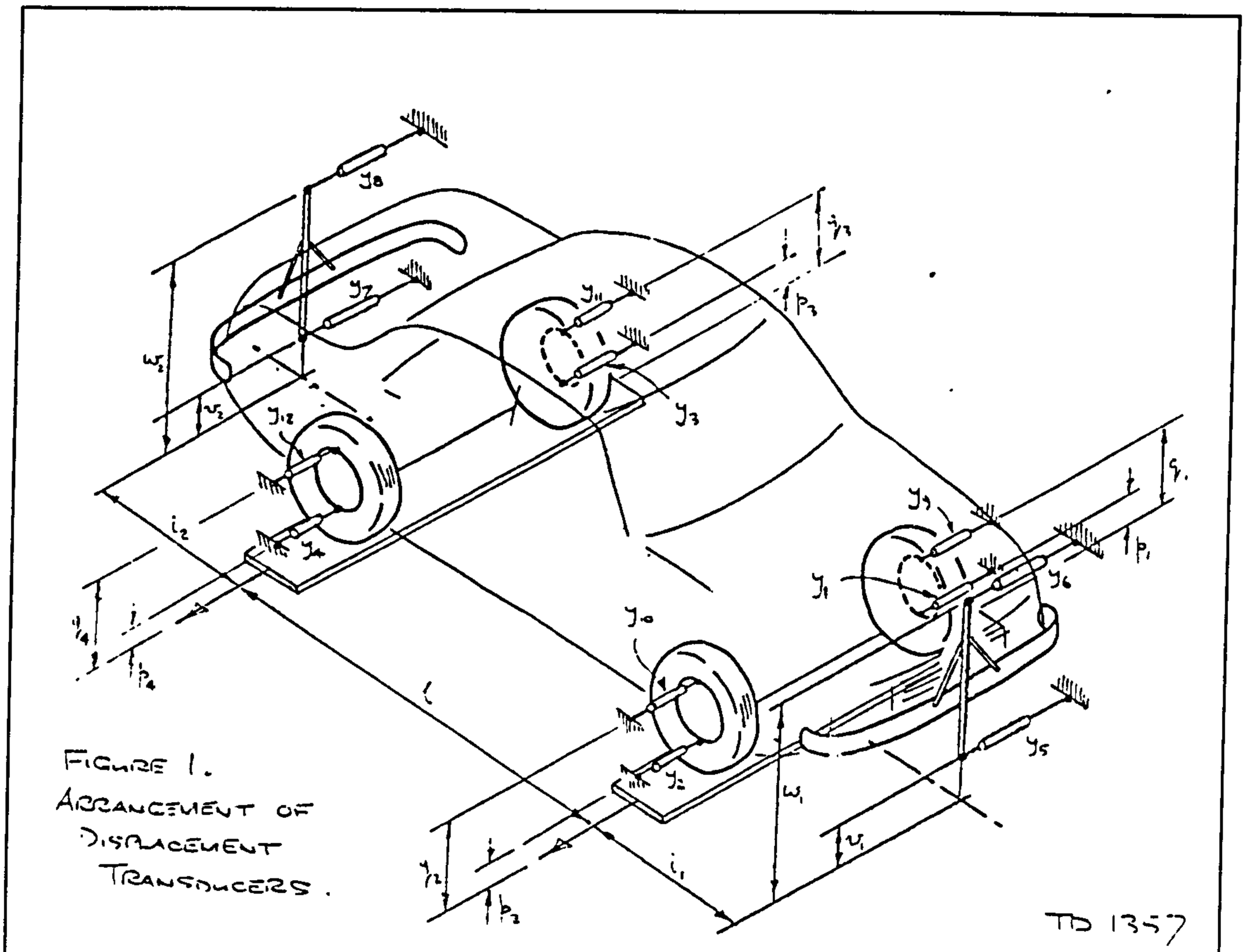

Fig. 4.1-1 inertia rig instrumentation /4.1.4/

4.1 Description of the SPUK Vehicle Inertia Rig

For any vehicle dynamics simulation input data are required describing the geometry of the vehicle, its inertia, damping and stiffness properties. Their number will be determined by the desired accuracy a particular type of simulation has to provide. These data are often difficult to obtain; it may not be available from the manufacturer, or the parameters needed cannot be derived simply from the drawings or design specifications, even by the manufacturer. Especially inertia characteristics of the sprung and unsprung masses are difficult to calculate and are usually determined experimentally on test rigs.

Since vehicle models are a simplified description of the actual design, their input data often consist of composite or lumped parameters, which characterise global quantities. These composite parameters include roll stiffness and damping of the sprung mass as well as suspension compliance effects. The latter represent the additional degree of steer, camber, track and wheelbase changes due to the forces and moments acting at

the wheel, which cause some elastic deformation of the various suspension components. These compliance effects are important issues with regard to refinement and limit handling.

At Fort Dunlop a test rig is available, the Inertia Rig /4.1.1-5/, by which certain parameters often needed for vehicle modelling purposes can be measured. It features two platforms on to which the front and rear axles of the test vehicle are driven. The specimen is instrumented with linear potentiometers as shown in fig. 4.1-1. Each platform can be oscillated laterally by hydraulic actuators underneath, exciting the vehicle's roll, yaw and lateral motion.

From the measurements recorded for the displacements of the body and the wheels, as well as for those of the forces acting vertically and laterally on the platforms, the parameters given in table 4.1-1 can be determined.

vehicle property
roll centre heights front and rear
camber change coefficients front and rear
centre of gravity height of sprung mass
roll & yaw inertia of the sprung mass (body)
product of inertia of the sprung and unsprung masses
roll stiffness and damping front and rear

Table 4.1-1 *estimated vehicle parameters*

On the other hand, rig testing is often employed to verify whether a design performs as expected and to quantify the effects of those components on the performance, which properties and tolerances were not fully known in the design process. The 'Kinematics and Compliance Rig' (K&C) at MIRA /4.1.6/, for instance, is used for these purposes. It facilitates the measurement of kinematic and compliance steering as well as suspension properties for the full suspension travel available.

While MIRA's K&C rig was developed to look into static suspension properties in great detail, the Inertia Rig was designed to obtain inertia properties of a test vehicle in addition to some basic suspension parameters. For that test, frequencies have to be much higher, in order to excite the roll and lateral motions of the car, compared to the quasi-static test procedure applied for the K&C rig. On the other hand, Inertia Rig tests are confined to fairly small perturbations about the nominal vehicle trim. The oscillations of the two plates are such that small roll and yaw angles are maintained to keep the suspension travel in its linear region, well away from bump and rebound stops. In this respect the Inertia Rig has its place in between suspension compliance rigs, as mentioned above, and those measuring mass distribution properties only, such as the rig available at Cranfield University /4.1.7/ and those described in /4.1.8-9/.

The rigs mentioned above and the Inertia Rig also differ in their approach to measuring the desired properties. Tests with the K&C rig provide the required information directly, whereas the Inertia Rig test results have to be matched to the output data of a corresponding vehicle model, simulated for the same input loads,

before the desired parameter values are made available. In general, this approach can be pursued in either time or frequency domain, as discussed in /4.1.10-11/. However, since the Inertia Rig method is designed to establish linear properties, their estimation is carried out in the latter.

4.2 Development of Inertia Rig

This section discusses some details of the Inertia Rig's design and operation as it was originally conceived, before the development work carried out during the project is summarised. The summary includes the findings of J.D. Rayner's MSc project work.

4.2.1 Inertia Rig testing in the past

Before proceeding to discuss the development work on the rig, it seems appropriate to outline the testing and evaluation methods as they were originally devised. This provides a reference to the work summarised in the following sections and, more importantly, some insight into the concept of vehicle parameter identification in the frequency domain.

After the test vehicle has been driven onto the two plates shown in fig. 4.1-1, it is aligned such that its longitudinal axis becomes perpendicular to both platforms. This is achieved by repositioning the platforms relative to each other, followed by some fore and aft movement of the car to take out any lateral preloads in the tyres. After that, the vehicle is instrumented with twelve linear potentiometers, four of which are attached laterally between the vehicle body and a reference on the ground, whereas the other eight are mounted in pairs to the wheels.

The lateral displacements of the four chassis mounted potentiometers define the roll and yaw angle and the lateral motion of the front axle. It is apparent that there is one redundant measurement for obtaining these three rigid body degrees of freedom (DoF), which would allow to distinguish between the vehicle roll at front and rear ends. However, for the analysis the average of the two was taken, assuming a torsionally rigid chassis.

The two displacements at each wheel determine the absolute lateral movement of its contact point and the absolute camber angle, provided that any steering motion during a test can be constrained. For that reason the steering rack or the steering wheel is locked.

An additional potentiometer underneath each plate records the plate motion. Furthermore, load cells inside each plate measure the vertical wheel loads as well as the lateral force driving the plate. In the original configuration a total of 20 signals was gathered; two input signals for the plate displacements, twelve lateral vehicle and wheel displacements and six forces.

Various test conditions can be set within a frequency range of 0-10 Hz, by adjusting the relative phase of the two plate motions as well as their individual amplitudes. Conventionally, tests were conducted at the same frequency with a pure sinewave platform motion at either end.

The original equipment included only a 16 channel data acquisition card, necessitating a two stage test procedure, in order to capture the complete set of 20 signals.

The rig's design, its original equipment and the test and analysis methods adopted were geared to extract a complete set of vehicle parameters for a simple handling model similar to those proposed by Segel /4.2.1/ and Ellis /4.2.2/. It has three DoF for the roll about a fixed roll axis, yaw and lateral motion. In contrast to the 'bicycle model', /4.2.3/, it allows analysing lateral load transfer effects.

In order to obtain sufficient test data for a successful estimation of those parameters listed in table 4.1-1, tests were conducted for plate motions of different individual amplitudes and phases, each at a frequency close to the roll eigenfrequency.

A first set of tests was carried out for obtaining data, which allowed the determination of the roll centre heights at the front and rear ends. For that, all potentiometer outputs were captured, from which the roll angle as well as the track changes were evaluated. It was assumed that the wheel travel is proportional to the roll angle, implying that the vertical tyre squash is of negligible magnitude, so that the roll centre heights could be estimated from a linear relationship between track change and roll angle established in a least square sense.

For the following tests only the six forces and the four vehicle body displacements were recorded. The test data was Fast-Fourier transformed and only the first harmonic content of each signal was used in the subsequent analysis.

Then, these data and the roll centre heights established beforehand, were submitted to a parameter estimation routine, which calculated a cost function, comprising the sum of the differences between measurement on the one hand, and the corresponding model response, based on Segel's vehicle dynamics equations, on the other. A regression algorithm was applied, which minimises this cost function by adjusting the remaining values of the parameter set given in table 4.1-1, and thus determines those values providing the best match between experiment and simulation as estimates.

4.2.2 Introduction of modified test and estimation methods

The introduction to this chapter addressed some issues concerning the development needed to make the Inertia Rig a fully operational facility. First of all, the data acquisition soft- and hardware had to be updated. Secondly, the work of J.D. Rayner /4.2.4/ inspired some more research into improving the testing procedure and the parameter identification method. Finally, the availability of a Jaguar XJ6 to the project, for which all properties concerned here were known, offered the opportunity to verify the rig results for the first time.

Jaguar Cars Ltd. provided the information about the suspension geometry, wheel rates and damping characteristics as well as inertia properties, which were established from rig testing at Cranfield University /4.1.7/. Having these 'benchmark' data available, alternative testing and estimation procedures could be analysed and verified. Any flaws had to be removed before a testing procedure could be devised that provided a reliable parameter estimation with a minimum of rig testing.

Equipment

The problems concerning the equipment deficiencies were resolved by installing the data acquisition package DIA-DAGO /4.2.5/ with a corresponding card into a PC. Further on in the project a second card was acquired accompanied by four more potentiometers. As shown in fig. 4.2-1, these were fitted vertically at each corner of the vehicle between the wheel centre and a suitable location on the bodywork. This arrangement allows measuring the wheel travel directly.

Fig. 4.2-1 instrumented Jaguar XJ6 on Inertia Rig

Following the implementation of the new equipment, the corresponding signal processing software was written, making use of some purpose written MATLAB /4.2.6/ routines for calibrating the signals, taking their Fourier transforms and checking the data against possible measurements errors.

Findings of the MSc project on the Inertia Rig

Some of J.D. Rayner's ideas were taken on board for designing a more efficient test procedure geared to gather just the data required for a robust parameter estimation. In his theoretical study he addressed two fundamental questions concerning the feasibility of the Inertia Rig testing in its original configuration.

Firstly, he investigated which vehicle properties could be estimated successfully, even in the presence of measurement noise. He identified five parameters, whose estimates would be rather sensitive to corrupted measurements.

Secondly, he defined a test procedure, which would provide sufficient data for a subsequent identification. This is an important matter for optimising the test procedure, since it is desirable to test as little as possible for obvious reasons, while on the other hand, one has to ensure that the measured data contains enough information, so that the estimator can distinguish between the contributions made by each of the individual parameters to the measured response characteristics. If this is the case, the measured responses can only be replicated by a model based on a unique set of parameters. For instance, the estimation of the individual wheel rates will be successful only if some of the measured signals are sensitive to either of these, such as the vertical wheel loads, rather than determined by their aggregate, such as the roll angle.

In his research he used AUTOSIM to create a linear model of a vehicle on the rig. In contrast to Segel's model, on which the original estimation approach was based, he also allowed for a pitch DoF in addition to the lateral, roll and yaw motions. Furthermore, each unsprung mass is given an independent DoF for the wheel travel. They are elastically connected to the chassis via spring/ damper elements and geometrically constrained by a radius arm. Also, the tyre forces are represented by spring/ damper units acting in parallel in the lateral and vertical directions. However, this introduces eight new tyre property parameters, requiring identification: stiffness and damping coefficients referring to the lateral and vertical directions for both front and rear end tyres. In contrast to this more detailed approach, the original method treated the forces as measured, hence known, inputs.

For identifying the vehicle parameters, he proposed a Nelder-Mead simplex method, which is a part of the MATLAB package. As other optimisation routines, it minimises a user-defined error criterion by adjusting the values of a set of variables, until a minimal error is established. In our case the error criterion is defined as the sum of differences between the measured and their corresponding predicted signals, while the set of variables comprises normalised starting values for the vehicle and tyre properties to be estimated. Normalisation of the initial parameter values ensures that all estimates are computed within the same percentage of accuracy. Also, the cost function has to be normalised to take account of the different units of the displacement and force data. In J.D. Rayner's work it considers the relative errors of twelve lateral potentiometer displacements as well as those of the six forces, according to:

$$error = \sum_{j=1}^{N} \left[\underbrace{\sum_{i=1}^{18} \frac{\left(real(\hat{y}_{i,j}) - real(y_{i,j})\right)^2}{\left(\hat{y}_{i,j}\right)^2}}_{\text{error of real parts}} + \underbrace{\sum_{i=1}^{18} \frac{\left(imag(\hat{y}_{i,j}) - imag(y_{i,j})\right)^2}{\left(\hat{y}_{i,j}\right)^2}}_{\text{error of imaginary parts}} \right]$$

where $\hat{y}_{i,j}$ denote measured and $y_{i,j}$

predicted force or displacement responses of the j'th test

His findings summarized here are based on an assumed test procedure including 20 tests, for which the plates moved either in or out of phase to each other at frequencies

between 15 and 20 rad/sec[1]. From the simulation results obtained, he concludes that all parameters given in table 4.1-1 can be identified, even taking measurement noise into account. Estimates for the tyre properties and the cross product of Inertia I_{xz} are found to be most sensitive to the influence of corrupted experimental data. As a measure to lessen their sensitivities, he suggests including further test data in the estimation scheme.

Conclusions from MSc project

Based on the findings published in Rayner's thesis /4.2.4/ and on the experience gained from testing a road and a touring car, some alterations regarding the test procedure and the parameter estimation scheme were introduced.

The rig was equipped with further instrumentation as pointed out earlier. It was believed that the additional four potentiometers, measuring the wheel travel, would provide data of sufficient accuracy to estimate the roll centre heights as well as the vertical tyre properties more reliably.

The test procedure was modified. It now comprises tests conducted within a frequency range of 0-7 Hz and includes recordings for at least four different phase settings. The reason for carrying out more tests than proposed by Rayner /4.2.4/ was to ensure a more robust estimation less sensitive to noise corrupted data.

Concerning the parameter identification approach, it was decided to utilise basically the same model and estimation algorithm as proposed in J.D. Rayner's thesis. However, some alterations to the vehicle model were made. The radius arm representation was replaced by introducing first order suspension derivatives for the relative scrub and camber, as described for the Steady State Handling Model in chapter 3.

The current version of the estimation method follows the approach proposed in /4.2.4/. The Nelder-Mead algorithm is employed for computing the estimates, based on a slightly modified error criterion. Rather than dividing the squares of each relative error by the square of the amplitude of the corresponding measurement, the following criterion was introduced:

$$error = \sum_{j=1}^{N} \left[\underbrace{\sum_{i=1}^{18} \frac{\left(real(\hat{y}_{i,j}) - real(y_{i,j})\right)^2}{\max_{j=1:N}\left(\hat{y}_{i,j}\right)^2}}_{\text{error of real parts}} + \underbrace{\sum_{i=1}^{18} \frac{\left(imag(\hat{y}_{i,j}) - imag(y_{i,j})\right)^2}{\max_{j=1,N}\left(\hat{y}_{i,j}\right)^2}}_{\text{error of imaginary parts}} \right]$$

where $\hat{y}_{i,j}$ denote measured and $y_{i,j}$

predicted force or displacement responses of the j'th test

Here, the relative errors for the real and imaginary parts are normalised by the maximal amplitude of the corresponding measurement of all tests considered. This

[1] this frequency range encloses the roll eigenfrequency of the baseline vehicle used in this study

ensures that errors for measurements of relatively small amplitudes are less weighted than those belonging to signals with high amplitudes.

Alternatively to the approach that estimates all parameters at once, including those representing the tyre properties, a sequential identification was tried too. In the first stage the suspension derivatives are established, based on the potentiometer measurements giving the wheel travel and the relative camber and track change. After that, the lateral and vertical tyre properties are estimated from the data providing the forces and their associated deflections. In the third stage, those parameters listed in table 4.1-1 are computed, based on the now constant values, which were obtained by the two previous identification steps.

After the introduction of the new instrumentation and analysis packages, the Jaguar XJ6 assigned to the project as well as a Nissan Primera were rig tested. These tests revealed some inconsistencies of the new approach, which will be discussed along with the results obtained in chapter 5.

4.3 Inertia Rig testing schedule

During the project five vehicles were tested on the rig, two of which on behalf of a SP Tyres customer. The other tests involved two different models of a Nissan Primera and a Jaguar XJ6. The first of the two Nissan vehicles was used to check the functioning of the rig and its by then updated data acquisition software as well as to collect some data for exploring the new parameter estimation approach described in 4.2. Before the other two vehicles were tested, the rig was equipped with additional instrumentation corresponding to the findings of the previous testing.

The dates for each vehicle test, the number of test runs conducted and their specification, along with some notes concerning the equipment used, can be found in table 4.3-1.

date	vehicle	no. of tests	test condition	notes
10/94	Audi A4	130	3.0 Hz 180 deg	original equipment & estimation approach employed; estimation for roll centre heights, roll stiffness and damping front and rear
26.10.95	Primera SLX	42	1.4-3.0 Hz 0 & 180 deg	original potentiometer equipment used; new estimation approach employed
31.10-1.11.95	Audi A4	107	3.25-4.6 Hz 0 & 180 deg	original potentiometer equipment used; new estimation approach employed
22.4-9.5.96	Jaguar XJ6	372	0.6-6.7 Hz 0, +/-90, 180 deg	new equipment estimation approach employed
19.8.-22.8.96	Primera GT	332	0.6-6.7 Hz 0, +/-30, +/-60, +/- 90, 120 deg	new equipment estimation approach employed

Table 4.3-1 Inertia Rig test schedule

In October 1994 an Audi A4 touring car was tested. The original test procedure was followed to obtain parameter values for the roll centre heights, the roll stiffness and damping for the front and rear axle. Inertia properties were not calculated.

In the following year data for a Nissan Primera was gathered using the original test equipment comprising twelve potentiometers measuring the lateral and roll motion of the sprung and unsprung masses. According to the theoretical study on the Inertia Rig /4.2.4/ tests at more than one frequency were conducted. The relative phase between front and rear end plate oscillation was kept at either zero or 180 degrees. The parameter estimation technique presented in 4.2 was employed for the first time.

Shortly after these tests were completed, the rig was used for the successor of the Audi A4 tested the year before. A similar test procedure was adopted as for the Primera. During two days, tests were carried out with five different anti-roll bar settings. Reasonable estimates for all parameters found in table 4.1-1 could be established /4.3.1/. Values for the front and rear roll stiffness corresponded with the different anti-roll bar settings tried.

During the data processing stage for the Primera as well as for the Audi, it became apparent that the roll centre height parameters varied considerably, depending on the frequency of the test, whose data was used for their estimation. In order to obtain more consistent results four additional potentiometers for measuring the wheel travel were acquired. The parameter estimates for the Audi A4 were computed for roll centre heights provided by the customer.

The Jaguar was the first car to be tested, for which the additional equipment was used and for which the new testing and parameter identification method was applied. More than 300 test runs were conducted, covering a frequency range from 0.6 to 6.7 Hz. The phase shift between the two plate motions varied between 0, +/-90 and 180 degrees. Unfortunately, the testing proved to be unsuccessful. Physically unreasonable parameters were estimated from the recorded test data and moreover, the agreement between some measured response characteristics and their corresponding predictions was poor.

Since no operational faults or flaws in the analysis were found explaining the failed parameter estimation exercise, another vehicle, a Nissan Primera GT was tested to gather additional data, which could either confirm or dismiss the assumptions made on the cause of the failure.

For this vehicle similar test conditions were defined. In comparison to the Jaguar testing, the data gathered includes results for 30, 60 and 120 degrees phase settings.

Although a much better agreement between measurement and prediction was achieved for the Primera, some doubt remains on the validity of the parameter values estimated.

5 Inertia Rig testing

After discussing the development work on the SPUK Inertia Rig in chapter 4.2, some results are presented which were obtained with the updated instrumentation and analysis approach. As pointed out in section 4.2.2, the availability of the Jaguar XJ6 and the data giving its mass, stiffness and damping properties, made it possible to verify the results obtained from the rig testing.

Its inertia properties and the centre of gravity height were established on the Cranfield rig /4.1.7/ for a 1991 model year Vanden Plas. Data concerning the suspension geometry, wheel rates and damper properties were disclosed in the form of graphs as well as an ADAMS model input deck, describing a 1993 model year XJ6.

Although a considerable amount of testing and analysis work was carried out, the parameter estimates obtained from the rig testing did not match these 'benchmark' values. However, the experience gained from the testing and analysis inspired some ideas about the possible causes of this mismatch, which are addressed in more detail in the last section of this chapter.

These ideas, supported by some test results, included that subframe and suspension compliance effects of this vehicle, which were neither considered in the testing nor in the vehicle model, were too pronounced and thus prevented a successful parameter estimation. Therefore another vehicle, a Nissan Primera, was tested as well. In this case, front and rear suspensions are directly mounted to the chassis rather than via a subframe. Also, the steering wheel lock was engaged for this vehicle during the testing, which was not the case for the Jaguar[1].

For this vehicle more reasonable parameter values were estimated, but unfortunately, these could not be verified against manufacturer's specifications. However, the following discussion of the results for both vehicles might contribute to a successful conclusion of the rig development, as it was envisaged.

5.1 Jaguar XJ6 test results

The Jaguar testing comprised tests at frequencies between 0 and 6.7 Hz. The frequency spacing was reduced for tests near the three rigid body resonances of the test car, while it was increased for tests in adjacent regions. Their spacing can be seen from the response plots shown further on. At each of these frequencies, tests were conducted with 0, +/- 90, and 180 degrees phase difference between front and rear plate

[1] Referring to 4.2.1 it seems obvious that this constraint has to be introduced, but at the time of the Jaguar testing only small steering motions of the road wheels were observed which did not seem to necessitate locking the rack or the steering wheel.

movements. The amplitudes were the same for both plates, but had to be adjusted at certain frequencies to prevent the vehicle from sliding off the rig.

	estimated vehicle parameters:	*Jaguar Cars data*
roll centre heights front and rear [m]	0.104/ 0.157	0.097/ 0.147
camber change coefficients front and rear [rad/m]	0.315 / 0.53	0.25/ 0.55
centre of gravity height of sprung mass [m]	0.404	0.57
roll & yaw inertia of the sprung mass (body) [kg m^2]	307.4/ 3177.5	321.3/ 2477.2
product of inertia of the sprung mass Ixz [kg m^2]	-71.7	n.a.
wheel rates front and rear [N/m]	38312/ 22769	21800/ 27300
damping coeff. [Nsec/m]	1243/ 1538	2383/ 2027

Table 5.1-1 Comparison of estimated properties vs. manufacturer's specification

As can be seen from the following plots, there are three eigenmodes, which determine the frequency response of the test vehicle within the bandwidth stated. The first mode occurs at about 1.9 Hz, which characterises an almost pure chassis roll motion in phase with the plate displacements. The second mode is excited most strongly for an anti-phase plate movement at about 3.3 Hz. For this condition the vehicle yaws heavily, but maintains a small roll angle. Finally, at about 4.3 Hz the third eigenmode, a combination of roll and lateral chassis motion in anti-phase to each other, becomes apparent.

The mismatch between the parameters estimated and those provided by Jaguar Cars can be established from table 5.1-1. The most striking differences are found for the centre of gravity height, the wheel rates and the damping coefficients.

These differences are considerable, and one would expect to see a corresponding discrepancy between measured vehicle responses and those predicted by the model based on the estimated parameters given in table 5.1-1. Surprisingly, this is not the case for the majority of the response characteristics, such as the amplitudes and phases for the roll, yaw and lateral DoF and those for the contact forces. In fact, most of them are well matched up to the second resonance.

5.1.1 Discussion of amplitude and phase graphs

The plots shown below indicate that, except for tests carried out near the third eigenfrequency, a good agreement for most of the characteristics is achieved. Discrepancies between model prediction and measurements are most pronounced for the lateral and especially for the front end vertical wheel loads.

The graphs 5.1-1a, b show the gains and phases of the three vehicle body DoF for in-phase plate oscillations. Note that the gains in this plot have different units: angles are given in radians, displacements in metres. For the plots presented here, a gain is defined by the ratio of the respective amplitude divided by the plate displacement amplitude. Phase angles[2] are given in radians. Points connected by broken lines refer to simulated data.

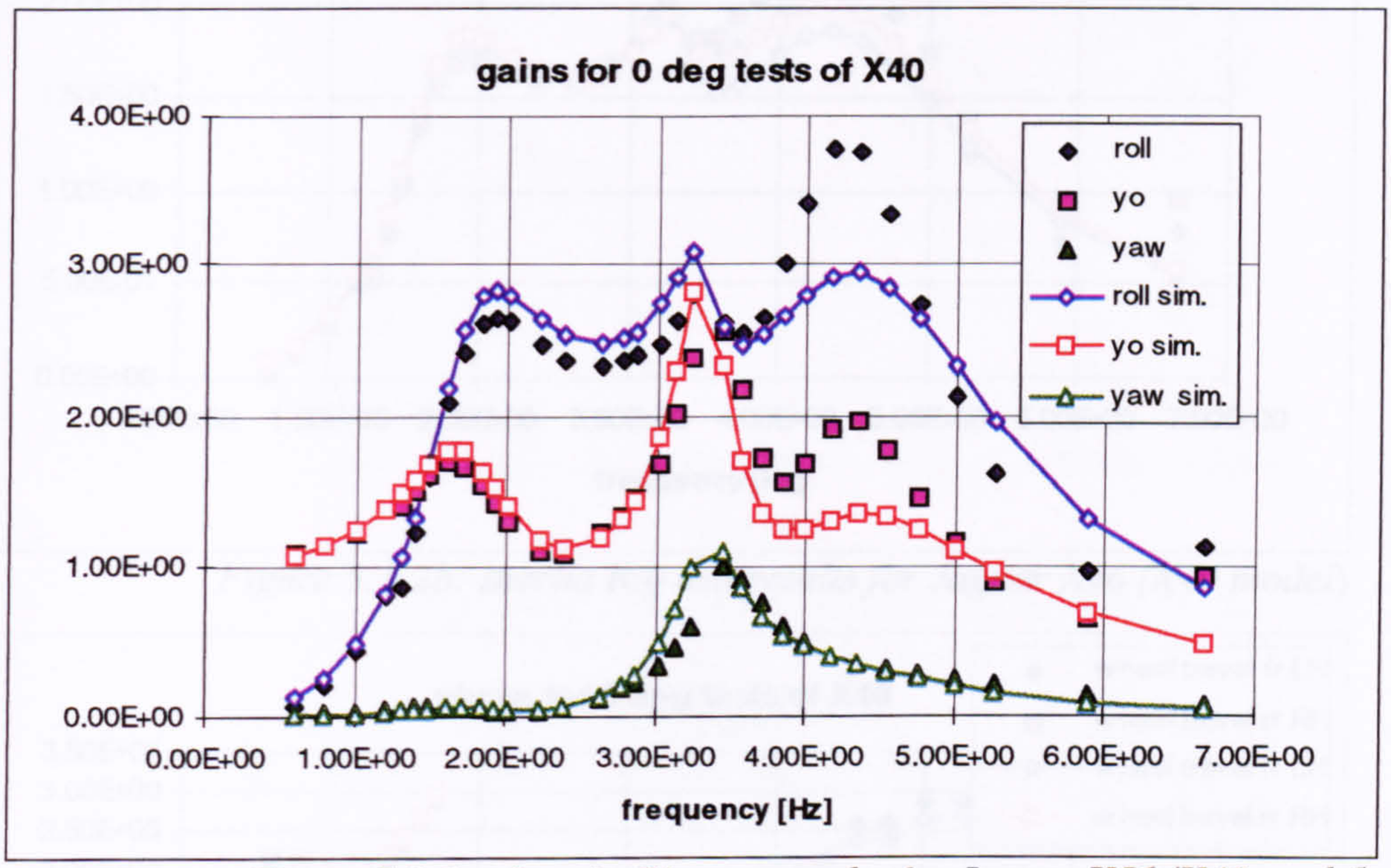

Figure 5.1-1a: Inertia Rig test results for Jaguar XJ6 (X40 model)

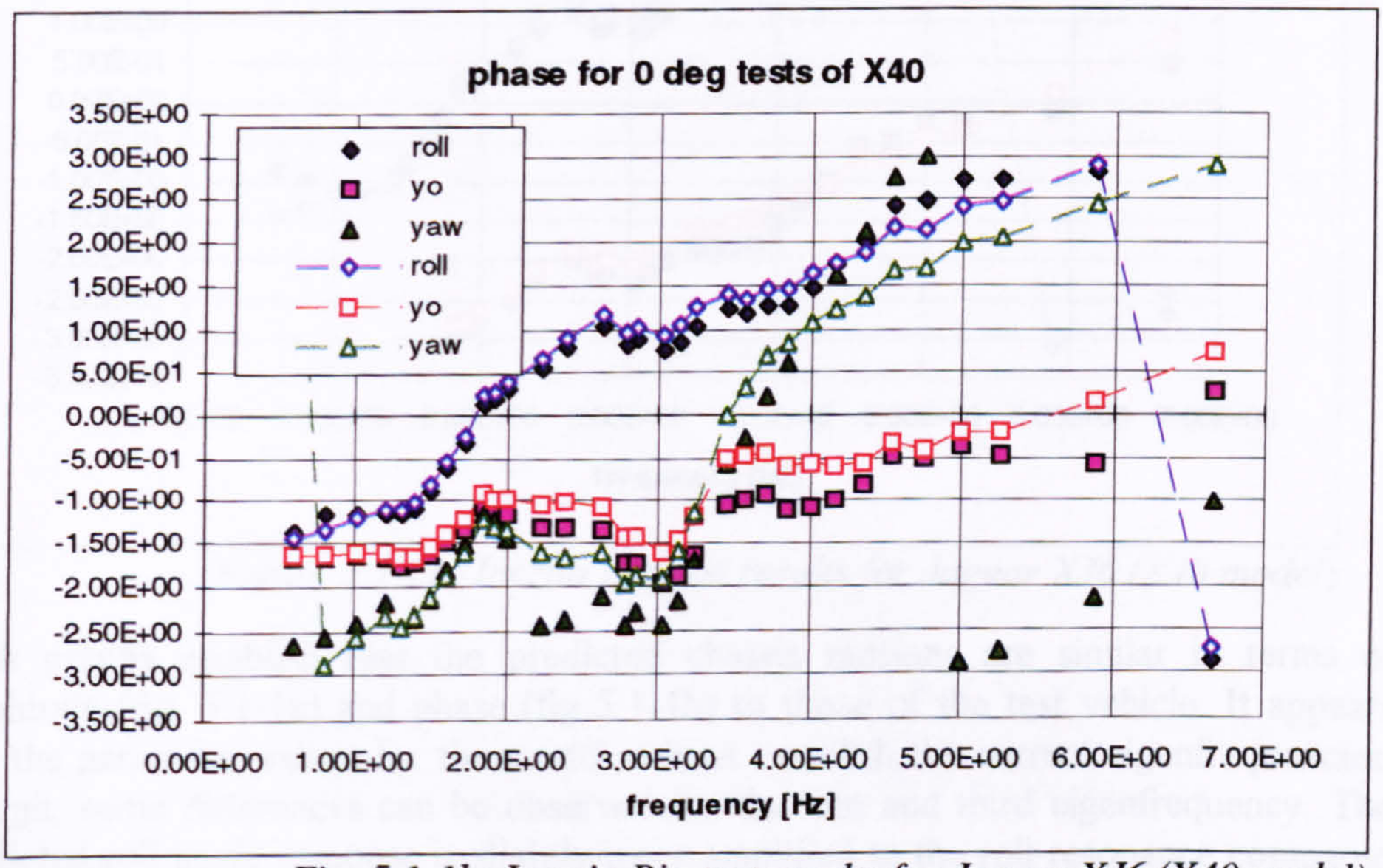

Fig. 5.1-1b: Inertia Rig test results for Jaguar XJ6 (X40 model)

[2] some of the data points given for the phase appear like outliers because of the 2π periodicity

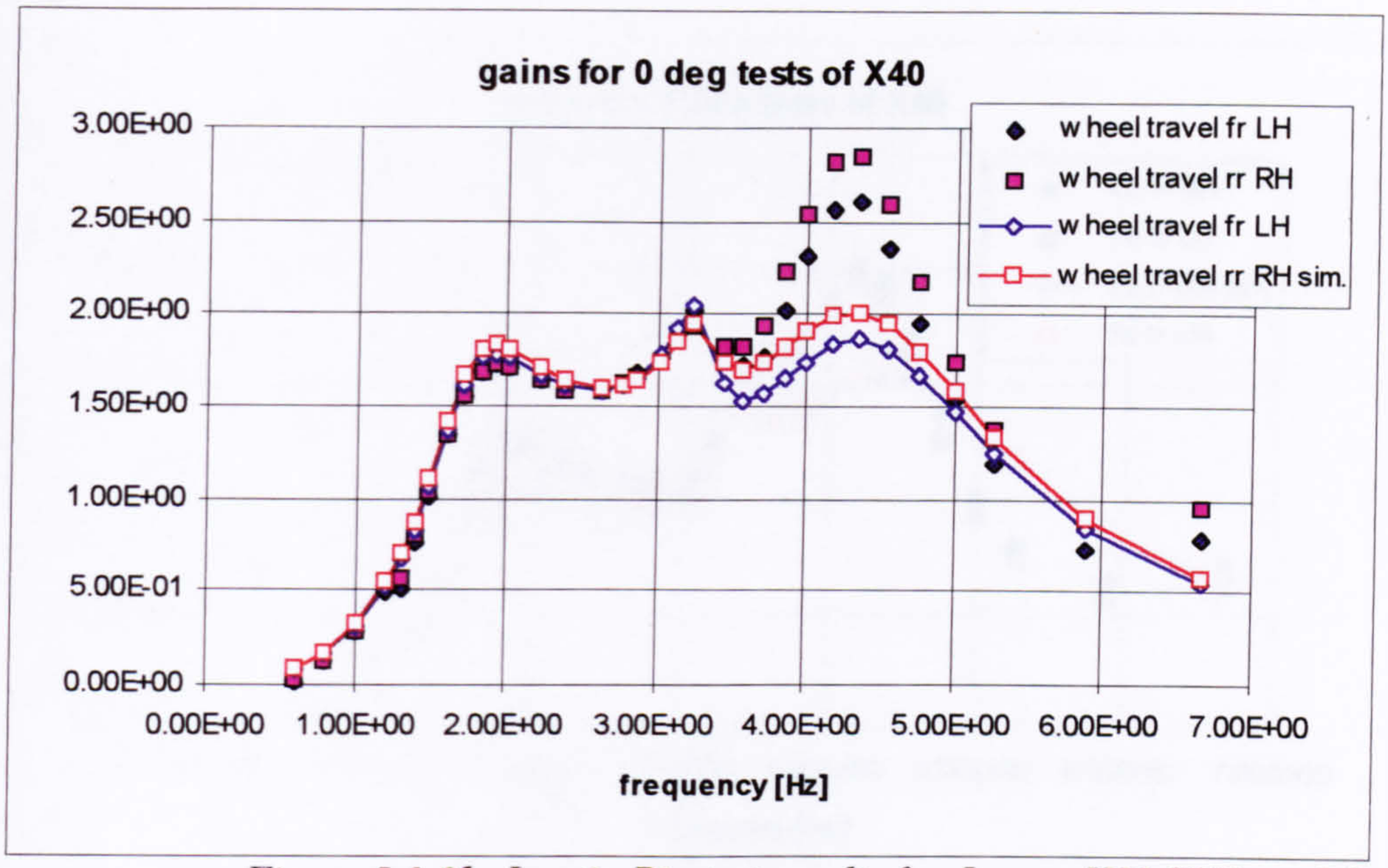

Figure 5.1-2b: Inertia Rig test results for Jaguar XJ6 (X40 model)

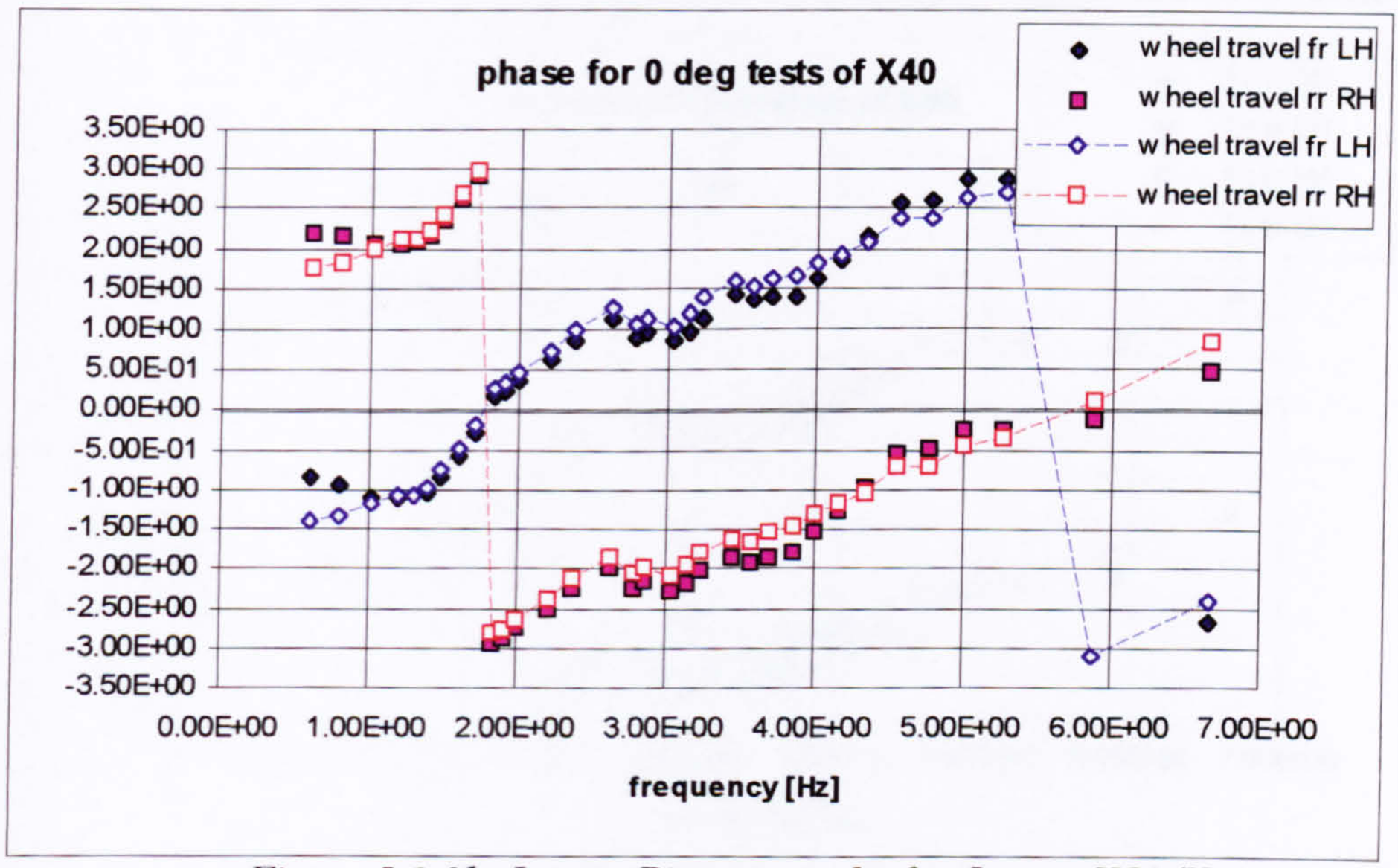

Figure 5.1-2b: Inertia Rig test results for Jaguar XJ6 (X40 model)

Both graphs establish that the predicted chassis motions are similar in terms of amplitude (fig. 5.1-1a) and phase (fig 5.1-1b) to those of the test vehicle. It appears that the parameter values for the model at least establish the correct eigenfrequencies, though, some differences can be observed for the first and third eigenfrequency. The predicted roll angle response is slightly more amplified at the roll resonance compared to the measurement. The opposite applies to the gains at the second resonance, for which the lateral movement of the front axle, yo, and the vehicle roll are much less pronounced for the model. Referring to fig. 5.1-1b, the phase angles are well matched

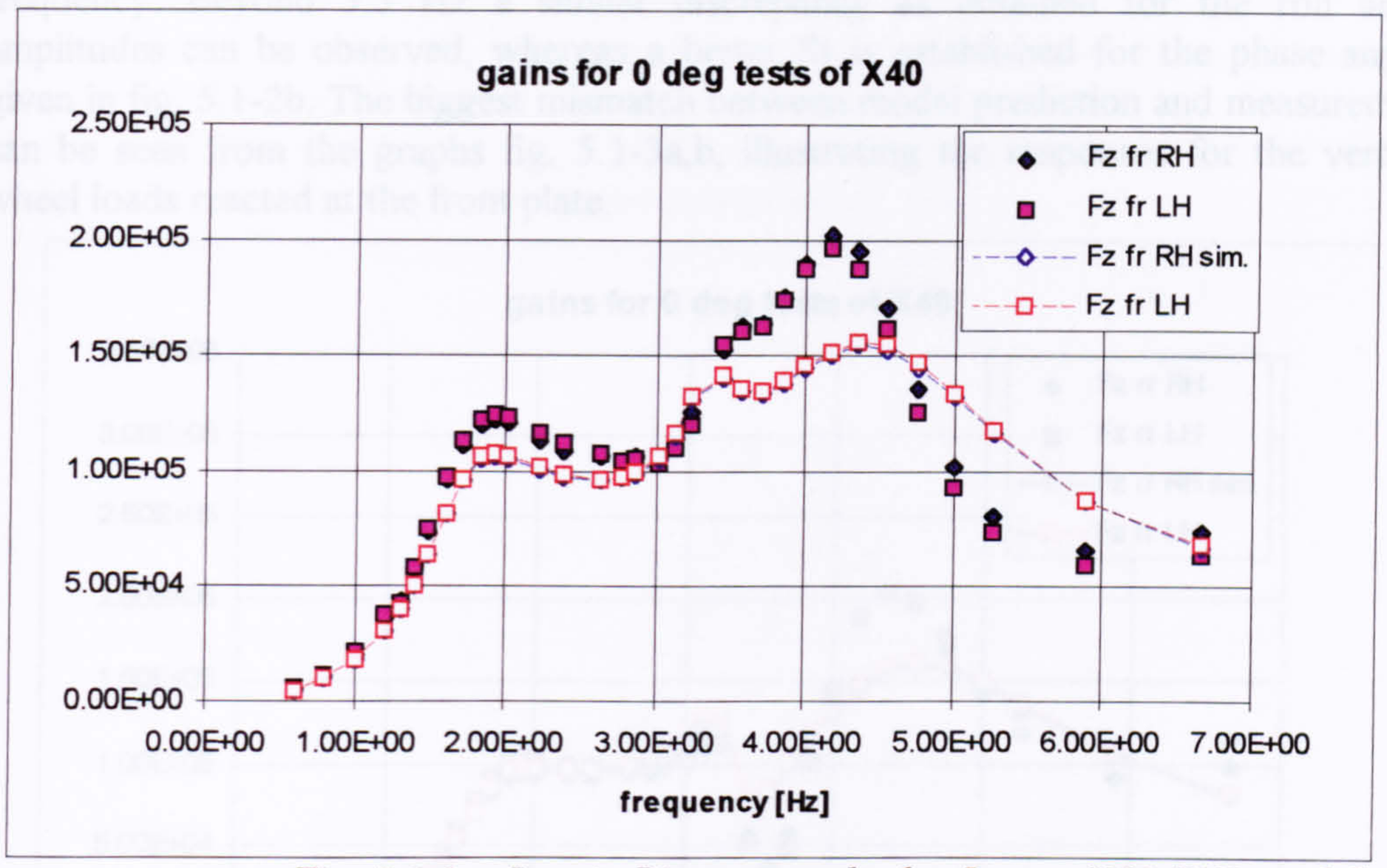

Fig. 5.1-3a: Inertia Rig test results for Jaguar XJ6 (X40 model)

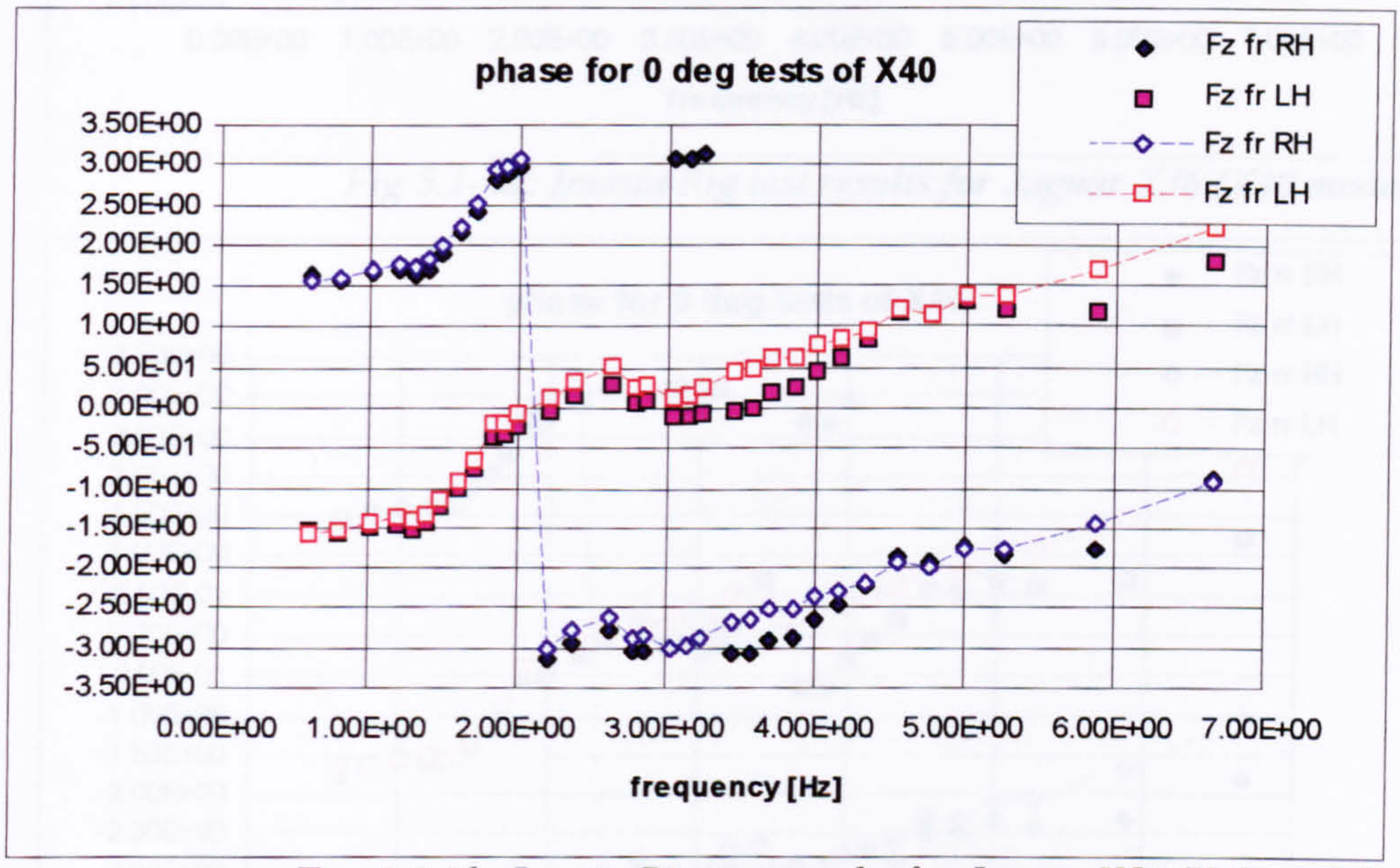

Fig. 5.1-3b: Inertia Rig test results for Jaguar XJ6 (X40 model)

for the lateral and roll DoF. Again, their disagreement is confined to tests at frequencies given above. The poor agreement for the yaw angle at low frequencies is a consequence of the low amplitudes produced by the in phase test condition.

A similar quality of fit is observed for the wheel travel response characteristics illustrated by fig. 5.1-2a,b. Corresponding to the higher roll angle amplification observed for the model, the wheel travel amplitudes are predicted to be slightly too large at the roll resonance. However, a good fit is maintained up to the yaw resonance

frequency. Beyond 3.3 Hz a similar discrepancy as obtained for the roll angle amplitudes can be observed, whereas a better fit is established for the phase angles given in fig. 5.1-2b. The biggest mismatch between model prediction and measurement can be seen from the graphs fig. 5.1-3a,b, illustrating the responses for the vertical wheel loads reacted at the front plate.

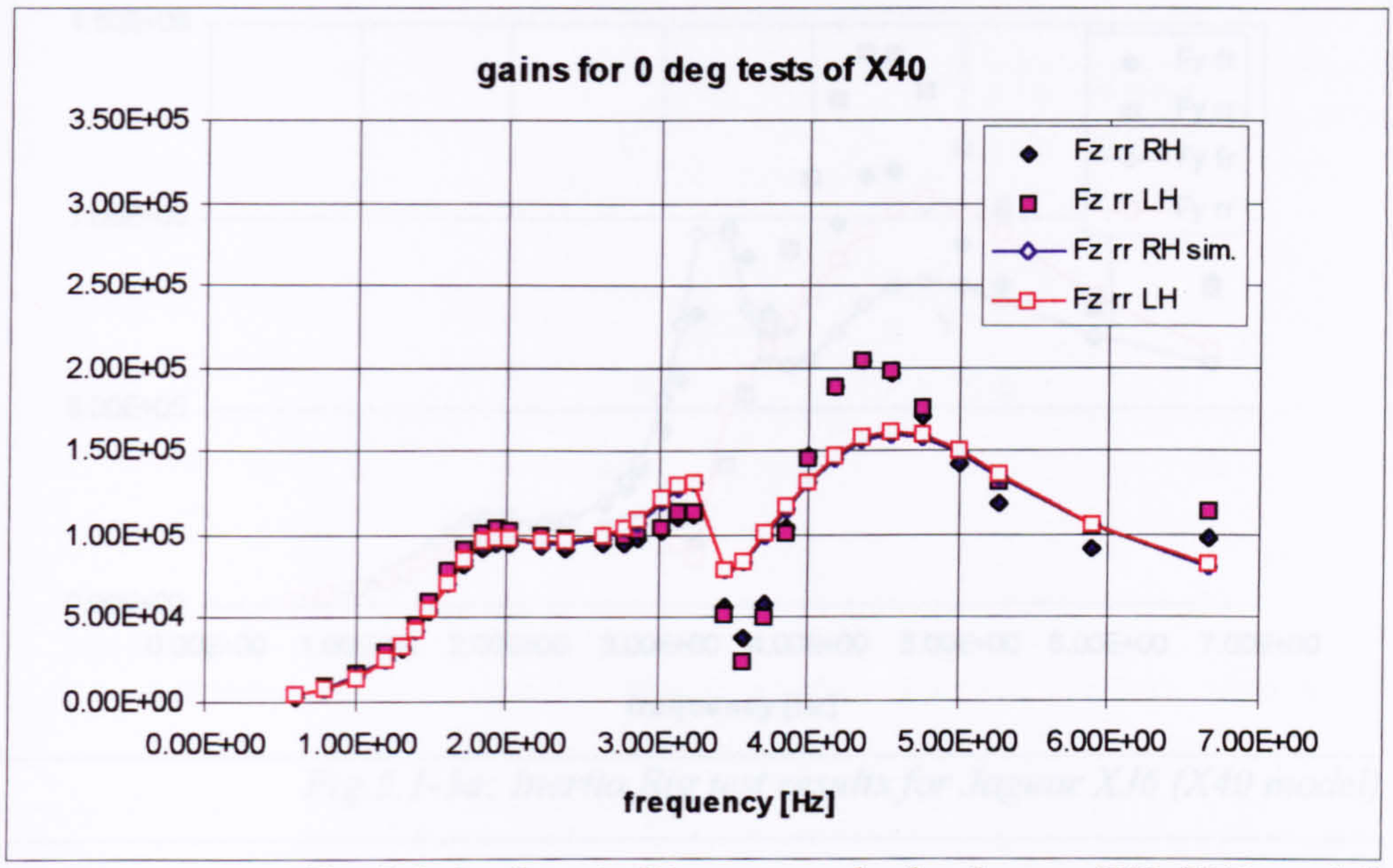

Fig 5.1-4a: Inertia Rig test results for Jaguar XJ6 (X40 model)

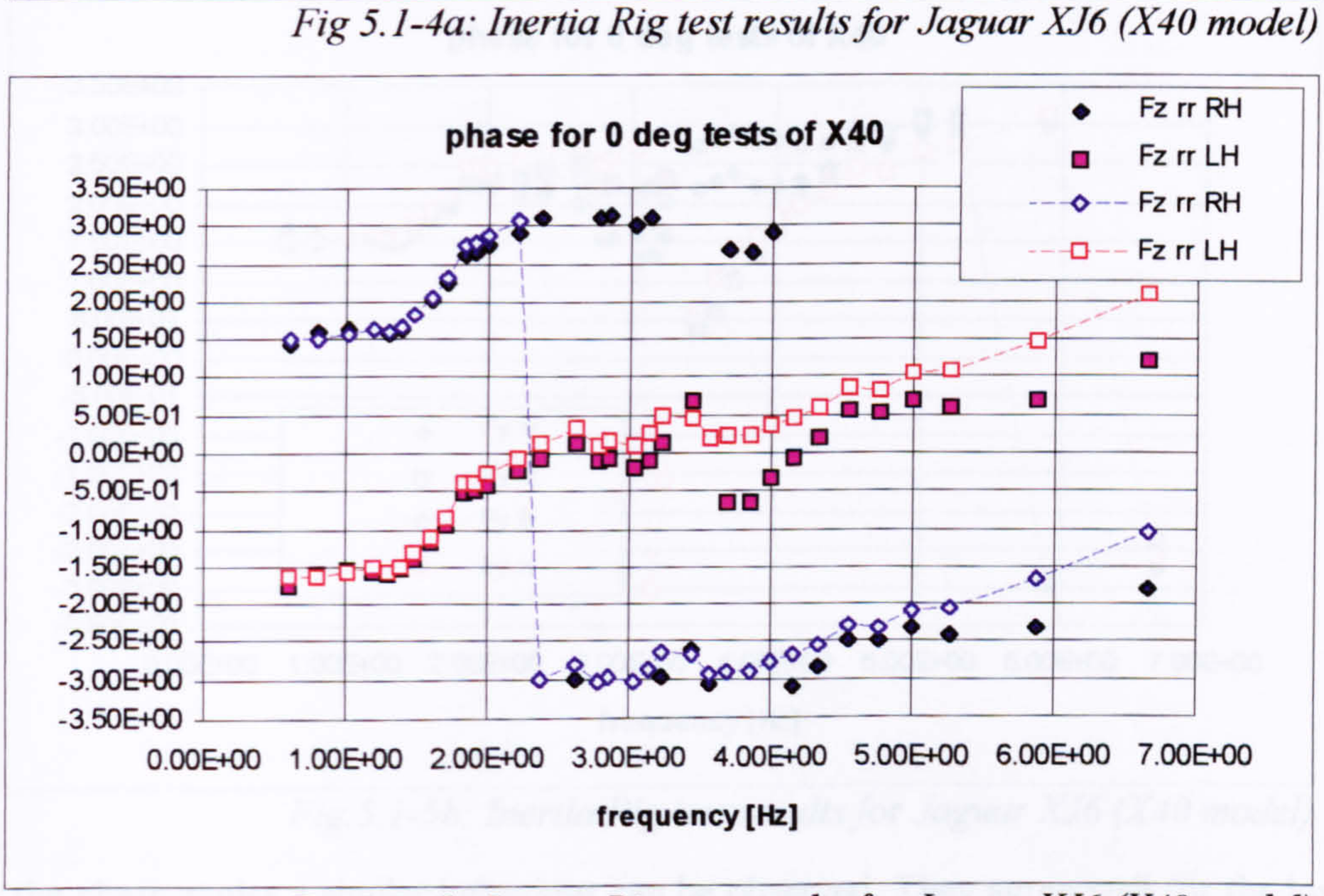

Fig 5.1-4b: Inertia Rig test results for Jaguar XJ6 (X40 model)

Although the basic shape of the curve describing the predicted gains looks right, the model amplitudes remain well below the measured ones, especially for tests beyond the

roll resonance. The largest discrepancy is found between the yaw and the third resonance, for which roll and lateral oscillations dominate. Also, the roll-off characteristics at high frequencies differ considerably from each other.

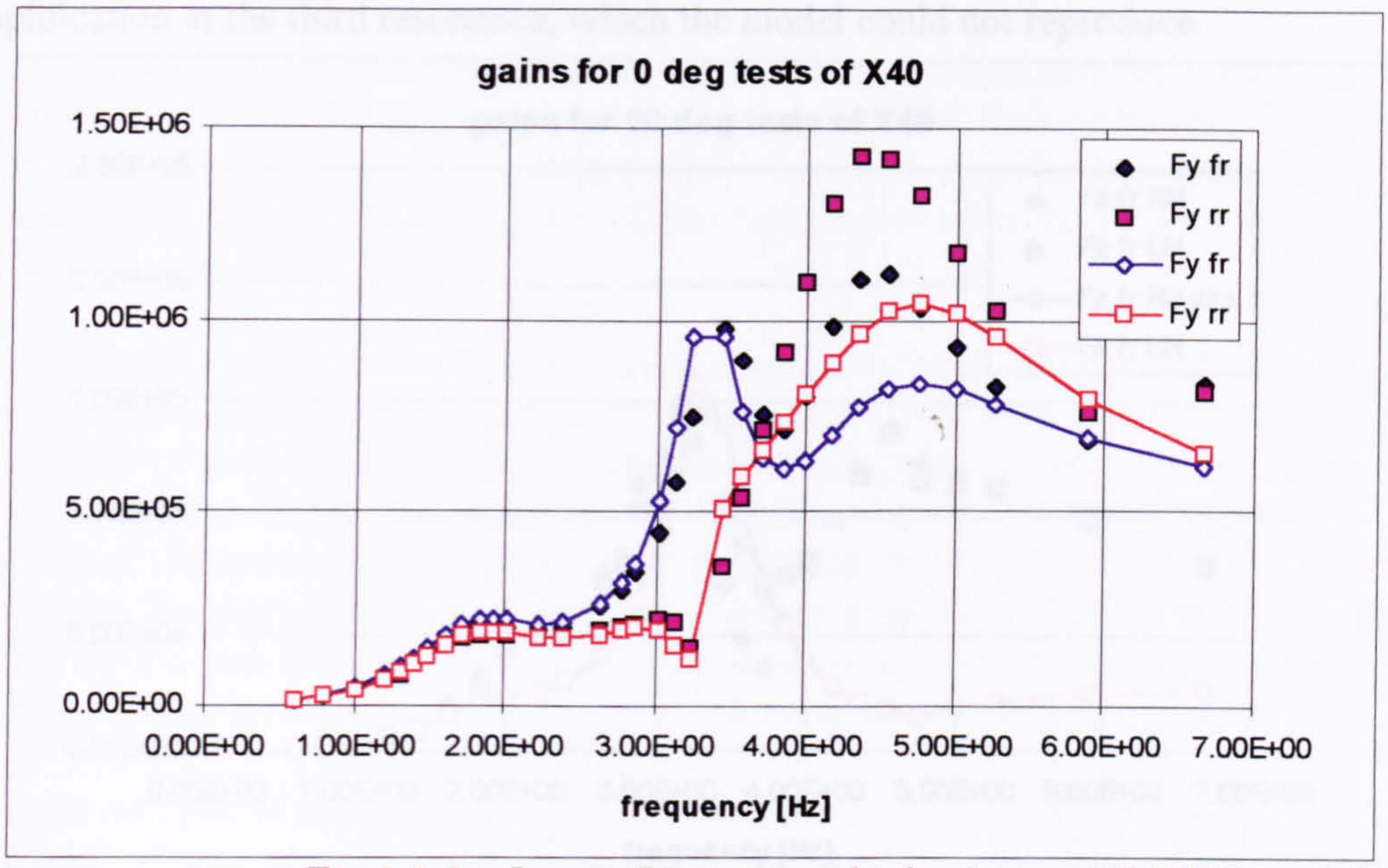

Fig.5.1-5a: Inertia Rig test results for Jaguar XJ6 (X40 model)

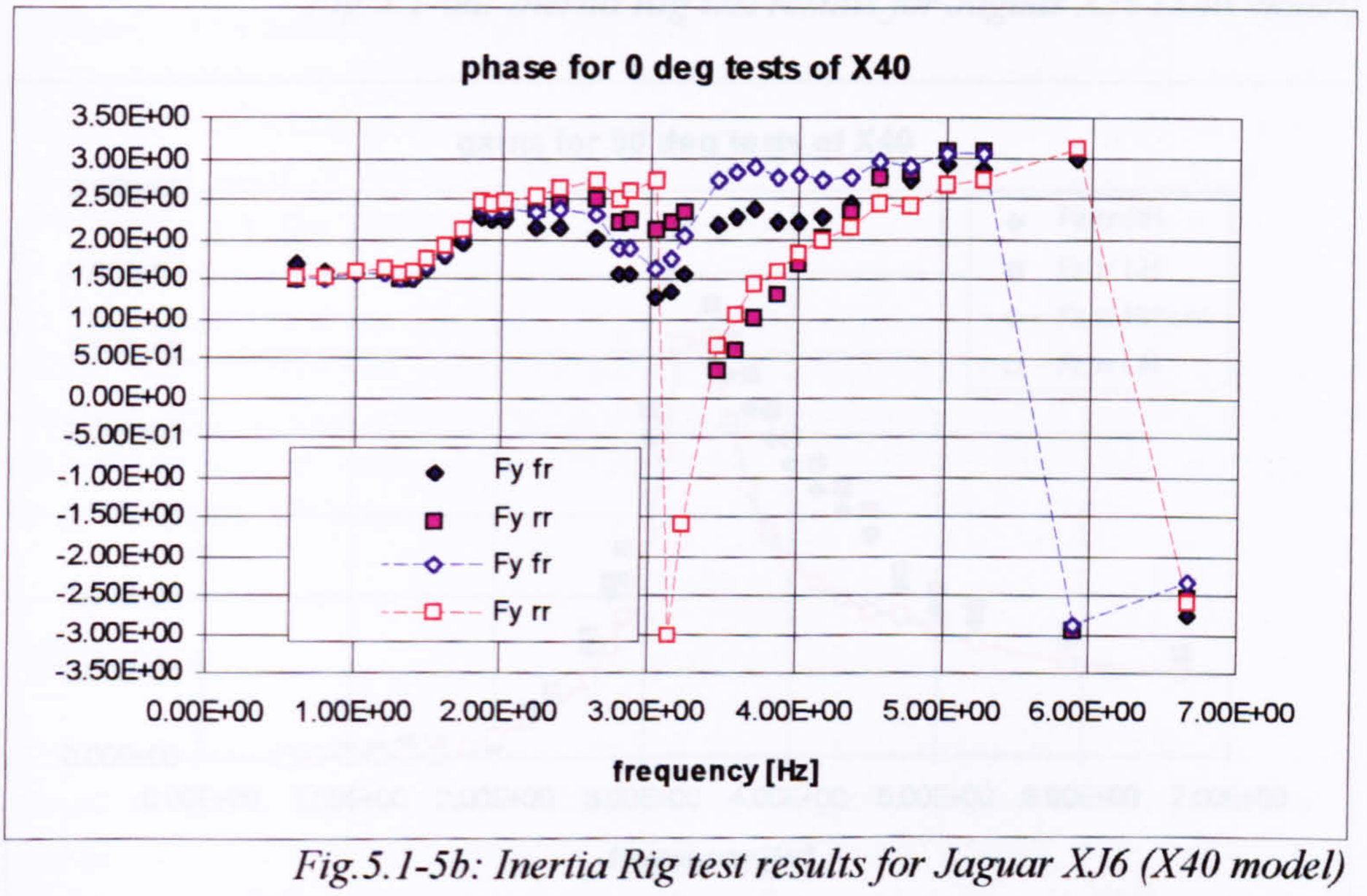

Fig.5.1-5b: Inertia Rig test results for Jaguar XJ6 (X40 model)

For the phase angles a similar behaviour can be observed. They agree well for the low frequency tests, up to the yaw eigenfrequency. At this resonance the largest mismatch occurs. Beyond this resonance measured and simulated phase angles converge toward each other.

In comparison to the front end vertical loads, a reasonable fit is obtained for those at the opposite end. Their magnitudes, as shown in fig. 5.1-4a, are well matched apart from the sudden roll off at the yaw eigenfrequency and a more pronounced amplification at the third resonance, which the model could not reproduce.

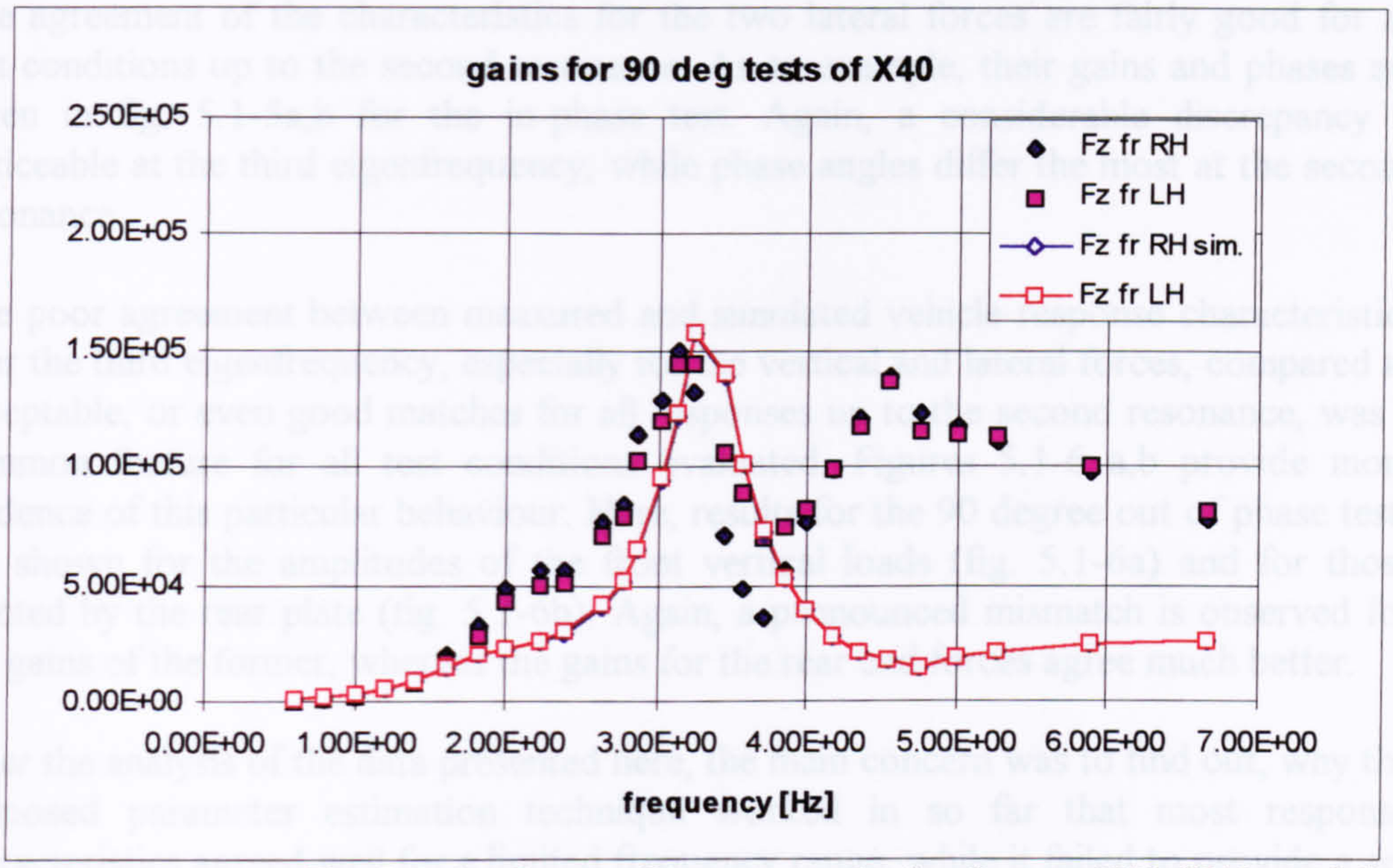

Fig.5.1-6a: Inertia Rig test results for Jaguar XJ6 (X40 model)

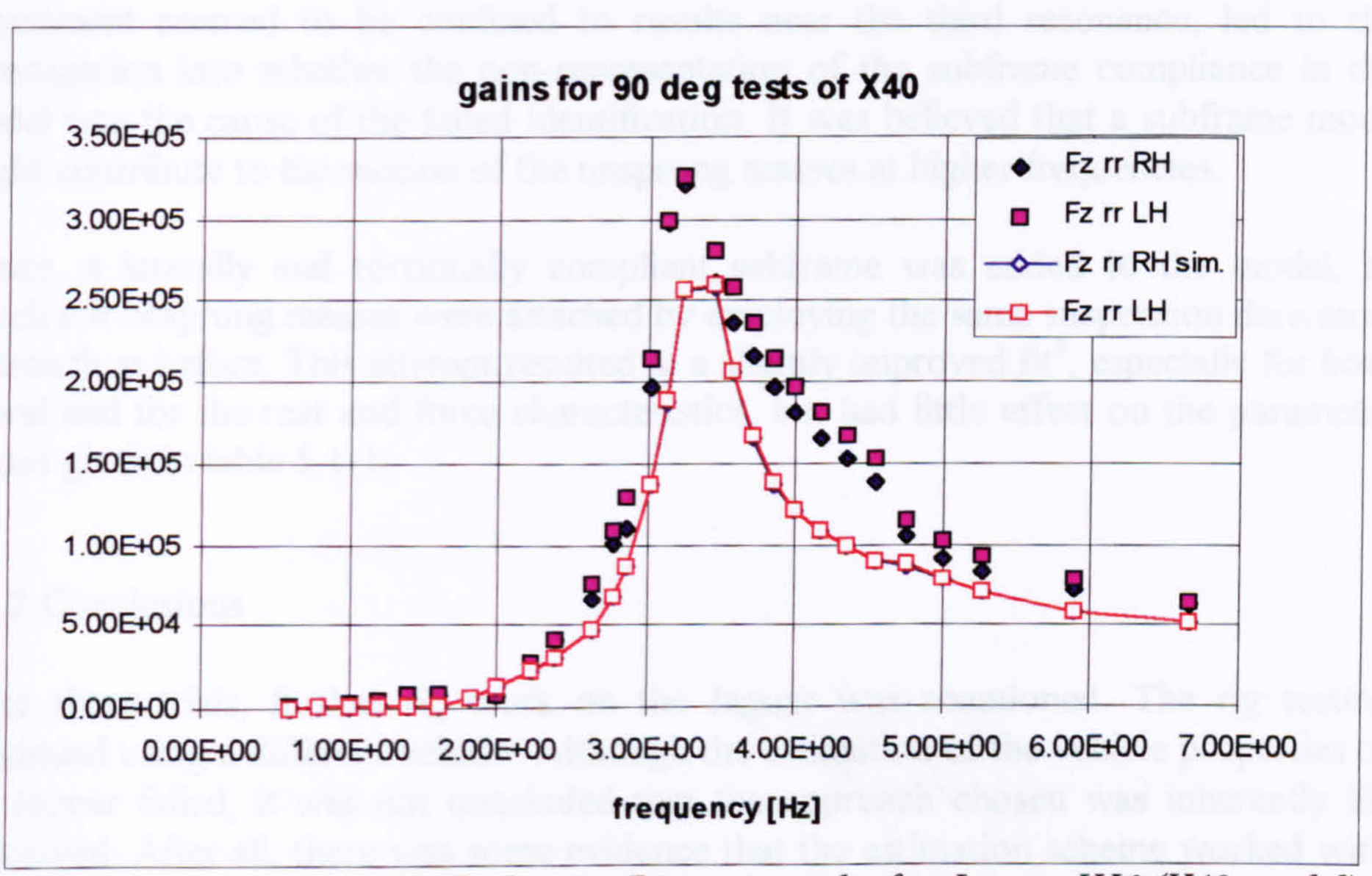

Fig.5.1-6b: Inertia Rig test results for Jaguar XJ6 (X40 model)

The mismatch near the yaw eigenfrequency becomes more apparent by comparing the phases shown in fig. 5.1-4. Also, an increase of the phase error with frequency can be observed here for test results beyond the third resonance.

The agreement of the characteristics for the two lateral forces are fairly good for all test conditions up to the second resonance. As an example, their gains and phases are given in fig. 5.1-5a,b for the in-phase test. Again, a considerable discrepancy is noticeable at the third eigenfrequency, while phase angles differ the most at the second resonance.

The poor agreement between measured and simulated vehicle response characteristics near the third eigenfrequency, especially for the vertical and lateral forces, compared to acceptable, or even good matches for all responses up to the second resonance, was a common feature for all test conditions evaluated. Figures 5.1-6 a,b provide more evidence of this particular behaviour. Here, results for the 90 degree out of phase tests are shown for the amplitudes of the front vertical loads (fig. 5.1-6a) and for those reacted by the rear plate (fig. 5.1-6b). Again, a pronounced mismatch is observed for the gains of the former, whereas the gains for the rear end forces agree much better.

After the analysis of the data presented here, the main concern was to find out, why the proposed parameter estimation technique worked in so far that most response characteristics agreed well for a limited frequency range, while it failed to provide a set of physically reasonable properties. The fact that the discrepancy between model and experiment seemed to be confined to results near the third resonance, led to the investigation into whether the non-representation of the subframe compliance in the model was the cause of the failed identification. It was believed that a subframe mode might contribute to the motion of the unsprung masses at higher frequencies.

Hence, a laterally and torsionally compliant subframe was added to the model, to which the unsprung masses were attached by employing the same suspension derivative approach as before. This attempt resulted in a slightly improved fit[3], especially for both lateral and for the rear end force characteristics, but had little effect on the parameter values given in table 5.1-1.

5.1.2 Conclusions

After these trials, further rig work on the Jaguar was abandoned. The rig testing continued using a different vehicle. Although the estimation of the vehicle properties of the Jaguar failed, it was not concluded that the approach chosen was inherently ill-conceived. After all, there was some evidence that the estimation scheme worked with regard to matching model output to the vehicle response measurements within a limited frequency bandwidth.

---

[3] which is hardly surprising considering that the estimator has additional variables to adjust for minimising the error cost function

The simplicity of the vehicle model, including its tyre representation, was seen as a possible reason for the failure to obtain reasonable estimates. However, it was not possible to study the influence of steering, compliance and nonlinearities on the robustness of the implemented estimation approach inside the project.

5.2 Nissan Primera test results

It was hoped that the Nissan Primera testing would establish either that the testing and estimation procedure works, at least for this specimen, or that, in the case of another failure, the whole idea of the present method had to be rethought. There was also the possibility, that further test results would reveal clues about what had prevented a successful conclusion earlier on.

Most of the parameter estimates for the rig tested Nissan Primera GT appear to be reasonable. They are given in table 5.2-1. In the adjacent column, some suspension parameter values for the standard version of this model are given.

	estimated vehicle parameters:	*Nissan Primera data*[1]
roll centre heights front and rear [m]	0.150/ 0.062	0.040/ 0.1295
camber change coefficients front and rear [rad/m]	0.42 / 0.23	0.2714/ 0.3386
centre of gravity height of sprung mass [m]	0.52072	n.a.
roll & yaw inertia of the sprung mass (body) [kg m^2]	289.6/ 1650	n.a.
product of inertia of the sprung mass Ixz [kg m^2]	-64.9	n.a.
wheel rates front and rear [N/m]	46452/ 84024	53743/ 44409
damping coeff. [N/m/sec]	3465/ 3427	n.a.

Table 5.2-1 Comparison of estimated properties vs. manufacturer's specification

The high figure for the rear end wheel rate has to be regarded with some doubt, though. On the other hand, for the centre of gravity height, which was the most obvious mismatched parameter for the Jaguar, a realistic value was calculated.

5.2.1 Discussion of amplitude and phase graphs

Measured and predicted response characteristics for this test vehicle agree reasonably well with a similar quality as established for the majority of the Jaguar test data. A mismatch confined to a limited frequency range, as observed especially for the lateral and vertical forces of the latter for all test conditions, was not replicated. However, the vertical wheel load characteristics showed the least quality of agreement in comparison to those of the vehicle DoF and those of the lateral forces. The latter were much better approximated than was the case for the Jaguar data.

In order to allow a qualitative comparison of the results obtained for the two vehicles, only those test results for the Primera are presented, which correspond to the same test

[1] The data for this vehicle were obtained from the Lotus Engineering Suspension Rig for a standard 1993 model year Primera

conditions on which the discussion in section 5.1.1 was based upon. Figures 5.2-1a,b show the gains and phases of the three vehicle DoF for a pure in-phase plate oscillation. As was the case for the Jaguar, experimental and simulated data agree very well up to the second resonance. As for the Jaguar, the predicted roll amplification at the last resonance is smaller than measured.

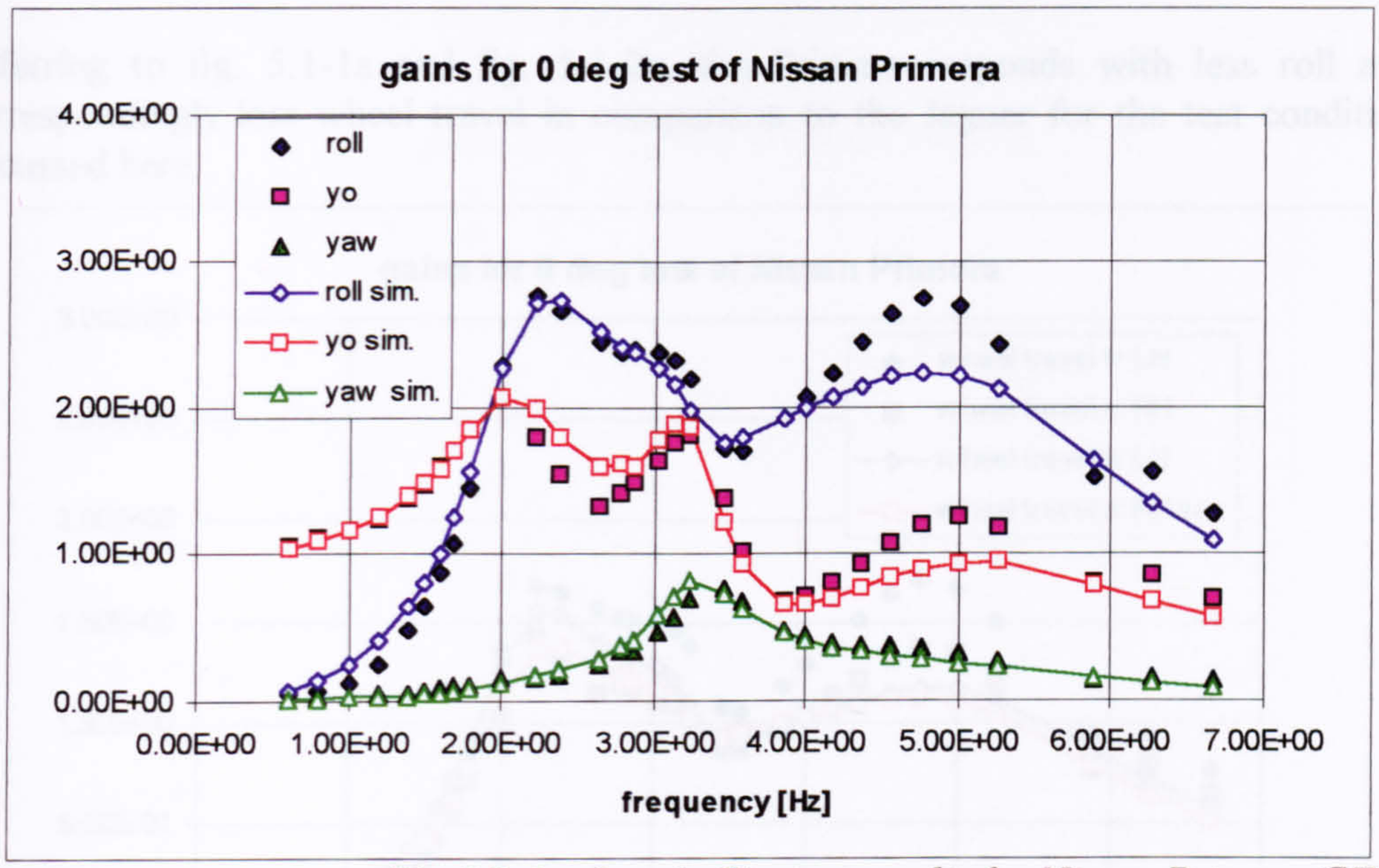

Fig 5.2-1a: Inertia Rig test results for Nissan Primera GT

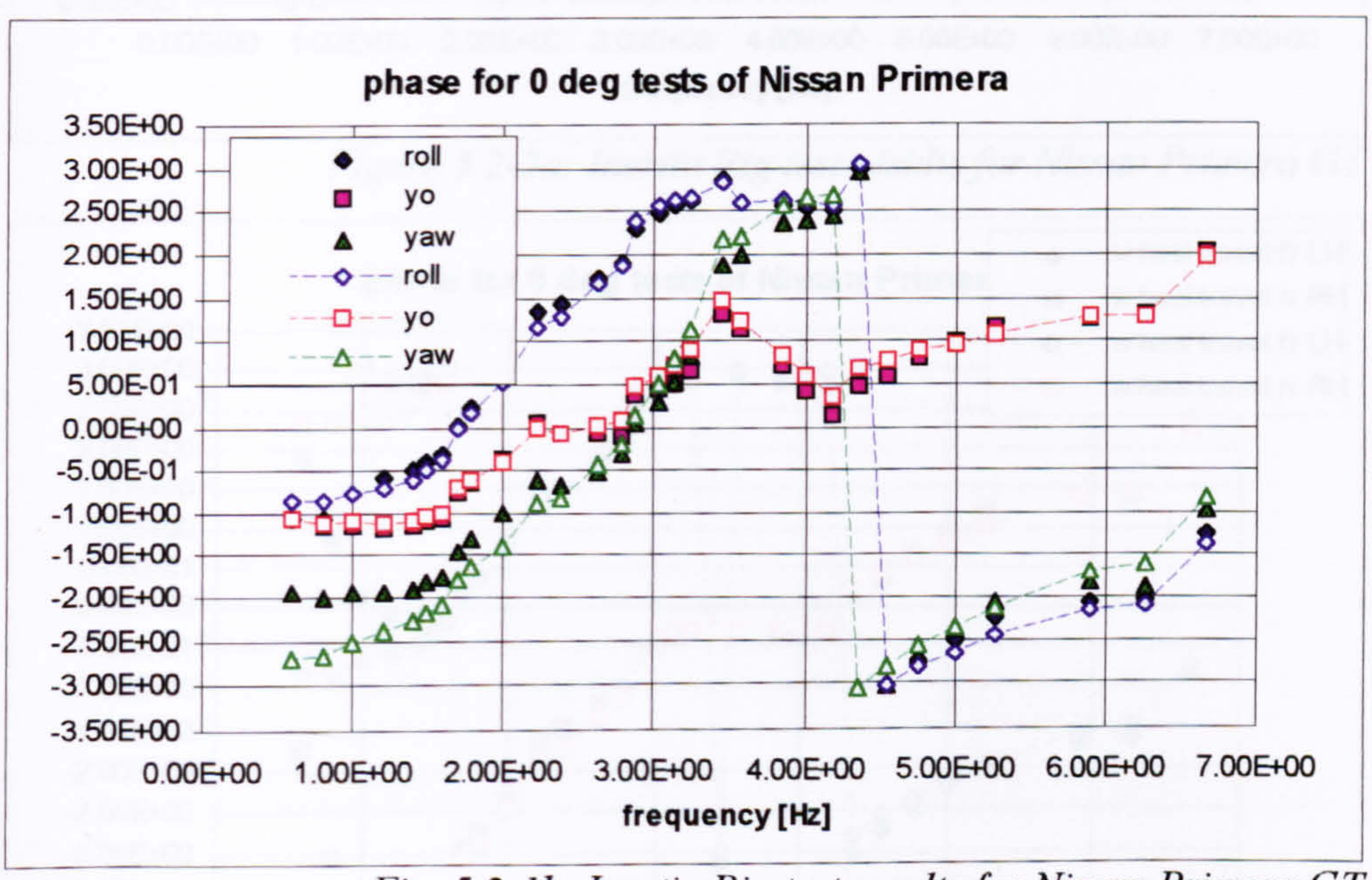

Fig. 5.2-1b: Inertia Rig test results for Nissan Primera GT

The correlation for the vertical wheel travel, shown in fig. 5.2-2a,b, is less good, especially in the neighbourhood of the third resonance, shortly before 5 Hz, as was the case for the Jaguar. Throughout the frequency range, the rear end amplitudes are far better approximated than those for the front end, whereas the graph for the phase (fig. 5.2-2b) indicates a good quality of fit, except for the low frequency tests.

Referring to fig. 5.1-1a and fig. 5.1-2a, the Primera responds with less roll and correspondingly less wheel travel in comparison to the Jaguar for the test condition discussed here.

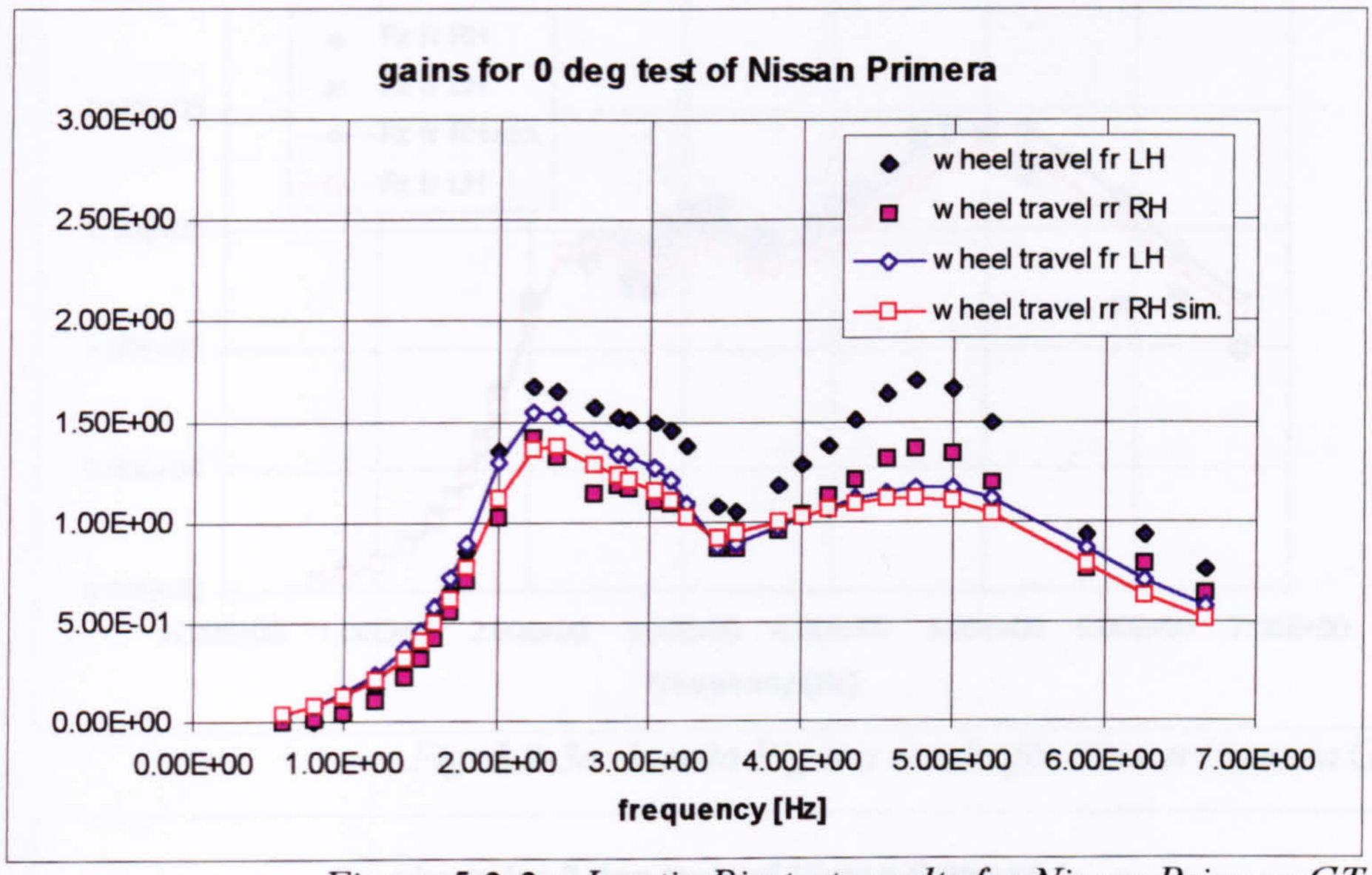

Figure 5.2-2a: Inertia Rig test results for Nissan Primera GT

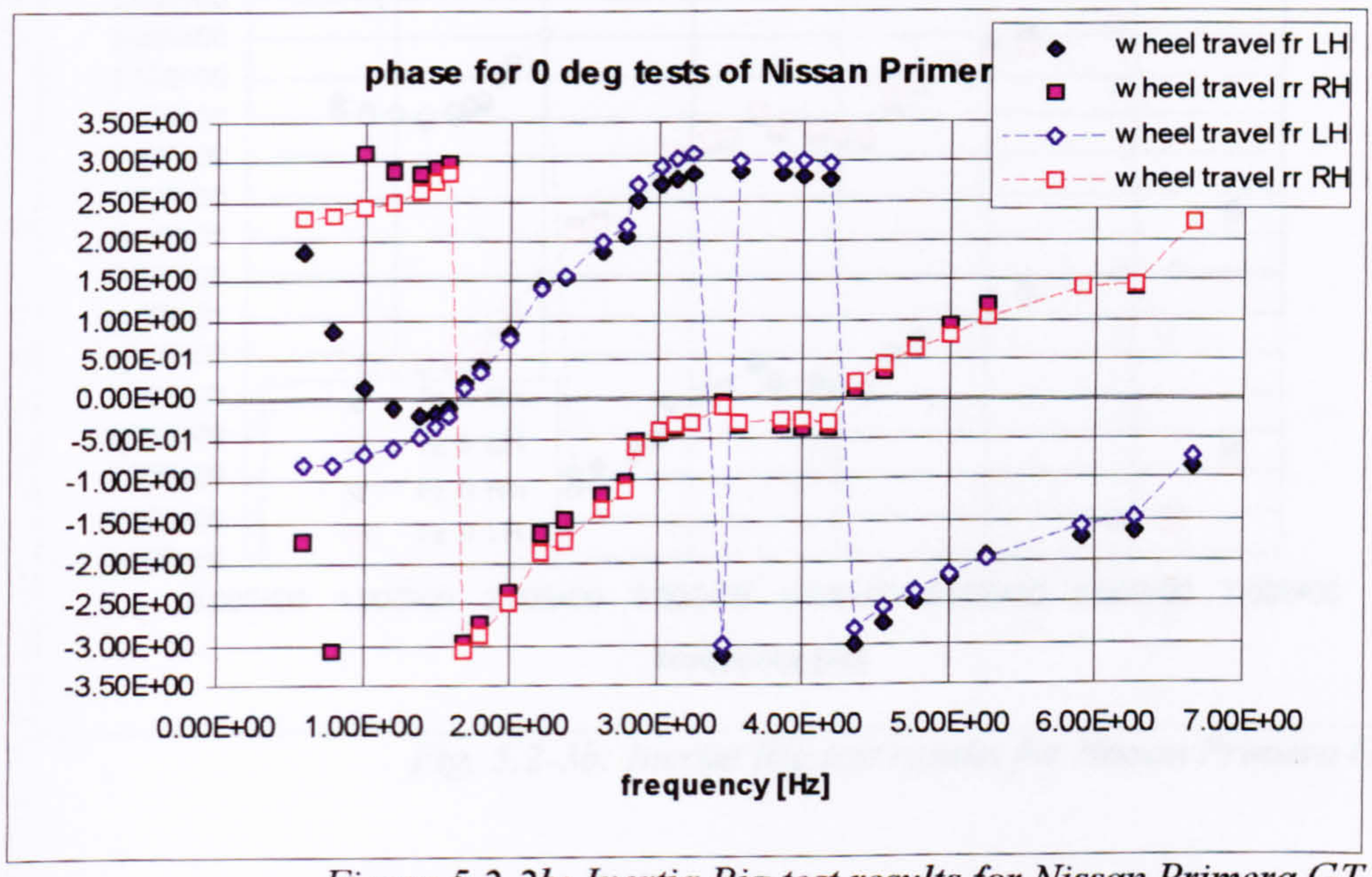

Figure 5.2-2b: Inertia Rig test results for Nissan Primera GT

In contrast to the Jaguar results, a rather good agreement is achieved for the vertical wheel loads front and rear, as shown in the fig. 5.2-3a,b and fig. 5.2-4a,b, respectively. This time, measurements and prediction differ more for the rear end load amplitudes, though, their mismatch is confined to frequencies between the first and second eigenfrequencies and is far less pronounced compared to the results obtained for the Jaguar shown in fig. 5.1-3a. Phases agree very well for these signals.

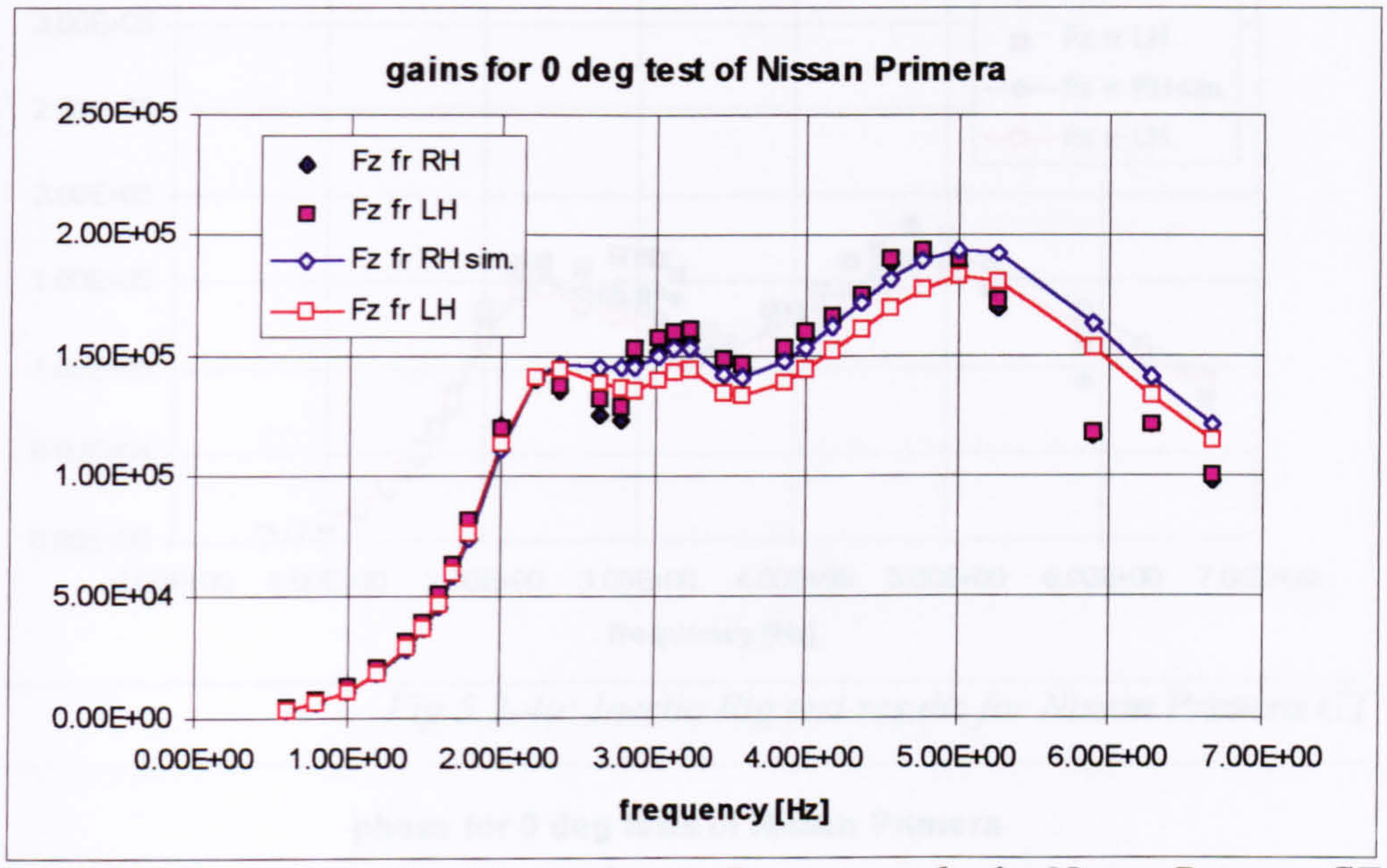

Fig. 5.2-3a: Inertia Rig test results for Nissan Primera GT

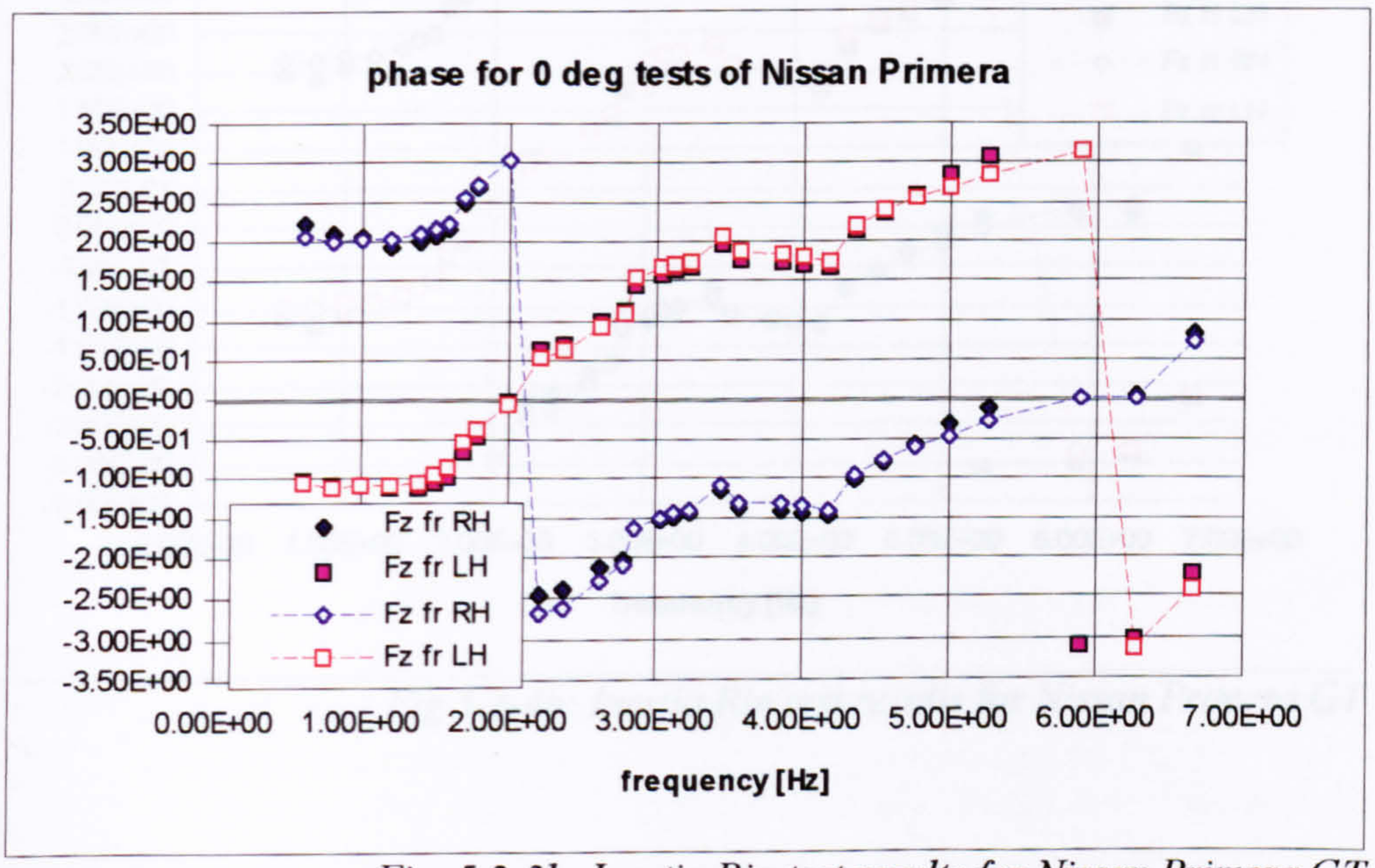

Fig. 5.2-3b: Inertia Rig test results for Nissan Primera GT

For completeness, an example for the lateral force characteristics is given by fig. 5.2-5a,b. A much improved agreement in comparison to the Jaguar data was achieved for all test conditions.

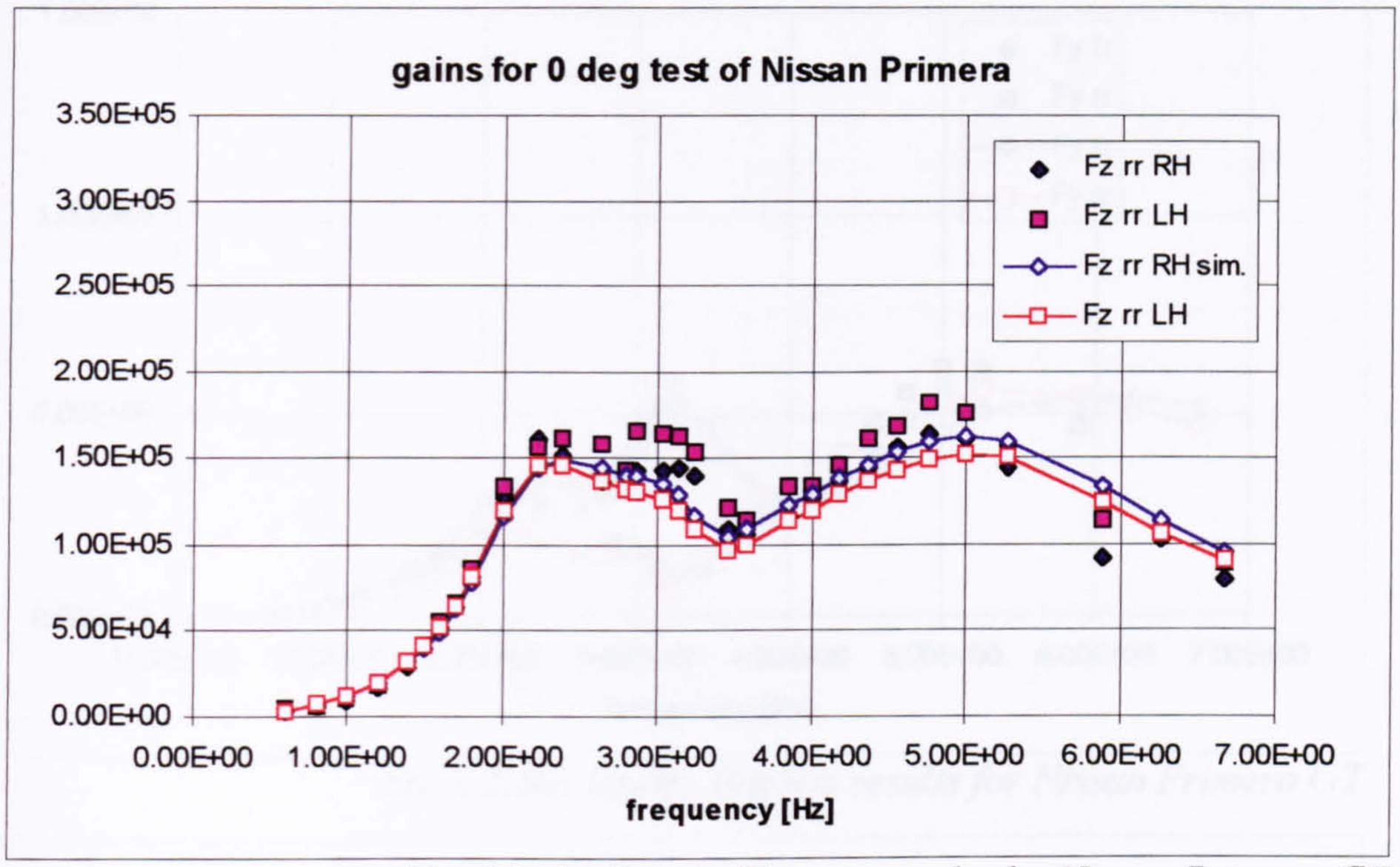

Fig 5.2-4a: Inertia Rig test results for Nissan Primera GT

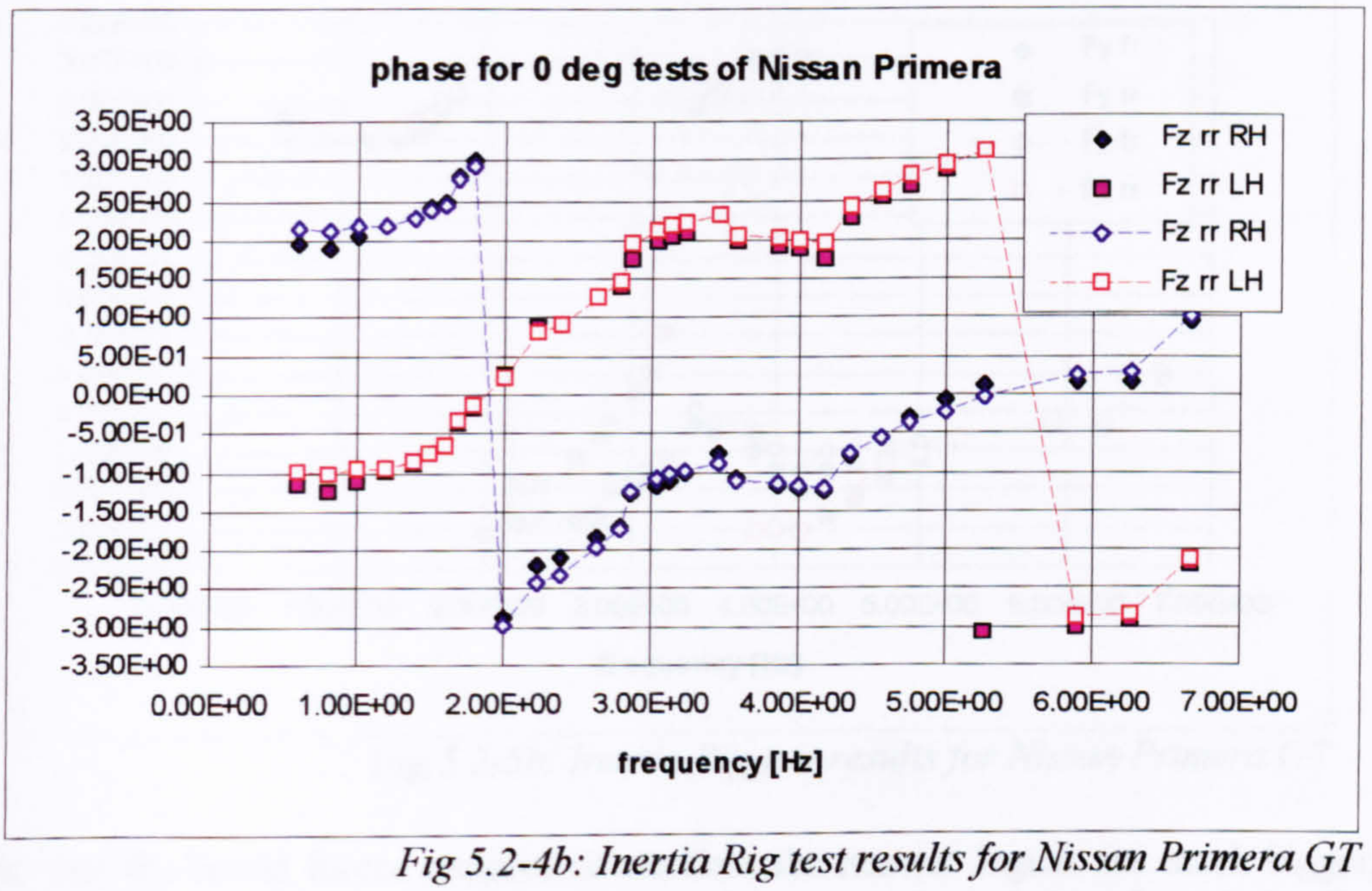

Fig 5.2-4b: Inertia Rig test results for Nissan Primera GT

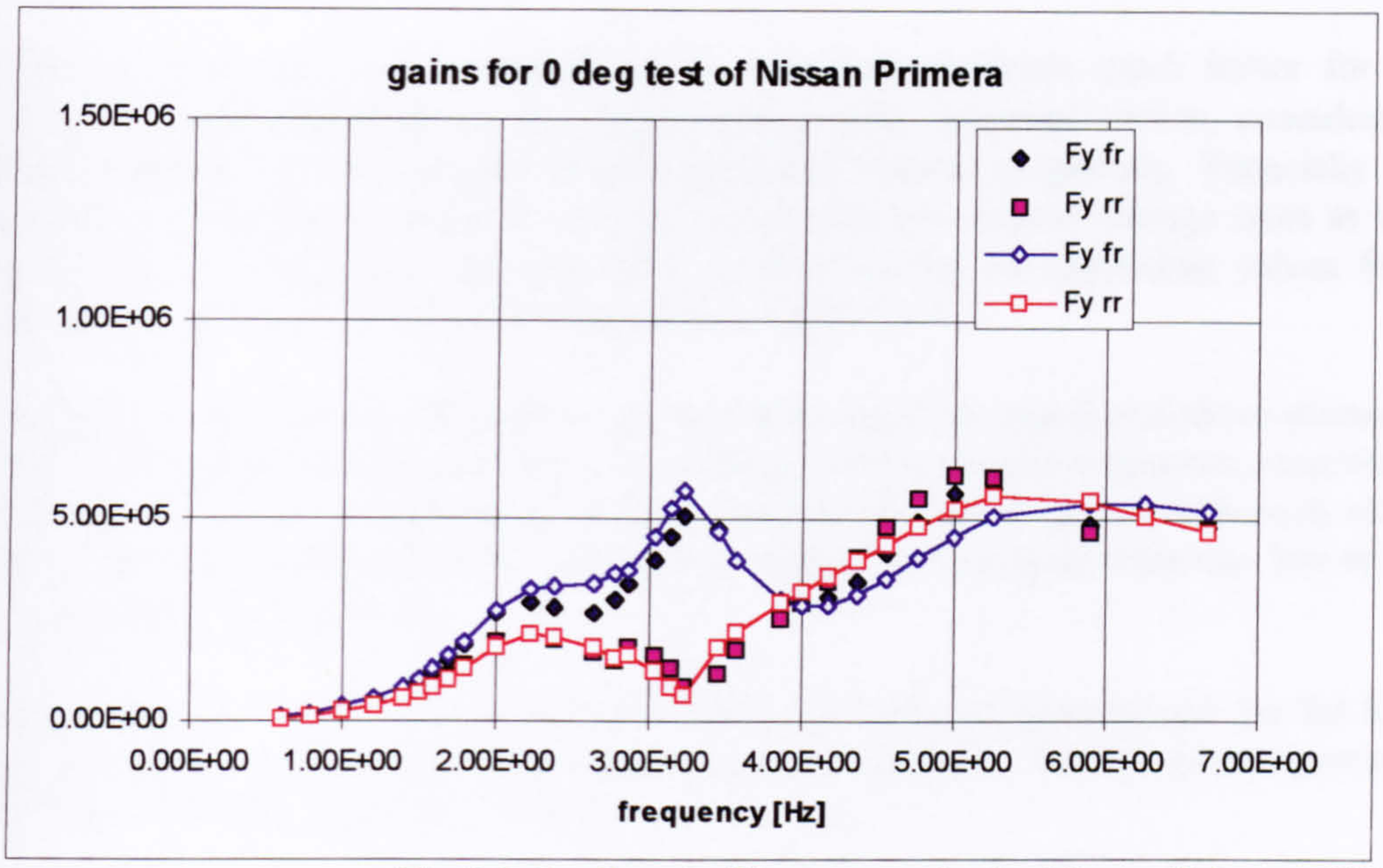

Fig.5.2-5a: Inertia Rig test results for Nissan Primera GT

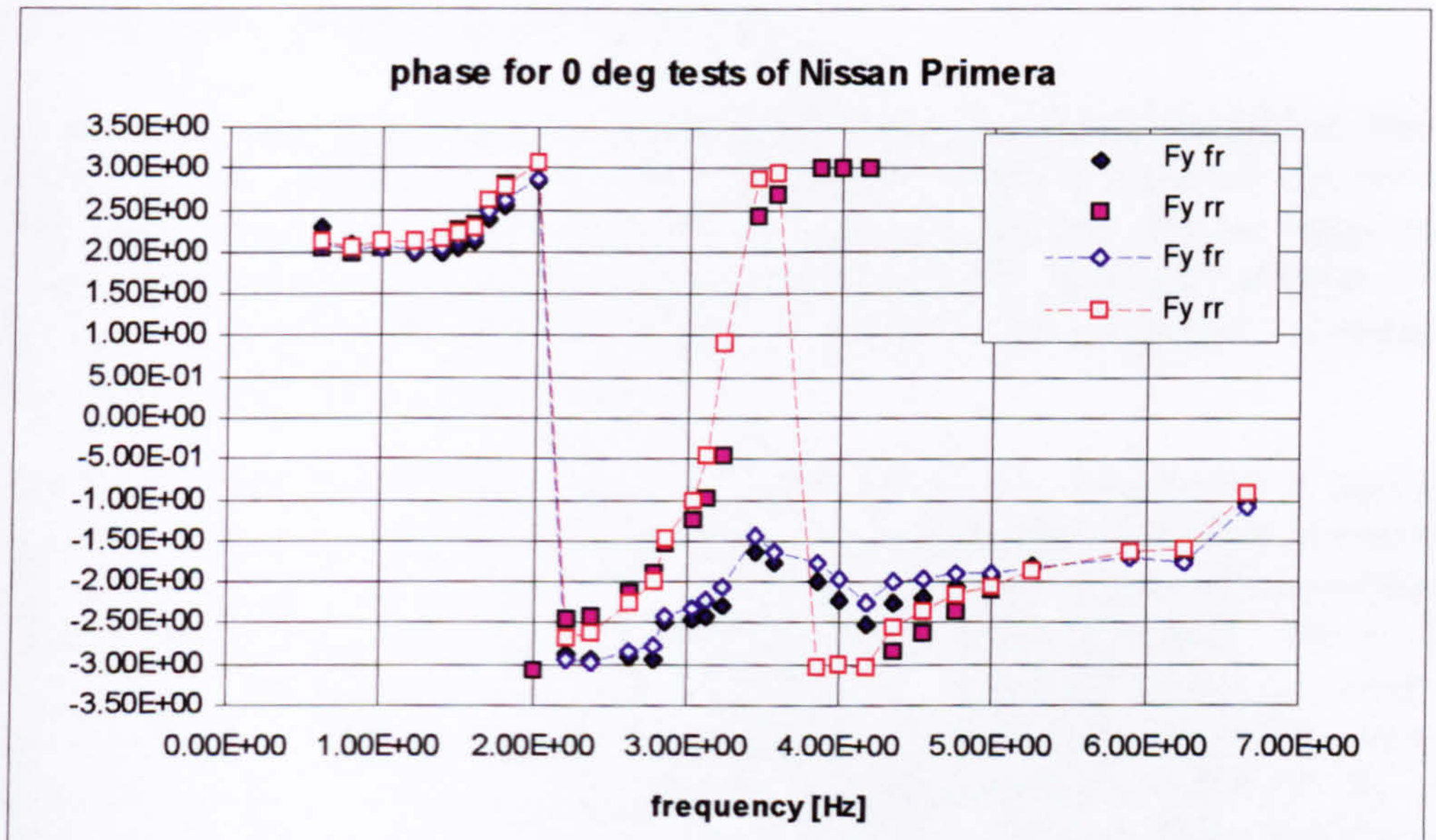

Fig.5.2-5b: Inertia Rig test results for Nissan Primera GT

Note that the lateral forces required to oscillate the heavier Jaguar are much bigger, especially in the frequency range between 4 and 5 Hz, as illustrated by fig. 5.1-5a. The shapes of the curves for the lateral force amplitudes are similar for both vehicles, although the peak rear end force at the third resonance is much more pronounced for the Jaguar.

5.2.2 Conclusions

Although measured and simulated vehicle responses correlate much better for the Nissan Primera compared to the Jaguar test results discussed earlier, considerable doubt remains on the validity of the estimated vehicle properties. Especially the geometric suspension parameters for the roll centres and camber change rates as well as the wheel rates appear unreasonable, considering the corresponding values for a comparable example of this vehicle as given in table 5.2-1.

There are similarities between some results obtained for the Jaguar and those discussed here. The biggest discrepancy between predicted and measured responses occurred at the third resonance, where lateral and roll motions are out of phase with each other. The predicted amplifications for the roll and wheel travel motions were too low at this frequency for both vehicles.

On the other hand, the huge mismatch found for the lateral and especially for the front end vertical force response of the Jaguar, was not repeated. A rather good agreement for these characteristics was obtained.

5.3 Conclusions from the Inertia Rig testing

Although J.D. Rayner's theoretical study of the Inertia Rig testing established that it is possible to carry out a successful vehicle parameter estimation based on the test data obtainable from this rig, test results of two vehicles did not provide experimental proof. Consequently, the testing and parameter estimation approach adopted for the two vehicles, which is discussed in chapter 4.2.2, has to be regarded as unsuitable for providing reliable parameter values.

However, from the theoretical point of view, there is no reason why a successful completion of the Inertia Rig development cannot be achieved. The results presented in this chapter suggest that a good agreement between measured and predicted response characteristics can be obtained, at least for a limited frequency range, as was the case for the Jaguar. In theory, that would establish that the vehicle model, on which the parameter identification is based, represents the vehicle tested on the rig. But the comparison between the estimated parameter values and those obtained by other means shows that this is not the case. In order to resolve this conflict of achieving a good agreement between prediction and measurement on the one hand and obtaining a set of unreasonable vehicle properties on the other, further research has to be carried out.

Concerning the testing procedure, it would be useful to investigate the sensitivity of the wheel displacement measurements to bump or compliance steer. For the testing carried out so far, a steering motion of the road wheels was thought to be negligible and no attempt was made to establish the magnitude of these effects. But it may be that the steer DoF is excited at certain test frequencies or by large platform forces. This

would introduce a systematic error for the track change measurement, which is obtained from two potentiometers fitted in parallel to each wheel. If it was established that the steering motion contributes to the lateral displacements measured by the two wheel sensors, an additional potentiometer would have to be fitted fore or aft the others to record the steering angle. On the other hand, if it could be established that steering motions occur only for high frequent inputs, tests at these conditions may be omitted.

In J.D. Rayner's work the robustness of the Nelder-Mead based estimation technique was investigated with respect to measurement noise. This study could be extended to analyse how a systematic measurement error and non-linear suspension and tyre characteristics would bias the estimated parameter values. Based on the results of this sensitivity analysis, test conditions could be specified more adequately, ensuring that the measurements taken are predominantly due to linear vehicle response and far less influenced by effects not considered in the estimation procedure.

6 MIRA proving ground testing

In this chapter some details concerning the MIRA proving ground testing are given. A short introduction to the vehicle testing, given in section 6.1, is followed by section 6.2, explaining the choice of test manoeuvres selected for the limit handling evaluation. Section 6.3 summarises the alterations made to the test car during the test program. In section 6.4 a brief summary of the vehicle instrumentation equipment can be found as well as some details on the processing of the test data.

6.1 Introduction to the proving ground testing

During the proving ground program a variety of vehicles and tyre constructions were tested for a selection of manoeuvres in wet and dry conditions. However, most of the testing was carried out with a fully instrumented Jaguar XJ6.

At the beginning of the project, when the Jaguar was not yet available, some subjective testing was carried out. The handling stability of four different vehicles were evaluated by a test, in which the vehicle travelled over a slat while cornering at limit speed on a constant radius of turn. Most of this work was done on the wet handling steering pad, after trials in dry conditions proved that the resulting disturbance was too small to influence the vehicle's cornering capability. Tests were conducted for various tyre inflation pressures.

Since no instrumentation was employed then, the handling assessment was based on the subjective impressions of the test driver. He assessed the magnitude of the vehicle's deviation from the intended course and its attitude changes. He commented on how much he had to correct the steering wheel to maintain the course.

In a similar test configuration, tests were carried out in which the car travelled across a high friction patch laid across the wet handling steering pad. Again, driver comments on the handling behaviour were recorded.

These tests were not aimed at collecting data, representing the response characteristics of the vehicle, but at giving the project participants a subjective impression on limit driving conditions and also some idea of how test drivers describe and judge the limit handling behaviour.

At the beginning of the test program, an understanding had to be developed for test driver comments and for the meaning of some terms often used in the handling assessment context. It was established that terms like 'stability' and 'under- and oversteer' have different or additional connotations for test drivers than for those approaching the subject theoretically. For instance, test drivers also use the terms 'understeer' and 'oversteer' to describe transient handling characteristics, whereas

these terms denote a steady state property in the vehicle dynamics literature. Moreover, a vehicle reported to respond in an 'unstable' manner does not necessarily imply that this vehicle was on the verge of spinning off the track due to saturating rear end grip. In vehicle testing, the term 'stability' seems to be associated with the amount of corrective steering control the vehicle requires during a transient manoeuvre and with the time taken for the car to settle to a steady state condition.

During the project two cars were equipped with a data acquisition system in order to monitor the driver's control inputs and the corresponding vehicle responses. The first vehicle used for instrumented handling testing was a Nissan Primera. The equipment used then comprised sensors recording the hand wheel angle and torque, the yaw rate and the lateral acceleration. In addition to that, the speed of a front wheel was measured.

Following these initial trials, it was decided to upgrade the instrumentation. It was found that test drivers, when performing a manoeuvre at limit conditions, tend to use additional throttle control either deliberately or subconsciously. In order to obtain consistent results a throttle position sensor was added to the instrumentation package, which allowed monitoring of the driver's dual steering and throttle control action. Furthermore, two more gyroscopes were employed for gathering data of the pitch and roll motions. Having the pitch and roll rates available allowed integrating their corresponding angles in the data postprocessing stage. The integrated time histories for the pitch and roll angle were used to correct the measurements of the lateral acceleration, so that the true performance of the car as well as the severity of the manoeuvre could be established. Details regarding the data processing can be found in section 6.4.

The Jaguar test vehicle was also fitted with a brake pedal force sensor. As for the throttle position, this allows monitoring the driver's consistency in carrying out specified test manoeuvres. For the analysis of the 'braking in a turn' test results, only those test runs are to be considered for which the driver could establish a constant brake pedal force after initiating the manoeuvre with a specified brake application speed.

Further on, the manoeuvres chosen for the limit handling assessment are discussed. Some of them are standard ISO tests. Others were well established in-house tyre evaluation procedures adopted by SP Tyres, and a few were devised by the project participants, inspired by test procedures found in the literature.

After that, some information is given regarding the vehicle and tyre specifications and the track and weather conditions. Some details concerning the data processing are discussed in the last section of this chapter.

6.2 Manoeuvres for limit handling evaluation

Corresponding to the project title, test manoeuvres were defined, in which the tyres of the vehicle are subjected to adverse conditions. Manoeuvres were chosen which led to the saturation of the tyre's shear force generation for dry as well as for wet track conditions. Test were conducted at low and at high speeds.

Some of the tests involved manoeuvres in which high longitudinal and lateral guidance forces are generated at the same time. These tests, such as 'braking in a turn', 'throttle off in a turn' and timed laps on the Dunlop handling circuit, establish how sensitively the vehicle responds to the interaction of longitudinal and lateral tyre forces.

Other test manoeuvres were designed to establish the influence of road surface effects on the limit handling response. These tests included cornering over slats and cornering over short strips of high friction layers.

The criteria adopted for deciding on a suitable test manoeuvre included:

- representation of a real life driving situation
- feasibility/ availability of equipment
- existence of well established procedures available
- reproducibility

The order of the list indicates their ranking. Representing a real life driving scenario was regarded as most important. Therefore, a high proportion of the tests carried out had to be performed in a closed control loop. Lane changes, simulating the avoidance of a very slow or stationary object in front of a fast approaching vehicle, demand a certain level of commitment and skill from the driver. During such a manoeuvre the driver has to monitor the vehicle response, providing the feedback according to which necessary corrections to the steering wheel and throttle are made. The interaction between driver and vehicle was seen as an important element determining the limit handling quality.

Although a closed loop test represents a real life manoeuvre rather well, it has to be accepted that the test data gathered and the absolute performance levels established depend to an extent on the test driver's skill.

However, the analysis approach adopted for this project puts less weight on absolute performance measures, such as lap times or maximum speeds for a lane change. For the evaluation of the handling quality more emphasis is placed on how well the vehicle response is matched to the driver's control input and how response characteristics change with manoeuvre severity.

Corresponding to the second criterion given in the list above, tests were chosen which could be performed on the circuits available at the MIRA proving ground. Tests which could be set-up easily with little equipment were preferred.

It was thought beneficial to incorporate as many well established test procedures as possible. It was decided to adopt the ISO lane change test for evaluating the transient limit performance and to use the ISO constant radius test to establish the steady state properties of the test vehicle. As an alternative to the latter a constant hand wheel angle test was also tried. In contrast to the corresponding ISO test, the hand wheel angle is held at a fixed position, while the forward speed is increased at a small rate until the vehicle reaches its limit cornering performance.

In addition to the ISO lane change which commences from straight ahead travelling, an alternative test was devised representing a double lane change on a turn. This test was carried out on the steering pad, where cones marked the layout of the lane change. Tests started at low speeds which were successively increased, until the vehicle failed the test by hitting one or more of the cones.

In order to ensure that the tyres are driven towards their saturation, the driver had to change lane towards the inside of the original circle, as illustrated by fig. 6.2-1. Travelling anti-clockwise, data was acquired after the car entered the first gate until it left the third gate. During the other three quarters of the circle, the vehicle speed was raised to the next higher level, ready for the following test run.

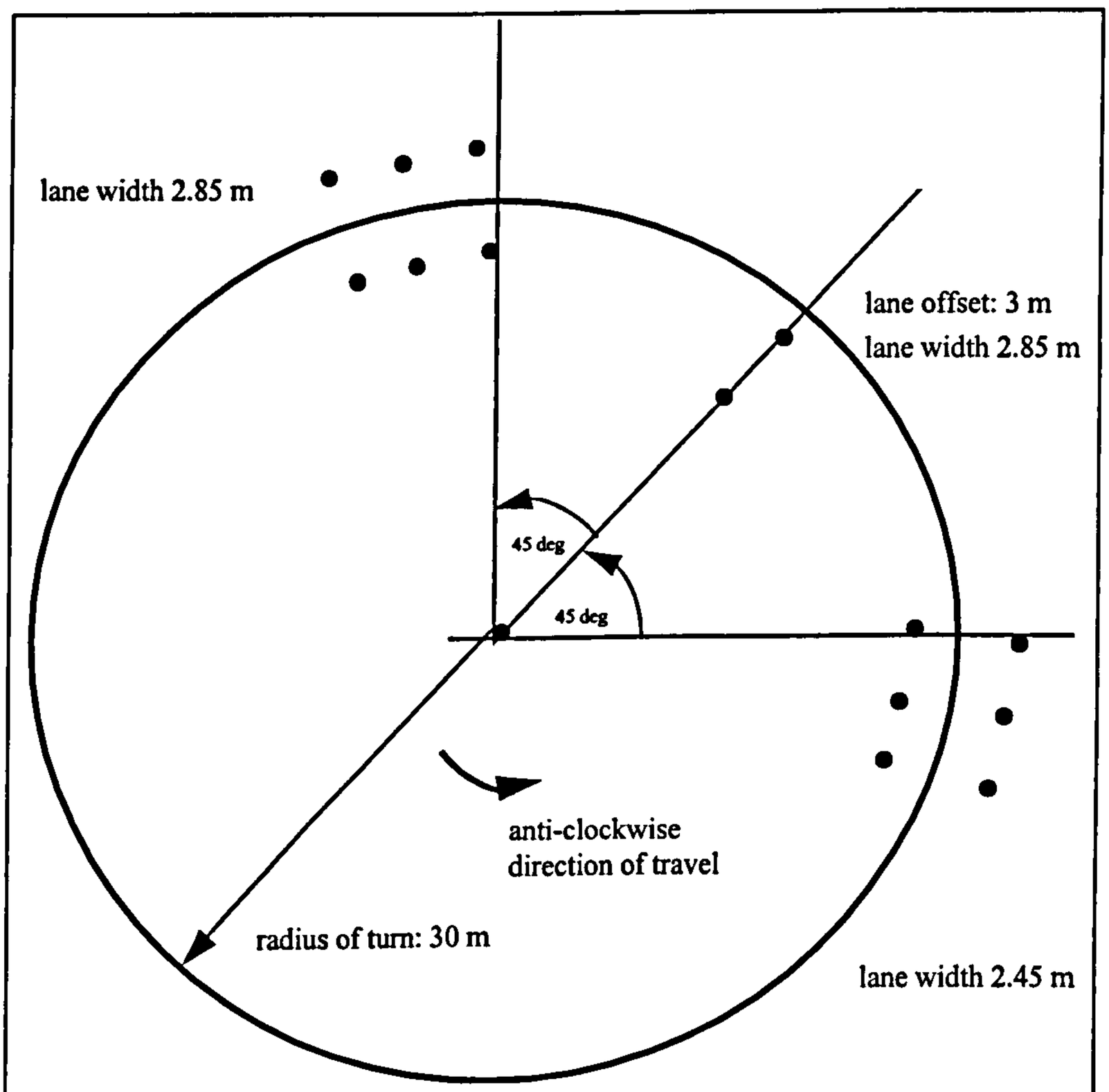

Fig. 6.2-1 lane change in a turn course layout

Lane changes on a turn as well as the standard ISO procedure were performed for a variety of speeds. A test sequence consisted of several runs performed with a constant throttle position, commencing at a fairly low speed. Speeds were increased gradually for each test run until the driver could no longer avoid the cones constraining the lane change course. After the limit speed was established for these constant throttle tests, the driver was asked to repeat the failed manoeuvre at the same entry speed, using the throttle as a second control input. Usually, the combined control of steering and throttle allowed the driver to exceed the limit speed established for the constant throttle tests considerably.

Other test procedures adopted from the ISO standards are the 'braking in a turn' and the 'throttle off in a turn' tests. These open loop manoeuvres, for which the hand wheel is held in a fixed position, were conducted on the dry steering pad.

test	standard	notes
steady state cornering test	ISO 4138-1982 (E)	Carried out on dry steering pad for a radius of 33 m; also performed on wet steering pad for three different road surfaces
steady state spiral out test	-	Equivalent to above; performed at a fixed hand wheel position; carried out on dry steering pad only
prolonged cornering at maximum speed	-	Carried out on dry steering pad for a radius of 33 m; also performed on wet steering pad for three different road surfaces
ISO double lane change	ISO/TR 3888-1975 (E)	Carried out on dry Dunlop handling circuit; test speeds started at 20 m/sec (72 kph) and were increased in increments of about 5-10 kph until vehicle hit cones
double lane change in a turn	-	Carried out on dry steering pad for an initial radius of 30 m (fig. 6.2.1); test speeds started at 5.5 m/sec (20 kph) and were increased in increments of about 2-5 kph until vehicle hit cones
braking in a turn test	ISO 7975-1985 (E)	Carried out on dry steering pad for a radius of 33 m;
throttle off in a turn test	ISO 9816:1993 (E)	as above
cornering over bump	-	Carried out on wet steering pad; an uncured truck tread laid across the full width of the track was used as an obstacle
cornering over high friction patch	-	Carried out on wet steering pad; strips of 3M safety walk were laid across full width of track
timed laps	-	six timed laps were recorded on the wet as well as on the dry handling circuit

table 6.2-1 limit Handling test used for CROVLA project

Timed laps on the wet and dry handling circuits were recorded for the Jaguar test vehicle fitted with sets of different tyre constructions. This is a well established in-house test adopted by SP Tyre's test drivers to assess the cornering and traction performance of the vehicle as well as its sensitivity to the combined action of longitudinal and lateral tyre forces. Although these tests do not represent a real life driving situation, these data were recorded to provide a reference for the skill and

judgement of professional test drivers, whose job it is to decide whether a vehicle or tyre meets the requirements of the customer, i.e. of ordinary motorists.

Tests involving prolonged cornering at the limit speed were performed on the wet and on the dry steering pad. The driver was asked to circle for three minutes, keeping the vehicle at the limit speed by correcting steering and throttle appropriately. This procedure was added to the test program in order to establish how drivers coordinate their steering and throttle control inputs during a limit manoeuvre. The test has to be regarded as an closed loop manoeuvre, involving subtle transients during which the driver compensates small deviations of the vehicle from the intended path. The control task involves tracking the given course and maintaining the appropriate attitude at the highest speed possible in the presence of saturating tyres. The driver's attention constantly changes from tracking the path to attempting a higher forward speed. After having established a steady state, the driver accelerates slightly to achieve a higher speed. The vehicle response to the throttle involves a deviation from the original radius of turn, which then requires additional steering and throttle inputs, until the vehicle reaches a steady state again. The interaction between longitudinal and lateral forces in combination with slight changes of the forward speed results in a complex, cross-coupled steering and throttle control action.

Instrumented tests concerning the effects of road irregularities on the wet handling behaviour were also included in the test program. They involved travelling over bumps as well as high friction layers laid across the track, as described in the introduction to this chapter.

One aspect regarding the criteria used for selecting suitable limit handling tests has not been mentioned so far. It concerns the reproducibility of test results. As has been said earlier, closed loop manoeuvres lend themselves less well for obtaining reproducible data. To some extent they reflect the skill and commitment as well as the personal driving style of a particular driver. Accepting the variability of test driver's talents and preferences, one can only try to ensure that other variables are as close to specification as possible.

However, there are some fundamental problems associated with limit testing. Tyres wear during a test, which affects their limit performance to some extent. Furthermore, the surface temperature also has an impact on the their peak performance. These effects are difficult to control, and the only sensible suggestion is to record tyre depth and weather conditions for each test.

The handling tests discussed here are summarised by table 6.2-1. Some keywords are added, explaining their configuration.

6.3 Test conditions

The testing program for the Jaguar XJ6 commenced in October 1996 and concluded in April 1997. Therefore, testing took place in varying weather conditions. The track surface temperature ranged from -3 degrees C in December up to 14 degrees C in April.

In order to quantify the influence of tyres, suspension design and vehicle load on the limit handling behaviour, several alterations were made to this car. These included fitting different tyre constructions to either the front or rear axle, removing the front anti-roll bar as well as placing a 90 kg load on the roof of the vehicle.

Tyre	notes
Dunlop SP2000 225/55R16	standard tyre used for all tests
Pirelli P6000 225/55R16	a worn set of tyres was used for steady state cornering testing
Dunlop SP8000 245/45R18	used for limited test program
Experimental tyre 'XY' 225/40 R18	slick tyre used for limited test program
Dunlop M2 Winter Sport 225/60R16	used for limited test program

Table 6.3-1 tyre designs tested on the Jaguar test vehicle

These modifications provided test data describing a variety of limit handling performances. The same test manoeuvres were carried out with poorly as well as well performing tyre-vehicle combinations. This approach allowed the investigation of their objective differences by analysing the recorded data and taking the comments of two test drivers into consideration.

The tyres fitted to the Jaguar are given in table 6.3-1. Tests included sets of mixed tyre constructions. The vehicle was tested with M2 winter tyres at the front and experimental slick tyres at the rear end. The opposite set-up was tried as well. Wear rates were recorded for some of the sets.

Tests with a roof rack carrying 90 kg of ballast and those for which the front anti-roll bar was removed were performed with standard Dunlop SP2000 225/55R16 tyres.

The test program involved several test drivers from SP Tyres. Two of them carried out the testing with the Jaguar. They are referred to as driver A and driver B in chapter 7 in which the test results are discussed. Driver A participated in the program until January 1997, before driver B succeeded him to complete the remaining tests.

The test schedule for the Jaguar is found in table 6.3.2. The headings in the first row indicate the type of test manoeuvre conducted, while those in the first column specify the test configuration.

Test / Tyre/Vehicle	Steady State (dry) ISO 4138-1982 (E)	Steady State (spiral)	Steady State (wet) ISO 4138-1982 (E)	Max. Speed (wet)	Max. Speed (dry)	Lane Change (linear) ISO/TR 3888-1975 (E)	Lane Change (in turn)	Accl. In Turn (brake) ISO 7975-1985 (E)	Accl. In Turn (throttle off) ISO 9816:1993 (E)	Wet (obstacle)	Wet (μ)	Timed Laps (dry)	Timed laps (wet)
Standard 225/55R16 SP2000J	10/11/96	10/11/96 26/11/96	14/11/96	14/11/96	10/11/96	11/11/96	10/11/96* 15/11/96 20/11/96	20/11/96	21/11/96	6/12/96	23/11/96	20/11/96 **	
Pirelli P6000 225/55/R16 OCP 5133/3	20/10/96	20/10/96	✗	✗	20/10/96	✗	20/10/96*	✗	✗	✗	✗	✗	✗
Dunlop 245/45R18 SP8000	9/12/96	9/12/96	10/12/96	9/12/96			9/12/96			✗	✗	9/12/96* *	10/12/96
F SP8000 R SP2000J	✗	✗	15/12/96	✗	✗	10/12/96	✗	✗	✗	✗	✗	✗	✗
F SP2000J R SP8000	✗	✗	✗	✗	✗	✗	✗	✗	✗	✗	✗	✗	✗
Dunlop 225/60R16 M2 Winter	15/1/96	15/1/96	16/1/96	16/1/96		15/1/96				✗	✗		
Special 'XY' 225/40R18 Plain	26/1/96		17/1/96	17/1/96		18/1/96	26/1/96			✗	✗	16/1/96	
F Special 'XY' R Winter	24/1/96					24/1/96	24/1/96			✗	✗	26/1/96	
F Winter R Special 'XY'	26/1/96					24/1/96	26/1/96			✗	✗	26/1/96	
SP2000J 1.5b / 2.5b	21/11/96 30/11/96	10/11/96	14/11/96	14/11/96	21/11/96	22/11/96	10/11/96* 20/11/96	20/11/96	21/11/96	6/12/96	23/11/96 6/12/96	20/11/96	
SP2000J 2.5b / 1.5b	21/11/96 30/11/96	30/11/96	17/11/96	17/11/96	21/11/96	22/11/96	10/11/96* 20/11/96	20/11/96	21/11/96	23/11/96 6/12/96	23/11/96	20/11/96	17/11/96^
SP2000J (60 kg) R Rack (90 kg)	2/12/96 6/12/96	6/12/96	✗	✗	6/12/96	6/12/96	2/12/96 2/12/96	✗	2/12/96	✗	✗	✗	✗
SP2000J No anti roll bar						17/4/97	17/4/97						

Table 6.3.2 proving ground test schedule for Jaguar

* Provisional Man.
** Observer sickness
^ Bearing noise
✗ Planned tests now abandoned

6.4 Some signal processing aspects

The data acquisition equipment, described in more detail in chapter 4.3 of the project report [1.0.1], recorded ten signals with a sampling rate of 50-100 Hz. The signals were calibrated to units given in the list below. Measurements were gathered for:

- hand wheel angle [deg]
- steering wheel torque [Nm]
- throttle position [%]
- wheel speed of an undriven wheel at the front axle [m/sec]
- yaw, roll and pitch rates in vehicle body coordinates [deg/sec]
- longitudinal and lateral acceleration in body coordinates [m/sec^2]
- brake pedal force [%]

An instrumented steering wheel from Sands-Whiteley Research & Development Ltd was employed to measure the first two signals. It contained a rotary potentiometer and strain-gauged blades connecting the hub and rim segments of the unit. The throttle position was established by a linear potentiometer measuring the throttle cable movement. A Kienzle pulse generator providing four pulses per wheel revolution gave the wheel speed. Three solid state gyroscopes of the type VSG provided by BASE recorded the angular vehicle motion, while two Monitran MTN/7000-5 DC accelerometers measured the forward and lateral motions. The strain gauging of the brake pedal was carried out by a specialist company.

Except for the brake and throttle signals, measurements were filtered by an eighth order Butterworth filter with a cutoff frequency of 20 Hz before the analog data was converted into digital format.

In a postprocessing stage these signals were digitally filtered using a Butterworth filter of fifth order with a cut-off frequency of 4 Hz. The low cut-off frequency was chosen to eliminate any high frequency effects from the data, which are unrelated to the low frequency steering and throttle control inputs exerted by the driver. This ensures that the vehicle response, which is analysed in the following chapter, can be entirely attributed to the driver's control inputs.

Furthermore, the accelerometer outputs had to be corrected for the pitch and roll angles established during a manoeuvre in order to obtain true measures of the forward and lateral acceleration of the vehicle. The accelerometers were mounted centrally in the passenger compartment. Each of their output is essentially composed of two components. The recording of the longitudinally installed accelerometer contains a component due to pitch, adding to the forward acceleration, while the laterally pointing accelerometer captures a component due to roll in addition to the centrifugal force. Since these angles could not be measured directly, their time histories had to be reconstructed from the measured angular rotations, captured by three gyroscopes.

Using the relationship between the angular velocities and the time derivative of their corresponding angles (angular rates), the pitch and roll angles could be integrated in the case of a transient manoeuvre or obtained by solving a simple algebraic equation for a steady state cornering test.

For three successive rotations, the relationship between the angular velocities, measured in a body fixed coordinate system, and their corresponding angular rates is given by:

$$\begin{bmatrix}\omega_z\\ \omega_x\\ \omega_y\end{bmatrix}=\begin{bmatrix}\cos\alpha_x\cdot\cos\alpha_y & \sin\alpha_y & 0\\ -\cos\alpha_x\cdot\sin\alpha_y & \cos\alpha_y & 0\\ \sin\alpha_x & 0 & 1\end{bmatrix}\cdot\begin{bmatrix}\dot\alpha_z\\ \dot\alpha_x\\ \dot\alpha_y\end{bmatrix} \qquad (6.4.1)$$

The vector on the left hand side gives the angular velocities for the yaw, roll and pitch motion, respectively, as measured by the gyroscopes. The vector on the right contains the corresponding rates. The transformation matrix relating the two vectors becomes rather simple, considering that only small roll and pitch angles, α_x and α_y, are established during a handling test. Equation (6.4.1) yields to:

$$\begin{bmatrix}\omega_z\\ \omega_x\\ \omega_y\end{bmatrix}=\begin{bmatrix}1 & \alpha_y & 0\\ -\alpha_y & 1 & 0\\ \alpha_x & 0 & 1\end{bmatrix}\cdot\begin{bmatrix}\dot\alpha_z\\ \dot\alpha_x\\ \dot\alpha_y\end{bmatrix} \qquad (6.4.2)$$

Assuming that the angular yaw velocity ω_z, measured in body fixed coordinates is approximately identical to the rate $\dot\alpha_z$, only two equations need to be solved for the angles α_x and α_y. These are

$$\dot\alpha_x=\alpha_y\cdot\omega_z+\omega_x \qquad (6.4.2a)$$

for the roll angle and

$$\dot\alpha_y=-\alpha_x\cdot\omega_z+\omega_y \qquad (6.4.2b)$$

for the pitch angle. The equations (6.4.2a) and (6.4.2b) establish a coupled system of linear first order differential equations. The roll and pitch angles, α_x and α_y, are integrated numerically, for which their rates are replaced by their first order differences, after removing any linear trends from the measured angular velocities. For steady state cornering, for which $\dot\alpha_x$ and $\dot\alpha_y$ are zero, the angles can be calculated simply from the respective ratio of the measured angular velocities. These are

$$\alpha_x=\frac{\omega_y}{\omega_z} \qquad (6.4.2c)$$

for the roll angle and

$$\alpha_y = \frac{-\omega_x}{\omega_z} \qquad (6.4.2d)$$

for the pitch angle.

The method described above is illustrated using three graphs, showing the three angular velocities measured by the gyroscopes in fig. 6.4-1, the integrated pitch and roll angles in fig. 6.4-2 and the measured and corrected lateral acceleration in fig. 6.4-3. The measurements were taken from a double lane change manoeuvre performed at 27 m/sec (97 kph). The angular velocity for the yaw motion is indicated by a thin line. Its peak values are slightly lower than those obtained for the roll motion, indicated by a thick line. The roll motion is in anti-phase to the yaw motion and features a less smooth characteristic. The output of the third gyroscope is hardly visible. It is negligible compared to the other two angular velocities for this type of manoeuvre.

Figure 6.4-2 gives the results of the integration process explained above. The roll angle assumes peak values of about 6 deg, while the pitch angle remained below 1 deg. For the latter, a slight linear trend is established, although the gyroscope signals were detrended before the numerical integration was executed. This behaviour may be due to an error in the initial conditions, which were assumed to be zero for the roll and pitch angles. However, this slight error for the pitch angle does not affect the correction of the measured lateral acceleration. Its measured time history is shown in fig. 6.4-3 by a thick line. The roll corrected signal assumes considerably lower peak values, while the shape remains the same. By comparing the roll angle and the lateral acceleration, it can be seen that they are almost perfectly in anti-phase to each other.

The integration method discussed in this section was applied to the test data obtained for transient manoeuvres, such as a double lane change. Recordings of the steady state cornering tests were corrected according to the roll angle established by (6.4.2c).

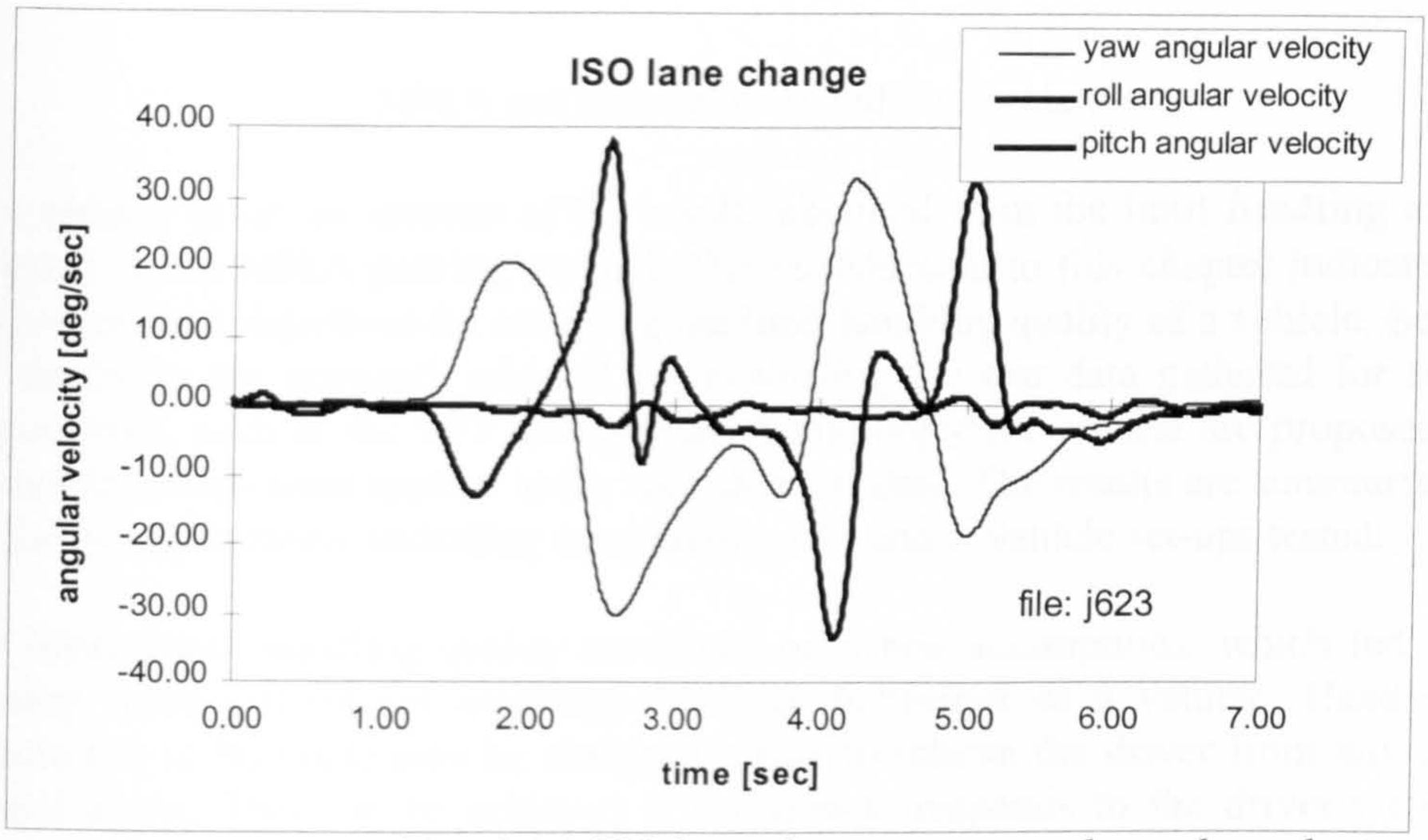

Fig. 6.4-1 ISO lane change: measured angular velocities

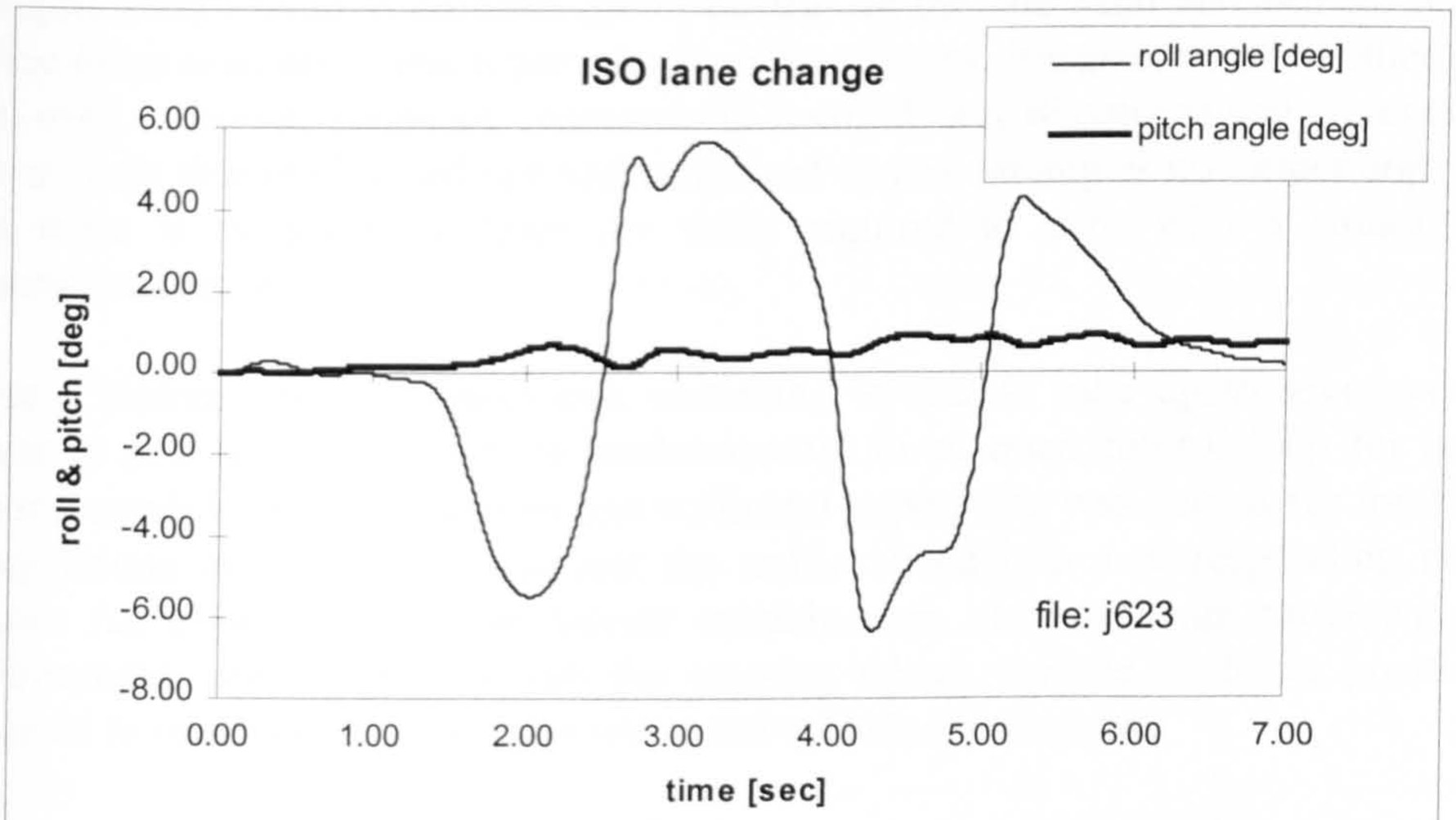

Fig. 6.4-2 ISO lane change: integrated roll and pitch angles

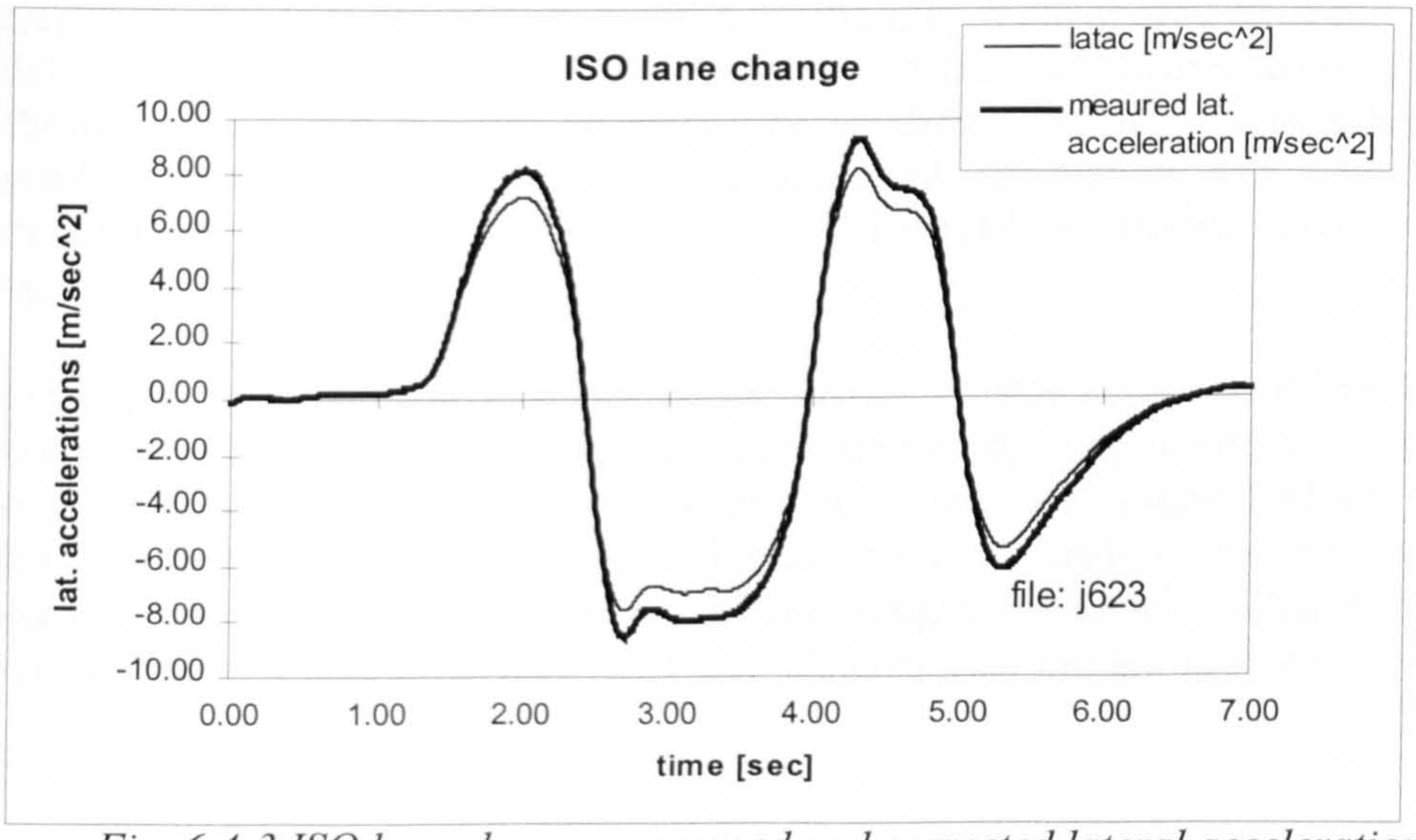

Fig. 6.4-3 ISO lane change: measured and corrected lateral acceleration

7 MIRA test data analysis and interpretation

This chapter gives an account of the results obtained from the limit handling testing program at the MIRA proving ground. The introduction to this chapter indicates the motivation and objectives for assessing the limit handling quality of a vehicle. Section 7.1 describes the approach adopted for evaluating the test data gathered for severe manoeuvres, such as the ISO lane change. Some objective criteria are proposed and discussed, which were applied to the recorded test data. The results are summarised in the following sections, including comparisons of various vehicle set-ups tested.

Our ideas about handling quality are based on a few assumptions, which led us to develop some criteria for assessing the limit behaviour of a vehicle. Handling a vehicle has to be made easy by design in order to relieve the driver from any tiring control strain. This can be achieved if the vehicle responds to the driver's control commands in a consistent and predictable manner throughout its operating range. A straightforward relation between driver control on the one hand and vehicle reaction on the other is desired, which prevails for all conditions, irrespective of whether dry or wet, even or bumpy roads are encountered. It could have disastrous consequences if a driver finds that the learned and well practised control strategies no longer apply, and that there is no scope to learn the skills required to cope with a situation not experienced before.

After a learning period, which can, according to /1.2.4/, take up to seven years, a driver is able to guide a vehicle predominantly in an open control loop for normal driving conditions. This requires that sufficient experience was gained for translating observations of the road layout and the traffic ahead into a corresponding control action. An experienced driver selects suitable cues obtained from previewing the environment, according to which the steering wheel, throttle or brake position is adjusted to maintain the desired position and attitude on the road.

If, for any reason, the desired vehicle response is not established, a driver has to superimpose additional control inputs, exerted in a closed loop, to compensate for the discrepancies between actual and required position, heading as well as speed of the vehicle. The driver uses the observed deviations to decide on whether steering, brake or throttle adjustments have to be made and on their respective magnitudes. The closed-loop control requires processing of additional information, and it has to be executed fairly quickly so that the less stressful open-loop driving mode can be pursued again.

A consistent response behaviour enables the driver to carry out a control task with little corrective intervention and demands less time for adjusting to and learning new driving situations. For instance, an inconsistent behaviour is established by a car, which is pulled to one side of the road due to its tyre's sensitivity to road camber. Moreover, excessive bump steer can disturb the straight line travel, so that persistent corrective steering has to be exerted. These disturbances, though undesired, can be

controlled easily, because driver and vehicle operate in the well practised region of their performance envelope. But cornering the same vehicle on a cambered and uneven road near the limit performance of its tyres, might establish such a complex control task, involving simultaneous steering and throttle adjustments, which the driver is unable to predict in time from the experience obtained through non-critical driving manoeuvres.

Another handling quality aspect mentioned earlier refers to a simple relation between driver control input and vehicle response. In mathematical terms, the simplest relationship between two quantities is a linear one. However, no evidence was found in the literature, indicating that human operators prefer this type of man-machine control in favour of a non-linear relation. But a linear system offers certain advantages with regard to the control effort as well as the learning period needed for becoming familiar with the system behaviour. A linear input/ output behaviour allows predicting any response gain the vehicle is able to produce with the lowest amount of previously obtained information, i.e. experience. Only a single pair of the input/ output relation has to be established and stored, whereas for the nonlinear system all possible states have to be either learned and stored by the operator and subsequently remembered in time, or extrapolated from known input/ output pairs, involving their differentiation.

Consequently, the control of a non-linear system demands a longer familiarisation, a larger storage capacity and fast accessing and processing of the gathered information. Especially the last requirement might be less well met by human operators and drivers, who have a limited ability in reacting in a short period of time to new circumstances.

In /1.2.4/ similar arguments favouring a fast linear vehicle response behaviour can be found. There it is argued that more accidents could be avoided if drivers were able to react earlier to an unexpected road or traffic situation ahead, by being able to rely entirely on quickly derivable control rules for accomplishing the appropriate driving task, rather than being exposed to a lengthy planning and decision-making process.

Furthermore, response times of the vehicle have to be regarded as properties relevant in determining the handling quality. It is obvious that long lag times between driver control and vehicle response render a vehicle uncontrollable, especially for high speed manoeuvering, for which a desired position or attitude correction has to be assumed in a short distance of travel. On the other hand, drivers cope well with short lag times and compensate the inherent vehicle response delays by adopting an anticipatory driving strategy. They predict the desired trajectory of travel as well as the traffic situation ahead, allowing them to steer with the necessary advance. For transient manoeuvres, such as entering a turn, the driver's steering control first leads to a yaw rotation of the vehicle, before the rear end tyres begin to support the front end in building up the cornering forces, which then leads to the desired change in trajectory. This applies to the standard front wheel steered vehicle, while for four wheel steered

vehicles (4WS) a concurrent force build-up can be achieved, so that the change in vehicle attitude matches that of its direction of travel.

Taking the research of /2.3.6, 2.3.7/ into consideration, short delay times seem to constitute a significant benefit for normal driving manoeuvres. Moderately long lag times may be compensated by an appropriate preview strategy. However, short response times are even more desirable for completing an emergency manoeuvre, for which the emphasis lies on fast closed-loop control, rather than on preview based open-loop driving.

The idea of a consistent vehicle response can be applied to its delay characteristics. Ideally, lag times should be constant throughout the operating range, allowing the driver to adopt the same preview strategy for all speeds and conditions.

In addition to a fast and predictable response, a driver needs an element of warning built into the vehicle design. The feedback through the steering or through other cues has to provide a reliable source of information, from which a driver can assess the road and tyre condition and whether the vehicle meets the expected response. It may well be that secondary response cues, such as the hand wheel torque or the roll angle, are well suited for this purpose. These are not essential for controlling the path or attitude of a vehicle, but can either reassure or alert the driver. For the steering feel, a non-linear behaviour may be desirable for encountering limit conditions. A hand wheel torque, sharply rolling-off when cornering on ice or snow, provides a warning about the limited friction available.

It was mentioned earlier that standard cars respond to a steering input by changing their attitude before an equilibrium for the lateral guidance forces acting at the front and rear end is established. The front tyres grip more or less instantaneously after the steering angle is set. The front end forces rotate the vehicle, which produces a slip angle at the rear axle, enabling the rear end tyres to balance the initial yaw moment. During a transient the yaw rate is no longer matched to the lateral acceleration, as is the case for steady state cornering. The lateral acceleration $\ddot{y}$, determining the path of the vehicle, is composed of the rates established for the yaw ψ and the vehicle's slip angle β according to:

$$\ddot{y} = \mathrm{v} \cdot (\dot{\psi} + \dot{\beta}) \qquad (7.0.1)$$

In order to maintain the given path curvature ahead, the driver has to control these two degrees of freedom by a single control input, exerted by the steering wheel. It is well known that for higher frequency manoeuvres the yaw rate is amplified in relation to the lateral acceleration /7.0.1/. A proportionally higher yaw rate gain has to be established to achieve a lateral acceleration matching the path radius. The difference between the lateral acceleration and the product of vehicle speed v and yaw rate is lost in the side slip motion of the vehicle. For normal driving conditions the lateral acceleration is still well correlated to the yaw rate, though slightly delayed. However, for higher forward speeds and more severe cornering, the yaw motions become less

damped, so that the vehicle, while perfectly following the curved path, oscillates about its vertical axis. The position and the attitude control of the vehicle then become two separate tasks to be accomplished with an appropriate steering wheel input.

It seems desirable that the transition from a single input-single output system, as established for low frequency manoeuvering, to a single input-dual output system assumes a smooth and predictable behaviour. For a high frequency evasive manoeuvre, the vehicle has to be able to produce sufficient lateral forces at the front and rear ends to avoid an impact with an object in its path. For this, these forces should build up quickly in phase with each other, enabling to initiate a lane change. Depending on the magnitude of their out-of phase components, the driver has to dampen the yaw oscillations, which might become the most difficult part of the manoeuvre.

Another way of controlling position and attitude at the same time can be performed by utilising more than one control input. In the literature examples of 4WS systems aimed at limiting the vehicle side slip /1.2.4/ can be found as well as systems applying brake forces to certain wheels of the car /1.2.5/ to prevent it from spinning out. The latter systems intervene if the measured vehicle response is not correlated to the driver's steering control input. On the other hand, skilled drivers might use the throttle or the hand brake to exert a second control input, allowing them to control vehicle position and attitude in the desired fashion.

In order to establish a predictable behaviour for a synchronised steering and throttle or braking control, one has to address the cross-coupling between the lateral and longitudinal vehicle dynamics. The additional throttle control while cornering enables a skilful driver to redistribute the cornering and traction forces of the driven tyres. In this case a strong, though predictable, cross-coupling between cornering and longitudinal control is desired. From another point of view one would try to minimise any cross-coupling effects, so that braking or throttle application would not impinge on the cornering stability. However, if the limit of tyre adhesion is reached it is inevitable that the interaction between longitudinal and lateral guidance forces becomes more and more pronounced. Anti-lock brake systems (ABS) help to overcome this problem in that they limit the longitudinal slip in order to allow the tyre to produce at least some of its lateral shear force, thus enabling the driver to use the steering advantageously.

Corresponding to the idea behind ABS, i.e. preventing wheel lock for maintaining lateral control, it can be said that it is paramount to provide a predictable steering response and that, if the driver decides to use a combination of steering and throttle or brake control, it should be to the benefit of the vehicle's stability, rather than causing an uncontrollable reaction. Some of the results concerning the ISO lane changes carried out during the research project indicate that a superimposed throttle control clearly improves the controllability, though this combined control strategy might have evolved from a lengthy learning period.

In summarising these ideas, it can be stated that a fast and predictable responding vehicle is required from the limit handling quality point of view. It was argued that a linear relation between driver control and vehicle response requires less time for acquiring the experience to handle a vehicle with ease. Also, a linear system behaviour allows its operator to predict its response in unfamiliar conditions from the behavioural patterns established earlier. On the other hand, non-linear steering torque characteristics may be suited to provide a warning signal about an imminent loss of adhesion. As has been said earlier, the two lateral degrees of freedom of a standard vehicle, its yaw rate and its side slip, have to be controlled by the steering, dividing the driver's attention into path and attitude control action. Finally, some remarks were made on the cross-coupling between longitudinal and lateral guidance forces. It has to be accepted that for limit conditions these interact strongly, and that their effects on the controllability of the vehicle are either determined by the driver's proficiency or by the capability of traction control systems.

7.1 Analysing limit handling behaviour

After the introduction, which outlined some basic principles defining a good limit handling behaviour, some test results obtained from the MIRA proving ground are summarised. Most of the testing was conducted with a fully instrumented Jaguar XJ6. The test schedule is given in chapter 6.3. Also, some notes concerning the test conditions and the layout of the manoeuvres performed can be found there.

In this section, criteria used to evaluate the limit handling quality of vehicles are described, while in the following sections test results for ISO lane changes, lane changes on a turn and for the steady state cornering performance are presented, as obtained for a variety of tyre designs as well as for modifications to the test vehicle. Where appropriate, test driver comments are added to the discussion of these results.

According to the principles established in the introduction to this chapter, some objective criteria were developed, which represent handling properties such as consistency and predictability. Based on an idea of Sharp /7.1.1/, the concept of correlation is applied, to look into the interaction between driver and vehicle for transient manoeuvres, such as lane changes. Recordings of the driver's steering, throttle and brake control action were correlated as input quantities to the corresponding vehicle responses, as measured by accelerometers and gyroscopes. Calculating the cross-correlation of two records reveals to what extent an input signal is translated into a corresponding response, as well as the delay time between these two. A correlation coefficient of one indicates that one signal is perfectly replicated, possibly after some time lag. On the other hand, a correlation of zero establishes that the two signals are unrelated.

Applying this principle to assessing the handling quality of a vehicle, the measured hand wheel angle and torque signals were correlated as input signals with the

recordings of the yaw rate and lateral acceleration. It was assumed that a high correlation prevails for normal driving manoeuvres between the steering wheel angle time histories and those of the yaw rate and lateral acceleration. For driving manoeuvres near the limit a loss of correlation between input and output quantities was expected, reflecting the effects of saturating tyres and higher frequency steering corrections not matched by the vehicle responses. In approaching the limit performance it is inevitable that the control effort increases, so that the limit handling performance has to be judged by the rate of quality loss. In order to study the behavioural transition from normal driving to the limit approach, test sequences were conducted in which the driving speed was raised by small increments.

Furthermore, some other measures, representing the severity of a manoeuvre and the corresponding complexity of the control effort involved, were computed from the experimental data. They reflect to what extent a driver has to control the yaw and side slip oscillations of the vehicle in addition to its position while tracking a lane change. They are explained using test data collected for the ISO lane changes. The layout of this double lane change manoeuvre is defined by 22 cones as shown in fig. 7.0-1.

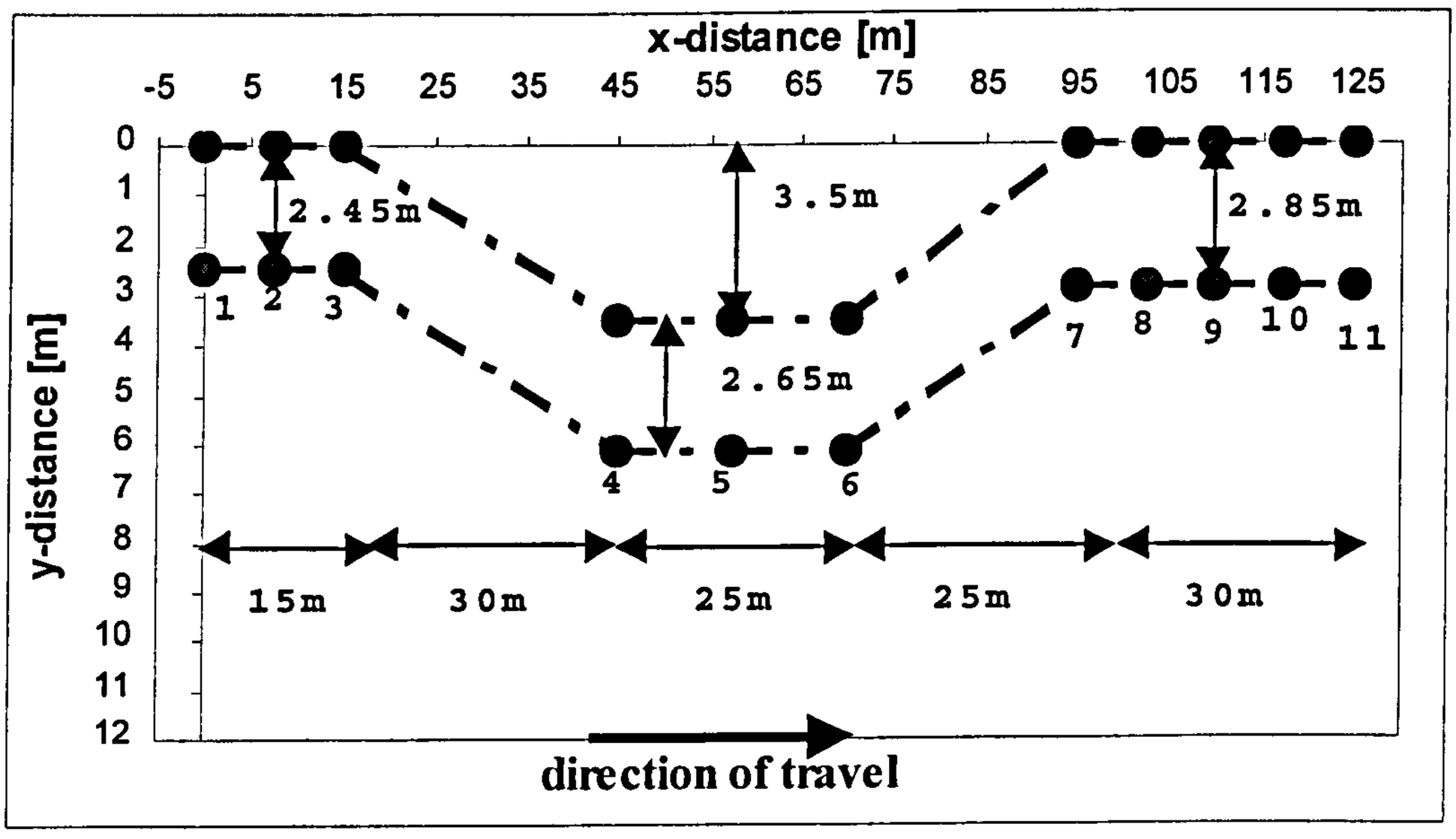

Fig. 7.0-1 ISO lane change layout

7.1.1 Correlation and time lags

The concept of correlation was applied for the analysis of the transient driver-vehicle interaction. Correlating time histories of the driver's controls to those of the vehicle responses establishes a measure of the vehicle's ability to follow the input commands faithfully. Computing the cross-correlation of two signals also gives a measure of the time expired between the input of the driver and the vehicle's reaction. These two measures of quality, correlation coefficient and time delay, are independent of the test driver's skill, whereas lap times or maximum speed for a successful double lane change would reflect the driver's ability to a great extent. While correlation coefficient and delay time are properties of the vehicle and its components, a quick lane change or lap time could be achieved by an experienced driver in spite of deficiencies in the vehicle's handling. Taking only absolute performance measures into consideration, such as maximum speed and lap time, might conceal handling deficiencies compensated by the driver during the test run. These criteria would not apply as a measure for the ease of control felt by a less skillful driver.

As an illustrative example of how the idea of correlation can be used for the handling assessment of a vehicle, some results obtained for ISO lane changes are presented. These results refer to the standard Jaguar fitted with standard tyres inflated to the manufacturer's recommended pressures. A lane change test session consisted of several runs starting at speeds between 70 and 80 kph. After a successful lane change the test speed was increased by 2-5 kph, until the driver failed to complete the manoeuvre by hitting one or more of the cones marking the course. The car was driven by a professional test driver. He was asked to complete each lane change with a constant throttle or speed. After the maximum speed was established, he was given the opportunity to carry out additional trials for which he was free to use the throttle to his advantage. For each test the following measurements were taken:

- hand wheel angle [deg]
- steering wheel torque [Nm]
- throttle position [%]
- wheel speed of an undriven wheel at the front axle [m/sec]
- yaw, roll and pitch rates in vehicle body coordinates [deg/sec]
- longitudinal and lateral acceleration in body coordinates [m/sec^2]
- brake pedal force [%]

This test data was digitally filtered with a cut-off frequency of 4 Hz to eliminate measurement noise and high frequency content, originating from the road unevenness. Since the roll angle could not be measured directly, it was integrated from the three rates measured by the gyroscopes as described in chapter 6. The measured lateral acceleration was then corrected for the roll angle, and this corrected signal will be referred to as 'lateral acceleration' (or 'latac') for the rest of this chapter. As a reference velocity the wheel speed sensor output was used.

Fig. 7.1-1 shows the W-shaped steering wheel angle and the corresponding yaw rate in one graph for a double lane change performed at 21 m/sec (76 kph). Their similar shape indicates a high cross-correlation. The time lag for the yaw rate relative to the hand wheel angle input can be estimated from the difference between their intersection of the abscissa. Similar conclusions can be drawn from the following graph, fig. 7.1-2, showing the steering wheel angle and lateral acceleration.

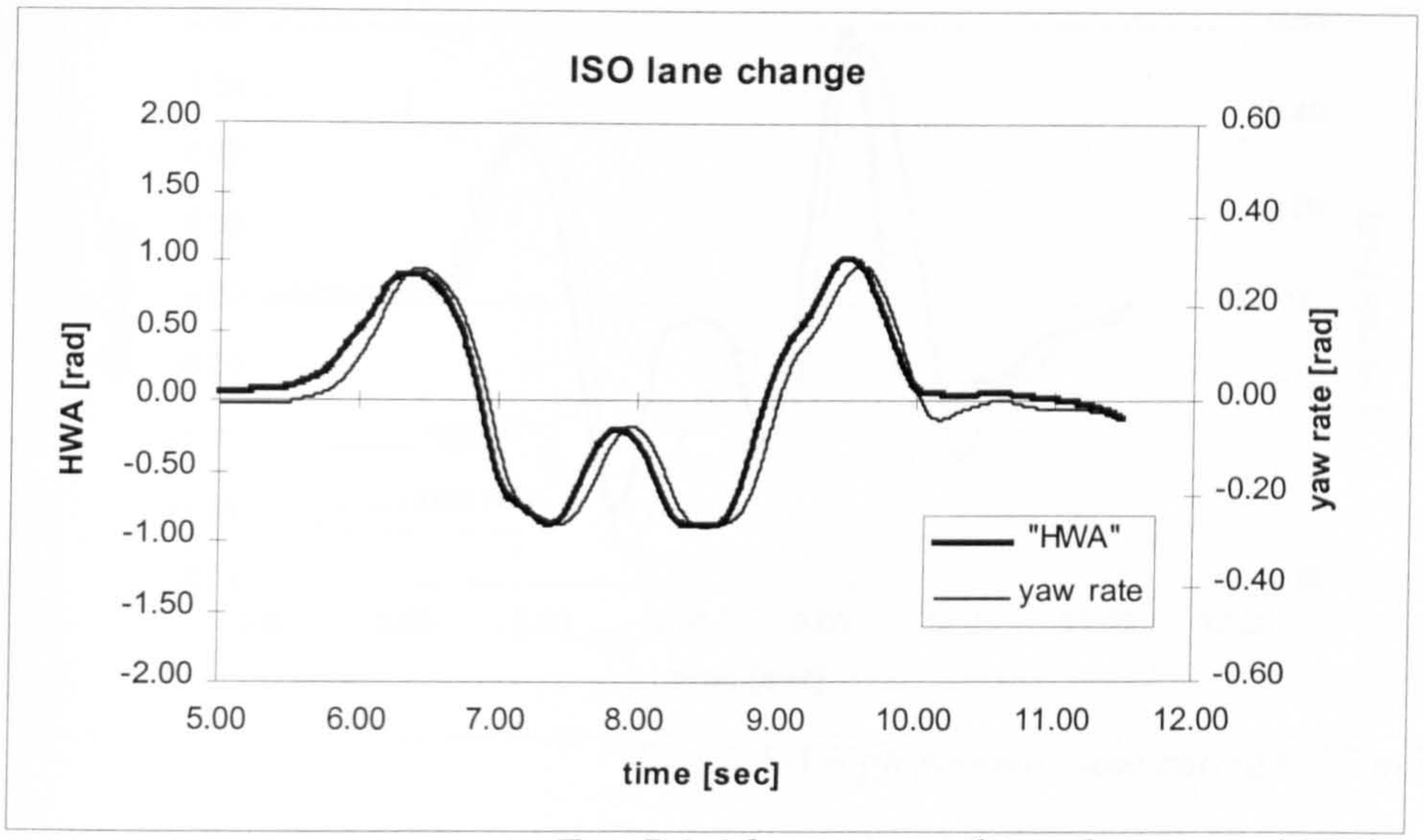

Fig. 7.1-1 low severity lane change: v=21 m/sec

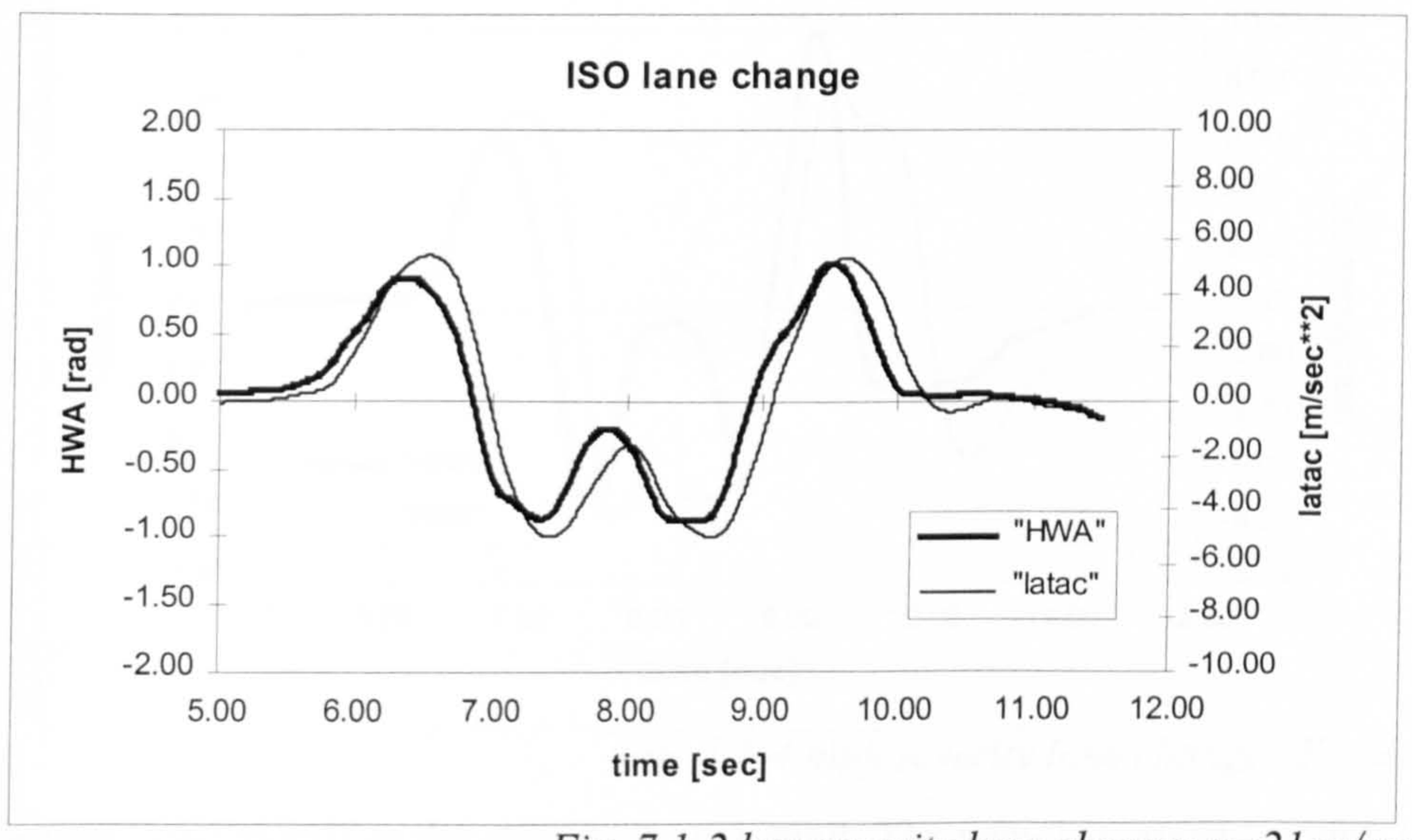

Fig. 7.1-2 low severity lane change: v=21 m/sec

From the two graphs, fig 7.1-1 and fig 7.1-2, it can be said that the yaw rate response matches the steering wheel input better than the corresponding lateral acceleration. Furthermore, the delay of the yaw rate is smaller than that of the lateral acceleration. These characteristic features become more apparent for a more severe lane change close to the limit velocity as illustrated by fig. 7.1-3 and fig.

7.1-4. The time histories shown there belong to a double lane change performed at 27 m/sec (97 kph), establishing the maximum speed for which the test could be performed successfully with a constant throttle position. It can be noticed that the W-shaped steering wheel input prevalent at lower speeds still applies for this limit manoeuvre. However, the lateral acceleration of the vehicle and thus its radius of turn

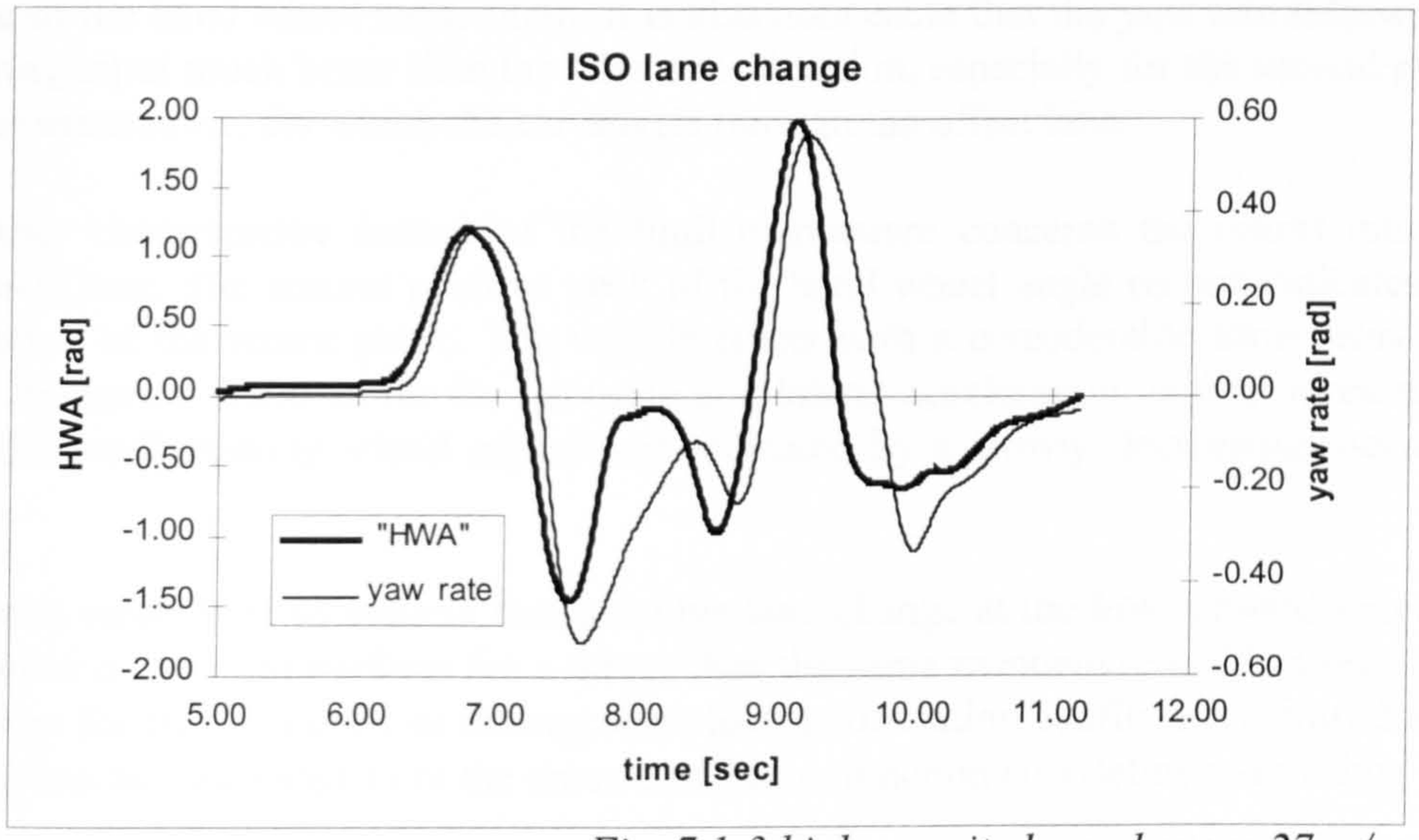

Fig. 7.1-3 high severity lane change: 27 m/sec

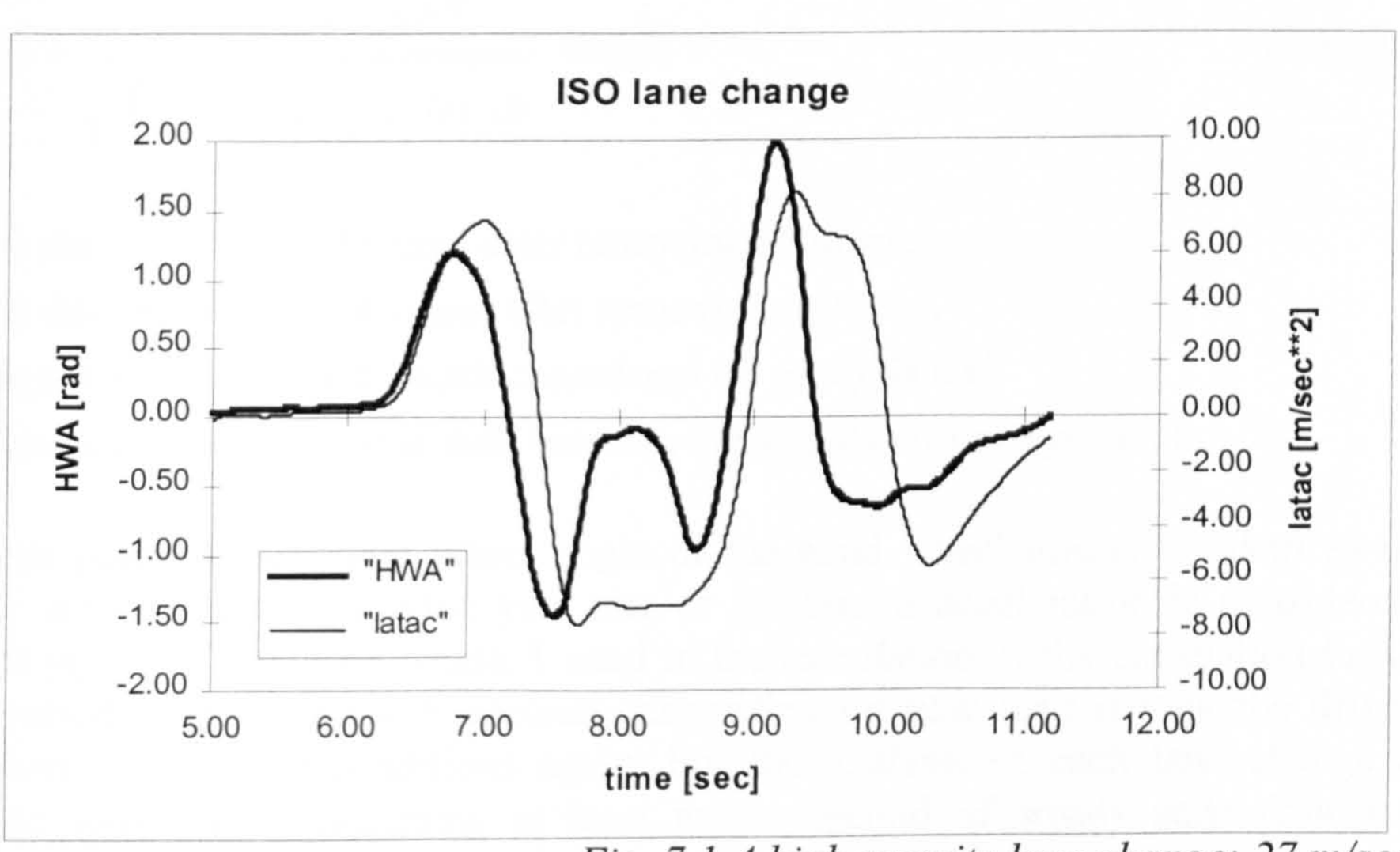

Fig. 7.1-4 high severity lane change: 27 m/sec

no longer corresponds to the steering wheel input. The vehicle corners through the second section of this double lane change, the lane offset from the original lane, with an almost constant lateral acceleration (7.7<time<8.7). The vehicle does not respond to the steering wheel reversal as it did for the low severity manoeuvre, for which a short straight ahead motion was established, as denoted by almost zero yaw rate and lateral acceleration in fig. 7.1-1 and fig. 7.1-2.

Comparing the shape of the input to each of the two output signals for the severe double lane change indicates how their cross-correlation has deteriorated. The mismatch between steering wheel actuation and vehicle response is most apparent for the second and third part of the manoeuvre, and it is further pronounced by a considerable time delay shifting the zero-crossings of the vehicle response behind those of the hand wheel angle input. It is also noticeable that the yaw rate follows the steering input much better than the lateral acceleration, especially for the second phase of the manoeuvre, for which the car travels through the offset lane.

Another characteristic feature of the limit manoeuvre concerns the return into the original lane. The second positive peak of the hand wheel angle record indicates the initiation of the return phase. The vehicle reacts with a considerable time delay and with distinct overshoots for the yaw rate and lateral acceleration, which necessitates an additional steering wheel adjustment indicated by a slowly decreasing, negative peak.

It seems reasonable to assume that a double lane change at the low forward speed of 21 m/sec is easier to perform for a driver than the same manoeuvre at 27 m/sec. As a measure for task difficulty or driving work load a correlation coefficient is introduced, which can be calculated from the cross-correlation function $c(\tau)$ defined according to:

$$c(\tau) = \frac{\int_0^T x(t) \cdot y(t+\tau) dt}{\sqrt{\int_0^T x^2(t)\ dt \cdot \int_0^T y^2(t)\ dt}}, \text{ where} \qquad (7.1.1)$$

$x(t)$ denotes the input signal after removing its mean,

$y(t)$ denotes the output signal after removing its mean,

T denotes the sequence length considered for analysis and

τ denotes the relative time shift between the signals $y(t)$ and $y(t+\tau)$

For our purposes the hand wheel angle or the hand wheel torque is taken as input signal x(t), whereas either the yaw rate or the lateral acceleration is considered as output y(t). The sequence length T used in the calculation of the correlation function $c(\tau)$ varied from 5.5 up to 9 seconds, depending on how long it took the driver to establish steady state conditions again. For the analysis of each lane change test, records were taken containing at least half a second of steady state data at the beginning and end of the manoeuvre.

The cross-correlation function $c(\tau)$ lies in between plus and minus 1 (one) depending on the lag time τ. A high magnitude of correlation between two signals at a certain lag time indicates that their shapes are well matched, so that one signal can be superimposed on the other after shifting one of them by the relative time delay and scaling its amplitude. Uncorrelated signals are denoted by a cross-correlation function

of zero for all time lags τ. For more details concerning the properties of the cross-correlation function $c(\tau)$, the reader is referred to /7.1.2/.

As an illustrative example, cross-correlation functions for the two manoeuvres described above are shown. In fig. 7.1-5 the cross-correlation coefficient for the hand wheel angle and yaw rate (thick lines) as well as those for the hand wheel angle and lateral acceleration (thin lines) are plotted against the time shift τ. It can be noticed that the magnitude of the yaw correlation peak hardly changes for the two manoeuvres considered, though it moves from τ= 0.1 sec towards a higher time lag of τ=0.15 sec. A similar behaviour can be observed for the cross-correlation between hand wheel angle and lateral acceleration. Their peak correlation coefficient occurs at a higher lag time for the high severity lane change. Corresponding to the poor agreement between the shape of the hand wheel angle time history and that of the lateral vehicle response, the peak correlation coefficient is reduced by about 20%.

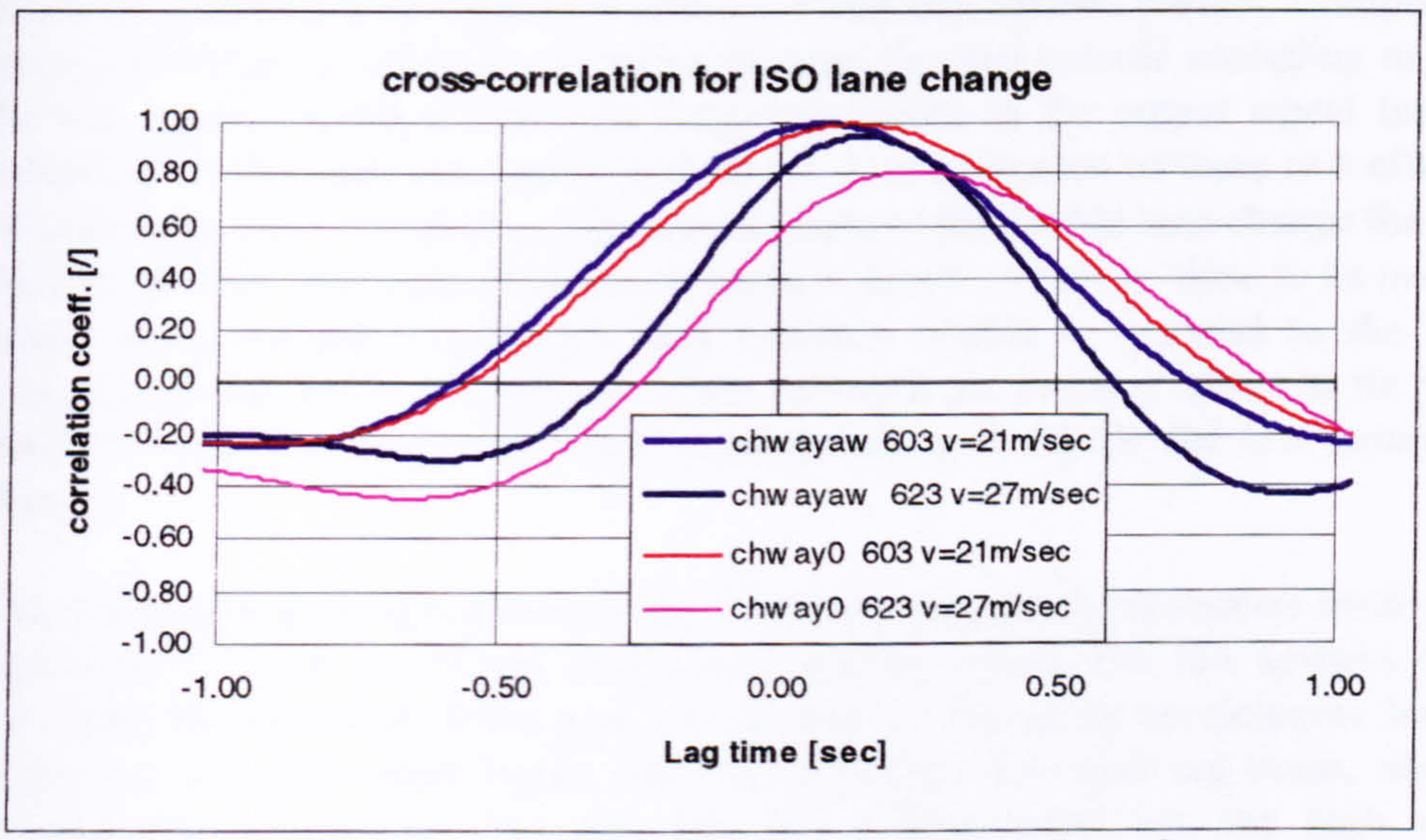

Fig. 7.1-5 cross-correlation between hand wheel angle and yaw rate ('chwayaw') and between hand wheel angle and lat. acceleration('chway0') for v= 21 & 27 m/sec

In addition to the peak correlation coefficient and its associated time lag, the correlation at zero time lag $c(\tau=0)$ provides another measure of how the input-output behaviour changes when approaching the limit performance. For low time lags and relatively low forward speeds, the peaks of the correlation functions remain fairly flat, giving a high correlation at τ=0. However, for high speeds their peaks become more pronounced, so that the values at τ=0 decrease considerably. Especially, if the peak correlation occurs at a high lag time, as it does for the lateral acceleration, the correlation loss at τ=0 is amplified.

As can be seen from the results presented in chapter 7.2, the approach of the limit vehicle performance is characterised by decreasing peak correlation coefficients as

well as increasing time lags. Both effects result in decreasing correlation coefficients at τ=0. The results also demonstrate that the correlation with regard to the yaw rate is usually far better maintained than that with respect to the lateral acceleration. Furthermore, the delay for the latter is longer than the yaw rate time lag. These two trends indicate that attitude control can be maintained with relative ease even in limit conditions, while controlling the vehicle path or radius of turn, as given by the lateral acceleration, becomes more demanding.

The decrease in peak correlation is inevitable and can be ascribed mainly to two factors. Firstly, the non-linear tyre behaviour limits the guidance forces required to complete a lane change at a given speed, which renders the saturating tyres indifferent to any steering corrections. The property of vehicles and their tyres to filter higher frequency steering inputs, provides the second reason for a non-perfect correlation of one (or -1). Beyond a certain frequency bandwidth, the vehicle attenuates these inputs and responds mainly to the slower steering wheel adjustments present. Computing the cross-correlation function by sweeping through the two records according to (7.1.1), the non-representation of the high frequency inputs in the output signal leads to a reduction for the peak correlation coefficient. A combination of these two effects can be seen from fig. 7.1-4. During the second phase of the double lane change the vehicle reaches its peak lateral acceleration of about 8 m/sec^2, which is close to its maximum steady state cornering capability, and becomes unable to respond to the quickly exerted steering wheel corrections. Even returning the steering wheel to its nominal position hardly decreases the lateral acceleration, as it did for the low severity lane change.

The correlation functions shown in fig 7.1-5 also indicate the transition from a single input-single output to a single input-double output system. For low severity driving, the correlation function of the yaw rate and that of the lateral acceleration, both with respect to the hand wheel angle, differ only slightly for small lag times, whereas a considerable discrepancy between the two is established for the high severity manoeuvre at 27 m/sec, indicating a rather poor cross-correlation coefficient between the yaw rate and the lateral acceleration. The latter is consistent with our observation that the yaw rate follows the steering input much better than the lateral acceleration signal.

A corresponding analysis can be conducted involving the cross-correlation between the hand wheel torque and the yaw rate and that between the former and the lateral acceleration. Although the steering feel is regarded as an important handling characteristic, it is not a primary control input like the steering wheel angle, which determines the magnitudes of the lateral guidance forces and thus the heading and direction of travel. It has to be considered that the hand wheel torque felt by a driver results from the aligning moments produced by the front tyres as well as those generated by the lateral and possibly longitudinal forces about their respective kingpin axis, and thereby indicates the performance level of the front end. However, the presence of power-assistance reduces the resulting moment transmitted through the

steering column into the hand wheel and may conceal the approach of front end tyre saturation to some extent.

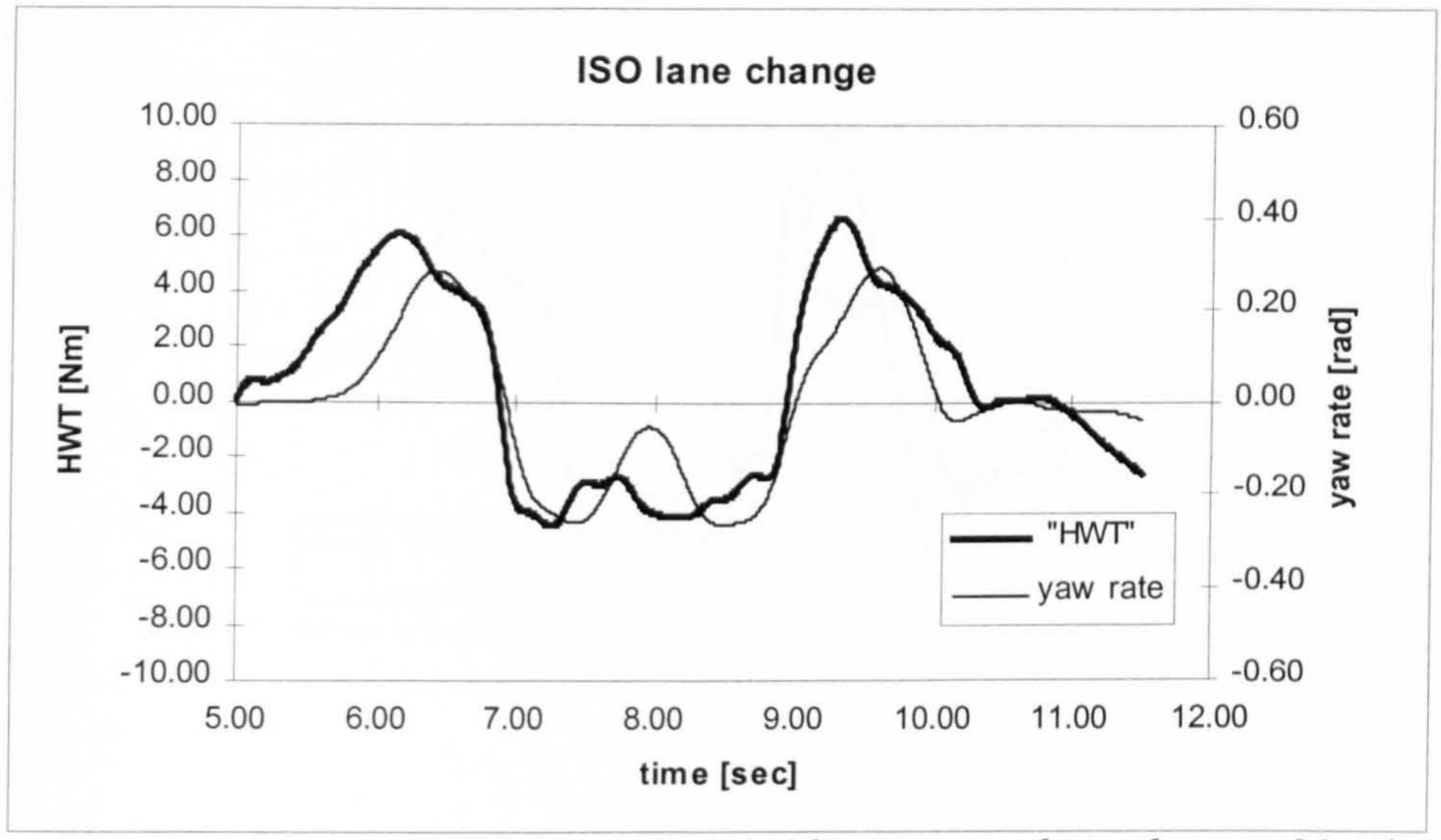

Fig. 7.1-6 low severity lane change: 21 m/sec

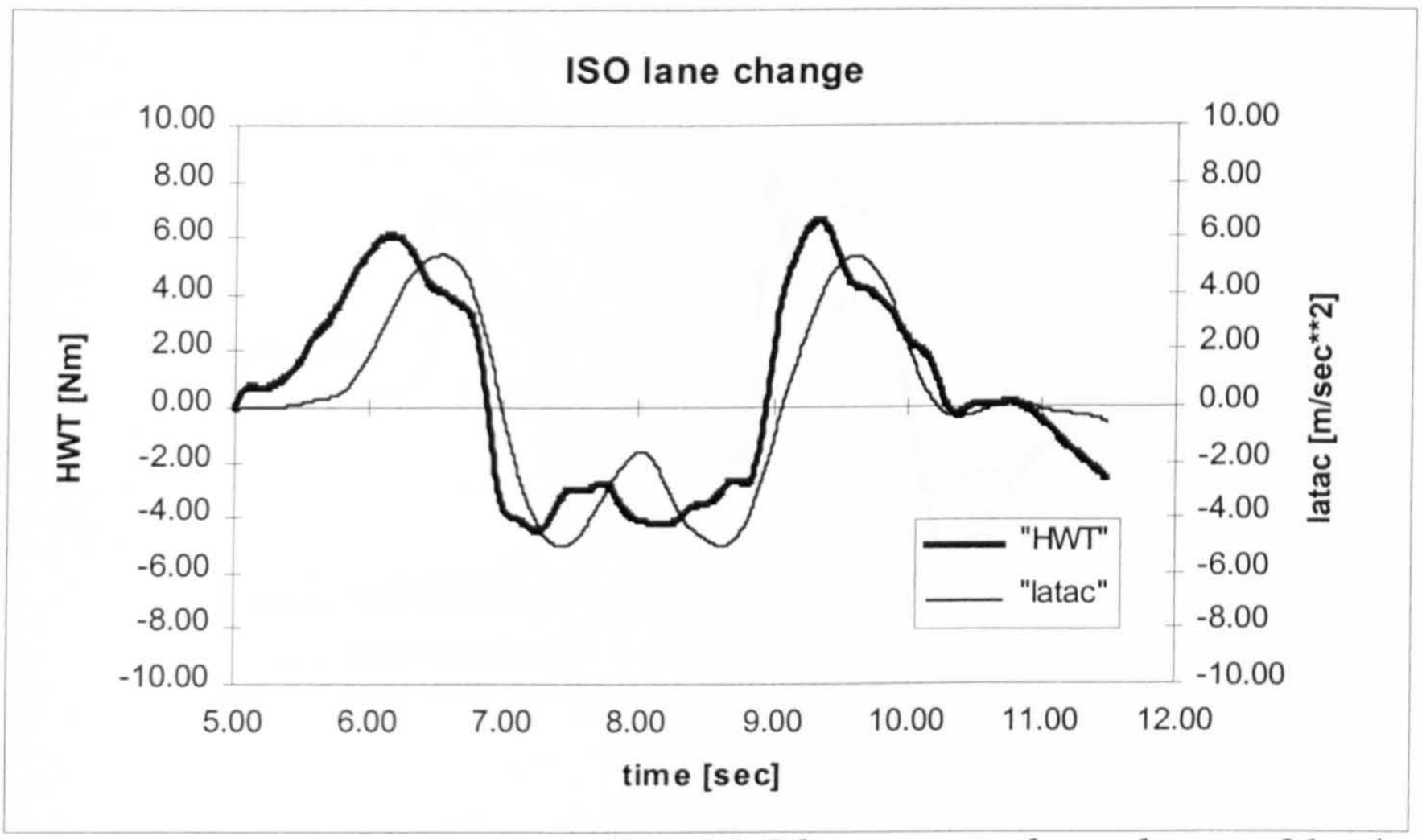

Fig. 7.1-7 low severity lane change: 21 m/sec

Fig. 7.1-6 and fig. 7.1-7 allow comparing the time histories for the hand wheel torque and yaw rate and those of the former and the lateral acceleration respectively, as obtained for the low severity lane change performed at 21 m/sec.

For the time histories shown in this chapter the sign of the hand wheel torque is reversed to allow a more convenient comparison to other measurements. It has to be said though, that the measurements for the hand wheel torque were sometimes corrupted by fluctuations about the nominal zero level. However, from the measured results presented here, it can be concluded that for low severity driving the agreement between the exerted hand wheel torque and lateral vehicle responses, i.e. yaw rate and

lateral acceleration, is clearly less compared to the input-output pairs shown in fig. 7.1-1 and fig. 7.1-2.

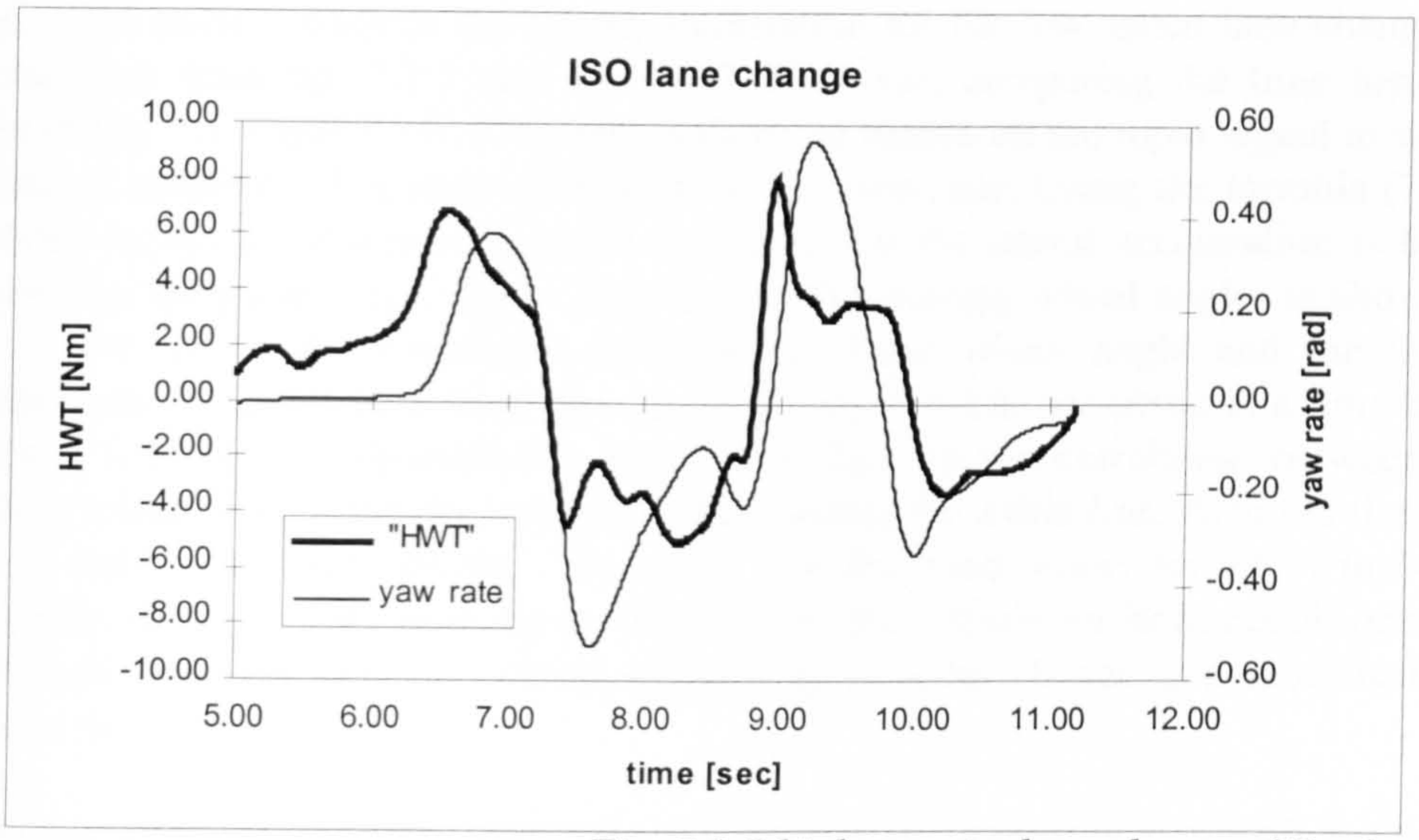

Fig. 7.1-8 high severity lane change: 27 m/sec

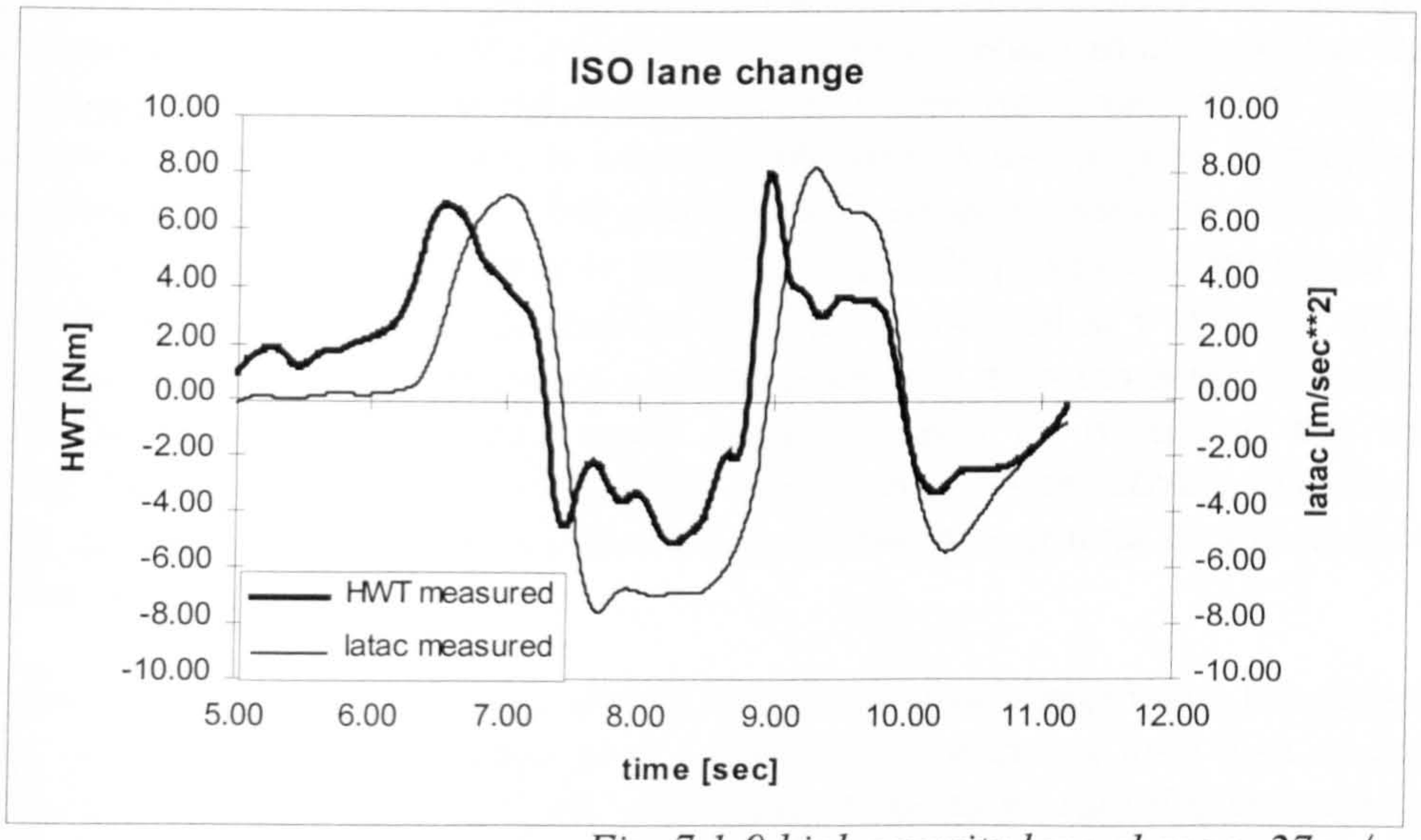

Fig. 7.1-9 high severity lane change: 27 m/sec

Also, it is more difficult to establish an average for the time lags between the response records and that of the hand wheel torque. From fig. 7.1-1 and fig. 7.1-2, relating the lateral vehicle responses to the hand wheel angle input, time delays can be estimated consistently, either by taking the drift between the corresponding peaks or by the shift between the intersections of the abscissa. The plots in fig. 7.1-6 and 7.1-7, referring to the hand wheel torque as input, indicate that the peaks are more offset than the intersections of the time axis. Fig. 7.1-8 and 7.1.9 show a similar result for the high severity manoeuvre.

By comparing fig. 7.1-1 and fig. 7.1-6 as well as fig. 7.1-3 and fig. 7.1-8 it can be seen that the yaw rate correlates much better to the hand wheel angle than to the torque input. The same applies to the lateral acceleration for the low speed lane change, as can be seen from fig. 7.1-2 and fig. 7.1-7. However, comparing the time histories given in fig. 7.1-4 and 7.1-9, it is more difficult to decide on the input signal to which the lateral acceleration is most correlated for the limit case. Using the formula (7.1.1) provides an objective measure, which indicates that the lateral acceleration is better matched to the hand wheel torque than it is to the steering wheel angle, as shown in fig. 7.1-10. Here, the correlation between the hand wheel angle and the lateral acceleration is plotted by a thick line. Its peak value of 0.8, occurring at a time delay of about 0.25 sec, is considerably lower than that for the correlation between the steering wheel torque and the response record plotted by a thin line. Also the time lag for the latter is slightly shorter. The result that the hand wheel torque is in better agreement to the lateral cornering performance of the vehicle for limit conditions was confirmed by other tests for which different tyres were chosen and modifications made to the vehicle.

These introductory examples show that the correlation concept is a suitable means to establish to what extent vehicle response follows faithfully the driver's steering angle and torque input. Therefore, the correlation coefficients obtained at zero time lag and for the peak value provide an objective measure of how much the vehicle's handling deteriorates when it approaches its limit performance. A loss of peak correlation was ascribed to the influence of non-linearities, mainly caused by saturating tyres, as well as to the indifference of a vehicle to translate higher frequency control inputs into a corresponding response. The correlation coefficient obtained at $\tau=0$ might represent the feedback a driver receives during severe closed-loop manoeuvering, for which the control action has to be continuously updated, based on observing the vehicle response according to the exerted steering wheel action. Alternatively, the time lags for the yaw rate and the lateral acceleration can be taken as criteria for the closed-loop limit handling quality.

It is certainly desirable to judge a vehicle's handling quality based on a few parameter values rather than trying to come to a conclusion by studying long data records as presented in this section, but on the other hand, it has to be said that the correlation coefficients and time lags only give an average quality measure in representing a fairly complex manoeuvre like the ISO lane change. Localised events during such a test, which might be noticed and taken account of in the vehicle's assessment by a test driver, may not be weighted sufficiently by the proposed concept.

Furthermore, the correlation coefficient does not necessarily provide a measure for the driver's control work load. Even in the case for which a high correlation and a low lag time are established, which may be recognised as beneficial properties, an unacceptably high control effort might have been required to complete a limit lane change. Conceptually, one can think of a vehicle with lowly damped response characteristics, which responds fast and well correlated to the input, but may require

very high frequency corrective steering action including many reversals.

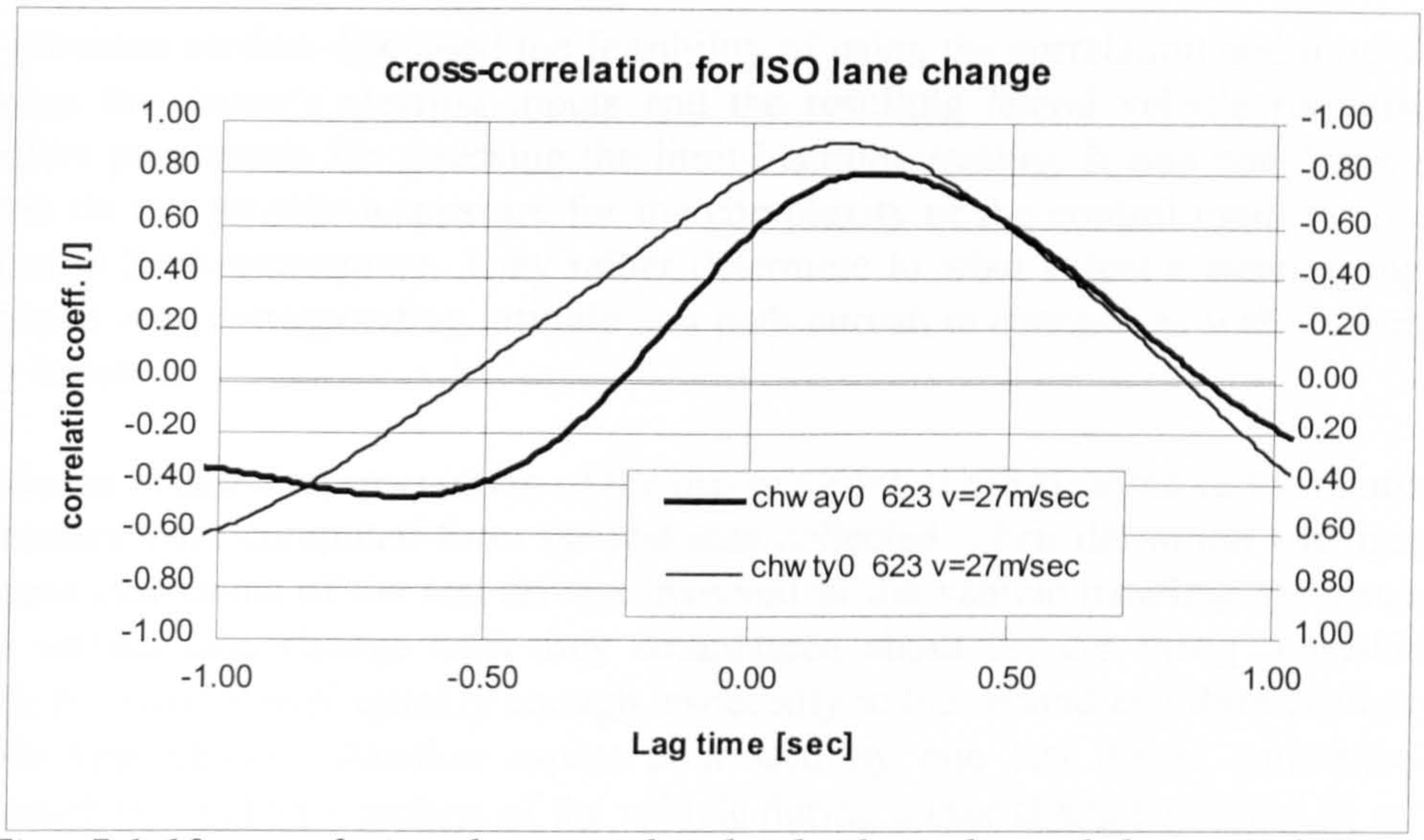

Fig. 7.1-10 correlation between hand wheel angle and lat. acceleration ('chway0') and between hand wheel torque and lat. acceleration ('chwty0'), v=27 m/sec

In order to provide a more complete handling quality analysis, some more parameters derived from the test data records are added. These parameters are defined to represent the steering control effort. They are discussed in the following section.

7.1.2 Other statistical handling parameters

The previous section discussed the feasibility of using the correlation and time delays between the driver's steering inputs and the resulting lateral vehicle responses as objective parameters for assessing the limit handling quality. It was noted that these criteria do not provide a measure for the complexity of the control input required to perform a limit manoeuvre. They rather determine to what extent a steering input is translated into corresponding attitude and path curvature changes as well as the time delay involved.

In order to obtain a representation of the driver's control effort, some further statistical parameters were computed from the test data collected. Their definition was inspired by some comments of the test drivers involved in the vehicle handling test program. After certain lane change tests they complained about the car being 'unstable' or unable to 'settle down' quickly enough, especially in the second and third section of a double lane change. Another aspect addressed by one test driver concerned the combined roll and yaw motion of the vehicle during a lane change, referred to as 'roll steer'. The driver associated the 'roll steer' characteristic with the vehicle's rear end stability, in that excessive roll and yaw gave him the impression of 'oversteer' or imminent rear end breakaway.

From these statements it was concluded that large roll angles and yaw rate overshoots are undesired responses, which have to be represented in the data analysis. Due to its tight layout, the lane change test requires the driver to concentrate most of all on establishing the appropriate position and path curvature rather than on setting the attitude of the car. For that the driver has to produce a steering wheel input giving the lateral acceleration, which corresponds to the desired course ahead. The test results given in section 7.1.1, referring to fig. 7.1-3 and fig. 7.1-4, indicated that the lateral acceleration becomes less correlated to the yaw rate response towards the limit. This can be ascribed to the increasing side slip motion of the car, which contributes to the lateral response according to equation (7.0.1). The presence of side slip or side slip acceleration $v\dot{\beta}$ requires to produce a yaw rate, disproportionate to the lateral acceleration, in order to achieve the cornering performance that allows to maintain the course. In contrast to steady state cornering for which the yaw rate is proportional to the lateral acceleration, only a part of the yaw rate generated by the steering wheel input is translated into a change of path curvature, while the remainder is lost in the side slip motion. The resulting yaw motion may be lowly damped and accompanied by pronounced roll oscillations. It is possibly this transition from a single-input/ single-output to a single input/ dual output control behaviour, which is addressed by test driver's comments on 'roll steer' and 'instability'.

The parameters chosen for representing the severity of a manoeuvre and complexity of the control effort are discussed below. It was decided to use the standard deviations of the measured lateral acceleration and yaw rate as measures for the severity and that of the hand wheel velocity as a parameter for the mental rather than physical control

effort. The standard deviations take account of the number of reversals as well as the magnitudes of the peaks contained in a data record by integrating the square of a signal before taking the root. Hence, the standard deviation assigns a single figure to the frequency content and the peak values of an event. It gives a high value for a record showing high peaks, which are maintained for longer periods of time, as is the case for the lateral acceleration in fig. 7.1-4, and thus indicates the severity of a manoeuvre. Furthermore, a high standard deviation is obtained for a higher frequency event for which peak values are assumed quickly for a short while, as shown for the hand wheel angle in the same graph. However, the parameter reflecting the control effort is calculated from the steering wheel angular velocity rather than from the angle. This is consistent with the approach of other researchers /2.3.6, 2.3.7, 7.1.3, 7.1.4/, who regard the derivative action as the mentally straining effort.

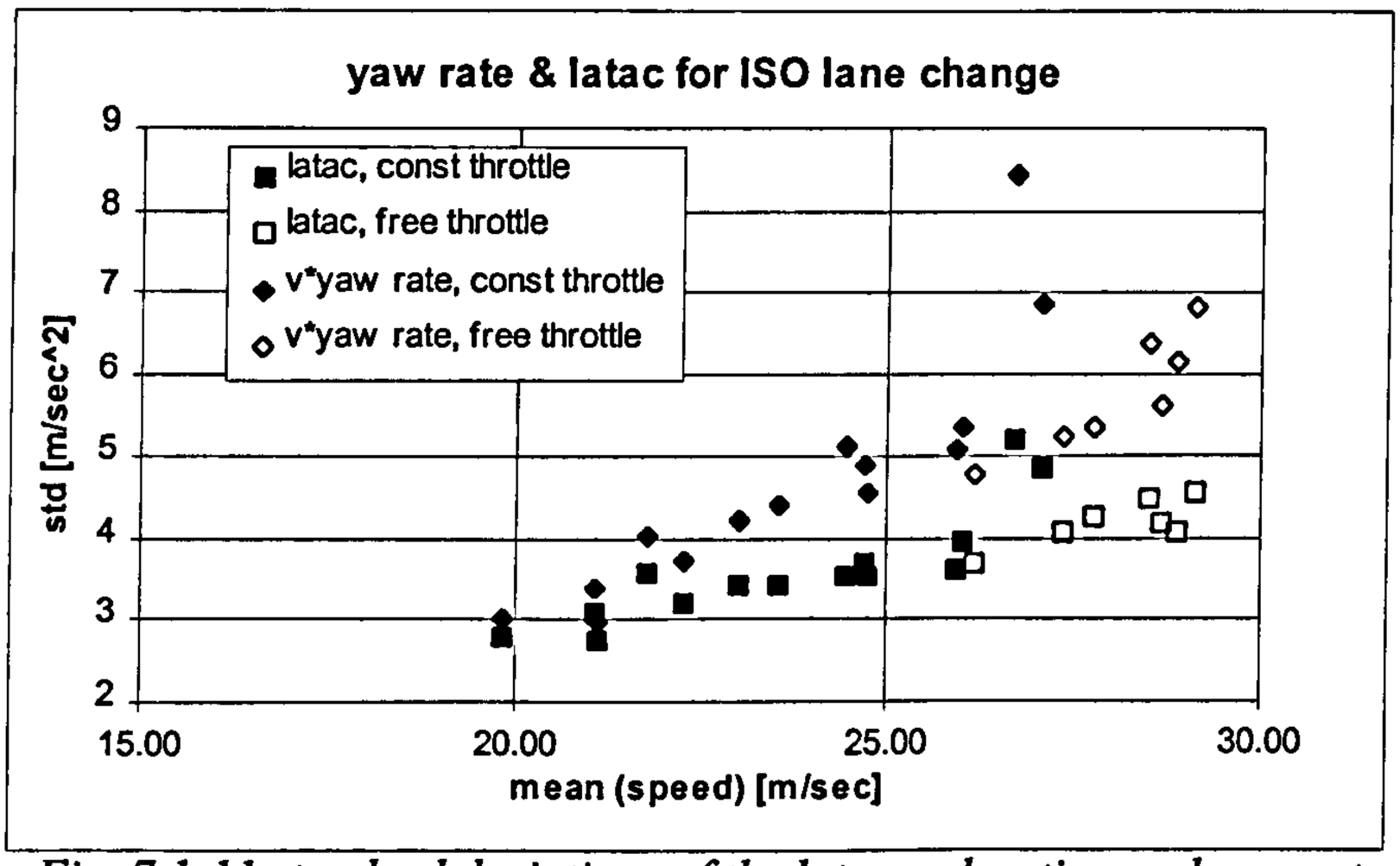

Fig. 7.1-11 standard deviations of the lat. acceleration and yaw rate as a function of vehicle speed

An example of the increasing severity of a lane change manoeuvre performed at constant speeds, approaching the limit by increments of 2-5 kph, is illustrated in fig. 7.1-11. It shows the standard deviations for the lateral acceleration and that for the product of the yaw rate and forward speed, plotted against the velocity during the manoeuvre.

As can be seen from the time histories in fig. 7.1-1 and fig. 7.1-2, these quantities are equivalent at low speeds, for which the steady state cornering behaviour prevails. At higher speeds the standard deviations differ from each other. As has been said earlier, the product of velocity and yaw rate assumes a steeper gradient than the resultant lateral acceleration. The difference between the two curves shown gives a measure for the vehicle's slip acceleration.

Results represented by filled markers represent tests for which the throttle was held almost constant, whereas their unfilled counterparts denote those for which the standard deviation of the throttle position signal exceeded a threshold value of 20% of its mean. It is apparent that for velocities beyond 27 m/sec the lane change could only

be performed with additional throttle control. The use of this second control input contained the yaw and corresponding side slip motions to manageable levels up to the limit speed. The limit speed for pure steering control appears to be 27 m/sec, as indicated by the sharp roll-off for the yaw rate standard deviation.

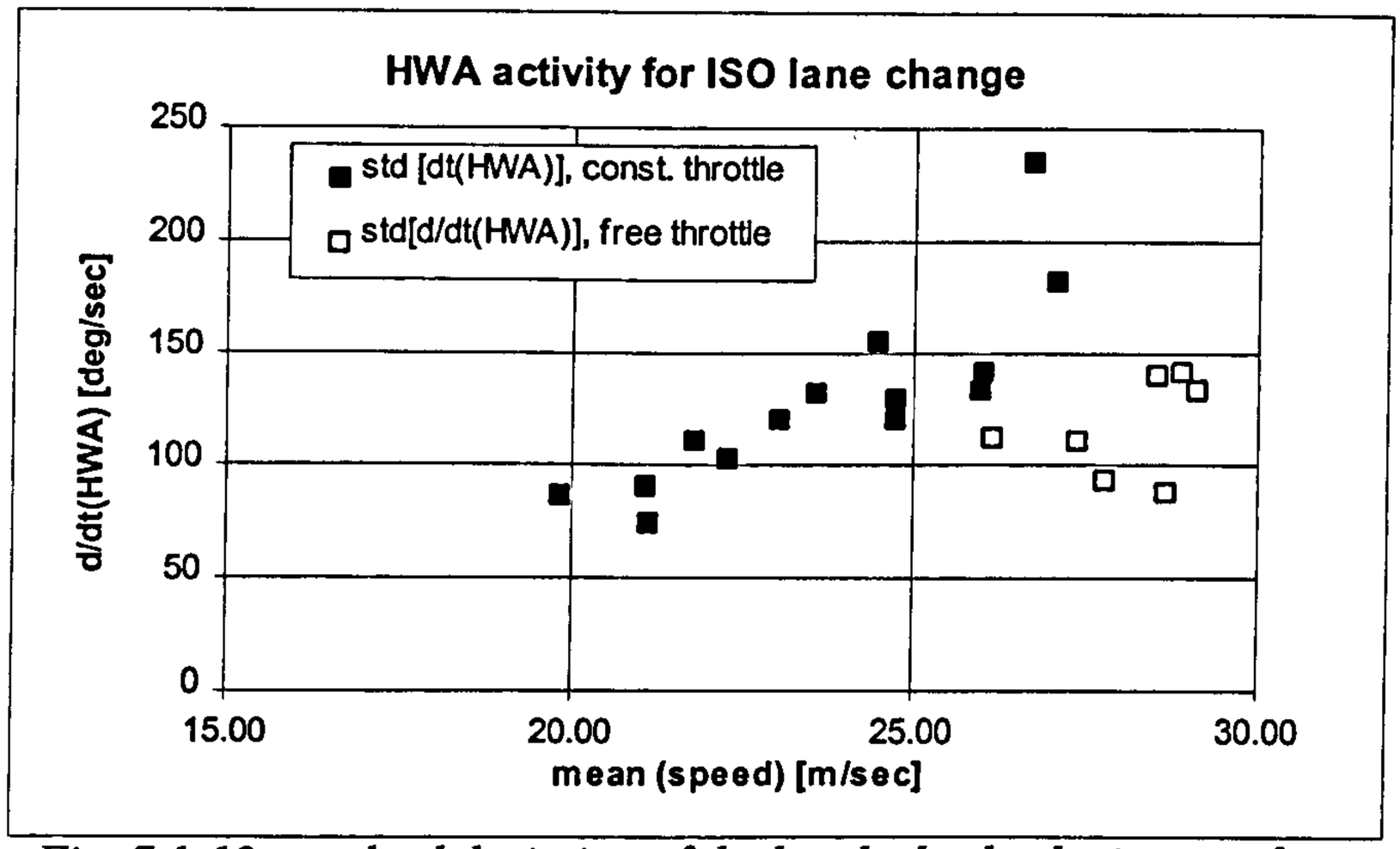

Fig. 7.1-12 standard deviation of the hand wheel velocity as a function of vehicle speed

From the handling quality point of view, a vehicle may be classified as good, if the approach to its limit performance involves gradually increasing severity levels. For that, oscillations of the lateral acceleration and yaw rate as well as long sustained peak values are undesired, unless they correspond to the wavelength and curvature of the track. The limit approach has to be predictable and should therefore assume a smooth transition.

The same applies for the control effort represented by the time derivative of the hand wheel angle[1], as shown in figure 7.1-12. Similar conclusions can be drawn from this graph, as was done with regard to the manoeuvre's severity. The complexity of the hand wheel angle input increases with speed until it assumes its peak value of approximately 240 deg/sec at a test velocity of 27m/sec. Successful tests beyond this speed involved considerable throttle application by which the steering effort could be reduced substantially.

In order to discriminate the steering effort devoted to controlling the attitude or yaw motion from that aimed at establishing the appropriate side slip, another parameter was derived that is based on the standard deviations shown in fig. 7.1-10-12. Considering that the yaw rate response correlates well to the steering input and assumes low time lags up to the limit performance, as shown in the previous section, the attitude control has to be seen as the easier control task. The more demanding effort has to be directed to the path or curvature tracking, which requires the

[1] the time derivative was established by taking the first order difference of the measured hand wheel angle signal

additional control of the increasing side slip motion near the limit. A measure for the side slip acceleration $v\dot{\beta}$ is easily calculated from the difference between those for the yaw rate and lateral acceleration according to:

$$\sigma_{\dot{\beta}} = v \cdot \sigma_{\dot{\psi}} - \sigma_{\ddot{y}}, \text{ where} \qquad (7.1.2)$$

The expressions in (7.1.2)[2] denote the standard deviations of the yaw rate and lateral acceleration as well as their corresponding means. The ratio between the parameter $\sigma_{\dot{\beta}}$ and the product $v \cdot \sigma_{\dot{\psi}}$, representing the side slip and yaw rate variations respectively, is then multiplied with the standard deviation of the hand wheel velocity. The steering wheel activity for controlling the side slip is thus defined according to:

$$\sigma_{\dot{\delta},\beta} = \frac{(v \cdot \sigma_{\dot{\psi}} - \sigma_{\ddot{y}})}{v \cdot \sigma_{\dot{\psi}}} \cdot \sigma_{\dot{\delta}}, \text{ where} \qquad (7.1.3)$$

$\sigma_{\dot{\delta}}$ denotes the standard deviation of the total hand wheel angle velocity. This parameter bears some resemblance to Bergman's test criterion of the 'normalised sideslip acceleration' given by (2.3.4.1). However, the standard deviation gives a reflection on the whole manoeuvre, while (2.3.4.1) indicates a peak value.

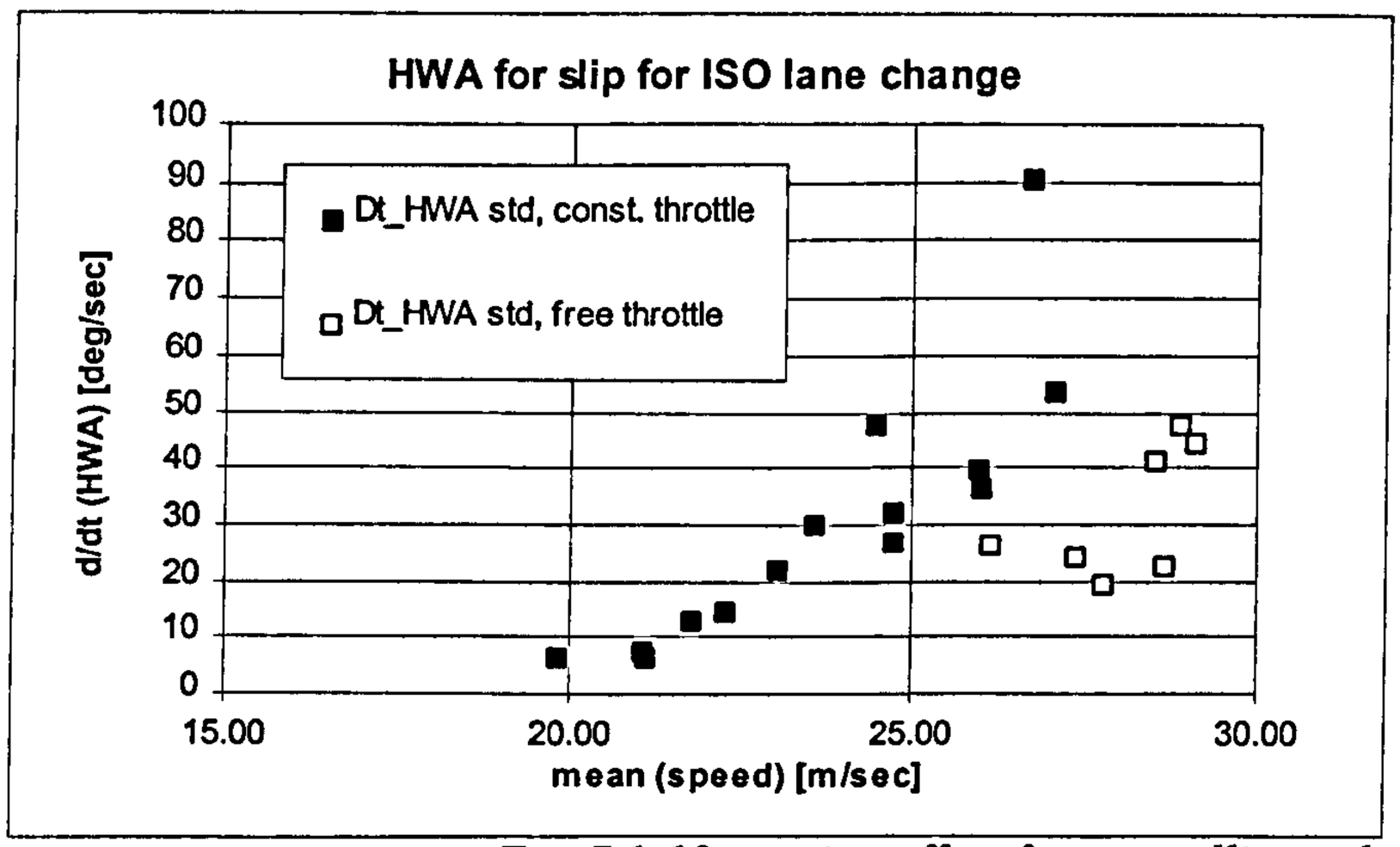

Fig. 7.1-13 steering effort for controlling side slip

As an example, some results are presented in fig. 7.1-13. These were obtained for the standard car fitted with standard tyres. The shape of the curve is similar to that shown for the standard deviation of the total hand wheel activity $\sigma_{\dot{\delta}}$. The steering effort for controlling the side slip motion, as denoted by $\sigma_{\dot{\delta},\beta}$, remains very low for the low speed tests, but rises to almost 40% of the total input at the limit velocity of 27 m/sec

[2] it has to be noted that (7.1.2) is not the definition for the standard deviation of the side slip acceleration

for the constant throttle tests. Again, the effect of a successful throttle operation can be noticed which reduces the side slip motion, as can be seen from the relatively small offset between the curves shown in fig. 7.1-11, as well as from the corresponding steering effort $\sigma_{\dot{\delta},\beta}$.

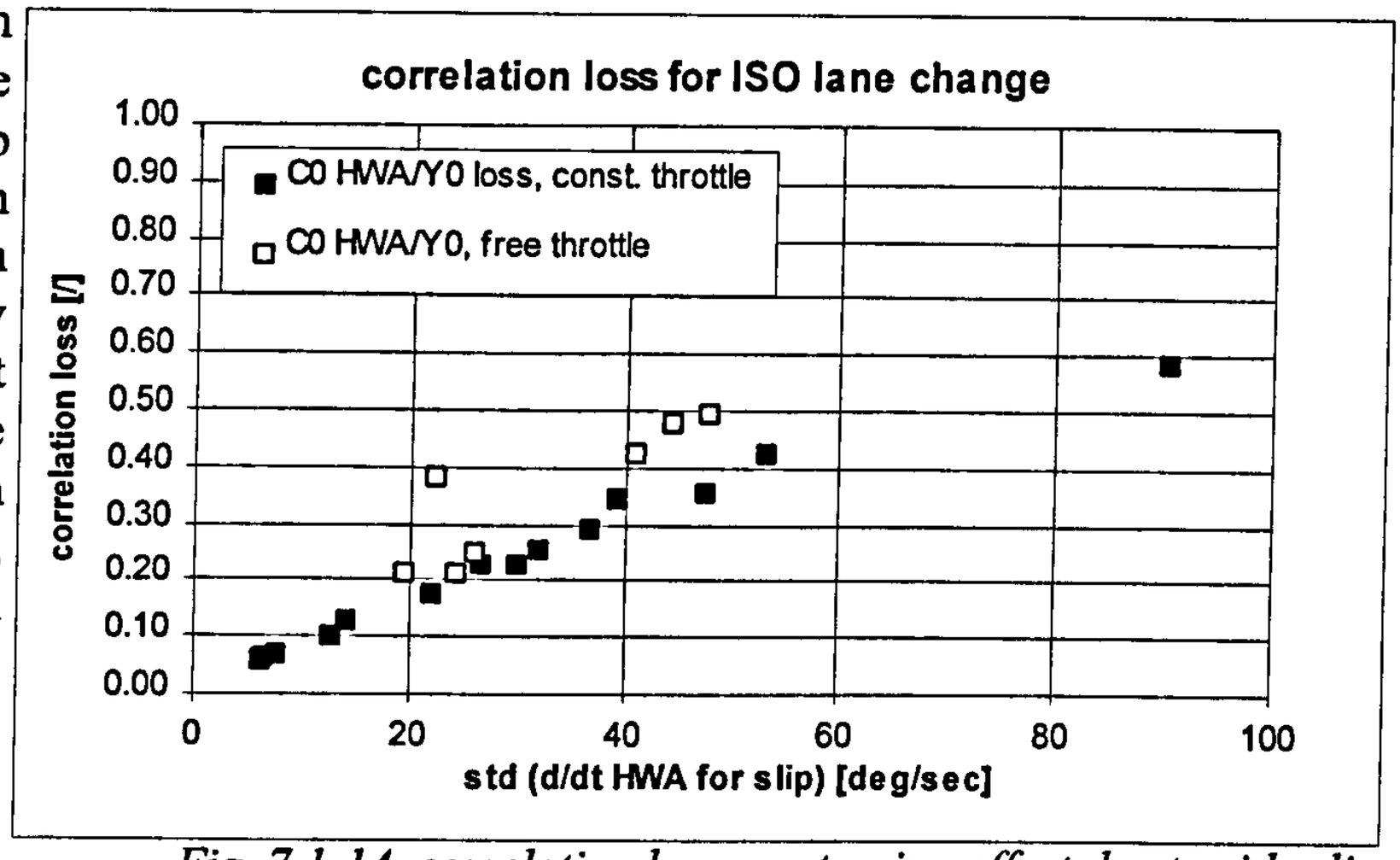

Fig. 7.1-14 correlation loss vs. steering effort due to side slip

The graph given in fig. 7.1-14 indicates the relation between the increasing loss of correlation computed for the hand wheel angle input - lateral acceleration output pair and the increasing steering effort $\sigma_{\dot{\delta},\beta}$ that is required to control the side slip as driver and vehicle approach the limit. This representation takes account of the two control challenges a driver is confronted with: the deteriorating correlation and the transformation of the single input/ single output system into a single input/ dual output one.

The correlation loss is simply the difference between the perfect correlation of one and the value established from the test data. The steering effort is computed for each test run according to (7.1.3).

The loss of correlation as well as the steering effort to control the side slip motion, as reflected by $\sigma_{\dot{\delta},\beta}$, remain low for low speed lane changes. An almost linear relationship between correlation loss and steering effort $\sigma_{\dot{\delta},\beta}$ is established for the results referring to the constant throttle tests ('diamonds'). A high correlation loss corresponds to a high control effort $\sigma_{\dot{\delta},\beta}$ at the limit. Results referring to tests, for which the driver was free to apply the throttle, assume lower values for the control effort than those for the constant throttle at the same level of correlation loss.

As documented in section 7.3, a favourable test driver rating for the limit handling was obtained for vehicles, for which a low gradient for the correlation loss with respect to the steering effort $\sigma_{\dot{\delta},\beta}$ was established. This suggests that the ability of the vehicle to change the curvature of its trajectory in agreement to the steering wheel input, as represented by the correlation coefficient, must not be too sensitive to the dynamic influence of the side slip motion. A well performing vehicle maintains a relatively high level of correlation between the control action of the driver and its lateral response, even in the presence of considerable side slip motion during a limit manoeuvre.

7.2 Results for ISO lane changes

After discussing the criteria used to compare and assess the limit handling of vehicles, some test results are presented which were obtained for the ISO lane change. Test were carried out with a fully instrumented Jaguar XJ6, which was equipped with various sets of tyres of different construction. Furthermore, the vehicle properties were modified in two ways. Firstly, the car was tested with a 100 kg ballast on its roof, while the second modification involved removing the vehicle's front anti-roll bar.

Section 7.2.1 discusses in detail the results obtained for the standard car fitted with standard tyres. These results will be used as a reference for the results referring to other tyre designs and those for the modified car, which are given in the proceeding sections.

7.2.1 ISO lane change with standard car fitted with standard Dunlop SP 2000

Tests with the standard set-up were carried out in November 1996 on a slightly damp test track. The average air temperature was 3 degrees Celsius. The tests were performed by test driver A. In total 21 successful double lane changes were recorded for a speed range starting from 20 m/sec up to 29 m/sec.

The handling performance is discussed using graphs showing correlation coefficients and time lags plotted against the mean of the speed maintained through the lane change. The graph in fig. 7.2-1 gives the peak correlation coefficients obtained for the hand wheel angle and yaw rate signals, denoted as 'Cm HWA/YAW', and those established for the hand wheel angle and the lateral acceleration, which is referenced as 'Cm HWA/Y0'. As in section 7.1, filled markers represent the free throttle tests, while unfilled markers depict those almost exclusively performed with steering control.

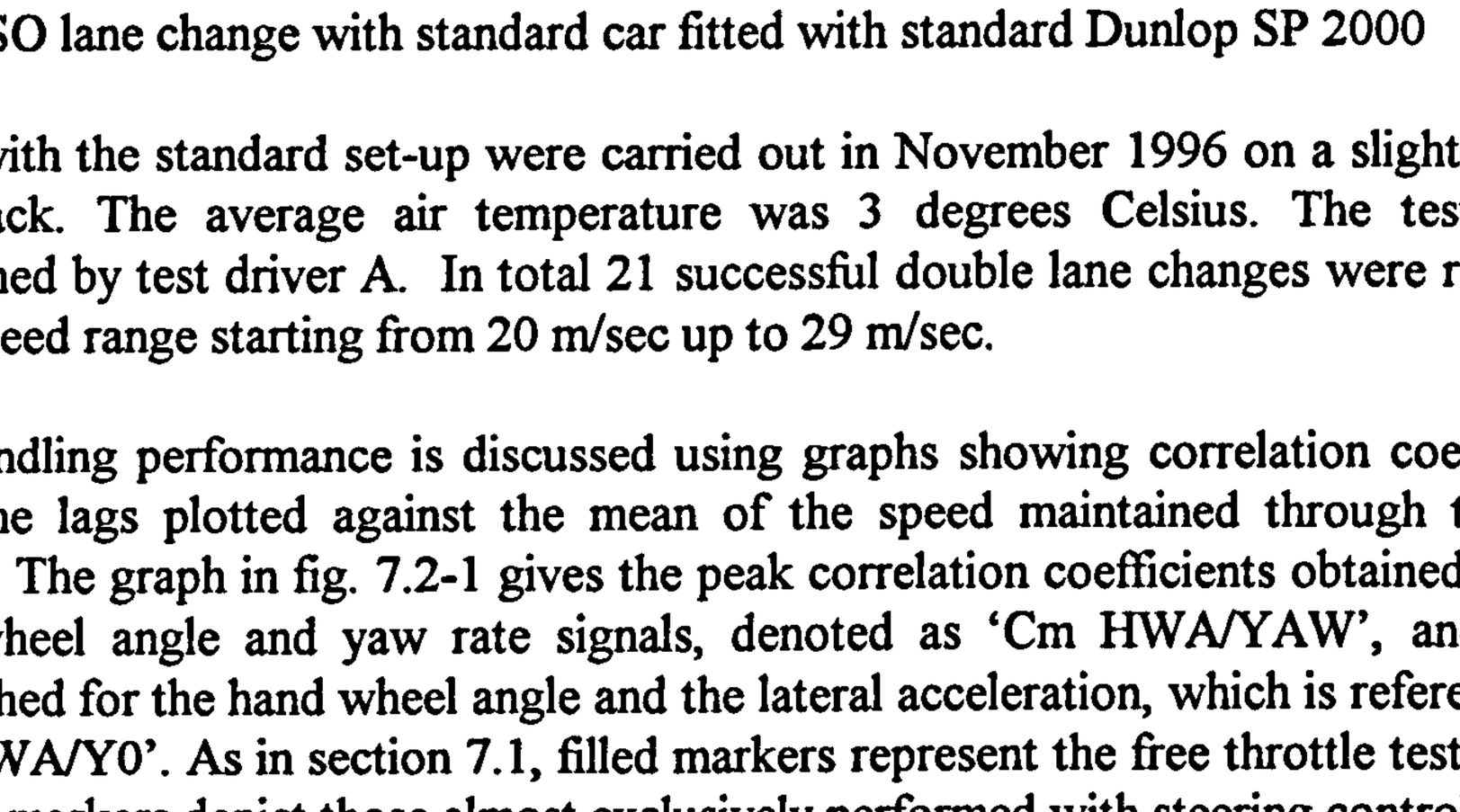

Fig. 7.2-1 maximum correlation for yaw rate and lat. acceleration response

As stated in the previous section the yaw rate response hardly deteriorates with

increasing severity. It remains well matched to the steering wheel input up to the limit speed of 29 m/sec. The peak correlation for the lateral acceleration though, decreases progressively up to a level of 0.8 at a velocity of 27 m/sec. Beyond this speed the manoeuvre could only be completed without hitting the cones by using considerable throttle operation. The additional throttle control enables the driver to regain a better match between his steering input and the lateral response at high speeds until the maximum speed of 29 m/sec, at which the correlation drops to the level established for the 'steering only' peak performance.

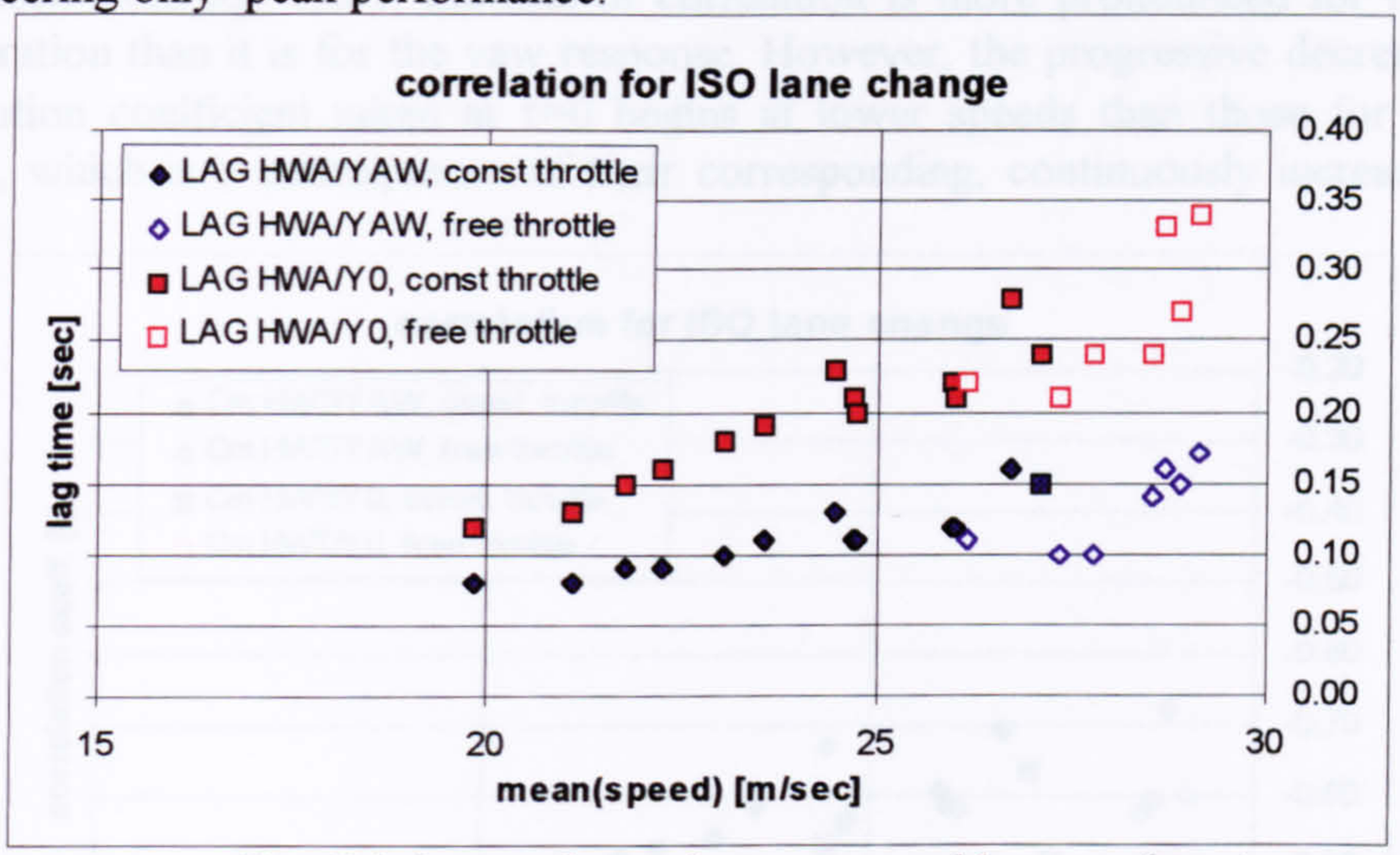

Fig. 7.2-2 time lags of yaw rate and lat. acceleration response

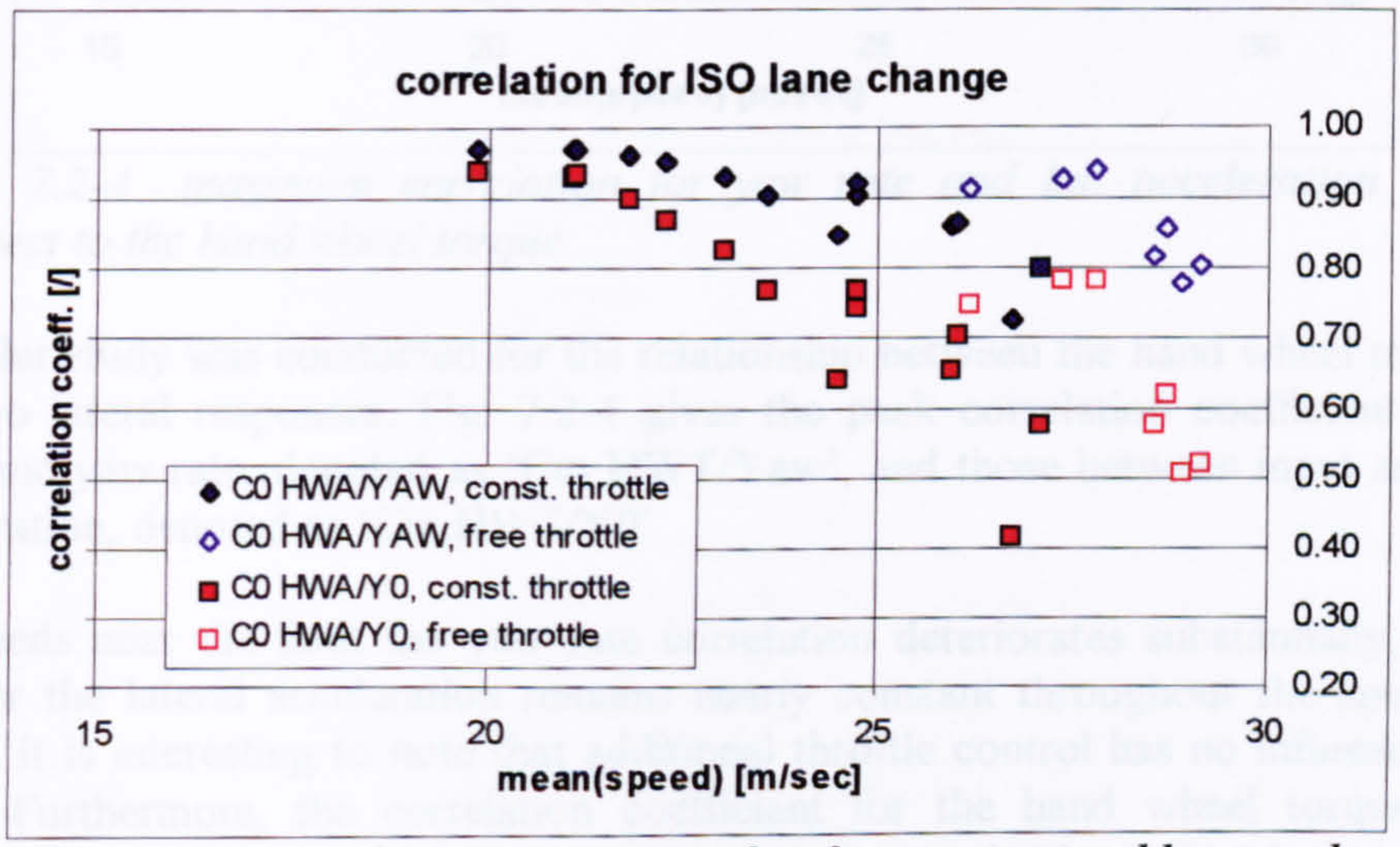

Fig. 7.2-3 correlation at zero time lag for yaw rate and lat. acceleration response

In section 7.1 lateral response time lags were proposed as quality criteria. They are given in the fig. 7.2-2. The graph shows that the yaw rate and lateral acceleration lag the steering angle increasingly with forward speed. However, the delay time associated with the lateral acceleration is more sensitive to an increasing severity. It is almost three times higher at the limit speed compared to its value assumed at 20

m/sec. A cross-coupled steering and throttle control appears to lessen the rise in lag time to a small extent.

As described in section 7.1, the composite effects of vehicle speed, non-linearities and time lags can be represented by the correlation coefficients at zero lag τ=0. This parameter may also be interpreted as the instantaneous feedback provided by the vehicle response to the steering wheel input. Their values are given in fig. 7.2-3. As we have seen from fig. 7.2-1, the loss of correlation is more pronounced for the lateral acceleration than it is for the yaw response. However, the progressive decrease of the correlation coefficient taken at τ=0 begins at lower speeds than those for the peak values, which is a consequence of their corresponding, continuously increasing, lag times.

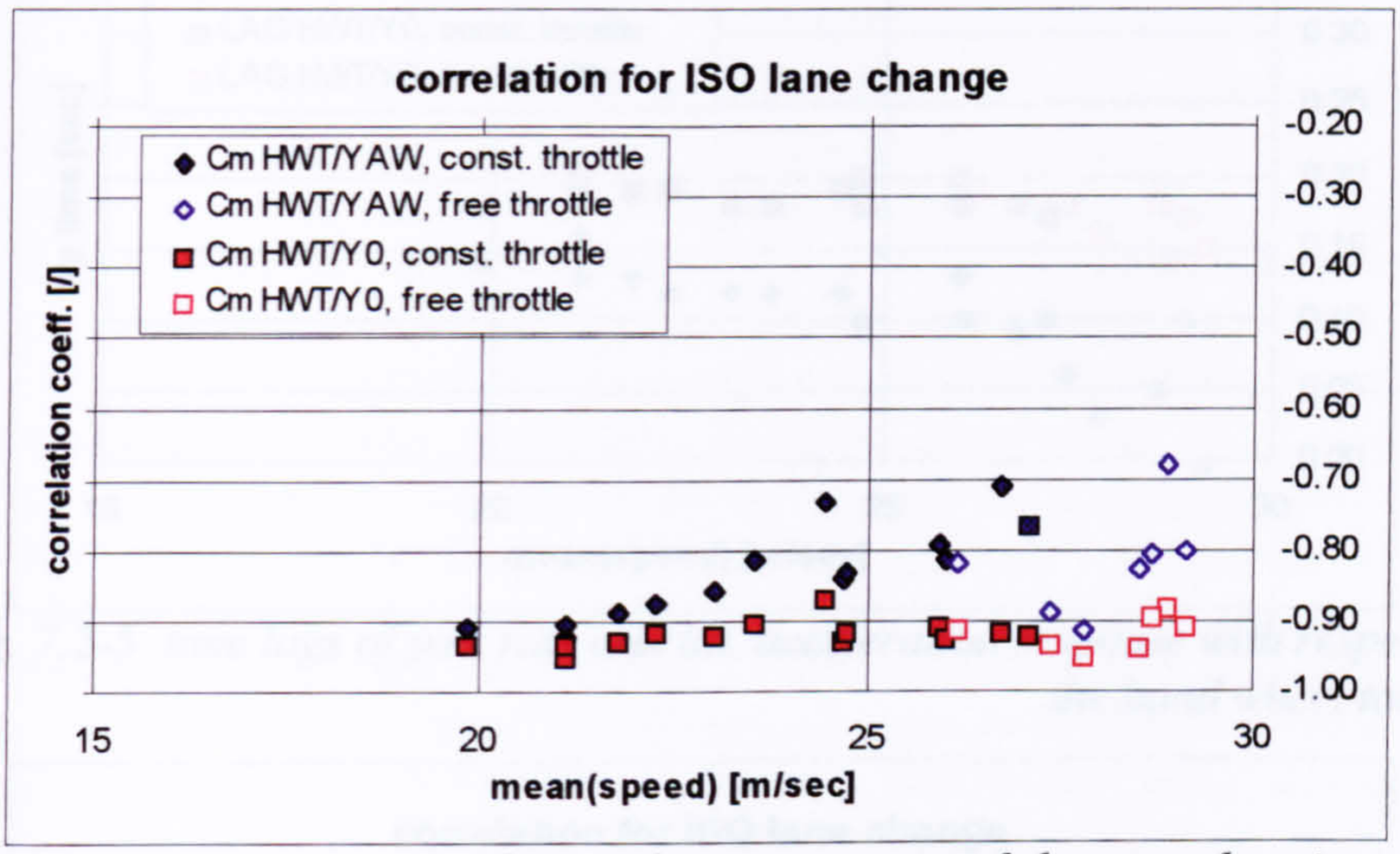

Fig. 7.2-4 maximum correlation for yaw rate and lat. acceleration with respect to the hand wheel torque

A similar study was conducted for the relationship between the hand wheel torque and the two lateral responses. Fig. 7.2-4 gives the peak correlation coefficient between input and yaw rate, denoted as 'Cm HWT/Yaw', and those between input and lateral acceleration, denoted as 'Cm HWT/Y0'.

At speeds near the limit the yaw rate correlation deteriorates substantially, whereas that for the lateral acceleration remains nearly constant throughout the speed range tested. It is interesting to note that additional throttle control has no influence on the latter. Furthermore, the correlation coefficient for the hand wheel torque/ lateral acceleration pair assumes a higher value at limit speeds than that obtained for the steering wheel angle/ lateral acceleration pair.

The lag times of the lateral responses relative to the hand wheel torque are shown in fig. 7.2-5. As for the peak correlation, the time lag associated with the lateral acceleration remains constant. The time lag for the poorly correlated yaw rate tends to decrease towards zero for increasing speeds.

The correlation analysis for the standard car is completed with fig. 7.2-6, showing the correlation coefficient at zero time lag. Correlation coefficients for the yaw rate and lateral acceleration, taken at $\tau=0$, are more similar to each other than their corresponding peak values as given in fig. 7.2-4. The correlation $c(\tau=0)$ for the lateral acceleration is offset to its corresponding peak correlation by about 0.1, due to the constant time lag of approximately 0.18 sec. The correlation at zero time lag for the yaw rate converges towards its peak correlation coefficient for the limit speed, for which the associated time lag becomes zero.

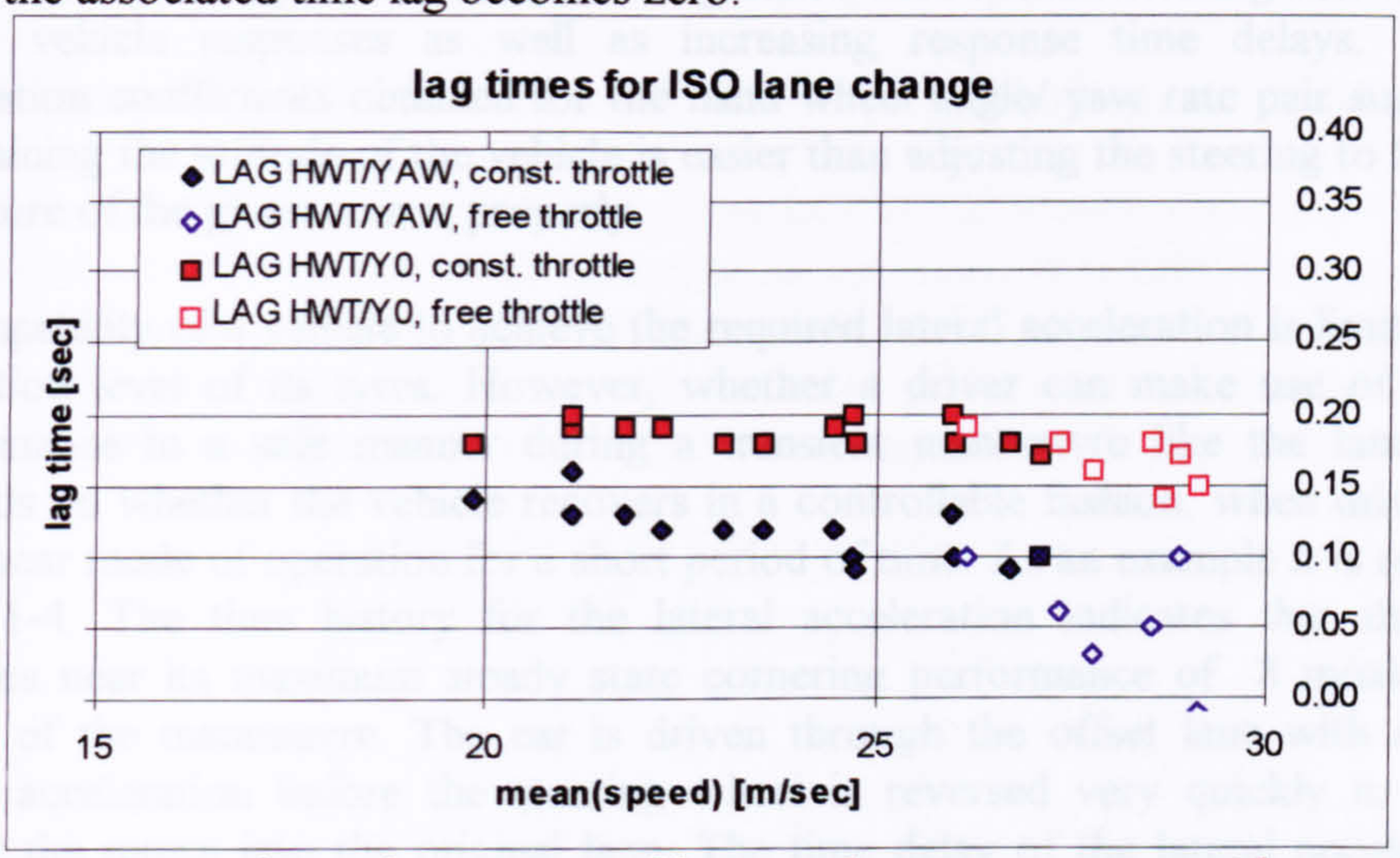

Fig. 7.2-5 time lags of yaw rate and lat. acceleration response with respect to the hand wheel torque

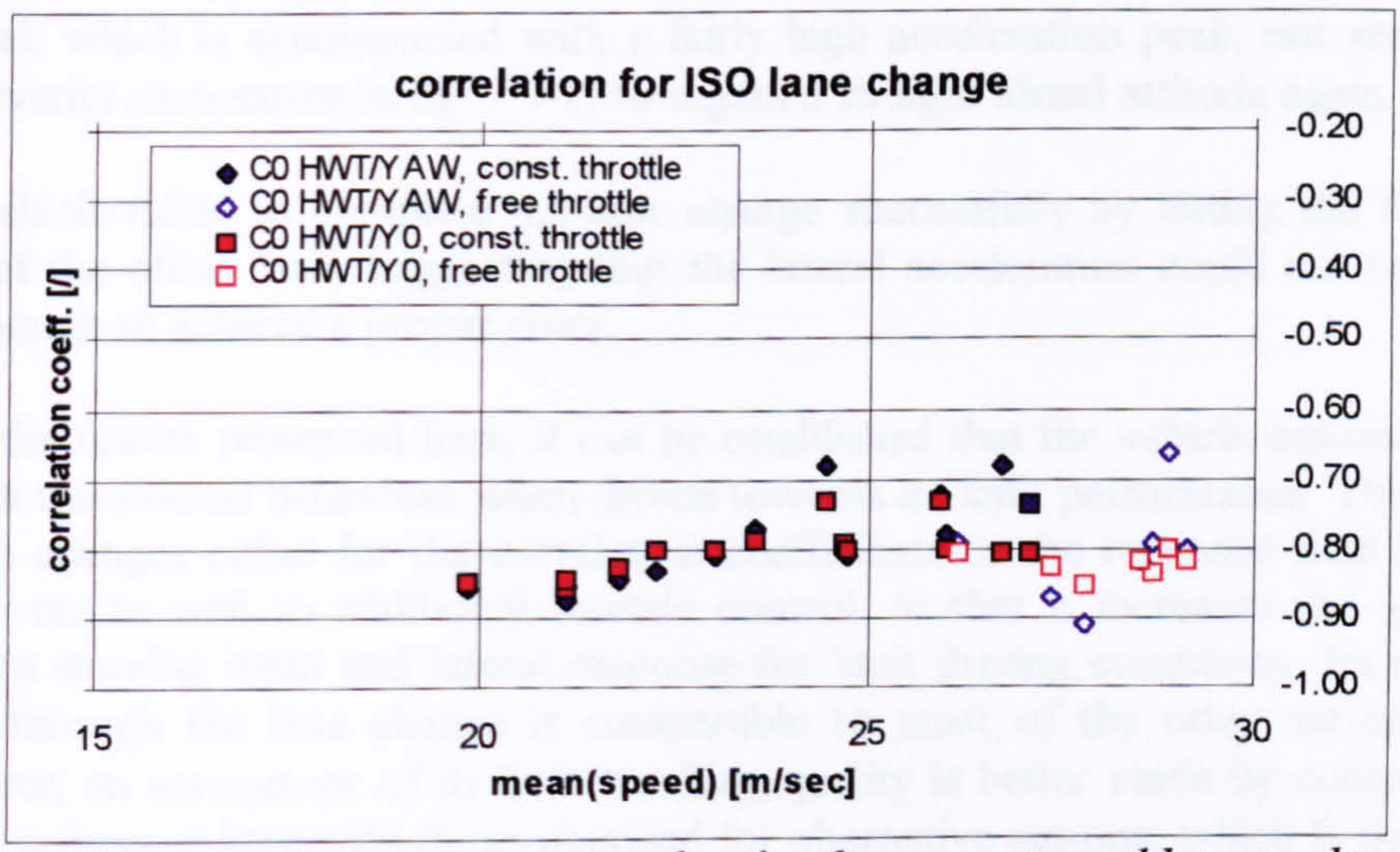

Fig. 7.2-6 correlation at zero time lag for the yaw rate and lat. acceleration response with respect to the hand wheel torque

The consistent behaviour for the correlation between the hand wheel torque and the lateral acceleration may provide a reliable feedback to the driver, indicating the level of front tyre saturation and cornering severity.

summary of test results

The graphs for the correlation coefficients and time lags presented in this section describe the transitional behaviour of a vehicle driven through a double lane change with speeds incrementally approaching the limit. They reveal how smooth or how sudden the input/ output behaviour changes for an increasing manoeuvre severity. A driver, attempting to perform such a manoeuvre at a higher velocity than previously practiced, has to cope with a deteriorating match between the steering control and the lateral vehicle responses as well as increasing response time delays. The high correlation coefficients obtained for the hand wheel angle/ yaw rate pair suggest that maintaining the attitude of the vehicle is easier than adjusting the steering to follow the curvature of the given course properly.

The capability of a vehicle to achieve the required lateral acceleration is limited by the saturation level of its tyres. However, whether a driver can make use of the peak performance in a safe manner during a transient manoeuvre like the lane change, depends on whether the vehicle recovers in a controllable fashion, when driven in the non-linear mode of operation for a short period of time. As an example it is referred to fig. 7.1-4. The time history for the lateral acceleration indicates that the vehicle operates near its maximum steady state cornering performance of 8 m/sec^2 at two stages of the manoeuvre. The car is driven through the offset lane with maximum lateral acceleration before the steering wheel is reversed very quickly in order to initiate the return into the original lane. The time delay of the lateral acceleration is considerable, so that the vehicle maintains a high lateral acceleration when it enters the straight ahead lane again. The slow response necessitates an additional steering wheel reversal, which is accompanied with a fairly high acceleration peak, not seen for the low severity manoeuvre in fig. 7.1-2, to regain a straight ahead attitude again.

The vehicle failed to complete the lane change successfully by hitting the first inside cone of the offset lane, suggesting that the lateral acceleration could not be built up fast enough to achieve a proper entry.

From the results presented here, it can be established that the vehicle assumes a fairly smooth transitional behaviour when driven towards its limit performance. There are no sudden changes either for the correlation coefficients or the response time lags. The vehicle reacts well to additional throttle control, in that it increases the agreement between steering input and lateral response for limit driving conditions. Its maximum speed through the lane change is comparable to most of the other set-ups tested. However, an assessment of its limit handling quality is better made by comparing the results presented here with those obtained for alternative set-ups, which is the content of following section.

7.3 Comparisons of ISO lane change performance

In this section test results obtained for alternative vehicle set-ups are discussed. They are presented such that they can be compared to the results established for the standard vehicle fitted with standard tyres inflated to their recommended pressures, as discussed in 7.2.1. Firstly, the influence of the tyre inflation pressure is analysed in 7.3.1, before further results are presented, representing the effects of different tyre constructions as well as chassis modifications on the limit handling behaviour.

7.3.1 Influence of inflation pressure on ISO lane change handling performance

In addition to the lane change tests summarised in the previous section, similar test sequences were carried out on the same day for two alternative inflation pressures. The same set of tyres was used. The pressure settings were changed from their nominal values of 2.0 bar for front and rear tyres to 2.5 bar at the front and 1.5 bar at the rear for the first test sequence, before the opposite setting was used for the second.

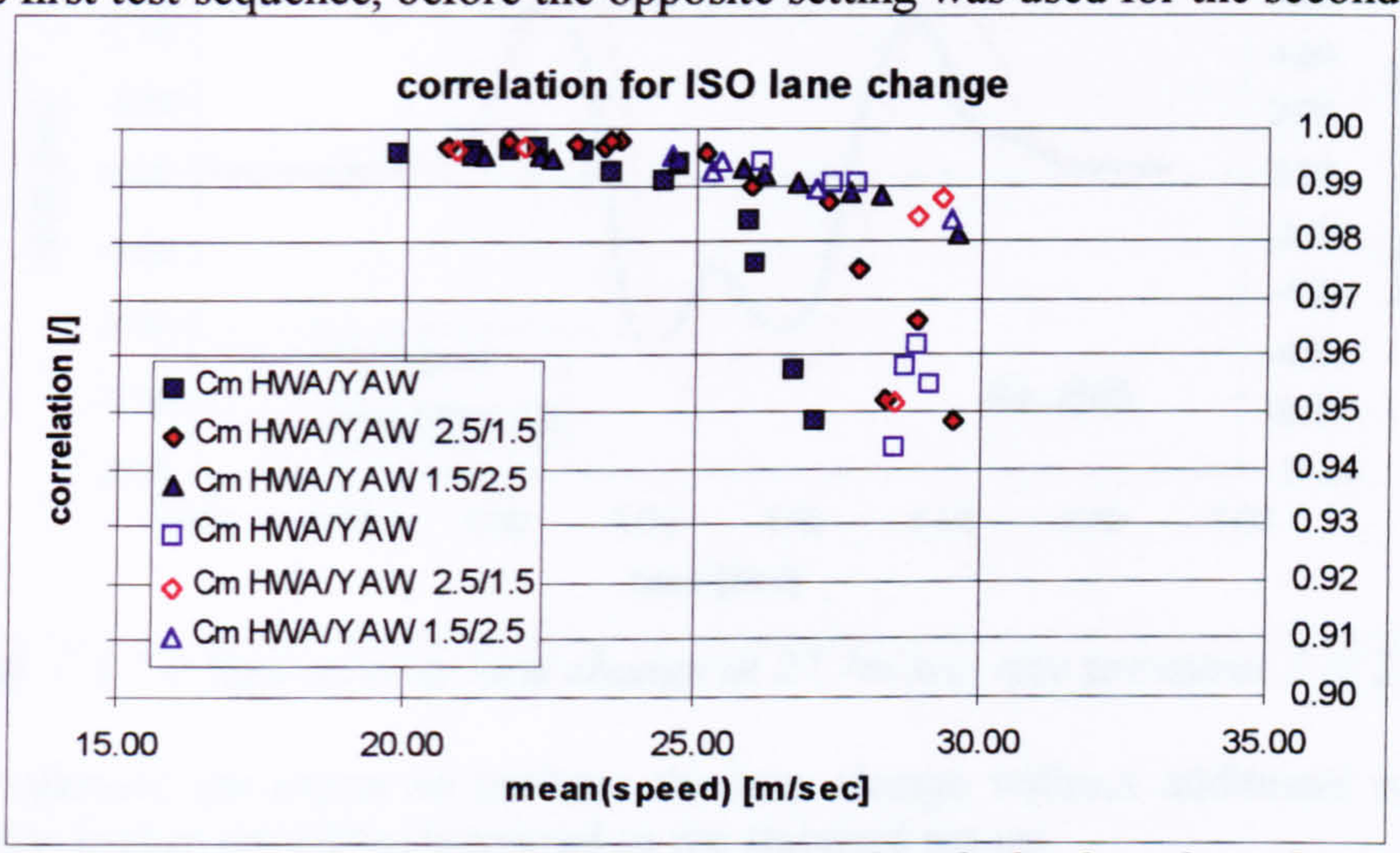

Fig. 7.3.1-1 maximum correlations between hand wheel angle and yaw rate

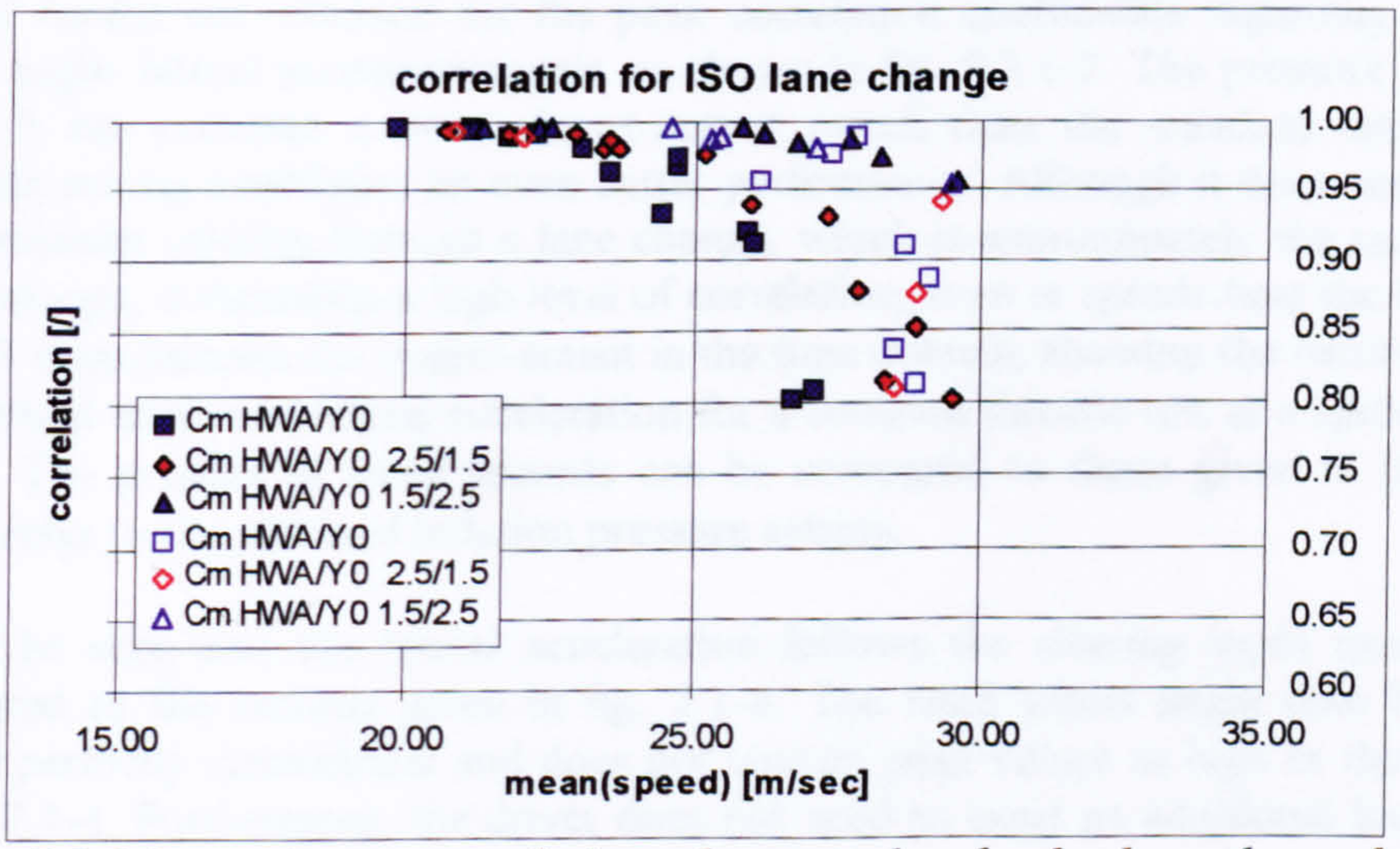

Fig. 7.3.1-2 maximum correlations between hand wheel angle and lat. acceleration

In fig. 7.3.1-1 the peak cross-correlation coefficients between hand wheel angle and yaw rate are plotted. Squares indicate test results obtained with tyres inflated to the nominal pressure, diamonds refer to the 2.5 bar front/ 1.5 bar rear setting and triangles to the opposite setting. Filled markers represent tests for which throttle application during the test was negligible, while their blank counterparts denote those for which the driver exerted additional throttle control. For all three settings the correlation coefficient remains above 0.9. However, the attitude control quality deteriorates slightly for the standard setting as well as for the low pressure setting at the rear, while the yaw rate correlation for the car fitted with higher inflated rear tyres remains almost unchanged. The setting with over-inflated front tyres establishes a smoother roll-off compared to the standard pressures.

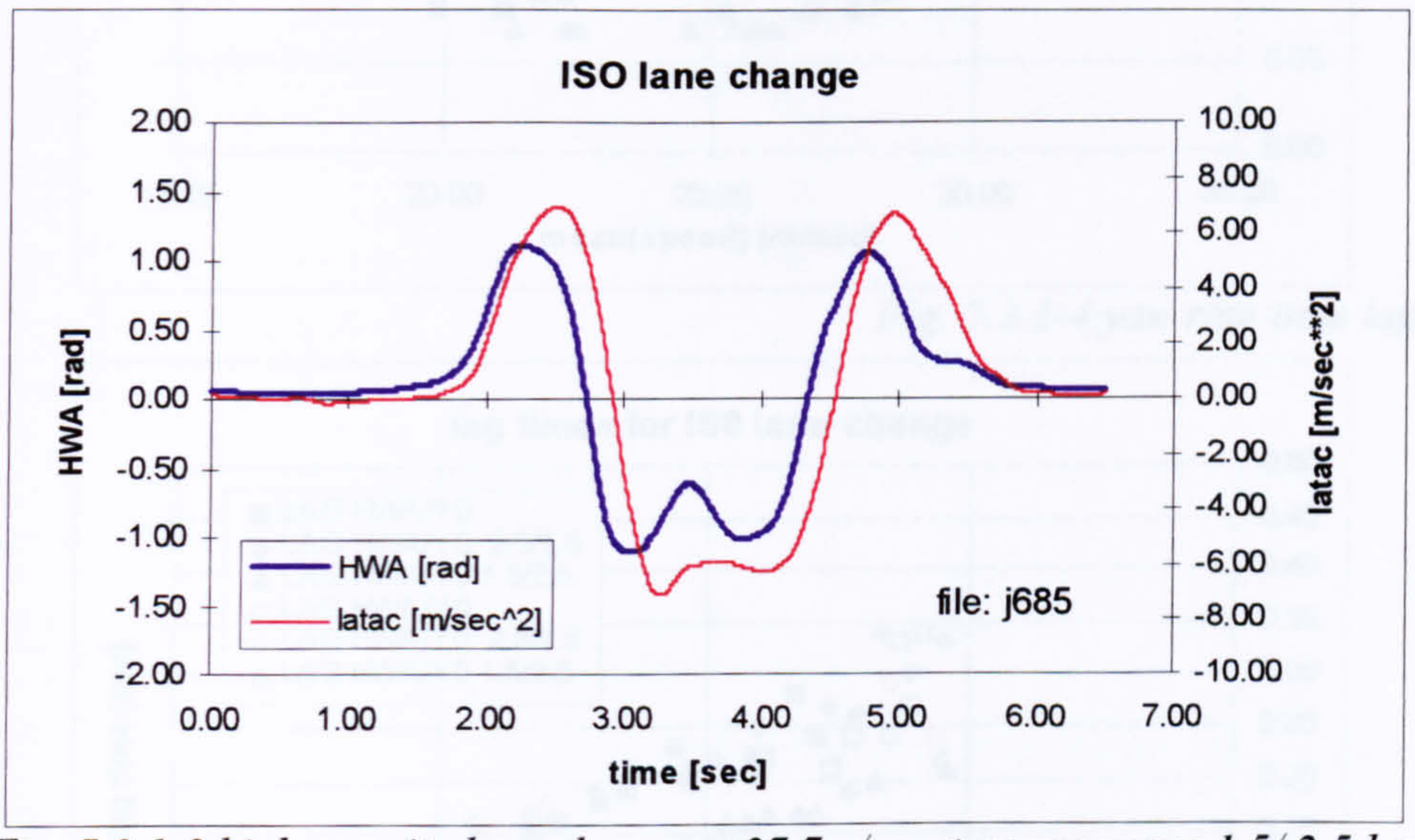

Fig. 7.3.1-3 high severity lane change at 27.7m/sec, tyre pressures 1.5/ 2.5 bar

It also allowed the driver to perform the lane change without additional use of the throttle at higher velocities compared to the standard set-up.

Similar results are obtained for the peak correlation coefficients regarding the hand wheel angle/ lateral acceleration pair, as shown in fig. 7.3.1-2. The pressure setting of 2.5/ 1.5 bar provides a better input-output match than the standard setting. The opposite setting establishes an even better performance. Although it does not improve the maximum velocity through a lane change, which is approximately the same for all three set-ups, it maintains a high level of correlation, even at speeds near the limit. Fig. 7.3.1-3 demonstrates the improvement in the time domain, showing the records for the hand wheel angle and lateral acceleration for a constant throttle test at a speed of 27.7 m/sec. The profiles of these records can be compared to those given in fig. 7.1-4, which refer to the standard inflation pressure setting.

It can be seen that the lateral acceleration follows the steering input much better compared to the records given in fig. 7.1-4. The hand wheel angle time history is almost perfectly symmetrical and does not contain peak values as high as those found in fig. 7.1-4. Furthermore, the driver does not need to exert an additional hand wheel

reversal after returning into the original lane, as he did when driving with the standard set-up.

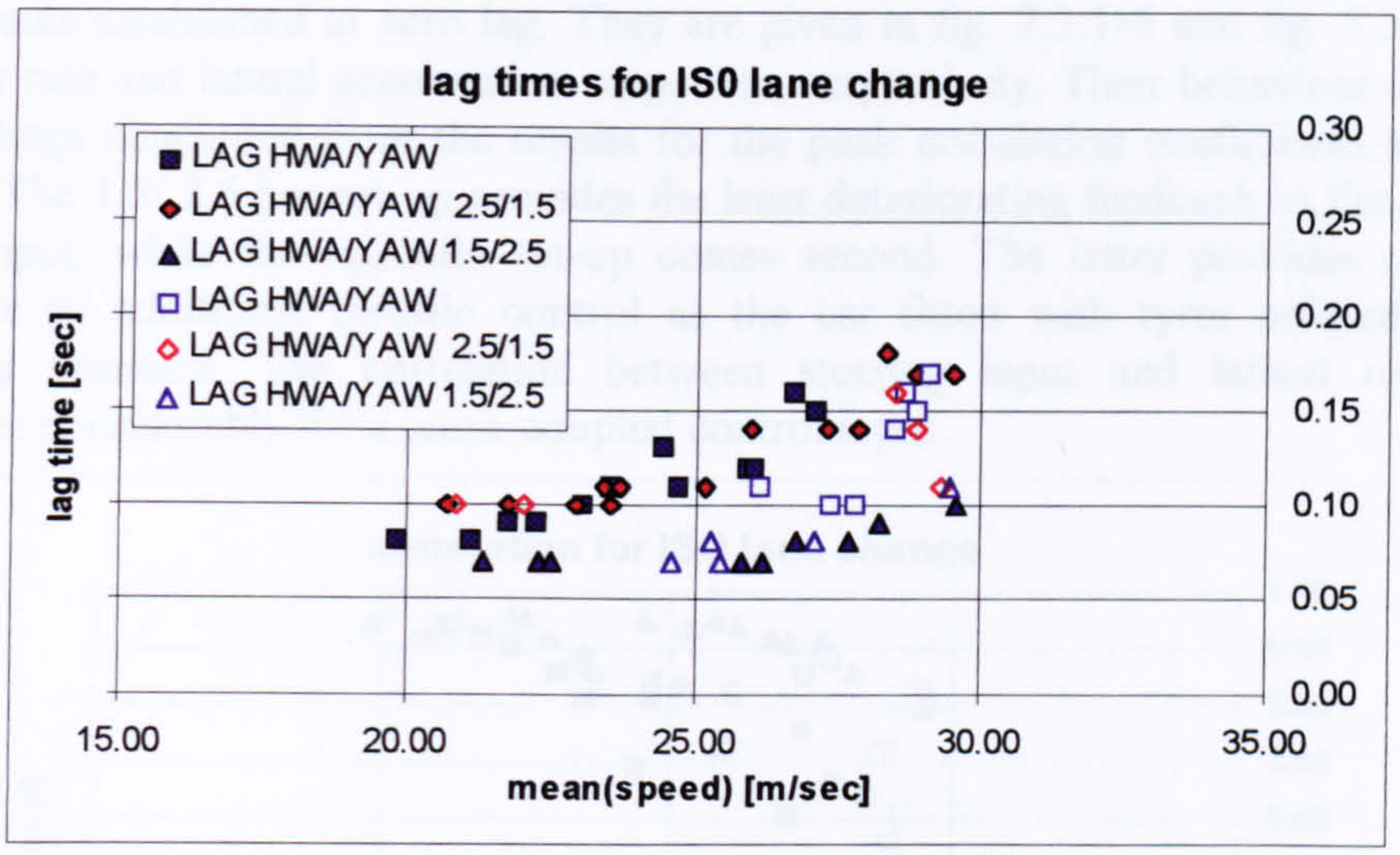

Fig. 7.3.1-4 yaw rate time lags

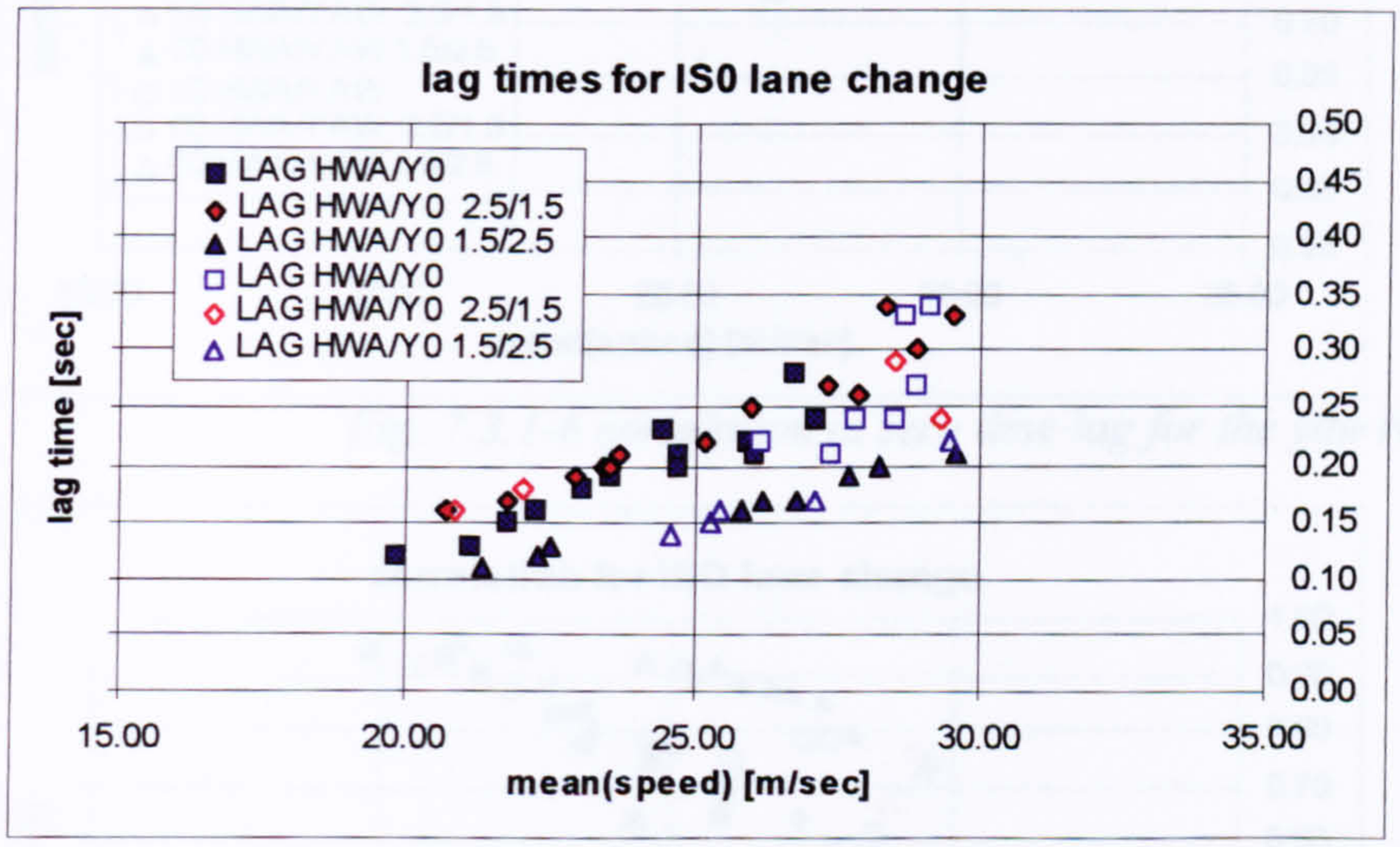

Fig. 7.3.1-5 lateral acceleration time lags

The graphs in figures 7.3.1-4 and 7.3.1-5 illustrate the differences for the three set-ups in their response delay characteristics. The 1.5/ 2.5 bar set-up provides the fastest yaw rate response to a steering wheel input, as can be seen from fig. 7.3.1-4. Its average time lag remains almost constant at a level below 0.1 seconds. There is little difference between the other two settings. For them the yaw rate time lag increases with forward speed up to 0.18 seconds at the maximum speed possible.

The lateral acceleration delays, given in fig. 7.3.1-5, behave in a very similar fashion, though they are longer than those for the yaw rate response. Again, the 1.5/ 2.5 bar setting establishes the fastest as well as the least sensitive response. The lag times for this setting increase only mildly with an increase in manoeuvre severity.

The effects of a deteriorating peak cross-correlation and increasing time delays in combination with increasing vehicle speeds are represented by the correlation coefficients established at zero lag. They are given in fig. 7.3.1-6 and fig. 7.3.1-7 for the yaw rate and lateral acceleration responses, respectively. Their behaviour confirms the findings concluded from the results for the peak correlation coefficients and time delays. The 1.5/ 2.5 bar set-up provides the least deteriorating feedback to the steering angle input, while the opposite set-up comes second. The latter provides a similar response to additional throttle control as the car fitted with tyres inflated to the standard pressure. The correlation between steering input and lateral responses increases considerably for a cross-coupled control input.

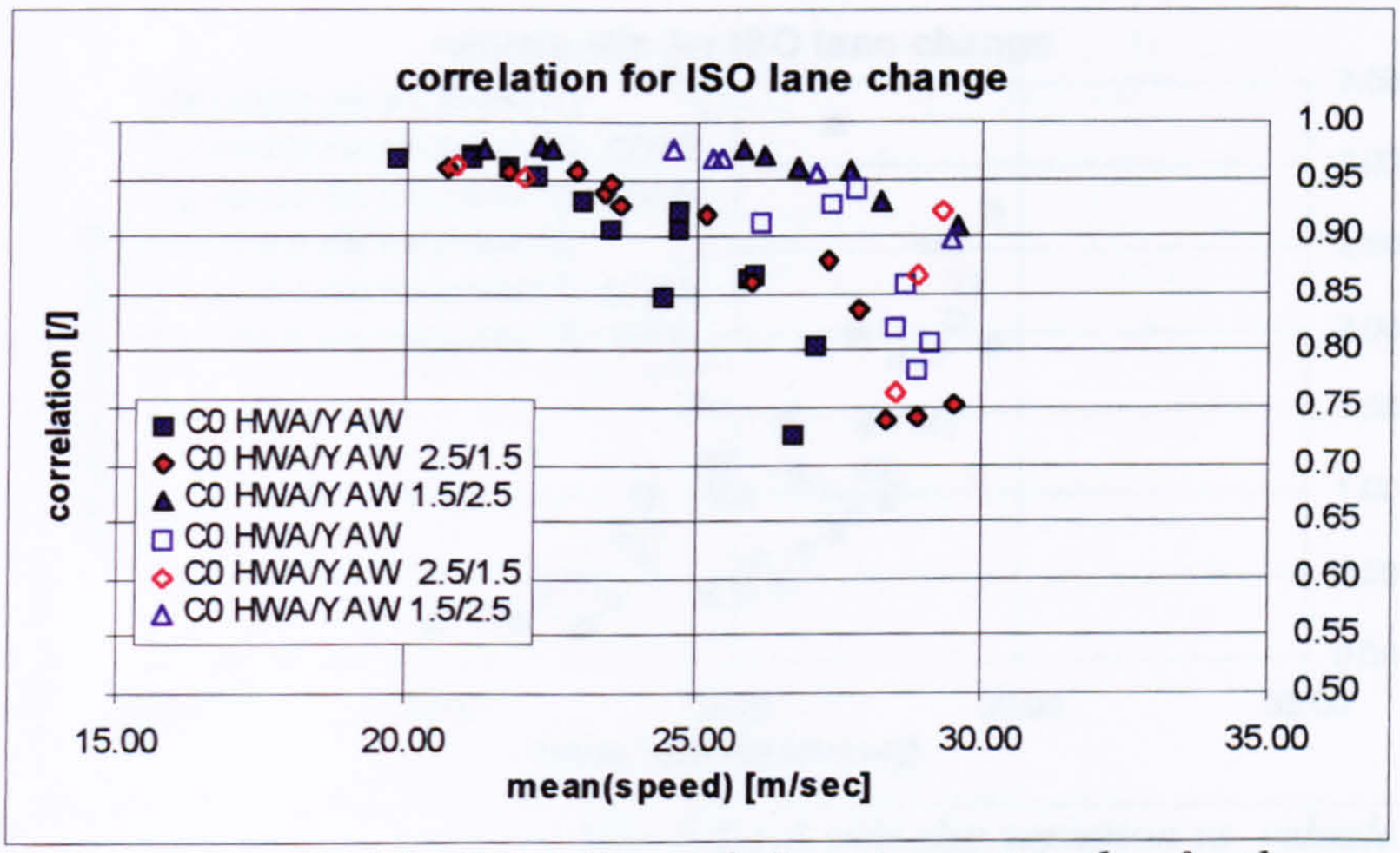

Fig. 7.3.1-6 correlation at zero time lag for the yaw rate

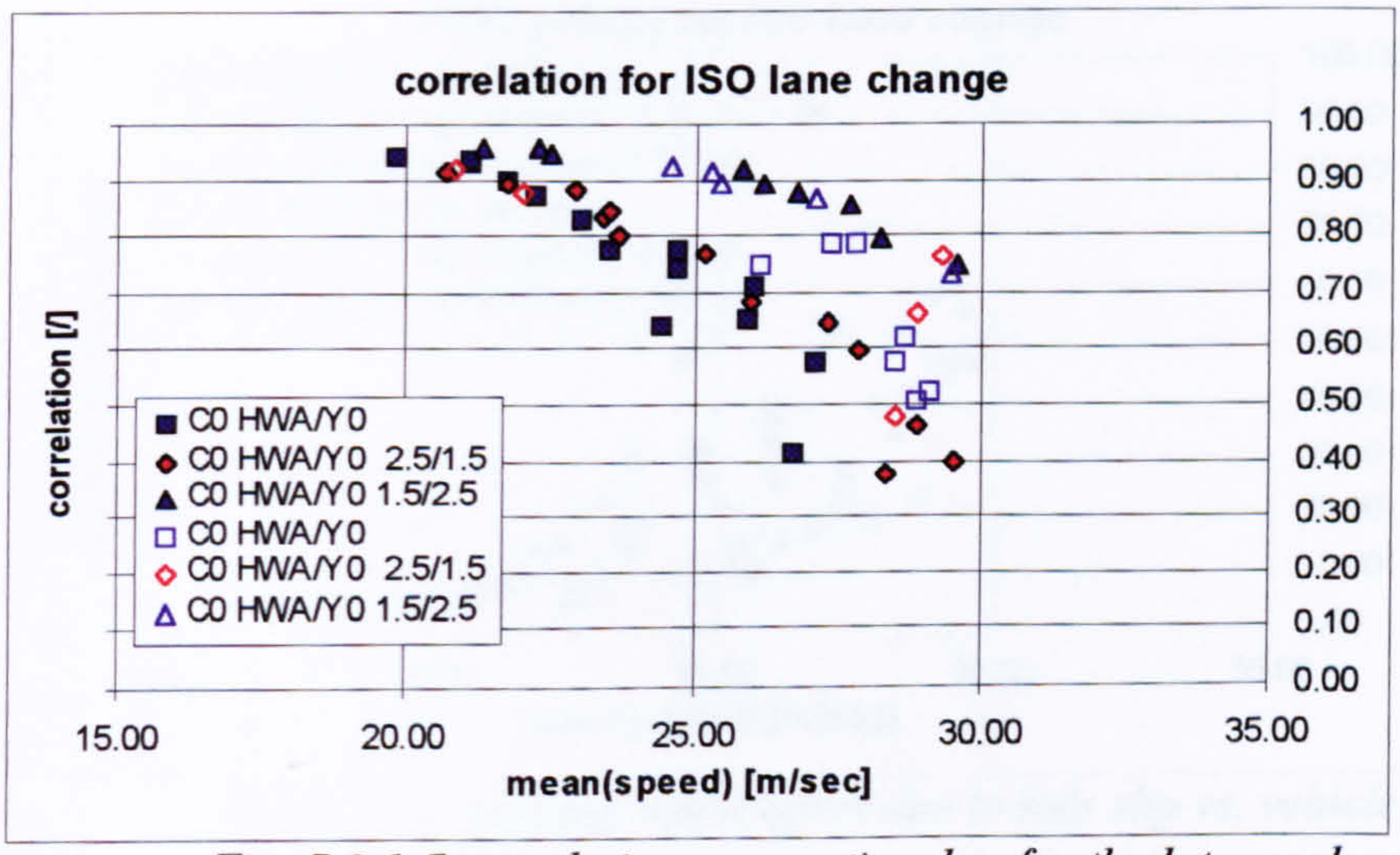

Fig. 7.3.1-7 correlation at zero time lag for the lat. acceleration

Results relating the hand wheel torque to the lateral responses are rather similar for the three set-ups and are therefore omitted. The following graphs address the influence of the increasing side slip motion on the limit controllability. Fig. 7.3.1-8 represents the side slip acceleration as defined by (7.1.2). The lateral acceleration is

in phase with the yaw rate response for low severity manoeuvering, indicated by a low value for the side slip variations $\sigma_{\dot{\beta}}$. Towards the limit the side slip increases for all three cases. However, the vehicle fitted with over-inflated rear tyres limits at a much lower level of side slip variation than was the case for the other two pressure settings. The most pronounced increase in side slip with manoeuvre severity is observed for the standard set-up. The side slip motion is contained effectively by some superimposed throttle application at tests near the limit speed. Its peak value of 3.25 m/sec^2, obtained for the standard set-up, is equivalent to approximately 40% of the acceleration established by the product of vehicle speed and yaw rate, $v \cdot \dot{\psi}$.

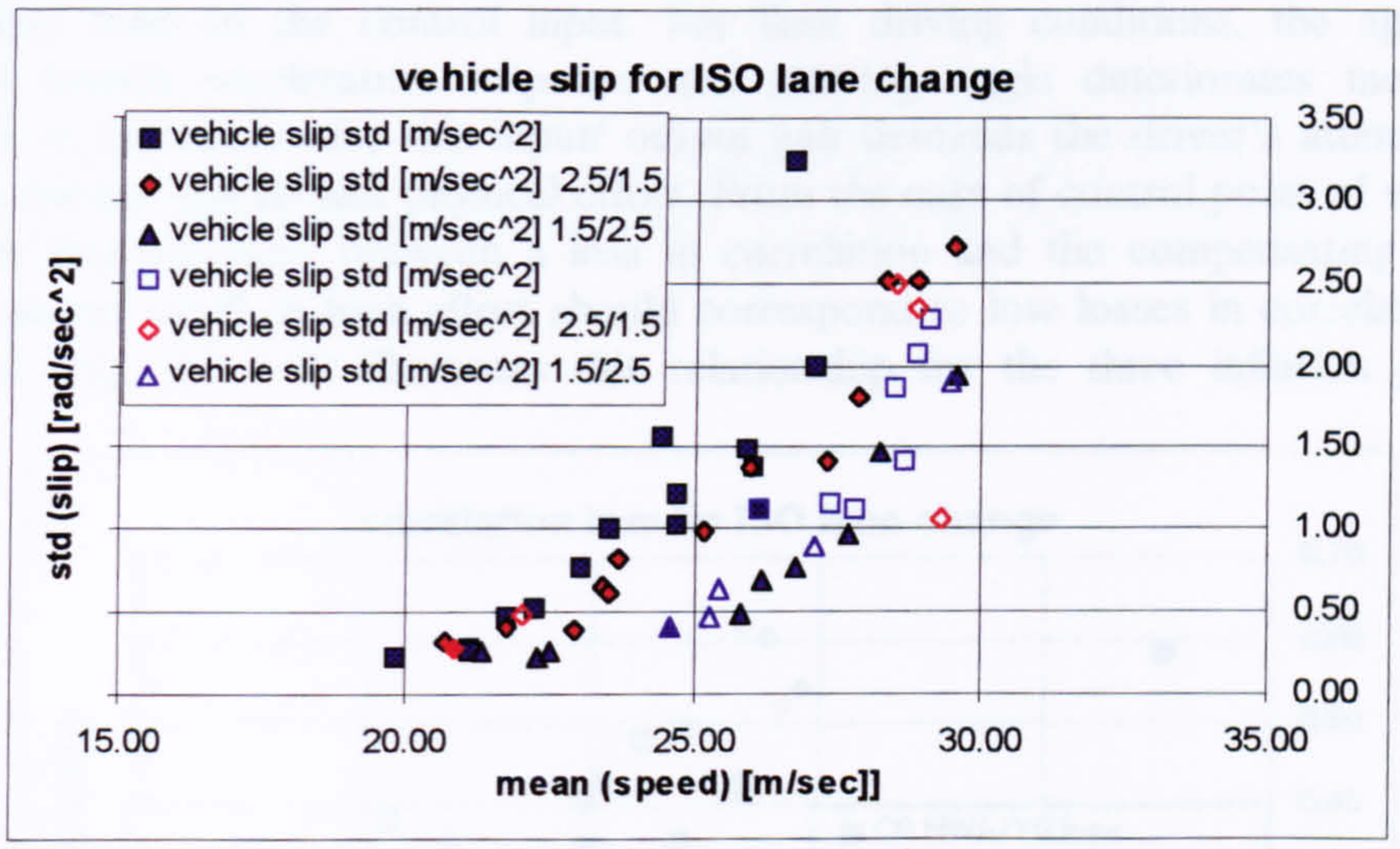

Fig. 7.3.1-8 side slip variation vs. vehicle speed

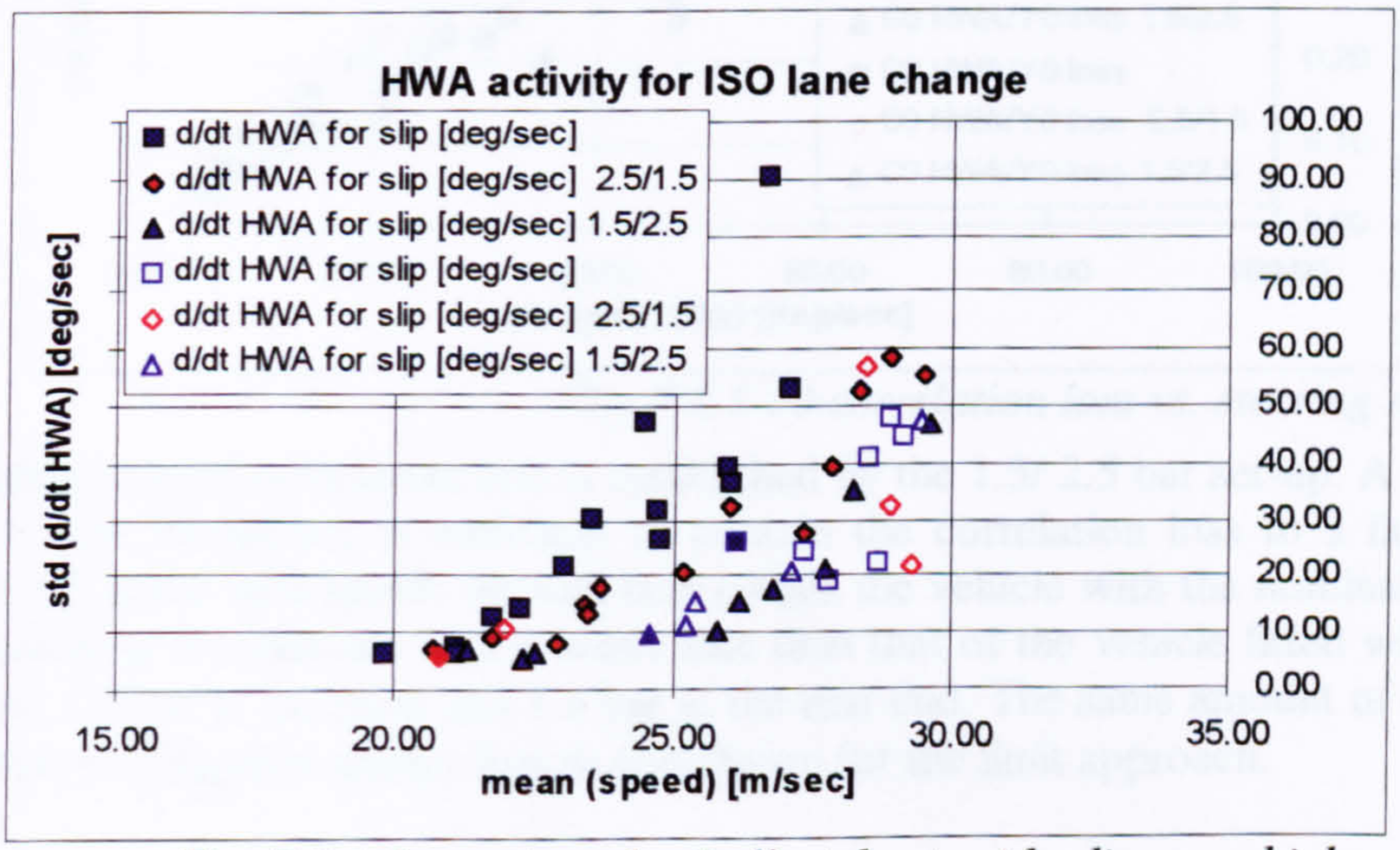

Fig. 7.3.1-9 steering wheel effort due to side slip vs. vehicle speed

The hand wheel angle activity associated with controlling the side slip motion, $\sigma_{\dot{\delta},\beta}$, which was proposed in section 7.1 as a measure for the control strain, is shown in fig. 7.3.1-9. It corresponds to the graph showing the side slip motion characteristics.

The standard set-up requires a comparatively high steering effort for controlling the side slip motion of the vehicle, especially for manoeuvres carried out with a constant throttle position. The 1.5/ 2.5 bar setting allows driving through the lane change with the lowest control effort.

Plotting the cross-correlation coefficient at zero time lag for the hand wheel angle/ lateral acceleration pair against the steering wheel activity $\sigma_{\dot{\delta},\beta}$ reveals how well the control feedback can be maintained by increasing the control effort. A driver performing a limit manoeuvre has to be most concerned about those responses, correlating least to the control input. For limit driving conditions, the agreement between lateral acceleration response and steering angle deteriorates most. The decrease in correlation for this input/ output pair demands the driver's attention and requires further mental and physical effort. From the ease of control point of view it is desirable that the ratio between a loss in correlation and the compensating control effort remains small. A high effort should correspond to low losses in correlation and feedback. Fig. 7.3.1-10 illustrates this relationship for the three inflation pressure settings.

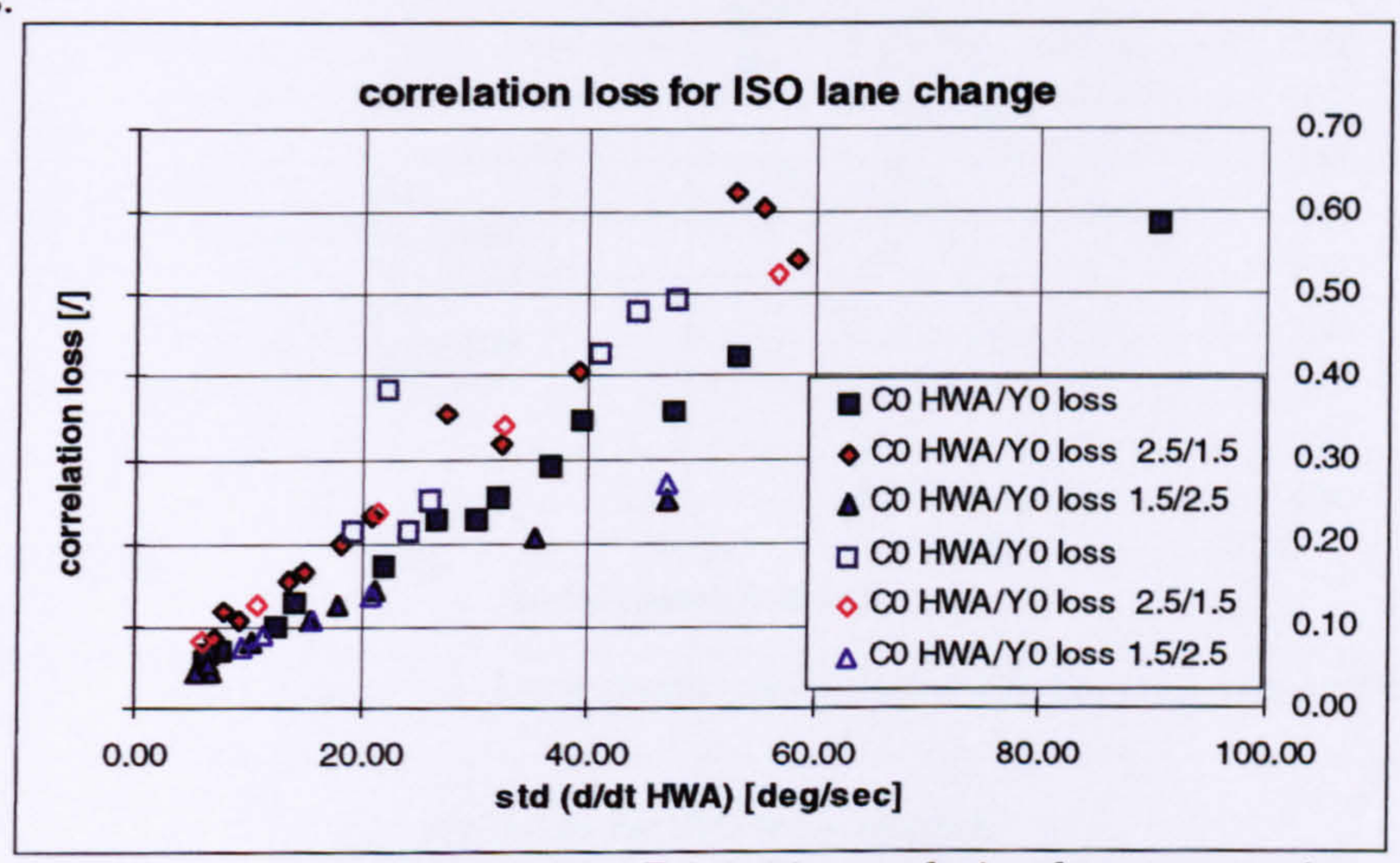

Fig. 7.3.1-10 correlation loss vs. steering effort

The smallest rate of correlation loss is established by the 1.5/ 2.5 bar set-up. A steering effort of only 50 deg/sec is sufficient to contain the correlation loss to a fairly low value of 0.3 at the limit speed. Second best comes the vehicle with the nominal set-up, whose handling deteriorates with a lower rate than that of the vehicle fitted with tyres inflated to 2.5 bar at the front and 1.5 bar at the rear end. The same amount of steering effort leads to a slightly smaller loss in correlation for the limit approach.

summary of test results

The results presented in this section demonstrate the influence of the inflation pressure on the limit handling performance. They establish noticeable differences in the limit behaviour. The vehicle with under-inflated front and over-inflated rear tyres performed significantly better than when it was equipped with tyres inflated according to the other

two pressure settings. This pressure setting provided a faster response, which deteriorated by a small rate with increasing severity. However, its maximum speed of 29.5 m/sec was matched by the car fitted with tyres inflated to the opposite pressures. Overinflating the front tyres and deflating the rear tyres by 0.5 bar enabled the driver to perform the lane change at higher speeds with the throttle held constant than he managed with the standard set-up. This improvement may be partly ascribed to the newly acquired skill obtained from practicing this manoeuvre more often. On the other hand, it may well be that the higher front tyre pressure increased the front cornering stiffness, thereby reducing the required slip of the front tyres, and also extended the limit grip of the front axle.

Although the standard set-up has a lower limit speed for tests, for which the throttle was kept constant, than the former, it provides a smoother limit approach. The rate by which the correlation between input and output deteriorates with steering control effort is slightly smaller.

7.3.2 Effects of tyre construction on ISO lane change handling performance

The proving ground program also involved testing of alternative tyre constructions. ISO lane changes were carried out for two of them. The test vehicle was tested fitted with a set of Dunlop M2 winter tyres of the size 225/60 R16 as well as with a set of experimental slick tyres (plain tread) on 18 inch rims. Further tests were conducted by fitting these tyres either to the front or rear axle. All these tests were performed by driver B.

This section summarises the handling performance of the Jaguar test vehicle fitted with a complete set of either of these tyre designs, whereas in the following section the mixed tyre set-ups are compared against each other. As in the previous section, results are compared to those of the standard car equipped with standard tyres inflated to the recommended pressure.

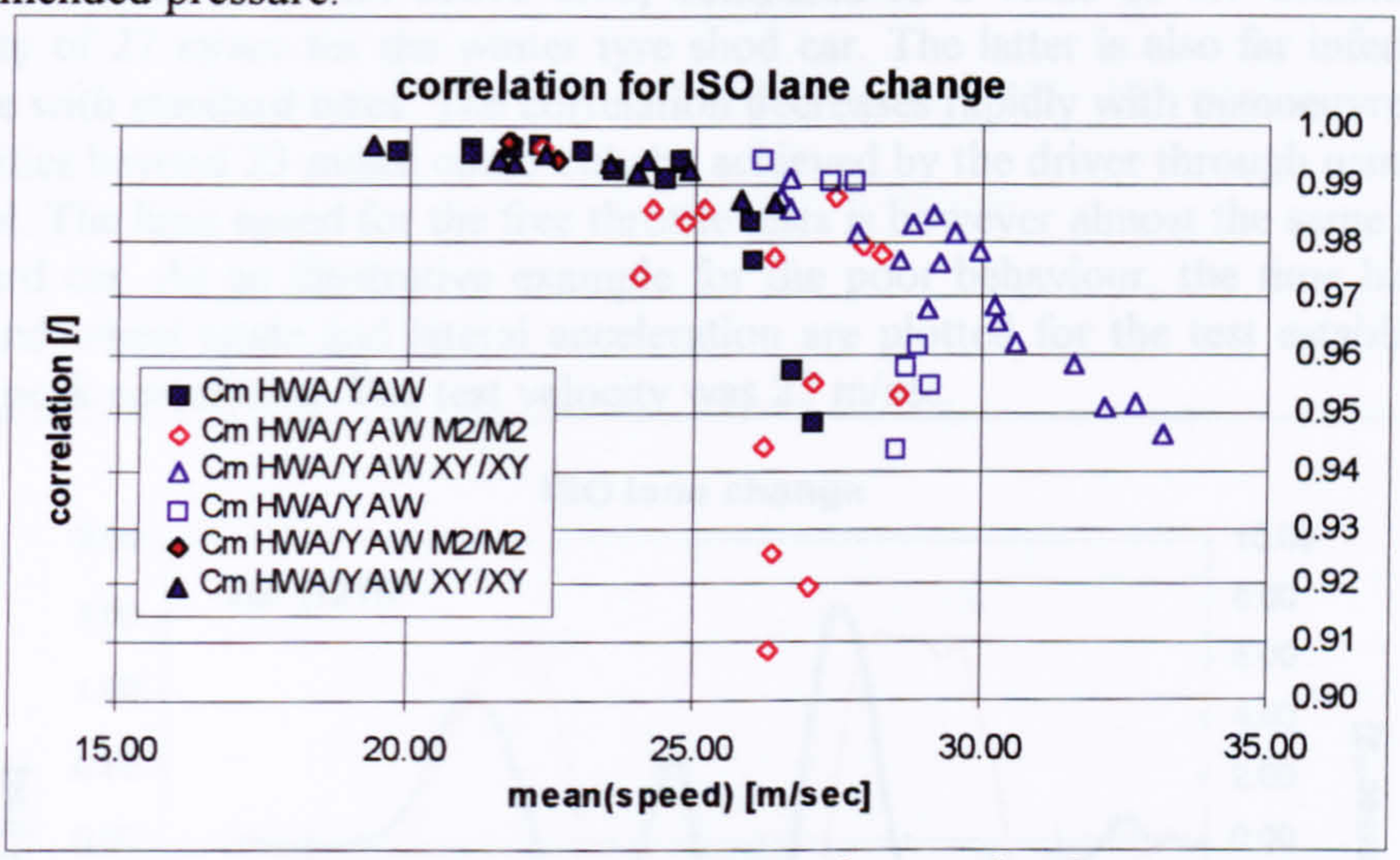

Fig. 7.3.2-1 maximum correlations for the yaw rate response

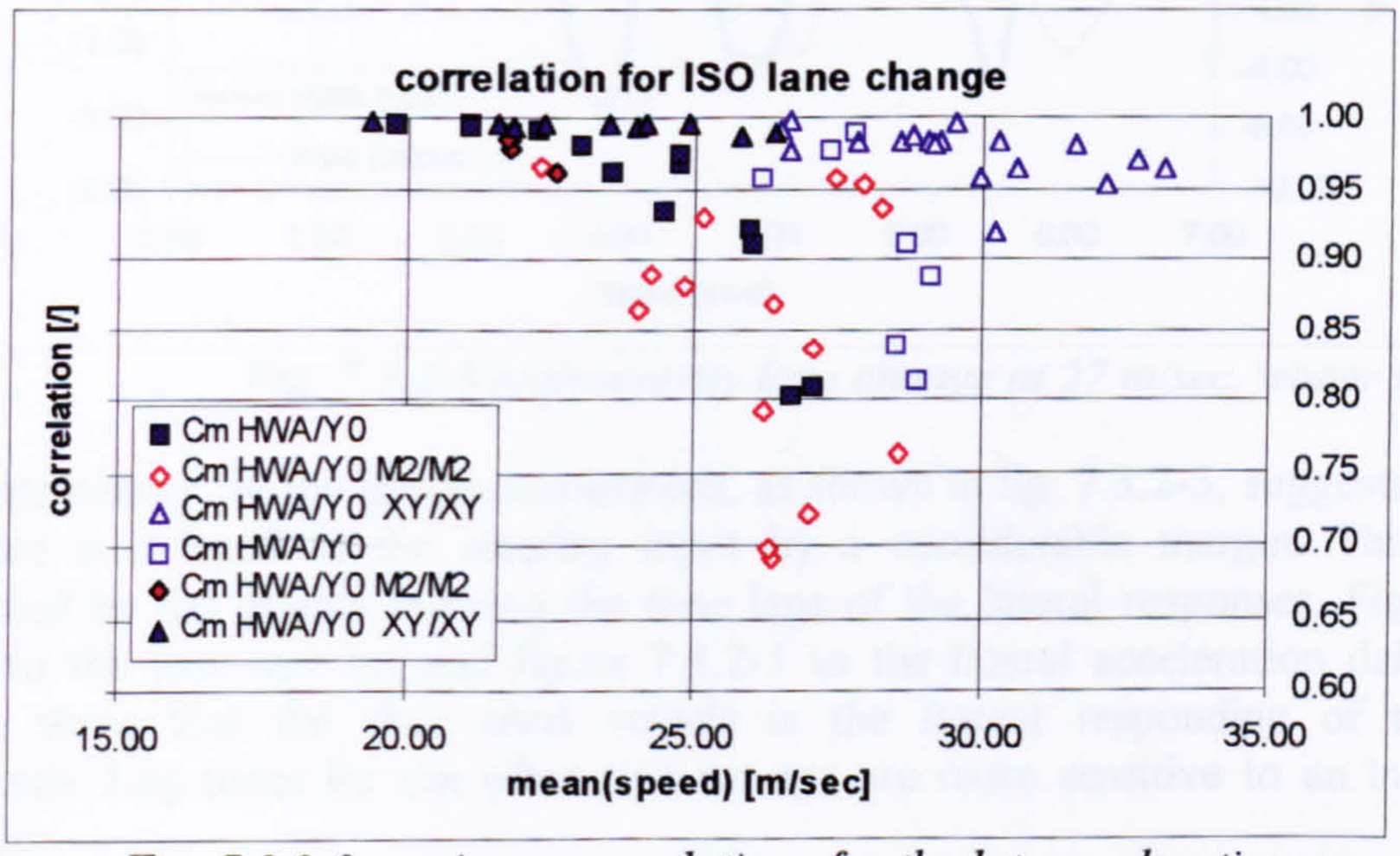

Fig. 7.3.2-2 maximum correlations for the lat. acceleration response

Fig. 7.3.2-1 and fig. 7.3.2-2 show the peak cross-correlation coefficients obtained for the two lateral responses, yaw rate and lateral acceleration respectively, with regard to the steering angle input. Results for the standard set-up are marked as before. The vehicle fitted with slick tyres is referenced by 'XY/XY', whereas results referring to the winter tyre shod vehicle are denoted by 'M2/M2'.

It is apparent that the slick shod vehicle has a marked performance advantage, in that it achieves by far the highest speed through the double lane change. However, the driver used a combination of steering and throttle control to achieve this goal. The limit speed established with a constant throttle is similar to that achieved with the standard tyres. The slick shod vehicle also distinguishes itself by maintaining a very high correlation between the control input and the corresponding responses. Especially, the correlation concerning the lateral acceleration remains at a very high level. At the limit speed of about 33 m/sec it is still above 0.95, compared to a value of 0.7 established at a velocity of 27 m/sec for the winter tyre shod car. The latter is also far inferior to the vehicle with standard tyres. The correlation decreases rapidly with manoeuvre severity. Velocities beyond 23 m/sec could only be achieved by the driver through using throttle control. The limit speed for the free throttle tests is however almost the same as for the standard car. As an illustrative example for the poor behaviour, the time histories of the hand wheel angle and lateral acceleration are plotted for the test establishing the worst peak correlation. The test velocity was 27 m/sec.

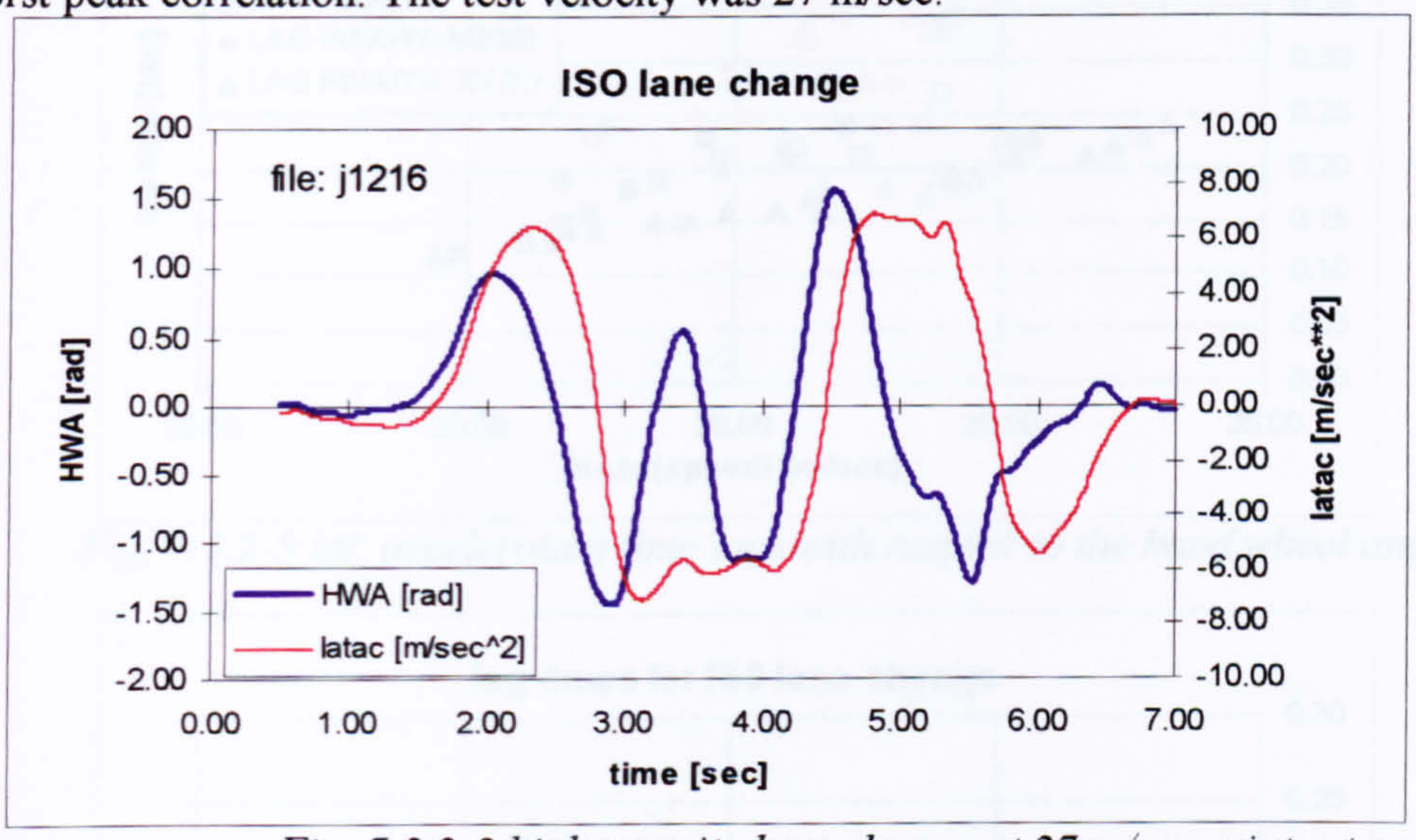

Fig. 7.3.2-3 high severity lane change at 27 m/sec, winter tyres

The time history for the lateral acceleration, as shown in fig. 7.3.2-3, suggests that this response is delayed to the steering input by a considerable margin. This can be confirmed by the graphs showing the time lags of the lateral responses. Fig. 7.3.2-4 refers to the yaw rate lag and figure 7.3.2-5 to the lateral acceleration delay. Both graphs show that the slick shod vehicle is the fastest responding of the three specimens. Lag times for the other two set-ups are more sensitive to an increase in severity.

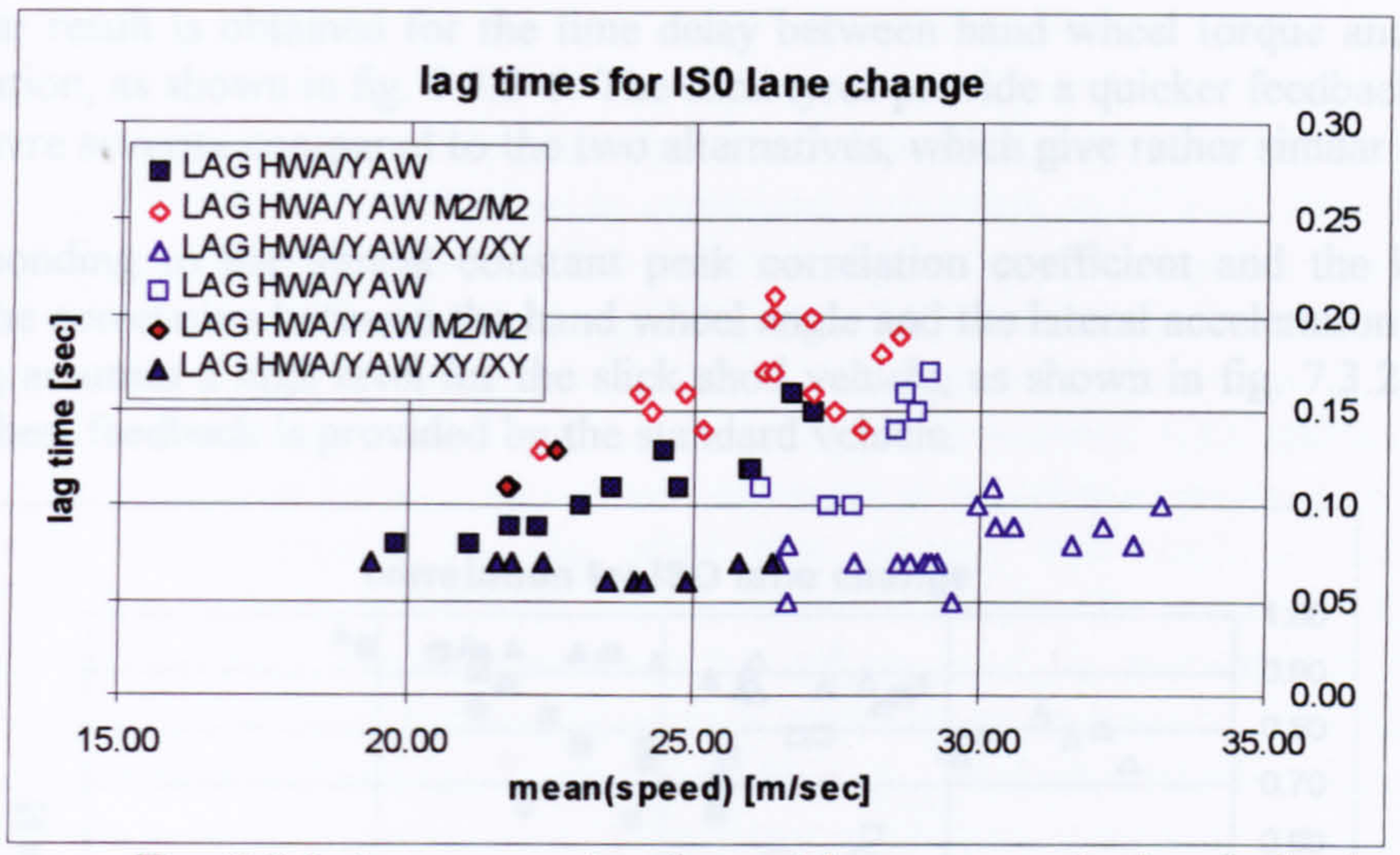

Fig. 7.3.2-4 yaw rate time lags with respect to the hand wheel angle

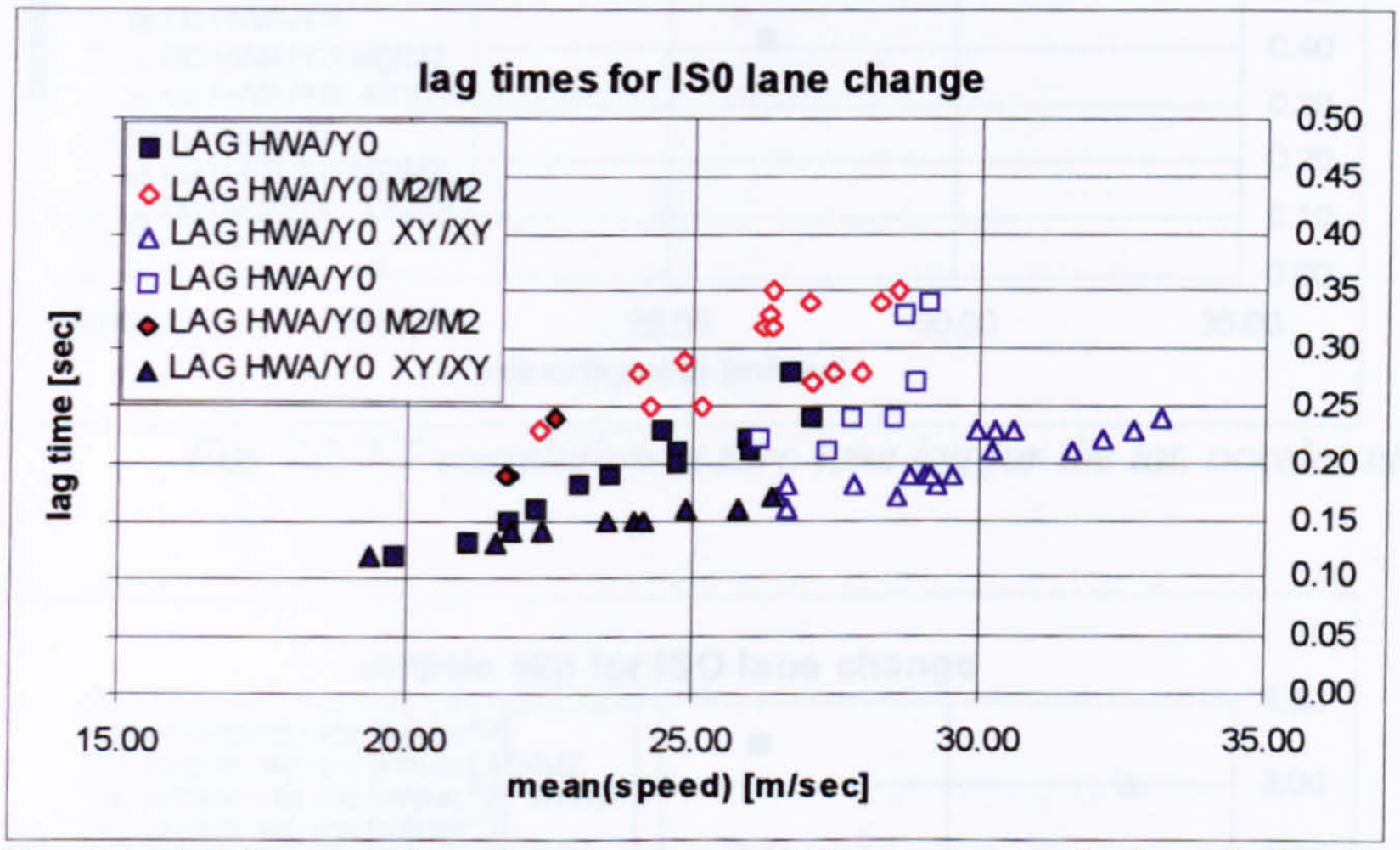

Fig. 7.3.2-5 lat. acceleration time lags with respect to the hand wheel angle

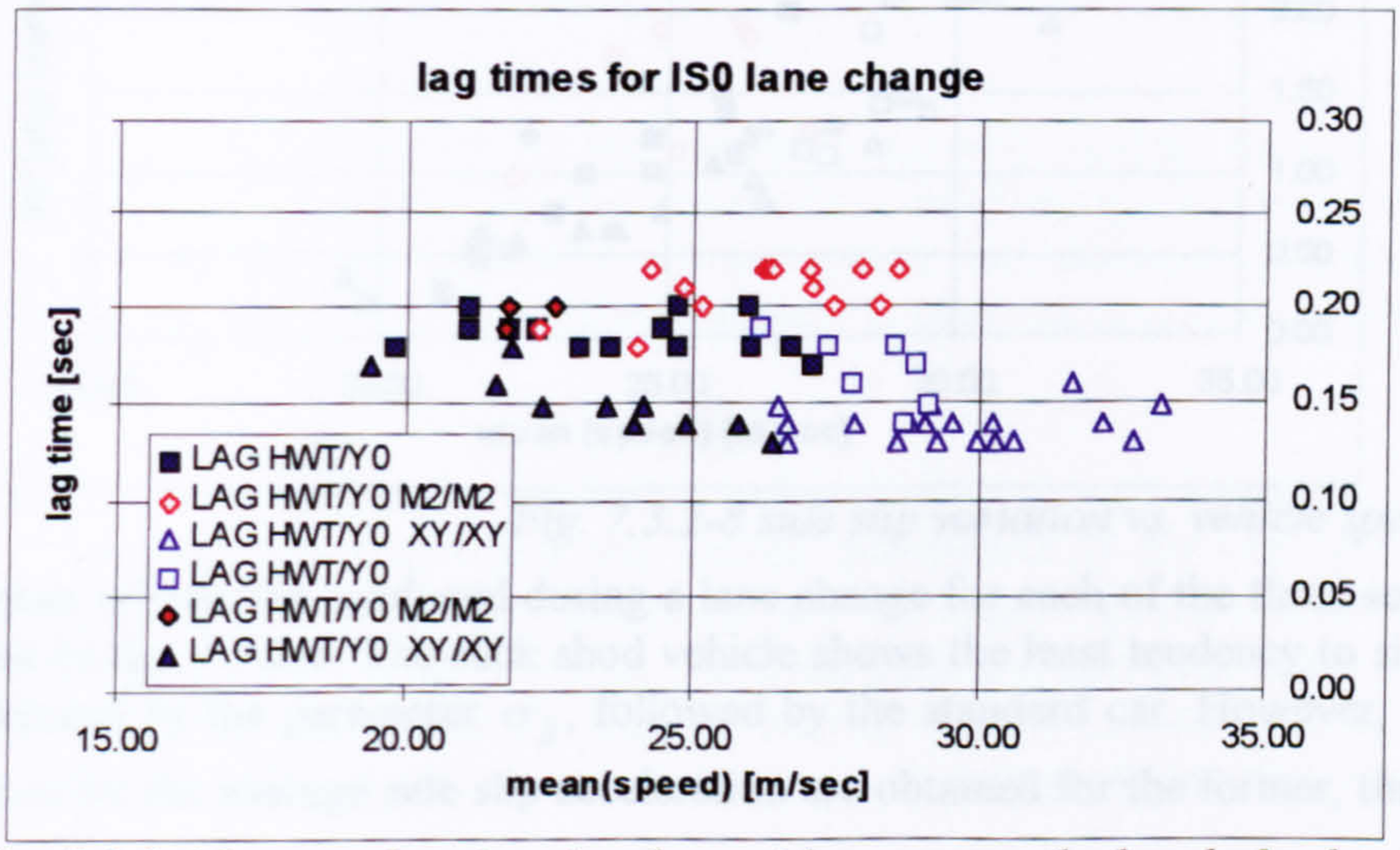

Fig. 7.3.2-6 lat. acceleration time lags with respect to the hand wheel torque

A similar result is obtained for the time delay between hand wheel torque and lateral acceleration, as shown in fig. 7.3.2-6. The slick tyres provide a quicker feedback of the manoeuvre severity compared to the two alternatives, which give rather similar results.

Corresponding to the almost constant peak correlation coefficient and the low lag times, the correlation between the hand wheel angle and the lateral acceleration at zero time lag assumes a high level for the slick shod vehicle, as shown in fig. 7.3.2-7. The second best feedback is provided by the standard vehicle.

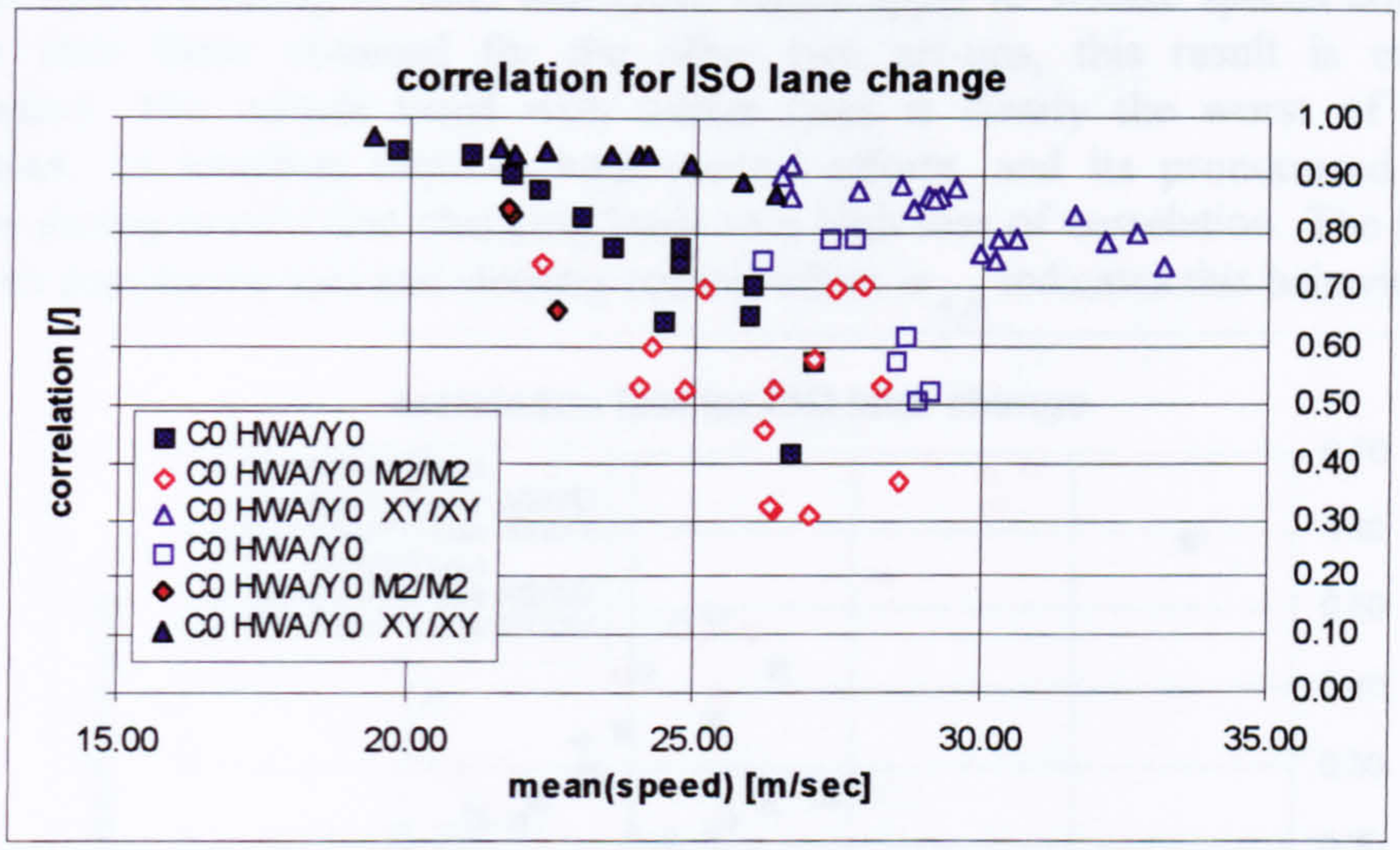

Fig. 7.3.2-7 correlation at zero time lag for the lat. acceleration

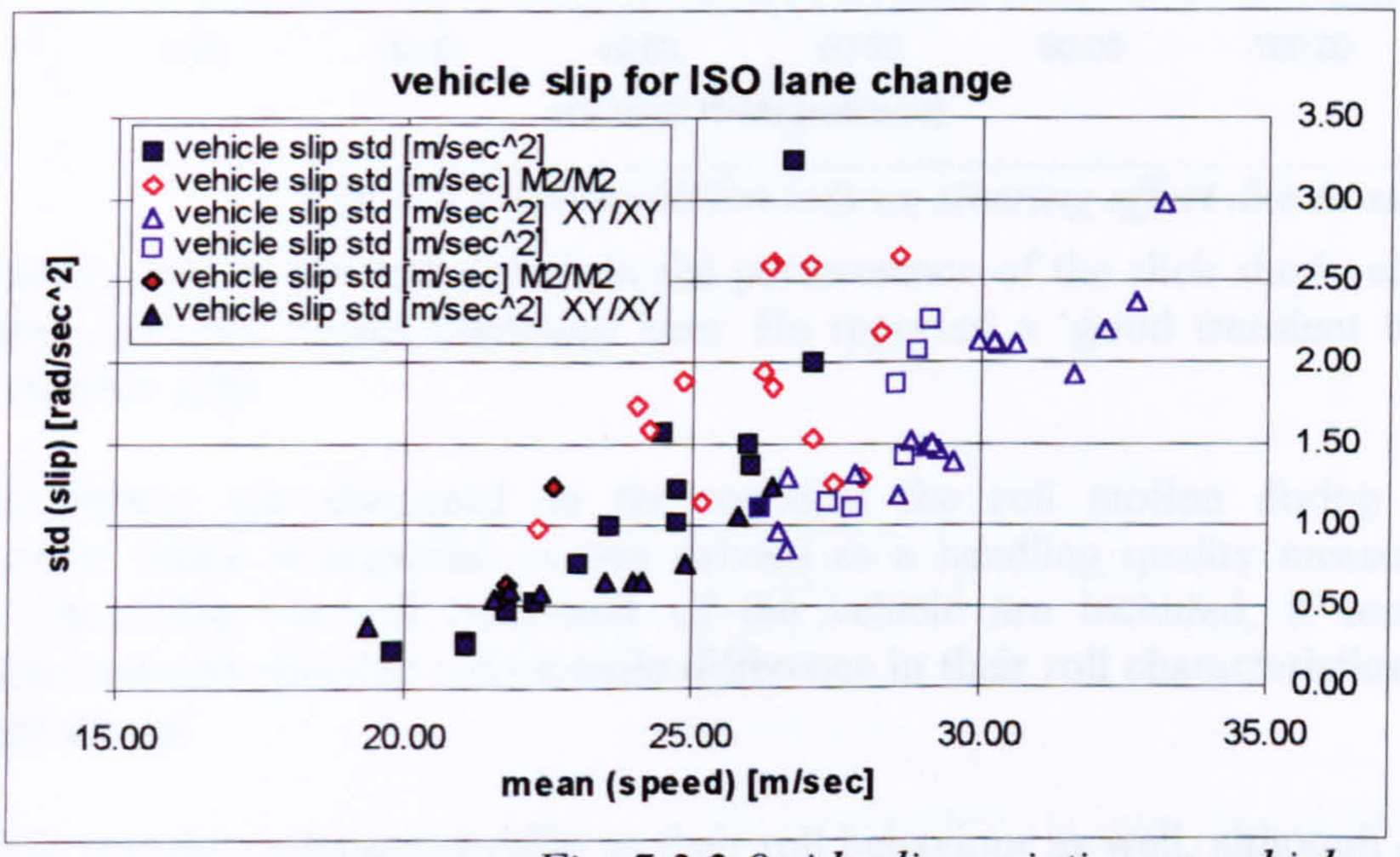

Fig. 7.3.2-8 side slip variation vs. vehicle speed

The amount of side slip produced during a lane change for each of the three set-ups is illustrated by fig. 7.3.2-8. The slick shod vehicle shows the least tendency to side slip, as represented by the parameter $\sigma_{\dot{\beta}}$, followed by the standard car. However, equally high values for the average side slip acceleration are obtained for the former, though at

higher forward speeds.

From the average side slip motion and the standard deviation of the hand wheel speed a measure for steering control effort is computed, according to (7.1.3). This measure, representing the steering activity due to side slip, is plotted against the loss of correlation between the hand wheel angle input and the lateral acceleration response, as shown in fig. 7.3.2-9. The graph illustrates the superior performance of the slick tyres. For limit conditions a low loss in correlation is maintained with relatively small control effort. Bearing in mind that these values apply to vehicle speeds considerably higher than those obtained for the other two set-ups, this result is even more impressive. The vehicle fitted with winter tyres is clearly the worst of the three examples. Its handling requires high control efforts, and its pronounced side slip motion during severe lane changing leads to a high loss of correlation. The high ratio between correlation loss and steering control effort $\sigma_{\dot{\delta},\beta}$ indicates this behaviour.

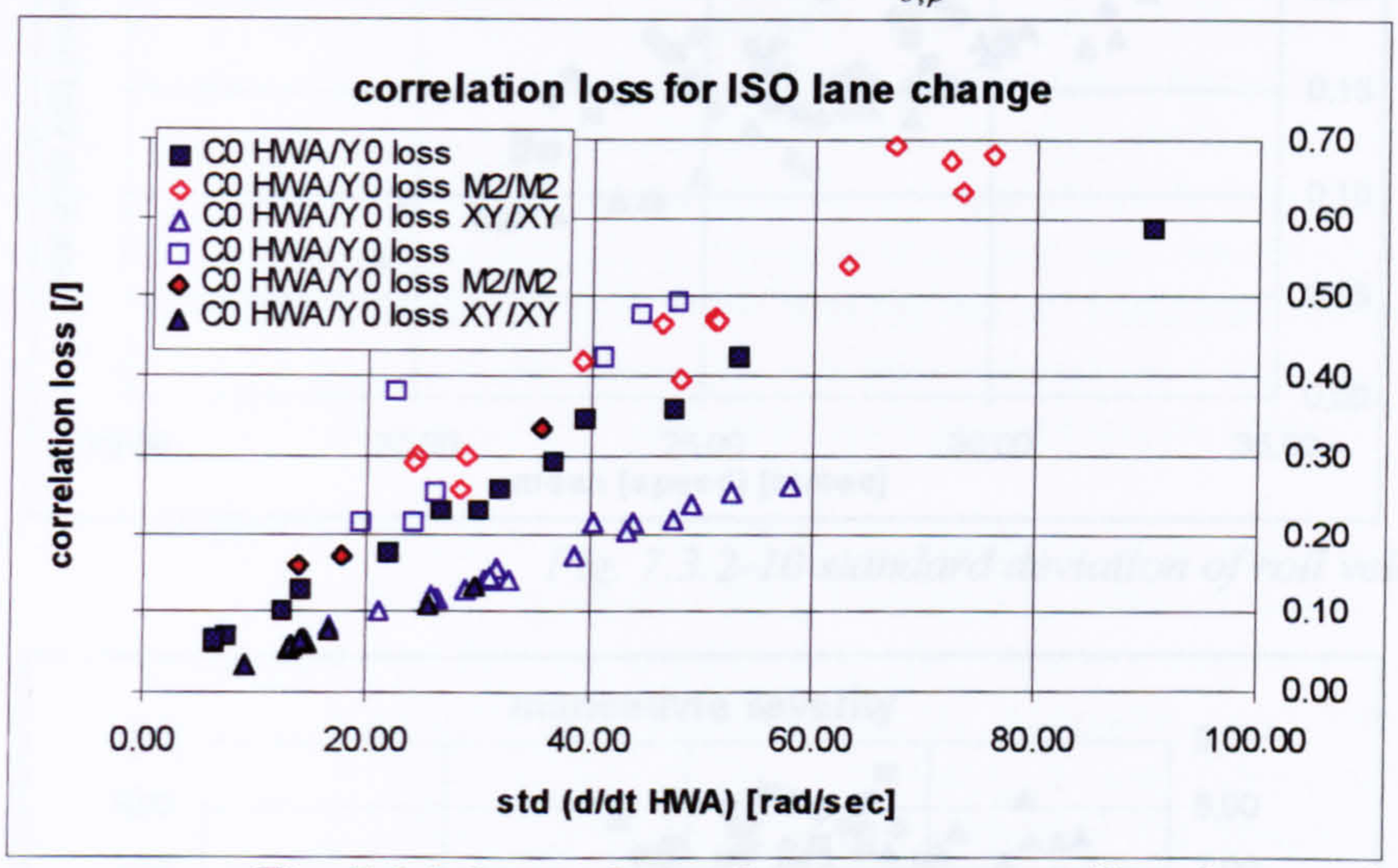

Fig. 7.3.2-9 correlation loss vs. steering effort due to side slip

Comments made by the test driver on the performance of the slick shod vehicle were consistent with the results discussed here. He reported a 'good transient behaviour' and a superior grip.

Another aspect not discussed so far concerns the roll motion during a severe manoeuvre, which is regarded by test drivers as a handling quality measure. Some results describing the roll behaviour of the vehicle are included, if tests of the alternative set-ups revealed a noticeable difference in their roll characteristics from the standard set-up.

The three set-ups investigated differ in their roll behaviour as well, although only their tyres are different. The suspension and weight distribution of the vehicle remained unchanged. The slick shod vehicle shows far less roll angle variations than the other two specimens, as shown in fig. 7.3.2-10. Here, the standard deviation of the roll angle derivative is plotted against vehicle speed. The roll velocity is used in order to put more emphasis on the speed by which the roll attitude changes. The lower roll

variations are not a consequence of a higher roll stiffness or damping, possibly provided by the slick tyres, but result from a smoother lateral acceleration profile. The slick tyres enable the driver to change lane with lower peak values and lower variations for the lateral acceleration. This can be seen from fig. 7.3.2-11, giving the peak values and standard deviation of the lateral accelerations. Those vehicle set-ups, featuring a more oscillatory lateral acceleration record, as illustrated by fig. 7.1-4 and fig. 7.3.2-3, tend to produce more roll angle variations.

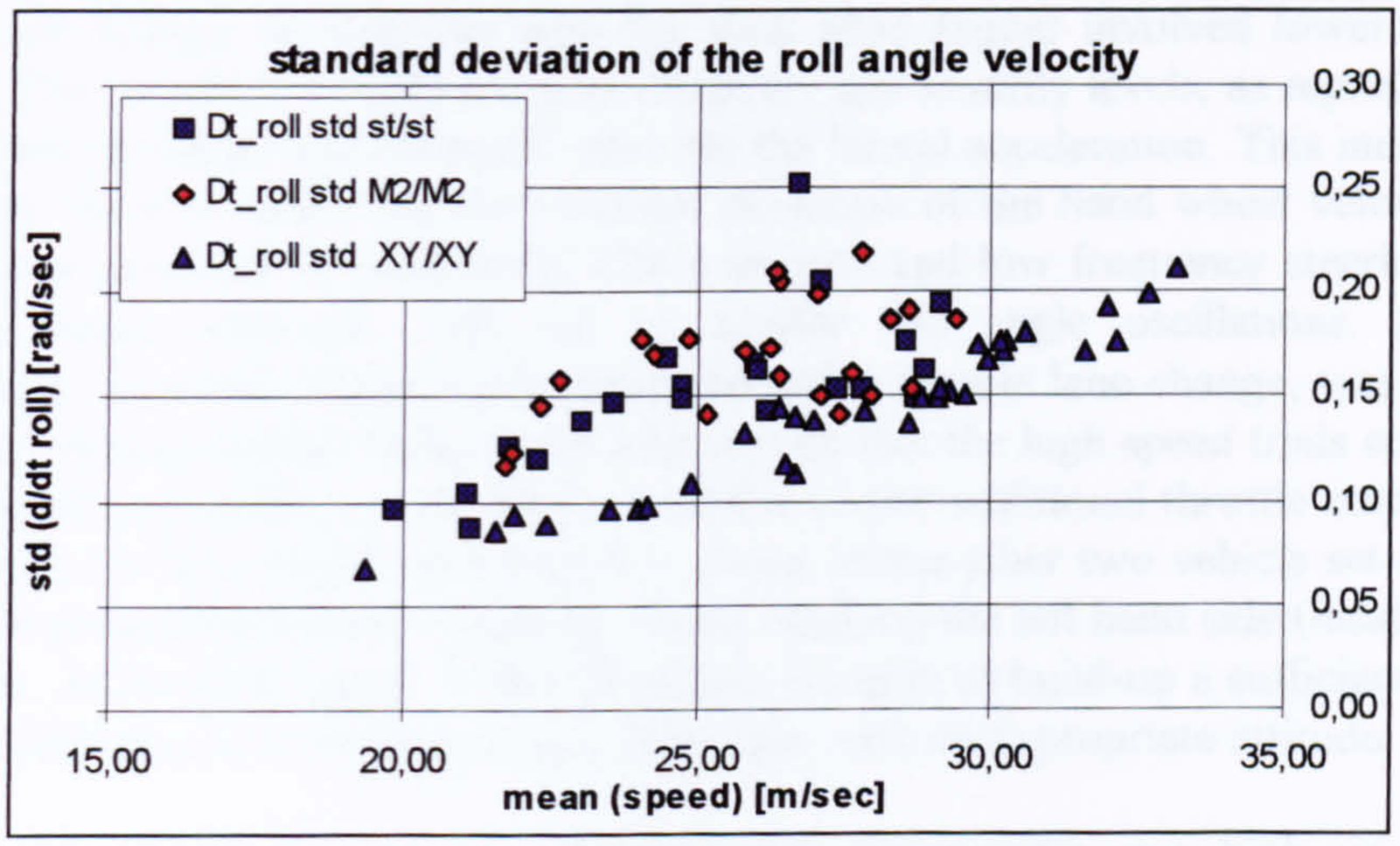

Fig. 7.3.2-10 standard deviation of roll velocity

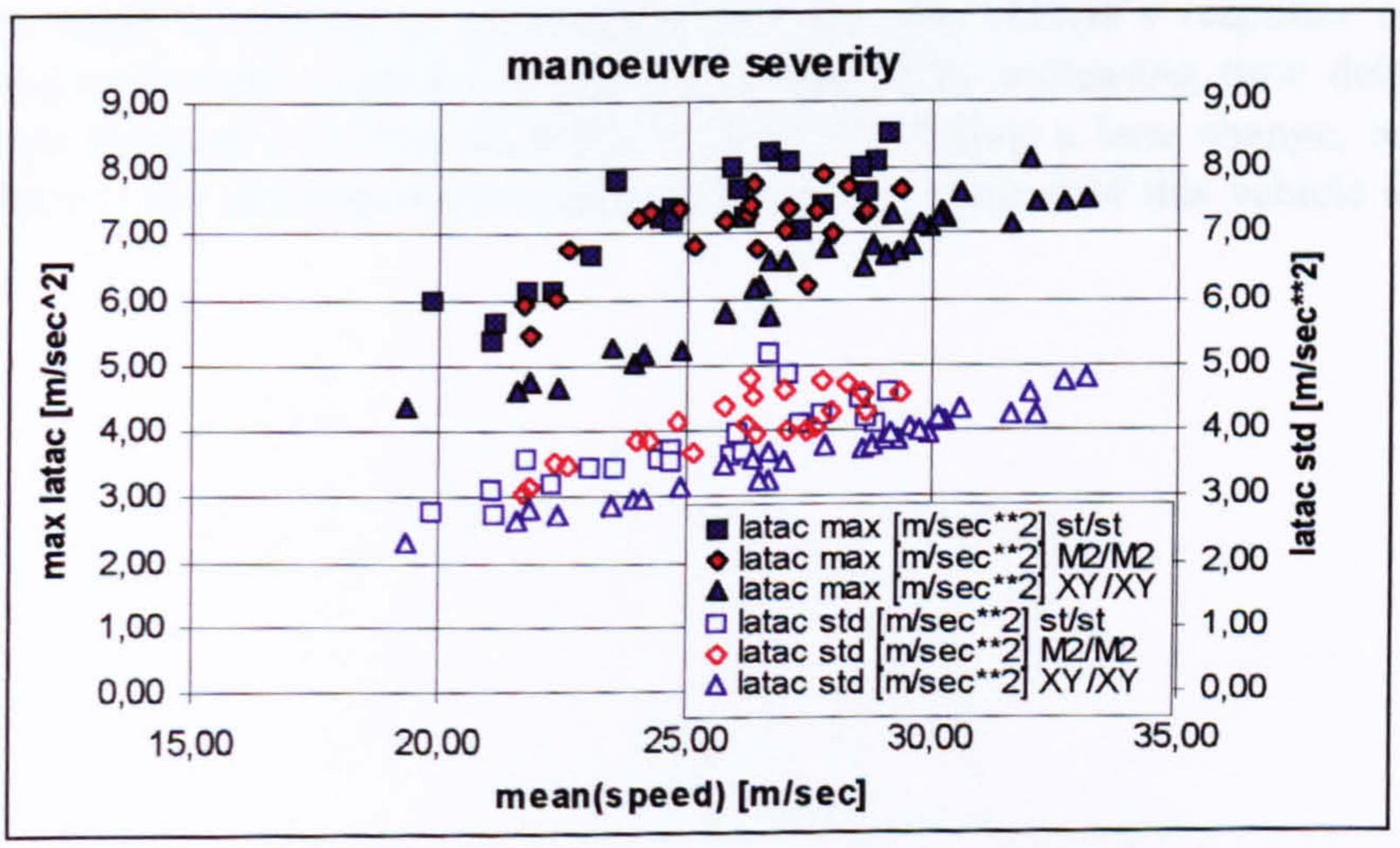

Fig. 7.3.2-11 manoeuvre severity vs. vehicle speed

summary of test results

The results discussed in this section indicate the influence of the tyre design on the transient limit handling behaviour. The tyres determine how fast the vehicle responds to the driver's steering and throttle control and how well correlated inputs and responses are maintained. Furthermore, they make a difference to the behavioural transition from low severity driving to limit manoeuvering. The slick tyre shod vehicle is far less sensitive to increased levels of severity compared to the other two set-ups. It maintains its capability to provide a fast and well correlated response up to the limit speed. Lane change manoeuvres with the slick shod Jaguar involved lower side slip motions. They could be completed with relatively low severity levels, as represented by the standard deviation and the peak value for the lateral acceleration. This indicates, in addition to the low values for the standard deviation of the hand wheel velocity, that the manoeuvres could be performed with a smooth and low frequency steering input, involving fewer reversals. This led to smaller roll angle oscillations. Its peak performance, in terms of maximum speed through a double lane change, was superior to all other set-ups tested. It has to be said though that the high speed trials could only be performed successfully, if the driver was free to use additional throttle control. The failure mode for this vehicle was similar to those of the other two vehicle set-ups. The car left the prescribed course by hitting a cone marking the left hand side (inside) of the offset lane. At the limit speed, it was obviously not able to build-up a sufficient level of lateral acceleration in time to enter the offset lane with an appropriate attitude.

The ability to match the driver's input faithfully deteriorates at a high rate for the winter tyre equipped vehicle. Although the driver managed to achieve almost the same maximum speed compared to the standard set-up, the vehicle's response behaviour showed a considerable correlation loss accompanied by increasing time delays. This vehicle also featured a strong tendency to side slip during a lane change, leading to high values for the steering effort associated with the control of this vehicle degree of freedom.

7.3.3 Effects of mixed tyre constructions on ISO lane change handling performance

This section summarises the handling performance of the Jaguar XJ6 fitted with a mixed set of tyre designs. Two experimental slick tyres, denoted as 'XY' in the previous section, were fitted either to the front or rear end of the vehicle, while winter tyres were mounted on the respective opposite end. As we did in the previous section, results are compared to those of the standard car equipped with standard tyres inflated to the recommended pressure.

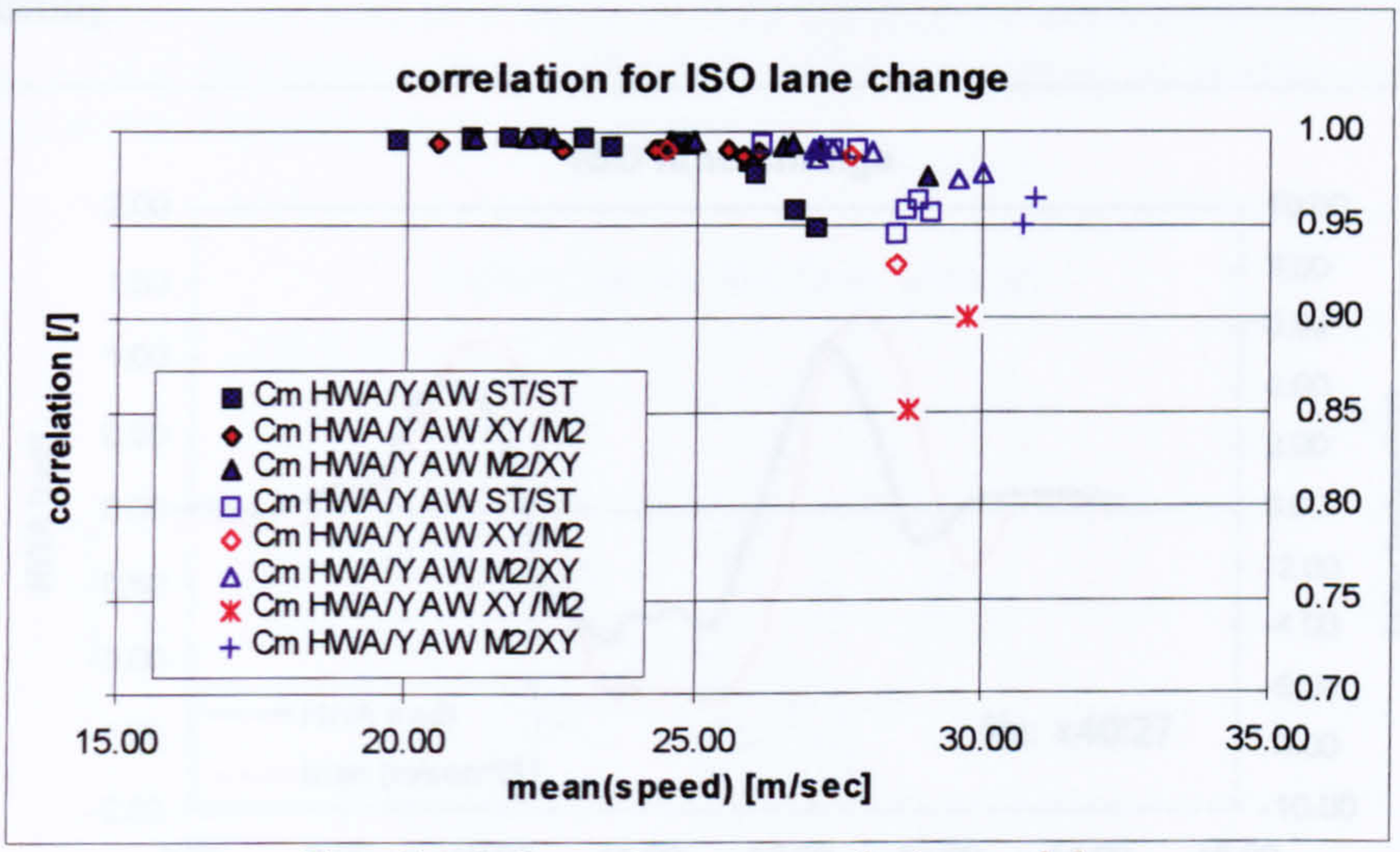

Fig. 7.3.3-1 maximum correlations of the yaw rate response

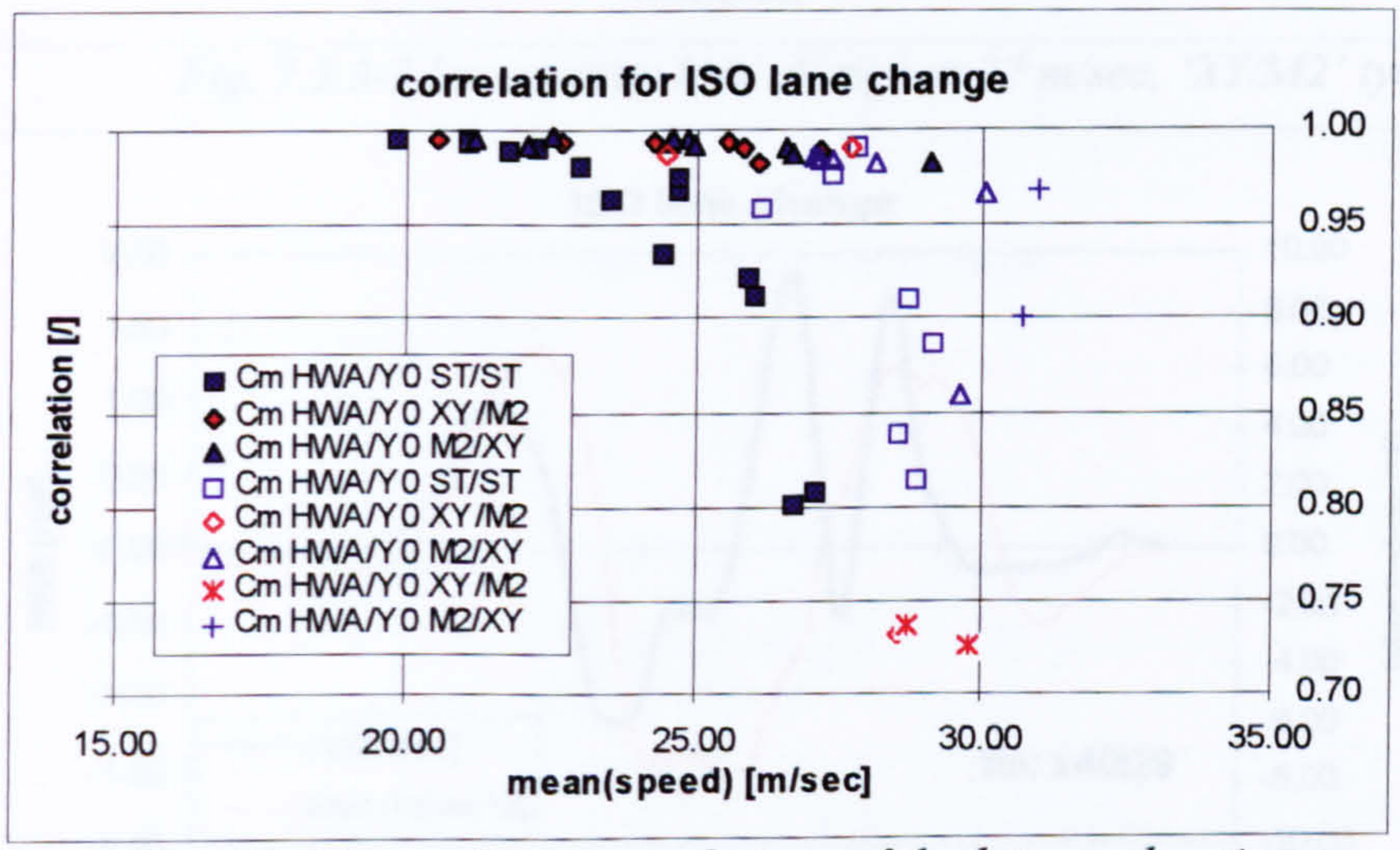

Fig. 7.3.3-2 maximum correlations of the lat. acceleration response

Fig. 7.3.3-1 and fig. 7.3.3-2 show the peak cross-correlation coefficients obtained for the two lateral responses, yaw rate and lateral acceleration respectively, with regard to the steering angle input. The standard set-up is marked as before. The vehicle fitted with slick tyres at the front and winter tyres at the rear end is referenced by 'XY/M2'. The inverse set-up is denoted by 'M2/XY'. In these graphs results representing a failed lane change manoeuvre are found as well. A failed test, for which one or more cones

were hit, is denoted by an asterisk (*) in the case of the former set-up, whereas a cross (+) refers to an unsuccessful test with the 'M2/XY' test configuration. These results are included to demonstrate the sudden deterioration in the response behaviour of the vehicle, which is equipped with race type front tyres and rather compliant winter tyres at the rear end. A pronounced loss in correlation occurs beyond a velocity of 28 m/sec, as can be seen from both graphs. For the other two tyre configurations a much more progressive performance roll-off is established. On the other hand, there is little difference in the maximum speed for which the manoeuvre could be completed successfully.

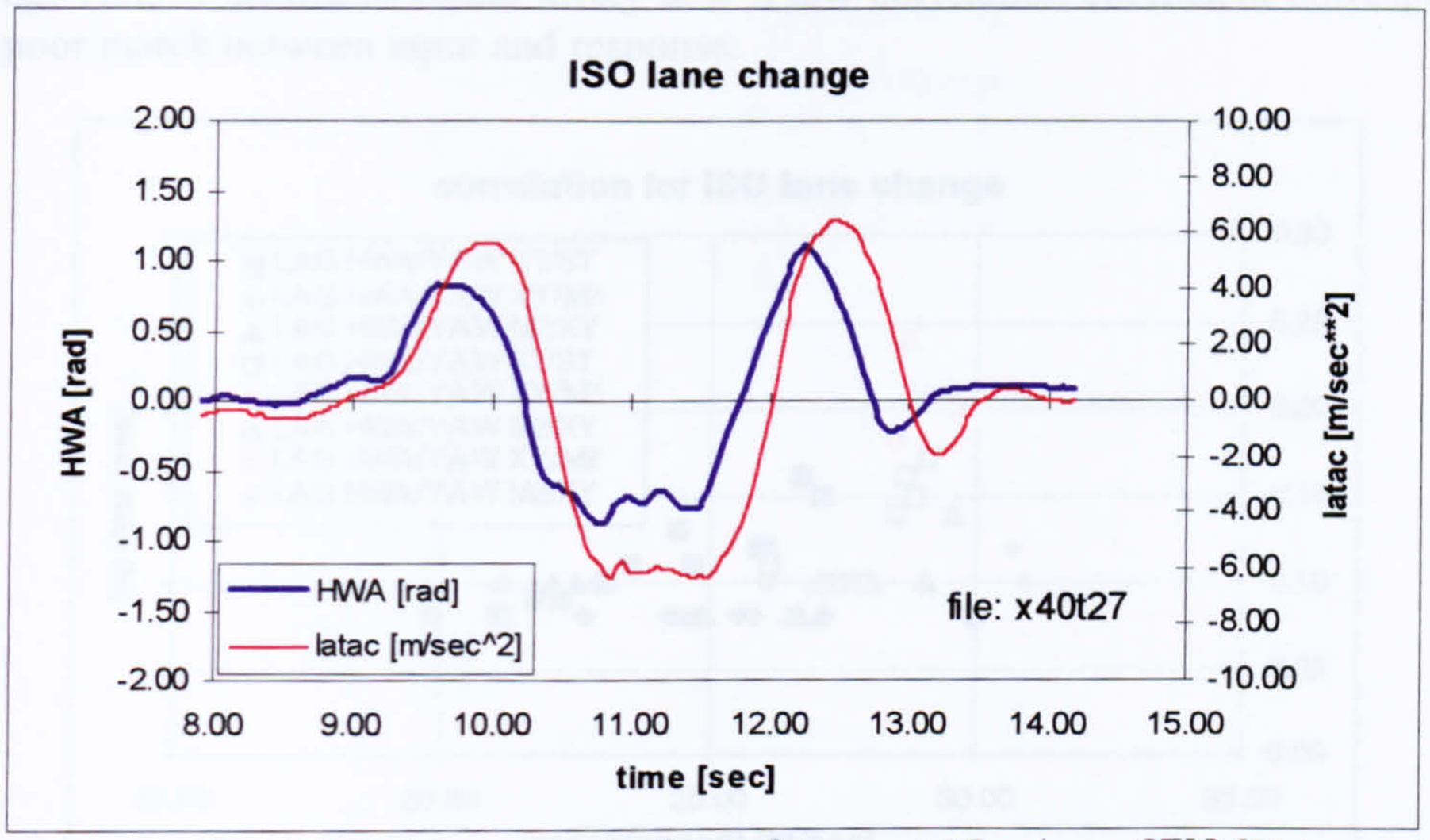

Fig. 7.3.3-3 low severity lane change at 27 m/sec, 'XY/M2' tyre mix

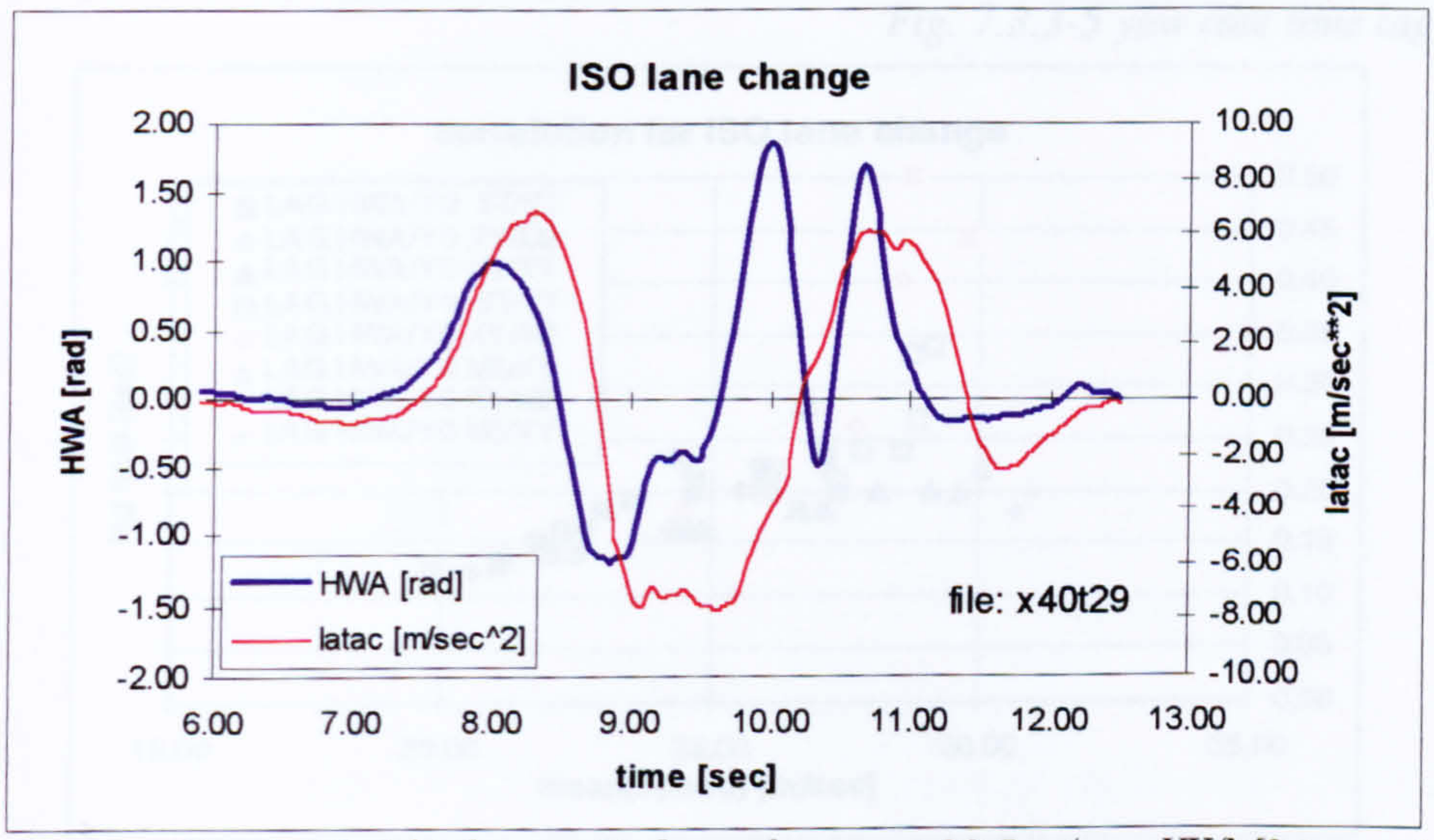

Fig. 7.3.3-4 high severity lane change at 28.5 m/sec, XY/M2 tyre mix

As an illustrative example for the rapid change in behaviour observed for the 'XY/M2' configuration, the time histories for the hand wheel angle and lateral acceleration are

plotted for two tests. The first test refers to an average speed of 27 m/sec and was performed with the throttle held constant. The peak cross-correlation coefficient for the two signals shown in fig. 7.3.3-3 is 0.99, which indicates that the hand wheel angle is perfectly replicated by the lateral acceleration response.

In fig. 7.3.3-4 the same signals are shown, but for the limit speed of 28.5m/sec. The peak correlation coefficients obtained for this particular test are denoted by unfilled diamond in fig. 7.3.3-1 and fig. 7.3.3-2. The peak correlation for the lateral acceleration has decreased to a value of 0.73 for a speed increase of only 1.5 m/sec, and fig. 7.3.3-4 illustrates rather nicely how a low correlation coefficient corresponds to a poor match between input and response.

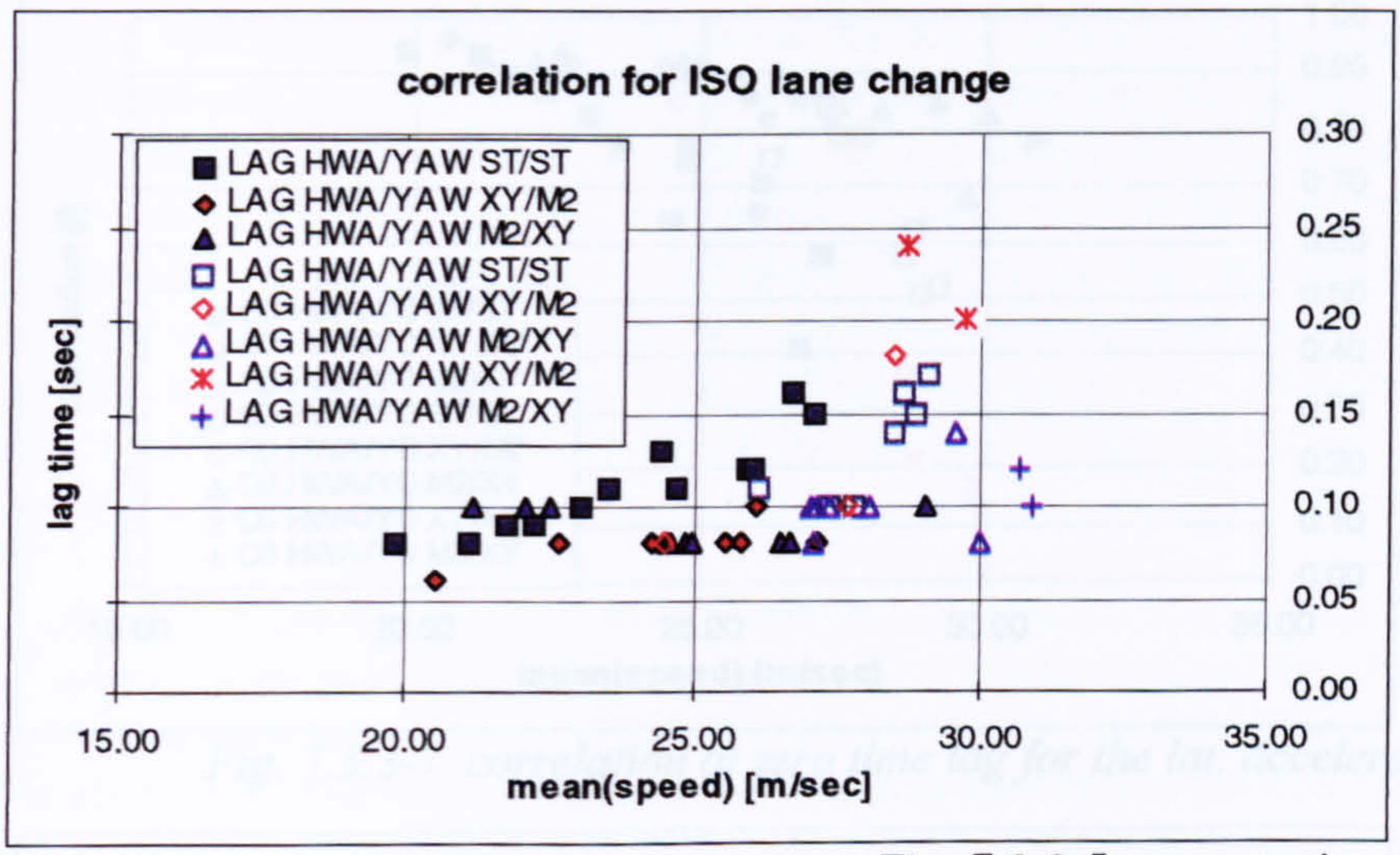

Fig. 7.3.3-5 yaw rate time lags

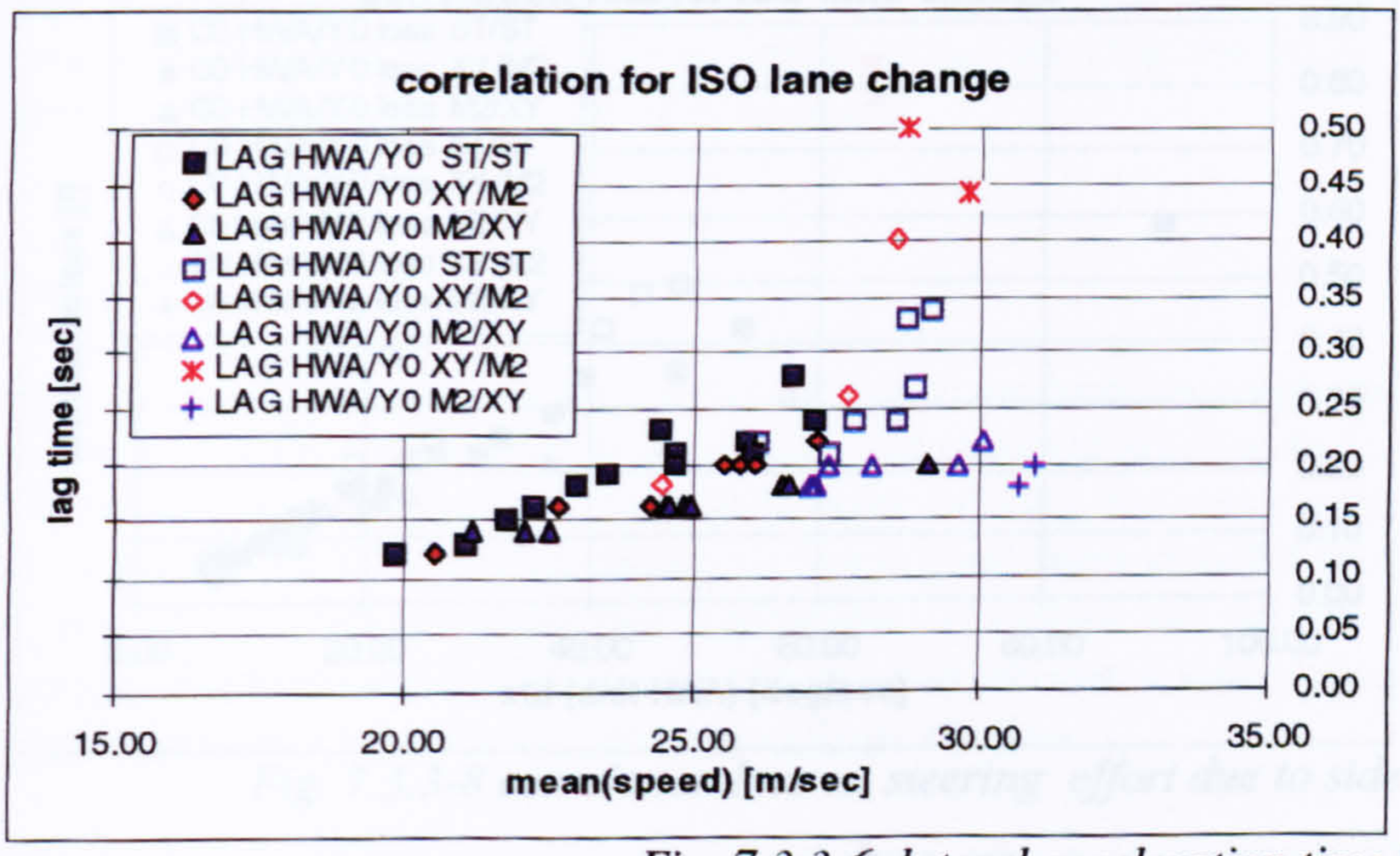

Fig. 7.3.3-6 lateral acceleration time lags

In comparison to the 'XY/M2' set-up, the inverse configuration maintains an input/ output relationship less sensitive to manoeuvre severity. It also enabled the highest limit speed of the three test configurations.

Graphs indicating the time delays between steering angle and vehicle responses show a similar behaviour as established for the corresponding cross-correlation coefficients. In fig. 7.3.3-5 those associated with the yaw rate response are given, and the lateral acceleration time lags are presented by fig. 7.3.3-6.

Corresponding to the sudden decrease in correlation, the average time lags for the 'XY/M2' set-up increase from a rather low level to high values beyond velocities of 28 m/sec. For the opposite configuration, time lags increase only slightly towards the limit speed. They remain at the same level or below those established for the standard set-up.

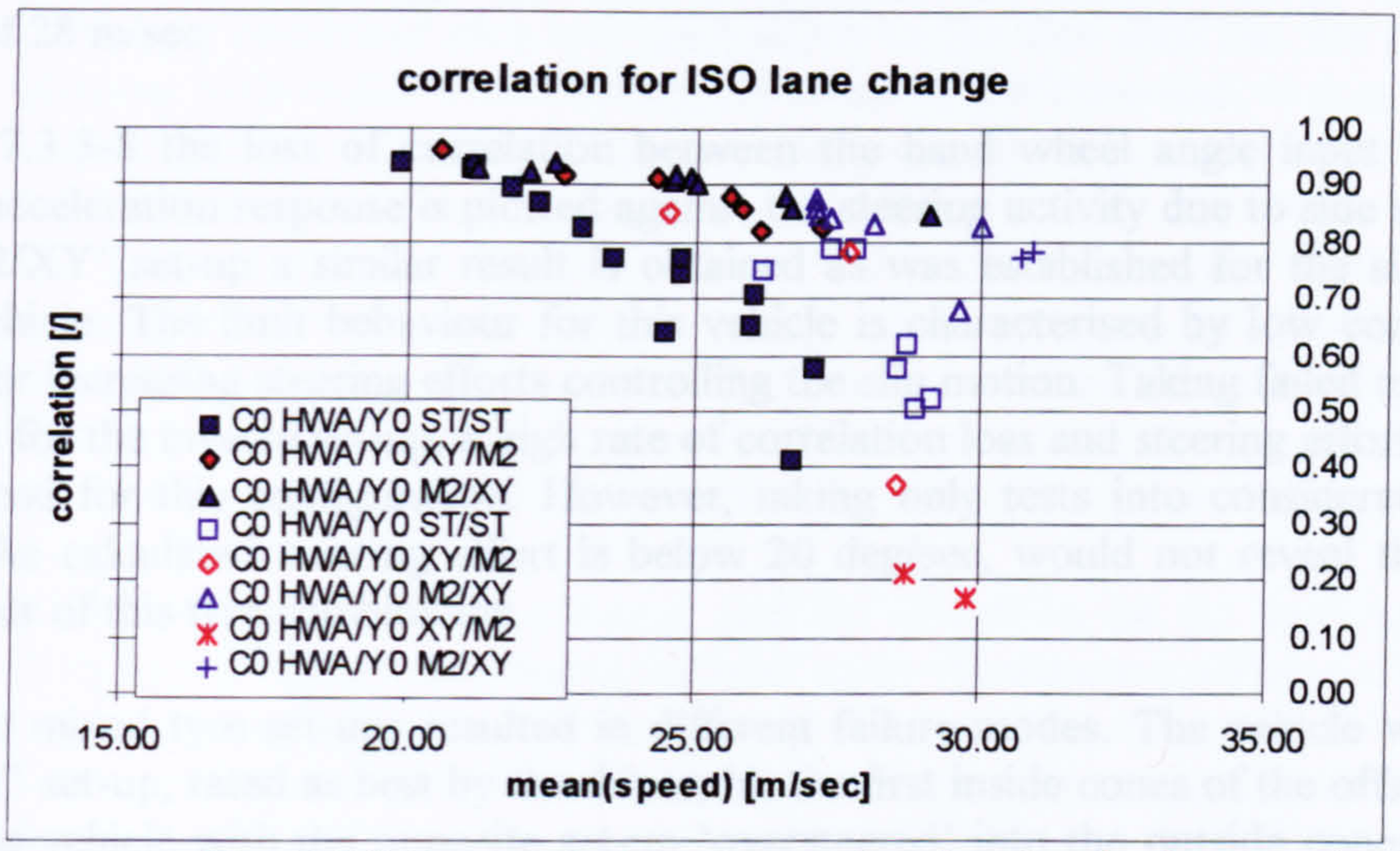

Fig. 7.3.3-7 correlation at zero time lag for the lat. acceleration

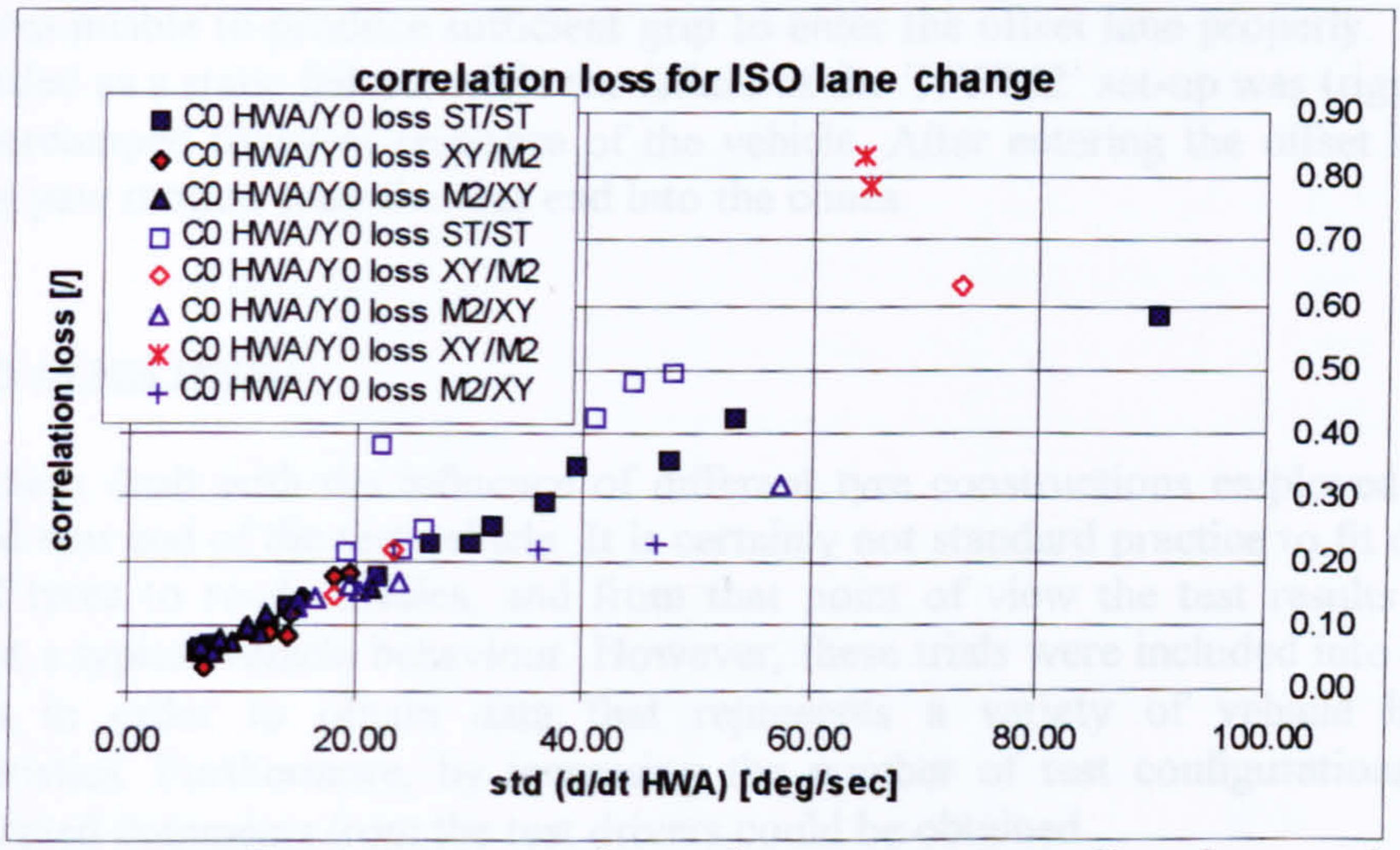

Fig. 7.3.3-8 correlation loss vs. steering effort due to side slip

The graph showing the cross-correlation coefficient between the hand wheel angle and the lateral acceleration at zero time lag is given in fig. 7.3.3-7. This parameter was associated with the instantaneous feedback the driver receives when having to correct

the position of the vehicle in a closed loop. A high value indicates that the vehicle can quickly translate a steering input into a change of direction. The proportion between the change of steering wheel angle and the change of direction gives the driver a feedback cue to readjust the steering input.

The correlation coefficient for the vehicle fitted with winter tyres at the front end behaves very similarly to that measured for the 'XY/XY' set-up, shown in fig. 7.3.2-7. For both cases, a smooth decrease in correlation is established. The standard set-up is much more sensitive to an increase in speed, while the 'XY/M2' configuration shows a rather discontinuous limit approach with a sudden decrease in correlation beyond a speed of 28 m/sec.

In fig. 7.3.3-8 the loss of correlation between the hand wheel angle input and the lateral acceleration response is plotted against the steering activity due to side slip. For the 'M2/XY' set-up a similar result is obtained as was established for the slick tyre shod vehicle. The limit behaviour for this vehicle is characterised by low correlation losses for increasing steering efforts controlling the slip motion. Taking failed tests into account for the inverse set-up, a high rate of correlation loss and steering effort can be established for this configuration. However, taking only tests into consideration for which the calculated steering effort is below 20 deg/sec, would not reveal the poor behaviour of this tyre combination.

The two mixed tyre set-ups resulted in different failure modes. The vehicle with the 'M2/XY' set-up, rated as best by the driver, hit the first inside cones of the offset lane, while the vehicle with the opposite set-up 'oversteered' into the outside cones at the end of the offset lane. The failure mode of the former is probably a result of saturating front tyres unable to produce sufficient grip to enter the offset lane properly. This can be regarded as a static failure, while the failure of the 'XY/M2' set-up was triggered by the underdamped transient response of the vehicle. After entering the offset lane, the resulting yaw motion spun the rear end into the cones.

<u>summary of test results</u>

This section dealt with the influence of different tyre constructions employed for the front and rear end of the test vehicle. It is certainly not standard practice to fit different types of tyres to road vehicles, and from that point of view the test results do not represent a typical vehicle behaviour. However, these trials were included into the test program in order to obtain data that represents a variety of vehicle handling characteristics. Furthermore, by increasing the number of test configurations, more differentiated comments from the test drivers could be obtained.

Test driver B rated the 'winter tyre front/ XY tyre rear' set-up as 'more precise to the limit' than any other set-up he tried. He assessed the steering characteristics of this configuration as being superior even to the vehicle fitted with slick tyres all around. The former configuration was regarded as most suitable for drivers with average skills,

although it is inferior in terms of limit speed through a lane change. His evaluation is matched by some objective properties derived from the recorded test data. The two best set-ups established the fastest responses and provided a vehicle response least sensitive to severity. Cross-correlation coefficients maintained a high level for the 'M2/XY' tyre combination as well as for the slick shod vehicle ('XY/XY'), representing a vehicle response well in agreement with the driver's control input. Correlation coefficients and response time lags changed only gradually for the limit approach.

However, from the criteria used here, it is not possible to establish why the test driver prefers the 'winter tyre front/ slick tyre rear' set-up to the slick shod car. He indicated that the steering feels better with winter tyres fitted to the front end. It may well be that these tyres provide a steering torque characteristic that indicates the approach of saturation in a more pronounced fashion than the slick tyres do. This property is not represented by the correlation coefficient alone, which quantifies how well the shapes of two signals agree with each other. A high correlation can be regarded as a precondition that an input/ output pair provides a useful feedback. In order to find out whether the gain between steering torque and lateral acceleration changes in a stronger way for the winter tyres, one would have to consult the time histories of these signals.

However, this approach was not pursued, and the discussion on the steering feel is completed by giving a graph containing the peak cross-correlation coefficients between hand wheel torque and lateral acceleration in fig. 7.3.3-9. This time the vehicle fitted with slick tyres all around ('XY/XY') is used as a reference. It can be said that there is little difference in terms of correlation between the 'M2/XY' and the 'XY/XY' set-up. A few results regarding the former configuration establish a slightly worse correlation for velocities near the limit speed for the constant throttle tests (27m/sec).

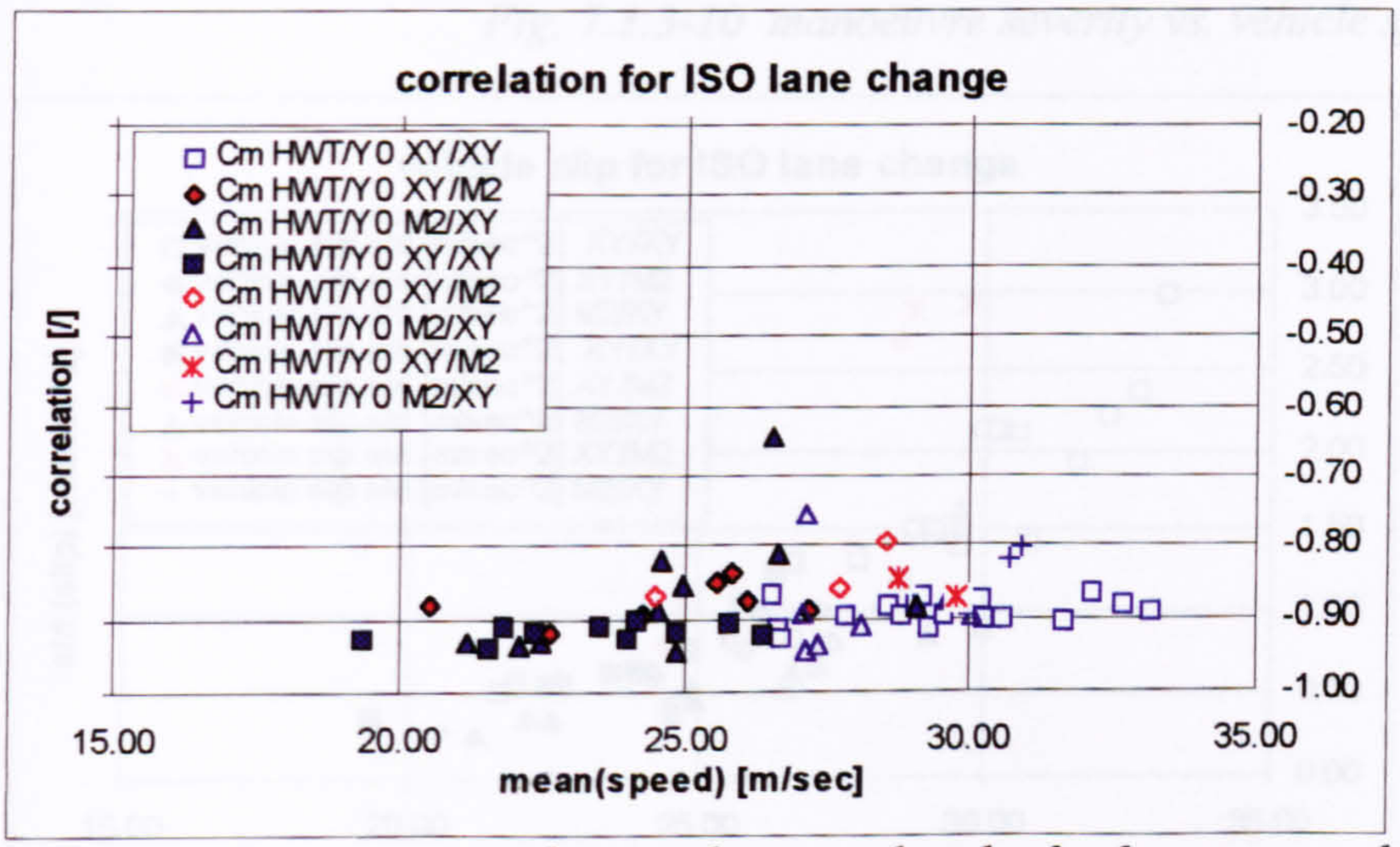

Fig. 7.3.3-9 maximum correlations between hand wheel torque and lat. acceleration

However, as has been said above, the small differences in the correlation coefficients,

indicated by fig. 7.3.3-9, do not allow to establish the quality of the steering feel experienced by the driver, and the question, why the driver preferred the steering feel of one vehicle to that of another, remains unresolved.

The two highly rated set-ups differ considerably in the standard deviations for the lateral acceleration obtained from the recorded lane change tests. This statistical parameter was introduced to assess the smoothness and severity of a manoeuvre performed at a constant speed. As can be seen from fig. 7.3.3-10 the standard deviation is lower for the 'M2/XY' set-up compared to the second highest rated configuration 'XY/XY'. The former set-up allowed the driver to change lane with fewer reversals and possibly lower peak values for the lateral acceleration at the same speed. A similar trend was established for the yaw rate standard deviation.

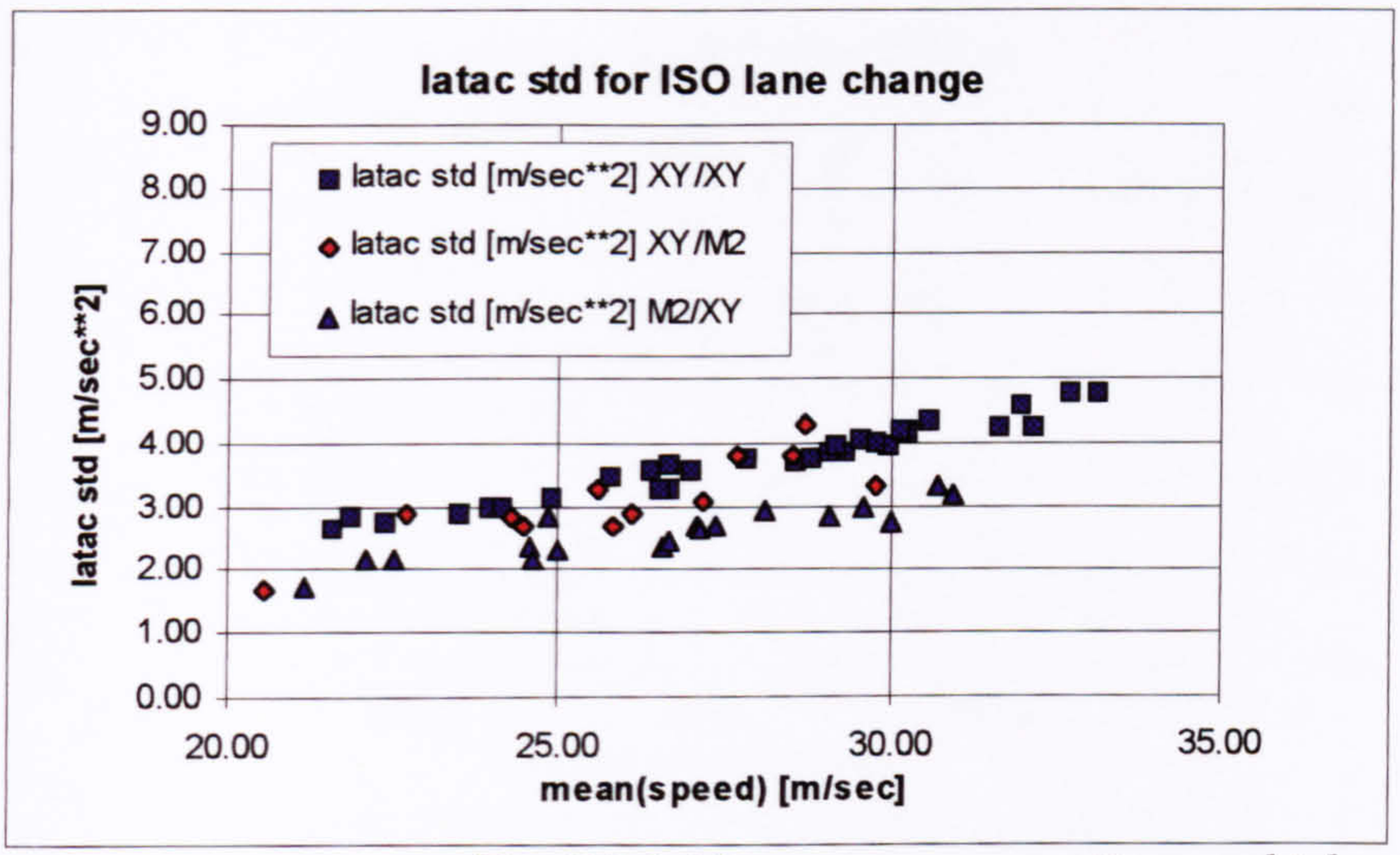

Fig. 7.3.3-10 manoeuvre severity vs. vehicle speed

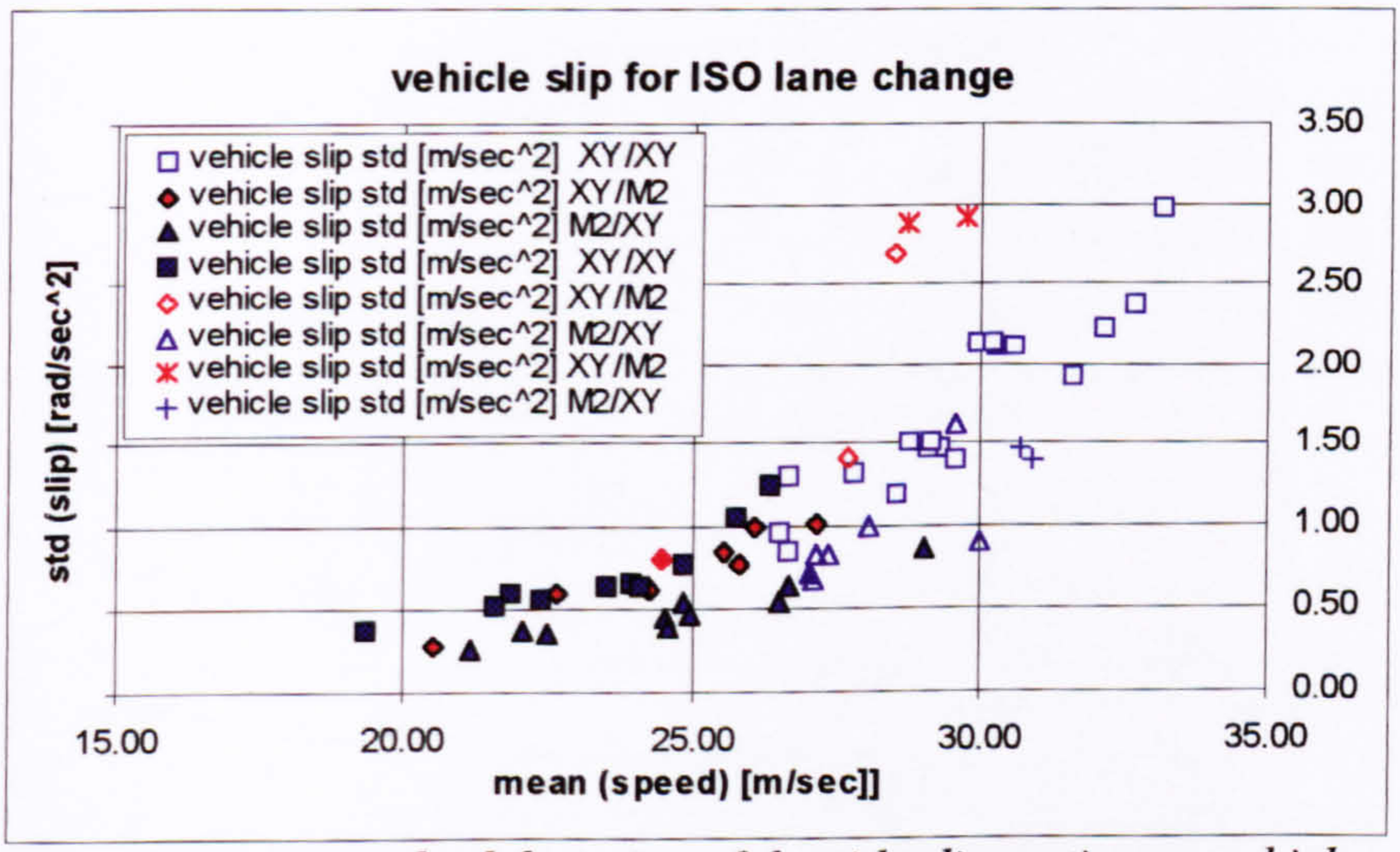

Fig. 7.3.3-11 standard deviation of the side slip motion vs. vehicle speed

The difference between the standard deviation obtained for the yaw rate, multiplied

with the forward speed, and that established for the lateral acceleration gives a measure of the side slip motion during the manoeuvre. Again, the mixed tyre set up showed less of a tendency to produce side slip than the slick shod vehicle, as can be established from fig. 7.3.3.-11.

7.3.4 Effects of vehicle modifications on ISO lane change handling performance

As stated in section 7.3 two modifications were carried out to the Jaguar test vehicle. Firstly, a rack carrying 90 kg of ballast was fitted to its roof. Double lane changes were performed by test driver A for this configuration in December 1996. The second chassis alteration involved the removal of the front anti-roll bar. Corresponding tests were conducted in April 1997 by test driver B. For the test program concerning these alternative chassis set-ups, sets of standard tyres of the specification Dunlop SP 2000 225/55 R16 were used. Since these tests were carried out in different seasons, for which different ambient and surface temperatures prevailed, it has to be considered that the results presented here reflect to some extent the temperature influence on the tyre performance.

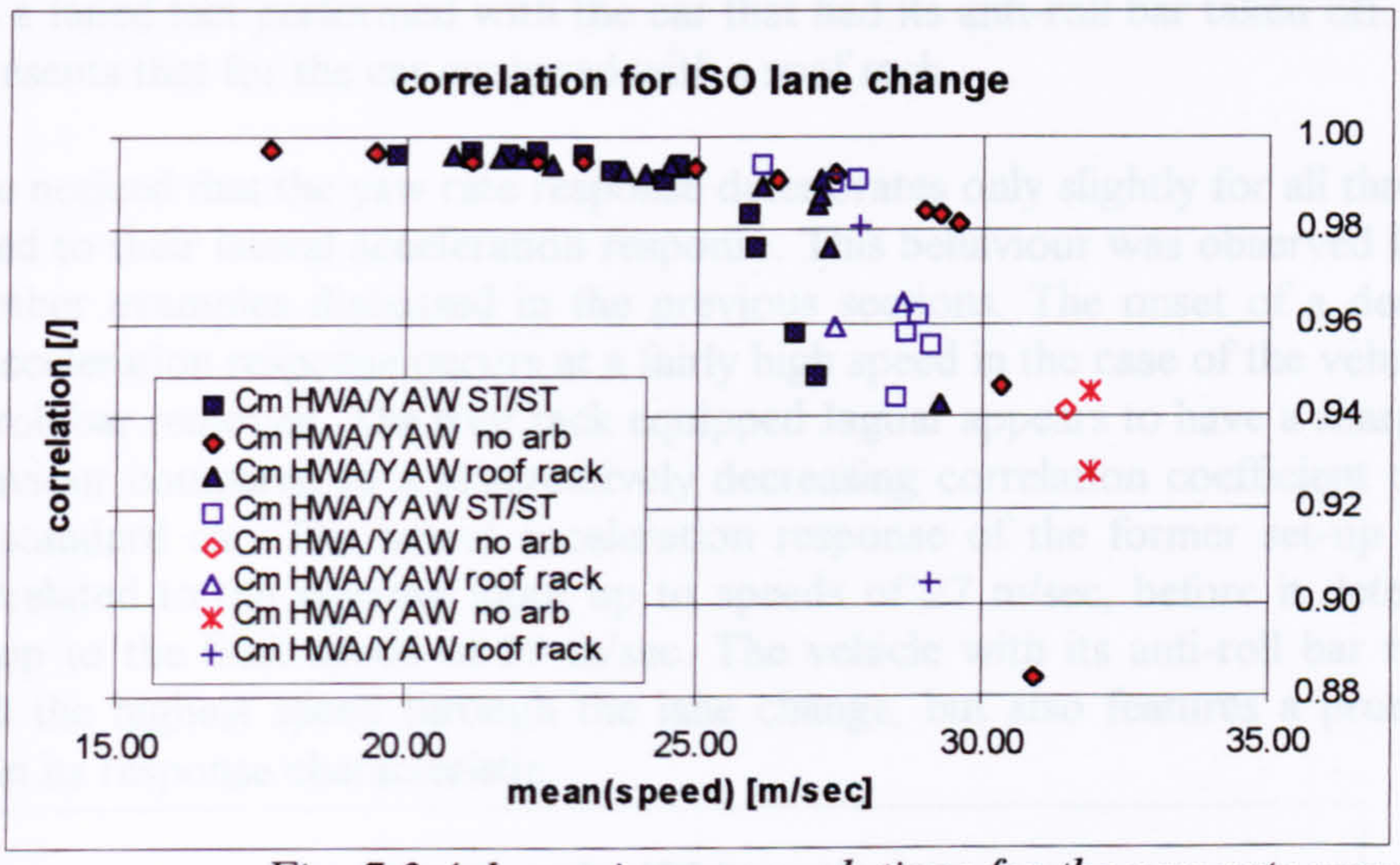

Fig. 7.3.4-1 maximum correlations for the yaw rate response

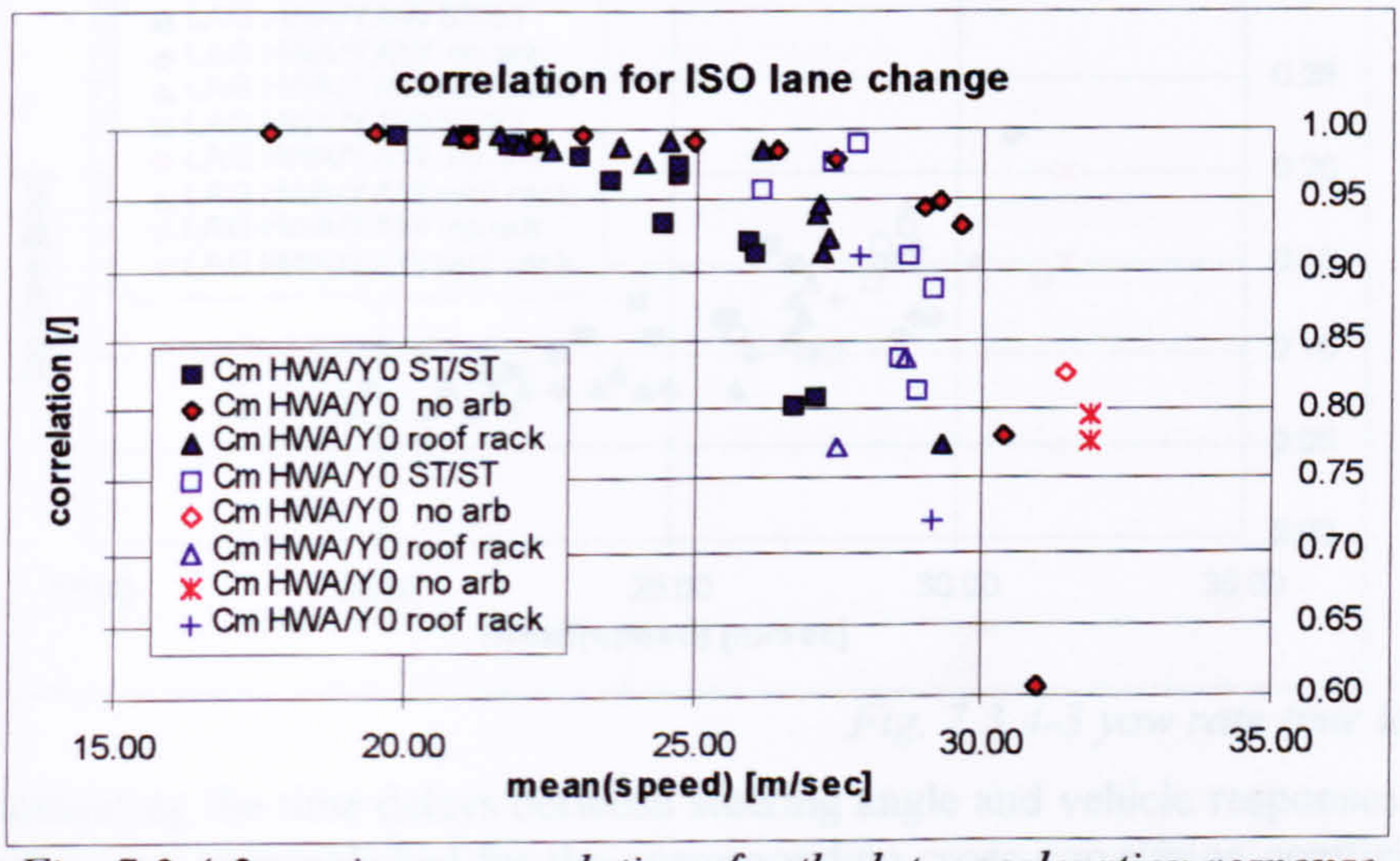

Fig. 7.3.4-2 maximum correlations for the lat. acceleration response

It was believed that these alterations would have detrimental effects on the limit handling, which would be reflected in corresponding driver comments as well as by

the recorded test data. As we did in the previous section, results are compared to those of the standard car.

Firstly, results for the peak correlation coefficients are presented which were established for the hand wheel angle/ yaw rate pair, as shown in fig. 7.3.4-1. Those for the hand wheel angle/ lateral acceleration pair are illustrated by fig. 7.3.4-2. Results concerning the vehicle for which the anti-roll bar was removed are denoted by diamonds, whereas triangles refer to the car fitted with the roof rack. Filled markers denote tests performed with a constant throttle, whereas blank ones indicate that the driver made considerable use of the throttle in attempting to complete the manoeuvre successfully. As was done in the previous section, results of two failed tests are included which were obtained for each of the alternative set-ups. An asterisk (*) denotes a failed test performed with the car that had its anti-roll bar taken off. A cross (+) represents that for the car equipped with a roof rack.

It can be noticed that the yaw rate response deteriorates only slightly for all three cases compared to their lateral acceleration response. This behaviour was observed for most of the other examples discussed in the previous sections. The onset of a decreasing lateral acceleration response occurs at a fairly high speed in the case of the vehicle with its anti-roll bar removed. The roof rack equipped Jaguar appears to have a sharper roll-off behaviour compared to a progressively decreasing correlation coefficient obtained for the standard car. The lateral acceleration response of the former set-up remains well correlated to the steering input up to speeds of 27 m/sec, before it deteriorates rapidly up to the limit speed of 29 m/sec. The vehicle with its anti-roll bar removed achieved the highest speed through the lane change, but also features a pronounced roll-off in its response characteristic.

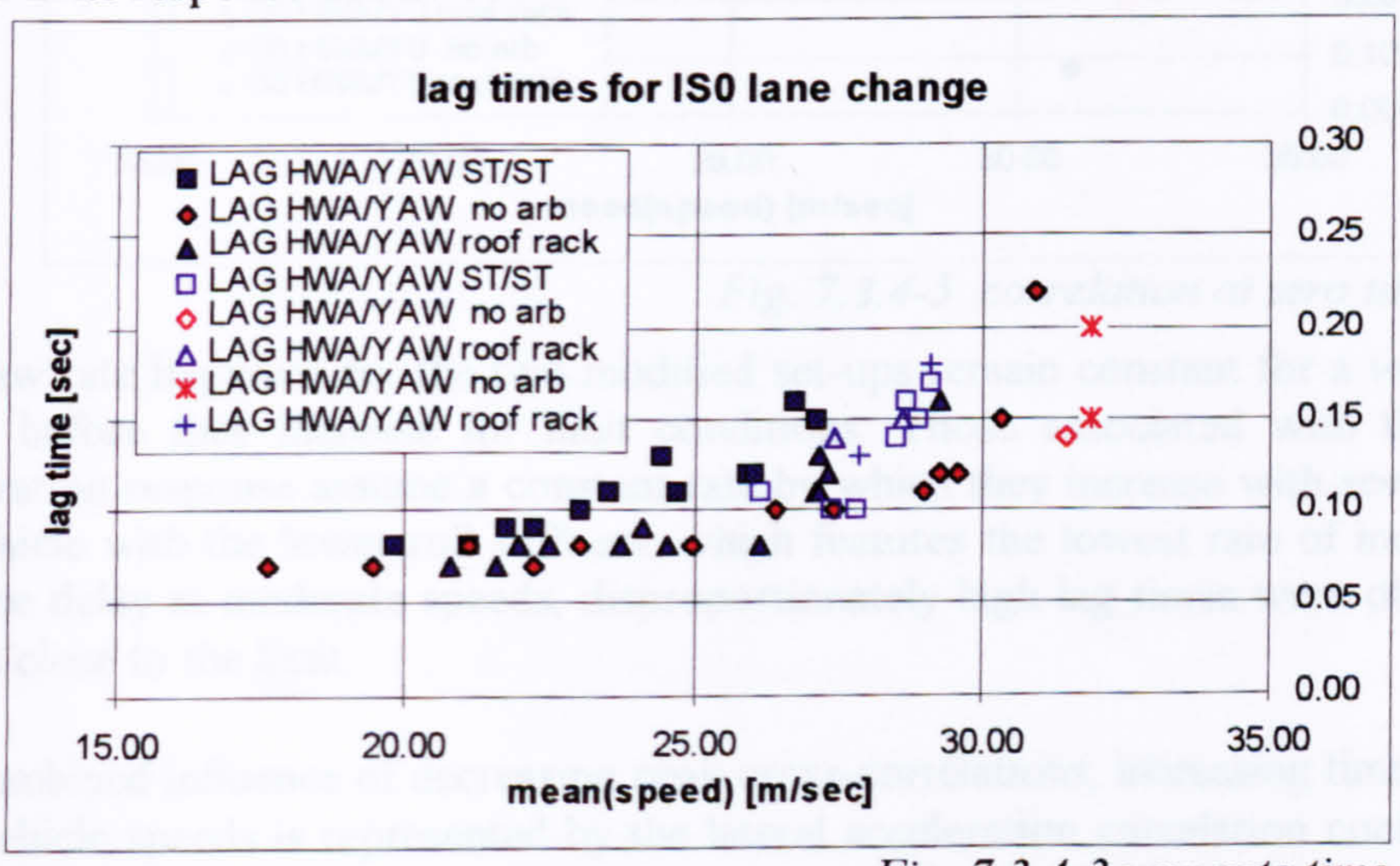

Fig. 7.3.4-3 yaw rate time lags

Graphs indicating the time delays between steering angle and vehicle responses show a similar behaviour as established for the corresponding cross-correlation coefficients. In fig. 7.3.4-3 those associated with the yaw rate response are given, and the lateral acceleration time lags are presented by fig. 7.3.4-4.

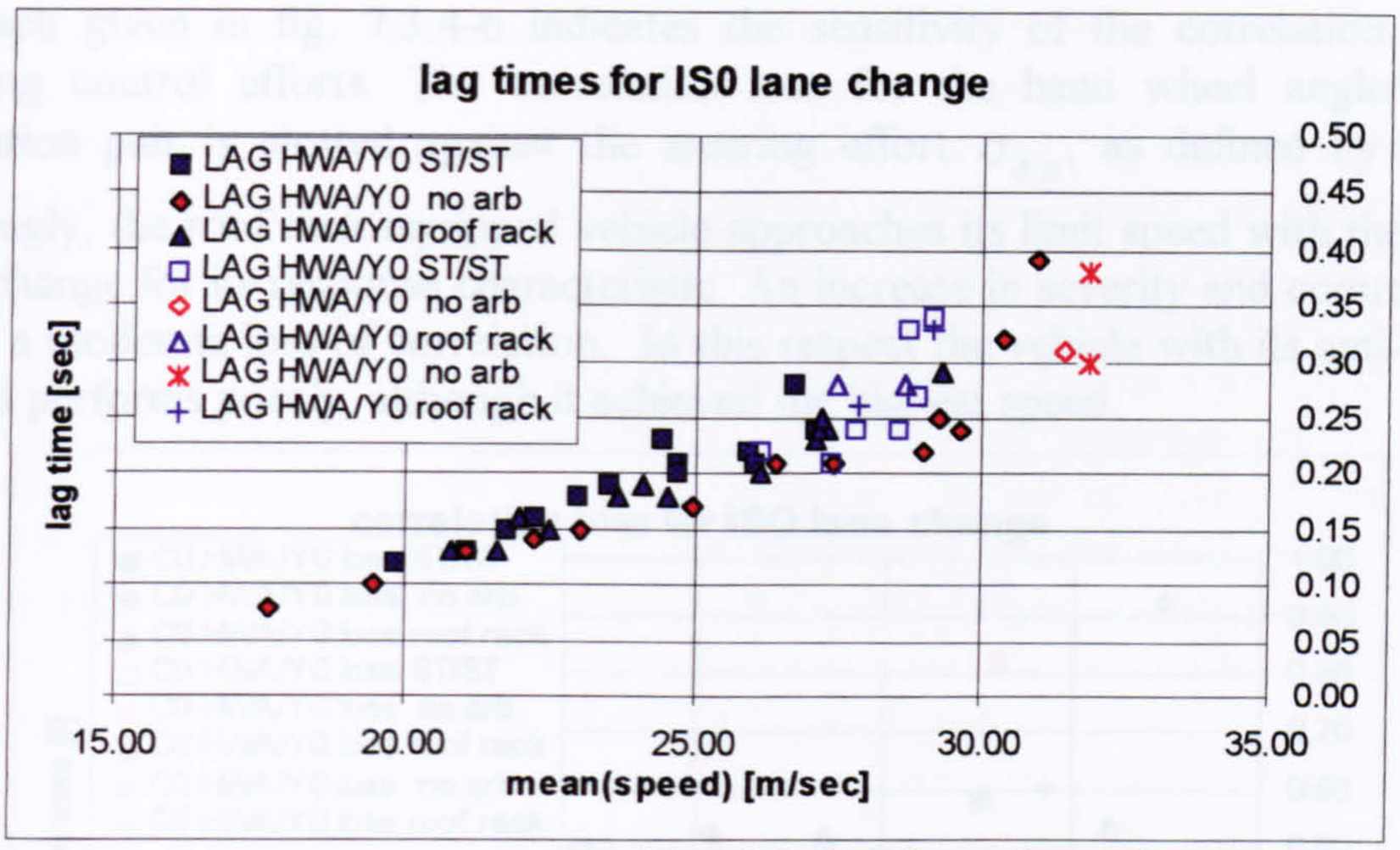

Fig. 7.3.4-4 lateral acceleration time lags

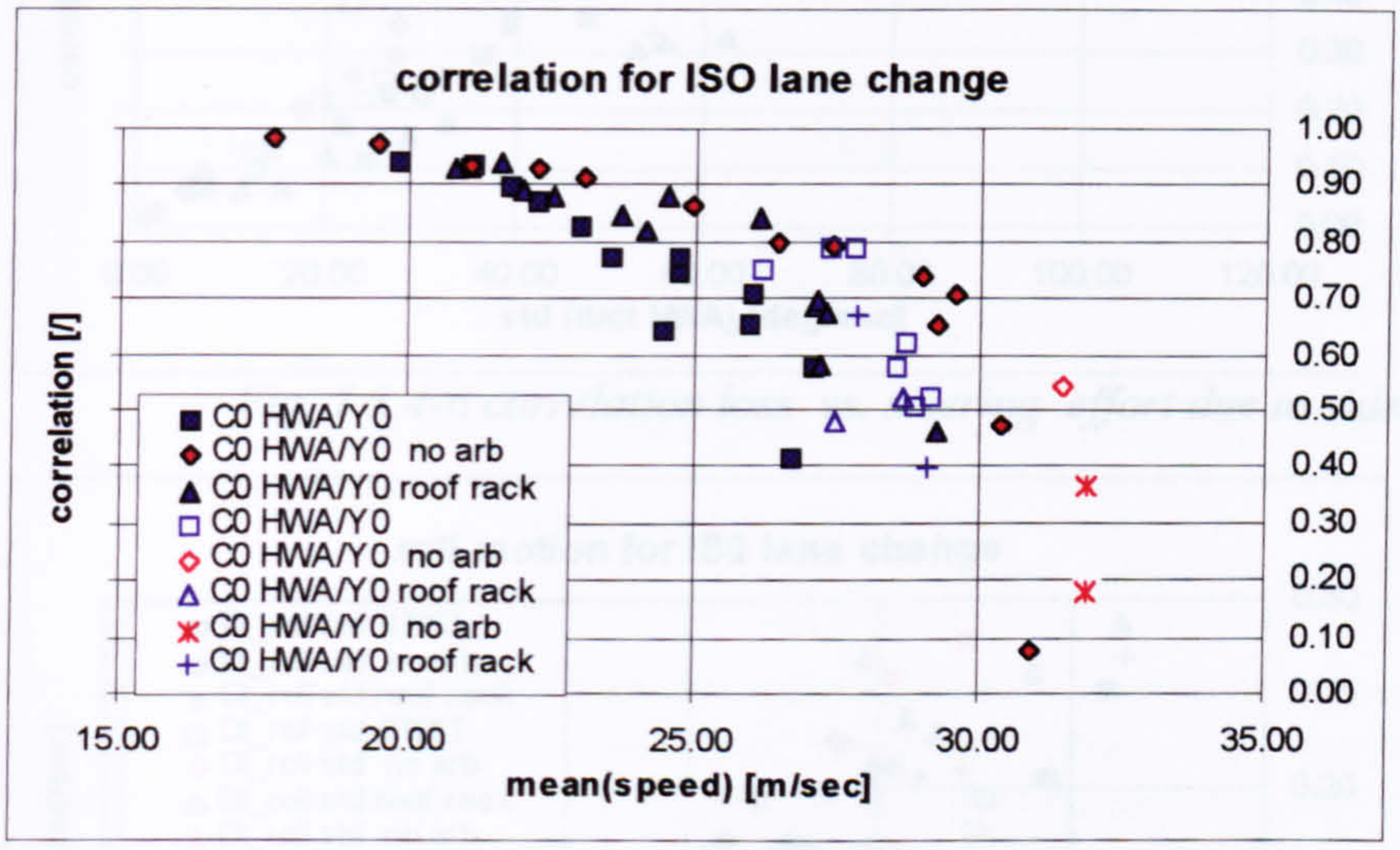

Fig. 7.3.4-5 correlation at zero time lag

The yaw rate lag times for the two modified set-ups remain constant for a wide speed range, before they increase for limit conditions. Those associated with the lateral acceleration response assume a constant rate by which they increase with severity. For the vehicle with the lower roll stiffness, which features the lowest rate of increase for the time delay at moderate speeds, disproportionately high lag times were obtained at speeds close to the limit.

The combined influence of decreasing peak cross-correlations, increasing time lags and high vehicle speeds is represented by the lateral acceleration correlation coefficient at zero time delay, shown in fig. 7.3.4-5. The vehicle with its anti-roll bar removed behaves in an inconsistent manner when approaching the limit speed. Its response behaviour deteriorates moderately up the 30 m/sec. Beyond this speed the lateral acceleration feedback rapidly rolls off.

The graph given in fig. 7.3.4-6 indicates the sensitivity of the correlation loss to increasing control efforts. The correlation loss for the hand wheel angle/ lateral acceleration pair is plotted against the steering effort $\sigma_{\dot{\delta},\beta}$, as defined by (7.1-3). Surprisingly, the roof rack equipped vehicle approaches its limit speed with the lowest rate of change for its response characteristic. An increase in severity and control effort leads to a moderate loss of correlation. In this respect the vehicle with its anti-roll bar removed performs poorly, although it achieved the highest speed.

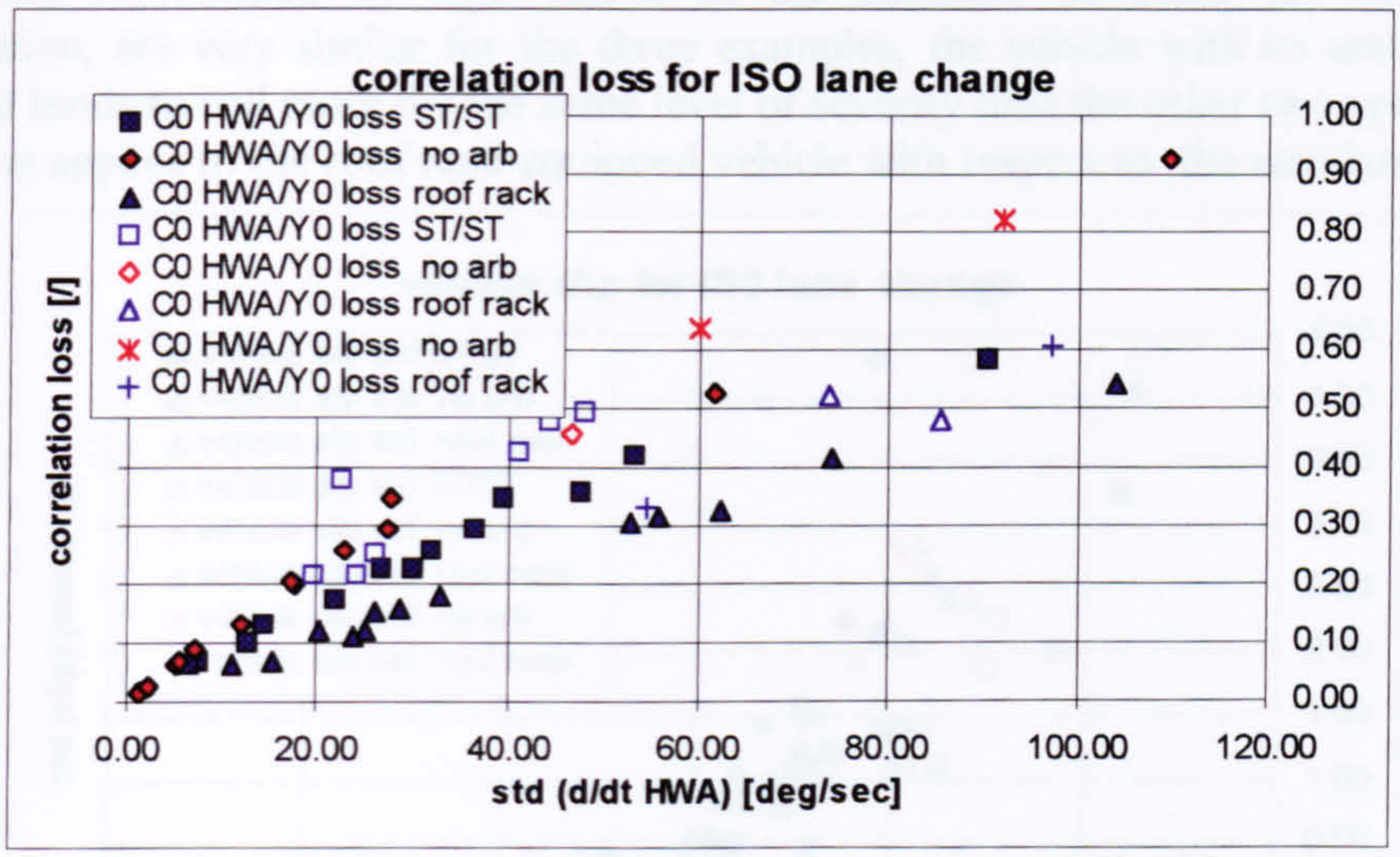

Fig. 7.3.4-6 correlation loss vs. steering effort due to side slip

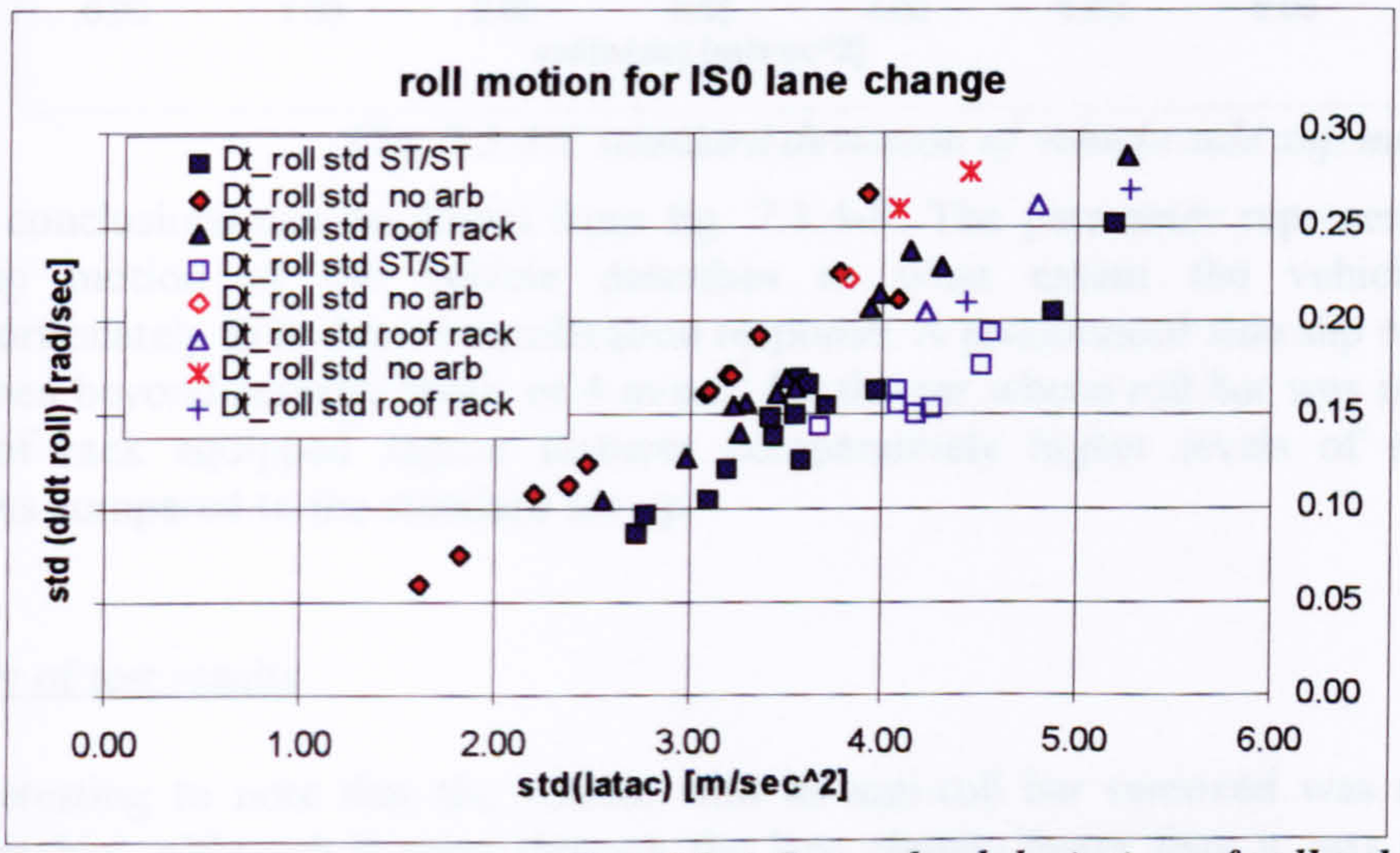

Fig. 7.3.4-7 standard deviation of roll velocity

The test driver found this vehicle set-up unacceptable. He rejected it, because it rolled too much during the manoeuvre. After inquiring whether the roll motion would prevent him maintaining the lateral control of the vehicle, he commented that the vehicle felt 'unstable' after it exited the first lane of the manoeuvre. He went on to explain that the front end felt 'loose' and that the vehicle was unable to 'settle down' quickly enough. He was concerned about a high degree of combined roll and

yaw oscillations ('corkscrewing'), after the vehicle joined the offset lane.

The observations of the driver can be illustrated with two graphs, showing the standard deviation for the roll motion (fig. 7.3.4-7) and the parameter for the slip motion of the vehicle (fig. 7.3.4-8), respectively. Their values are plotted against the standard deviation of the lateral acceleration, which was introduced to represent the severity as well as the smoothness of the manoeuvre. Although, values for the roll motion at limit conditions, represented by high values of the standard deviation for the lateral acceleration, are very similar for the three examples, the vehicle with its anti-roll bar removed tends to roll more for the same level of severity than the other two specimens. The same applies to the roof rack equipped vehicle with respect to the standard car.

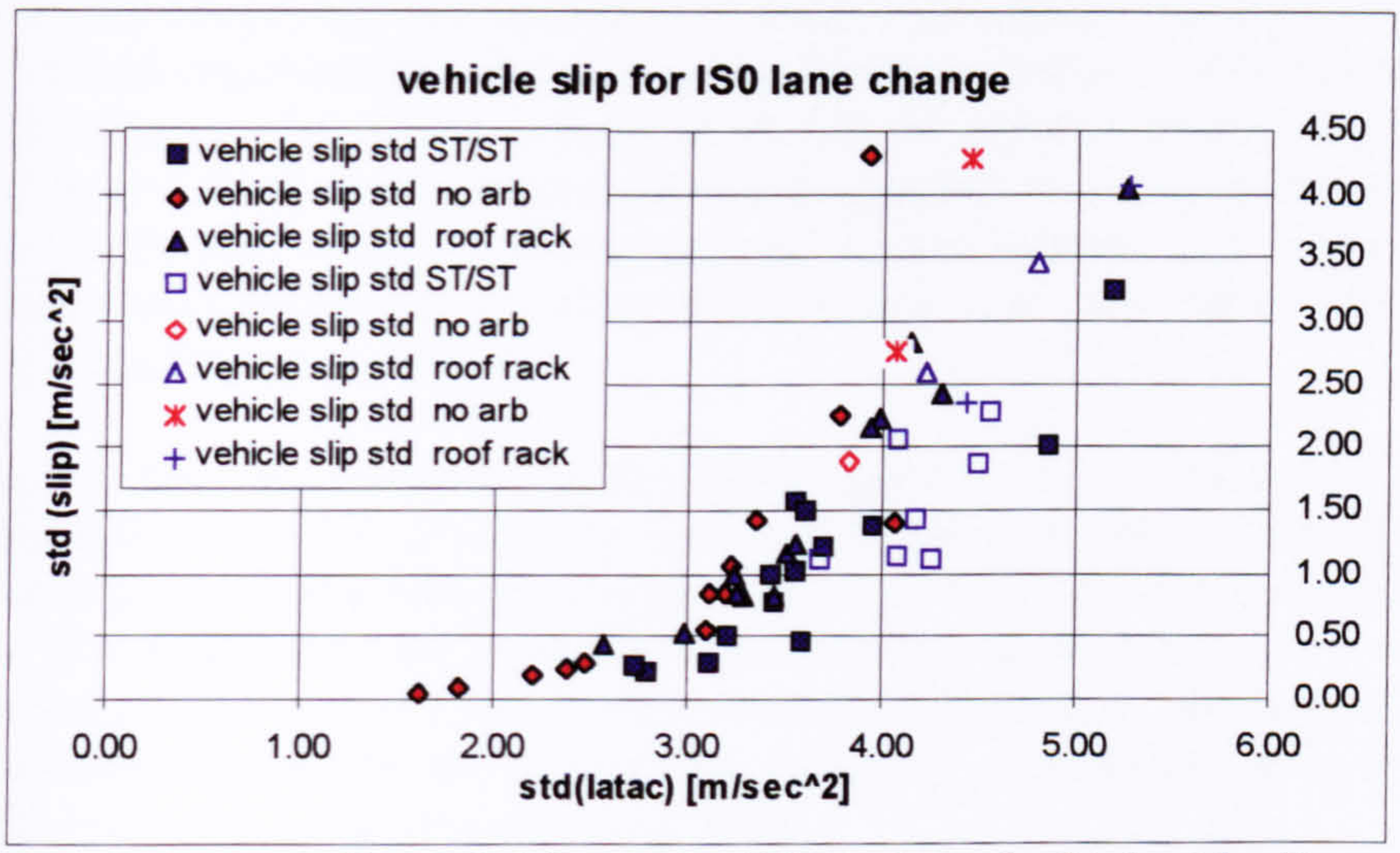

Fig. 7.3.4-8 standard deviation of vehicle side slip motion

Similar conclusions can be drawn from fig. 7.3.4-8. The parameter representing the side slip motion of the vehicle describes to what extent the vehicle yaws disproportionately to its lateral acceleration response. A pronounced side slip motion is established beyond severity levels of 4 m/sec^2 for the car whose roll bar was removed. The roof rack equipped Jaguar features comparatively higher levels of side slip variations compared to the standard set-up.

summary of test results

It is interesting to note that the vehicle with its anti-roll bar removed was rated as 'unacceptable', although it went through the lane change faster than it was possible with the other two set-ups. It appears that test drivers take more notice of the rate of change in the response behaviour of a vehicle than of their absolute performance. This vehicle set-up was mainly rejected on the grounds of producing too much roll during the manoeuvre. As established from the test data, its roll variations are more pronounced for the same level of manoeuvre severity. Secondly, the test driver objected to the yaw oscillations, preventing him to position the car properly in the offset lane. This comment corresponds to the vehicle's tendency to side slip relatively

more for the same severity. The vehicle with its anti-roll bar removed responds with a disproportionately high yaw rate in relation with the lateral acceleration generated.

Fitting a roof-rack containing a 90 kg ballast to the vehicle, did not deteriorate its lateral response characteristics. In fact, the test results indicate that its feedback characteristic, represented by the correlation loss for the lateral acceleration at zero time lag, is less sensitive to severity. Its roll and side slip characteristics assumed higher values than obtained for the standard vehicle, though.

7.4 Results for lane changes in a turn

This section summarises some of the test results obtained for lane change in a turn manoeuvres. This test is described in chapter 6. In contrast to the ISO lane change this test was performed on the MIRA steering pad. Due to its limited diameter of 76 m, tests could be conducted only at comparatively low speeds. A maximum speed of approximately 65 kph for steady state circling was achieved for the Jaguar test vehicle. Lane change in a turn manoeuvres commenced from circling on a constant radius of about 30 m, which left a sufficient run-off area towards the edge of the steering pad. The highest recorded entry speed was 55 kph.

The basic idea behind this test specification was to investigate the sensitivity of the vehicle's lateral response characteristics to the increasing influence of tyres operating in their non-linear performance envelope. Similar to the 'throttle off in a turn' test, the test starts from a steady state cornering condition, possibly involving tyres operating at high slip angles, followed by a transient event. It was believed that performing an evasive manoeuvre with tyres, operating relatively near their performance limit, would constitute a challenging control task.

However, the test data recorded for the Jaguar suggests that velocities achieved for this manoeuvre are too low to trigger a significant transient response. Even though the vehicle was driven to the limit performance of its tyres, its response remained well damped. The limit behaviour, established by this test procedure, was determined predominantly by the vehicle's steady state characteristics. Usually, the vehicle failed to complete the manoeuvre in the entry phase, because it was already operating at its steady state limit and could not turn in any more.

Consequently, results obtained by this test for different tyre constructions and for the alternative vehicle set-ups discussed in 7.3.4 discriminate differences in the limit behaviour to a far lesser extent than those established by the ISO lane change tests. Therefore, only a few examples of the test data gathered for this manoeuvre are presented.

In the first set of results, presented in 7.4.1, the effects of three different tyre designs on the limit behaviour of the standard Jaguar are compared. In section 7.4.2 the influence of sets of mixed tyre constructions is discussed, as was done in section 7.3.3 for the ISO lane change tests.

7.4.1 Effects of tyre construction on the lane change in a turn performance

In this section some results are presented, which were obtained for three different tyre designs. Lane change in a turn tests were conducted, using a set of the standard SP 2000 design, a set of Dunlop SP8000 245/45 R18 and one of the experimental slick tyres, which were referenced by 'XY/XY' in the previous sections.

The standard set-up is denoted as before. The tests for the experimental tyres are

denoted by diamonds and those for the SP 8000 design are referenced by triangles. Except in one case, tests were performed with an almost constant throttle position.

In fig. 7.4.1-1 and 7.4.1-2 results for the cross-correlation coefficients between the hand wheel angle and the lateral responses at zero time lag are found. The magnitude of the decrease in correlation is similar to that established by ISO lane change test results, shown in fig. 7.2-3 for the standard set-up. However, the response characteristics deteriorate within a much smaller speed range. There is hardly any difference between the three test configurations up to a speed of 12 m/sec. Beyond this velocity, the yaw rate response to the hand wheel angle (fig. 7.4.1-1) and the lateral acceleration response (fig. 7.4.1-2) roll off towards the limit speed of 14 m/sec. The smoothest roll-off is established by the slick tyre shod vehicle, which also achieved the highest average speed through the double lane change. The SP 8000 set-up provides almost the same peak performance, but at a lower level of input/ output correlation.

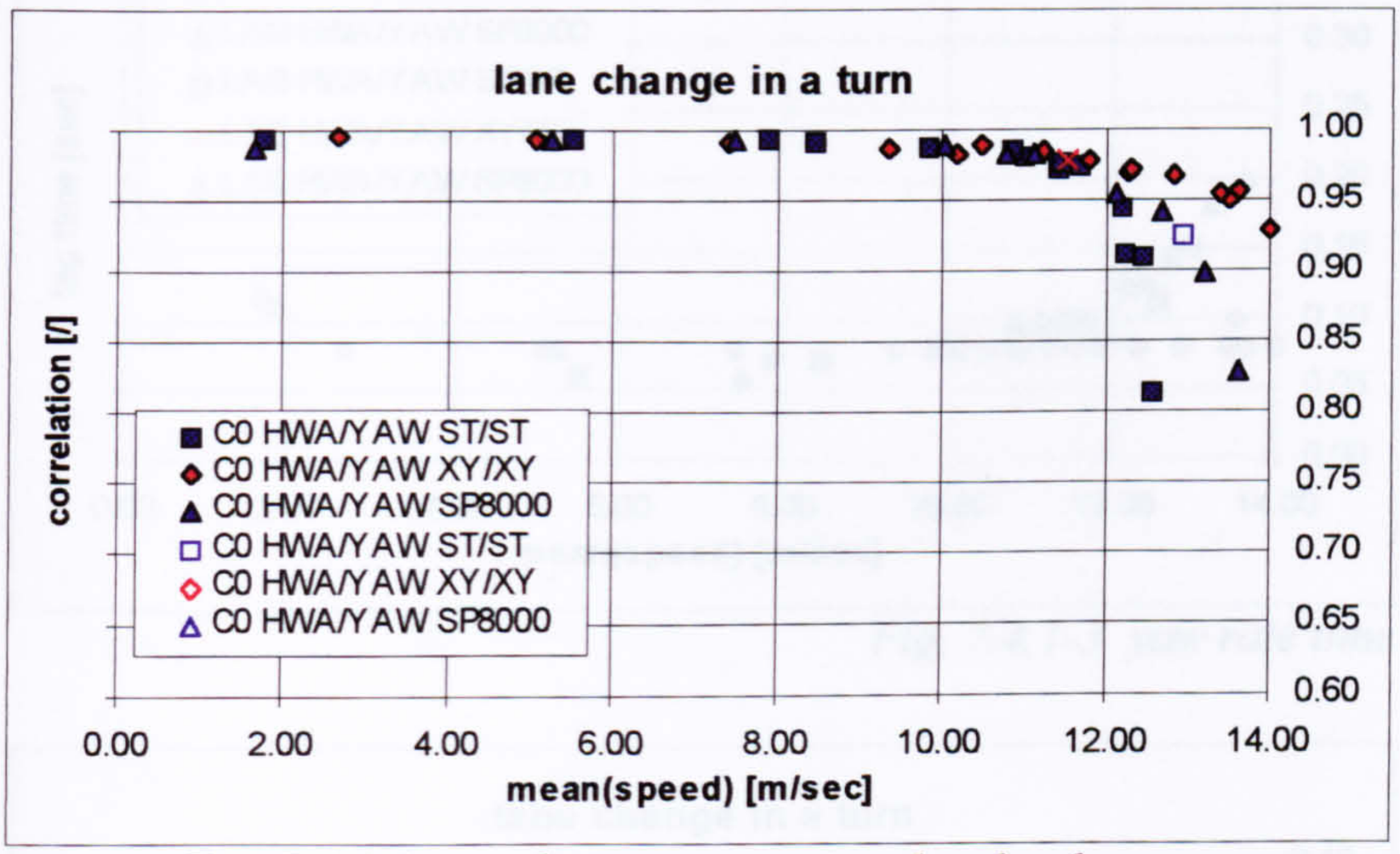

Fig. 7.4.1-1 correlation at zero time lag for the yaw rate response

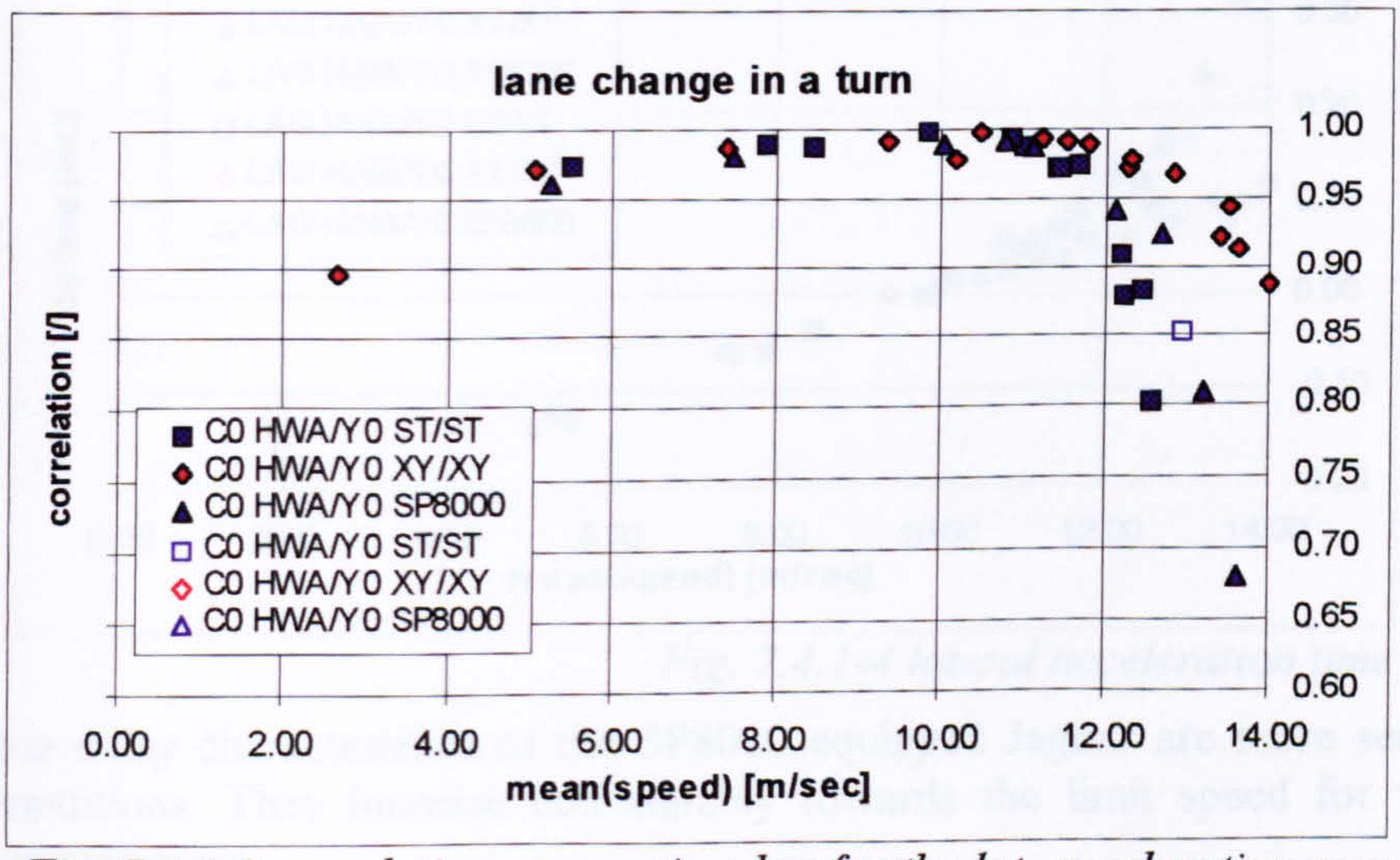

Fig. 7.4.1-2 correlation at zero time lag for the lat. acceleration response

The sharpest roll-off is found for the standard tyres, for which the lowest limit speed was recorded.

The corresponding response time lags are shown in fig. 7.4.1-3 and fig. 7.4.1-4. Again, the values established for limit speeds are similar to those obtained from the ISO lane change tests. The average yaw rate lag time is shorter than that for the lateral acceleration response. Lag times established for the standard car and especially those for the slick tyre set-up behave in a consistent manner for the limit approach. They remain constant in the case of the yaw rate and maintain a constant rate of change for the lateral acceleration response.

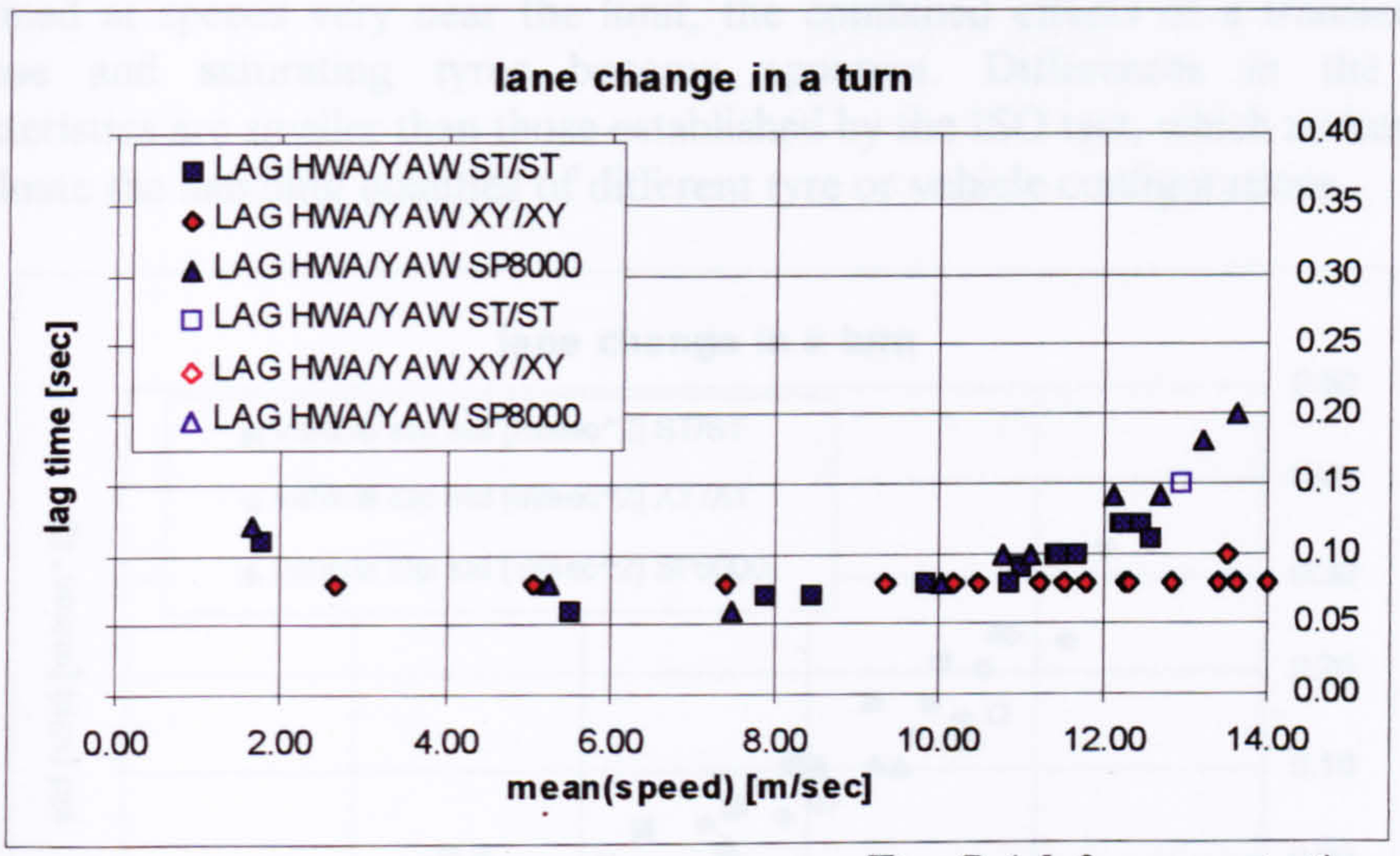

Fig. 7.4.1-3 yaw rate time lags

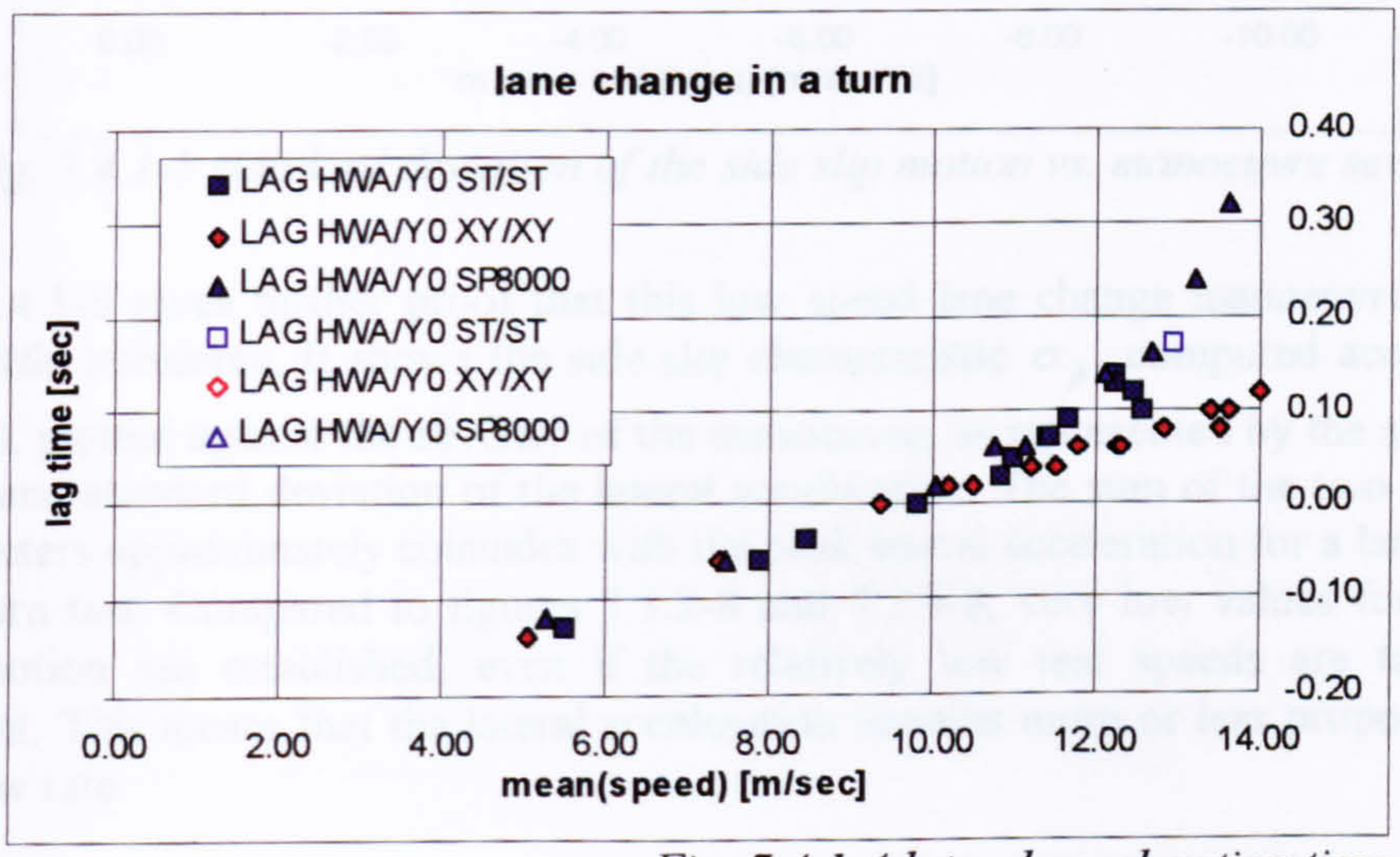

Fig. 7.4.1-4 lateral acceleration time lags

The time delay characteristics of the SP8000 equipped Jaguar are more sensitive to limit conditions. They increase considerably towards the limit speed for the more severe manoeuvres.

The negative delay times of the lateral acceleration, established for tests of low severity, may suggest that the lateral acceleration response leads the steering input. One has to consider though, that the delay time, as computed from correlating one signal to another, represents an average time shift for which the highest correlation is obtained. It is not to be confused with time delays computed from frequency response data.

The results, shown for the correlation coefficients and their corresponding time delays, illustrate the steady state nature of the lane change in a turn test. Only for tests performed at speeds very near the limit, the combined effects of a transient vehicle response and saturating tyres become apparent. Differences in the handling characteristics are smaller than those established by the ISO test, which makes it harder to evaluate the handling qualities of different tyre or vehicle configurations.

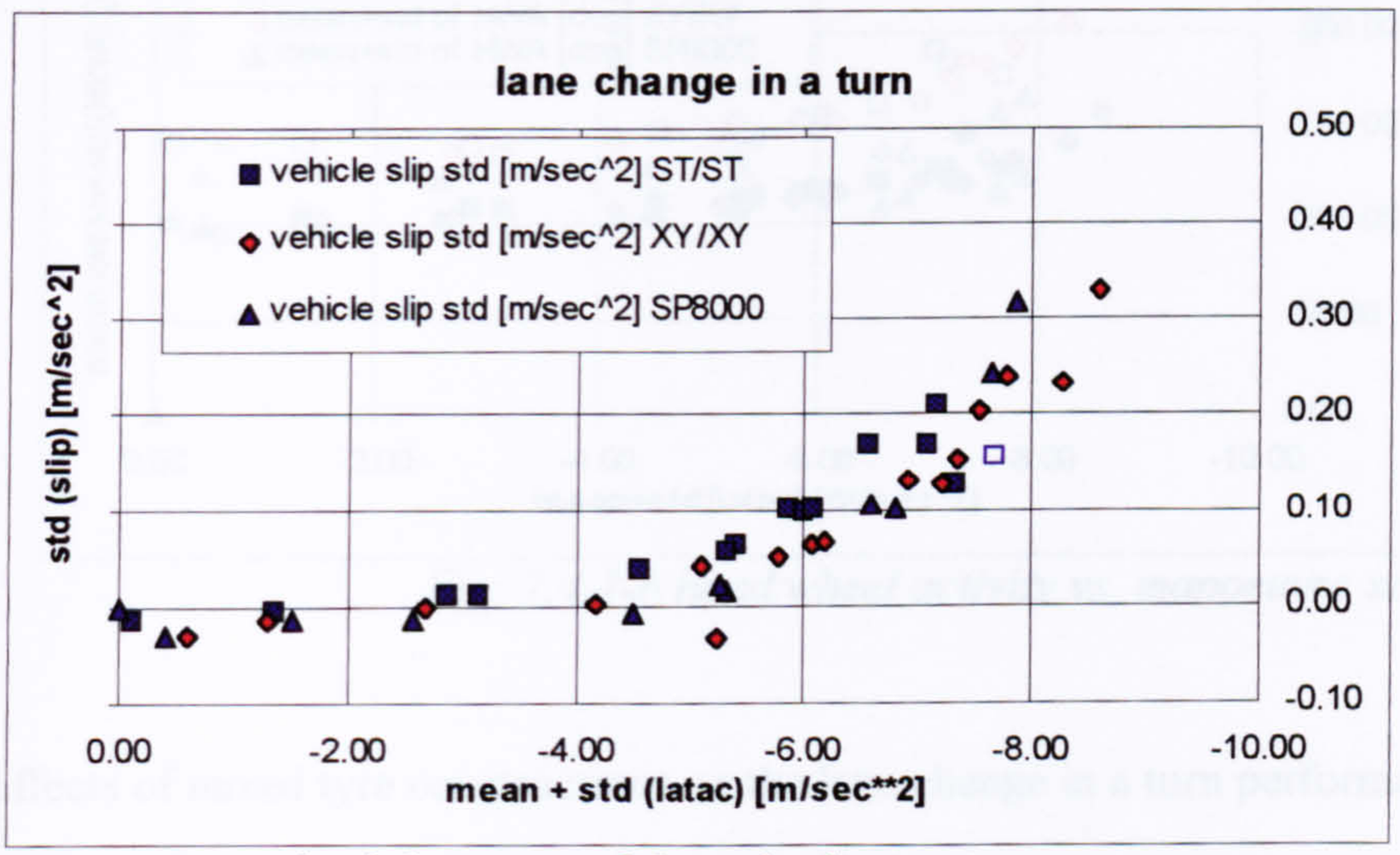

Fig. 7.4.1-5 standard deviation of the side slip motion vs. manoeuvre severity

Fig. 7.4.1-5 gives further proof that this low speed lane change manoeuvre involves very little transients. It shows the side slip characteristic $\sigma_{\dot{\beta}}$, computed according to (7.1.2), plotted against the severity of the manoeuvre, as represented by the sum of the mean and standard deviation of the lateral acceleration. The sum of the two statistical parameters approximately coincides with the peak lateral acceleration for a lane change in a turn test. Compared to figures 7.3.2-8 and 7.3.4-8, very low values for the side slip motion are established, even if the relatively low test speeds are taken into account. This means that the lateral acceleration remains more or less proportional to the yaw rate.

As this test predominantly reflects the steady state performance of a vehicle, it is appropriate to summarise the steering characteristics by a handling diagram, similar to

that used for describing the steady state cornering performance. In figure 7.4.1-6[1] two measures for the hand wheel angle activity are plotted against the parameter representing the severity of the manoeuvre, as used in fig. 7.4.1-5. Data points denoted by filled markers give the mean of the steering wheel angle. Those represented by blank ones refer to the sum of the mean and standard deviation of the of the steering wheel angle ('mean+std'). The graph indicates that the SP8000 set-up provides the most neutral steering characteristic. The limit steering characteristics of the other two are typical for understeering vehicles, for which an increasingly higher steering angle is needed for maintaining course at higher speeds.

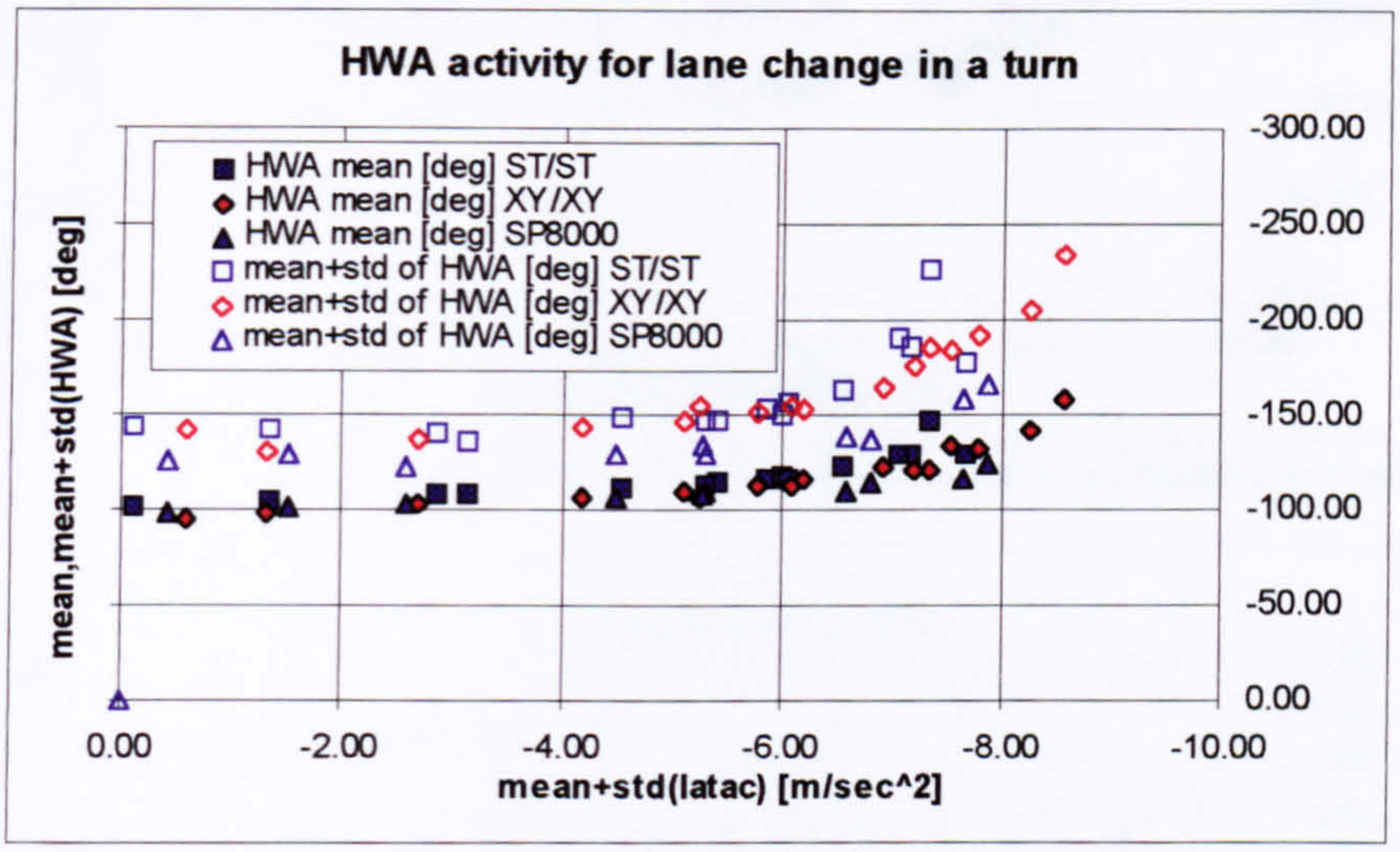

Fig. 7.4.1-6 hand wheel activity vs. manoeuvre severity

7.4.2 Effects of mixed tyre constructions on the lane change in a turn performance

This section concludes the discussion on the results obtained for the lane change in a turn tests. Some results are given, which were obtained for two sets of mixed tyre constructions. As for the ISO lane changes, the testing involved trials for which the Jaguar was fitted with winter tyres at the front and experimental slick tyres at the rear. The inverse set-up was tested as well.

In the results plots, the 'slick tyre front/ winter tyre rear' configuration is referred to by diamonds, whereas the 'winter tyre front/ slick tyre rear' fitment ('M2/XY') is denoted by triangles. The slick tyre all around fitment ('XY/XY') is used as a reference. Since there is very little difference between the three configuration regarding their correlation and time lag characteristics, the corresponding graphs are omitted.

The 'handling diagram' is shown in fig. 7.4.2-1. It indicates that there is no difference in the steering characteristics for the three set-ups up to a severity level of about 7.5

[1] negative values for the steering and severity measures indicate that the corresponding tests were performed anti-clockwise

m/sec^2. The limit speed was lowest for the 'slick tyre front/winter tyre rear' configuration, which corresponds to a comparatively low peak severity. At the limit speed the mean steering wheel angle is slightly lower than for the test performed at the

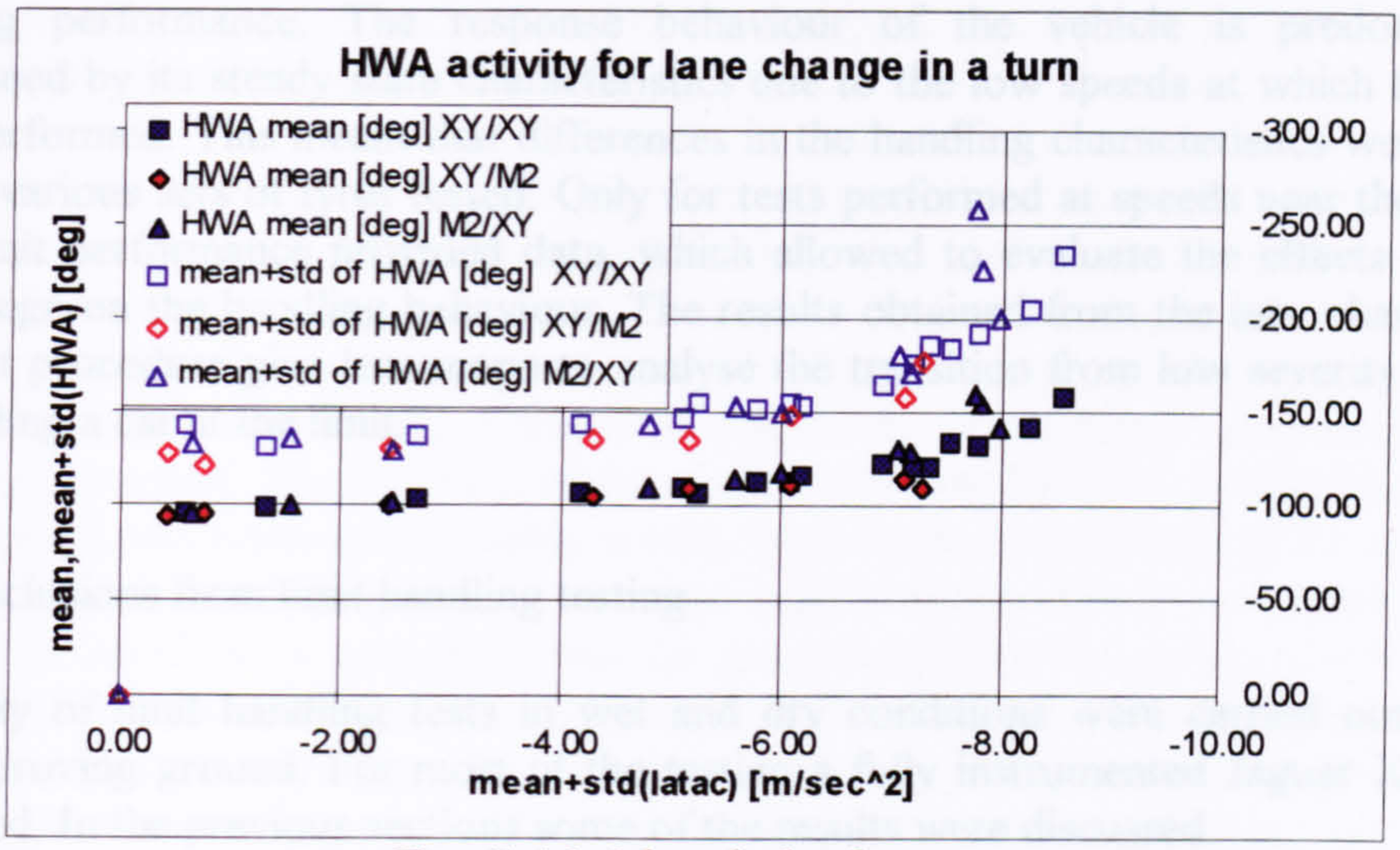

Fig. 7.4.2-1 hand wheel activity vs. manoeuvre severity

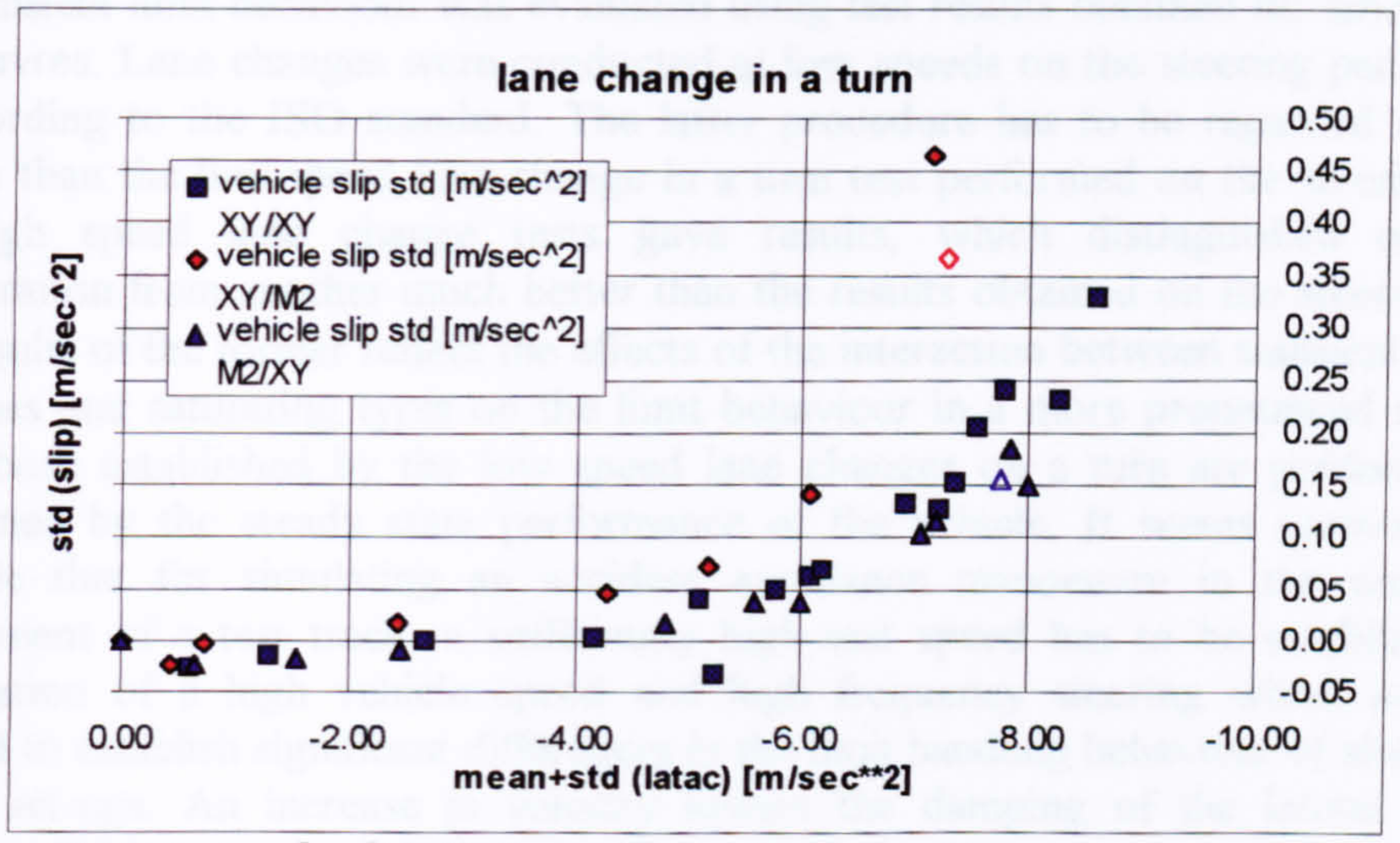

Fig. 7.4.2-2 standard deviation of the side slip motion vs. manoeuvre severity

second highest level of severity, while the sum of the mean and standard deviation increased by a small margin. The 'M2/XY' set-up understeers considerably more at the limit than the 'XY/XY' benchmark.

Finally, results indicating the side slip motion are given as in fig. 7.4.1-5. Although small in magnitude, the 'XY/M2' arrangement tends to side slip more for low severity lane changes, as can be seen from fig. 7.4.2-2. For tests near the limit, the discrepancy between yaw rate and lateral acceleration response increases at a large rate.

7.4.3 Conclusions

The lane change in a turn test proved to be less suitable for evaluating the limit handling performance. The response behaviour of the vehicle is predominantly determined by its steady state characteristics due to the low speeds at which the tests were performed. This meant that differences in the handling characteristics were small for the various sets of tyres tested. Only for tests performed at speeds near the steady state limit performance provided data, which allowed to evaluate the effects of each tyre design on the handling behaviour. The results obtained from the lane change in a turn test procedure give less scope to analyse the transition from low severity driving to handling a car at the limit.

7.5 Conclusions from limit handling testing

A variety of limit handling tests in wet and dry conditions were carried out at the MIRA proving ground. For most of the testing a fully instrumented Jaguar XJ6 was employed. In the previous sections some of the results were discussed.

The transient limit behaviour was evaluated using test results obtained for lane change manoeuvres. Lane changes were conducted at low speeds on the steering pad as well as according to the ISO standard. The latter procedure has to be regarded as more suitable than the low speed lane change in a turn test performed on the steering pad. The high speed lane change tests gave results, which distinguished one test configuration from another much better than the results obtained on the steering pad. Test results of the former reflect the effects of the interaction between transient vehicle responses and saturating tyres on the limit behaviour in a more pronounced manner, while those established by the low speed lane changes on a turn are predominantly determined by the steady state performance of the vehicle. It seems reasonable to conclude that for simulating an accident avoidance manoeuvre in the controlled environment of a test track, a sufficiently high test speed has to be established. A combination of a high vehicle speed and high frequency steering wheel inputs is required to establish significant differences in the limit handling behaviour of alternative chassis set-ups. An increase in velocity lowers the damping of the lateral vehicle responses. Increasing hand wheel speeds combined with saturating tyres excite the non-linear dynamic response of the vehicle. The interaction of these effects determine the difficulty of the control task the driver faces in a limit manoeuvre, as well as the assessment of the vehicle or its tyres.

The results for the ISO lane change test presented in the previous sections show that significant differences in the handling behaviour of a vehicle can be established, depending on tyre design, inflation pressures and on suspension properties. The criteria used to evaluate the limit handling quality included cross-correlation coefficients and time lags. The former represent the rate of agreement between the driver's control input and the vehicle response, while the latter describes the average delay in the vehicle's reaction. Most of the test results established that the correlation between

steering wheel input and lateral vehicle response deteriorates accompanied by increasing time delays for approaching the limit performance of the vehicle in small increments. However, inflation pressures and tyre design can make a big difference to the magnitude of the correlation coefficients and time lags as well as to their rate of change with increasing manoeuvre severity.

Although it is believed that these measures are suitable to discriminate a well handling vehicle from a car behaving in an unpredictable fashion, further handling characteristics have to be included in the evaluation. Test driver comments suggest that they place some emphasis on the roll response of a vehicle. Especially, the combination of roll and amplified yaw motion during a transient manoeuvre is regarded as an undesirable response behaviour. The handling of the Jaguar was rated poorly, mainly because of the excessive roll experienced during a test, when a roof rack carrying 90 kg ballast was fitted and when its anti-roll bar was removed. For these two cases, cross-correlation coefficients and lag times do not establish a deficiency in the lateral response behaviour. However, additional results indicate that the two vehicle modifications resulted in larger roll and side slip motions compared to the standard set-up for the same manoeuvre severity. Representative parameters for these characteristics were introduced and subsequently used as additional handling quality measures.

8 Tyre - Suspension interaction for steady state cornering

From the basic literature it is well known that the guidance forces produced by a tyre in the longitudinal and lateral directions depend on the respective slip quantities, the camber angle and the vertical load. These variables are controlled by the vehicle's steering and suspension systems. The suspension's geometry and its load transfer characteristics determine to a great extent the shape and pressure distribution of the contact patch and thereby the performance of tyre and vehicle. Before looking into the transient vehicle behaviour, the interaction between tyre and suspension is analysed for steady state cornering manoeuvres. The results show how tyres and suspension influence each other, yielding either a more or a less satisfactory limit handling behaviour, depending on the various properties involved in the tyre and suspension design. Using the 'Steady State Cornering Model' discussed earlier, different suspension designs as well as tyre characteristics were analysed with respect to their effect on the limit handling quality. In the next section a short introduction into the basic mechanics of the steady state cornering condition is given and followed by some information about the simulation and data preparation, before results and conclusions are presented.

8.1 Basic mechanics of the steady state cornering condition

Many different vehicle suspension designs can be found on current production cars. There are rather simple designs such as the McPherson strut, often employed for small and medium sized front wheel driven vehicles, and there are more elaborate types, such as the five link suspension used for luxury vehicles. In any case, the suspension geometry defines how relative camber and scrub (or track change) properties change with the wheel travel going from full rebound to full bump. Furthermore, roll or bump steer and the amount of Ackermann steering, i.e. how much the inside wheel is turned in more than the outside, has to be considered too for the steered front wheels. For the general three dimensional case, other design parameters, such as the wheelbase and castor, may alter as well, due to the corresponding vertical motion of the wheel. Apart from the kinematic properties, compliance characteristics of a suspension design are important. Since suspension elements such as wishbones, links and struts are attached to the hub or to the chassis

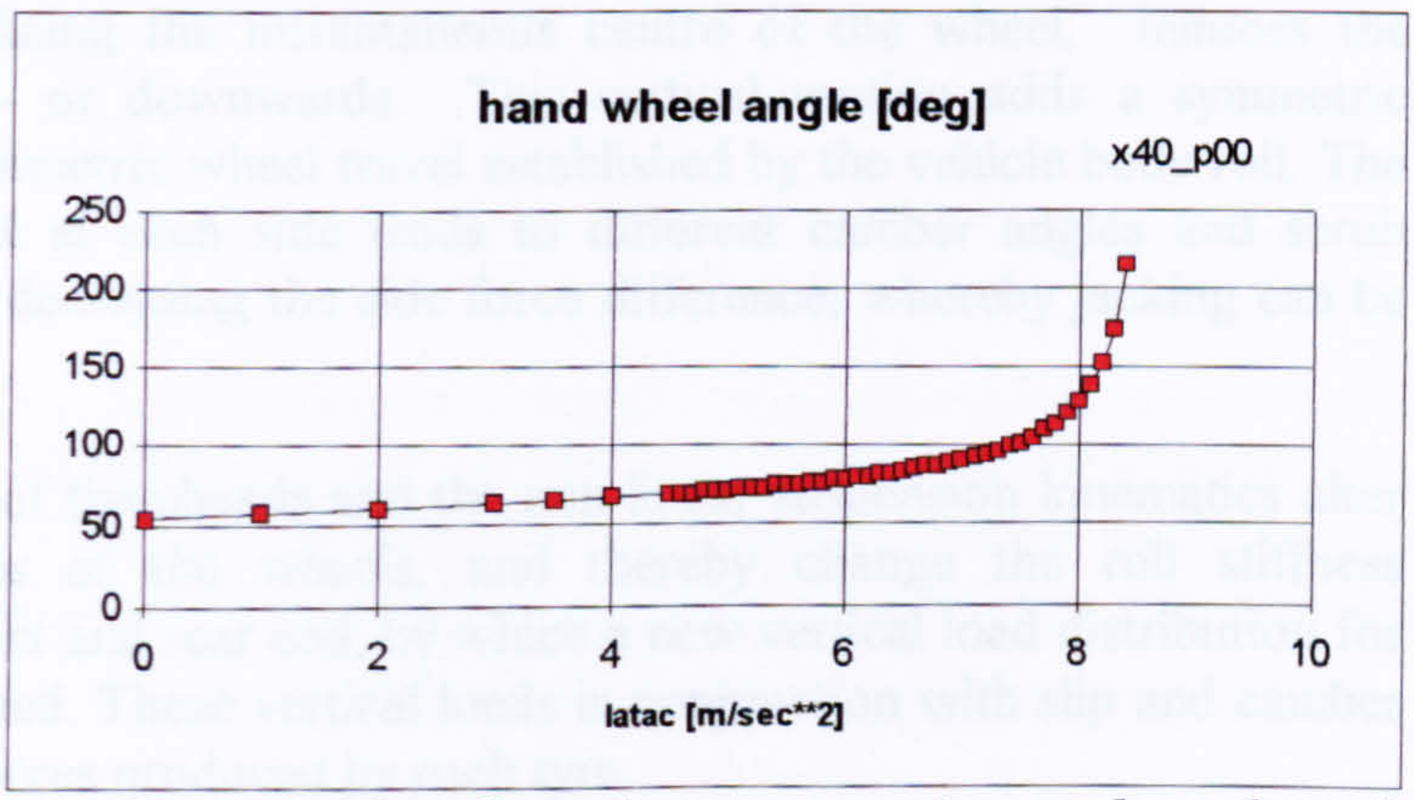

Fig. 8.1-1 handling diagram: steering angle vs. lateral acceleration

by flexible rubber bushes, additional side force steer and/ or longitudinal force steer affect the balance of the car.

Other important features of a suspension design are the bump and rebound stops, which limit the relative wheel travel in either direction. After their engagement they act in parallel to the usually linear springs.

The steady state cornering performance of a vehicle is best represented by the handling diagram (fig. 8.1-1), showing the hand wheel angle against lateral acceleration, from which a linear and a non-linear region can be distinguished.

The linear behaviour up to 0.5 g for that example represents a vehicle, which has a constant ratio of lateral load transfer between front and rear and an almost linear relation between side force and slip as well as camber angle. The former is determined by the spring and anti-roll bar stiffness as well as by constant roll centre heights front and rear.

From fig. 8.1-1 it can be seen that the lateral load transfer does not affect the linear response of the vehicle up to 0.5 g, since the loss of side force at the inside tyre is accounted for by an equivalent gain at the heavier loaded outside tyre. But it will be shown that for the limit region one has to abandon the notion of linear tyre and suspension behaviour. Both systems start to interact strongly, and it is hard to trace which design features are the most influential on the limit handling performance.

In a constant radius cornering test the vehicle travels with a constant speed, which is equivalent to a certain lateral acceleration. The driver has to adjust the hand wheel in such a way that side forces at each end are produced, which match the centrifugal forces corresponding to the forward speed. Starting from the tyres upwards, which are loaded differently at each side, the outside wheel produces more side force under a similar slip angle than its counterpart at the inside. This force difference together with the scrub derivative, defining the instantaneous centre of the wheel, induces the vehicle body to jack up- or downwards. This vertical motion adds a symmetric component to the anti-symmetric wheel travel established by the vehicle body roll. The difference in wheel travel at each side leads to different camber angles and scrub derivatives, increasing or decreasing the side force difference, whereby jacking can be reduced or pronounced.

Furthermore, the jacking of the chassis and the non-linear suspension kinematics alter the instantaneous centres of the wheels, and thereby change the roll stiffness contributions from the front and rear end, by which a new vertical load distribution for all four wheels is established. These vertical loads in conjunction with slip and camber angles define the lateral forces produced by each tyre.

The difficulty in analysing limit handling behaviour does not arise exclusively from the nonlinear relation between lateral tyre force and slip angle, which would determine, given the vehicle mass distribution, the slip angles at the front and rear end of a bicycle

type vehicle, and hence the degree of under- or oversteer. Moreover, one has to resolve the cross-coupling between lateral forces, camber, and vehicle roll, pitch and heave established by certain suspension properties, which will be analysed in some detail in the following sections. The basic dependencies are explained using the formulas derived for the 'Steady State Cornering Model' in chapter 3.

Apart from the slip angle, the resultant side force each tyre produces depends on the camber angle and on the vertical load. The camber angles influence the performance of the tyres to some extent. They increase or decrease the cornering force depending on their sign and magnitude. Additionally, the peak performance can be reduced by the presence of camber, which can be ascribed to a less favourable pressure distribution in the contact patch, reducing the friction coefficient.

The camber angle present at each wheel depends on the relative wheel travel established by a combination of roll, pitch and heave motion of the chassis. According to the equations describing the 'Steady State Cornering Model', based on the assumptions that the wheel contact points remain at ground level, and secondly, that tyre deflections can be neglected, the wheel travel is composed of a symmetric part equivalent to the vehicle heave, and an anti-symmetric part proportional to the vehicle body roll. The symmetric part is given by (3.1.9) and (3.1.36-37), and can be approximated[1] by:

$$\Delta z^B \approx \frac{-\sum_1^4 y_i' \cdot F_{y,i}}{\sum_1^4 K_i \cdot (\frac{\partial_i}{\partial z})^2}$$

The body roll can be approximated using (3.1.10), (3.1.36-37) as follows:

$$\varphi^B \approx \frac{-\sum_{i=1}^4 (h + y_i' \cdot t_i) \cdot F_{y,i}}{\sum_{i=1}^4 K_i \cdot (\frac{\partial_i}{\partial z_i})^2 \cdot t_i^2 + \sum_{j=1}^2 c_{\varphi,j}^{RB}}$$

In contrast to the equations concerning the 'Steady State Cornering Model', the vehicle degrees of freedom (DoF) are given for the whole system rather than for only the front or rear half, and therefore the index 'f' is omitted. We recognise that both vehicle DoF are proportional to the sum of the products of side force $F_{y,i}$ and the corresponding scrub derivative y_i ', as well as inversely proportional to the wheel rates given by spring stiffness K_i, spring length derivative $(\frac{\partial_i}{\partial z})$ and anti roll bar stiffness

[1] for the approximations it is assumed that the unsprung masses are negligible, and that the wheel rates at each side for each end are equal

$c_{\varphi,j}^{RB}$. This means that either high differences between the side forces on the outside and inside, or very different scrub derivatives increase the jacking tendency of the chassis. Jacking would not occur for the theoretical case, for which the side forces remain equal, and the track changes behave equal opposite for the left and right hand wheel of each axle.

For limit cornering at high lateral acceleration, the non-linear vertical load effect on the cornering performance of the tyre becomes apparent. The loss of cornering power at high loads can only be compensated by even higher slip angles. The vertical load distribution is again a function of suspension and tyre properties, as can be seen from:

$$\Delta F_{z,i} \approx K_i \cdot (\frac{\partial_i}{\partial z})^2 \cdot z^B + (K_i \cdot (\frac{\partial_i}{\partial z})^2 \cdot t_i + \frac{c_{\varphi,j}^{RB}}{2 \cdot t_i}) \cdot \varphi^B - y_i \cdot F_{y,i}$$

Again we notice the influence of the wheel rates and the anti-roll bar and that of the scrub derivative. A high negative value of the latter, which would indicate a rather high roll centre height for the static case, leads to an increase of the wheel load.

Summarising it can be said that these simple approximations indicate the complexity of the tyre-suspension interface rather well, even so they are not valid for the true limit case, where bump or rebound stops are engaged, leading to high wheel rate differences on one axle. They show that lateral and vertical forces as well as wheel travel and camber are strongly coupled, and that their relations are determined by parameters giving the scrub derivative and wheel rate.

It becomes obvious that controlling the wheel travel is important to control the camber angles and their corresponding side forces as well as the wheel rates, since these give the constraints according to which each tyre has to produce its guidance force. If these constraints are such, that the necessary side forces at the rear end can only be produced at higher slip angles than at the front, the limit handling behaviour would be oversteer and for the opposite it would be understeer.

8.2 Vehicle and tyre data used for simulation

In order to highlight some of the effects of the tyre-suspension interface and their impact on the vehicle's handling, a case study was carried out, in which some suspension types and their combinations were analysed. The following sections summarise the vehicle, suspension and tyre data used for the simulation.

8.2.1 Vehicle data

For the experiment two baseline data sets were developed, which represent two rather different vehicles. The first vehicle modelled is the Jaguar X40 (table 8.2-1) of 1993 and the second one a Rover 2.0 litre estate from 1995 (table 8.2-2). For all steady state cornering simulations tyre data was used from a measured Dunlop D8 195/65 R15 (2.0 bar). It has to be said that this tyre is not original equipment for either of the cars mentioned above. But it is a typical specimen fitted to cars of the same class and weight as the Rover. In order to make the heavy Jaguar compatible to this tyre, its total mass was lowered to 1708 kg, which is a representative load value for the tyre as original or replacement product. Analogous to the mass the static wheel rates were changed too, to give similar ride frequencies as the original.

- **vehicle data for X40 93MY data**
-
- **total mass : 1708 kg**
- **wheelbase: 2.87 m**
- **half track width: 0.75m front, 0.764 m rear**
- **CoG height: 0.57 m**
- **wheel load: 4350 [N] front, 4027 [N] rear (52%:48%)**
- **roll rate adjusted to give 7.5deg/g**
- **lateral load transfer ratio front to rear: 1.25**
- **original tyre: Pirelli P4000 225/60 R16**
- **original suspension: double wishbone front & rear**
- **roll centre heights: 9cm front, 14cm rear**

Table 8.2-1 Jaguar XJ6 vehicle data

- **Rover 2.0 litre**
-
- **total mass : 1350 kg**
- **wheelbase: 2.50 m**
- **half track width: 0.73m front, 0.73 m rear**
- **CoG height: 0.50 m**
- **wheel load: 3973 [N] front, 2650 [N] rear (60%:40%)**
- **roll rate adjusted to give 7.5deg/g**
- **original tyre: Dunlop D8 185/55 R15**
- **original suspension:**
- **lateral load transfer ratio front to rear: 1.15**
- **McPherson strut front, twist beam axle rear**

Table 8.2-2 Rover 2 litre vehicle data

The handling of these vehicle models were simulated for different suspensions fitted to the front and rear end. The analysis involved combinations of two McPherson Strut and two double wishbone suspensions, a trailing arm rear, and a swing axle rear design. In order to make the simulation results for all these vehicles with different suspension systems comparable, it was decided to introduce two constraints, which all derivatives of each baseline vehicle have to comply with. Firstly, all specimen have a static roll stiffness distribution to give a roll resistance of about 7.25 deg of roll per 1g

lateral acceleration for the Jaguar derivatives and 7.5 deg/g for the Rover derivatives. Secondly, their static lateral load transfer ratio is set to 1.25 and 1.15 respectively. These constraints reduce the number of possible simulations and make sure that the limit handling of each vehicle specimen is not determined almost exclusively by the static load or roll stiffness distribution. Hence, the sensitivity of the tyres to load changes are of the same order, whatever suspension combination is investigated and compared to another one. In the end it does not make sense to compare a sports car like vehicle with a high roll stiffness against a soft sprung saloon car.

8.2.2 Suspension data

A wide range of suspension types were analysed including a McPherson strut, double wishbone, tailing arm and swing axle designs. As an example of the first type, the Ford Escort front suspension of the 1995 model year was chosen as described in /8.2.1/.

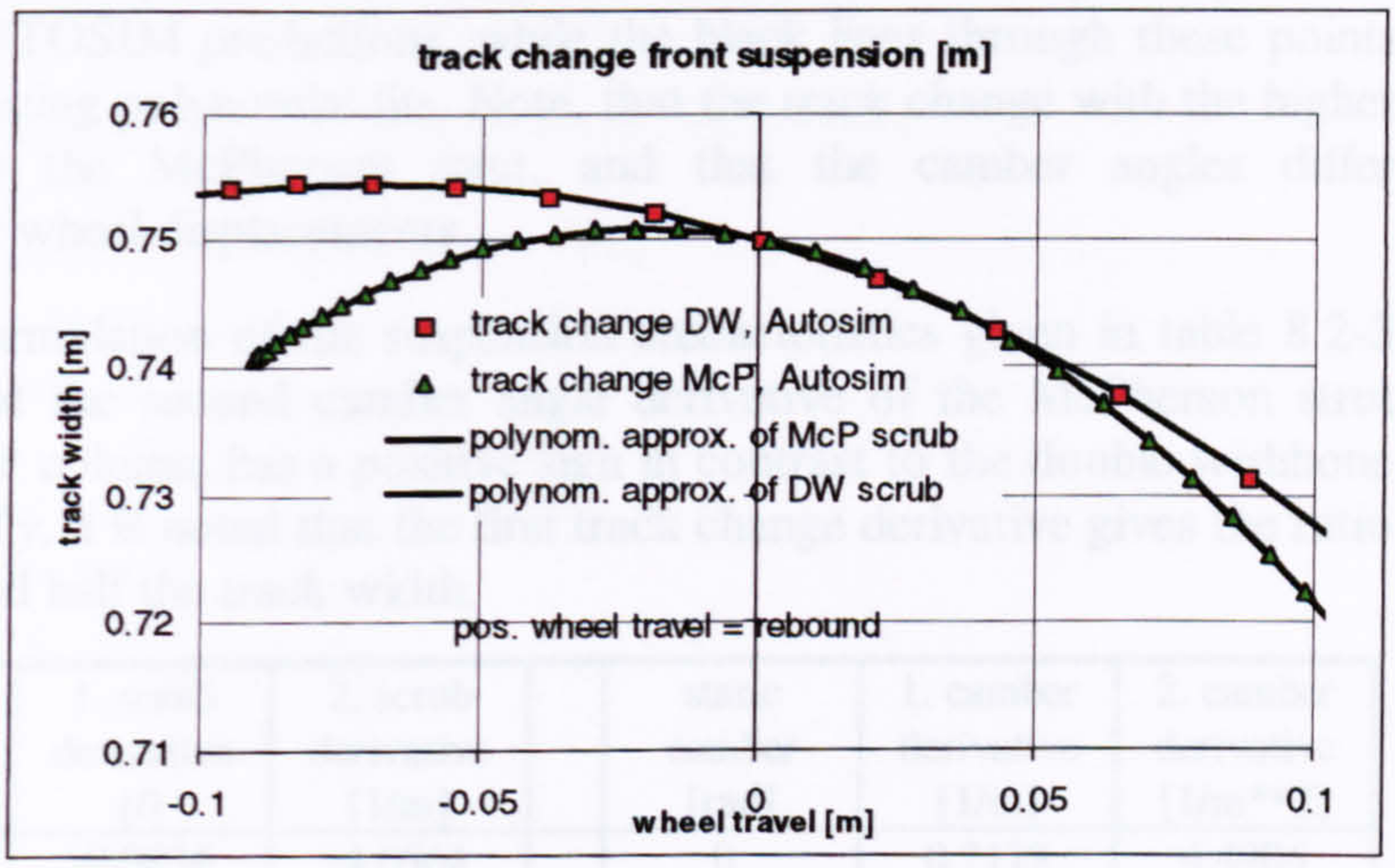

Fig. 8.2-1 track change vs. wheel travel

The geometry of the front and rear double wishbone suspension of the X40 was obtained from an ADAMS full vehicle model that contained the relevant geometry data /8.2.2/. In addition to that, Jaguar Cars supplied information on weights, wheel rates, roll centre heights, bump steer characteristics and all the other model input parameters discussed in sections 3.1 and 3.2.

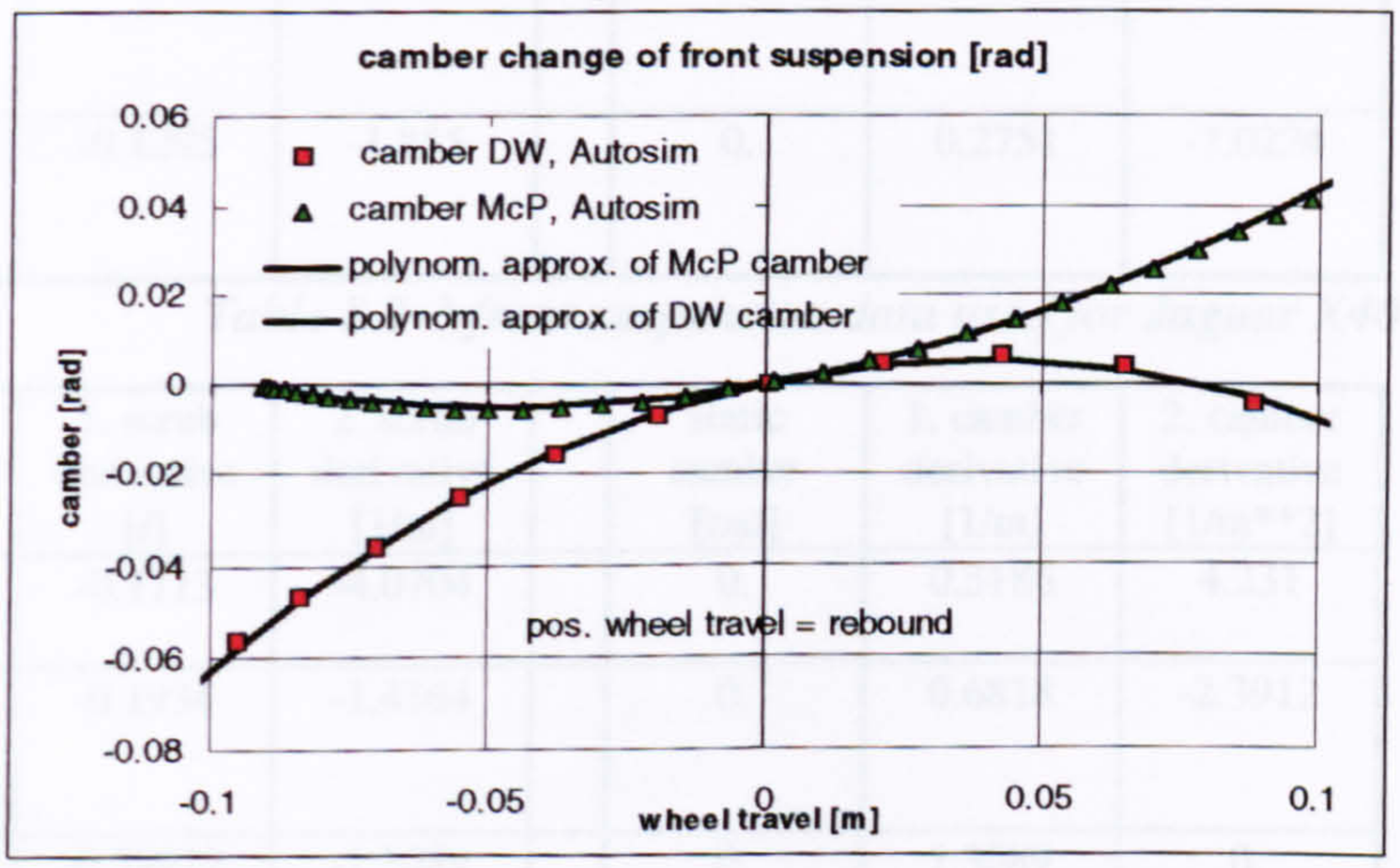

Fig. 8.2-2 camber change vs. wheel travel

As representatives of trailing arm and swing axle designs,

the simplest configurations were selected, which are a trailing arm pivoting about a horizontal axis in front of the wheel centres, and a pendulum axis with a common pivot on the vertical centre line of the vehicle.

The geometric data of these suspensions had to be transformed into formulations for the track and camber change with respect to the wheel travel, after which it can be used in the 'Steady State Cornering Model'. Using AUTOSIM, two-dimensional models of a McPherson and a double wishbone suspension were created to extract these suspension properties. Subsequently, second order polynomials were fitted to the data of the track and camber change for wheel displacements of 10 cm in bump and rebound. Their coefficients were used as input data for the 'Steady State Cornering Model'. For the two simple suspension designs of a trailing arm and a swing axle, these polynomial coefficients were found analytically. In the plots fig 8.2-1 and fig. 8.2-2 the track and camber changes of the Jaguar double wishbone and those of the Escort McPherson strut suspension are compared. Points indicated by triangles and boxes refer to the AUTOSIM predictions, while the black lines through these points represent the well agreeing polynomial fits. Note, that the track change with the higher curvature belongs to the McPherson strut, and that the camber angles differ considerably for larger wheel displacements.

From the analytical formulation of the suspension characteristics given in table 8.2-3 and 8.2-4, we see that the second camber angle derivative of the McPherson strut design, given in the last column, has a positive sign in contrast to the double wishbone suspension. Additionally, it is noted that the first track change derivative gives the ratio of roll centre height and half the track width.

suspension type	half track width [m]	1. scrub derivative [/]	2. scrub derivative [1/m]		static camber [rad]	1. camber derivative [1/m]	2. camber derivative [1/m**2]
McPherson strut (Ford Escort 95MY)	0.75	-0.0834	-4.0564		0.	0.2119	4.4906
double wishbone (X40 93MY)	0.75	-0.1295	-1.855		0.	0.2751	-7.0224

Table 8.2-3 front suspension data used for Jaguar X40

suspension type	half track width [m]	1. scrub derivative [/]	2. scrub derivative [1/m]		static camber [rad]	1. camber derivative [1/m]	2. camber derivative [1/m**2]
McPherson strut	0.764	-0.1713	-4.0704		0.	0.3186	4.231
double wishbone (X40 93MY)	0.764	-0.1934	-1.4164		0.	0.6818	-2.3912
swing axle	0.764	-0.39922	-1.3089		0.	1.3089	0.
trailing arm	0.764	0.	0.		0.	0.	0.

Table 8.2-4 rear suspension data used for Jaguar X40

The same first and second suspension derivatives as given in the tables 8.2-3 and 8.2-4 were used for the simulations concerning the Rover baseline vehicle.

Bump and rebound stops were introduced, in order to limit the wheel travel to up to 12 cm in either direction. Since original data describing the characteristics of the latter were not available, it was presumed that both bump and rebound stops are engaged at 7 cm wheel travel, and that their characteristics can be based on the same force-displacement relation. This generic description was used for both front and rear end.

8.2.3 Tyre data

As mentioned in section 8.2.1, measured tyre data of a Dunlop D8 195/65 R15 were used to extract the 'Magic Formula' coefficients for the lateral force-slip angle and aligning torque-slip angle relationships. Data describing the influence of camber on these were not available, so that 'default values' as published in the first paper dealing with the 'Magic Formula' /2.4.6/ had to be chosen.

$$F_y = D \cdot \sin\left(C \cdot \arctan\{(Bx - E \cdot (Bx - \arctan(Bx)))\}\right)$$

$$D = \left[(a_1 F_z + a_2) \cdot (1 - \mathbf{a_{15}} \gamma^2)\right] \cdot F_z$$

$$BCD = a_3 \cdot \sin\left(\left[2 \cdot \arctan\left\{F_z / a_4\right\}\right] \cdot (1 - \mathbf{a_5} \cdot |\gamma|)\right)$$

$$E = (a_6 F_z + a_7) \cdot \left\{1 - (\mathbf{a_{16}} \gamma + a_{17}) \cdot \mathrm{sgn}(\alpha + S_{hy})\right\}$$

$$S_{hy} = a_8 \cdot F_z + a_9 + \mathbf{a_{10}} \cdot \gamma$$

$$S_{vy} = a_{11} \cdot F_z + a_{12} + (\mathbf{a_{13}} \cdot F_z^2 + \mathbf{a_{14}} \cdot F_z) \cdot \gamma$$

$a_5 = 1.261$

$a_{10} = 0.028$

$a_{13} = 0.0$

$a_{14} = 0.848$

$a_{15} = 10.0$

$a_{16} = 0.0$

Table 8.2-5 camber coefficients in 'Magic Formula'

In table 8.2-5 those coefficients relating to camber proper-ties of the side force-slip angle relation are highlighted, and their values as used in the experiment are given. The corresponding plot for a vertical load of 4000 N is shown in fig. 8.2-3. In the linear region the side force increases with camber, which can be ascribed to a_{14} coefficient, while for high slip angles the camber effect is less obvious. The detrimental effect of camber on the peak force

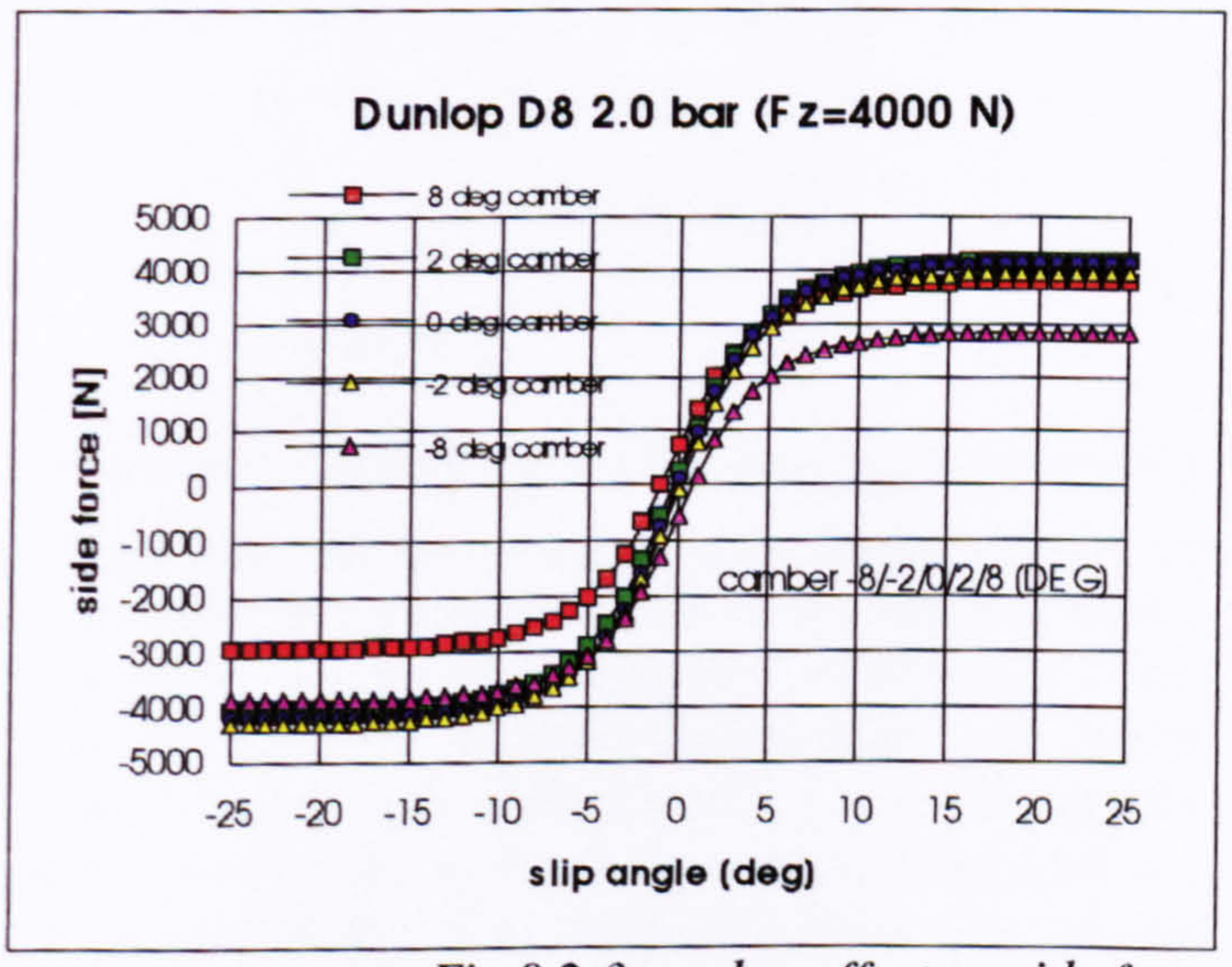

Fig 8.2-3 camber effect on side force

represented by a_{15} cancels out the gain made in the linear region. On the other hand we can see that an adverse camber angle leads to a considerable loss of side force for the sliding condition. In the literature plots can be found stating a different camber behaviour for high slip angles /8.2.3, 8.2.4/. There, the linear side force-camber relation seems to hold even for high slip angles.

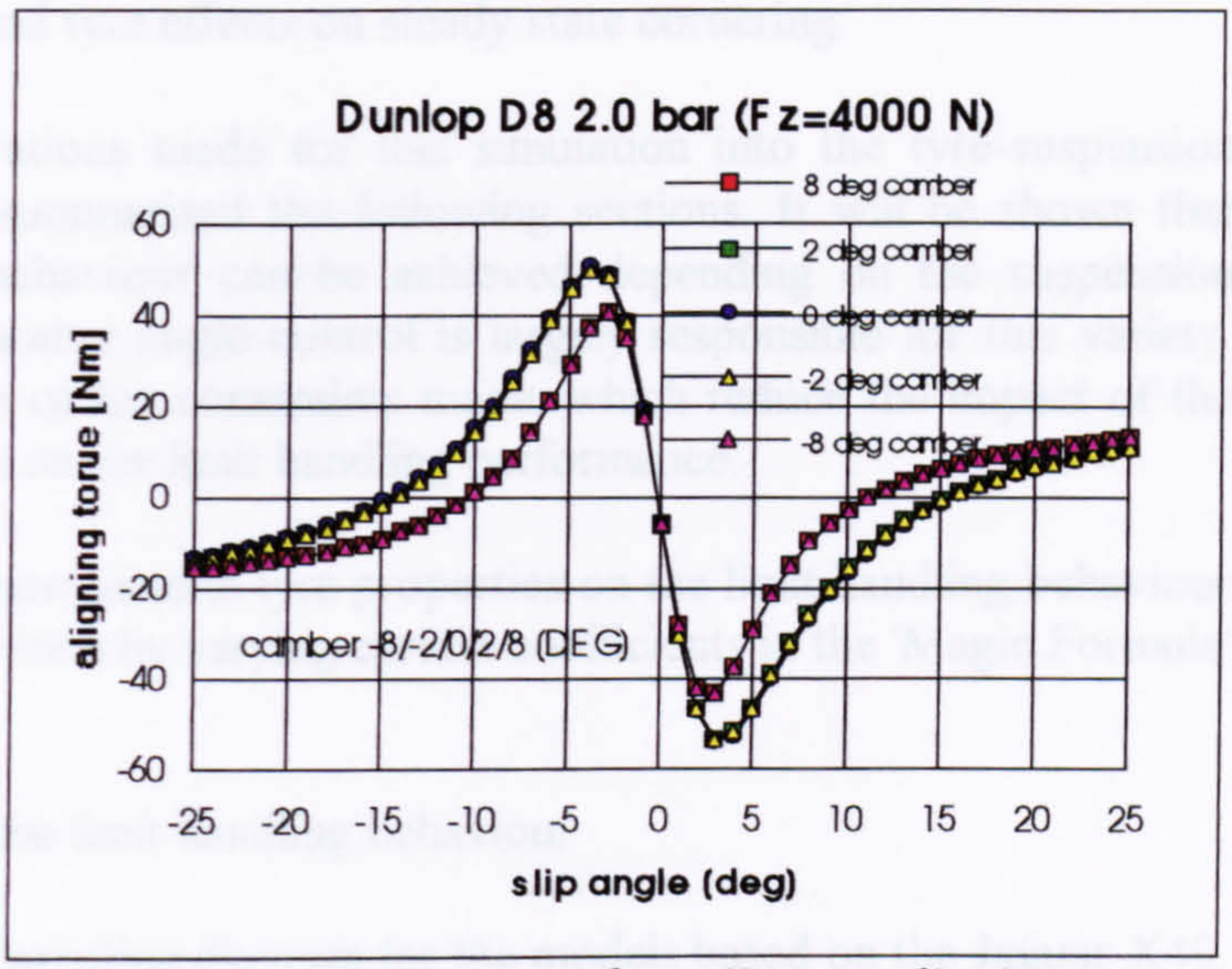

Fig. 8.2-4 camber effect on aligning torque

The aligning torque, as shown in fig. 8.2-4, behaves less sensitive to camber (at least for the model data used here), especially to the angle's orientation. It needs rather large angles to reduce the peak values, which occur at slightly lower slip angles.

8.3 Analysis of suspension and tyre effects on steady state cornering

After discussing the preparations made for this simulation into the tyre-suspension interface, some results are summarised the following sections. It will be shown that almost any limit handling behaviour can be achieved depending on the suspension combination utilised. The camber angle control is largely responsible for this variety. This is partly a consequence of the constraints made, which reduce the impact of the tyre's vertical load sensitivity on the limit handling performance.

Furthermore, the effect of some generic tyre properties on the limit handling behaviour are analysed, which is easily done by varying certain coefficients in the 'Magic Formula' tyre model.

8.3.1 Suspension effects on the limit handling behaviour

The analysis begins with the handling diagram for the models based on the Jaguar X40. In fig. 8.3-1 the hand wheel angle against the lateral acceleration is shown for all

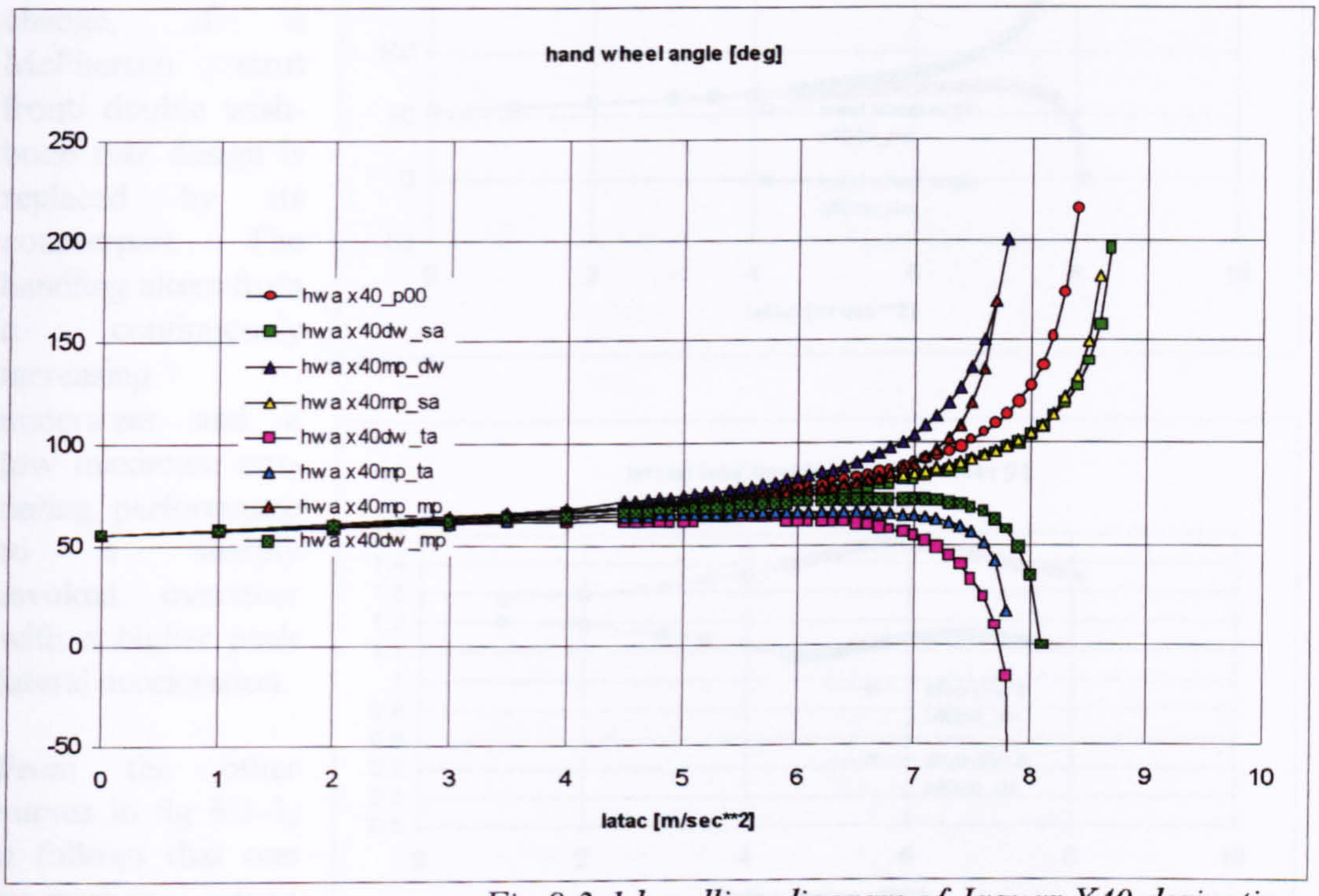

Fig.8.3-1 handling diagram of Jaguar X40 derivatives

investigated suspension combinations. The abbreviations used in the legend refer to the suspension type. For instance, x40dw_mp depicts the car with the original double wishbone design at the front and a McPherson strut configuration similar to that of the Escort front suspension at the rear. Subsequently, 'sa' stands for the swing axle and 'ta' for the trailing arm rear suspension design, both given in table 8.2-4, whereas the 'x40p00' refers to the original design with double wishbone type suspensions front and rear. It can be seen that the original version as well as those with swing axle rear and McPherson front suspensions give final understeer behaviour, whereas a trailing arm

design for the rear as well as a double wishbone front and a McPherson rear suspension combination lead to final oversteer.

It has to be noted that the constraints concerning the roll stiffness distribution and the lateral load transfer ratio could not be met for the vehicles with a swing axle rear suspension. The reason is, that a swing axle design provides a high roll centre giving a higher roll resistance, even without anti roll bars, than defined for all other model variants. At the same time this design promotes more lateral load transfer to occur at the rear. As a consequence comparatively smaller roll and thereby smaller camber angles are encountered at high lateral accelerations, which explains that the swing axle shot model achieves even a higher cornering performance.

Apart from the rather odd example of the swing axle, we notice a dramatic handling change, if a McPherson strut front/ double wishbone rear design is replaced by its counterpart. The handling alters from a continuously increasing understeer and a low maximum cornering performance to a sharply invoked oversteer with a higher peak lateral acceleration.

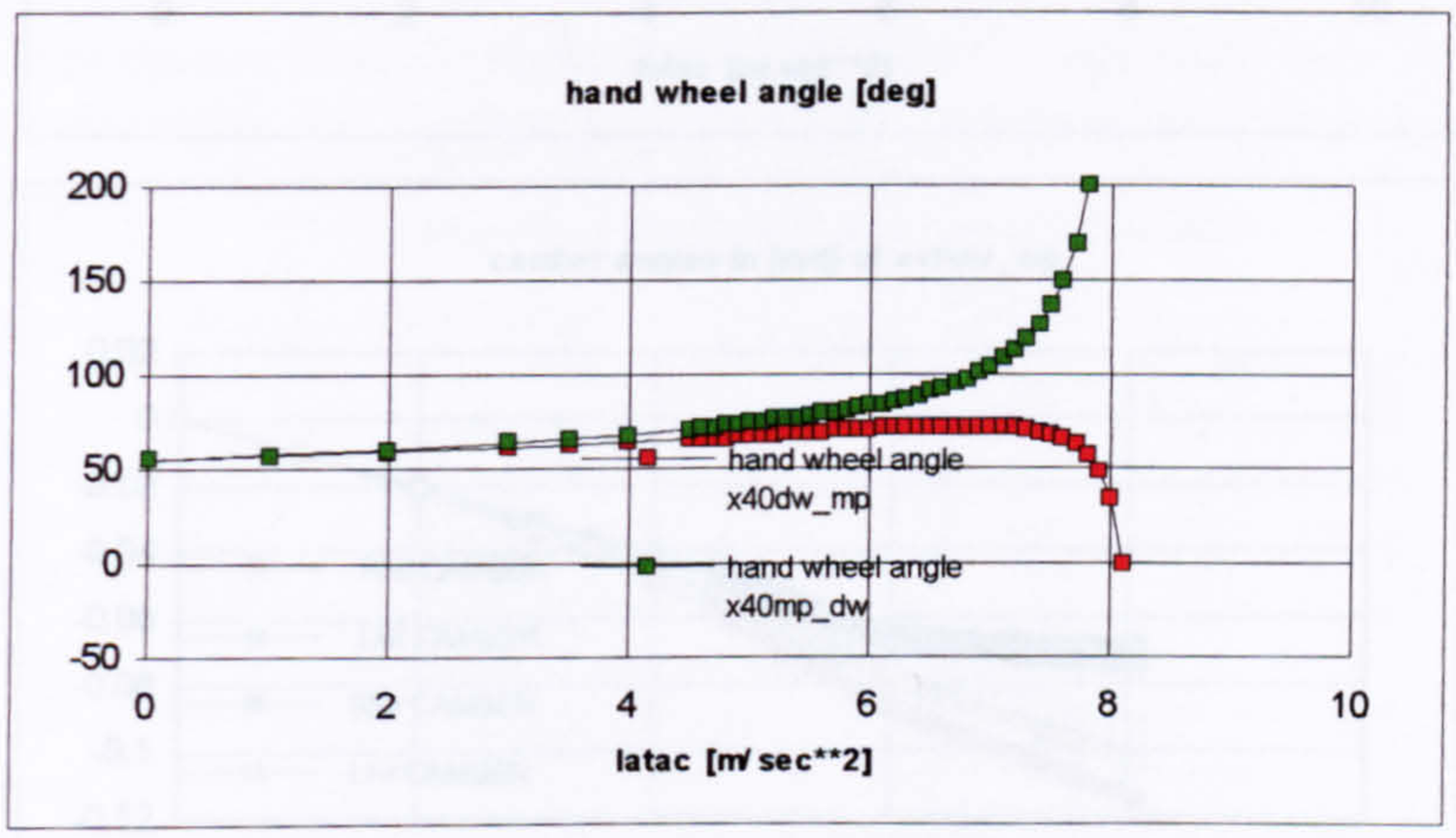

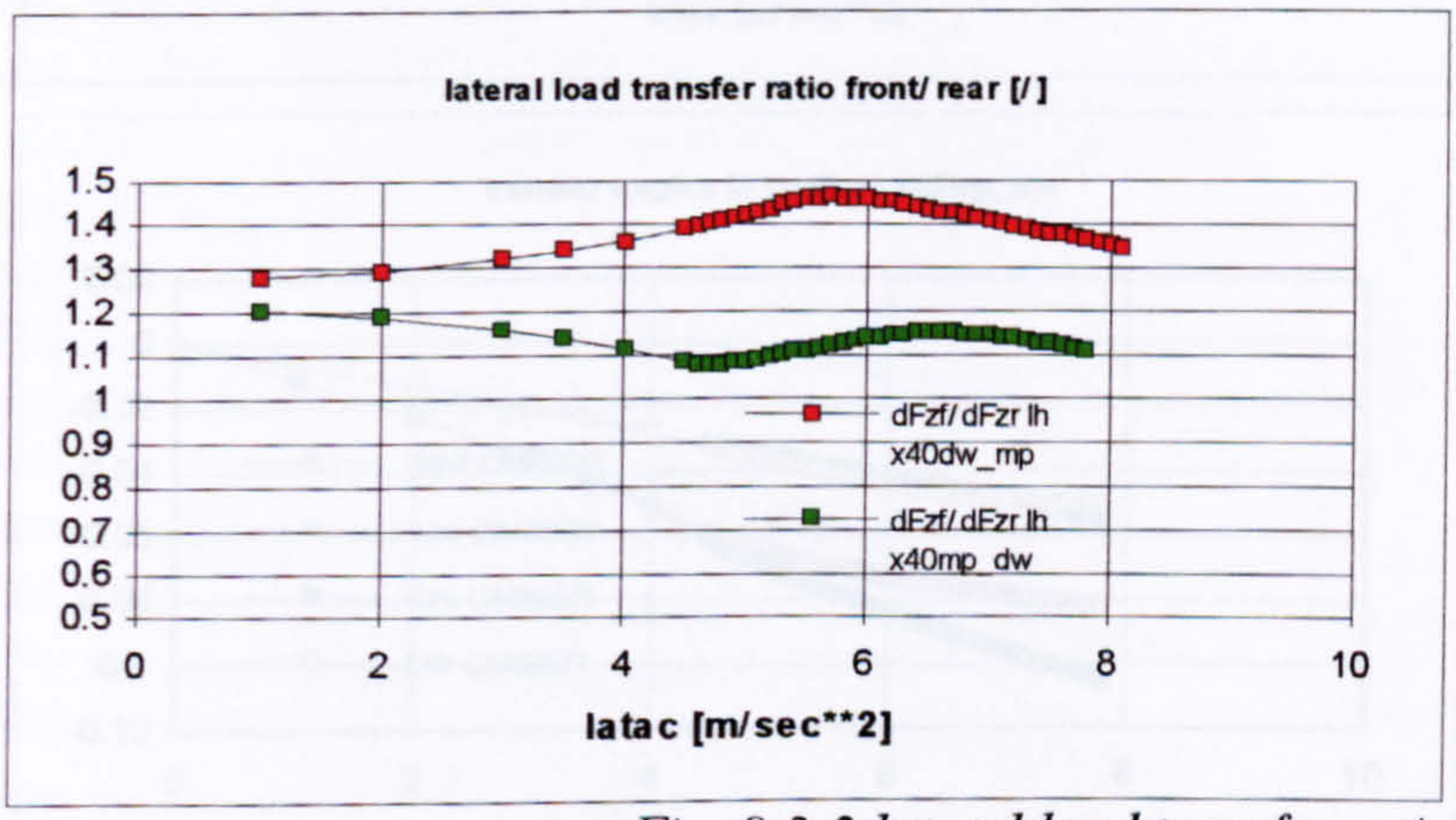

Fig. 8.3-2 lateral load transfer ratio for the double wishbone/ McPherson strut (x40dw_mp) and for the McPherson strut/ double wishbone (x40mp_dw) models

From the other curves in fig 8.3-1, it follows that one suspension type alone cannot be responsible for this phenomenon, since one can find at least one example of an understeering vehicle which features one of the two designs at either front or rear end. In order to find out which effects cause the difference in handling behaviour, as given again in the upper plot of fig. 8.3-2, the changes of the major suspension characteristics of these two vehicle variants are compared. Firstly, let

us look how the lateral load transfer ratio differs from its static value for a severe cornering manoeuvre. This ratio denotes the quotient of the load additional to the nominal load carried by the front outside and that of the rear outside wheel, and is shown in the second plot of fig 8.3-2. For moderate cornering up to 0.5 g these two designs feature an opposite tendency in distributing the moment of the centrifugal force, from which it can be concluded that a McPherson strut design decreases the effective roll stiffness at its end, and consequently pronounces the load transfer at the opposite end. The peaks, indicating the minimum and maximum of the load transfer ratios, coincide with the engagement of the bump stop on that end, where the McPherson strut is located. For a further increase in lateral acceleration, the lesser laden wheel of the double wishbone suspended axle is send into the rebound stop, reversing the load transfer distribution modestly for both cases.

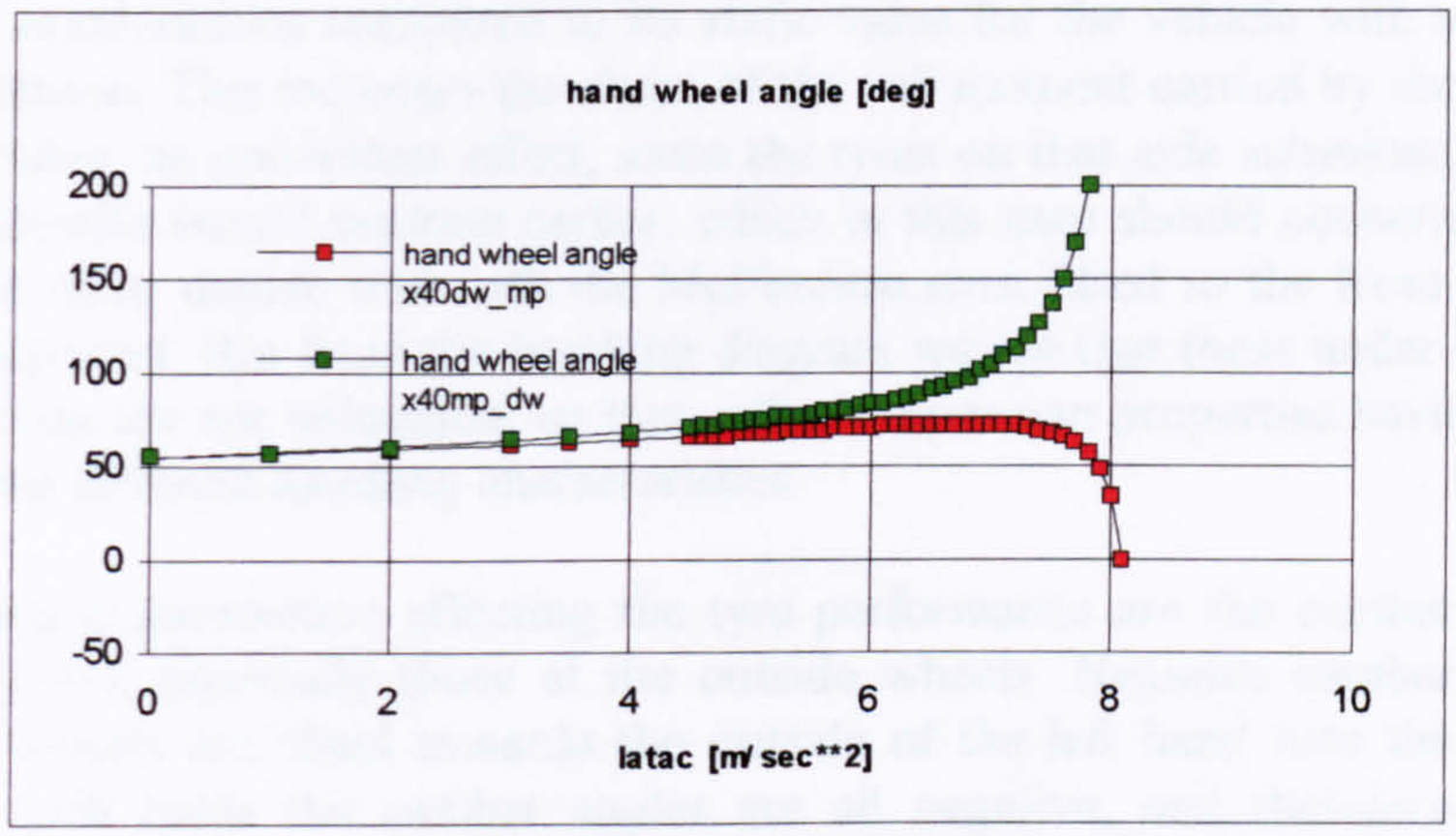

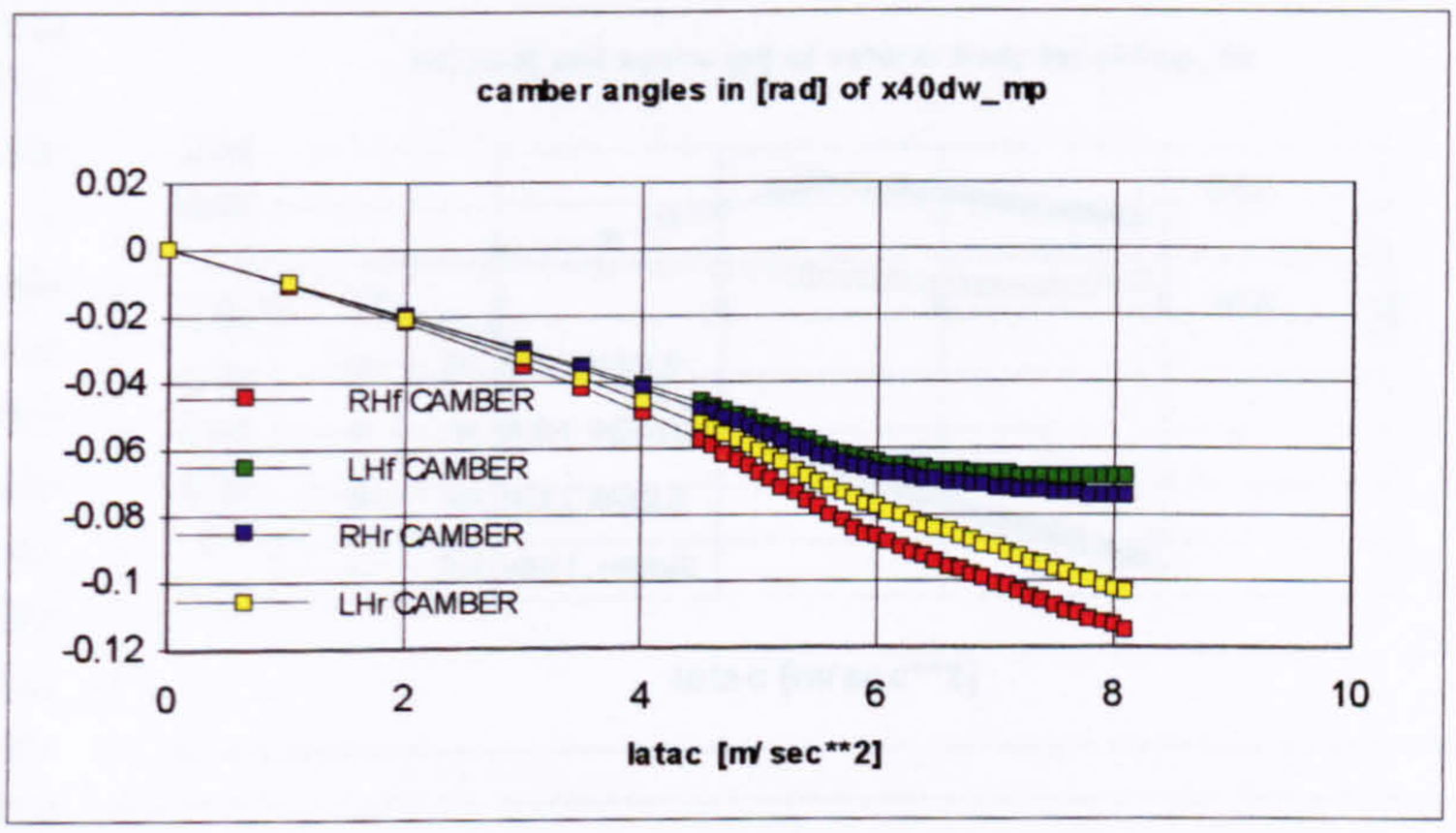

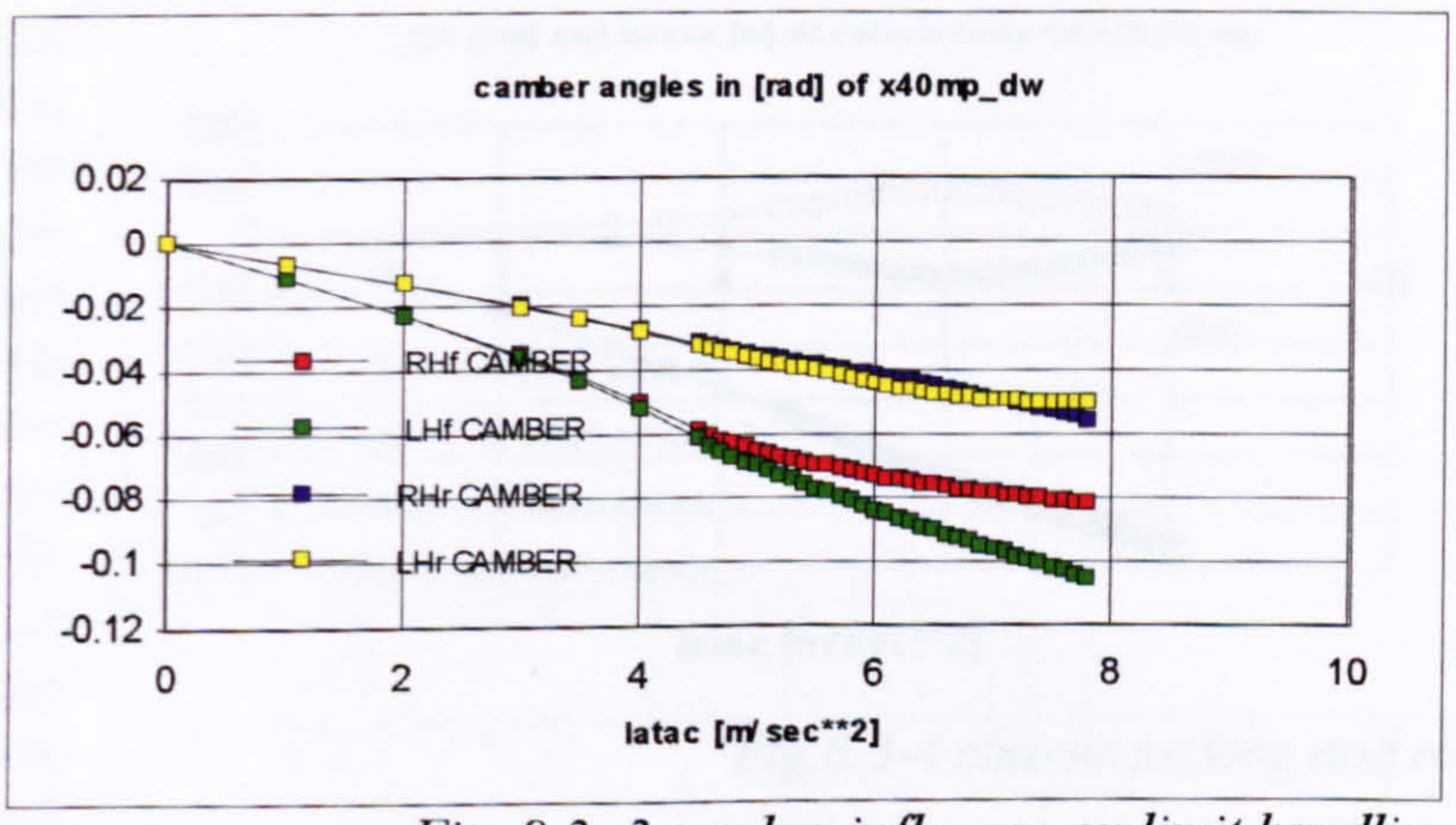

Fig. 8.3.-3 camber influence on limit handling

However, the plots for the lateral load transfer indicate a contrary effect concerning the vehicle response than established by the handling diagram. The load transfer ratio has increased at limit accelerations compared to its static value for the vehicle with a McPherson rear suspension. This increases the share of the roll moment carried by the front end. This constitutes an understeer effect, since the tyres on that axle submitted to more lateral load transfer would saturate earlier, which in this case should concern the front end. For the other model, that with the McPherson strut fitted to the front, the opposite can be expected. But from the handling diagram we see that these under- or oversteer contributions are not influential, so that other suspension properties have to be responsible for the different handling characteristics.

The only other suspension parameters affecting the tyre performance are the camber angles shown in fig. 8.3-3, especially those at the outside wheels. Negative camber angles mean that the wheels are tilted towards the outside of the left hand turn the vehicle follows. For both cases the camber angles are all negative, and therefore reducing the cornering power of each tyre. The camber angle of the outside rear wheel is smaller in magnitude than its counterpart at the front end for the understeering vehicle indicated by 'x40mp_dw', whereas for the oversteering car 'x40dw_mp' the opposite holds. This explains the vehicle behaviour shown by the handling diagram, and demonstrates that the camber control exerted by the two suspension types determines the limit response. Larger adverse camber at the rear end as established by the double wishbone suspension than at the front end provides limit understeer, whereas the design 'x40dw_mp' with diametrical properties is characterised by limit oversteer.

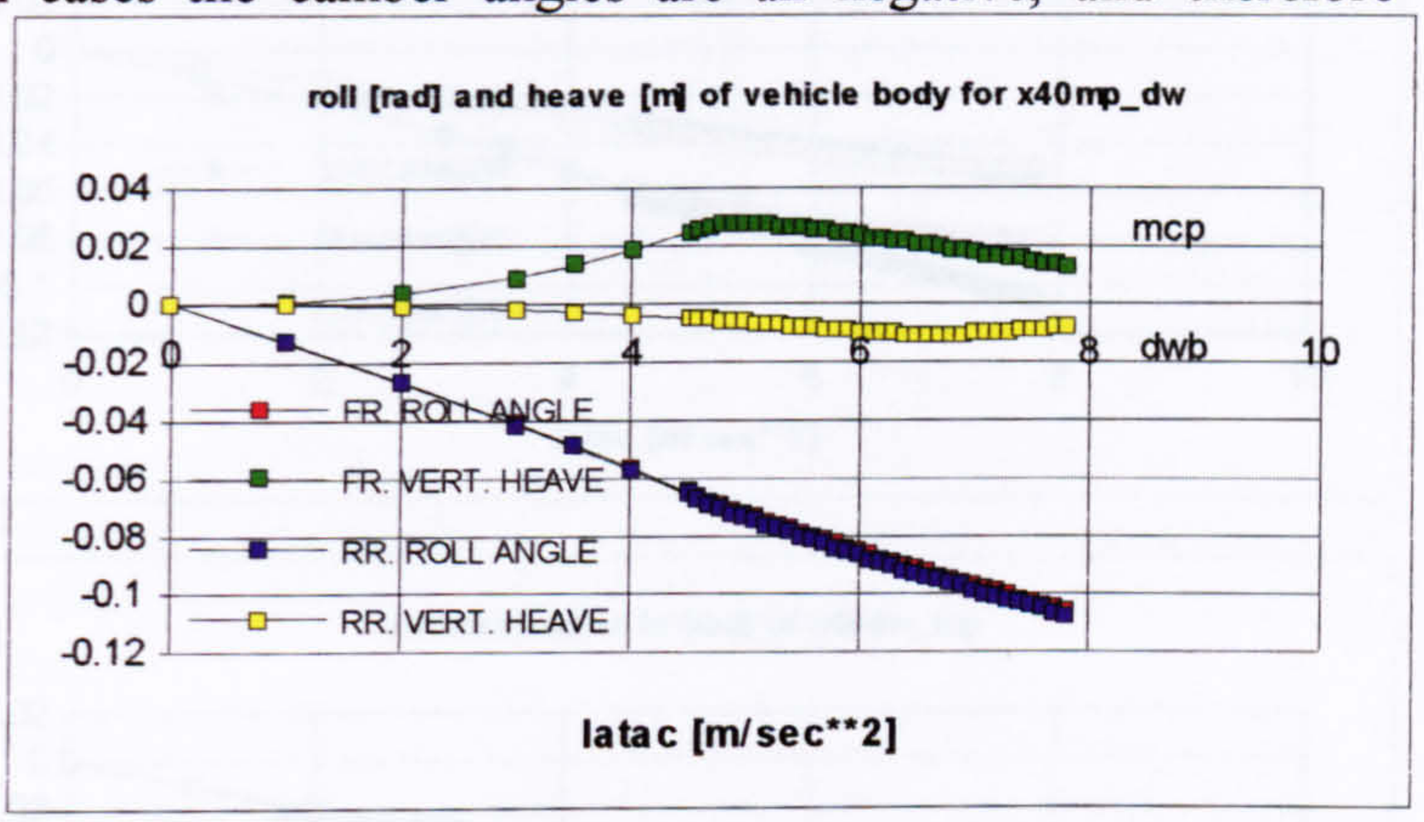

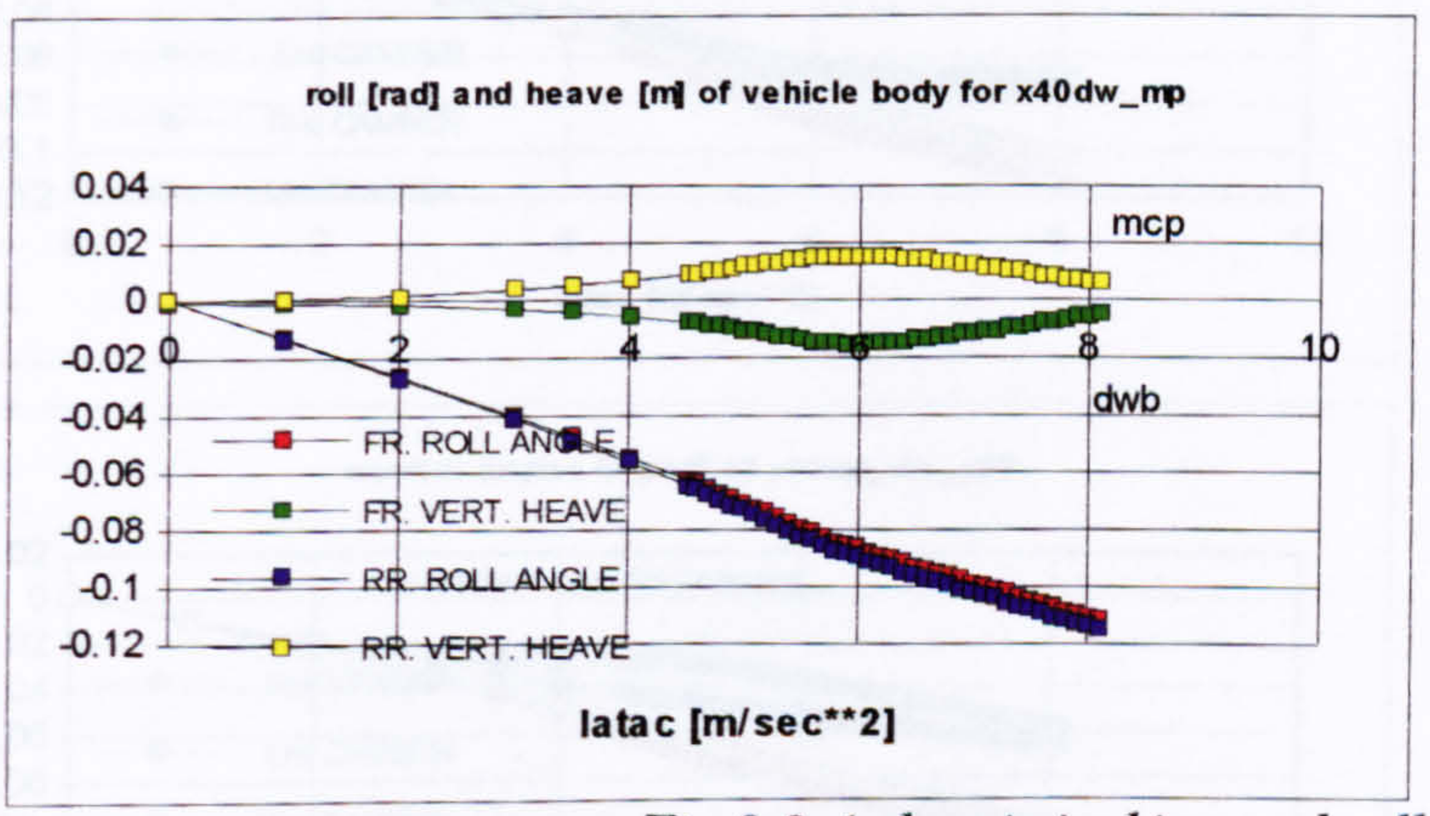

Fig.8.3-4 chassis jacking and roll

Other results not shown here indicate that the McPherson strut type suspension, used in those combinations analysed here, tends to promote a rather high wheel travel in the bump direction for the outside wheel, while the double wishbone design pronounces the inside wheel travel into rebound. This is caused by adverse jacking tendencies, as shown in fig. 8.3-4. For both cases (x40mp_dw, x40dw_mp) the end fitted with a McPherson strut design jacks downwards, whereas the double wishbone suspension leads to an upwards motion of the chassis. This phenomenon is not a consequence of large differences in the static instantaneous centres, which lie above ground level for both suspension types, as can be seen from the data in table 8.2-3 and 8.2-4, but a result of all issues involved in the tyre-suspension interface, such as camber angle and scrub control as well as load transfer and various tyre properties. The downwards jacking of the chassis, superimposed on the roll motion

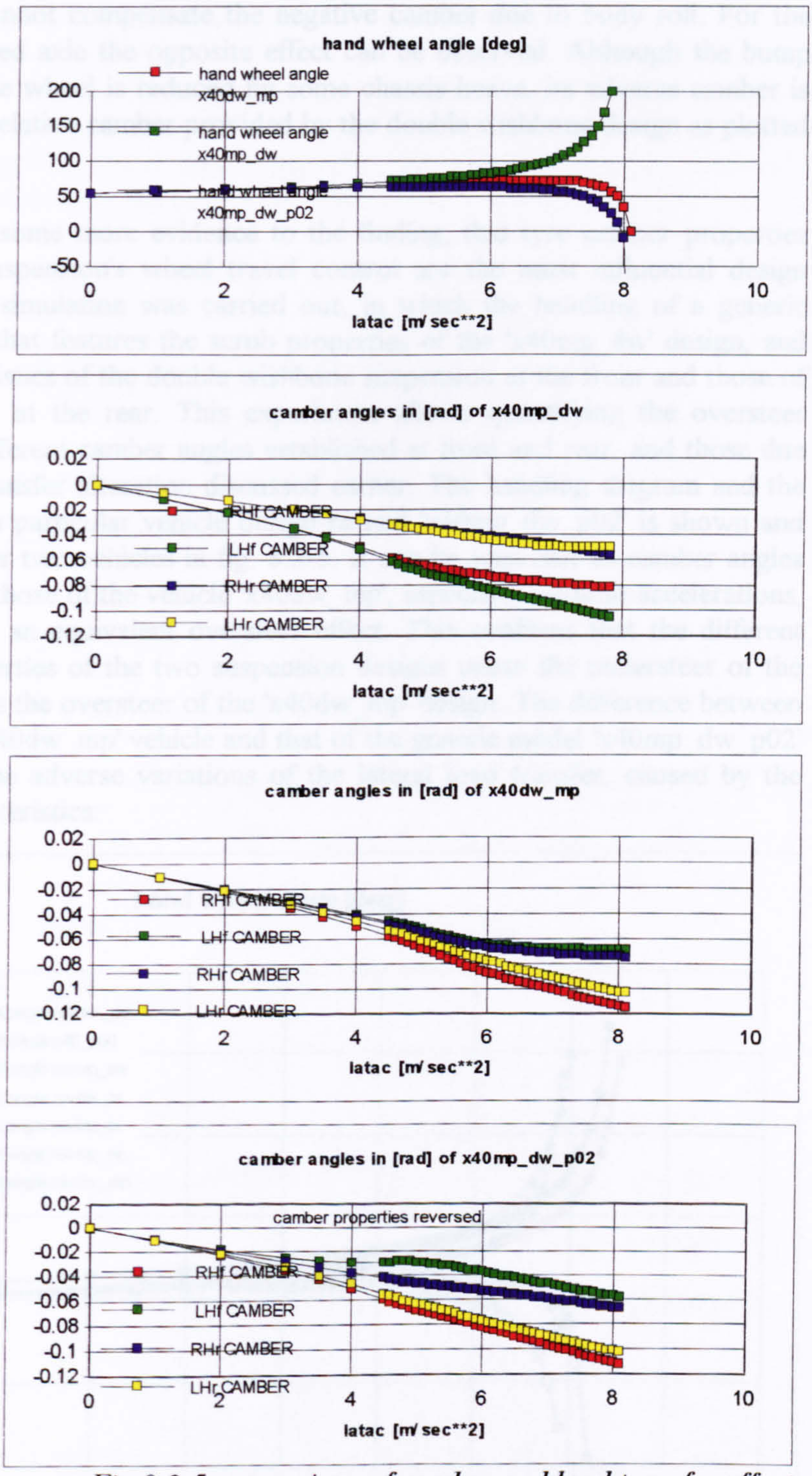

Fig 8.3-5 comparison of camber and load transfer effects

also shown in fig. 8.3-4, results in a large wheel travel in the bump direction. The bump travel produces, according to fig. 8.2-2, relative camber angles of small magnitude, which cannot compensate the negative camber due to body roll. For the double wishbone fitted axle the opposite effect can be observed. Although the bump motion of the outside wheel is reduced by some chassis heave, its adverse camber is decreased by larger relative camber provided by the double wishbone design as plotted in fig. 8.2-2.

In order to provide some more evidence to the finding, that tyre camber properties together with the suspension's wheel travel control are the most influential design parameters, another simulation was carried out, in which the handling of a generic vehicle was studied that features the scrub properties of the 'x40mp_dw' design, and the camber characteristics of the double wishbone suspension at the front and those of the McPherson strut at the rear. This experiment allows quantifying the oversteer effects due to the different camber angles established at front and rear, and those due to the lateral load transfer alteration discussed earlier. The handling diagram and the camber angles of this particular vehicle design named 'x40mp_dw_p02' is shown and compared to the other two vehicles in fig. 8.3-5. It can be seen that its camber angles are indeed similar to those of the vehicle 'x40dw_mp', especially for limit accelerations, and thereby produce an equivalent oversteer effect. This confirms that the different camber control properties of the two suspension designs cause the understeer of the 'x40mp_dw' as well as the oversteer of the 'x40dw_mp' design. The difference between the handling of the 'x40dw_mp' vehicle and that of the generic model 'x40mp_dw_p02' can be ascribed to the adverse variations of the lateral load transfer, caused by the reversed scrub characteristics.

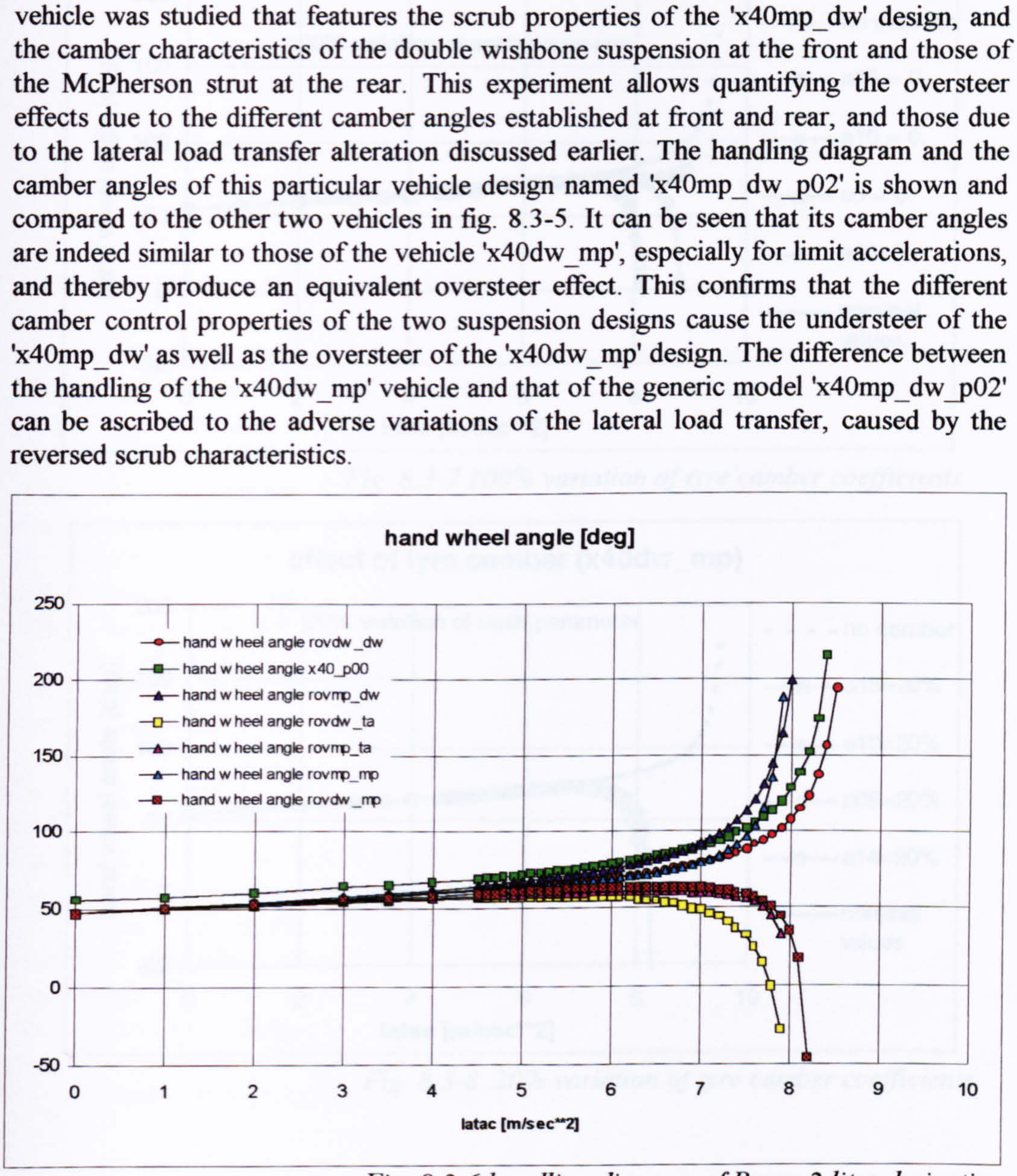

Fig. 8.3-6 handling diagram of Rover 2 litre derivatives

Results very similar to those for the Jaguar X40 based vehicle were obtained for the second baseline model, and are given as handling diagrams in fig. 8.3-6. Note, that the hand wheel angle is also plotted for the Jaguar X40 baseline model.

All the examples presented so far indicate on the one hand, how influential the tyre's camber properties are on the limit handling, and on the other the role of the suspension design, in controlling the wheel travel and thus the camber angle to achieve a predictable vehicle response to the hand wheel input.

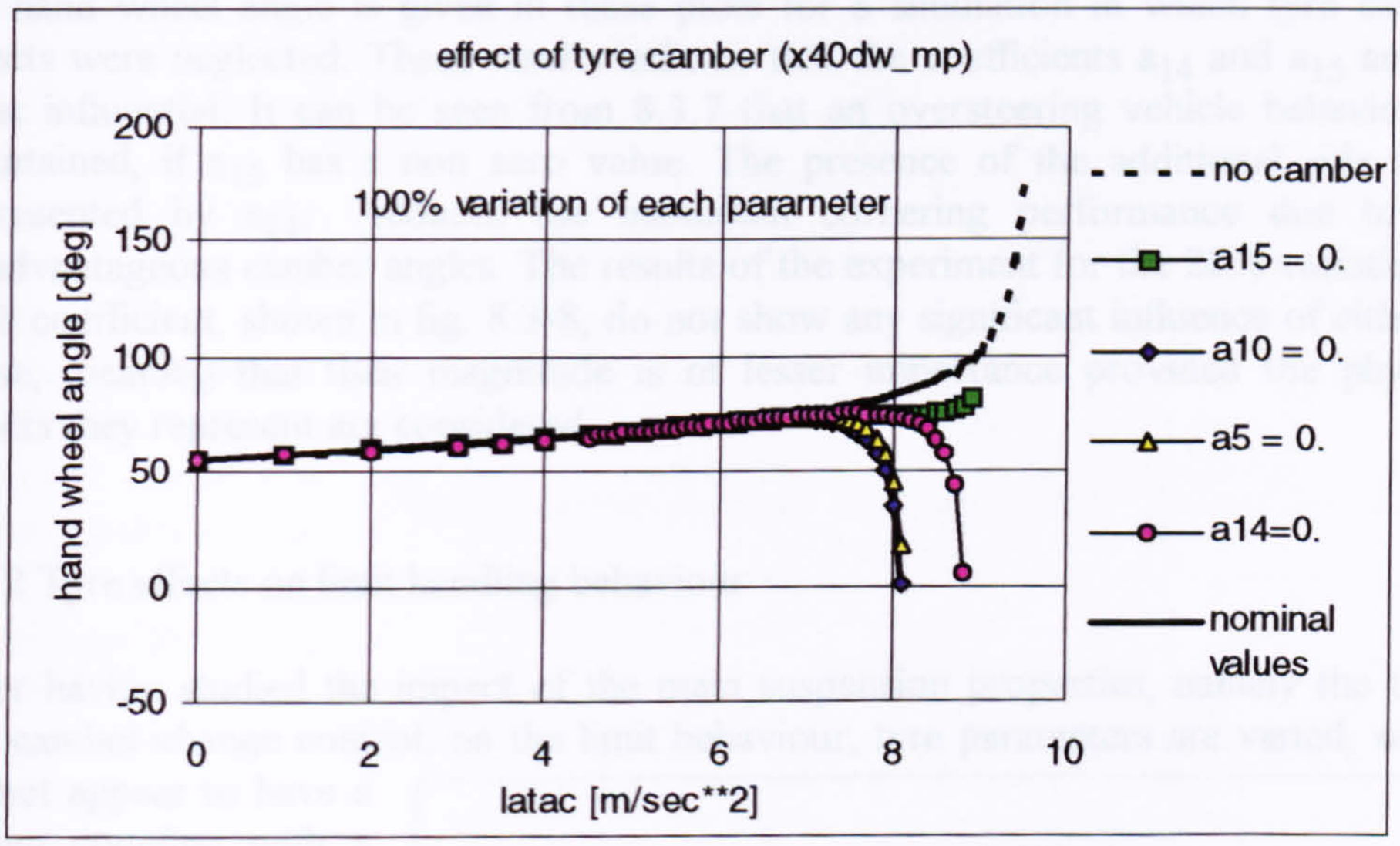

Fig. 8.3-7 100% variation of tyre camber coefficients

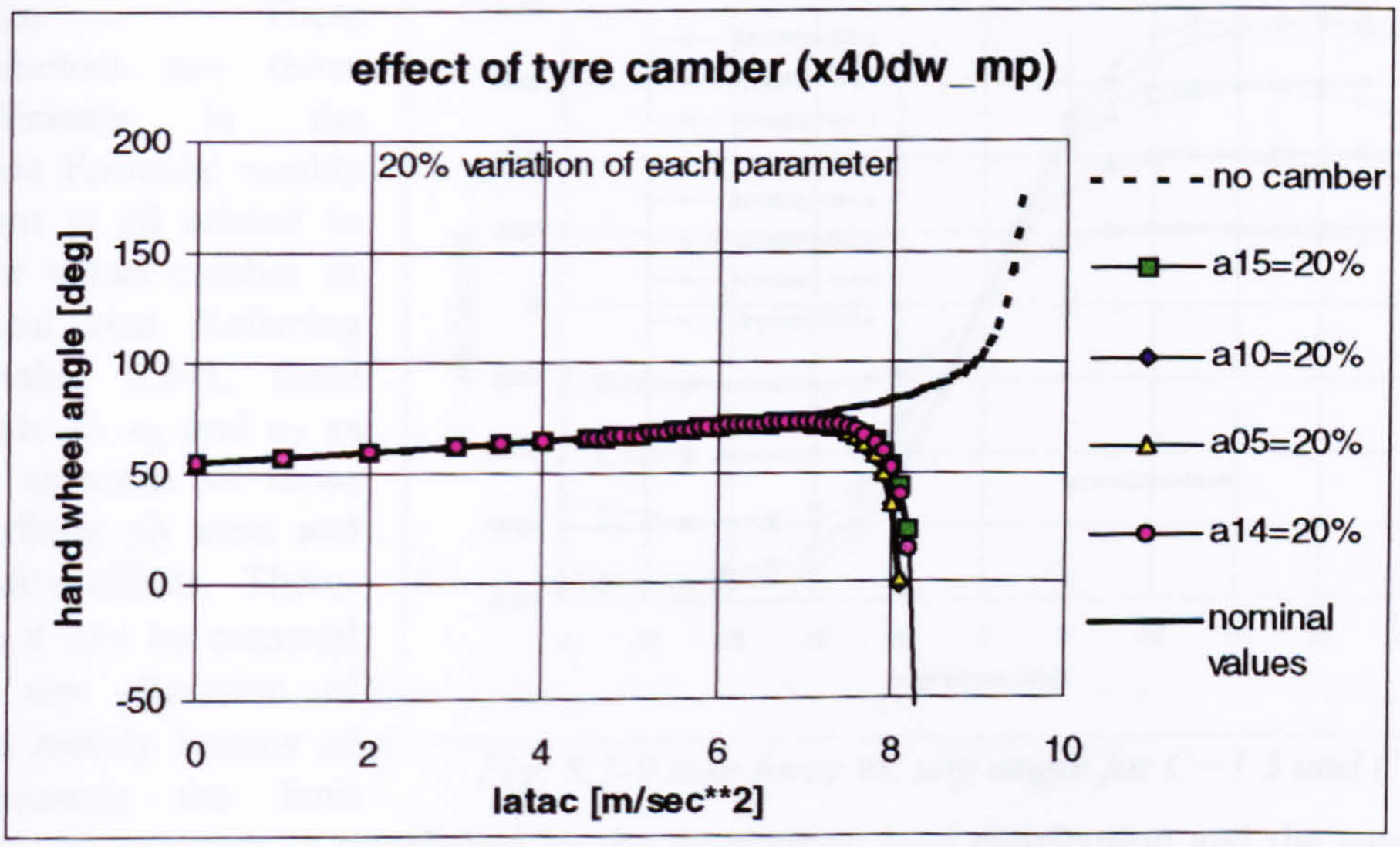

Fig. 8.3-8 20% variation of tyre camber coefficients

Subsequently, the tyre camber properties, given by the highlighted coefficients in the 'Magic Formula' stated in table 8.2-5, were analysed in more detail. In the first experiment simulations were carried out, in each of which one of those coefficients was set to zero, and all others were kept to their nominal value. In order to overcome some of the uncertainty caused by relying on 'default' rather than measured tyre data, a second similar experiment was conducted, in each of which one of the coefficients was lowered by 20% instead of being set to zero. The corresponding handling diagrams for the oversteering vehicle 'x40dw_mp' are shown in fig. 8.3-7 and 8.3-8. Additionally, the hand wheel angle is given in these plots for a simulation in which tyre camber effects were neglected. These results indicate that the coefficients a_{14} and a_{15} are the most influential. It can be seen from 8.3.7 that an oversteering vehicle behaviour is maintained, if a_{15} has a non zero value. The presence of the additional side force represented by a_{14}, reduces the maximum cornering performance due to the disadvantageous camber angles. The results of the experiment for the 20% variation of each coefficient, shown in fig. 8.3-8, do not show any significant influence of either of those, meaning that their magnitude is of lesser importance provided the physical effects they represent are considered.

8.3.2 Tyre effects on limit handling behaviour

After having studied the impact of the main suspension properties, namely the track and camber change control, on the limit behaviour, tyre parameters are varied, which do not appear to have a strong coupling with a particular suspension design. These parameters are those coefficients in the 'Magic Formula' weakly or not at all related to either wheel camber or vertical load. Referring to table 8.2-5, these include C, a_3 and a_7 as well as some of those describing ply steer and conicity effects. Therefore, it can be assumed that any alteration of these merely lessens or pronounces the limit under- or oversteer as established by the dominating load distribution and the camber control provided by the suspension design.

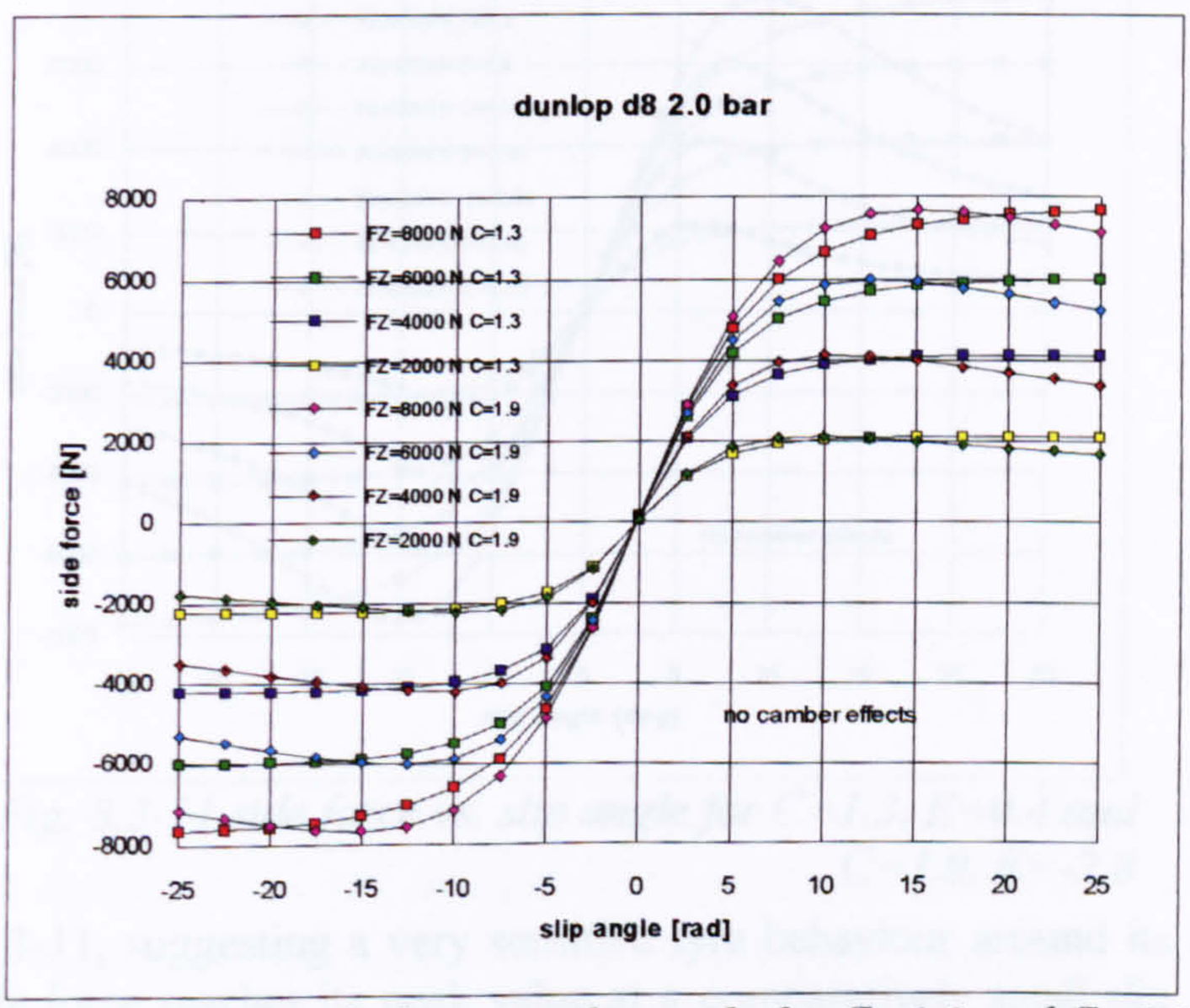

Fig. 8.3-9 side force vs. slip angle for C=1.3 and C=1.9

The tyre characteristics were altered by varying the curvature parameters C and E from their nominal values 1.3 and 0.4 at nominal vertical load, respectively. The latter was adjusted by redefining coefficient a_7, which seems to be the more important one determining E. Increasing parameter C from 1.3 to 1.9 shifts the occurrence of the maximum side force to lower slip angles, as shown in fig. 8.3-9. At the same time, it leads to a constantly declining force beyond its peak value, which is emphasised at higher loads. Adjusting factor E from 0.4 to -1.84 extends the linear region of the side force-slip curves leading to a rather sudden breakaway close to the peak side force, as illustrated in fig. 8.3-10. An extreme setting, given by C=1.9 and E=-2.8, is shown in fig. 8.3-11, suggesting a very sensitive tyre behaviour around its peak performance. The side force reaches its peak value at a comparatively small slip angle, and decreases strongly afterwards.

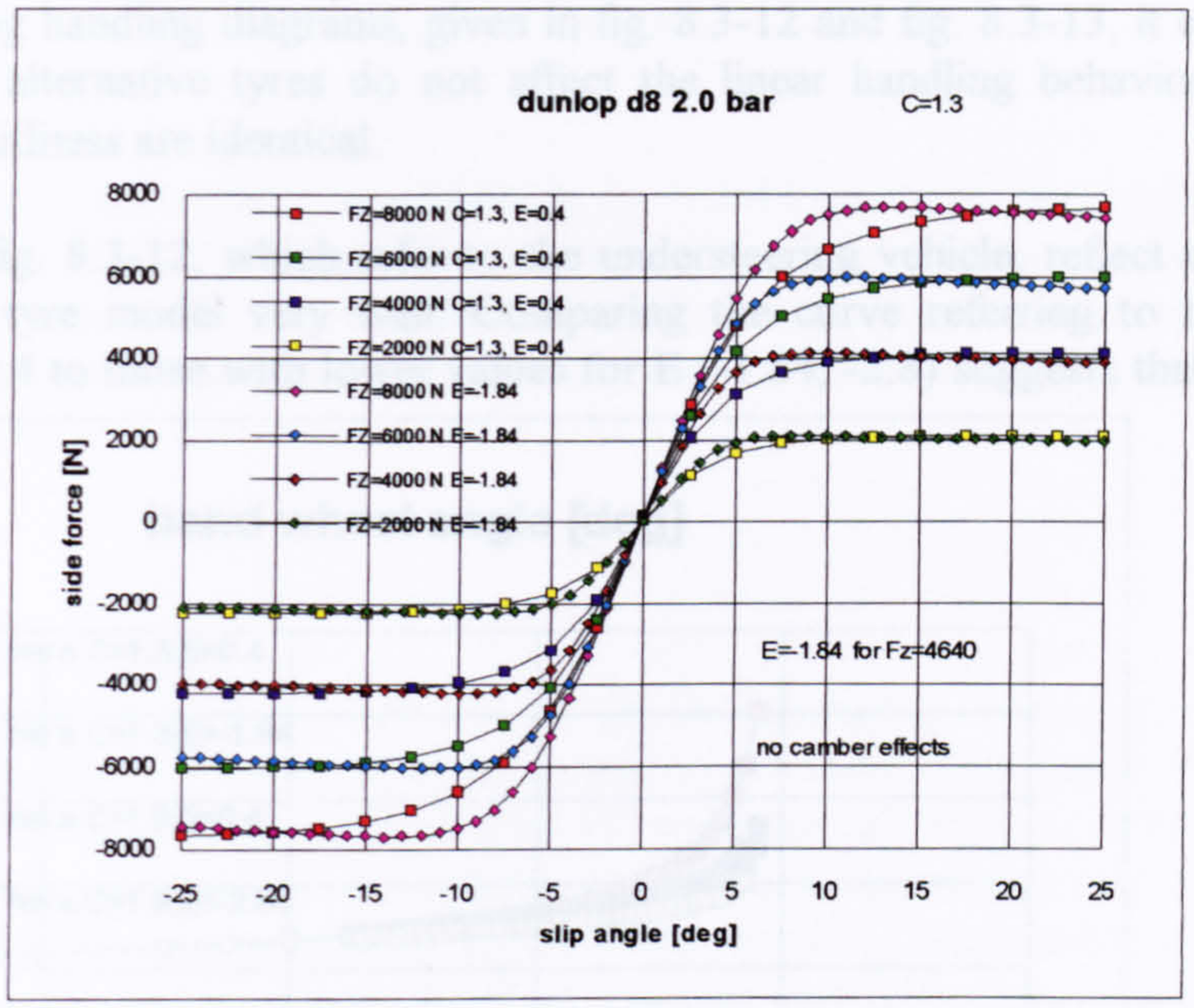

Fig.8.3-10 side force vs. slip angle for E=0.4 and E=-1.84

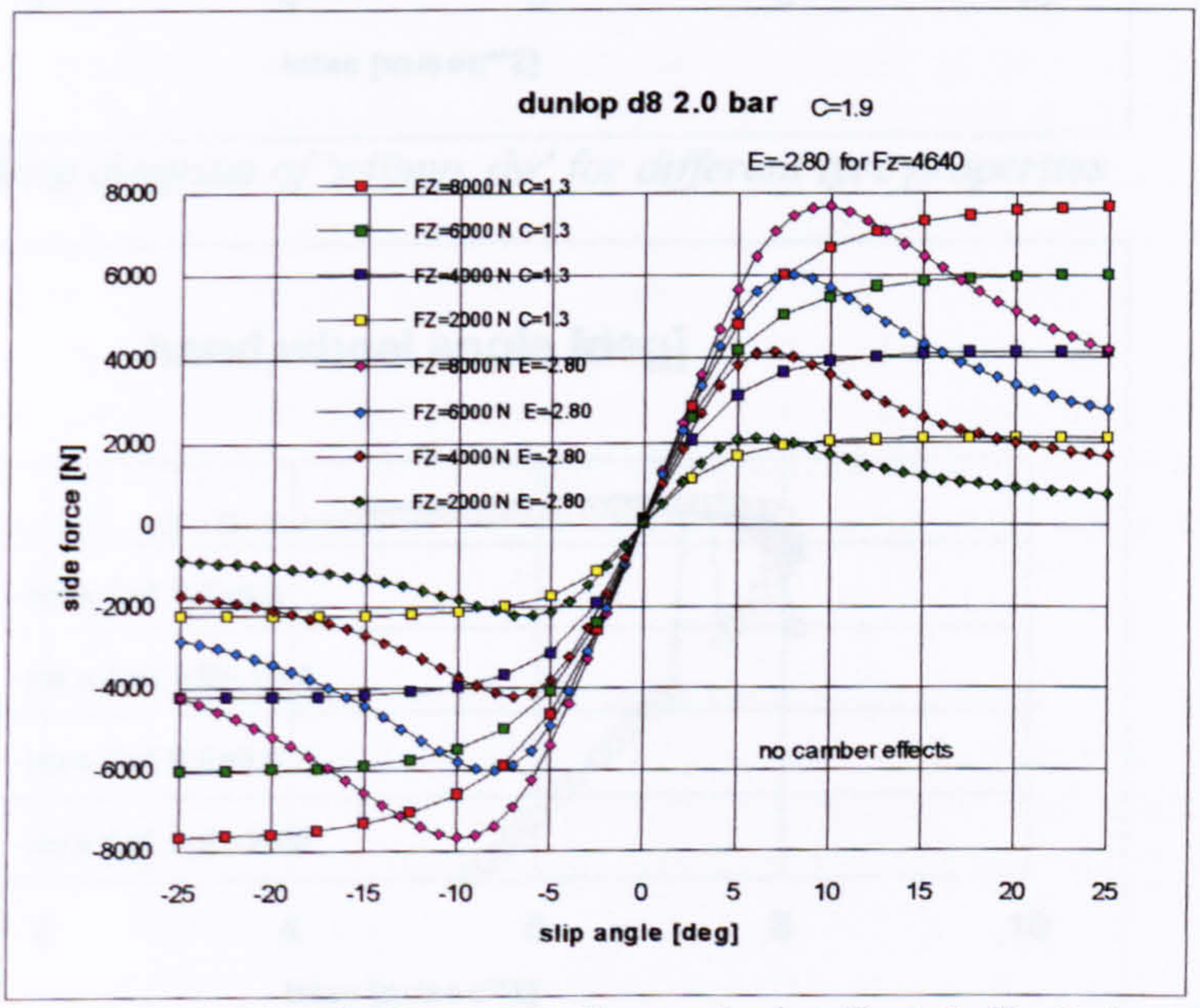

Fig. 8.3-11 side force vs. slip angle for C=1.3, E=0.4 and C=1.9, E=-2.8

The vehicle handling resulting from these generic tyres was simulated for the two models 'x40mp_dw' and 'x40dw_mp', discussed in detail in the previous section, which provide an example of an under- and oversteering vehicle, respectively.

From the corresponding handling diagrams, given in fig. 8.3-12 and fig. 8.3-13, it can be noticed that these alternative tyres do not affect the linear handling behaviour, confirming that their stiffness are identical.

The curves shown in fig. 8.3-12, which refer to the understeering vehicle, reflect the changes made to the tyre model very well. Comparing the curve referring to the standard E setting of 0.4 to those with lower values for E (-1.84, -2.8) suggests that a

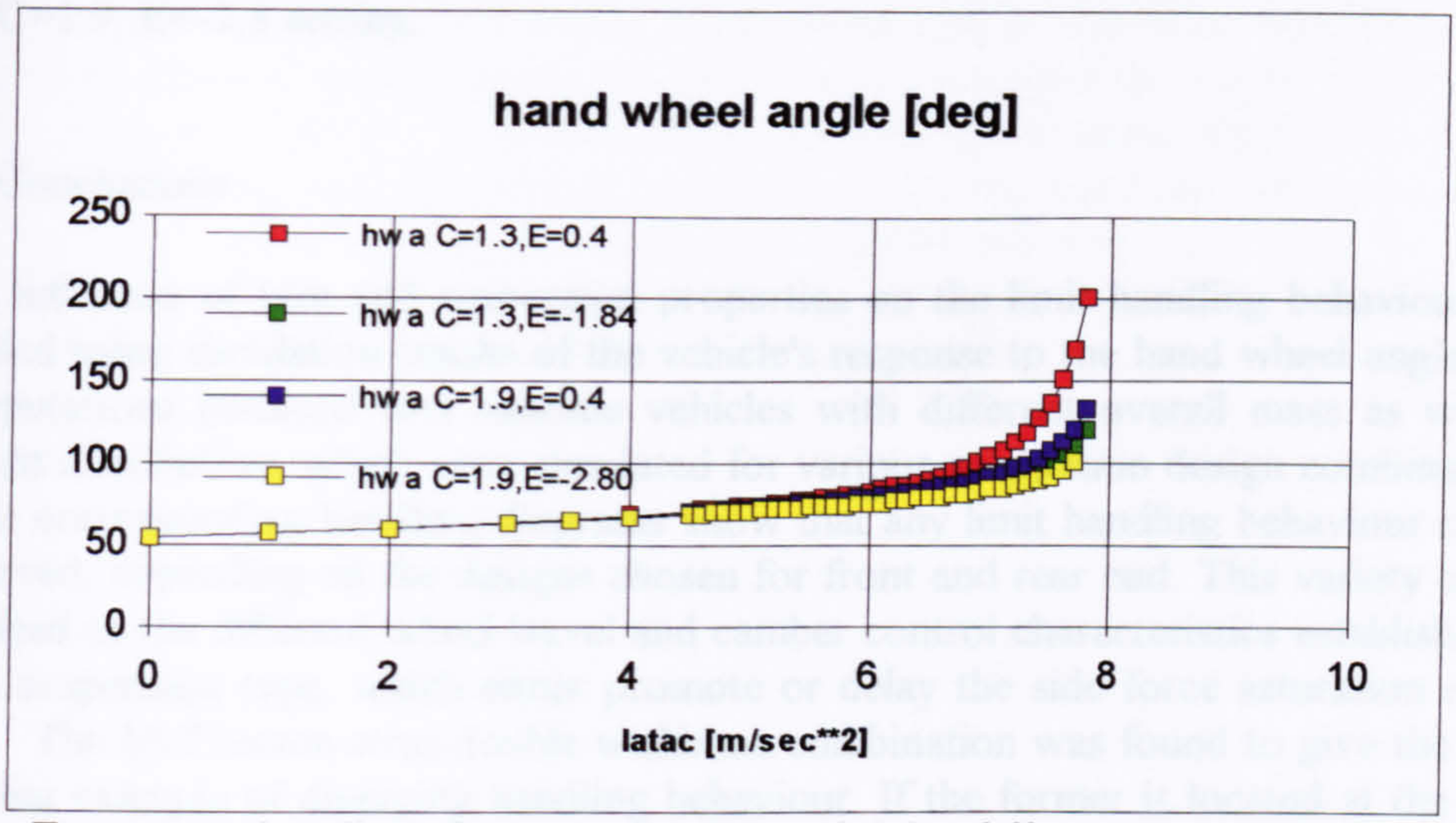

Fig. 8.3-12 handling diagram of 'x40mp_dw' for different tyre properties

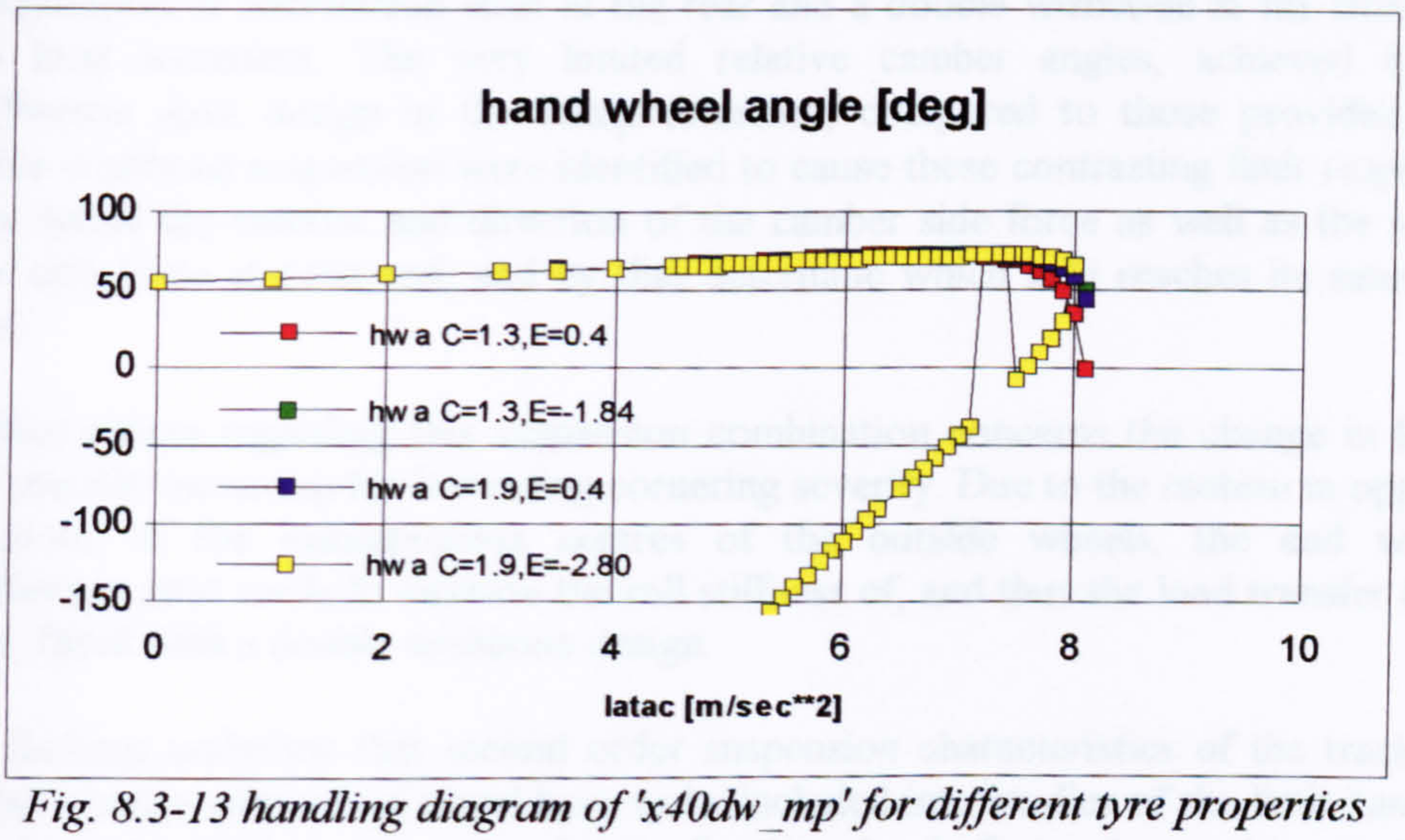

Fig. 8.3-13 handling diagram of 'x40dw_mp' for different tyre properties

tyre with an extended linear behaviour, as modelled by the latter setting, enlarges the linear vehicle response as well as increases the curvature of the breakaway region. An equivalent tendency can be observed for an increase of the curvature factor C by comparing the curves regarding constant values of C to each other. Unfortunately, the off-peak handling behaviour could not be computed, but from the plots illustrating the different tyre and vehicle behaviour, it can be concluded that all tyre variants provide a very similar result for the maximum lateral

acceleration, and that the vehicle's breakaway behaviour just reflects that of the saturated tyre.

Similar conclusions can be drawn from the graphs in fig. 8.3-13 regarding the handling of the oversteering vehicle 'x40dw_mp'. The smoothest transition from the linear response to the breakaway of the car is obtained for the standard tyres, whereas a sudden oversteer onset is produced by those with a distinct side force peak given by the C=1.9, E=-2.8 setting.

8.4 Conclusions

The influence of tyre and suspension properties on the limit handling behaviour was studied using simulation results of the vehicle's response to the hand wheel angle. The computations involved two baseline vehicles with different overall mass as well as weight distribution, which were simulated for various suspension design combinations. Their corresponding handling diagrams show that any limit handling behaviour can be achieved, depending on the designs chosen for front and rear end. This variety can be ascribed to the different wheel travel and camber control characteristics established by each suspension type, which either promote or delay the side force saturation of the axle. The McPherson strut-double wishbone combination was found to give the most striking example of diverging handling behaviour. If the former is located at the front end, the baseline vehicles understeered at the limit, whereas those vehicles, featuring a configuration of McPherson strut at the rear and a double wishbone at the front end, give limit oversteer. The very limited relative camber angles, achieved by the McPherson strut design in the bump direction, compared to those provided by a double wishbone suspension were identified to cause these contrasting limit responses. They define the amount and direction of the camber side force as well as the loss in peak side force at each end, and by that determine which axle reaches its saturation force.

Another aspect regarding this suspension combination concerns the change in lateral load transfer occurring for increasing cornering severity. Due to the motion in opposite directions of the instantaneous centres of the outside wheels, the end with a McPherson strut tends to increase the roll stiffness of, and thus the load transfer at the other, fitted with a double wishbone design.

The findings underline that second order suspension characteristics of the track and camber change with wheel travel have to be included into studies of the limit handling behaviour. A vehicle model with a fixed roll axis and only first order camber properties cannot describe the characteristics of independent suspension designs accurately enough to represent the strong interaction between the latter and some major tyre properties.

Other simulation results obtained for several tyres with theoretical behaviour show how their properties emphasise the sharpness of the vehicle's breakaway at limit

cornering. In the investigated cases the vehicle response reflected the shape of the side force-slip angle relation near the peak force. Those vehicles simulated with tyres, giving a distinct peak rather than a constant side force at high slip angles, are more sensitive in their response, which corresponds to an increased curvature of the transition region from the linear to the limit behaviour, as shown in the handling diagrams.

The examples presented indicate to what extent the steady state handling can be altered by alternative suspension and tyre designs. In order to match these two by using numeric methods, it is crucial to provide an accurate description of the suspension camber and track change properties on the one hand and camber properties on the other, additional to the customary vehicle and tyre data used in vehicle dynamics. It remains to be seen, which of the two areas, suspension or tyre design, allow more variability to improve a particular product.

8.5 Tyre - suspension interaction for steady state cornering / design rules

The simulation results presented in the previous sections of this chapter suggest that almost any degree of either limit under- or oversteer can be achieved depending on the choice of suspension and tyre designs employed for the front and rear axles of the vehicle.

The variety in the limit handling behaviour, as shown in the handling diagrams fig. 8.3-1 and fig. 8.3-6, highlights the importance of second order suspension properties, which describe the rate at which scrub and camber change with wheel travel. These properties become more and more important in determining the extent to which each wheel travels into bump or rebound as well as its camber with respect to the road.

Also some tyre camber properties, as defined by the 'Magic Formula', were identified having a strong effect on limit handling.

Unfortunately, the complex nature of the vehicle cornering problem, which involves balancing the front with the rear ends, as well as the left with the right hand side, prevented deriving design rules for suspension and tyre.

So far, it was only demonstrated what the handling would be like for a car with different suspension and tyre designs at its front and rear ends. But this can only be the first step towards developing design recommendations, whose application would enable tuning the vehicle with regard to its maximum cornering acceleration, its degree of limit understeer as well as the smoothness of the transition from linear to limit cornering conditions.

In order to overcome this deficiency, the complexity was reduced by analysing the cornering performance of a single axle. For this one axle vehicle the same constant radius test is carried out, as discussed in the previous sections. This approach allows studying the effects of design changes made to either tyre or suspension on the maximum cornering performance of a certain axle, i.e. its maximum possible lateral acceleration. More importantly, some basic design rules can be derived for maximising the cornering power analytically due to the much simpler mathematics of the single ended vehicle problem. On the other hand, the performance can no longer be assessed in terms of under- or oversteer, since the single ended problem is equivalent to a perfectly symmetrical double ended vehicle giving a neutral response throughout its performance range.

Therefore, a single axle design is compared to another by a 'lateral force coefficient diagram', which shows, analogous to the side force-slip graphs for tyres, the normalised lateral force against the slip angle of the axle. From these diagrams, the peak force as well as the rate of roll-off towards the peak can be obtained.

8.5.1. Good and bad cases of limit cornering performance

In the first stage of this study, good and bad cases of an axle design were established. A high lateral force coefficient and a smooth transition from the linear to the peak region of the curve are understood as criteria for an advantageous design. A bad case is represented by low peak coefficient and a rapid roll-off at higher slip angles.

The swing arm suspension is known as a design with a quickly deteriorating limit performance. For this study, a horizontal swing arm of 0.55 m was modelled; the wheel diameter is 0.3 m. This design features a high roll centre giving a relatively high roll stiffness.

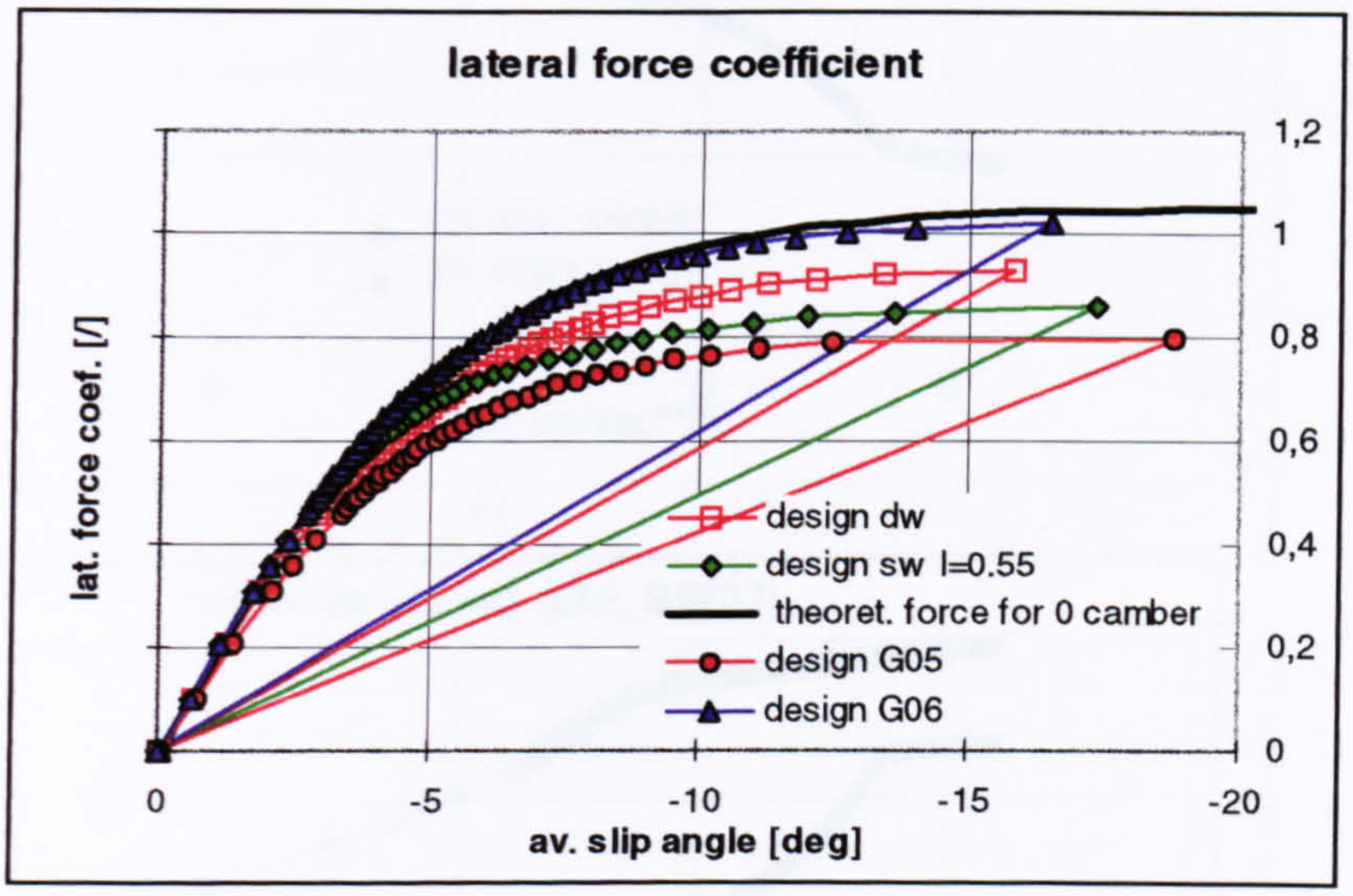

Fig. 8.5-1 lateral force coefficient vs. average side slip

Corresponding to a high roll centre, the wheel contact points tend to scrub rather strongly for bump and rebound travel, which changes the track width and, in combination with lateral load transfer, promotes an upwards jacking motion of the chassis.

As shown in fig. 8.5-1, the maximum coefficient of this design is 0.88, and falls well below the theoretical limit of 1.05, as established by the maximum tyre force at nominal load and zero camber. The limitations of this design example can be explained by the following three graphs in fig. 8.5-2, showing the roll and heave body motions for increasing lateral acceleration, the vertical travel for the outside (LH) and inside (RH) wheel, and the corresponding camber angles relative to the road.

The first graph illustrates the tendency of the swing arm suspension to jack up the chassis progressively with increasing cornering speeds. On the other hand, the high roll centre established by high scrub gradients, limits the vehicle's body roll to small angles, which, after increasing linearly for moderate cornering, decrease to zero at the maximum speed.

Fig. 8.5-2 roll, jacking, wheel travel and camber for swing axle vehicle

a)

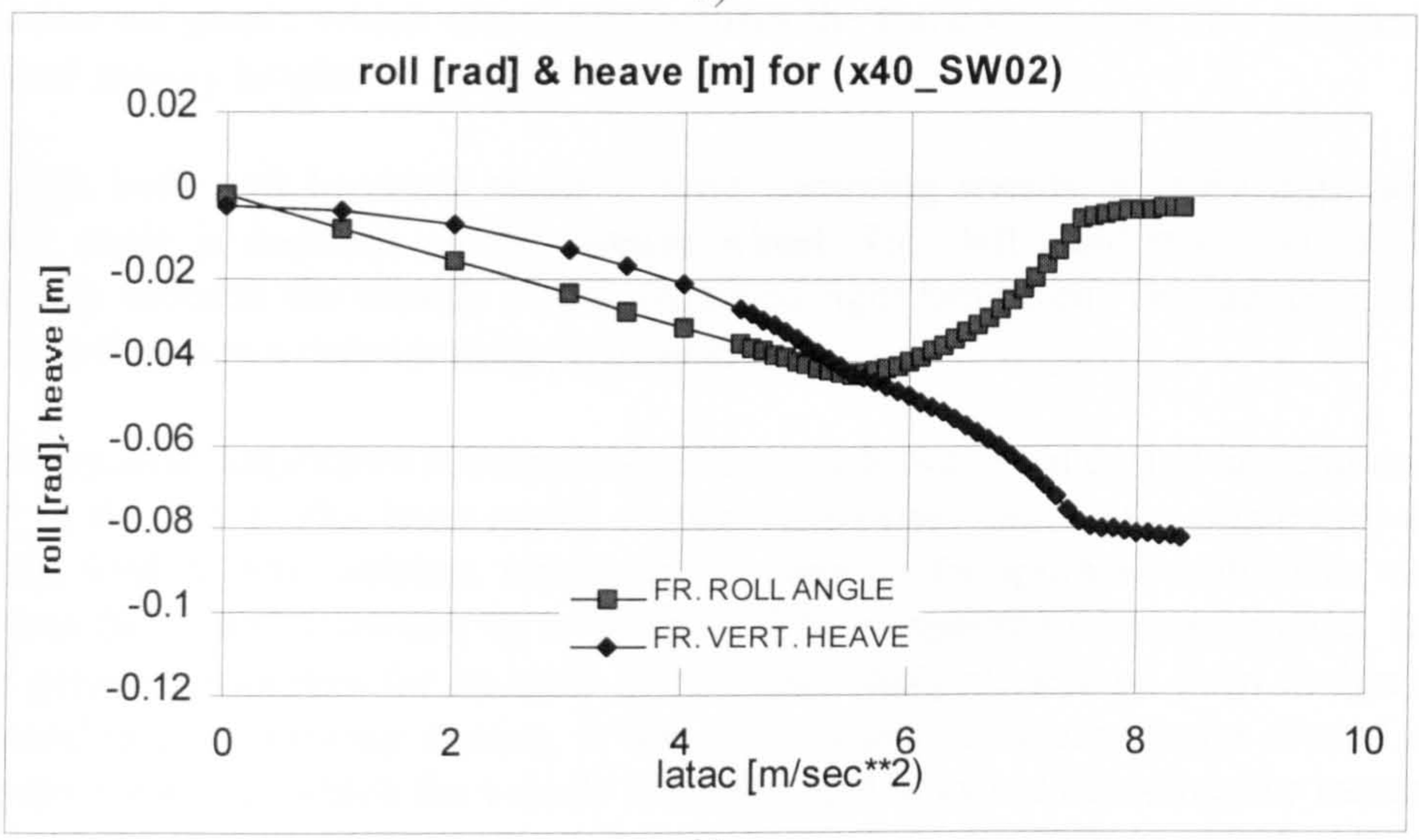

b)

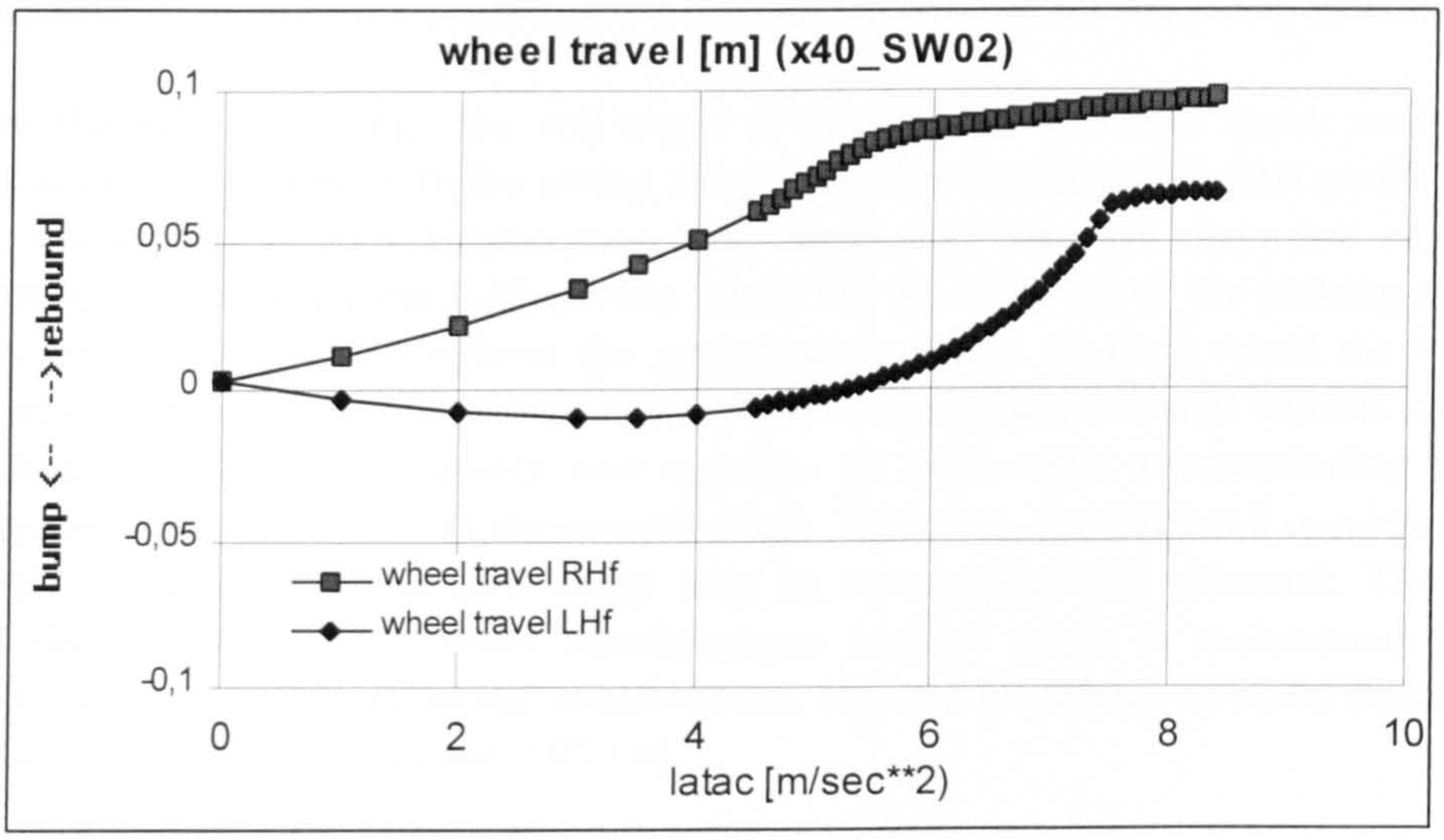

c)

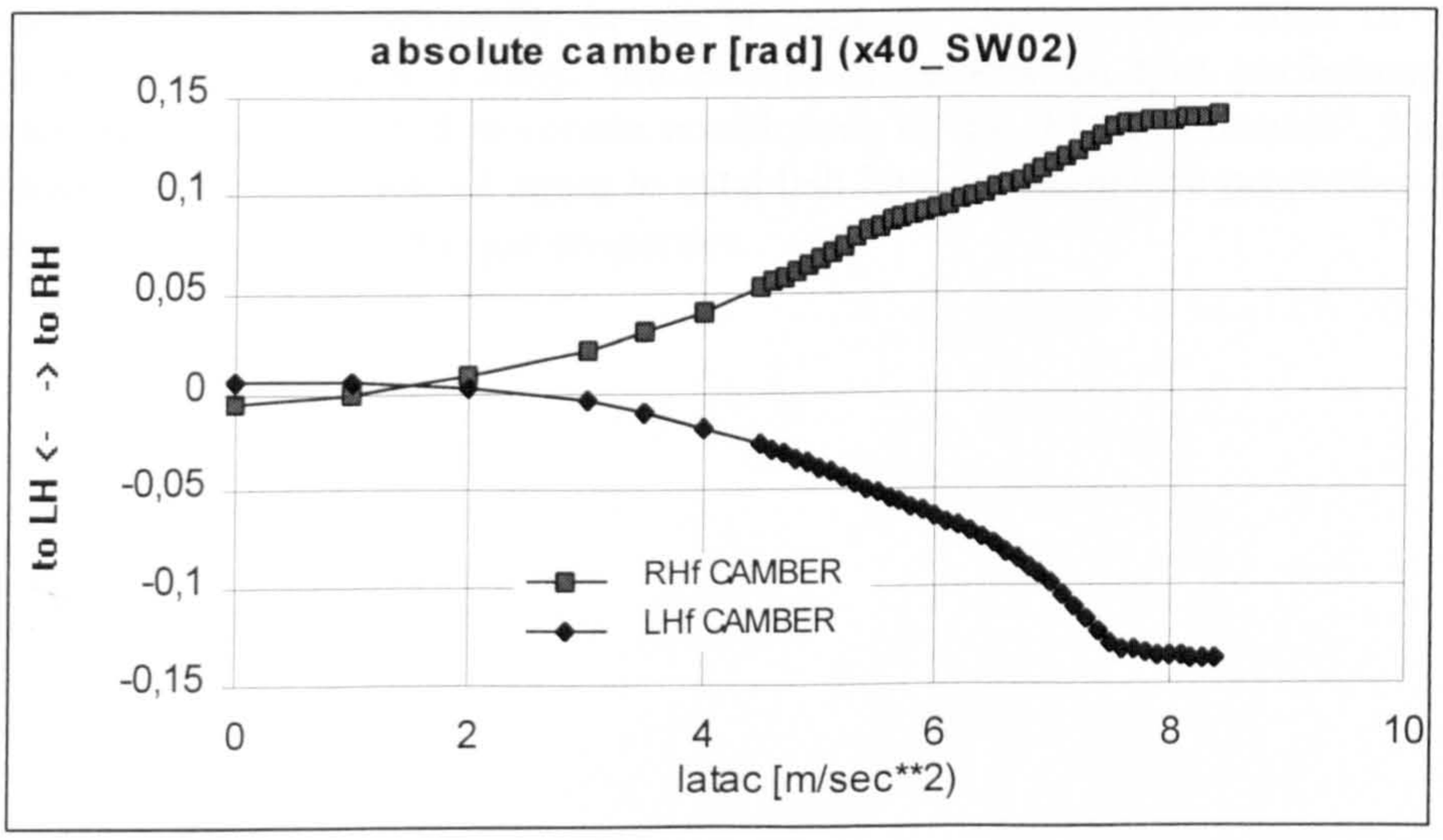

However, the excessive heave moves both wheels into the rebound direction as shown in the second graph, which effectively reduces the track width and also increases the centre of gravity height.

Although body roll becomes small at limit cornering speeds, a fairly high adverse camber angle is imposed on the outside wheel. This left hand wheel is cambered negatively towards the outside of the simulated right hand turn. This adverse camber also contributes to a deteriorating performance.

The swing axle suspension is compared with a much improved design as denoted with 'G06' in fig. 8.5-1. The latter nearly matches the performance of a single tyre under nominal load at zero camber, which can be seen as an optimal result. This design increases the effective friction by more than 10 % compared to the swing axle. It was given generic properties for its track and camber changes, derived from design rules discussed in the following section. It was given a low roll centre and a second order scrub derivative, by which the vehicle is encouraged to jack downwards for increasing lateral load transfer. Furthermore, the suspension accomplishes a full roll angle compensation, as well as a progressively increasing camber for the bump direction.

Due to the low roll centre, the roll angle of the chassis increases much more with lateral acceleration than with the swing axle, as can be seen from the first graph in fig. 8.5-3. Close to the limit acceleration, the bump and rebound stops are engaged, preventing the vehicle from rolling even more. On the other hand, the jacking motion is very well contained throughout the performance range. At limit speed the vehicle jacks down only a few millimetres. Since there is hardly any vertical chassis motion, the wheels travel almost equally and opposite to each other, corresponding to the vehicle roll angle, as shown in the second graph. However, the left hand outside wheel has travelled slightly more into bump than its counterpart into rebound. The third graph shows that a much more advantageous camber angle is maintained at the outside wheel. At high cornering accelerations, the outside wheel cambers negatively into the right hand turn at about 0.05 rad.

After these introductory examples, the tyre-suspension matching problem is approached more fundamentally in an attempt to derive some rules of thumb applicable to their design. Firstly, the effects of camber on tyre performance are summarised and then related to certain coefficients of the 'Magic Formula'. Then the suspension design is addressed again to establish how its geometric properties can be matched or mismatched with tyre properties.

Fig. 8.5-3 roll, jacking, wheel travel and camber for 'G06' vehicle

a)

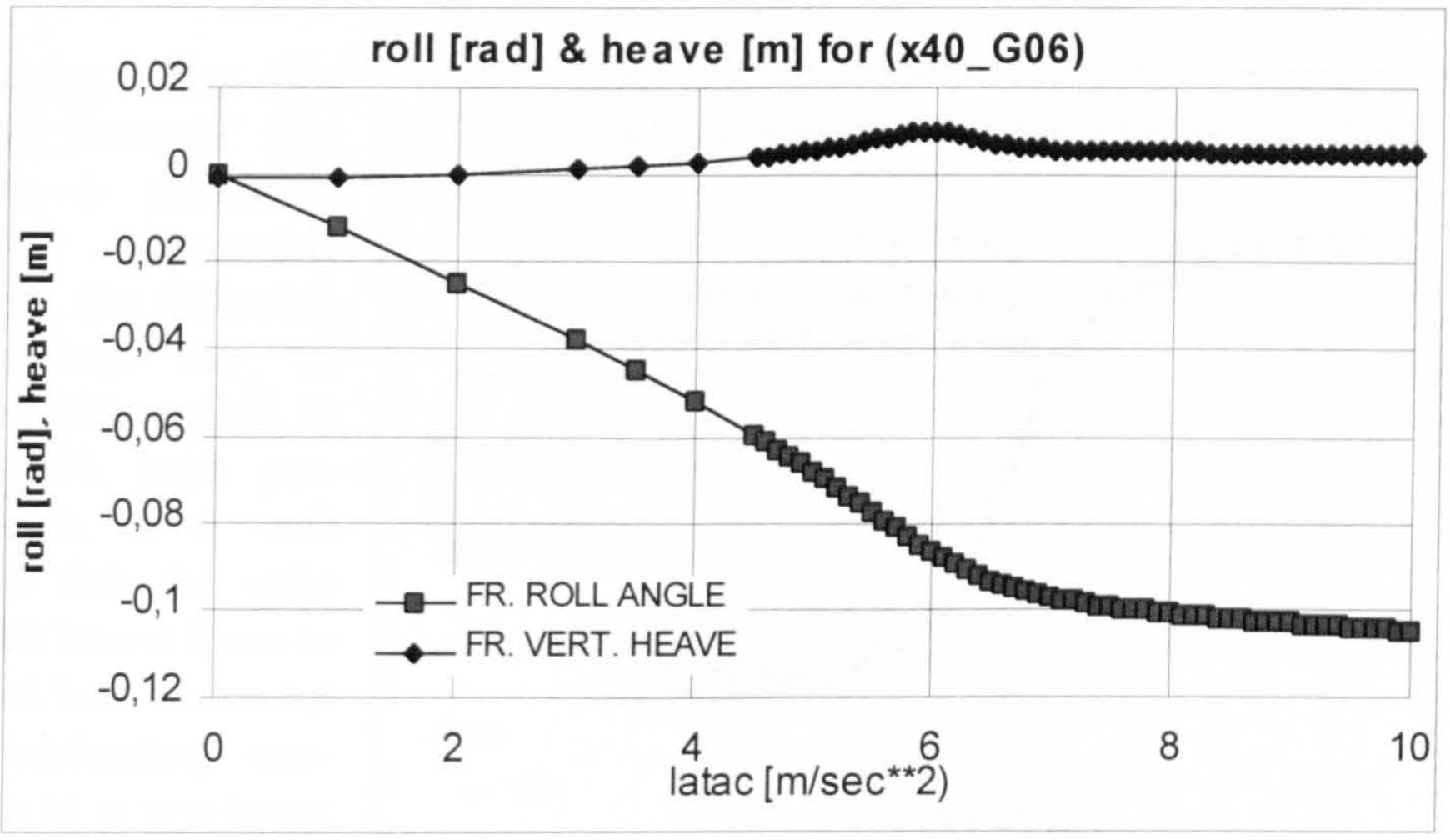

b)

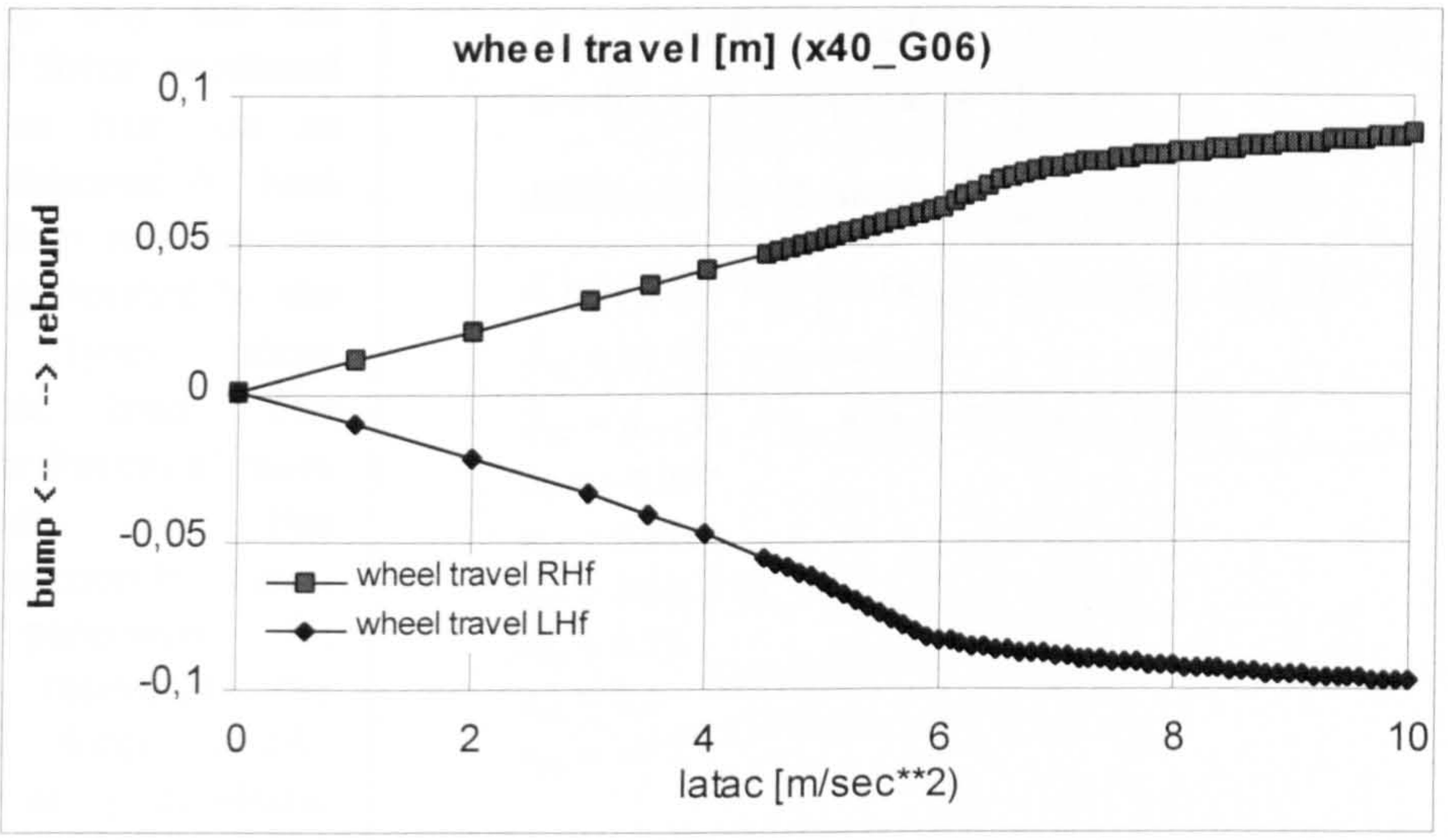

c)

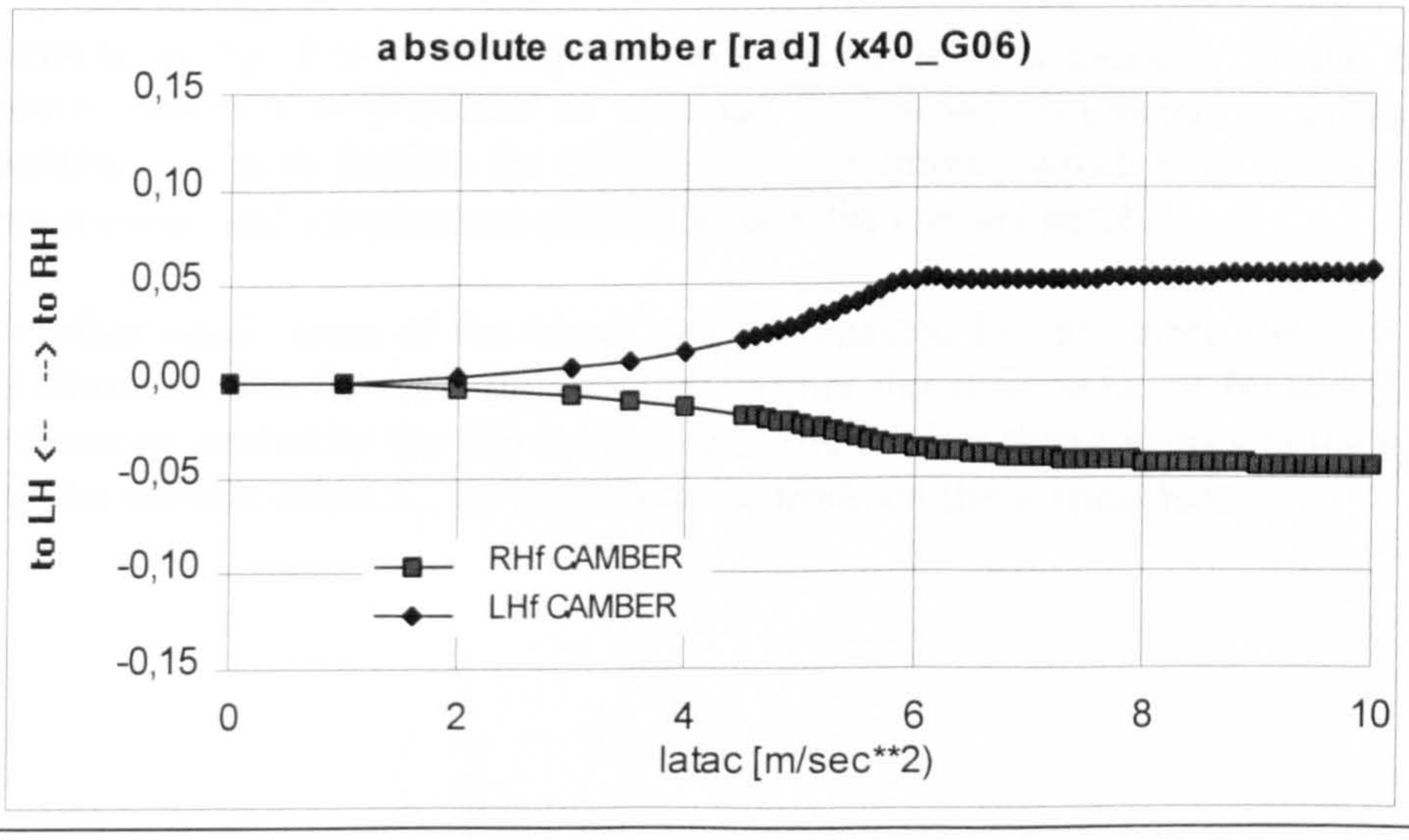

8.6 Effects of tyre camber on limit handling performance

Presuming that the 'Magic Formula' represents a pneumatic tyre accurately enough, the following conclusions can be drawn with regard to the tyre's peak performance. It is well known that the ratio of peak lateral force to vertical load decreases for overloading conditions in a non-linear fashion. This is the reason, why the net lateral force produced by two tyres on an axle exposed to load transfer is less than the force generated by the same tyres under nominal load. The 'Magic Formula' takes account of this phenomenon by defining parameter D, which represents the lateral force amplitude, as a quadratic function of the vertical load F_z. Referring to the formula in fig. 8.6-1, the expression in brackets is a measure of the friction coefficient, which is proportional to the load F_z. Usually, coefficient a_1 is negative, representing a loss in friction for overloading conditions, which may correspond to adverse pressure and temperature distributions in the contact patch.

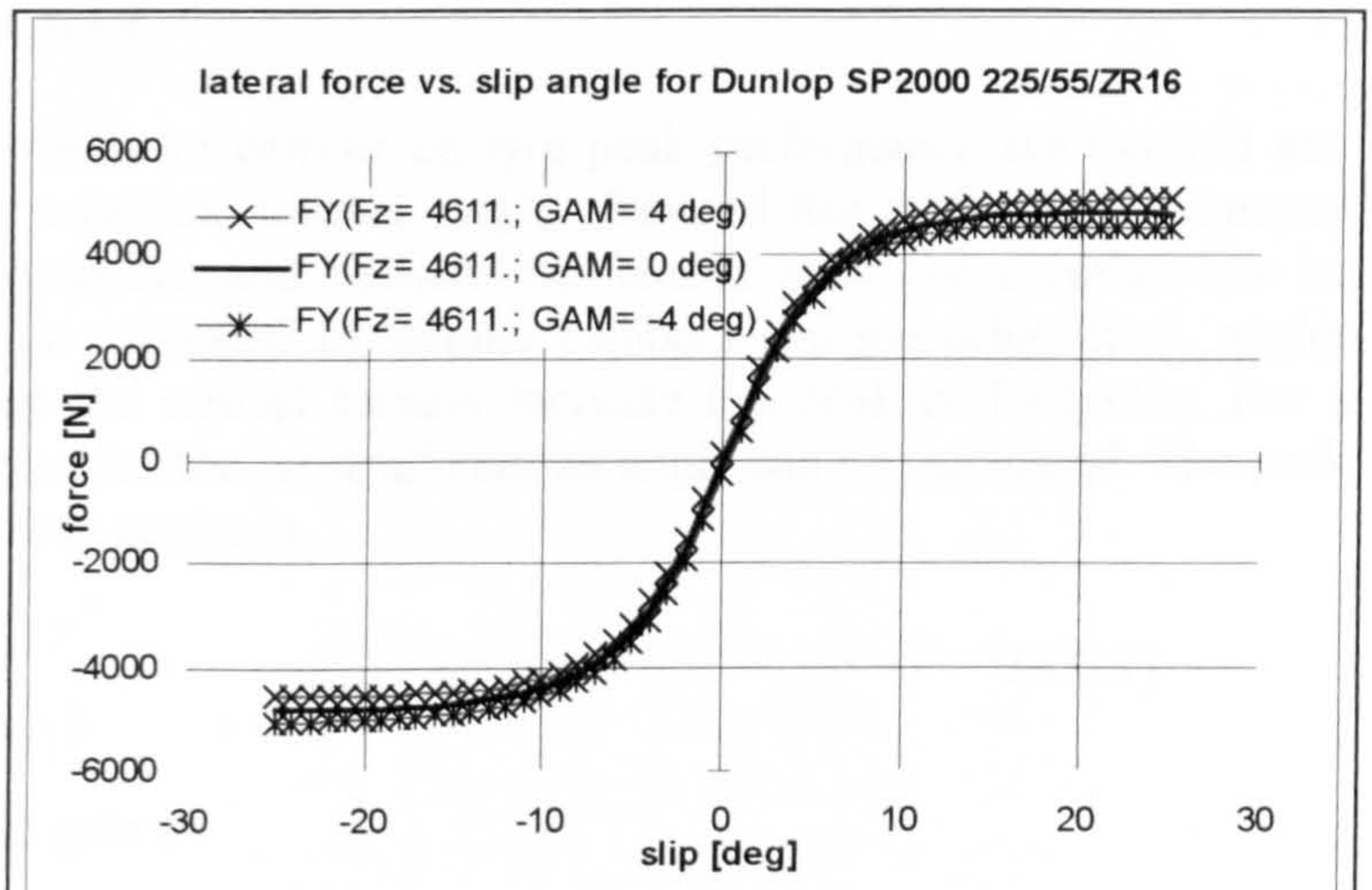

$$F_y = D \cdot \sin\left\{C \cdot \arctan\left\{(Bx - E \cdot (Bx - \arctan((Bx))\right\}\right\}$$

$$D = \left[(a_1 F_z + a_2) \cdot (1 - \mathbf{a}_{15}\gamma^2)\right] \cdot F_z$$

$$BCD = a_3 \cdot \sin\left\{2 \cdot \arctan\left\{F_z / a_4\right\}\right\} \cdot (1 - \mathbf{a}_5 \cdot |\gamma|)$$

$$E = (a_6 F_z + a_7) \cdot \left[1 - (\mathbf{a}_{16}\gamma + a_{17}) \cdot \mathrm{sgn}(\alpha + S_{hy})\right]$$

$$S_{vy} = a_8 \cdot F_z + a_9 + \mathbf{a}_{10} \cdot \gamma$$

$$S_{hy} = a_{11} \cdot F_z + a_{12} + (\mathbf{a}_{13} \cdot F_z^2 + \mathbf{a}_{14} \cdot F_z) \cdot \gamma$$

$$a_5 = -0.097$$

$$a_{10} = 0.016$$

$$a_{13} = 2.0E-05$$

$$a_{14} = 0.73$$

$$a_{15} = 0.4$$

$$a_{16} = -9.7$$

Fig. 8.6-1 tyre camber properties

On the other hand, some of the losses can be regained by cambering the tyre in the proper direction. The formula suggests that camber thrust force has to be added to the lateral force generated by the slip mechanism. The camber thrust occurs in the expression for the vertical offset S_v. Its magnitude depends on the vertical load.

According to the formula, camber also has a detrimental effect on the maximum available friction as denoted by a positive value for coefficient a_{15}. Again, this loss might be ascribed to disadvantageous pressure and temperature distributions of the rubber in contact with the road.

It is concluded that the effects of camber on tyre peak performance are twofold and cancel each other out for a certain 'critical' angle. Beyond this angle, the detrimental effect on the friction dominates and reduces the lateral peak force (otherwise an infinite side force could be produced by infinite camber). On the other hand, angles smaller in magnitude than the critical camber increase the peak performance. For a single tyre an approximation for the 'critical' camber angle can be calculated. The peak side force loss due to camber angles is:

$$\Delta F_y^- = \mu_0 \cdot F_z \cdot \mathbf{a_{15}} \cdot \gamma^2 \qquad (8.6.1)$$
$$\text{with } \mu_0 = (a_1 F_z + a_2)$$

whereas the camber thrust gain is

$$\Delta F_y^+ \approx F_z \cdot \mathbf{a_{14}} \cdot \gamma \qquad (8.6.2)$$

assuming that $\mathbf{a_{13}} \cdot F_z$ is much smaller in magnitude than a_{14}. In order to maintain some gain over the inevitable losses, the following inequality applies, defining a critical ratio of a_{14} to a_{15}, i.e. the already mentioned 'critical' camber angle:

$$\Delta F_y^- \le \Delta F_y^+ \Leftrightarrow \mu_0 \cdot |\gamma| \le \frac{\mathbf{a_{14}}}{\mathbf{a_{15}}} \qquad (8.6.3)$$

Note that the 'critical' camber angle would be inversely proportional to the nominal friction coefficient, which allows slightly higher camber at the more loaded outside wheel than at its lightly laden partner.

Another camber effect not discussed here refers to the curvature of the transition region, which is heavily dependent on parameter E. Since this parameter has no influence on the peak force, it will not be considered in this study.

These preliminary considerations illustrate how tyre properties on the one hand, e.g. those describing camber characteristics, and the ability of the suspension to position the contact patch favourably to the road on the other, are related to each other. Furthermore, some of the coefficients in the 'Magic Formula' can be employed as constraints for the suspension design or as a 'property' to be optimised by a tyre designer.

In the following section some basic rules for the suspension design are established. These rules relate tyre properties in the form of 'Magic Formula' coefficients to geometric suspension design characteristics. Although the discussion concentrates on matching suspension geometry to tyre camber properties, some other design considerations are summarised briefly.

8.7 Design rules for tyre and suspension

The 'Magic Formula' coefficients used in this investigation were derived from steady state testing of a DUNLOP SP 2000 tyre of the size 225/55 ZR16. Specimens of this tyre were tested for slip angles ranging from -14 up to 14 degrees at four loads, including three camber angle settings (+/-10, 0 deg) for each load. The surface material of the indoor test rig was '3M resin bond', which provides high friction. The camber coefficients derived from the raw test data are listed in fig. 8.6-1. Note that both coefficients a_{13} and a_{14} are positive, and thus define a progressively rising camber thrust for increasing loads. The agreement between the 'Magic Formula' approximation of the side force and the aligning torque and the corresponding test data is illustrated by figures B2-1-3 which can be found in appendix B2.

It was already stated that lateral load transfer limits disproportionately the cornering performance of a vehicle or an axle on a vehicle. This detrimental effect can be reduced or worsened by cambering the wheels to the road, so that the tyres can produce some camber thrust. In order to use this additional force to maximise the cornering performance of an axle, the suspension design has to be tuned to achieve favourable camber angles at the limit. It was established that for limit conditions small camber angles are desired, by which a high friction is maintained. Given the tyre properties described by the 'Magic Formula', principles for designing a performance enhancing suspension geometry can be defined. Considering that the outside and inside wheels corner under different loads as well as different camber angles, two conditions can be derived from the 'Magic Formula', which have to be met in order to generate a favourable net camber thrust force. For our study only the linear camber thrust associated with a_{14} is taken into account. This is a reasonable simplification provided that second order camber thrust effects as described by a_{13} are small, as was the case for the tyre data considered here, or if these effects even contribute to a side force gain. Applying equation (8.6.2) to the inside and outside tyre, a net camber thrust side force gain is obtained. It is composed of two parts of similar magnitude, and reads:

$$\Delta F_Y = \underbrace{a_{14} \cdot F_{Z,stat} \cdot (\gamma_{out} + \gamma_{in})}_{\text{'bicycle camber thrust'}} + \underbrace{a_{14} \cdot \Delta F_Z \cdot (\gamma_{out} - \gamma_{in})}_{\text{'static camber thrust'}} \qquad (8.7.1)$$

In the first part we find the sum of the outside and inside camber angles weighted by the static wheel load. The second part contains their difference, weighted by the load transfer. In accordance with the sign convention used earlier, an additive camber thrust is positive for a right hand turn. Provided that the product of a_{14} and the static wheel load $F_{z,stat}$ is positive, the sum of the camber angles has to be positive:

condition (a) for a right hand (RH) turn: $\hat{\gamma}^{LH} + \hat{\gamma}^{RH} \geq 0 \qquad (8.7.2)$

which means, that the average of the two wheel camber angles has to lean towards the inside of the turn, analogous to a cornering bicycle. The second condition (b) requires the outside wheel camber to be bigger in magnitude than at the inside:

condition (b) for a right hand (RH) turn: $\hat{\gamma}^{LH} - \hat{\gamma}^{RH} \geq 0 \qquad (8.7.3)$

This gain corresponds to the idea of providing a static camber, whereby a net force is produced as soon as the axle is submitted to load transfer ('static camber thrust').

Both conditions are met, if the outside wheel is cambered more towards the centre of the turn than its counterpart. In short we can write for a RH turn:

$$\hat{\gamma}^{LH} \geq \left|\hat{\gamma}^{RH}\right| \qquad (8.7.4)^{1}$$

Hence, camber on the outside wheel has to be positive for a right hand turn. In order to establish, which suspension design satisfies these two conditions, we substitute the absolute camber angles in (8.7.2) and (8.7.3) by the roll angle and those polynomials defined in section 3.1.5, which give the relative camber between wheel and chassis as a function of the wheel travel. The right hand side relative camber is defined by:

$$\gamma^{RH} = c_{\gamma,1} \cdot z_W^{RH} + c_{\gamma,2} \cdot (z_W^{RH})^2 \qquad (8.7.5)$$
$$z_W^{RH} \geq 0 \text{ for rebound}$$

The suspension derivative parameters $c_{\gamma,1}$ and $c_{\gamma,2}$ respectively define the rate of camber change with wheel travel z_W^{RH} and its progression towards full bump and rebound. The anti-symmetric left hand side relative camber reads:

$$\gamma^{LH} = -[c_{\gamma,1} \cdot z_W^{LH} + c_{\gamma,2} \cdot (z_W^{LH})^2] \qquad (8.7.6)$$
$$z_W^{LH} \geq 0 \text{ for rebound}$$

The following equations give the absolute camber angles between wheel and road, taking the vehicle roll into account.

$$\hat{\gamma}^{RH} = \phi + c_{\gamma,1} \cdot z_W^{RH} + c_{\gamma,2} \cdot (z_W^{RH})^2$$
$$\hat{\gamma}^{LH} = \phi - [c_{\gamma,1} \cdot z_W^{LH} + c_{\gamma,2} \cdot (z_W^{LH})^2] \qquad (8.7.7,\ 8.7.8)$$
$$z_W^{RH},\ z_W^{LH} \geq 0 \text{ for rebound}$$

The vertical motion of each wheel is composed of a symmetric part due to jacking and an anti-symmetric part corresponding to the vehicle roll. Neglecting vertical tyre deflections, each vertical wheel travel is defined as:

$$z_W^{RH} = -(z_B + T_W \cdot \phi) \qquad (8.7.9,\ 8.7.10)$$
$$z_W^{LH} = -(z_B - T_W \cdot \phi)$$

with :

T_W: half track width

$z_B \geq 0$ jacking downwards

$\phi \geq 0$ rolling to LH side

---

[1] Note, that this inequality is consistent with (8.6.3), by which we established that higher camber is acceptable at the heavier laden outside wheel

By putting (8.7.9) into (8.7.7) and (8.7.10) into (8.7.8), and introducing the resulting equations for the absolute camber angles into (8.7.2) and (8.7.3), we obtain for condition (a):

$$\hat{\gamma}^{LH} + \hat{\gamma}^{RH} \geq 0$$

$$\Leftrightarrow \underbrace{2 \cdot (1 - c_{\gamma,1} \cdot T_W) \cdot \phi}_{\text{body roll compensation}} + \underbrace{c_{\gamma,2} \cdot (4 \cdot z_B \cdot T_W \cdot \phi)}_{\text{camber due to body jacking}} \geq 0 \qquad (8.7.11)$$

$\hat{\gamma}^{RH}$ is camber of inside wheel for RH turn

Condition (b) yields to:

$$\hat{\gamma}^{LH} - \hat{\gamma}^{RH} \geq 0$$

$$\Leftrightarrow \underbrace{c_{\gamma,1} \cdot (2 \cdot z_B)}_{\text{camber difference due to jacking}} - 2 \cdot c_{\gamma,2} \cdot \underbrace{[z_B{}^2 + (T_W \cdot \phi)^2]}_{\text{positive camber difference}} \geq 0 \qquad (8.7.12)$$

$\hat{\gamma}^{RH}$ is camber of inside wheel

Note, that both inequalities contain a linear as well as a second order term associated with vehicle body motions ϕ and z_B. Whether both conditions can be satisfied depends on the geometric camber characteristics of the suspension as well as, whether the vehicle jacks downwards or upwards, and whether it rolls towards the outside or inside of the negotiated turn. The jacking and rolling motions of the chassis are hard to predict as the swing axle example illustrated. However, the inequalities (8.7.11) and (8.7.12) allows establishing at least the signs of the suspension properties depending on the jacking tendency of the axle. For instance, condition (b) is always met, if the terms in each parenthesis are positive, from which it can be concluded that the second order camber property has to be negative, whereas the first order property has to be positive for an axle with the tendency to jack downwards at limit cornering speeds.

The findings are summarised as follows:

$$c_{\gamma,1} \begin{cases} \geq 0, \text{ if } z_B \geq 0: \text{jacking down} \\ \leq 0, \text{ if } z_B \leq 0: \text{jacking up} \end{cases} \qquad (8.7.12a), \text{ and}$$

$$c_{\gamma,2} \leq 0 \qquad (8.7.12b)$$

In order to fulfil condition (a) as well, the sign of the roll angle has to be considered. Assuming that the vehicle rolls conventionally towards the outside of the corner, which gives a negative angle for a right hand turn, the inequality (8.7.11) requires:

$$\underbrace{(1 - c_{\gamma,1} \cdot T_W)}_{\text{body roll compensation}} \leq 0 \text{ and}$$

$$\underbrace{c_{\gamma,2} \cdot (4 \cdot z_B \cdot T_W)}_{\text{camber due to body jacking}} \leq 0$$

These inequalities are met by a suspension design, for which

$$c_{\gamma,1} \geq {}^{1}\!/_{T_W} \tag{8.7.11a}$$

$$\text{and} \quad c_{\gamma,2} \begin{cases} \leq 0, \text{ if } z_B \geq 0 \text{: jacking down} \\ \geq 0, \text{ if } z_B \leq 0 \text{: jacking up} \end{cases} \tag{8.7.11b}$$

holds. The first of the two inequalities (8.7.11a) and (8.7.11b) requires a suspension design accomplishing at least full body roll compensation. This design principle is represented by a positive value of the first order camber derivative with a magnitude of the inverse half track width. A less formal description of this principle is a suspension geometry, giving an equivalent radius arm smaller in length than half the track width, as indicated in fig. 8.7-1.

Furthermore, it can be established that the principles (8.7.11a) and (8.7.12a) as well as (8.7.11b) and (8.7.12b) contradict each other for an axle jacking upwards at the limit. Consequently, only an axle with a jacking downwards tendency at the limit is able to make full use of the tyre's camber thrust, provided that the design principles laid down for the suspension geometry in (8.7.11a) and (8.7.11b) are applied. If the vehicle jacks upwards, at best, one of the two parts of the camber thrust as defined in (8.7.1), is generated, which might be just too little to cancel out the adverse contribution of the second part.

The jacking motion of the axle can be controlled by a suspension geometry, which changes the track width only mildly for bump and rebound wheel travel. Contrary to that behaves a swing axle with a short radius arm. As demonstrated in section 8.5, this design is prone to large track changes, i.e. high scrub gradients, which, in combination with different side force levels at the inside and outside wheels, lead to a progressive vehicle heave. Conversely, the axle with the best performance, denoted by 'G06' in fig. 8.5-3, features a fairly low roll centre (10 cm above ground), which corresponds to a low first order scrub derivative and subsequently small track changes with bump and rebound. Furthermore, suspension scrub was defined to decrease with bump travel. This built in progression in combination with bump and rebound stops engaging at 6 cm wheel travel ensured, that the centre of gravity was pulled slightly below its static level, as required.

Before the findings are quantified in the following section by a few simulation results, the tyre and suspension principles established in this section as well as the assumptions made are summarised. The objective to optimise the cornering performance of a single ended vehicle led to design constraints, involving tyre as well as suspension properties. It was presumed that additive tyre camber thrust is still available even for high slip cornering, which seems reasonable considering the efforts made in setting up a race car suspension to establish a favourable wheel camber. It was also considered that high camber has an adverse effect on the effective friction. However, the simulations results presented here are based on tyre data, which was derived from rig tests on a high friction surface (3M resin bond), so that some uncertainty remains, whether the results reflect the on the road behaviour of tyre and vehicle.

It was shown, that a suspension geometry jacking the chassis downwards at limit accelerations, makes full use of the camber thrust generated by the two tyres. This design constraint requires to tune the scrub, i.e. track change properties, accordingly. It leads to a geometry giving a low roll centre (low first order scrub derivative). For a design with its roll centre above ground (negative scrub derivative for RH side), it might be appropriate to introduce some progression for the scrub, such that the scrub gradient decreases in magnitude with bump travel. In other words, the instantaneous centre of the wheel should move downwards for bump travel, and by that reducing the radius arm inclination. This configuration contains jacking to small levels, and forces the outside wheel to use slightly more suspension travel in bump than its counterpart does in rebound, by which an anti-symmetric camber setting is pronounced. Unfortunately, designs with a low roll centre come with the disadvantage of giving rise to comparatively high roll angles at moderate cornering accelerations, which have to be contained by anti-roll bars.

The other design principles found refer to the camber characteristics of the suspension. An ideal suspension, ideal in matching the tyre's camber thrust properties, more than compensates the vehicle roll angle by employing a short radius arm, whose length is inversely proportional to the first order camber derivative, and by a progressively increasing relative camber for bump travel. This progression, i.e. shortening of the radius arm, ensures, that the outside wheel in bump is cambered slightly more than the one on the inside ('static camber gain principle'). On the other hand, full roll compensation implies that the suspension camber is very sensitive to wheel travel variations, which might compromise straight line driving due to undesired camber forces disturbing the vehicle's heading. Furthermore, such a suspension would change its static camber for different static loading, which might affect its handling adversely. And it might not comply with the required axial play and inclination of the drive shafts.

But even if full roll angle compensation cannot be achieved by a suspension, some camber thrust can still be maintained by designing a strong jacking down tendency into the suspension. This would maintain a beneficial 'static camber gain', as defined by (8.7.12), due to the camber difference established between outside and inside wheel. Furthermore, the second order term in (8.7.11) would reduce the loss of a non roll compensating geometry.

A practical example and the benefits of using the camber thrust is discussed in /8.7.1/. A rear suspension that actively controls the camber angle is said to improve stability considerably for double lane changes and other transient manoeuvres.

design parameter/ tyre	preferred value	notes
a_{13} non-linear camber thrust property in 'Magic' Formula'	> 0	a positive value would extend performance range
a_{14} linear camber thrust property in 'Magic Formula'	> 0 as big as possible	none
a_{15} penalty coefficient representing loss in friction	as small as possible	ratio of a_{14} and a_{15} defines a 'critical camber' depending on nominal friction
design parameter/ suspension		
first order scrub (ratio of roll centre height and half the track width)	either positive or negative, but small in magnitude	leads to high vehicle roll
second order scrub	to be tuned to contain jacking	none
first order camber (inverse length of radius arm)	$> 1/Tw$	full roll compensation
second order camber	< 0	'more beneficial camber in bump than in rebound'

Table 8.7-1: design principles for ideal suspension and tyre properties

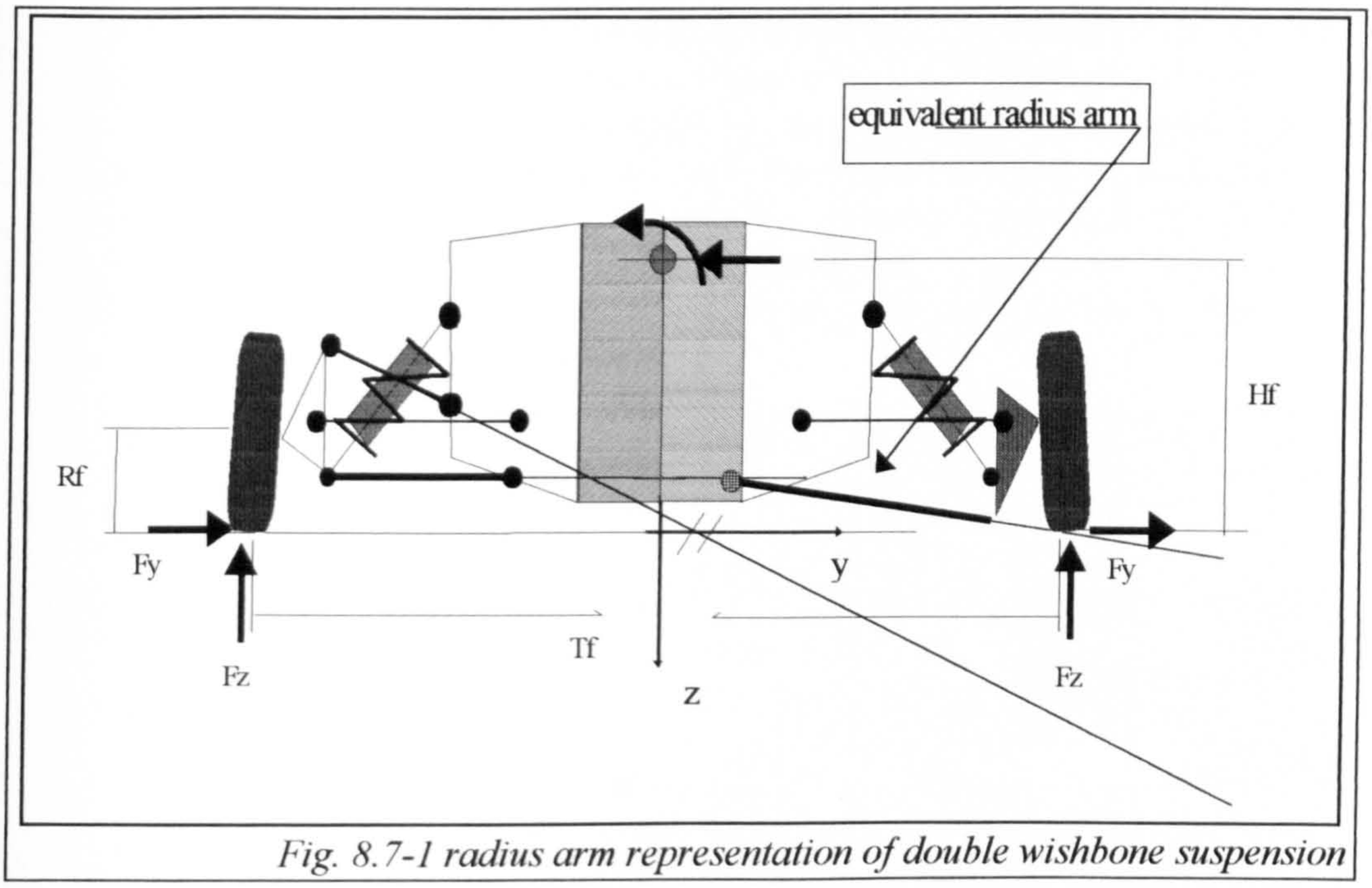

Fig. 8.7-1 radius arm representation of double wishbone suspension

It probably does not make much sense to try to establish baseline values for either the second order camber or scrub derivatives, firstly because we could not tell, whether such a generic design property could be transferred into a proper suspension drawing, and secondly because they will depend on the actual tyre camber properties, the static suspension camber and bump stop characteristics. It can be said, though, that they need to be tuned to contain the camber at moderate levels as defined by (8.6.3).

Finally, the design principles discussed in this section are summarised in table 8.7-1. A geometry corresponding to these rules is sketched in fig. 8.7-1. On the left hand side a double wishbone configuration is shown, which gives a low roll centre, full roll compensation as well as the required progressive scrub and camber behaviour. On the right hand side its equivalent radius arm is shown, which represents the suspension kinematics for small perturbations from a nominal configuration.

8.8 Simulation results of steady state cornering

In the last section some suspension design rules were presented, by which camber and scrub characteristics of the suspension design are matched with tyre camber properties. In this section some more simulation results are given, in order to quantify the findings. Firstly, it is established how influential each of those four suspension derivatives is on the cornering performance. Secondly, the findings are verified for a tyre, whose peak force is more sensitive to camber than presumed for the study summarised in section 8.5. Finally, the effect of static suspension camber as an additional tuning parameter is discussed.

Some more simulations were carried out for various generic suspension designs, in order to quantify the contribution of each of those four suspension derivatives on limit performance. Some of these are presented in fig. 8.8-1, for which the corresponding suspension parameters are given in table 8.8-1. Fig. 8.8-1a shows the performance diagram of seven suspensions. These have the roll centre height in common, whereas second order scrub derivative and both suspension camber parameters were varied. The highest cornering acceleration is achieved by design 'G06', as discussed in section 8.5, which also maintains a smooth transition from the linear to the limit state. Compared to the double wishbone suspension of a Jaguar X40 (93 model year, 'front dw'), the performance gain established by this generic design appears to be considerable, but so are the changes made to the suspension geometry. The generic suspension fully compensates the roll angle compared to approximately 20 % roll compensation for the X40. The former also differs in the second order characteristics, which define the anti-symmetry (progression) of scrub and camber for bump and rebound wheel travel.

suspension type	half track width [m]	1. scrub derivative $c_{y,1}$ [/]	2. scrub derivative $2 \cdot c_{y,2}$ [1/m]		static camber [rad]	1. camber derivative $c_{\gamma,1}$ [1/m]	2. camber derivative $2 \cdot c_{\gamma,2}$ [1/m**2]
double wishbone (X40 93MY)	0.75	-0.1295	-1.855		0.	0.2751	-7.0224
'G01'	0.75	-0.1295	-1.855		0.	0.2751	7.0224
'G03'	0.75	-0.1295	1.855		0.	1.3333	-7.0224
'G04'	0.75	-0.1295	-1.855		0.	1.3333	-7.0224
'G05'	0.75	-0.1295	-1.855		0.	-1.3333	7.0224
'G06'	0.75	-0.1295	-2*1.855		0.	1.3333	-2*7.0224

Table 8.8-1 alternative suspension layouts

The quantitative effect of these two second order properties can be estimated by comparing the curves for 'G03' and 'G04', and those for 'dw' and 'G01', respectively. The two former designs differ in the second order scrub, whereas the latter two feature equal, but opposite second order camber. Their contribution appears

to be small in relation to the improvement made by an increased first order camber derivative, as can be seen by comparing designs 'dw' and 'G04', considering though, that this parameter is more than four times higher than the camber derivative for the X40, whereas the values of the second order parameters for the generic designs were only doubled.

It was mentioned that a tyre is limited in producing beneficial camber thrust. Using the 'Magic Formula', one can calculate an optimal camber angle for which the maximum saturation side force occurs. Neglecting second order camber thrust effects (a_{13}=0), it reads:

$|\gamma_{OPT}| = \frac{\mathbf{a_{14}}}{2 \cdot \mu_0 \cdot \mathbf{a_{15}}}$, which is half of the 'critical angle' as defined by (8.6.3).

This ideal saturation camber angle becomes small for tyres, whose friction loss is represented by a high 'friction loss factor' a_{15}. In order to verify, whether our design rules still hold for this type of tyre behaviour, the simulations were repeated with a tyre characterised by a ten times higher value for a_{15} than before (a_{15}=0.4). Fig. 8.8-1b illustrates, that this more camber sensitive tyre hardly affects the performance of our benchmark design 'G06'. Such a tyre would only slightly reduce the limit acceleration[1], as can be seen by the relatively higher slip angles needed to establish the same amount of lateral force. This result is not surprising, considering that the 'G06' design maintains small wheel camber (fig. 8.5-3c), still below the 'critical' value, up to the limit. The swing axle, however, promotes adverse camber angles, as shown in fig. 8.5-2c, so that the limit friction is further reduced by a more camber sensitive tyre.

The third 'lateral force coefficient diagram' in fig. 8.8-1c shows the effect of a static camber angle that was introduced to compensate some of the adverse effects of the camber sensitive tyre (a_{15}=4). There is little improvement for the 'G06' benchmark design, while the performance envelope of the swing axle design increased slightly.

Other simulations confirmed a trend, according to which, static camber and a low friction loss a_{15} are more influential to designs not complying with those principles laid out in table 8.7-1 than to those adhering to them.

[1] Since the program could not compute any solution for the swing axle (0 deg camber, a_{15}=4) beyond 8 deg slip, we have to assess the performance by comparing the magnitude of slip necessary to establish equal levels of side force

Fig. 8.8-1 tyre camber effects on lateral force coefficient

a)

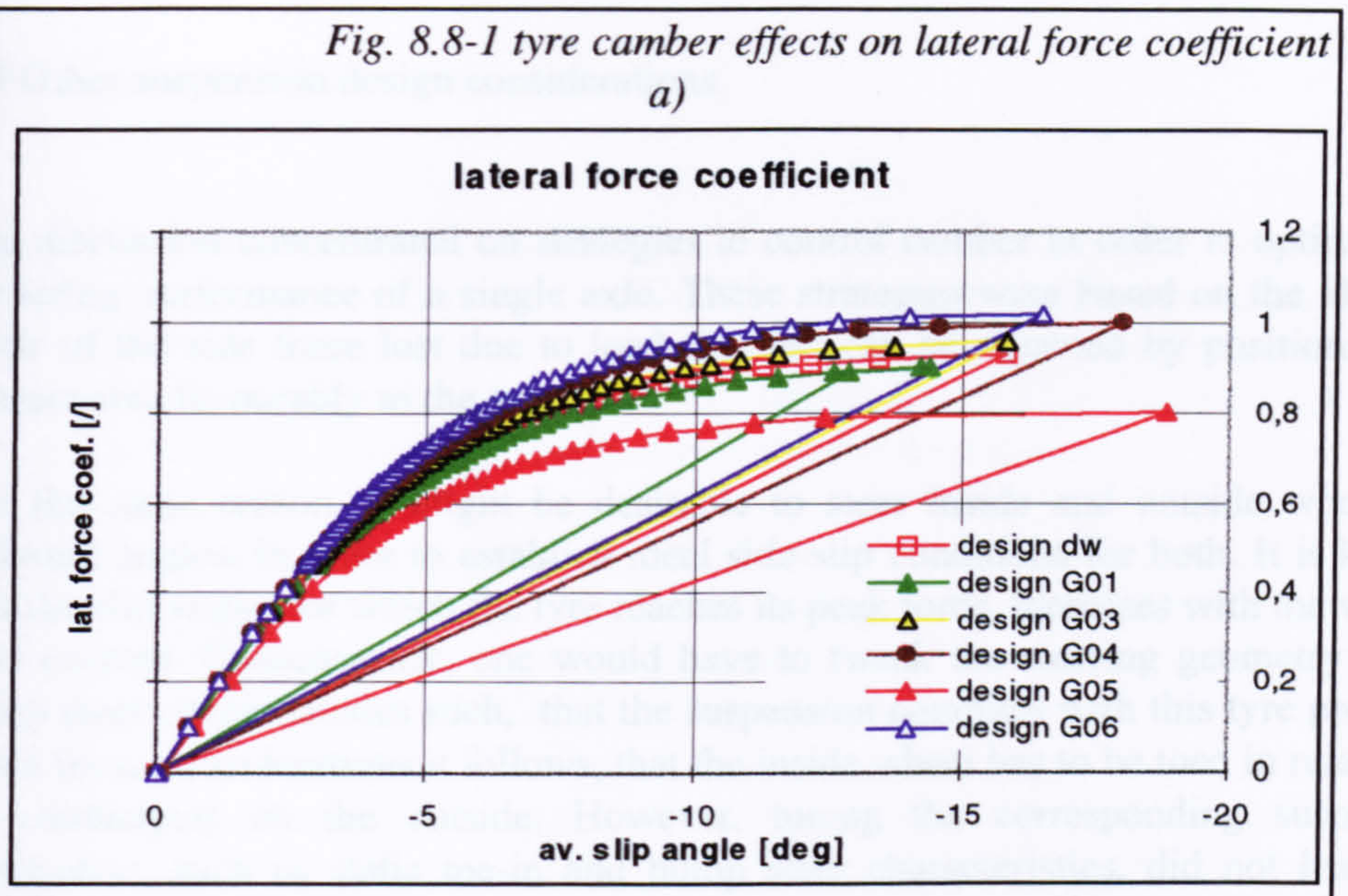

b)

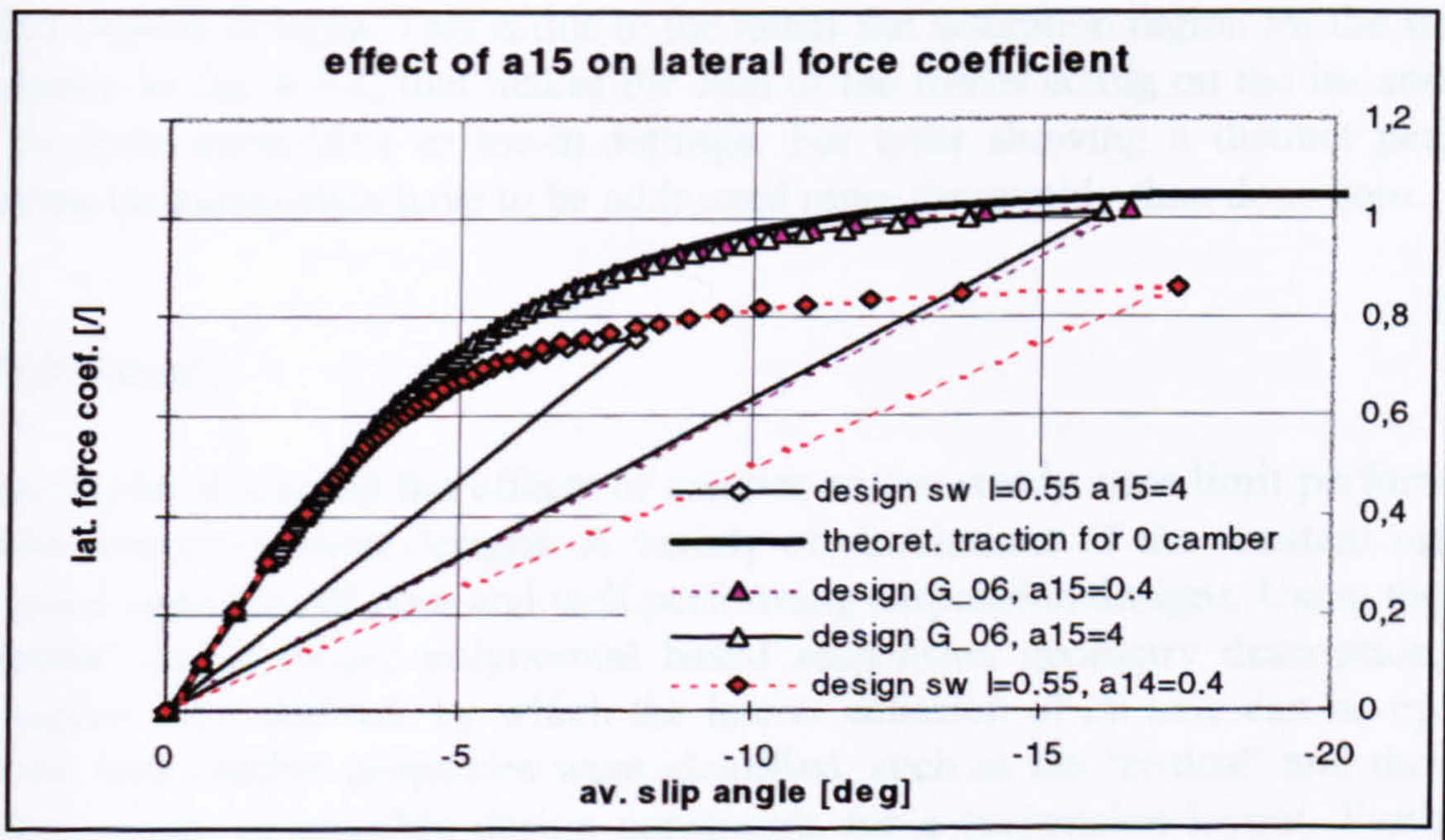

c)

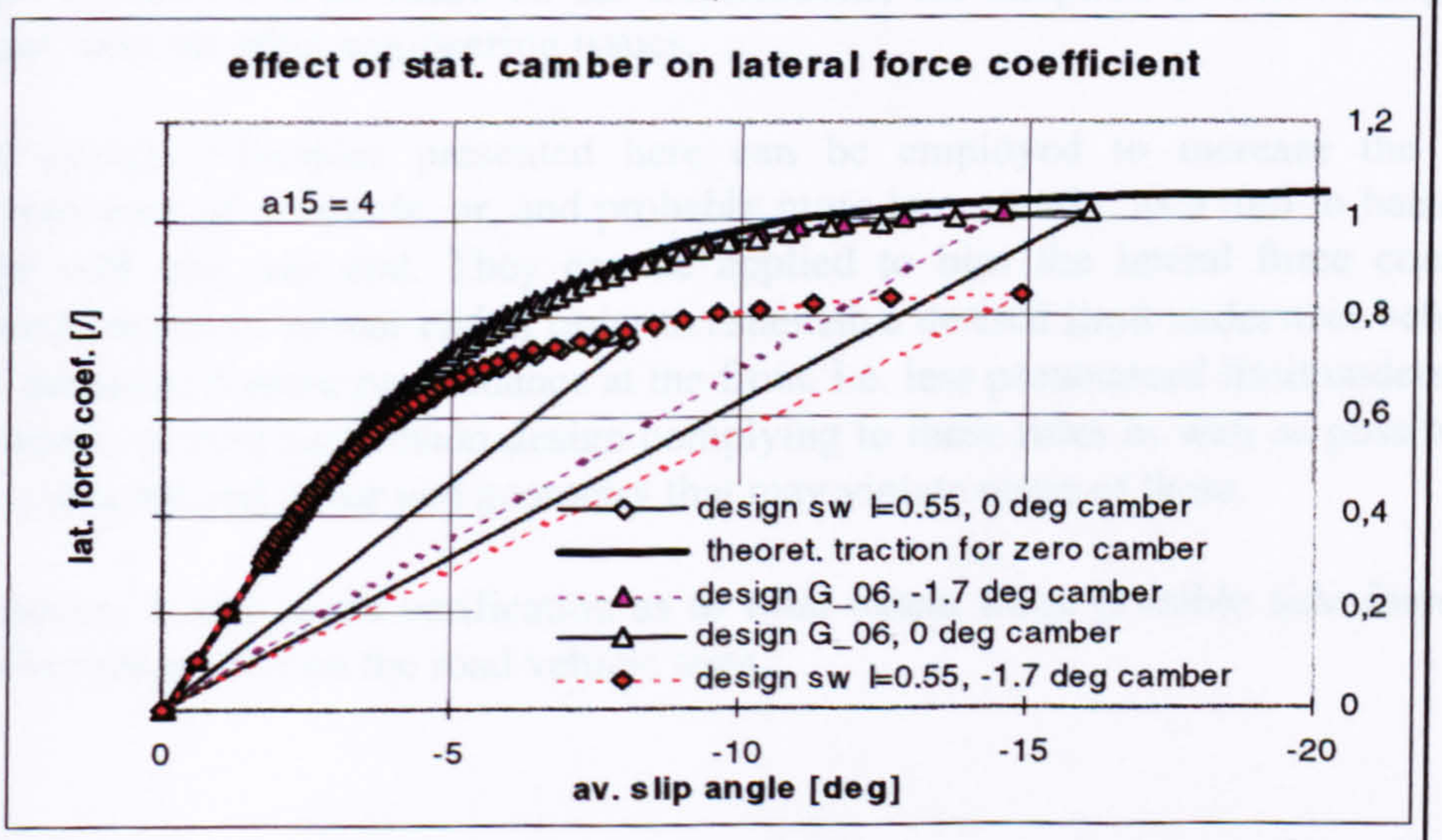

8.9 Other suspension design considerations

The discussion concentrated on strategies to control camber in order to optimise the cornering performance of a single axle. These strategies were based on the idea that some of the side force lost due to load transfer, can be regained by positioning the contact area favourably to the ground.

For the same reason, it might be desirable to steer inside and outside wheels by different angles, in order to establish ideal side slip conditions for both. It is known, that the slip angle, for which the tyre reaches its peak force, increases with the vertical load exerted. Consequently, one would have to tweak the steering geometry or the bump steer characteristics such, that the suspension complies with this tyre property. From these considerations it follows, that the inside wheel has to be toed in relative to its counterpart on the outside. However, tuning the corresponding suspension parameters, such as static toe-in and bump steer characteristics, did not lead to a significant improvement in cornering performance for any of the simulated single-ended vehicle designs. This is due to the rather flat saturation region for the side force, as shown in fig. 8.6-1, that makes the sum of the forces acting on the in- and outside of the axle insensitive to toe-in settings. For tyres showing a distinct peak, these steering characteristics have to be addressed more thoroughly than done here.

8.10 Summary

This chapter discussed the effects of camber on the steady state limit performance of automotive suspension designs. A variety of simulations of the constant radius test provided examples of poor and well performing suspension designs. Using the 'Magic Formula' and a simple polynomial based suspension geometry description, design principles were derived, by which the lateral adhesion of an axle can be optimised. Certain tyre camber properties were identified, such as the 'critical' and the optimal camber angle, as possible design constraints for a suspension layout. Furthermore, some comments were made on the implications, the adoption of those design rules might have on other engineering issues.

The design principles presented here can be employed to increase the overall performance of a vehicle, or, and probably more importantly, as a tool to balance the front with the rear end. They can be applied to bias the lateral force coefficient towards the front or rear end in order to establish a desired limit understeer behaviour. For instance, if more performance at the front, i.e. less pronounced limit understeer, is required, a front suspension design complying to these rules as well as possible may be employed and a rear end geometry that may violate some of these.

However, it still needs verification as to what extent those possible side force gains can be realised for on the road vehicle tests.

9 Vehicle dynamics simulation using AUTOSIM

The previous sections dealt with the steady state vehicle behaviour in some detail. In the following sections of this chapter, the discussion will concentrate on the transient limit handling performance of a vehicle. Corresponding to the parameter study conducted for the steady state cornering behaviour, certain suspension and tyre characteristics were altered with respect to a nominal setting.

During the project a fairly elaborate vehicle model was developed for this purpose, using the commercially available software package AUTOSIM. Details concerning this multi-body simulation code were given in chapter 3, along with a description of the vehicle model used for the limit handling simulations discussed in this chapter.

The vehicle model was validated against some of the data captured during the proving ground testing for the Jaguar vehicle. Some graphs, showing the degree of agreement obtained between experiment and simulation, are included in section 9.1. In the following section some simulation results of a parameter study are presented. The influence of suspension and tyre properties were investigated for transient limit driving.

Lane change manoeuvres were simulated corresponding to the proving ground tests carried out with a Jaguar XJ6 test vehicle. In section 9.2 some results are presented which were obtained from ISO lane change simulations for which the driver model described in section 3.2.3 was employed. As will be demonstrated in section 9.1, this model proved unsuitable for representing a driver's steering wheel input for severe manoeuvres. The results give further evidence of this finding. However, some of these results may illustrate how a vehicle responds to the closed loop control action of a driver with very limited experience and skill.

Results of limit handling manoeuvres simulated for an open loop steering input are given in section 9.3 and 9.4. Instead of using the driver model, a hand wheel angle input was defined, resembling to some extent the time histories measured for the lane changes performed on the proving ground. Section 9.3 deals with the effects of suspension properties, while section 9.4 discusses the impact of tyre properties on the limit handling performance.

Results are discussed using the handling criteria introduced in chapter 7. Correlation coefficients and time lags along with other statistical parameters are presented for a variety of vehicle and tyre characteristics. The nominal values of the vehicle and tyre parameters are given in the appendix B1 and B2. The values of the varied parameters are given in the text.

9.1 Vehicle model validation

Some suitable recordings were chosen from the proving ground test data for validating the AUTOSIM vehicle model. These recordings include steady state cornering tests, ISO lane changes and lane changes in a turn. The test data considered for the validation of the model was obtained from tests involving the standard Jaguar fitted with standard tyres of the type Dunlop SP 2000 225/55R16. For the simulations tyre properties were used, which were derived from the force and moment test data of this tyre design. The data describing the tyre properties as well as those used for the vehicle model /4.1.7, 8.2.2/ can be found in the appendix B1 and B2.

In the following section results for the steady state cornering performance are compared. This is followed by a comparison of time histories obtained from low speed lane change in a turn manoeuvres. The vehicle model is validated against measured time histories of the yaw rate, lateral acceleration, roll angle and the hand wheel torque. The same procedure is adopted for the validation against data referring to high speed lane changes. The measured hand wheel angle input is used in the corresponding vehicle simulation. Furthermore, cross-correlation coefficients and time lags were calculated from the simulated data and compared to those established from the corresponding recordings. These parameters were introduced in chapter 7 as limit handling quality criteria.

In addition to validating the model for the open loop case, some attempts were made to achieve the same level of agreement for the closed loop case. For that, the predefined hand wheel angle time histories used for the previous simulations were replaced by a driver model. The driver model, described in chapter 3.2.3, produces a steering angle input according to previewed path, as defined in the input file. However, the driver model proved to be unable to reproduce a similar hand wheel angle time history as measured for the test driver, unless the manoeuvre involved only moderate levels of severity.

9.1.1 Vehicle model validation for steady state cornering

The Jaguar vehicle model was validated against test data obtained for a steady state cornering test. This test was performed on the steering pad according to the ISO standard. In contrast to the proving ground procedure a constant speed test was defined for the simulation. The forward velocity was fixed at 12 m/sec, and the hand wheel angle was increased in steps of 23 deg and then held constant for four seconds, before it was increased again. Although this test involves short transients, it provides the same information as a constant radius test, as it is performed on the proving ground or simulated by the 'Steady State Cornering Model'. This constant speed procedure employed for the AUTOSIM simulation avoids having to define a controller tracking the course, which would have added an unnecessary complication.

The handling diagrams are compared in fig. 9.1.1-1. They show the understeer angle, representing the steering angle, which has to be added to the Ackermann angle to maintain a constant radius or lateral acceleration, plotted against the lateral acceleration. Proving ground results obtained for the standard tyres are indicated by squares, while those obtained with a set of worn Pirelli P6000 of the same size are denoted by diamonds.

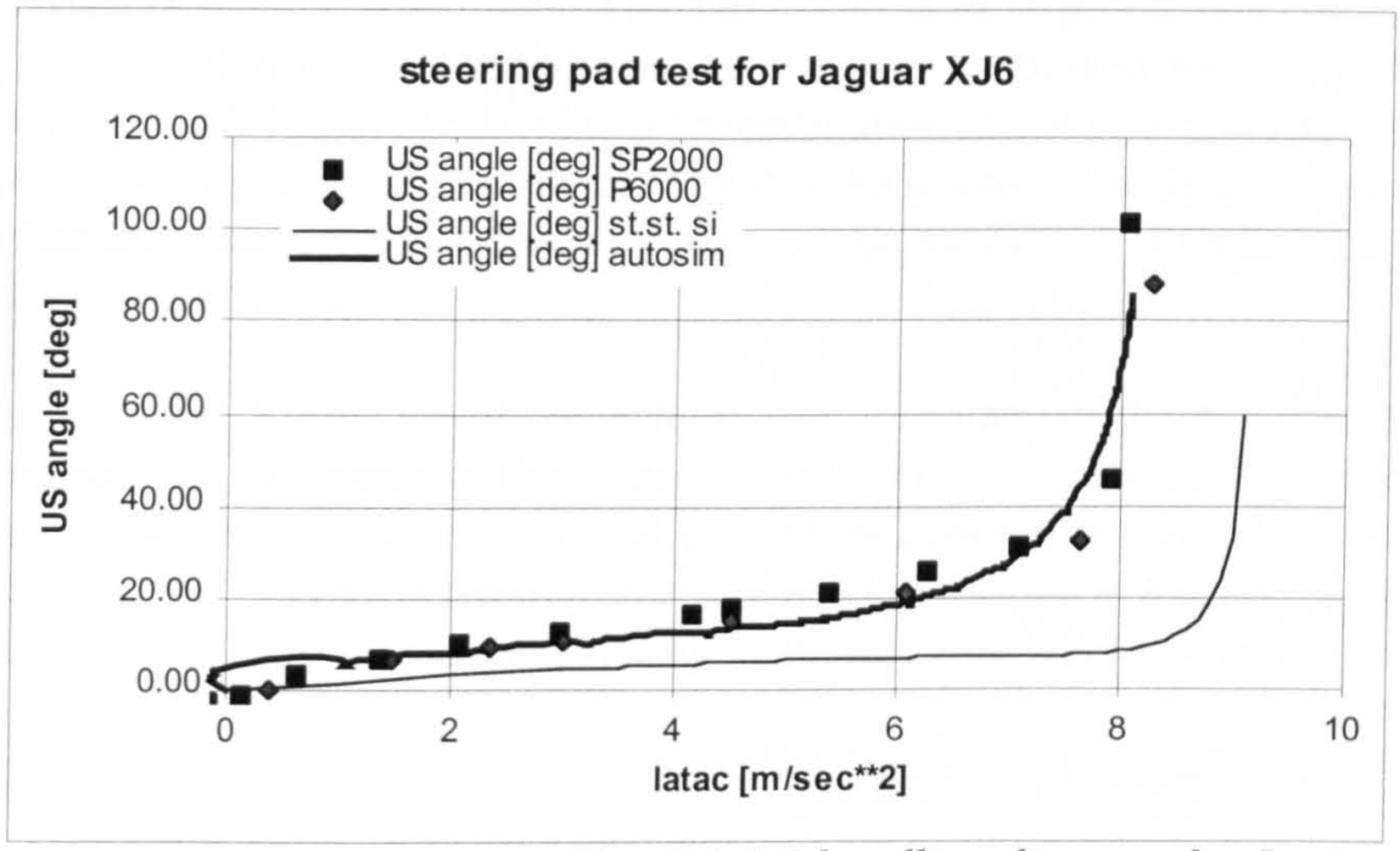

Fig. 9.1.1-1 handling diagram for Jaguar XJ6

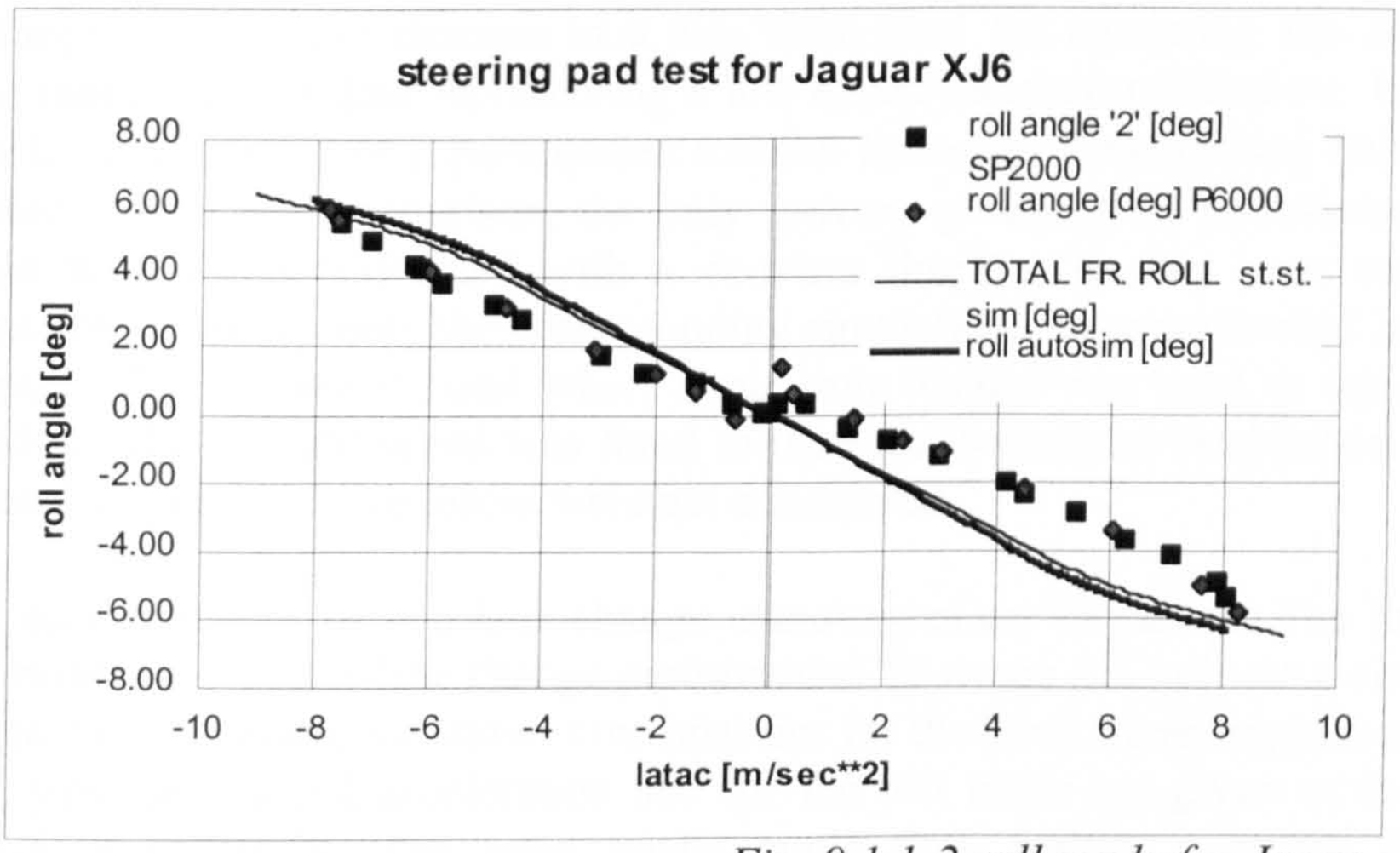

Fig. 9.1.1-2 roll angle for Jaguar XJ6

In addition to the AUTOSIM simulation results, those computed by the 'Steady State Cornering Model' are also included. The former are denoted by a thick line. The graphs indicate that an excellent agreement was achieved for the steering characteristics. The AUTOSIM model matches the linear behaviour (up to 6 m/sec^2) as well as the limit approach of the tested vehicle. Even the limit lateral acceleration of about 8 m/sec^2 was predicted accurately. This is a surprisingly good agreement, considering that the tyre data used in the model is based on test results obtained from

a force and moment measurement on a drum with a high friction 3M Safety Walk surface.

The agreement in the case of the 'Steady State Cornering Model' is clearly inferior. Neither the linear nor the limit behaviour is predicted as accurately as by the AUTOSIM model. The linear understeer is too low, whereas the maximum cornering performance prediction is too high. This behaviour is most probably a consequence of the lack of detail with regard to the steering system employed for the 'Steady State Cornering Model'. It includes neither a representation of the power assistance nor of a compliant steering rack. This explains why it gives a smaller understeer gradient. The reason for the discrepancy in the prediction of the maximum cornering performance was not established.

The graph in fig. 9.1.1-2 gives the vehicle roll, as established for a constant lateral acceleration. The roll angle of the Jaguar was derived from the measurements of the pitch and yaw rates according to (6.4.2c). Measurements and predicted behaviour agree far less for this characteristic. The predicted roll angle is too big, especially for the low severity tests. Experimental data obtained from Jaguar Cars confirmed the measured results.

9.1.2 Vehicle model validation for low speed lane change in a turn

Recordings of four lane changes in a turn were used for validating the AUTOSIM vehicle model against data representing a low speed transient manoeuvre. In order to eliminate the influence of superimposed traction forces on the cornering behaviour of the vehicle from the comparison, the only proving ground tests considered for this exercise were those performed with a constant throttle. As has been said in the introduction to this section, the corresponding simulations were performed in an open loop mode. The measured hand wheel angle time history was used as input for the simulation. The forward speed was fixed to the measured mean established from the test data. Longitudinal tyre forces were not considered.

In this section results of two lane change manoeuvres are discussed. The first set of results refers to a double lane change performed at 10 m/sec (36 kph) on a circle of 30 m radius. Simulated and measured time histories for the hand wheel angle, hand wheel torque, yaw rate, lateral acceleration and for the roll angle are given in the figures 9.1.2-1-5, respectively. The hand wheel angle time history indicates the three characteristic phases of this manoeuvre. After travelling on a constant radius the driver increases the steering angle to join a smaller radius of turn. In the second phase the steering is decreased while driving through the offset gate shown in figure 6.2-1. In the third section of the manoeuvre the steering angle is increased again to join the original circle.

As can be seen from fig. 9.1.2-2, there is hardly any resemblance between the measured and simulated hand wheel torque signals. Large, high frequency torque variations were recorded for the tests used in this validation exercise. The measured signal is indicated by a thin line. It compares to a simulated steering torque that is smooth and well matched to the low frequency hand wheel angle. This huge discrepancy is more probably due to a faulty torque sensor than to a misrepresentation of the steering system.

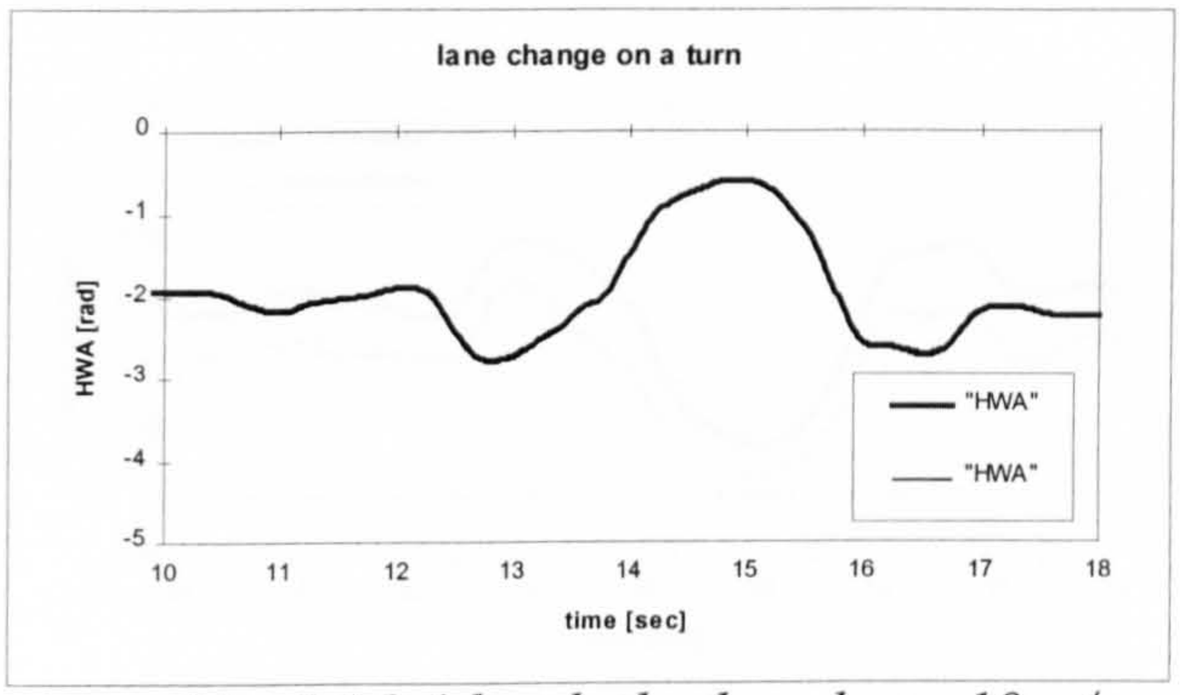

Fig. 9.1.2-1 hand wheel angle, v=10 m/sec

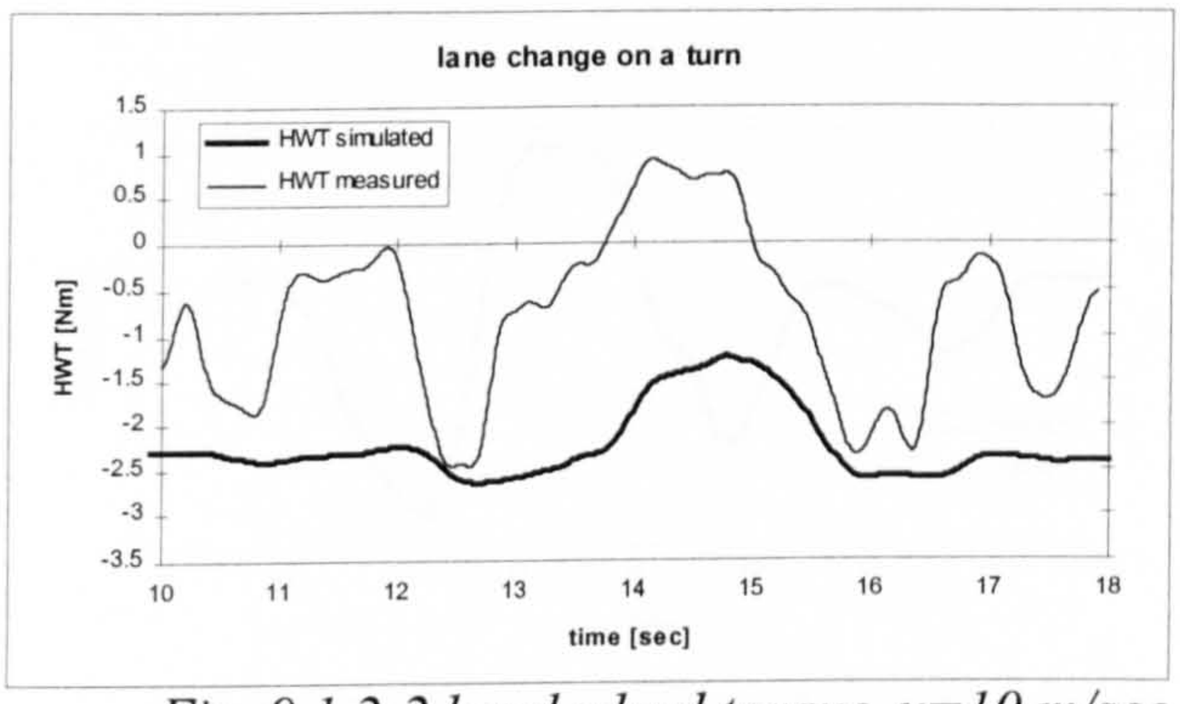

Fig. 9.1.2-2 hand wheel torque, v=10 m/sec

In contrast to the hand wheel torque behaviour an excellent agreement for the yaw rate and lateral acceleration response was achieved. From the initial and peak values of the lateral acceleration, it can be established that the vehicle operated in the linear part of its performance envelope throughout this test.

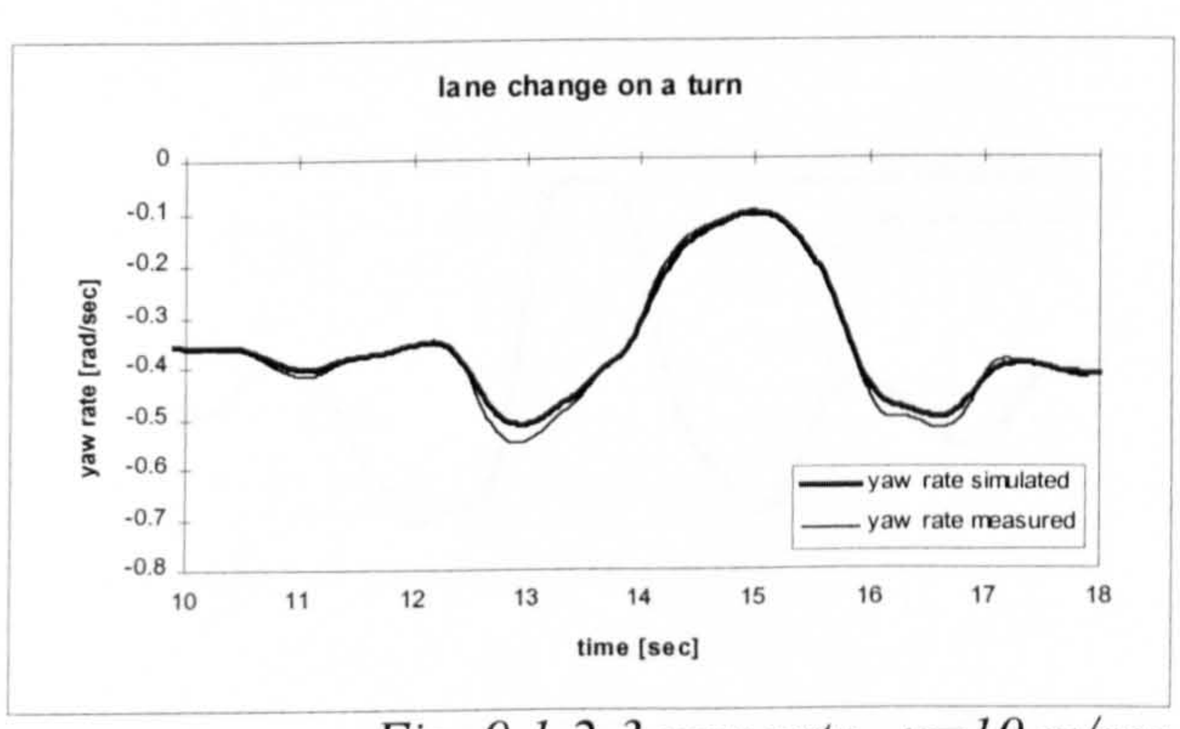

Fig. 9.1.2-3 yaw rate , v=10 m/sec

Roll angles are compared in fig. 9.1.2-5. As was established by the steady state cornering results, the model predicts a higher roll than actually measured. Apart from an offset equivalent to 1 deg a good agreement can be stated.

The following graphs refer to a limit manoeuvre. The average speed was 12.5 m/sec (45 kph). This time the hand wheel torque time histories are

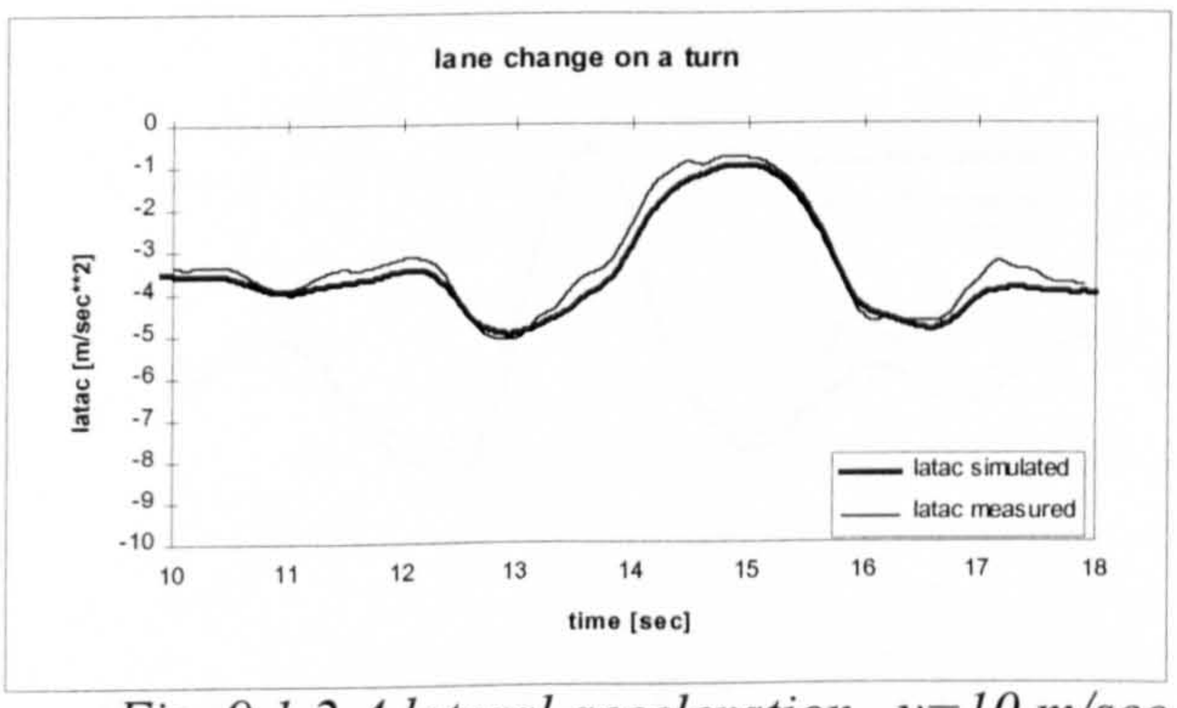

Fig. 9.1.2-4 lateral acceleration , v=10 m/sec

omitted. In Fig. 9.1.2-6 the hand wheel angle is given, while figures 9.1.2-7-9 allow comparisons of the yaw rate, lateral acceleration and roll angle. For this limit lane change, steering angle adjustments have to be exerted more quickly. Its time history assumes considerably higher amplitudes. Some of the symmetry is lost compared to fig. 9.1.2-1, and the third phase of the manoeuvre involves an additional reversal.

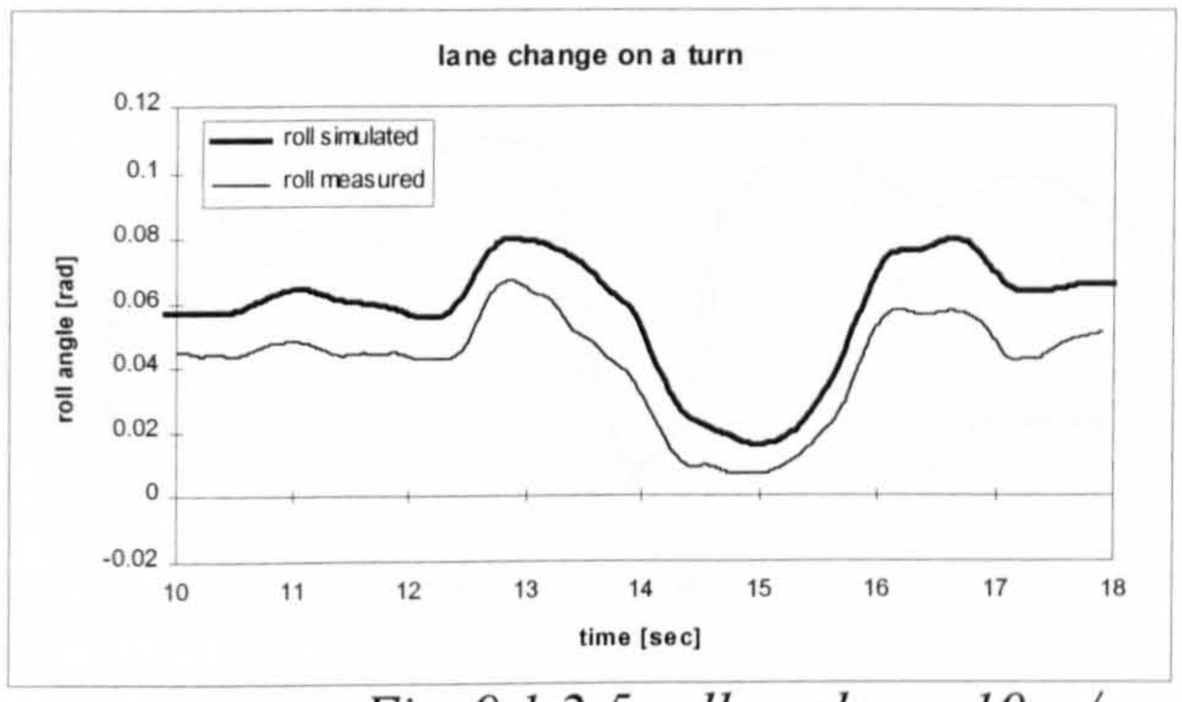

Fig. 9.1.2-5 roll angle, v=10 m/sec

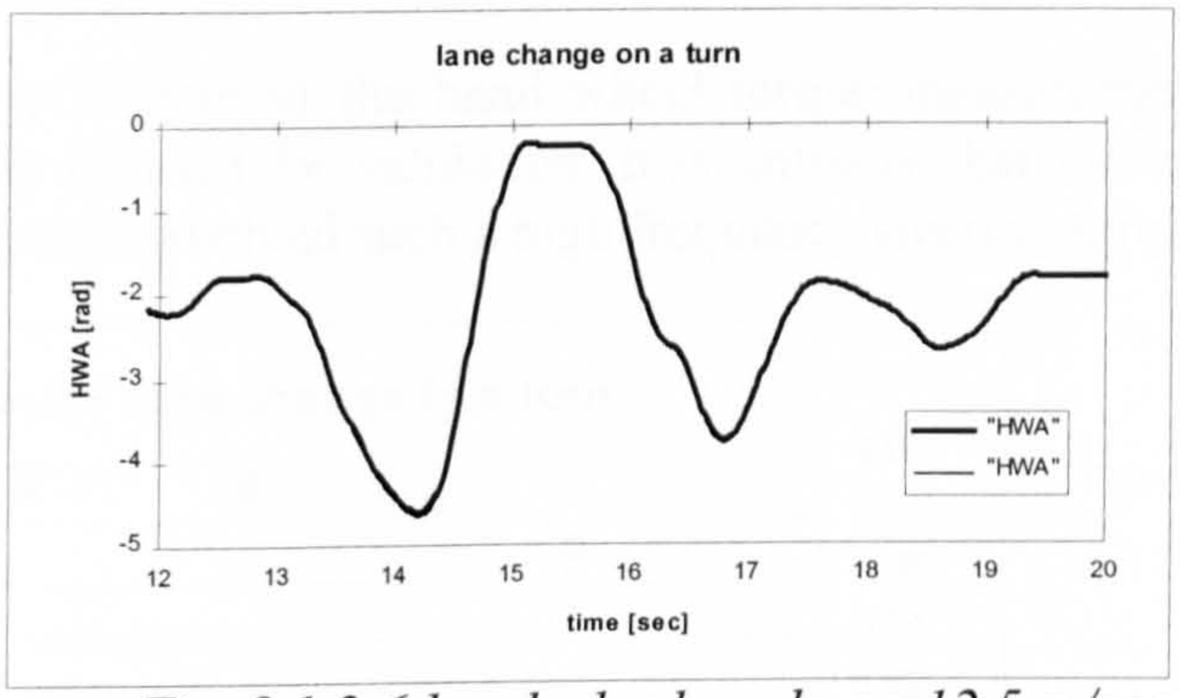

Fig. 9.1.2-6 hand wheel angle, v=12.5 m/sec

The yaw rate response is very well matched by the model, whereas some discrepancies for the lateral acceleration can be observed. The model vehicle seems to be better damped. The peaks for the simulated result are less pronounced, especially for the oscillations occurring after the reentry into the original lane. As can be seen from the peak values, the vehicle operates at times at its steady state cornering limit of 8 m/sec^2.

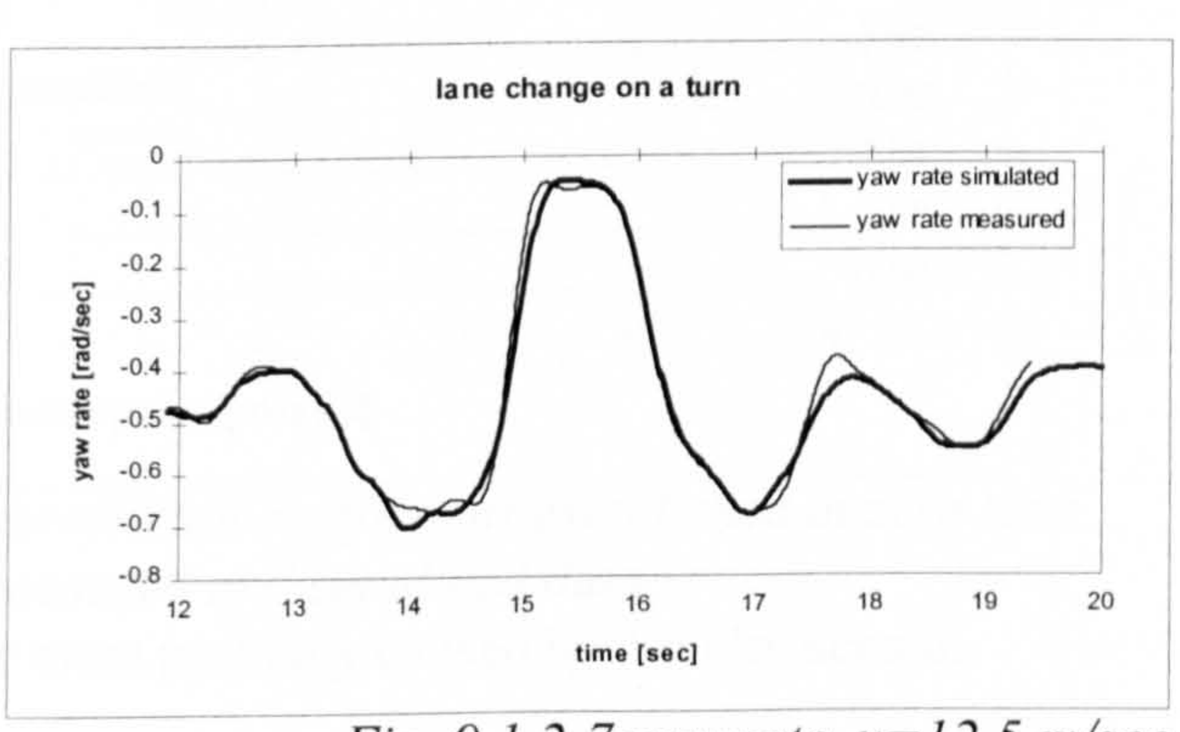

Fig. 9.1.2-7 yaw rate, v=12.5 m/sec

The roll angle time histories are offset from each other, as observed for the low severity lane change. Corresponding to the less oscillatory nature of the simulated lateral acceleration, the roll motion is better damped as well.

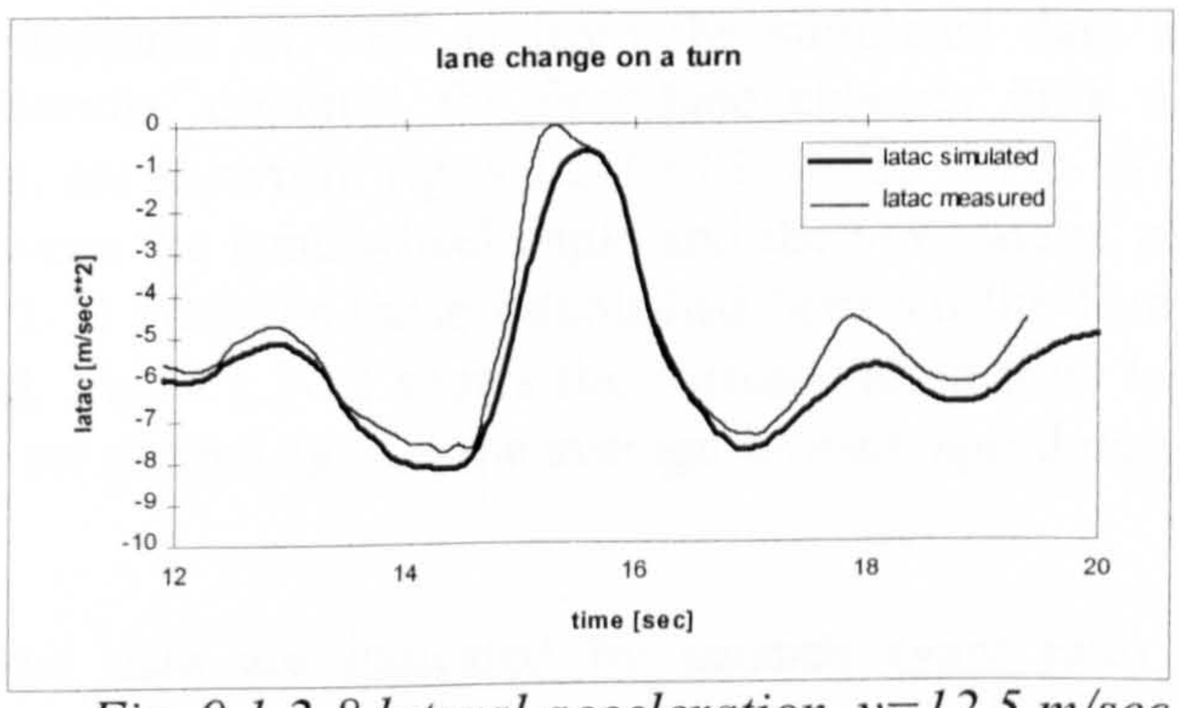

Fig. 9.1.2-8 lateral acceleration, v=12.5 m/sec

Summarising this validation exercise, it can be said that the level of agreement is encouraging for the major vehicle

response characteristics. An excellent match was obtained for the yaw rate and a satisfactory agreement was established for the lateral acceleration, even for the limit case. The vehicle model seems to describe the roll behaviour rather well, apart from an offset, which was already established for the steady state cornering results.

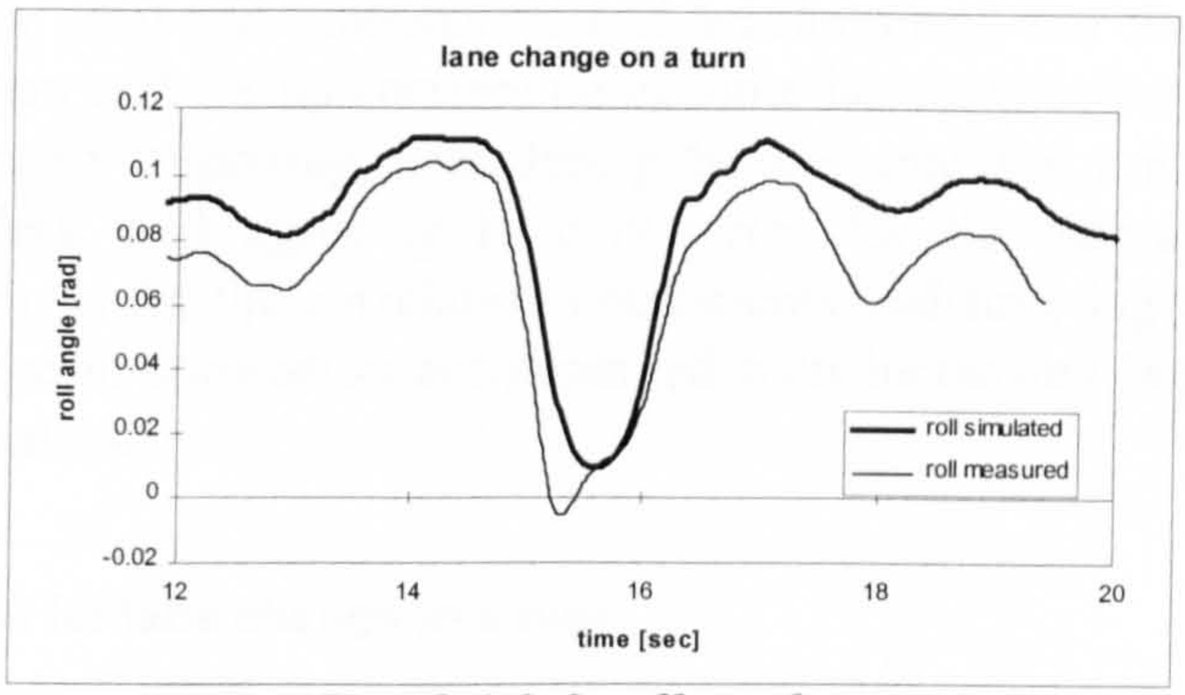

Fig. 9.1.2-9 roll angle, v=12.5 m/sec

Unfortunately, the high frequency content of the hand wheel torque measurements meant that they could not reliably be used for validation. It is unlikely that the low frequency manoeuvre of a lane change involved such a high frequency steering torque.

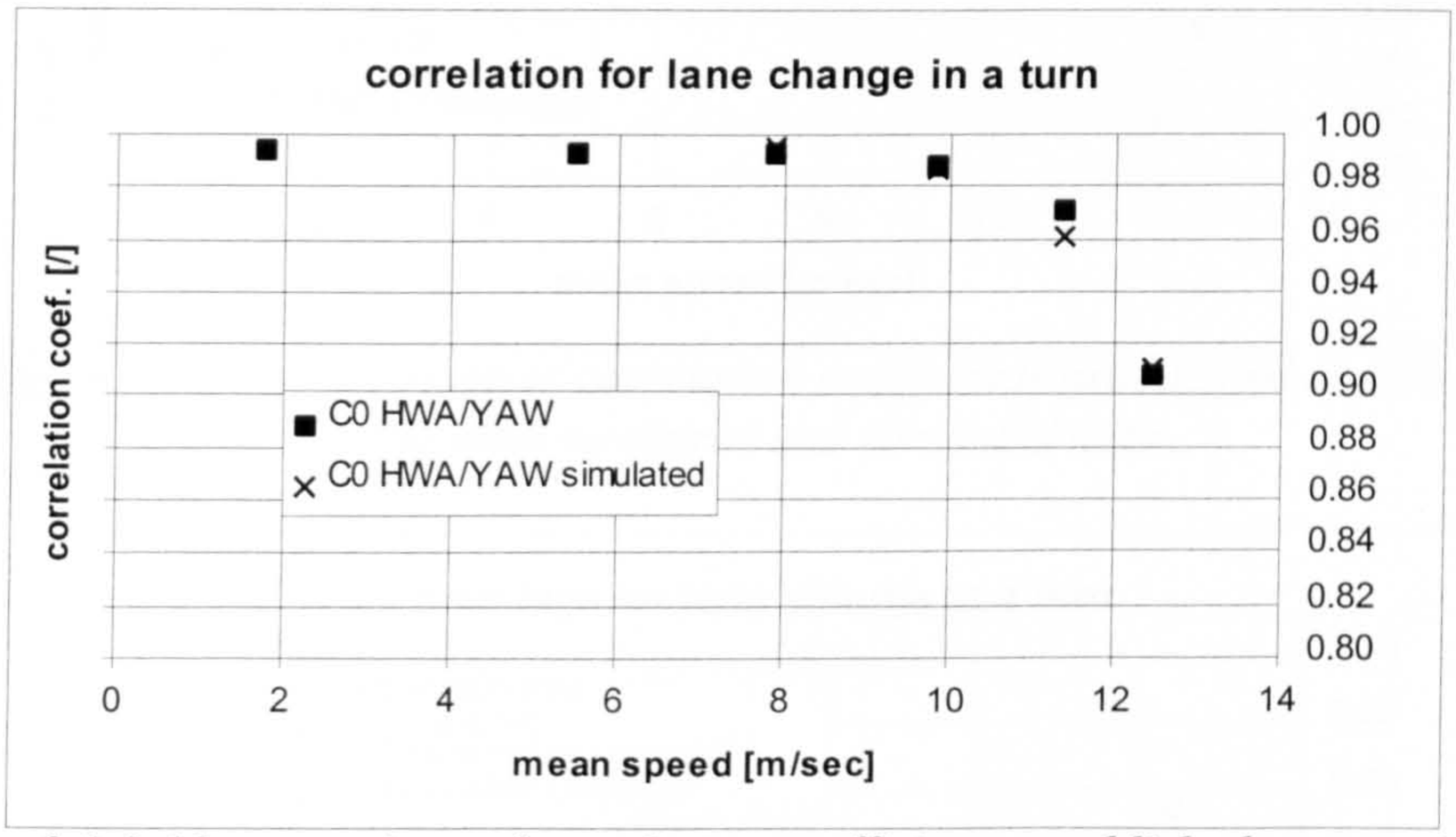

Fig. 9.1.2-10 comparison of correlation coefficients established at zero time lag from measured and simulated data

The high frequency contents were most probably caused by a faulty sensor.

In addition to the comparison of time histories, cross-correlation coefficients and time lags were computed from the measured as well as from the simulated data and compared against each other. Results, obtained for four lane changes in a turn performed with increasing speeds, are shown in fig. 9.1.2-10-12. In fig. 9.1.2-10 the cross-correlation coefficients between the hand wheel angle and the yaw rate at zero time lag is given, while fig. 9.1.2-11 contains those established between the former and the lateral acceleration signal. Fig. 9.1.2-12 shows the corresponding time lags. As in chapter 7, these parameters are plotted against the average forward speed during the manoeuvre.

Results computed from measured data are indicated by squares (yaw rate) or diamonds (lateral acceleration), whereas those calculated from the simulated time

histories are given by crosses (yaw rate) and asterisks (lateral acceleration). For the yaw rate cross-correlation coefficient and for its corresponding time lag an excellent agreement can be stated. This is hardly surprising, considering the well matched time histories presented above. The less well agreeing time histories for the lateral acceleration result in small differences for the correlation coefficients and time lags. However, the characteristic decrease in correlation accompanied with increasing lag times is replicated by the simulated data.

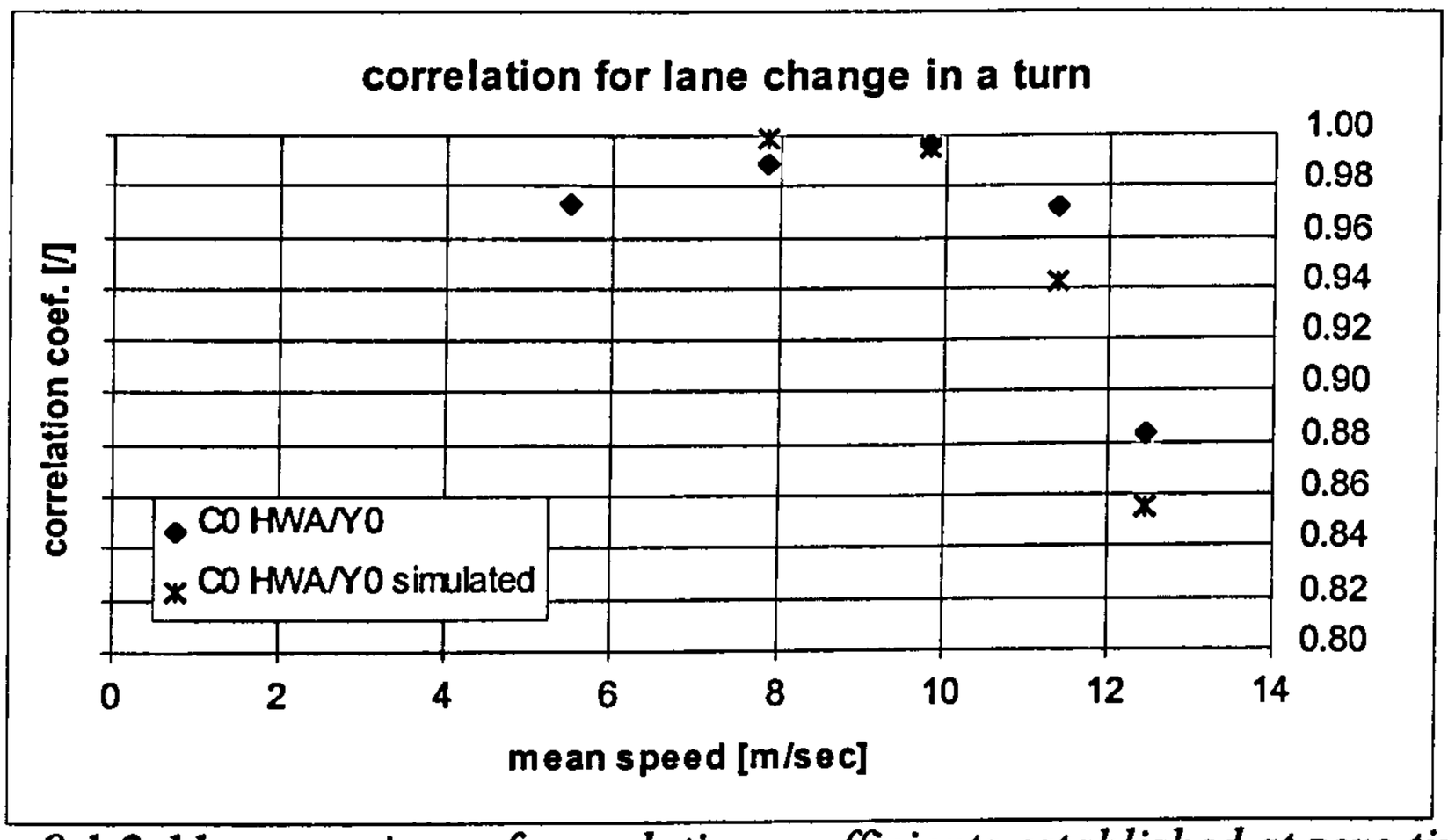

Fig. 9.1.2-11 comparison of correlation coefficients established at zero time lag from measured and simulated data

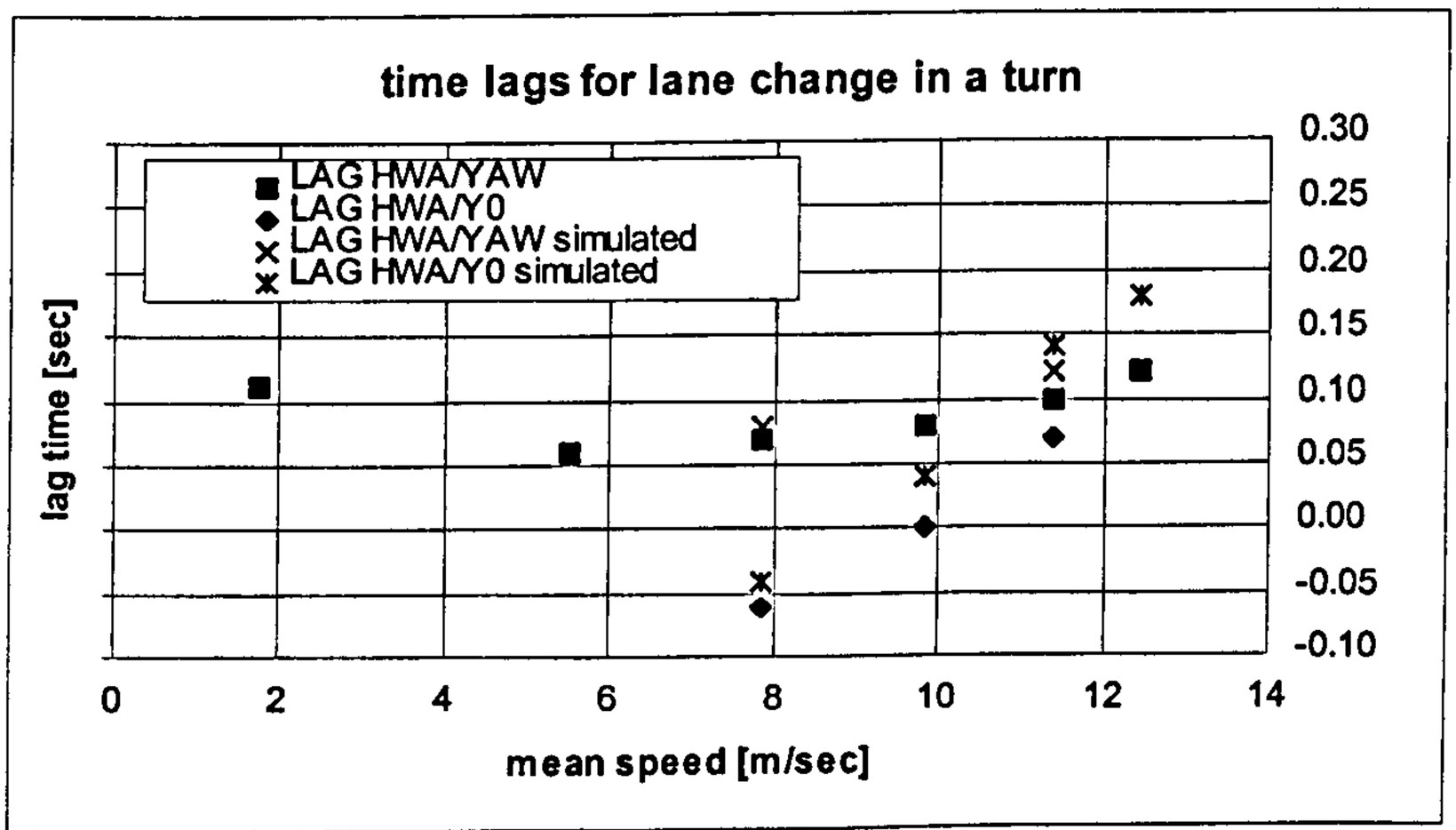

Fig. 9.1.2-12 comparison of time lags established from measured and simulated data

9.1.3 Vehicle model validation for high speed ISO lane change

In addition to validating the model against recordings taken from low speed lane change in a turn tests, simulations were carried out representing high speed double lane changes. High forward speeds result in less damped lateral vehicle responses to

the steering wheel input. Records of four ISO lane changes were used for validating the AUTOSIM vehicle model for high speed conditions. As was the case for the low speed lane changes in a turn, only constant throttle tests were considered. The simulations were carried out in the open loop mode by taking the measured hand wheel angle time history as input. The forward speed was defined as the measured mean established from the test data. Longitudinal tyre forces were not considered. Time histories representing lane changes of low and high severity are shown. Further-more, some graphs indicating the influence of additional throttle control on the quality of agreement between measured and simulated response are included. The graphs shown in figures 9.1.3-1-5 refer to a low severity lane change performed at 21m/sec (76 kph). They allow comparison of the hand wheel angle, steering torque, yaw rate, lateral acceleration and roll angle, respectively. Simulation results are drawn in thick lines. For the hand wheel torque, the least agreement was established, as was the case for the low speed lane change in a turn. The validity of the measured result is doubtful, since the record contains unreasonable torque variations of a similar magnitude as measured for the lane change in a turn test (fig. 9.1.2-2).

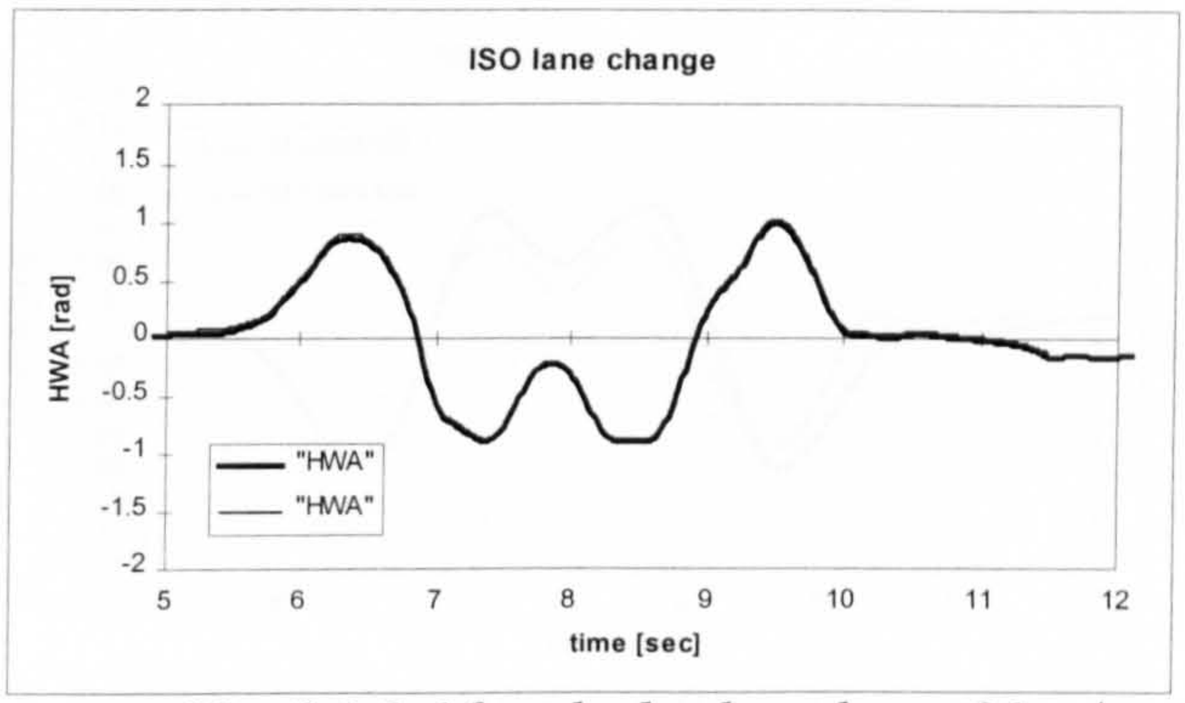

Fig. 9.1.3-1 hand wheel angle, v=21 m/sec

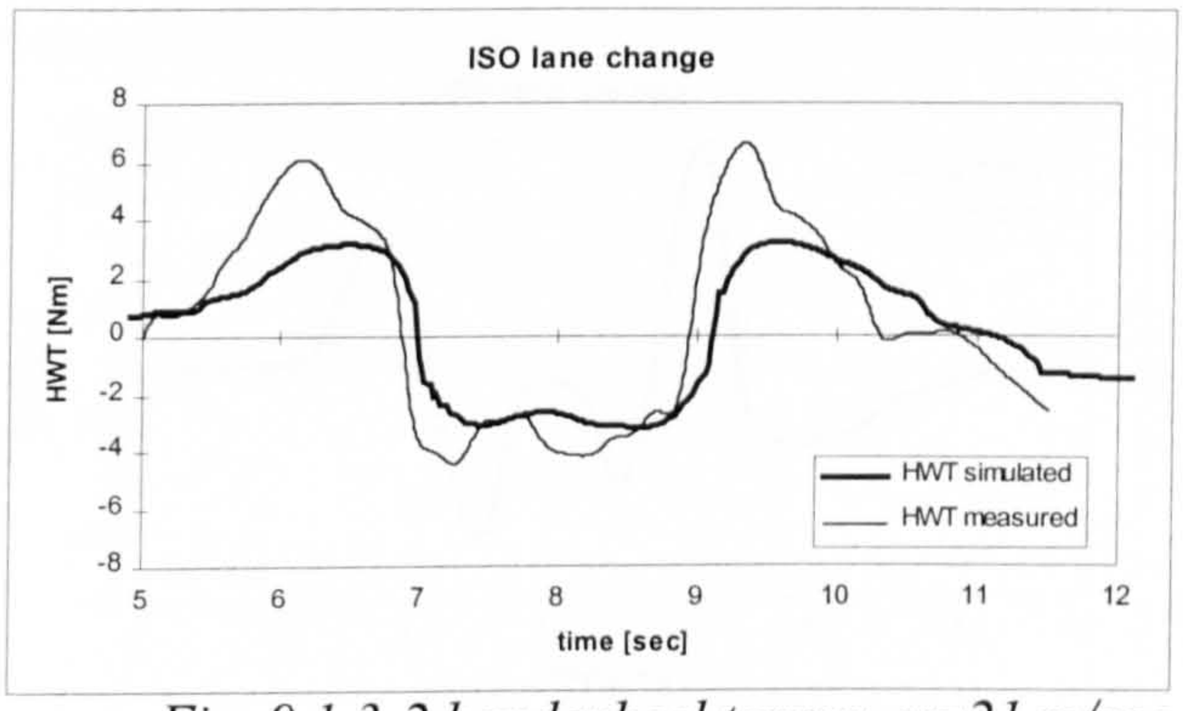

Fig. 9.1.3-2 hand wheel torque, v=21 m/sec

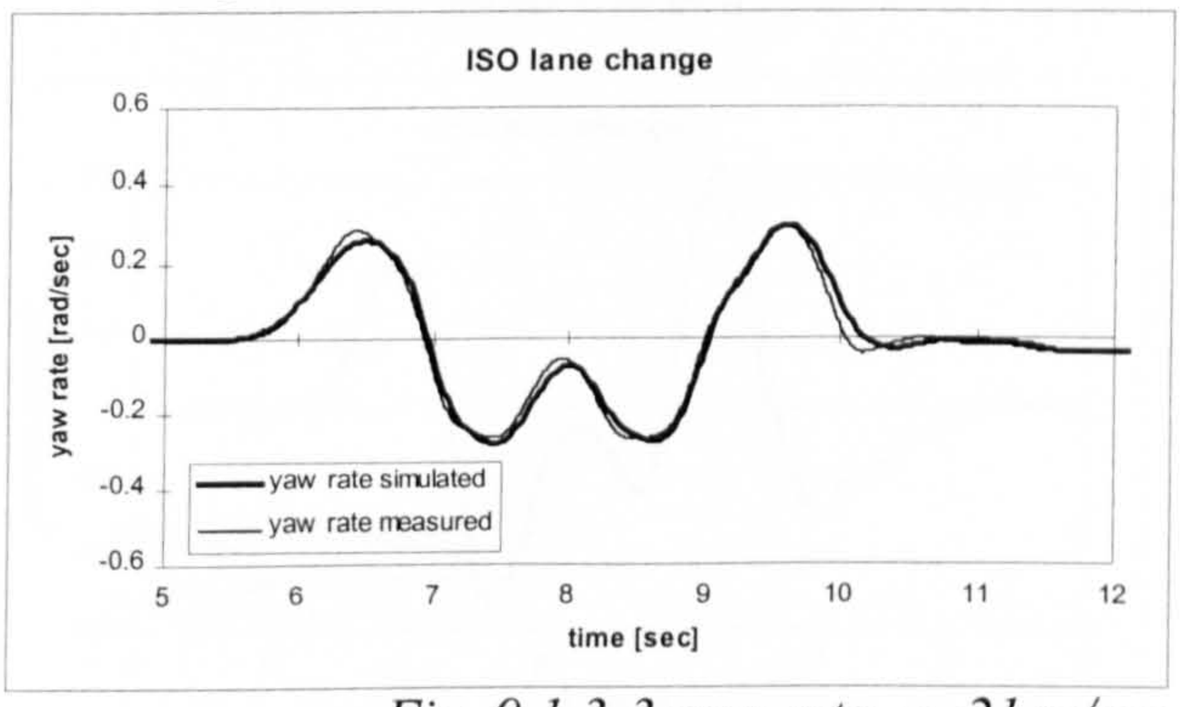

Fig. 9.1.3-3 yaw rate, v=21 m/sec

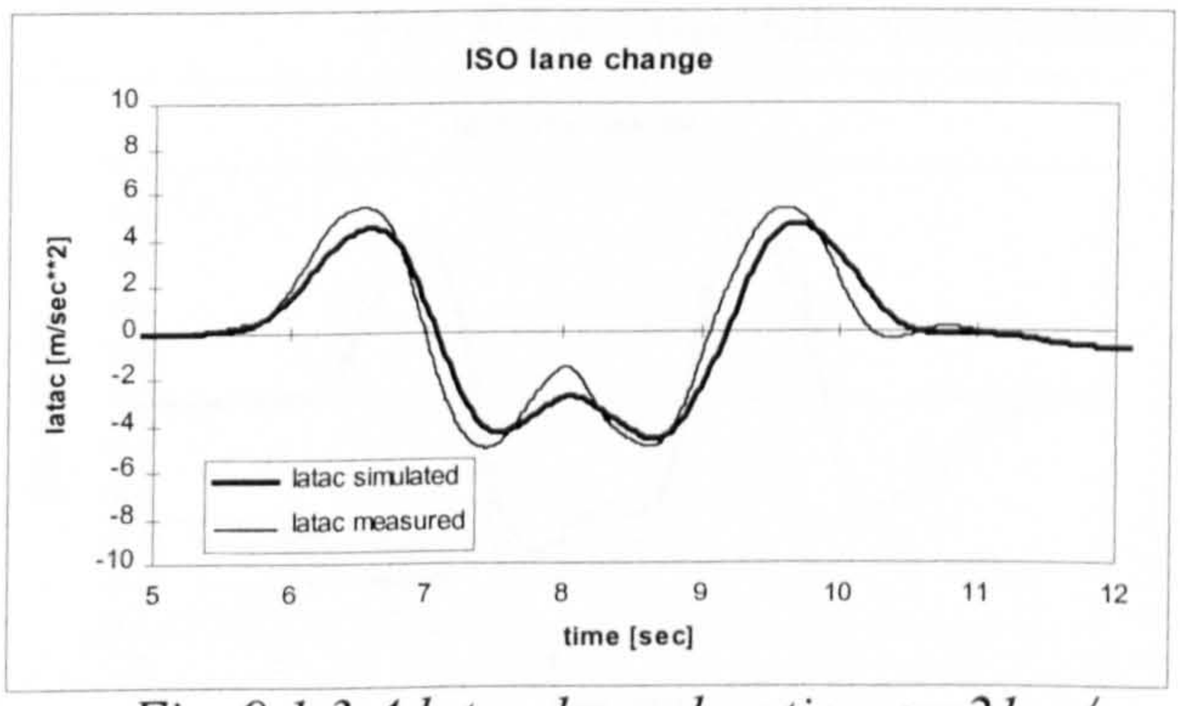

Fig. 9.1.3-4 lateral acceleration, v=21 m/sec

The simulation result for the yaw rate is almost identical to the measured signal, while the simulated lateral acceleration is less well matched. The predicted lateral acceleration response is more damped, as can be seen from the slightly lower peak values.

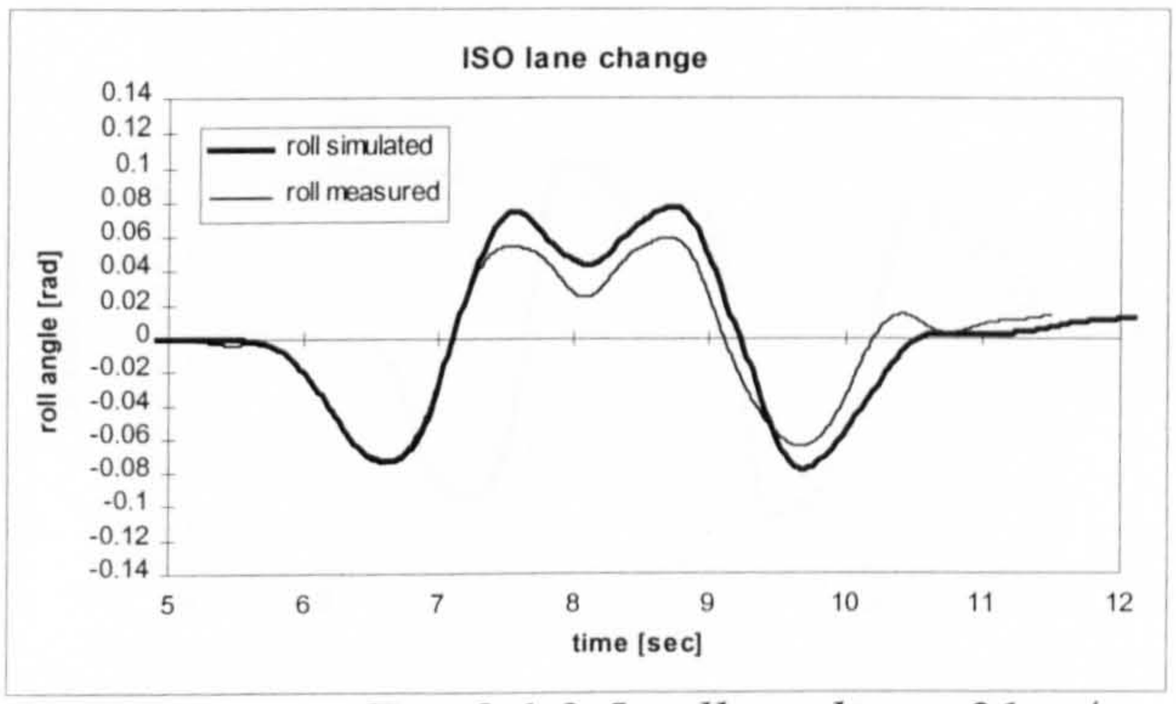

Fig. 9.1.3-5 roll angle, v=21 m/sec

The roll angle signals are perfectly matched for the first phase of the manoeuvre, but differ in the magnitude of the following peaks. The simulated results assume peak values considerably higher than measured.

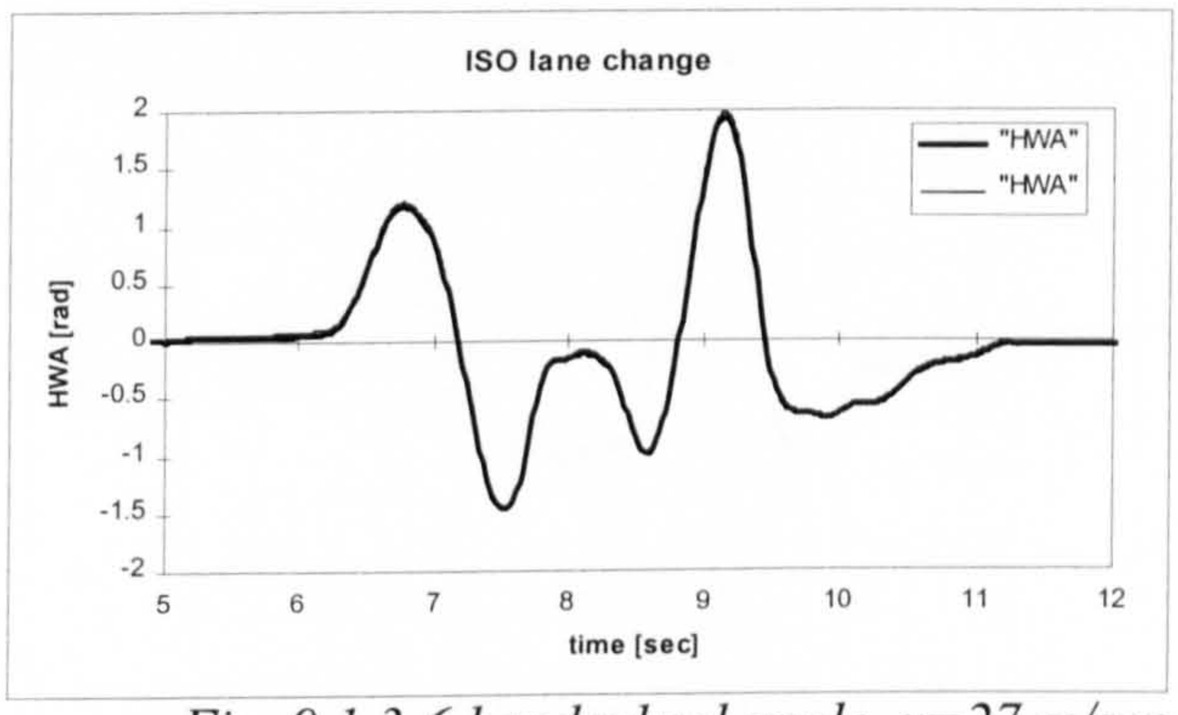

Fig. 9.1.3-6 hand wheel angle, v=27 m/sec

The following graphs shown in the figures 9.1.3-6-9 refer to a severe double lane change performed at 27 m/sec. The predicted yaw rate remains very well matched to its measured counterpart, as indicated by fig. 9.1.3-7. The peak values for the lateral acceleration are well approximated, as can be seen from fig. 9.1.3-8. However, the simulated lateral acceleration response remains better correlated to the hand wheel angle input than is the case for the measured response. The simulation result bears more resemblance to the w-shaped hand wheel angle established during the time interval of 7.5 and 9 seconds than the corresponding measurement, which features a distinct trough.

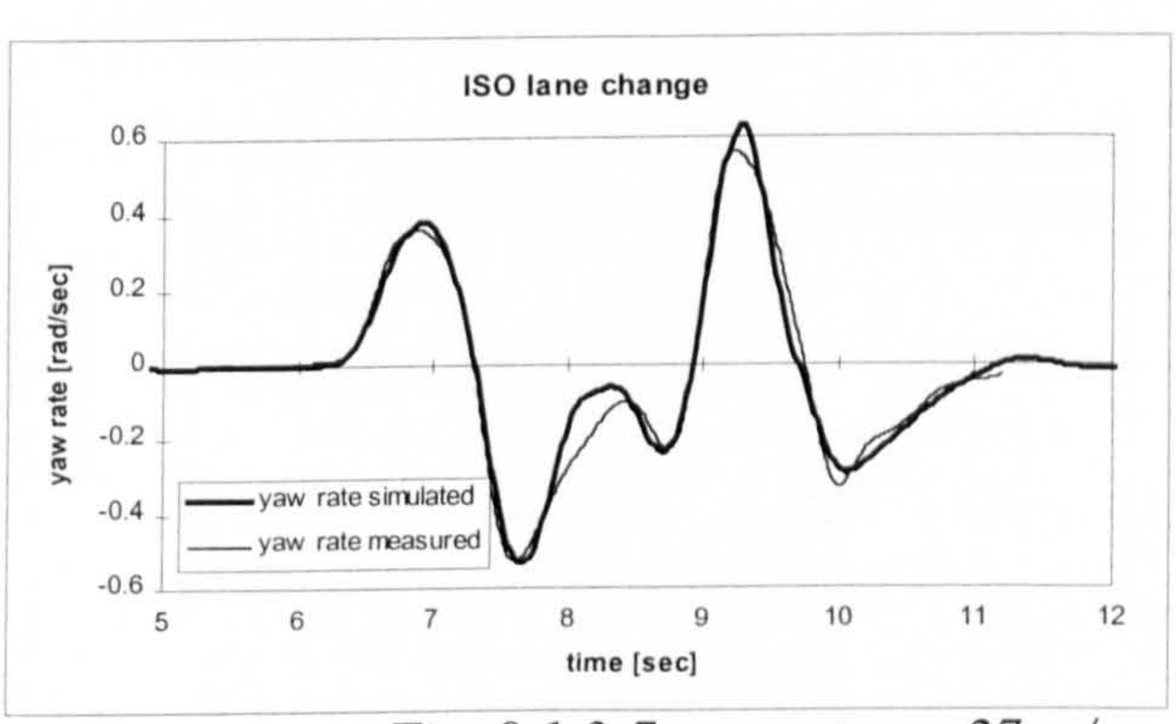

Fig. 9.1.3-7 yaw rate, v=27 m/sec

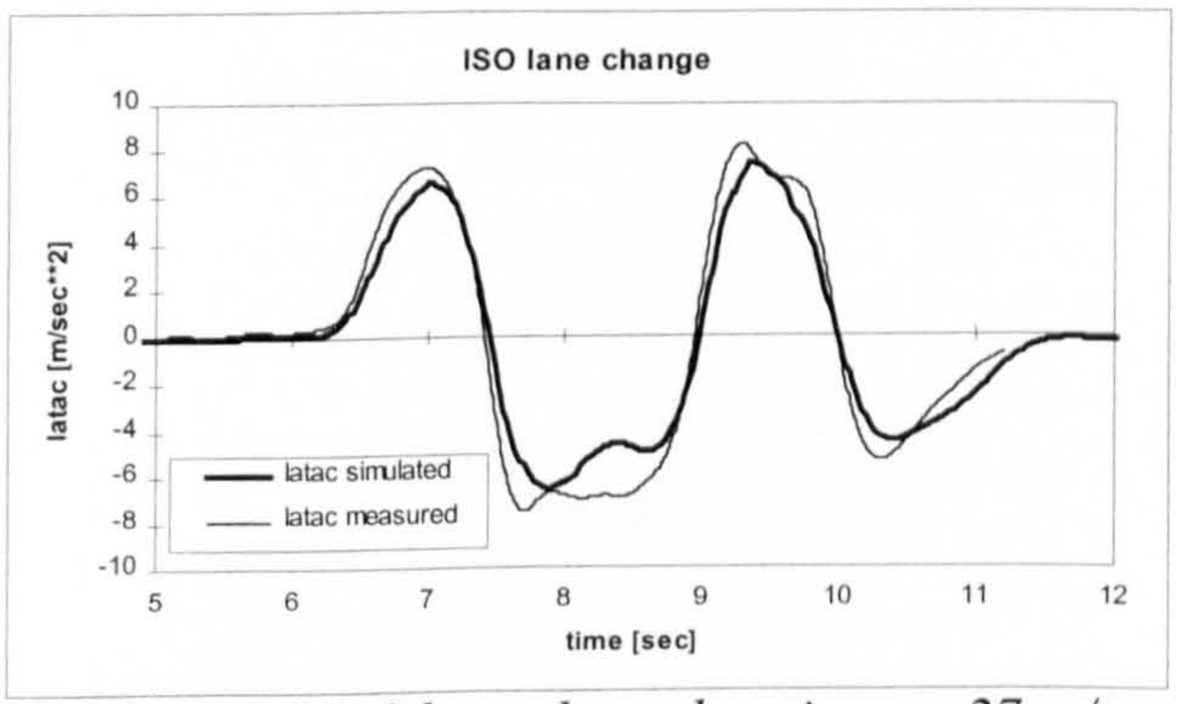

Fig. 9.1.3-8 lateral acceleration, v=27 m/sec

A similar level of agreement is

obtained for the roll angle, as given in fig. 9.1.3-9. The peak roll angles are closely matched, while the discrepancies between the measured and the predicted time history replicate those observed for the lateral acceleration.

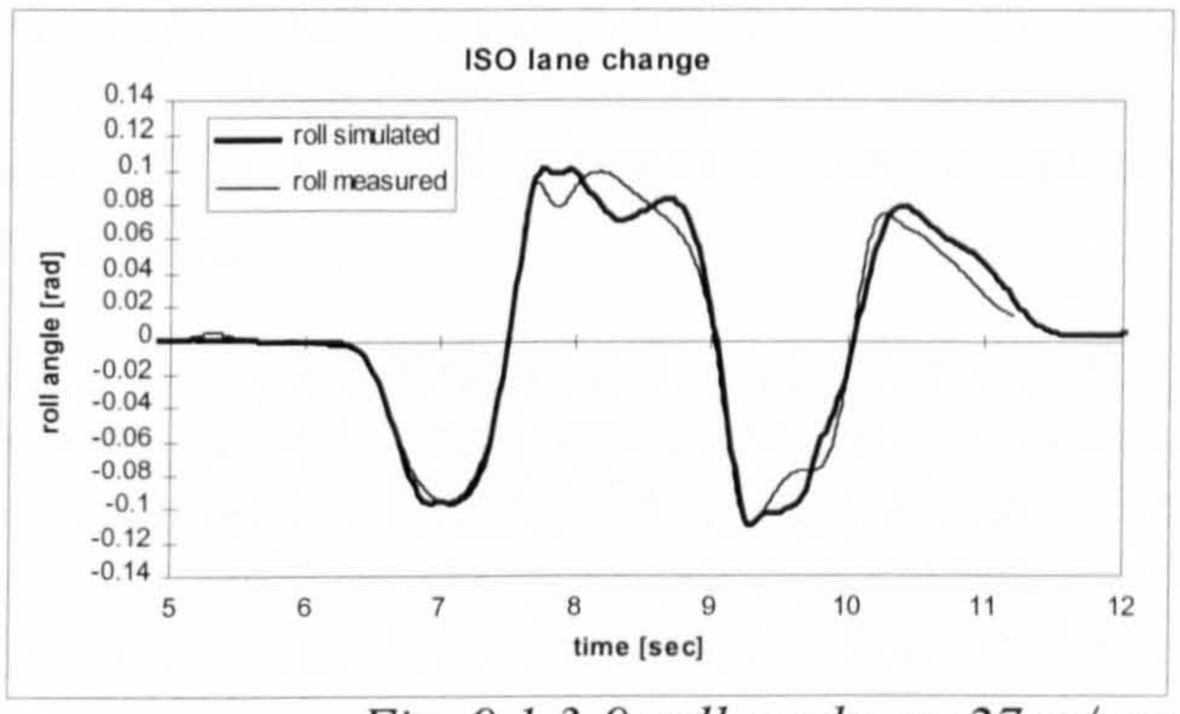

Fig. 9.1.3-9 roll angle, v=27 m/sec

Considering that these time histories represent a limit manoeuvre, a reasonably good agreement can be stated overall. The discrepancies observed for the lateral acceleration response may be related to the rear end cornering stiffness. The cornering stiffness used for the simulation might be too big, which would explain the more damped response behaviour established in fig. 9.1.3-4.

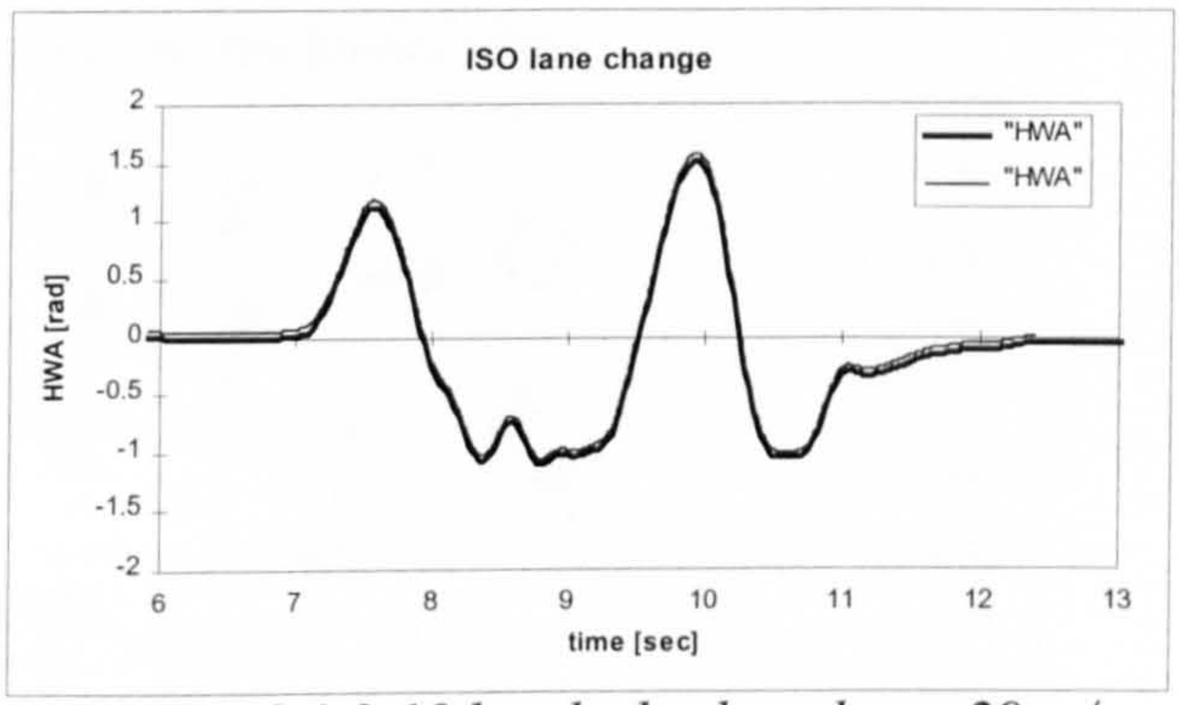

Fig. 9.1.3-10 hand wheel angle, v=29 m/sec

Three further graphs are included representing a manoeuvre performed at 29 m/sec. The driver was free to use the throttle as a second control in this test. The graphs illustrate the effects of redis-tributing the longitudinal and lateral forces by the use of the throttle. The corresponding simulation results, however, were computed for the meas-ured, slightly variable, speed profile. The interaction of the guidance forces was not considered. As can be seen in fig. 9.1.3-10, the driver no longer adopts a w-shaped steering input at the maximum speed. The time history of the hand wheel angle resembles that of the lateral acceleration

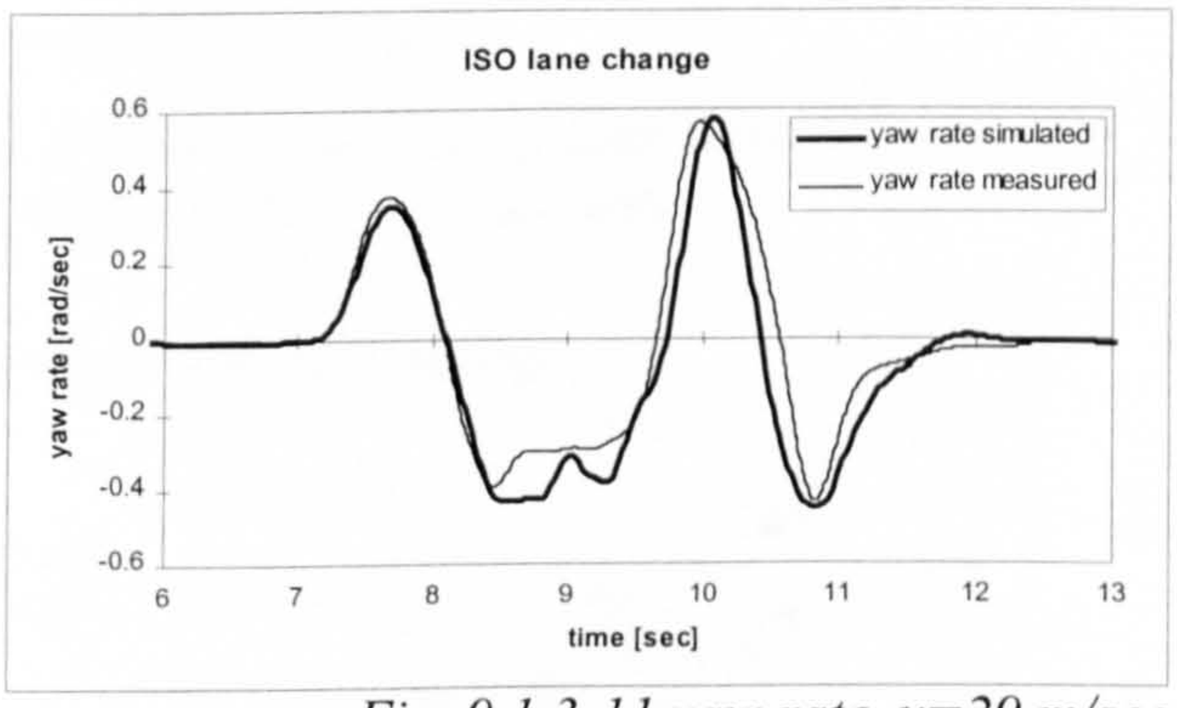

Fig. 9.1.3-11 yaw rate, v=29 m/sec

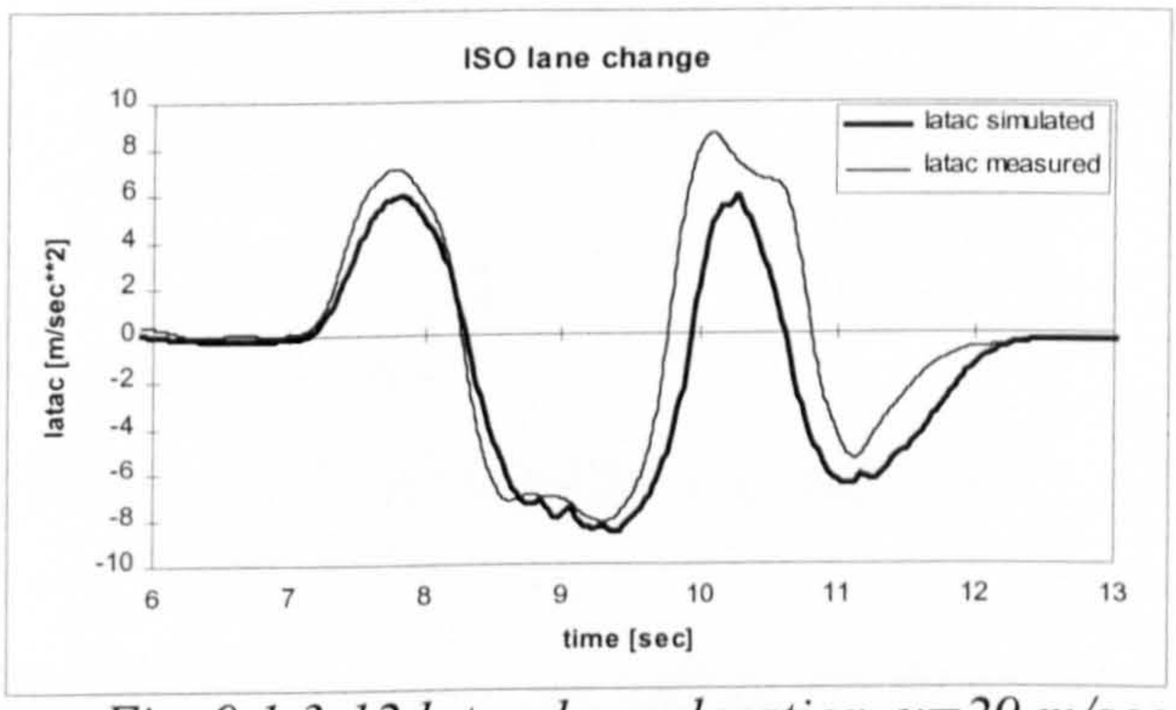

Fig. 9.1.3-12 lateral acceleration, v=29 m/sec

shown in fig. 9.1.3-8. The driver might have noticed that the vehicle no longer responds to the high frequency contents of the w-shaped steering input, and decided to corner through the offset lane rather than trying to establish a straight and level vehicle attitude in the middle of this section.

The graphs showing the yaw rate (fig. 9.1.3-11) and the lateral acceleration (fig. 9.1.3-12) illustrate that the mismatch between simulation and measurement increases considerably if the effects of the superimposed longitudinal traction forces are not represented in the simulation. The discrepancies are especially pronounced for the later stages of the manoeuvre and more so for the lateral acceleration than for the yaw rate.

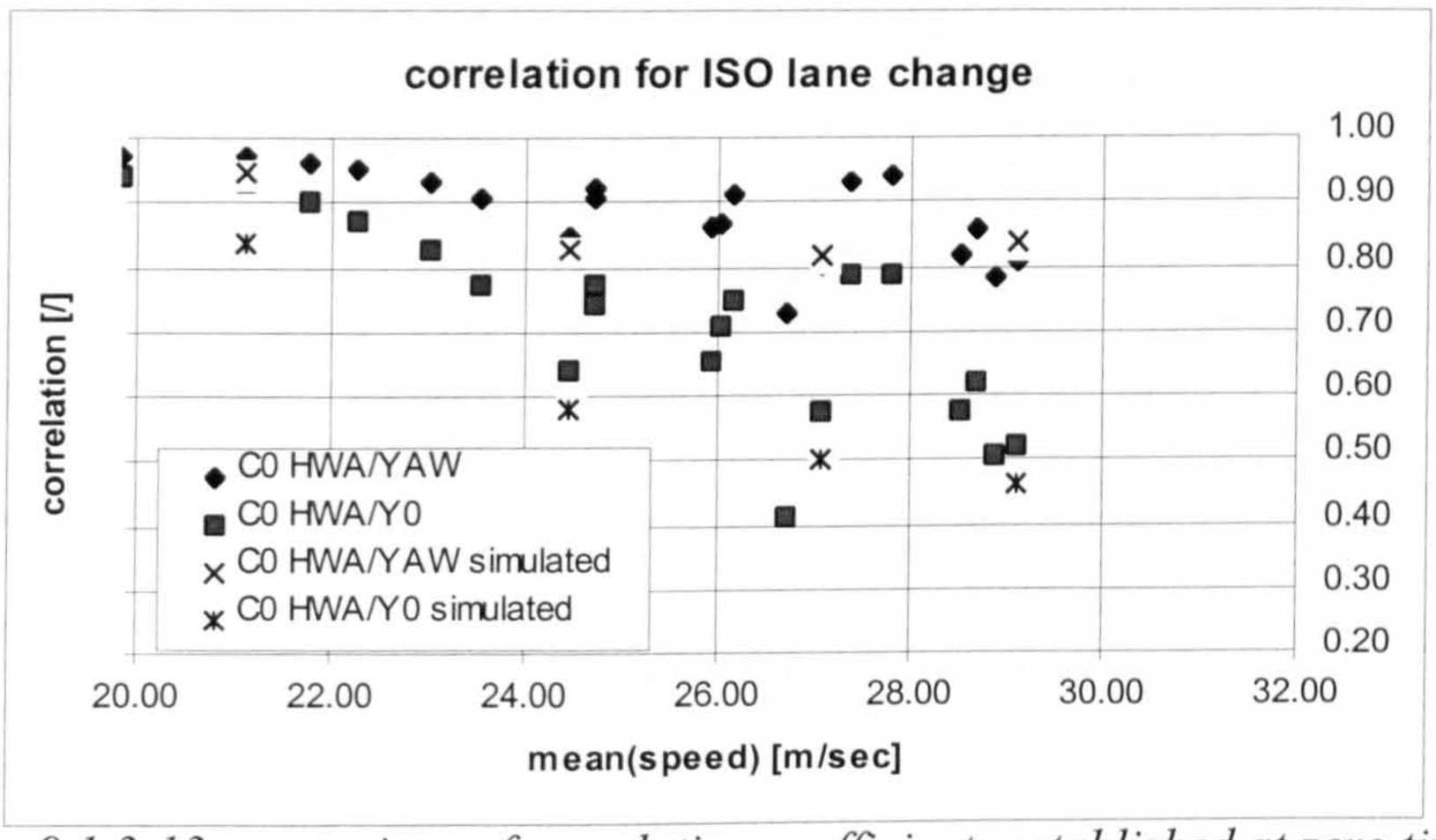

Fig. 9.1.3-13 comparison of correlation coefficients established at zero time lag from measured and simulated data

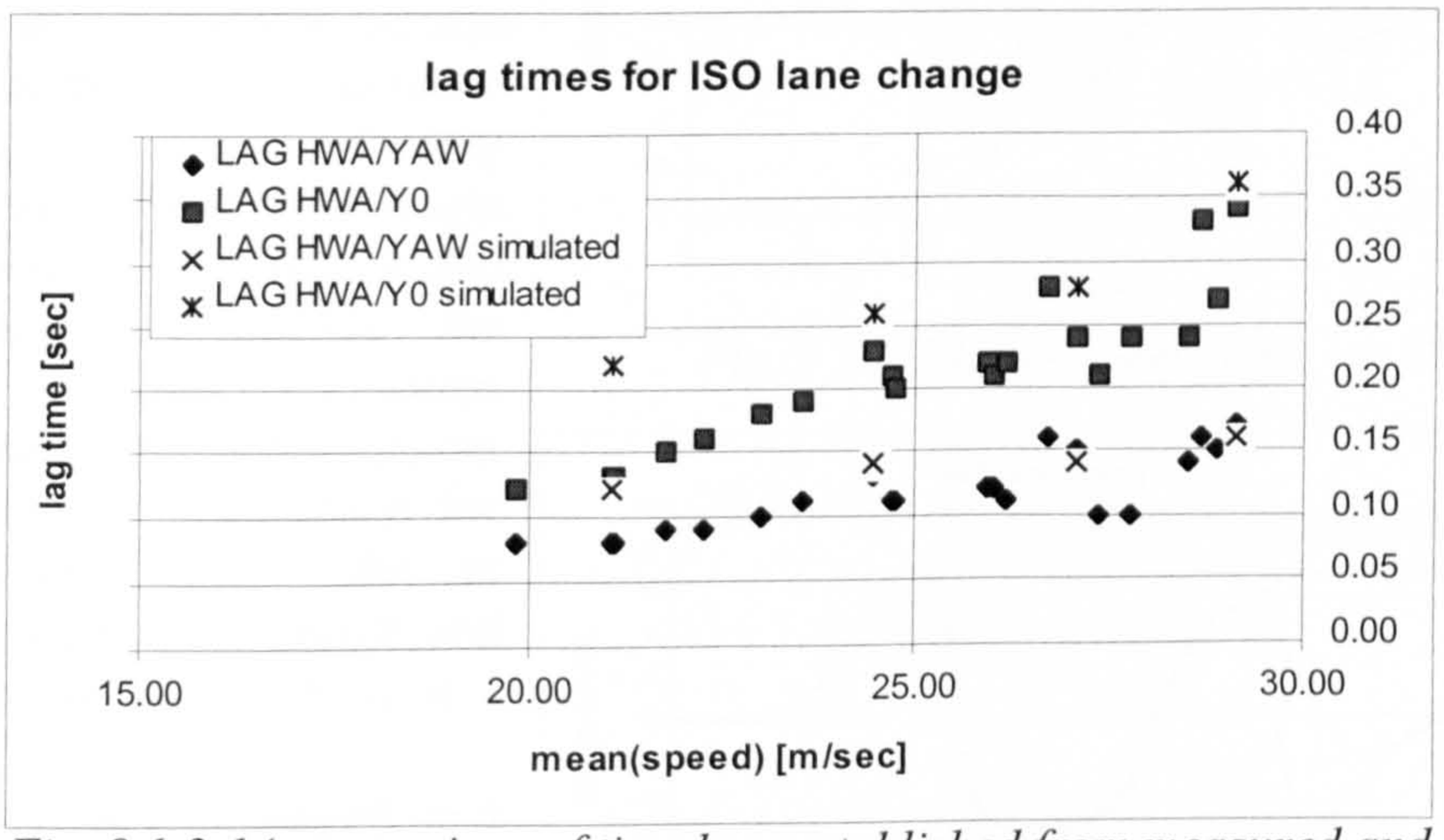

Fig. 9.1.3-14 comparison of time lags established from measured and simulated data

Finally, two graphs are given indicating the quality of agreement for the correlation coefficients and time lags. Applying the technique presented in chapter 7.1 to the

measured and to the simulated records, cross-correlation coefficients for the yaw rate and lateral acceleration were obtained with respect to the hand wheel angle input. Their values established at zero lag time are given in fig. 9.1.3-13. The corresponding time lags are presented in fig. 9.1.3-14. The same notation applies as introduced in section 7.2.1. A reasonable agreement is established for these properties. The trend of decreasing correlation coefficients and increasing lag times, as established from the measured data, is matched by the results obtained from the simulated data.

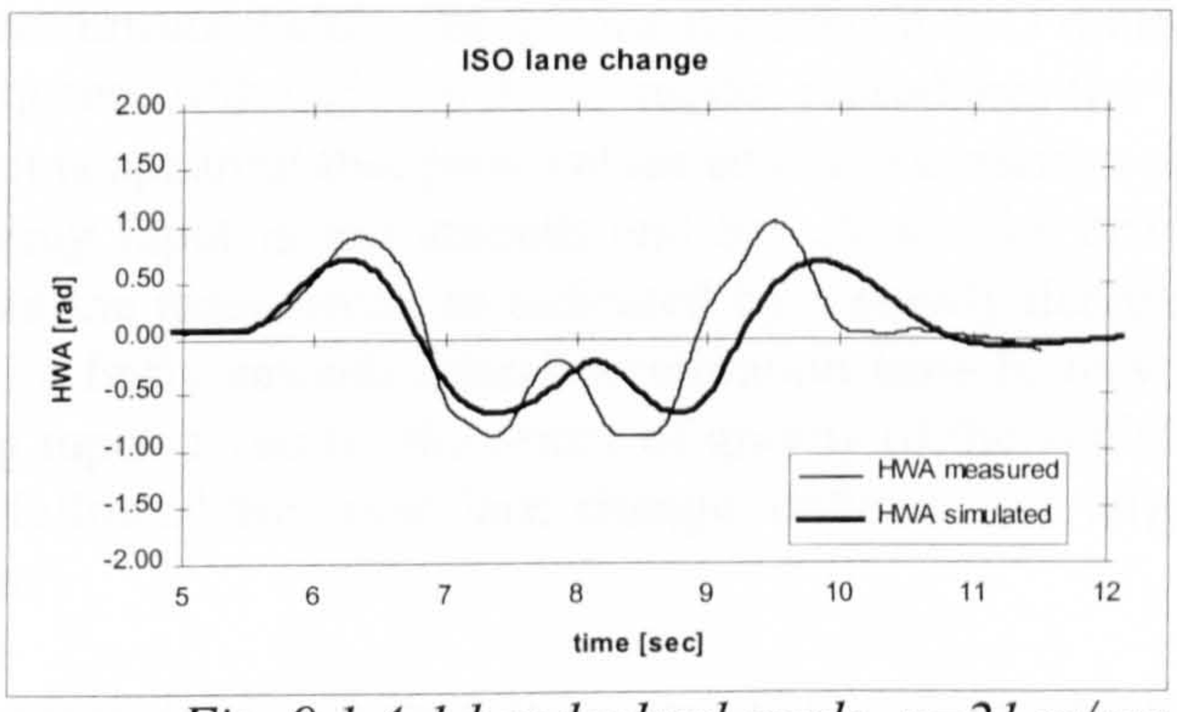

Fig. 9.1.4-1 hand wheel angle, v=21 m/sec

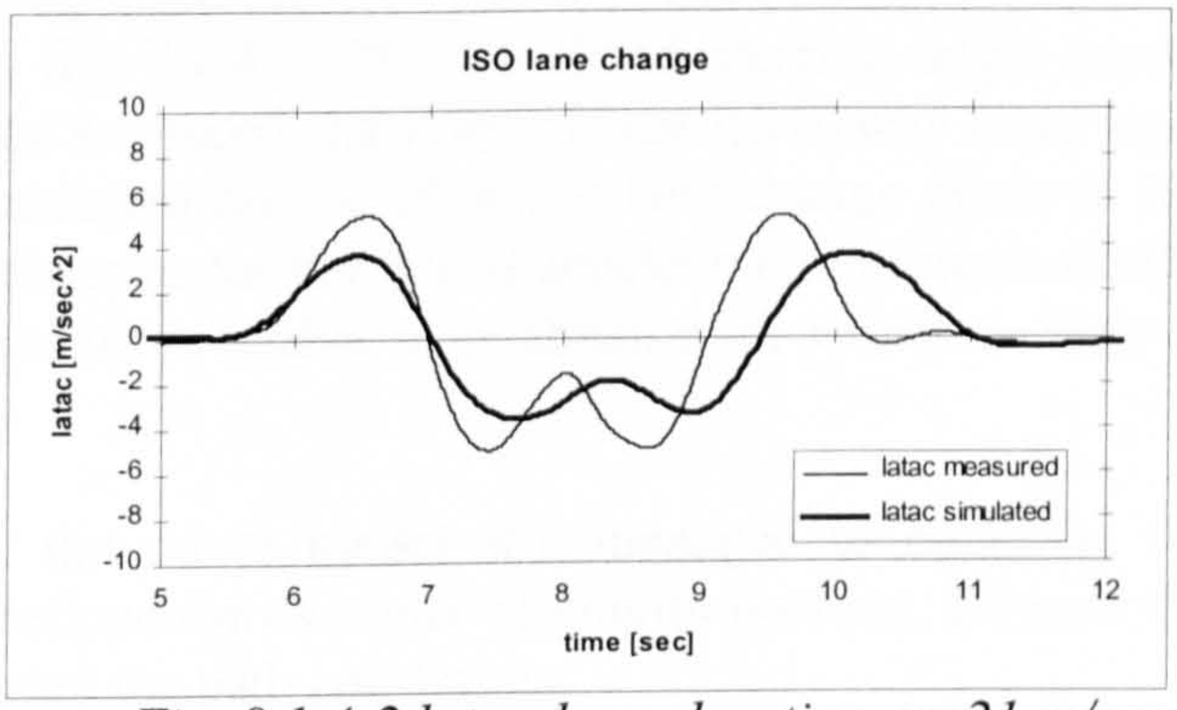

Fig. 9.1.4-2 lateral acceleration, v=21 m/sec

9.1.4 Validation of driver model

Some attempts were made to validate the AUTOSIM vehicle model for the closed loop mode of operation. Instead of using the measured hand wheel angle time histories, a driver model was used to simulate the steering wheel actuation according to the course layout ahead. Details concerning the driver model are found in chapter 3.2.3. The vehicle and tyre data remained unchanged.

Comparing the measured and simulated time histories of the steering wheel angle and the lateral acceleration, as shown in fig. 9.1.4-1 and fig. 9.1.4-2

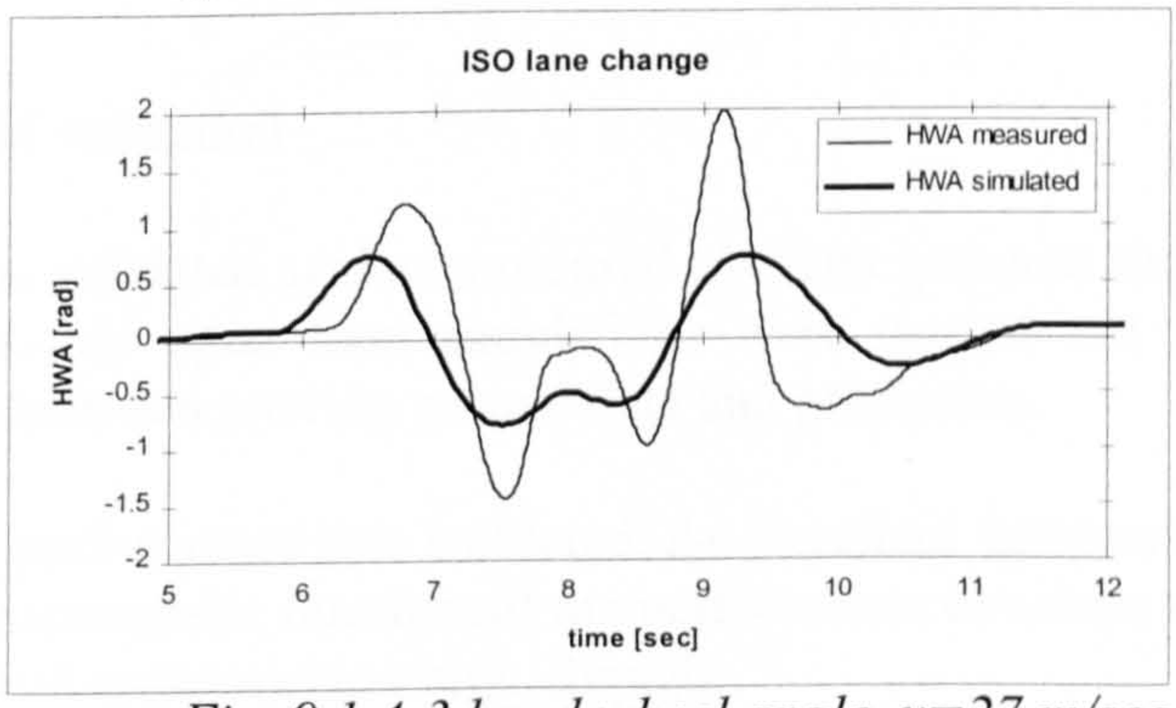

Fig. 9.1.4-3 hand wheel angle, v=27 m/sec

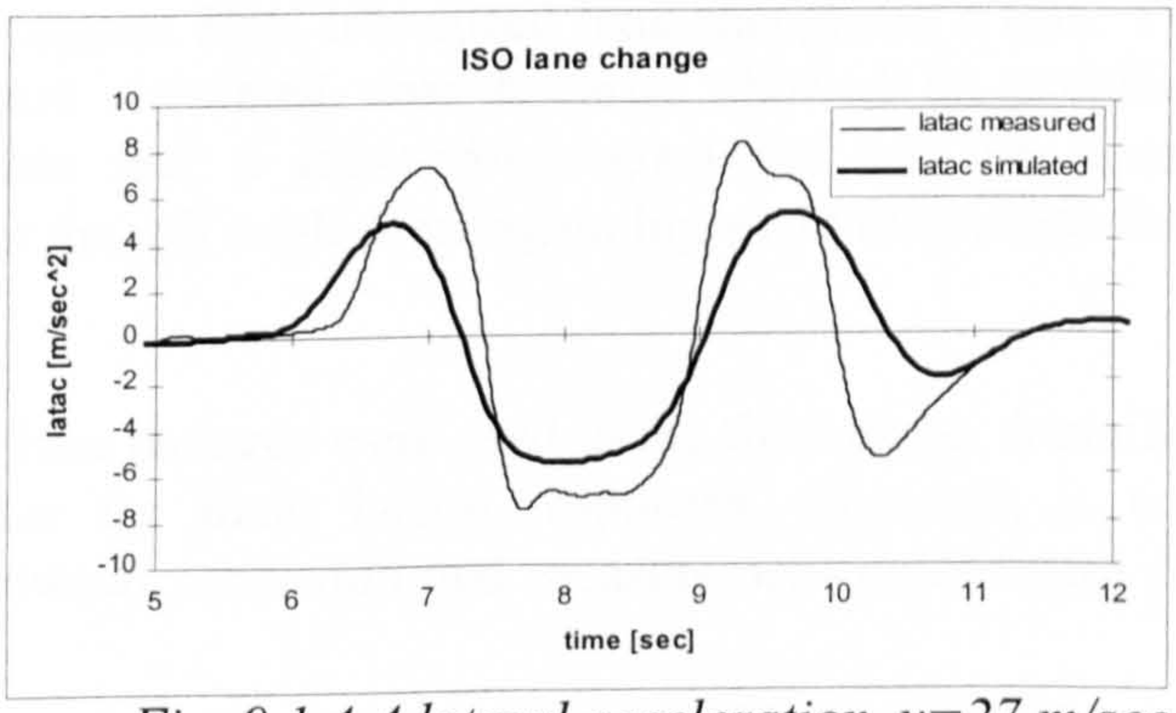

Fig. 9.1.4-4 lateral acceleration, v=27 m/sec

establishes that these attempts were unsuccessful. The graphs refer to an ISO double lane change test performed at 21 m/sec. Although the driver model reproduces the w-shaped steering input (thick line), it is apparent that peak values and zero crossings are not matched. The simulated steering input is too smooth and too slow. The driver model takes more time to complete the manoeuvre, as indicated by a slowly decreasing final peak. As a consequence, a fairly smooth lateral acceleration time history is obtained for the simulated steering input. Even so, the centre of gravity of the vehicle, simulated with the driver model, followed the given lane change, defined by a target line, within a tolerance of +/- 0.4 m[1].

The discrepancy between the measured driver steering input and that produced by the model becomes more apparent for the limit case at 27 m/sec. The corresponding plots are shown in fig. 9.1.4-3 and in fig. 9.1.4-4. The simulated steering angle hardly resembles its measured partner. The w-shaped characteristic has given way to an input more akin to the time history established for the 29 m/sec lane change given in fig. 9.1.3-10. The shapes of the time histories for the lateral acceleration are more similar to each other, though the driver model is unable to establish peak values as high as those in the measurement.

However, the vehicle steered by the driver model still managed to complete the manoeuvre within the tolerances defined for its centre of gravity position. Beyond the speed of 27 m/sec the vehicle violated the path constraints.

9.1.5 Conclusions from AUTOSIM validation

The AUTOSIM vehicle model was validated against measured test data gathered for a small variety of manoeuvres. Mainly open loop simulations were carried out to establish the quality of agreement between proving ground data and prediction.

Firstly, the steady state cornering performance was validated. An excellent agreement was obtained for the understeer characteristic throughout the performance envelope of the Jaguar vehicle. The predicted roll angle was too high, though.

The second stage involved data obtained from low speed lane changes in a turn. The comparison between measured and simulated time histories showed an excellent match for the yaw rate response and a reasonable agreement for the lateral acceleration. Simulation results for the roll angle were again higher in magnitude than measured.

Data captured for high speed ISO lane changes were used in the third stage. A similar quality of fit was established for the main lateral responses. However, it was established that the agreement between prediction and measurement deteriorates for

[1] this tolerance is equivalent to the difference between exit lane and vehicle width, as specified in ISO/TR 3888-1975 (E)

limit manoeuvres involving additional throttle control. The cross-coupled interaction between longitudinal and lateral tyre forces, not represented in the model, was given as the likely reason for this behaviour.

Unfortunately, inconclusive results were obtained for the steering torque characteristics. The agreement between measurement and simulation was poor. The measured signals contained high frequency components not replicated by the model. Some doubt on the reliability of the torque sensor seems appropriate.

The validation for the closed loop case, for which a simple driver model was used, was unsuccessful. Although the driver model managed to manoeuvre the vehicle through a lane change with reasonable tracking accuracy, it was unable to establish the lateral acceleration levels measured for a corresponding test on the proving ground. The driver model is too smooth and too slow for a proper simulation of limit conditions. The reasons for that are probably found in its inability to recognise and adjust to changes in the vehicle behaviour. It seems that the model cannot be adjusted sufficiently to the frequency response characteristics of a vehicle by its three defining parameters, the steering gain and the two establishing the preview window. Therefore, it cannot be used for simulating limit manoeuvres as performed by experienced drivers. However, it could be used for 'worst case' simulations, in which the driving has to be accomplished by a driver with little experience and skill.

The majority of results presented in chapter 9.1 suggests that the vehicle model can be used for limit driving simulations with some confidence. It has to be said, though, that the results do not include manoeuvres in which heavy use of throttle or brake was made in addition to the steering wheel input.

9.2 Lane change results using a simple driver model

Some lane change manoeuvres were simulated using the driver model described in chapter 3, before it became apparent that this model could not replicate the steering angle input as measured for such a manoeuvre.

As demonstrated by the time histories given in section 9.1.4, the driver model failed to produce hand wheel angle amplitudes and velocities of sufficient magnitude to match the signals, recorded for lane change manoeuvres on the proving ground. Although a reasonable tracking performance was achieved up to forward speeds near the measured limit speed, the corresponding peak lateral accelerations remained far too low compared to the measurements.

However, this simple driver model may be used for simulating 'worst case' scenarios. It might provide some insight into how a less skilful driver copes with a driving situation involving higher frequency steering inputs and higher peak lateral accelerations not experienced before. The model given by (3.2.3.3) implies that the control strategy of this 'inexperienced' driver is based on the low severity steady state driving performance of the vehicle. This driver assumes that the steady state vehicle behaviour applies for any driving condition. The delay characteristics of the vehicle are compensated by an appropriate preview strategy. The driver adjusts to the vehicle dynamics by choosing a suitable preview distance, but remains unable to adjust to system non-linearities in time.

The driver model was used for three cases. ISO lane changes at six speeds were simulated for the standard vehicle, the standard vehicle with its front anti-roll bar removed and for the standard vehicle with a considerably softer rack mounting. The corresponding parameter values are found in table 9.2-1. The second alteration results in a softer composite stiffness c_{comp} for the steering column, calculated according to (3.2.2.1).

vehicle set-up	front anti roll bar stiffness [Nm/rad]	composite column stiffness [Nm/rad]
standard	18000.0	25.0
standard/ anti-roll bar removed	0.	25.0
standard/ soft rack mounting	18000.0	15.2

Table 9.2-1 vehicle set-up for ISO lane change simulation

yaw rate gain at 20 m/sec [sec^{-1}]	max. preview time $\tau_{PV,max}$ [sec]	min. preview time $\tau_{PV,min}$ [sec]
4.3	0.85	0.80

Table 9.2-2 driver model parameters

Parameters for the driver model remained unchanged for each simulation. The values defining the yaw rate gain and the preview window are given in table 9.2-2. The value given for the yaw rate gain can also be expressed as an understeer gradient of 4.3 deg

sec^2/m, which compares to a value of 3.3 deg sec^2/m, as established by fig. 9.1.1-1.

Corresponding to chapter 7, results for the correlation coefficients and lag times are presented. Figure 9.2-1 shows the values computed for the maximum correlation between the hand wheel angle and the yaw rate. Results referring to the standard vehicle are denoted by squares, and those for the vehicle with a softer rack bush are indicated by triangles.

There is very little difference between the three set-ups. Similar results, not shown here, were obtained for the cross-correlation between the hand wheel angle and the lateral acceleration. The yaw rate as well as the lateral acceleration response hardly deteriorate with increasing speeds through the lane change, whereas measurements indicated a deteriorating response behaviour for speeds beyond 25 m/sec, as can be seen from the figures 7.3.4-1, 2.

As for the correlation coefficients, the average time delays between the hand wheel angle and lateral acceleration response, shown in fig. 9.2-2, differ very little from each other. They are of similar magnitude as established by measurements shown in fig. 7.3.4-4. The lateral acceleration lag times for the vehicle with its anti-roll bar removed are equal to those of the standard set-up, whereas test results established slightly shorter lag times. The vehicle with a more compliant steering arrangement responds slightly quicker than the other two. Corresponding to the almost constant peak correlation coefficients and to the almost identical time lags, very similar values for the correlation coefficient established at zero time lag were obtained, as can be seen from fig. 9.2-3.

There, results for the correlation between the hand wheel angle and the lateral acceleration are given. The predicted values are considerably higher for the limit manoeuvres than those established from the measurements, given in fig. 7.3.4-5. In contrast to the measured results, the simulation predicted lower correlation coefficients for the vehicle with its anti-roll bar removed than for the standard car.

However, a similar trend, as established by the measured results, was predicted for the rate of correlation loss with increasing steering effort. Corresponding to fig. 7.3.4-6, the loss of correlation at zero time lag is plotted against the steering effort parameter $\sigma_{\dot{\delta},\beta}$ defined by (7.1.3). Fig. 9.2-4 indicates that the correlation of the lateral acceleration with the hand wheel angle input deteriorates by a slightly higher rate in the case of the vehicle without the front anti-roll bar, compared to the alternative vehicle set-ups. For a speed of 29 m/sec a correlation loss of 0.34 for a steering effort of 19 deg/sec is established. At the same speed lower correlation losses as well as lower steering efforts are established for the other two vehicles.

Compared to the test data given in fig. 7.3.4-6, very low steering efforts $\sigma_{\dot{\delta},\beta}$ were predicted, corresponding to comparatively low hand wheel angle velocities and low vehicle slip accelerations. This mismatch between measured and predicted results was

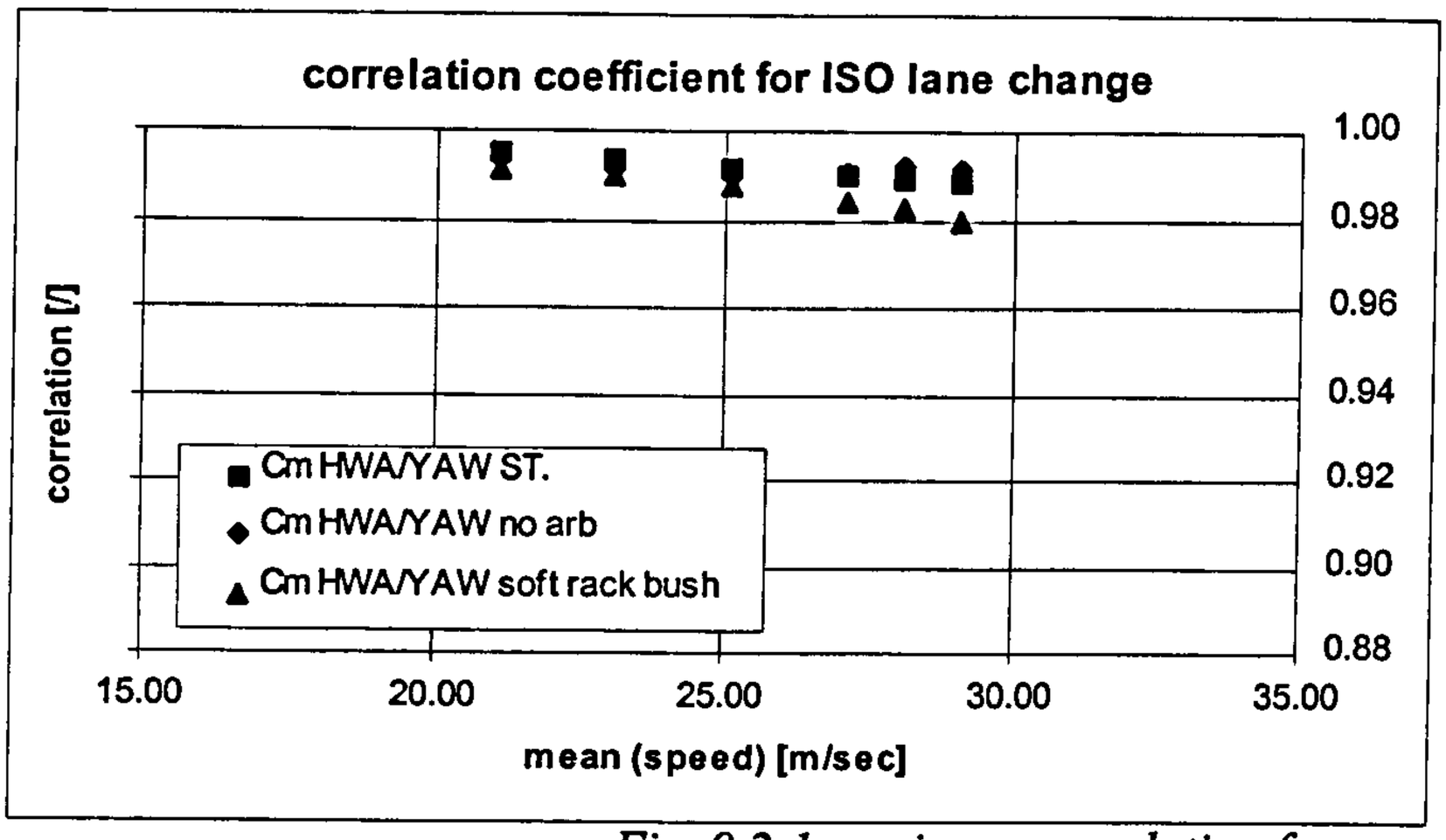

Fig. 9.2-1 maximum correlation for yaw rate

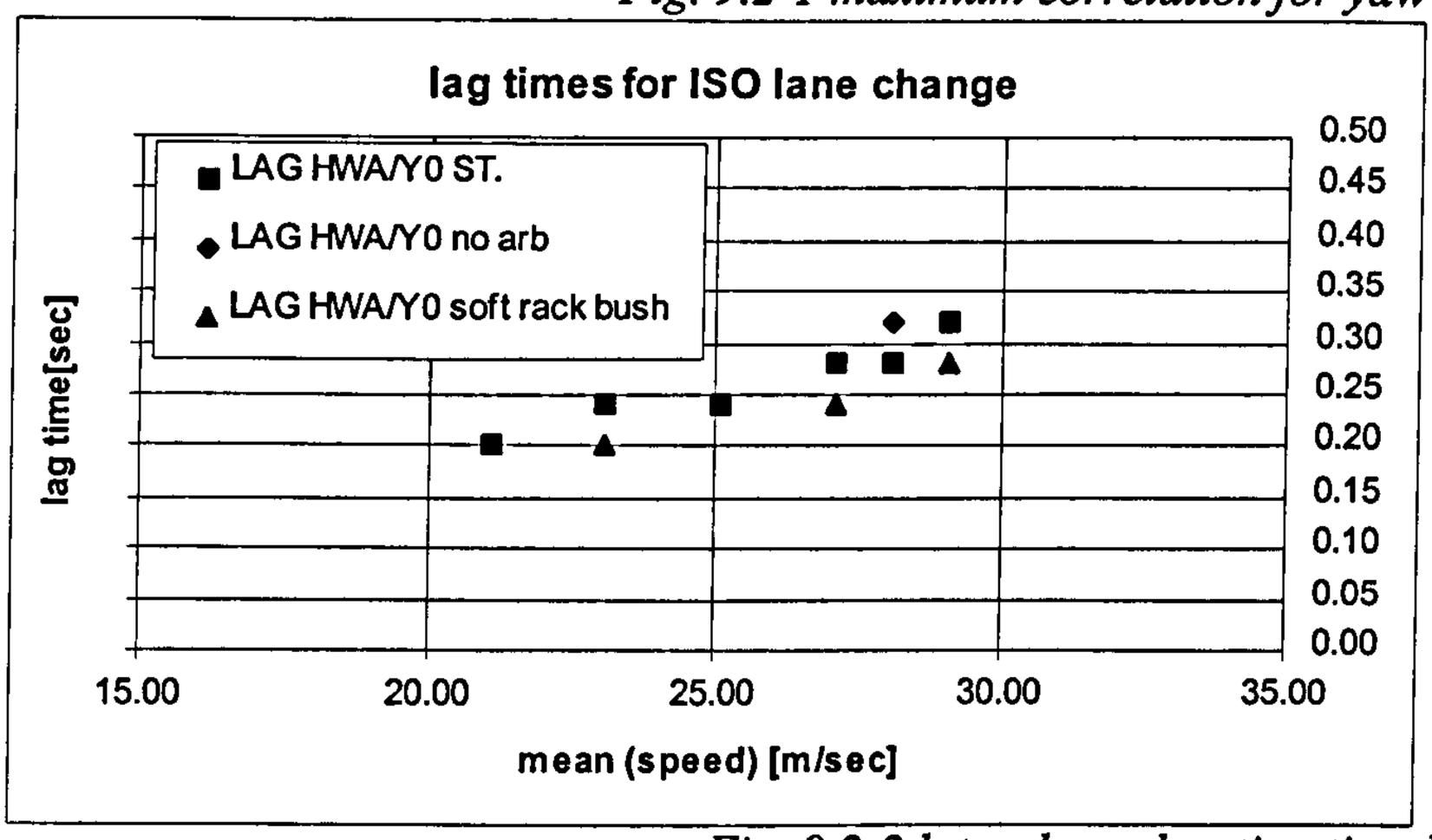

Fig. 9.2-2 lateral acceleration time lags

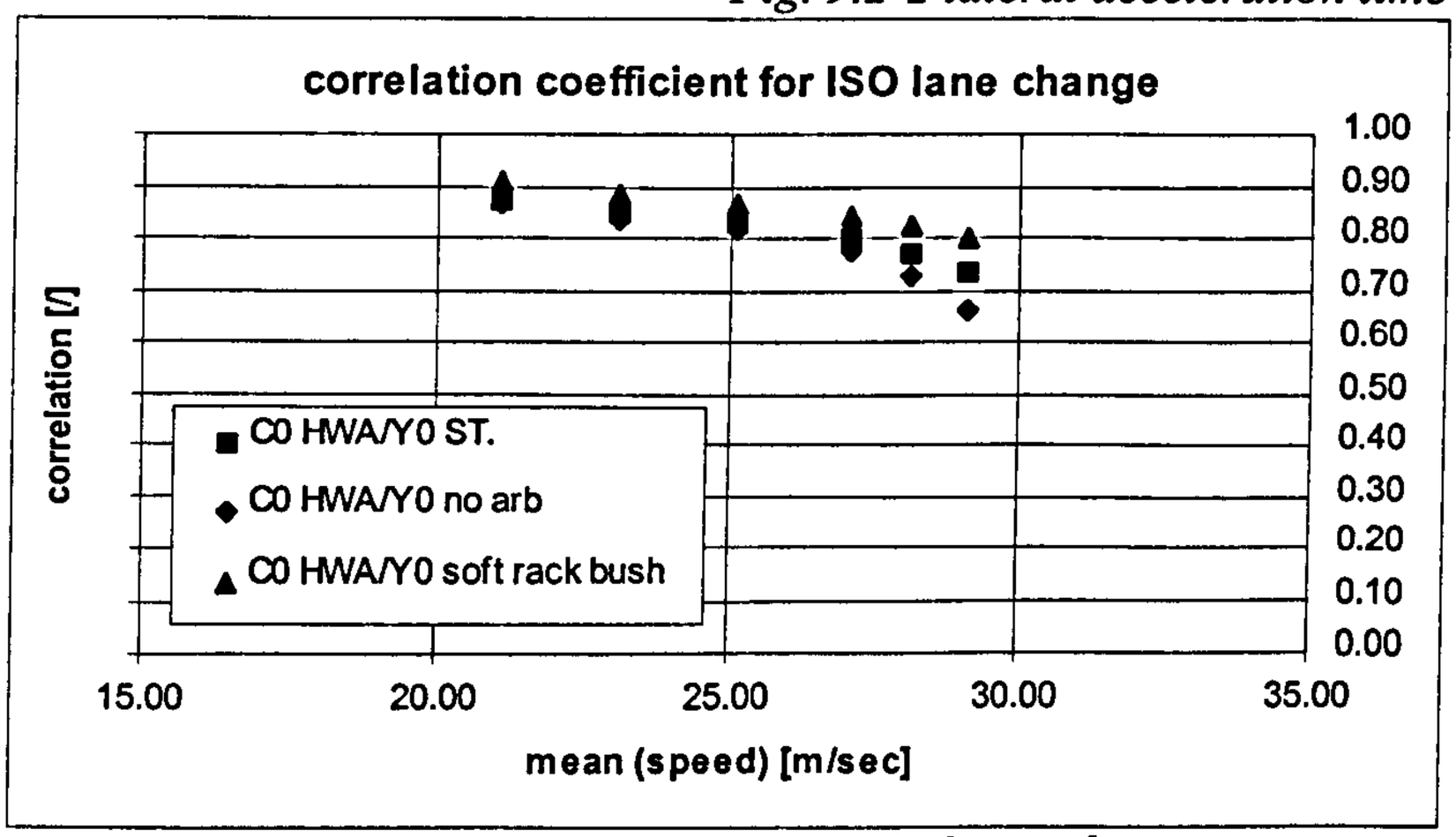

Fig. 9.2-3 correlation at zero time lag

already discussed in section 9.1.4. Simulated lane changes were of far lower severity compared to the corresponding proving ground tests, due to the deficiencies in the driver model.

The results given above seem to indicate that there is little difference in the response behaviour between the three vehicle configurations. The corresponding time histories for the hand wheel angle and the lateral responses, however, demonstrate that these small differences established for the correlation coefficients and lag times correspond to significant changes in the vehicle handling performance.

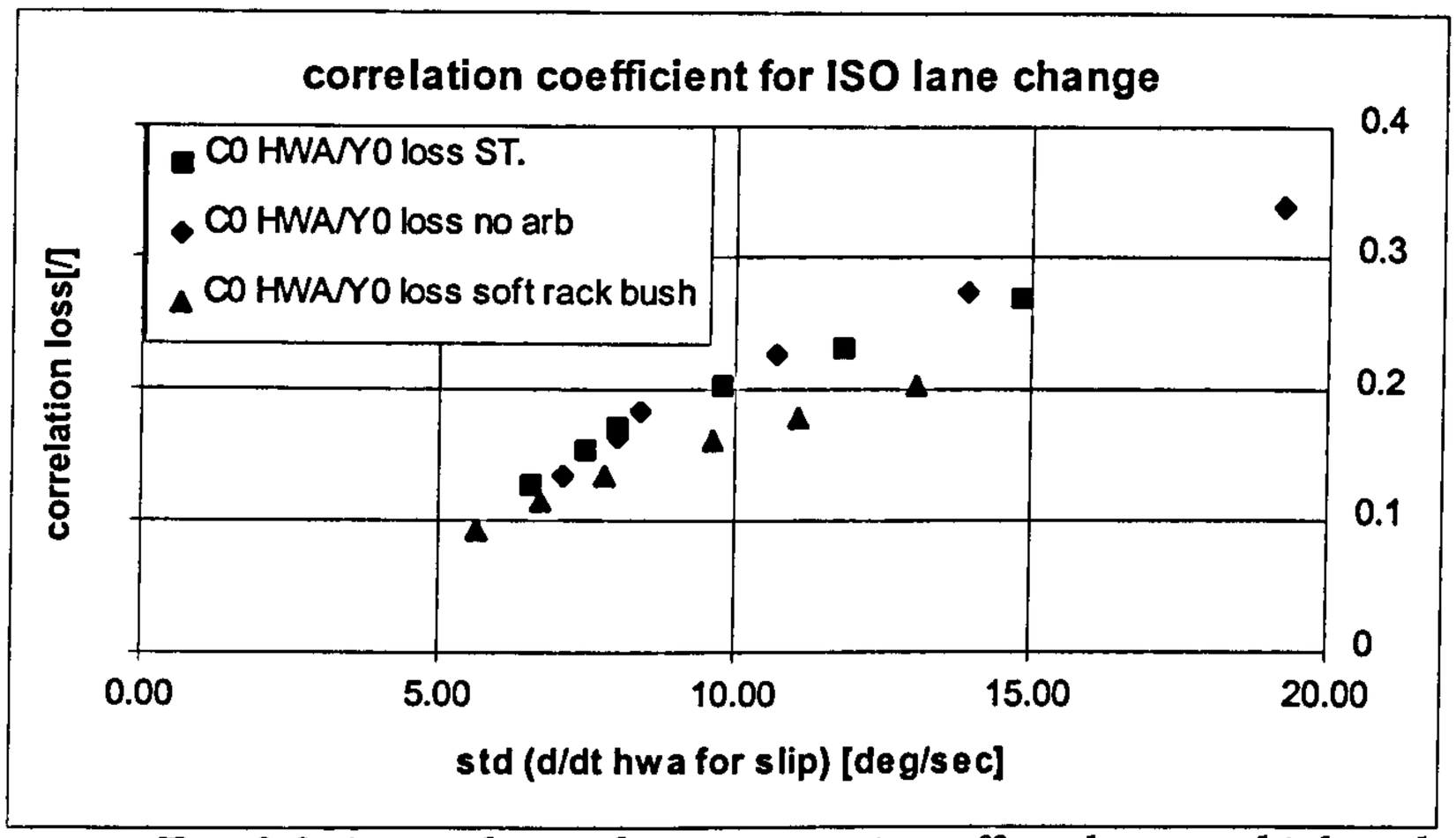

Fig. 9.2-4 correlation loss vs. steering effort due to vehicle side slip

Fig. 9.2-5 shows the trajectories for a double lane change of two of the vehicles investigated here. The centre of gravity position of the vehicle with a softer rack mounting is indicated by a thick line. The thin line refers to the vehicle with its anti-roll bar removed. The former vehicle just manages to travel through the course without exceeding the track limits indicated by small dots. The vehicle for which the anti-roll bar was removed violates the path confines when exiting the offset lane and when entering the original lane again. It oscillates strongly for a considerable distance after rejoining the original lane.

The corresponding time histories for the hand wheel angles and for the lateral accelerations are given in the figures 9.2-6,7. The steering wheel inputs differ little until the vehicle exits the offset lane (~4.5 sec). The steering wheel input for the vehicle with its anti-roll bar removed is slightly faster, as can be seen from small offsets between the zero crossings. The time histories differ considerably for the return phase of the manoeuvre, in which the vehicle rejoins the original lane. The beginning of the return phase is characterised by a second positive peak. The hand wheel angle for the vehicle with a more compliant steering system assumes a smaller peak, followed by a further negative peak until a steady state is established.

The return phase for the other vehicle involves a higher second peak, followed by further steering reversals of considerable magnitude. The oscillatory behaviour of the vehicle with its anti-roll bar removed is also illustrated by the lateral acceleration response shown in fig. 9.2-7. This vehicle establishes a similar lateral acceleration response to the vehicle with a more compliant steering until it joins the original lane. The following peaks assume fairly high magnitudes and decay slowly.

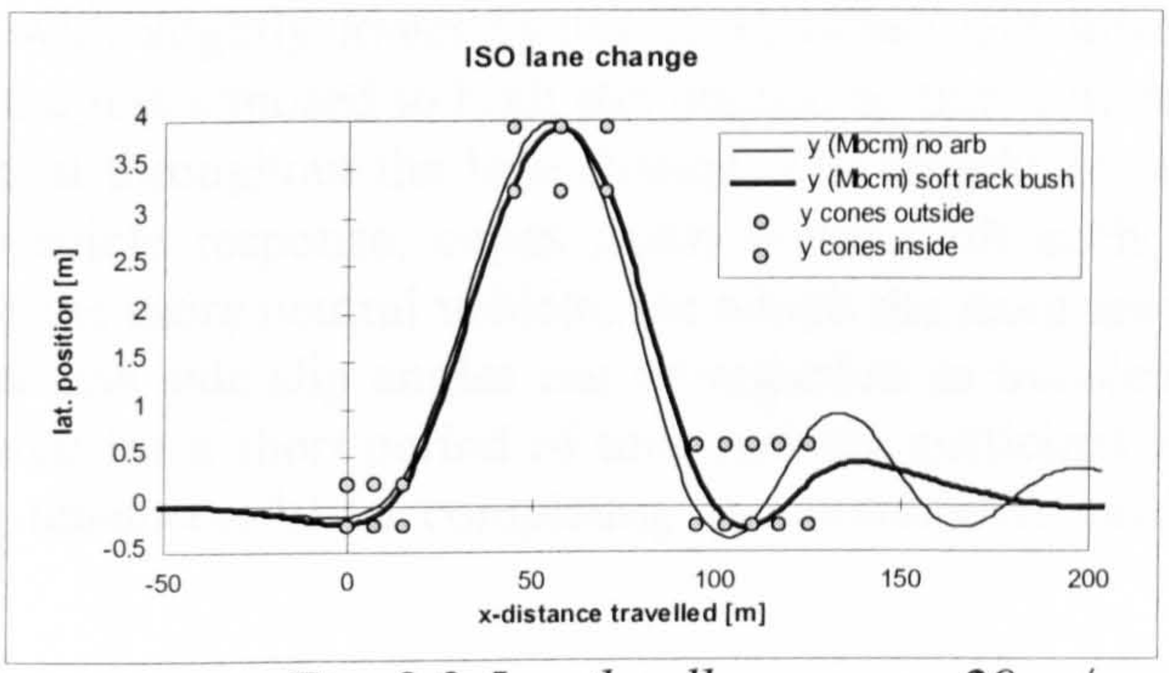

Fig. 9.2-5 path adherence v=29 m/sec

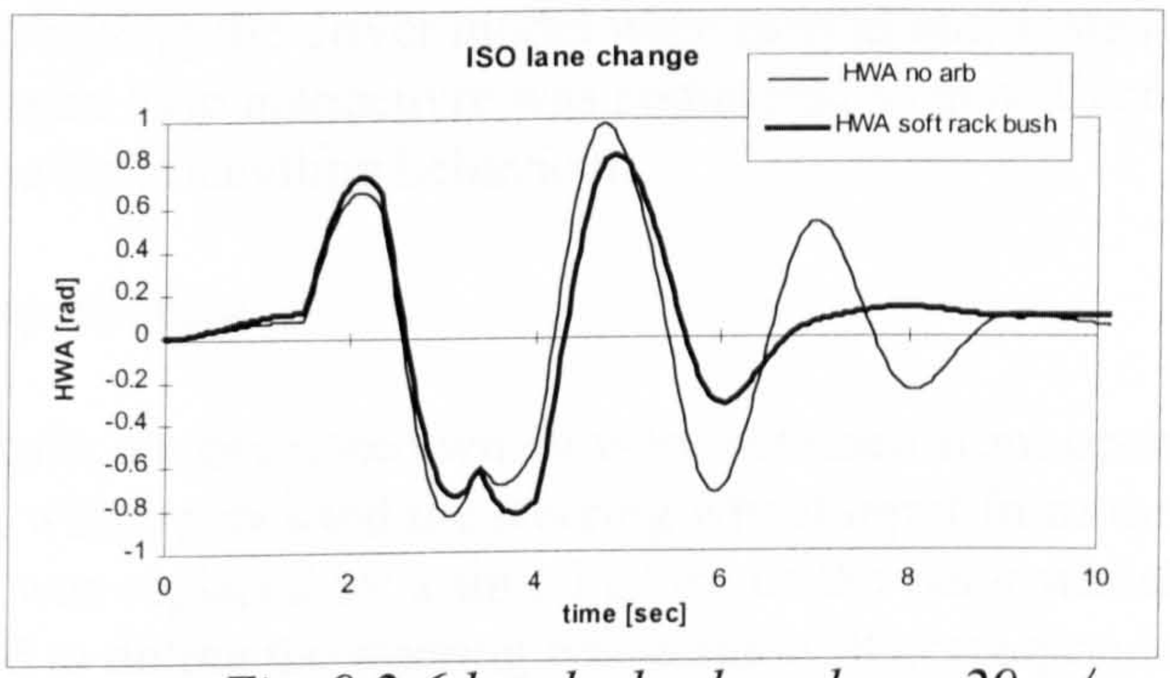

Fig. 9.2-6 hand wheel angle, v=29 m/sec

The graph for the vehicle slip angle shown in fig. 9.2-8 gives an indication why these two vehicles behave so differently in the return phase, while performing rather similarly during the first sections of the lane change. The vehicle with a lower roll stiffness assumes higher vehicle slip angle peaks, which correspond to larger side slip angles for the rear tyres. The rear tyres operate well in their non-linear region when the vehicle travels at a high lateral acceleration. Obviously, the driver model does not cope very well with this transient non-linearity, which results in a lightly damped yaw oscillation.

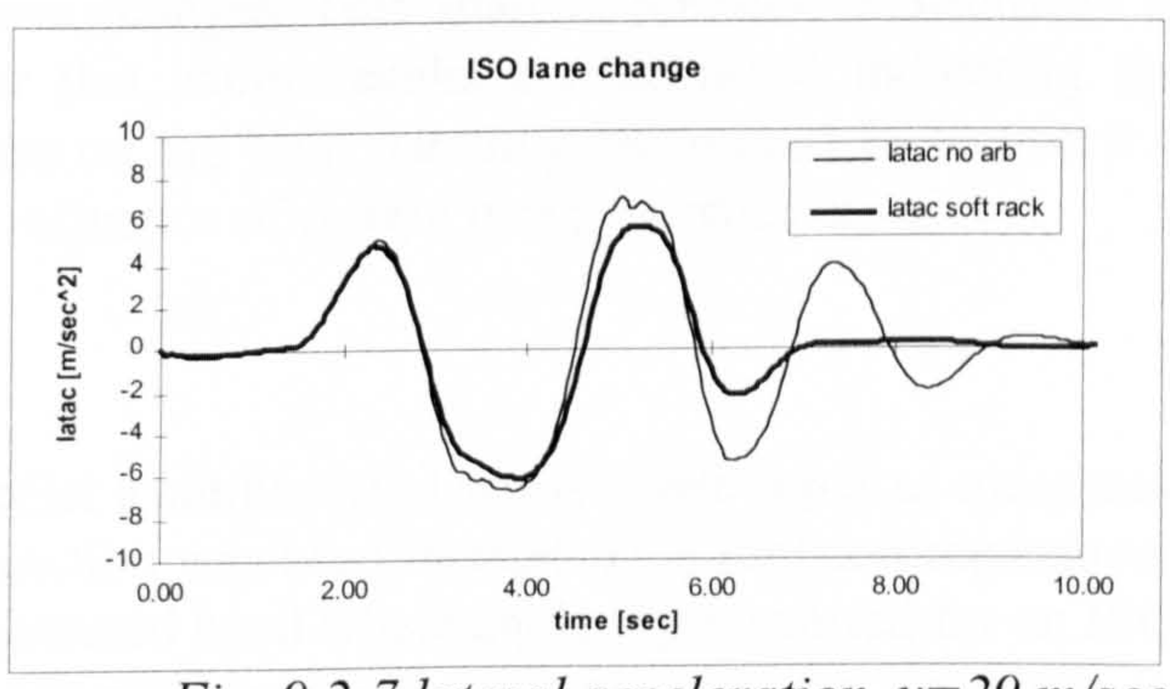

Fig. 9.2-7 lateral acceleration, v=29 m/sec

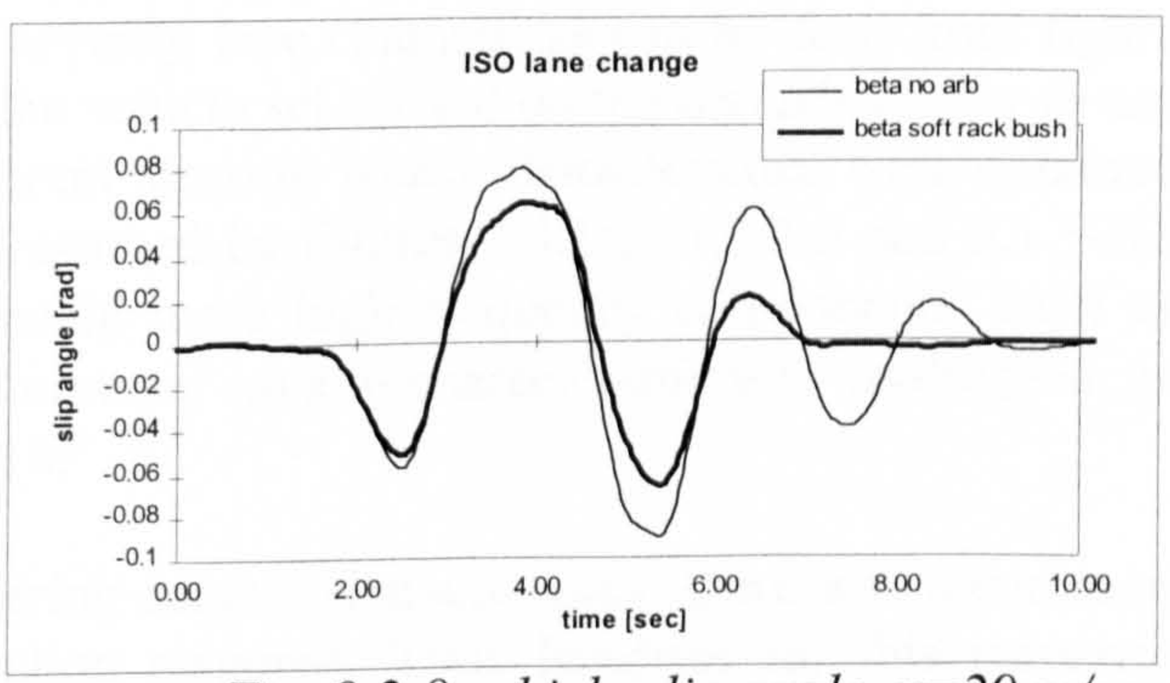

Fig. 9.2-8 vehicle slip angle, v=29 m/sec

Conclusions

This example may illustrate that small differences in the response behaviour can have significant benefits or disadvantages. The more understeering vehicle, the one with a more compliant

steering, performs the manoeuvre with slightly lower lateral acceleration and lower side slip peaks. The rear end tyres are less exposed to high slip angles, so that a linear vehicle response is maintained almost throughout the lane change. The simple driver model, which presumes a linear vehicle response, copes much better with such a behaviour than with the response of the more neutral vehicle, for which the front anti-roll bar was removed. The high rear end side slip angles can be regarded as transient non-linearities. These are encountered for a short period of time and are sufficient to render this 'inexperienced' driver unsuccessful in completing the manoeuvre with sufficient accuracy.

Since the validation for closed loop manoeuvres was unsuccessful for limit manoeuvres, no more simulations involving the driver model were carried out. Instead a series of simulations based on an open loop manoeuvre was completed to investigate suspension and tyre influences on the limit handling behaviour.

9.3 Lane change results for open loop steering

In this and the following section results are presented which were obtained from open loop simulations. The driver model, which predicted the steering wheel input from the course layout ahead of the vehicle, was replaced by a time history of the hand wheel angle. An analytic function was used to define the steering wheel input. It corresponds to some extent to the characteristic shape of the hand wheel angle time histories measured for the proving ground lane changes. This analytic function is discussed at the beginning of the section. After that, some results are discussed indicating the effects of various suspension designs on the limit handling behaviour. In section 9.4 simulation results which reflect the influence of certain tyre properties are given.

Definition of steering wheel input

Since the driver model failed to predict a similar hand wheel angle input as measured for limit manoeuvres, an analytic function was used instead. This function reproduces some of the characteristics of the measured hand wheel angle input exerted for an ISO lane change. Some examples of measured steering angle time histories are given in chapter 7 and in section 9.1.3. The typical steering angle input assumed a w-shaped characteristic for low and medium severity lane changes, as can be seen from figure 9.1.3-1 and 9.1.3-6. Depending on the vehicle set-up and on the driver's ability to use the throttle during a test, very different steering wheel characteristics were obtained for high severity manoeuvres, as illustrated by figures 7.3.1-3, 7.3.2-3 and 9.1.3-10. Some time histories seemed to contain more high frequency components, such as illustrated by fig. 7.3.2-3, while for others a smooth characteristic was established, as shown by figures 7.3.1-3 and 9.1.3-10.

In contrast to the variety of the steering control characteristics, there was a common trend regarding the lateral acceleration response. Time histories for this response seemed to contain less high frequency content with increasing severity. This trend is

illustrated by figures 9.1.3-4, 9.1.3-8 and 9.1.3-12. The w-shaped response at the low speed of 21 m/sec develops into a u-shaped characteristic at higher speeds. For limit manoeuvres the lateral response no longer follows those rapid steering wheel reversals exerted during the centre stage of the double lane change. Instead of momentarily establishing a straight ahead attitude in the offset lane, the vehicle corners at a constant lateral acceleration through this section. Fig. 9.1.3-10 suggests that the driver noticed this change in the vehicle response and adapted the steering input, as well as the throttle control, to the vehicle behaviour. In this case steering and vehicle response are well matched.

An analytic function for the steering wheel input was defined, which simulates to some extent the transitional changes in the steering wheel input, which were observed for increasing levels of severity. The w-shaped characteristic, which prevails at moderate severity levels, can be expressed by two cosine functions with equal and opposite amplitudes. The frequency of the first cosine function is adjusted to the vehicle speed and to the wavelength of the manoeuvre. The frequency, or the inverse of the wavelength, of the second cosine function has to be three times higher than the base frequency. The function reads:

$$\delta_{HW} = \delta_1 \cdot \cos\{2 \cdot \pi \cdot (f_2 - f_1) \cdot t\} - \delta_2 \cdot \cos\{2 \cdot \pi \cdot (f_2 + f_1) \cdot t\} \qquad (9.3.1)$$

with $f_0 = (f_2 - f_1)$ defining the base frequency and
$(f_2 + f_1) = 3 \cdot f_0$ defining the second harmonic

The amplitudes δ_1 and δ_2 have to be equal in order to establish a zero steering wheel angle at the beginning of the manoeuvre. As a result a w-shaped time history is obtained with five peaks of equal magnitude.

Since the layout of a lane change defines the wavelength of the manoeuvre, the frequencies have to be a linear function of the vehicle speed. This is expressed by:

$$f_0 = \mathrm{v}(t) / \lambda_0 \qquad (9.3.2a)$$
$$(f_2 + f_1) = 3 \cdot \mathrm{v}(t) / \lambda_0 \text{ , where} \qquad (9.3.2b)$$

λ_0 defines the wavelength or length of the course and
$\mathrm{v}(t)$ is the forward speed of the vehicle

If the vehicle response did not change with frequency and speed, and if no non-linearities were involved, the function given by (9.3.1) would represent a proper lane change steering input for any level of severity. The amplitudes could remain constant. But since vehicle response characteristics change with frequency as well as with vehicle speed, the amplitudes have to be adjusted accordingly.

A w-shaped input is used for low severity manoeuvres, which are simulated for a velocity of 20 m/sec. The amplitude δ_1 is defined to give 4 m/sec^2 lateral acceleration.

The corresponding value was taken from the handling diagram obtained for steady state cornering, such as the one given in fig. 9.1.1-1.

The limit speed was defined as 35 m/sec at which 8 m/sec^2 had to be established. The corresponding hand wheel angle amplitude was again established from the steady state data.

Taking account of the fact established by the test results, that the high frequency lateral acceleration response deteriorates, less weight is placed on the corresponding amplitude δ_2 and more is placed on the low frequency input determined by the amplitude δ_1. It is assumed that the high frequency contribution vanishes at a speed of 40 m/sec, and that only one harmonic input remains for the steering control. For the amplitudes δ_1 and δ_2 the following relationships were defined:

$$\delta_1 = \delta_0 \cdot \left\{1 - \left(\frac{v(t) - v_0}{v_{max} - v_0}\right)^2\right\} + \delta_{max} \cdot \left(\frac{v(t) - v_0}{v_{max} - v_0}\right) \qquad (9.3.3a)$$

and

$$\delta_2 = \delta_0 \cdot \left\{1 - \left(\frac{v(t) - v_0}{v_{max} - v_0}\right)\right\}, \text{ where} \qquad (9.3.3b)$$

δ_0 determines the amplitude at the the lowest speed v_0, and

δ_{max} defines the amplitude at the the highest speed v_{max}

The steering wheel input is then defined by the equations (9.3.1) and (9.3.3a, b). In order to allow a convenient data analysis, a series of 'lane changes' was simulated in one run. Within 80 seconds the vehicle speed increased linearly from 20 m/sec to 35 m/sec. The frequencies and amplitudes were adjusted continuously according to the increasing speeds. The peak amplitude for the steering wheel angle increased from a value giving 4 m/sec^2 at 20 m/sec to a value giving a lateral acceleration of 8 m/sec^2 at 35 m/sec. The steering angle time history used for the standard vehicle is defined by the parameters given in table 9.3-1.

parameter	*value*
wavelength [m] λ_0	100.0
initial speed [m/sec] v_0	20.0
max. speed [m/sec] v_{max}	40.0
long. acceleration [m/sec^2]	0.4
steer. amplitude δ_0 at initial speed v_0 [rad]	0.5
steer. angle δ_{max} at max. speed v_{max} [rad]	1.72

Table 9.3-1 parameters defining steering angle

Fig. 9.3-1 indicates the transitional change of the steering wheel input for this 'lane change sweep' manoeuvre. The thick line refers to the steering wheel angle assumed for the first 20 seconds (20-24 m/sec) of the manoeuvre during which five 'lane changes' are performed in succession. The second curve, plotted by a thin line, gives the steering angle established between 40 and 60 seconds (28-32 m/sec). The simulation commences with the typical w-shaped steering wheel input. The peak amplitudes increase slightly, while the high frequency component decreases with time.

The w-shaped input develops into a u-shaped characteristic, which is illustrated by the second curve. The amplitudes are less distinct and are maintained for longer. At higher speeds, the high frequency content decreases even more, and the steering wheel input approaches the shape of a cosine wave. At the same time the amplitude increases.

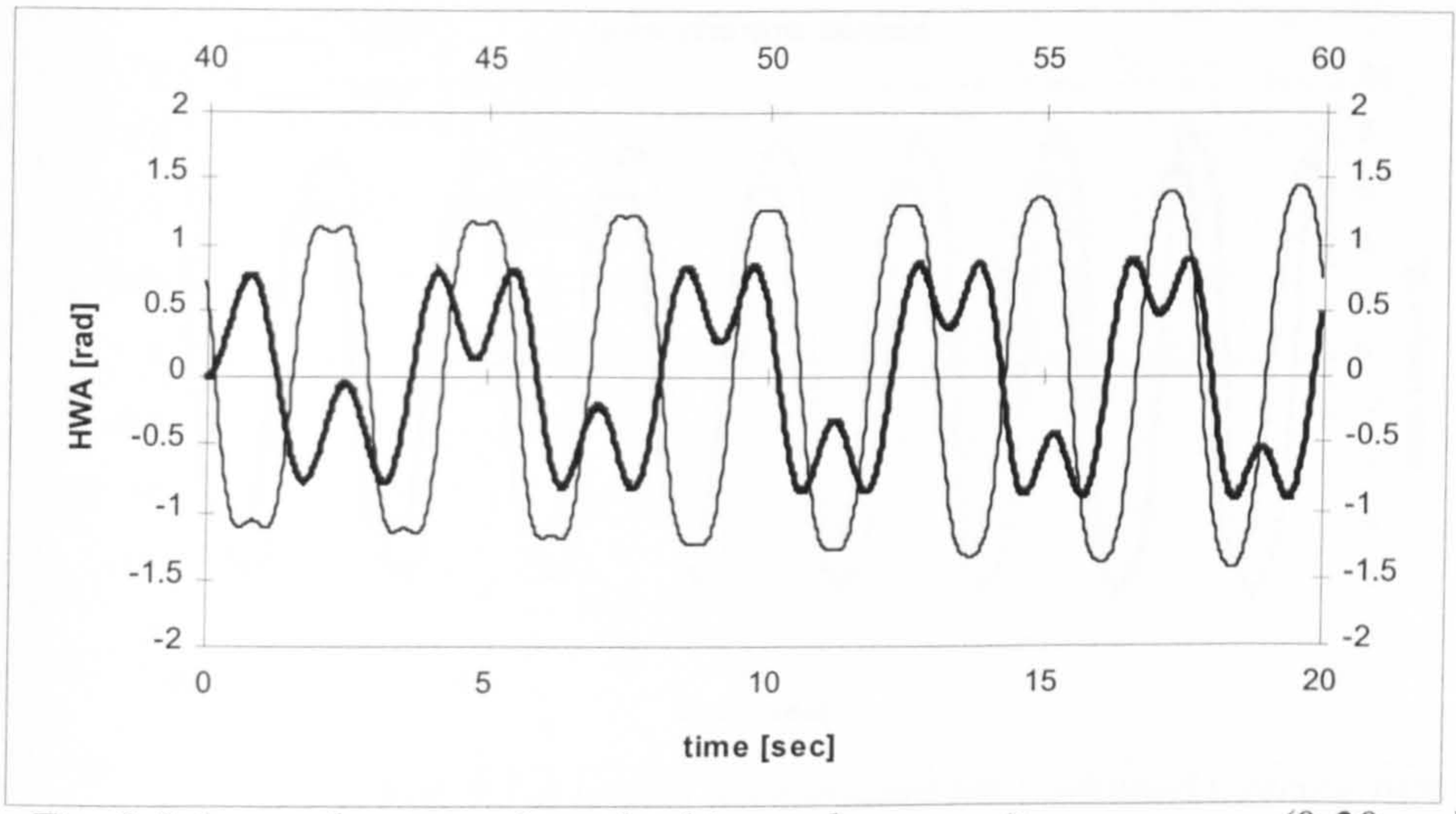

Fig. 9.3-1 open loop steering wheel input: low severity manoeuvre (0-20 sec) and high severity manoeuvre (40-60 sec)

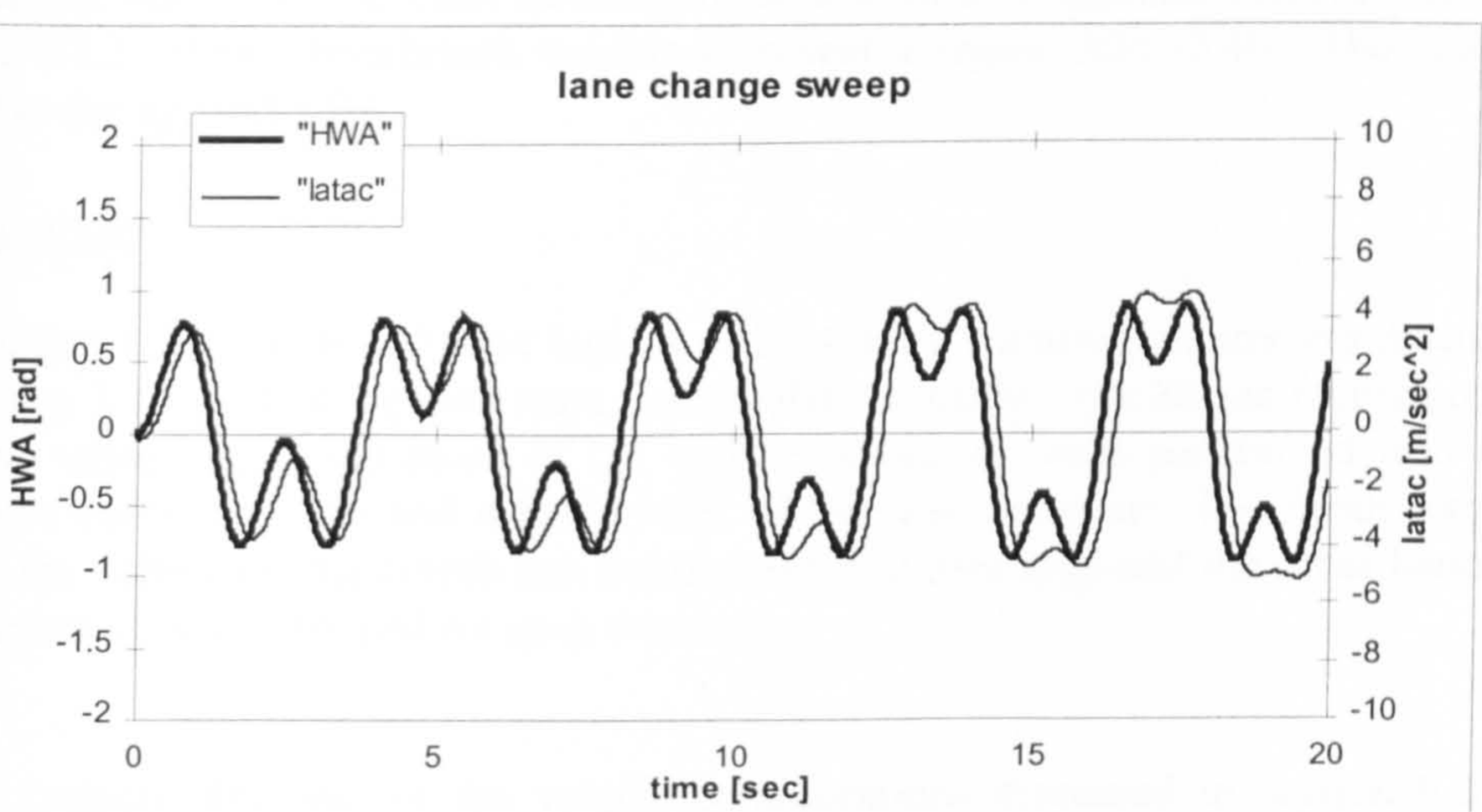

Fig. 9.3-2 lateral acceleration for W-shaped steering input

The corresponding time histories for the lateral acceleration are shown in the figures 9.3-2 and 9.3-3. The first of the two graphs illustrates that the high frequency component of the lateral acceleration (thin line) decreases disproportionately to that of the steering wheel angle (thick line). Fig. 9.3-3 shows that the shape of the lateral response becomes better matched to steering input when the high frequency component of the latter decreases. It also shows an increasing time delay. The ripples around the lateral acceleration peaks are due to the bump and rebound stop impacts.

A similar way of simulating the limit approach is suggested in /1.2.4/. There, the limit handling is assessed from the response data established at a constant speed for an oscillating steering wheel input with a continuously increasing, step-like amplitude.

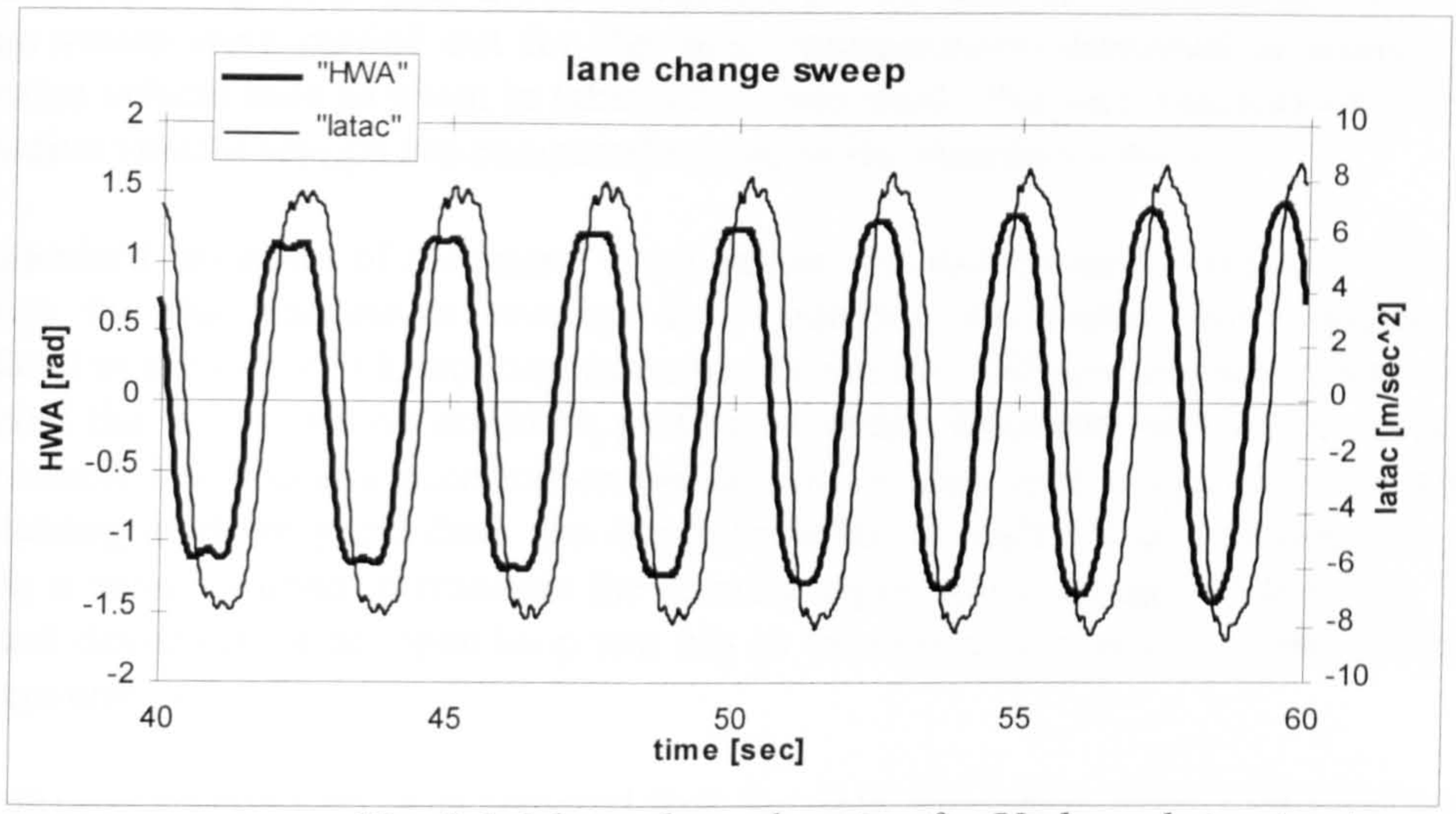

Fig. 9.3-3 lateral acceleration for U-shaped steering input

The steering angle input defined in this section was used for a parametric study into suspension effects on the limit handling behaviour of a benchmark vehicle. The data /4.1.7, 8.2.2/ of this benchmark vehicle represent a Jaguar XJ6 (X40). They can be found in the appendix B1.

Data analysis

Correlation coefficients and time lags as well as those handling parameters discussed in section 7.1.2 were computed from the simulation results. The 80 sec records of the steering wheel input and those of the vehicle responses were partitioned into time windows containing one and a half cycles of the first harmonic. The mean forward speed, the values for the correlation coefficients and time lags and the other handling parameters were established for each window.

Firstly, results obtained for the vehicle configurations discussed in section 9.2 are presented. The response characteristics of the standard vehicle are compared to those of the vehicle with its anti-roll bar removed and to those of the vehicle with a softer steering rack mounting. After that, some results are presented indicating the influence of certain suspension types. Finally, some results are used to demonstrate the effect of the vehicle's mass distribution and inertia properties.

9.3.1 Effects of steering compliance and roll stiffness

The effects of a more compliant steering system and those of a reduced roll stiffness on the limit handling behaviour are investigated in this section. Simulations of a lane change sweep were carried out for the three configurations discussed in section 9.2. The same vehicle data as given in table 9.2-1, was used. The performances of the two alternative vehicle set-ups are compared to that of the standard vehicle.

The standard deviation of the lateral acceleration was introduced in section 7.1.2 as a measure for the manoeuvre severity. Low standard deviations were regarded as beneficial in the case of closed loop manoeuvres like the ISO lane change. A low value indicated that a manoeuvre could be performed rather smoothly with fewer reversals and possibly lower lateral acceleration peaks. For an open loop manoeuvre, for which the steering angle is prescribed, the opposite holds. A high value indicates that the vehicle is more inclined to translate the steering input into a change of direction. The standard deviation for an open loop test has to be seen as a measure of the vehicle's manoeuverability.

For a proper comparison, it is required that for each simulation similar severity levels are established. This can be demonstrated by fig. 9.3.1-1, showing the standard deviation of the lateral acceleration as well as the peak lateral acceleration as a function of the vehicle speed in one graph. The graph indicates that very similar peak accelerations were achieved by the three set-ups. However, lower standard deviations were computed for the vehicle with its anti-roll bar removed.

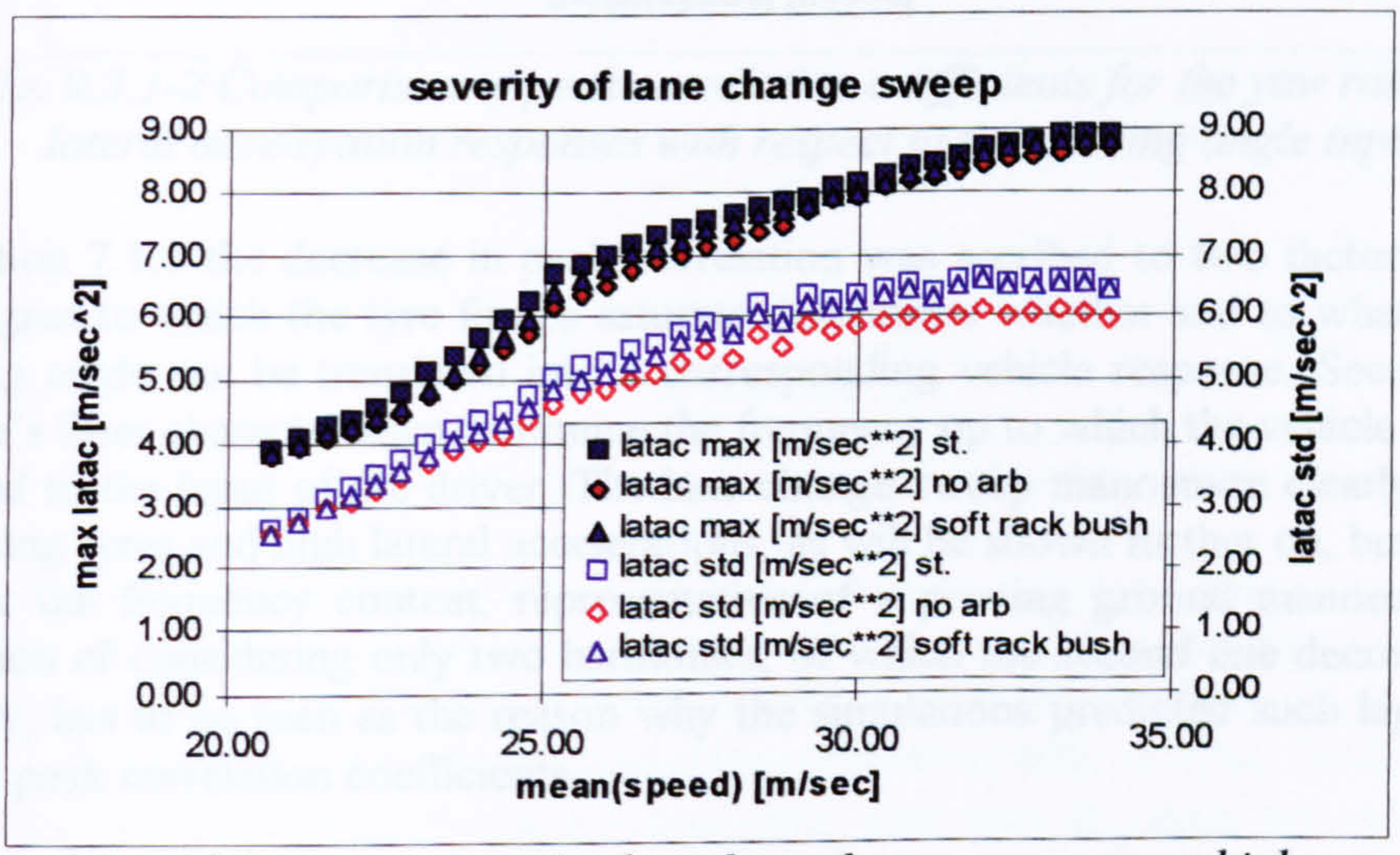

Fig. 9.3.1-1 Manoeuvre severity for a lane change sweep vs. vehicle speed

The more neutral steering vehicle, as established by the removal of the front anti-roll bar, fails to match the peak lateral acceleration with a correspondingly high standard deviation compared to the other two configurations.

Cross-correlation coefficients and time lags are given in figures 9.3.1-2-4. The peak

correlation coefficients are given in fig. 9.3.1-2, while those established at zero time shift are shown by fig. 9.3.1-3.

As can be seen from fig. 9.3.1-2, the peak correlation coefficients for the two lateral responses with respect to the steering angle remain almost constant. This was a common feature of all results obtained from simulations of a lane change sweep. This stands in contrast to the results obtained from the proving ground data, which indicate a continuous decrease in peak correlation with severity, as can be established from the corresponding graphs presented in chapter 7. The lane change sweep simulation established values of not less than 0.96 for the peak correlation coefficients of the hand wheel angle/ yaw rate pair and of the hand wheel angle/ lateral acceleration pair.

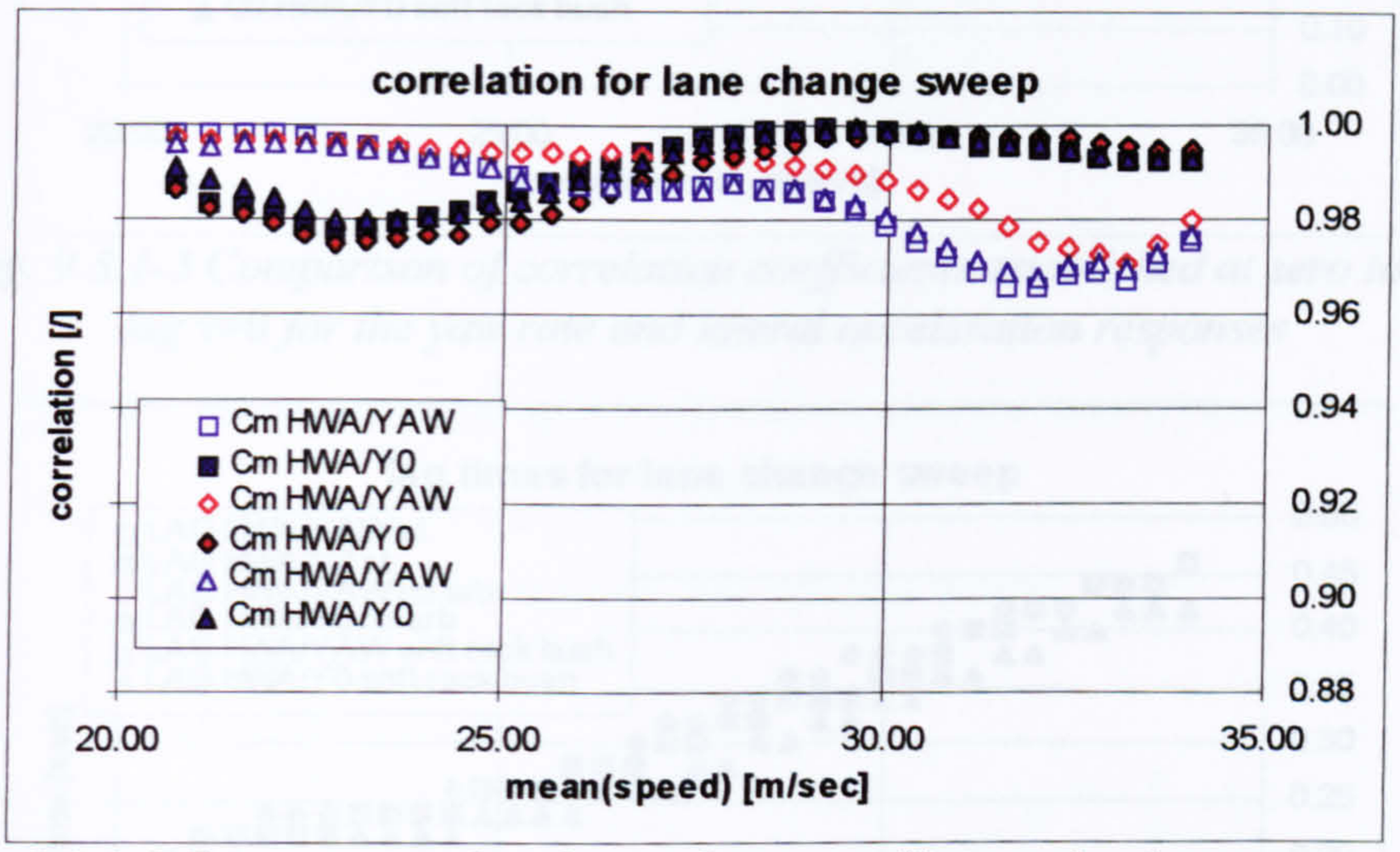

Fig. 9.3.1-2 Comparison of peak correlation coefficients for the yaw rate and lateral acceleration responses with respect to the steering angle input

In section 7.1.1 the decrease in peak correlation was ascribed to two factors. Firstly, the degree to which the tyre forces saturate determines whether and to what extent a steering angle can be translated into a corresponding vehicle response. Secondly, the vehicle's filter characteristics determine the frequency up to which the vehicle is able to respond to the input of the driver. The lane change sweep manoeuvre clearly leads to saturating tyres and high lateral accelerations, as will be shown further on, but it seems to lack the frequency content, representative of a proving ground manoeuvre. The limitation of considering only two harmonics, of which the second one decreases with severity, has to be seen as the reason why the simulations predicted such high values for the peak correlation coefficients.

However, the results for the correlation coefficients established at zero time lag, $\tau=0$, as shown in fig. 9.3.1-3, and the corresponding time delays show a similar behaviour to that obtained from the proving ground results discussed in chapter 7. The magnitudes of the correlation coefficients established at zero time lag decrease as severity increases. The coefficients of the hand wheel angle/lateral acceleration pair ('C0HWAY0') decrease at a higher rate than those of the wheel angle/yaw rate pair

('C0HWAYAW').

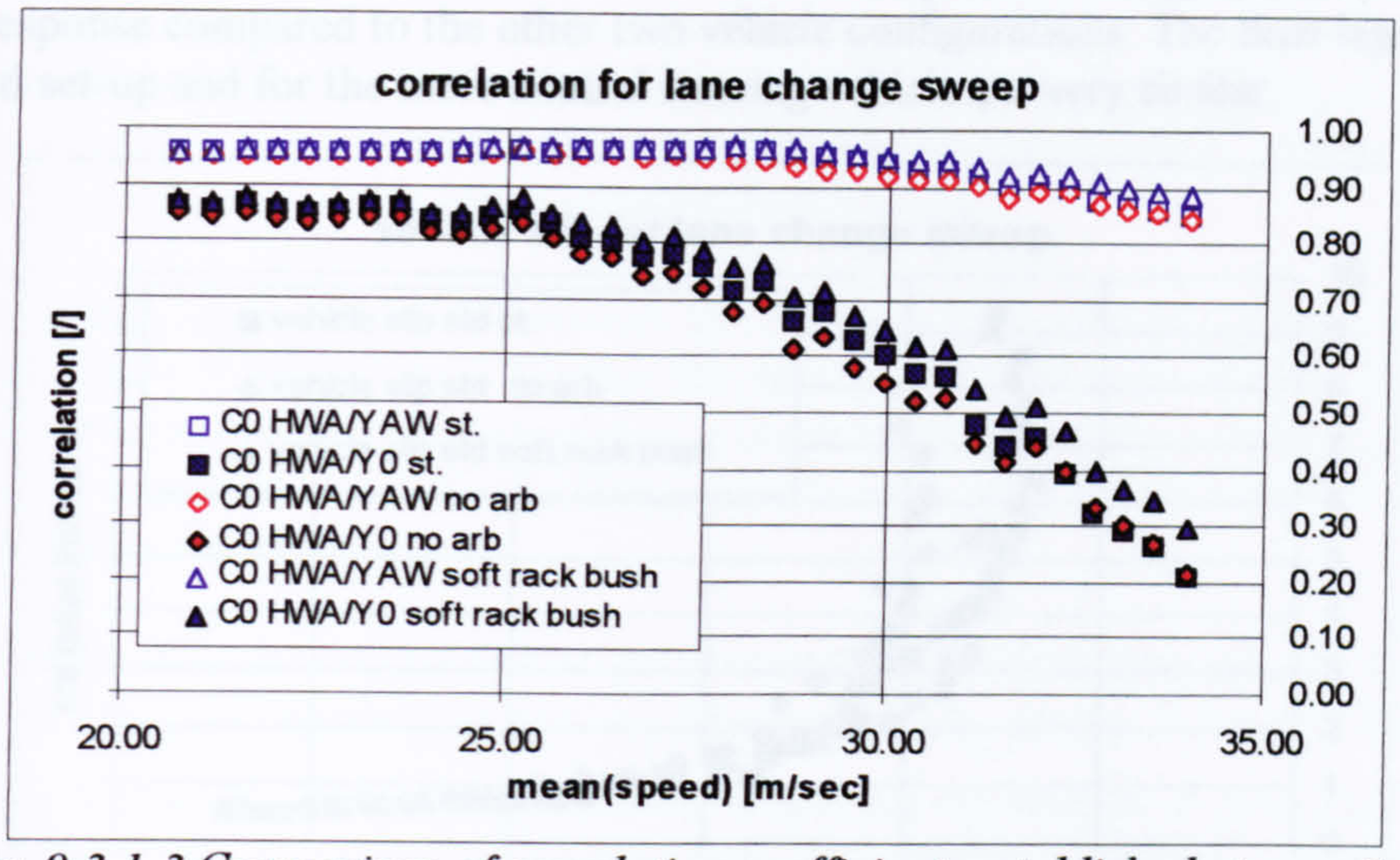

Fig. 9.3.1-3 Comparison of correlation coefficients established at zero time lag τ=0 for the yaw rate and lateral acceleration responses

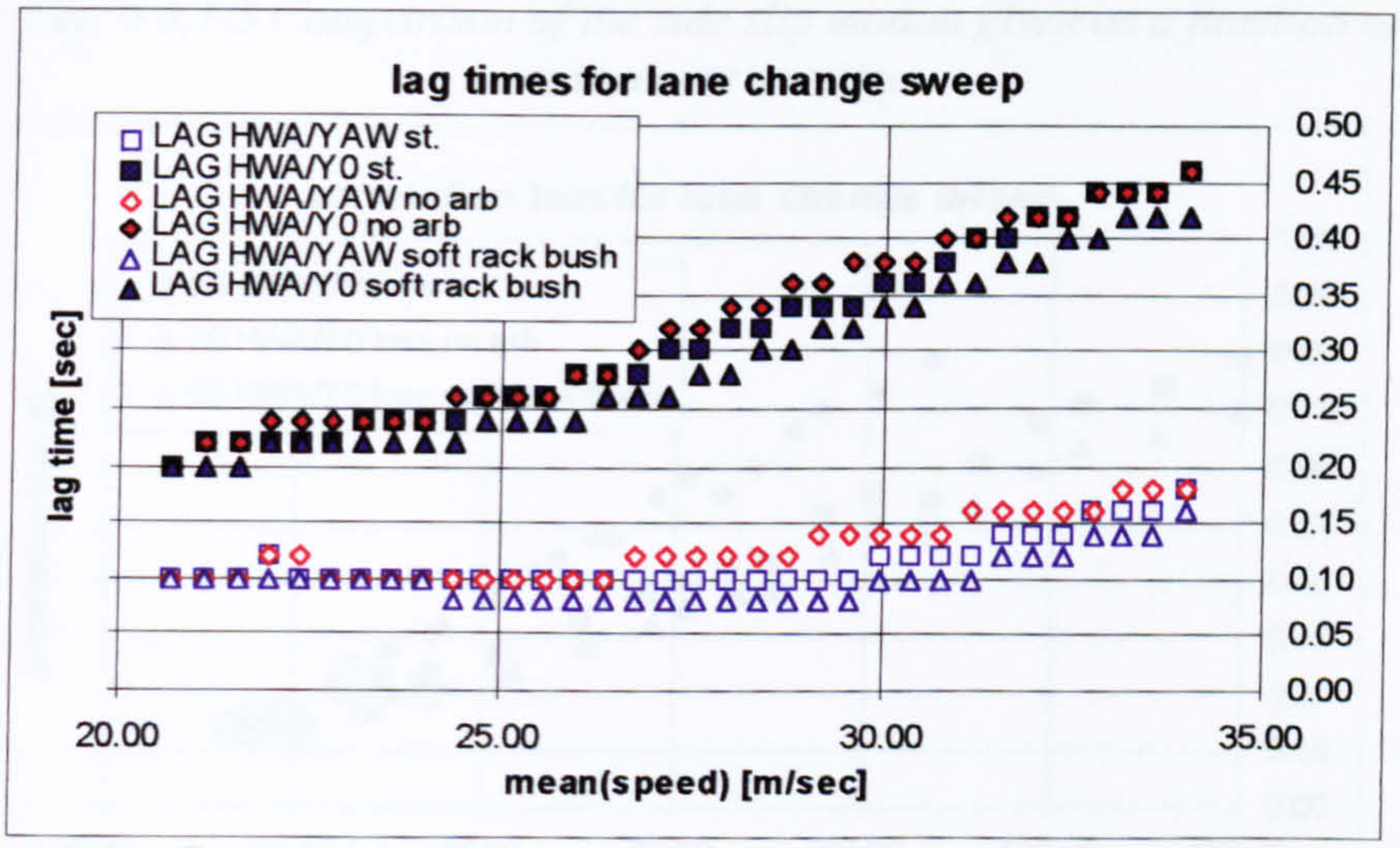

Fig. 9.3.1-4 Comparison of lag times for the yaw rate and lateral acceleration responses

Since the peak correlation coefficients remain fairly constant, the time delays computed for the input-output pairs correspond to the characteristics established by the cross correlation coefficients at zero time lag. As can be seen from fig. 9.3.1-4, the delay times for the yaw rate increase only moderately with severity, while those for the lateral acceleration rise at a higher rate. The rates at which the time lags increase and the rates at which the correlation coefficients at zero time lag decrease are comparable to those given in figures 7.3.4-3, 4 and fig. 7.3.4-5 for the proving ground tests.

Fig. 9.3.1-4 indicates that the vehicle with a more compliant steering system provides a faster response compared to the other two vehicle configurations. The time lags for the standard set-up and for the more neutral steering vehicle are very similar.

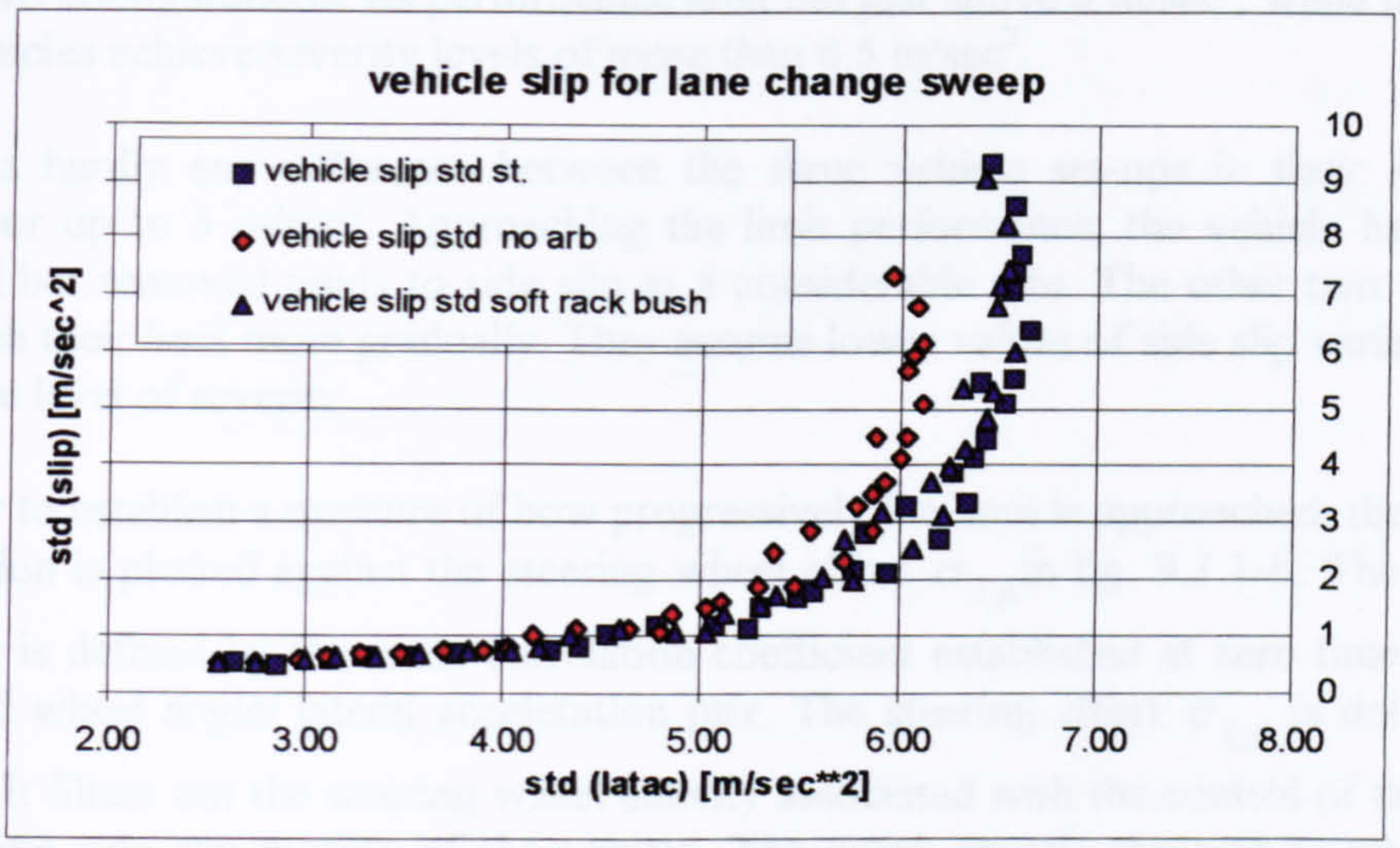

Fig. 9.3.1-5 Comparison of the side slip motion given as a function of manoeuvre severity

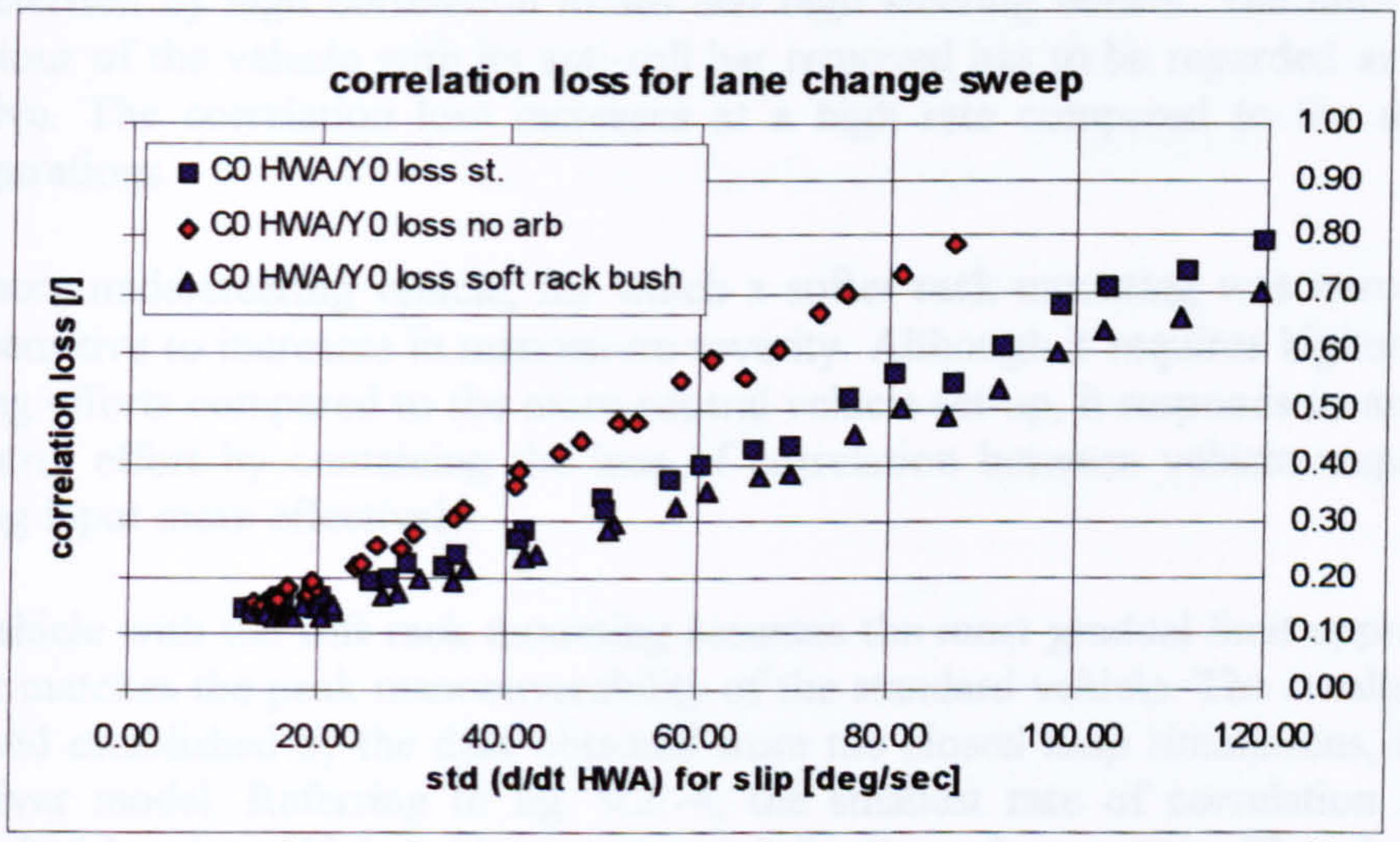

Fig. 9.3.1-6 correlation loss for the lateral acceleration vs. steering effort due to vehicle side slip

Fig 9.3.1-5 gives an indication of each vehicle's side slip motion during the lane change sweep manoeuvre. The side slip parameter $\sigma_{\dot{\beta}}$ was introduced in section 7.1.2 to establish a measure of the yaw motion in relation to the lateral acceleration. In fig. 9.3.1-5 the values of the side slip variation $\sigma_{\dot{\beta}}$ are plotted against the manoeuvre severity, as defined by the standard deviation of the lateral acceleration. It resembles the handling diagram used for describing the steady state cornering performance. It indicates the rate of change of the vehicle's side slip response with severity, as well as the peak performance, as given by the maximum standard deviation of the lateral

acceleration.

The graph shows that the more neutral vehicle is less manoeuvrable compared to the other two configurations. Its performance limit lies just above 6 m/sec^2, while the other two vehicles achieve severity levels of more than 6.5 m/sec^2.

There is hardly any difference between the three vehicle set-ups in their side slip behaviour up to 5 m/sec^2. Approaching the limit performance, the vehicle having its anti-roll bar removed tends to side slip at a considerable rate. The other two vehicles approach their limit more gradually. They assume lower values of side slip variations at the same level of severity.

In order to establish a measure of how progressively the limit is approached, the loss of correlation is plotted against the steering wheel effort $\sigma_{\dot{\delta},\beta}$ in fig. 9.3.1-6. The former quantity is defined by the cross-correlation coefficient established at zero time lag for the hand wheel angle/ lateral acceleration pair. The steering effort $\sigma_{\dot{\delta},\beta}$ is defined by (7.1.3). It filters out the steering wheel activity associated with the control of the more demanding side slip motion of the vehicle. The graph reveals the rate at which the vehicle's response quality deteriorates with severity. The more severe manoeuvres are characterised by high correlation losses and high steering efforts. The limit response behaviour of the vehicle with its anti-roll bar removed has to be regarded as the most sensitive. The correlation loss increases at a high rate compared to the alternative configurations.

The more understeering vehicle, for which a softer rack mounting was introduced, is least sensitive to increases in manoeuvre severity. Although it requires higher absolute steering efforts compared to the more neutral vehicle set-up, it responds to an increase in control effort by containing the loss of correlation between vehicle response and steering input more effectively.

The vehicle with the soft rack mounting assumes the most gradual limit approach and almost matches the peak manoeuverability of the standard vehicle. The results confirm the trend established by the data obtained from the closed loop simulations, involving the driver model. Referring to fig. 9.2.-4, the smallest rate of correlation loss was established by the vehicle with a more compliant steering system. The closed loop simulations also established that this set-up provides the fastest lateral acceleration response, as can be seen from fig. 9.2.-2.

Referring back to the summaries of the test results, given in sections 7.3.3 and 7.3.4, it can be concluded that the more understeering vehicle set-up would be rated highest. There, it was said that the assessment of vehicle handling is predominantly based upon the rate of change in the response behaviour rather than on the limit performance. The two highly rated vehicle set-ups tested on the proving ground ('M2/XY', 'XY/XY') responded quickly to the steering input. Their response times were low and increased only by a small rate with severity. Furthermore, these two vehicle set-ups were

characterised by a low gradient of the correlation loss with steering effort.

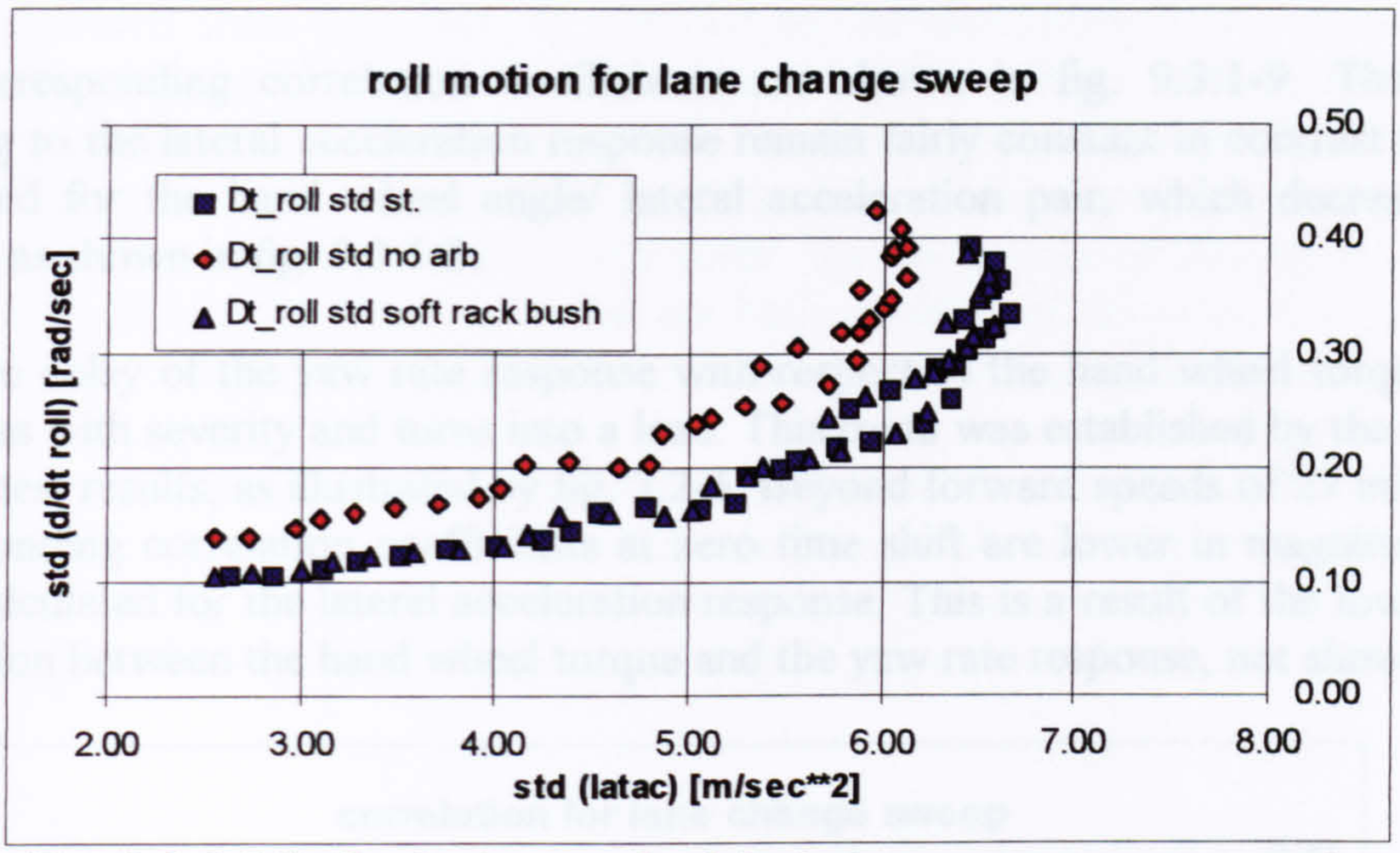

Fig. 9.3.1-7 Roll velocity standard deviation vs. manoeuvre severity represented by the standard deviation of the lateral acceleration

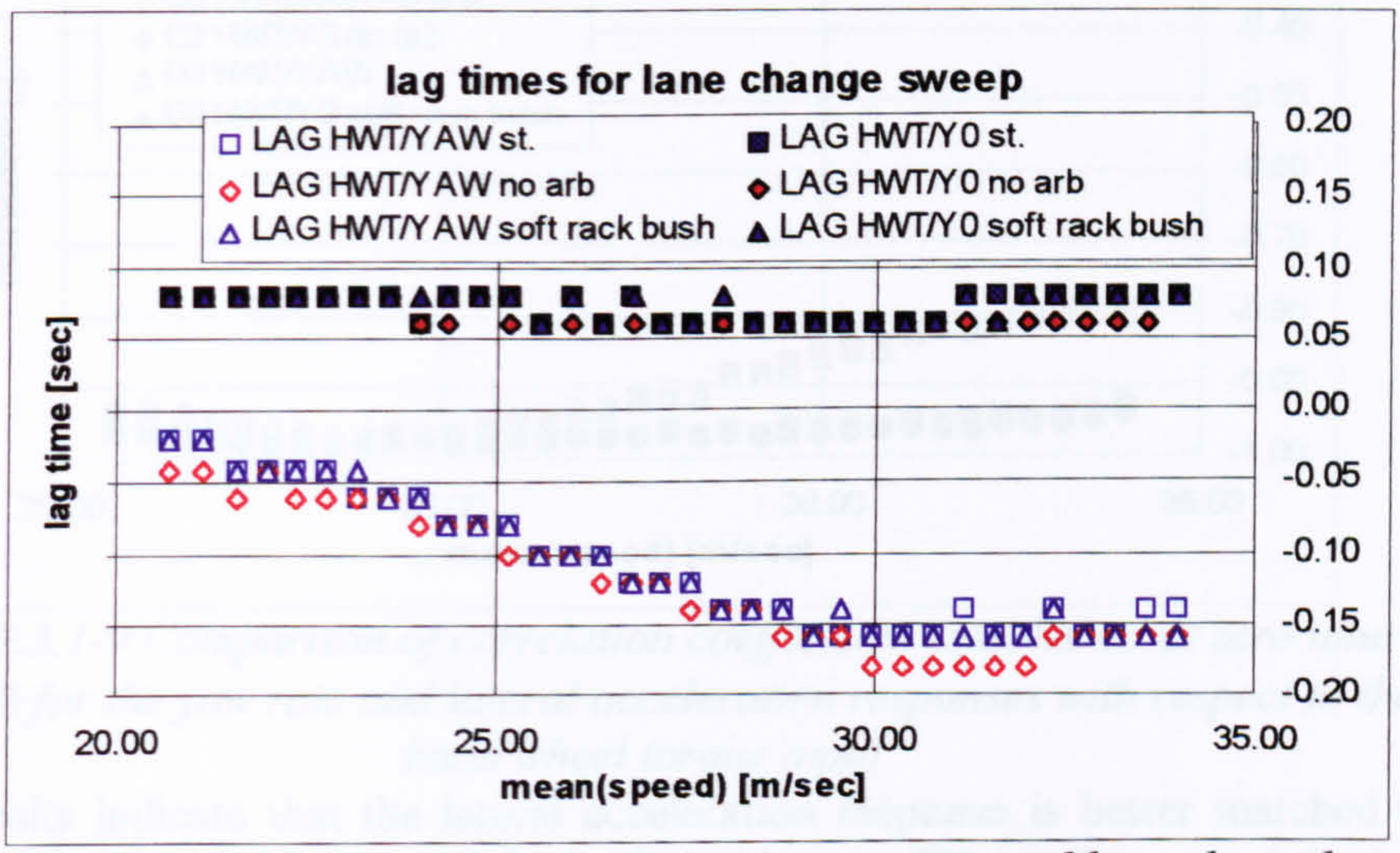

Fig. 9.3.1-8 Comparison of lag times for the yaw rate and lateral acceleration responses with respect to the hand wheel torque input

The increase of the roll motion for the vehicle with its anti-roll bar removed is illustrated by fig. 9.3.1-7. The standard deviation of the roll velocity is plotted against the manoeuvre severity.

So far, the discussion concentrated on the response behaviour with respect to the steering angle input. Correlation coefficients and time lags with regard to the hand wheel torque are given below. Figure 9.3.1-8 indicates that the response delay of the lateral acceleration is shorter with respect to the torque input compared to the corresponding characteristic established for the steering wheel input shown in fig. 9.3.1-4. The response time lag with respect to the hand wheel torque remains constant throughout the speed and severity range, yielding a relatively higher correlation at $\tau=0$

than established for the steering wheel angle/ lateral acceleration pair.

The corresponding correlation coefficients are shown in fig. 9.3.1-9. The values referring to the lateral acceleration response remain fairly constant in contrast to those calculated for the hand wheel angle/ lateral acceleration pair, which decrease with severity as shown in fig. 9.3.1-3.

The time delay of the yaw rate response with respect to the hand wheel torque input decreases with severity and turns into a lead. This trend was established by the proving ground test results, as illustrated by fig. 7.2-5. Beyond forward speeds of 27 m/sec, the corresponding correlation coefficients at zero time shift are lower in magnitude than those calculated for the lateral acceleration response. This is a result of the lower peak correlation between the hand wheel torque and the yaw rate response, not shown here.

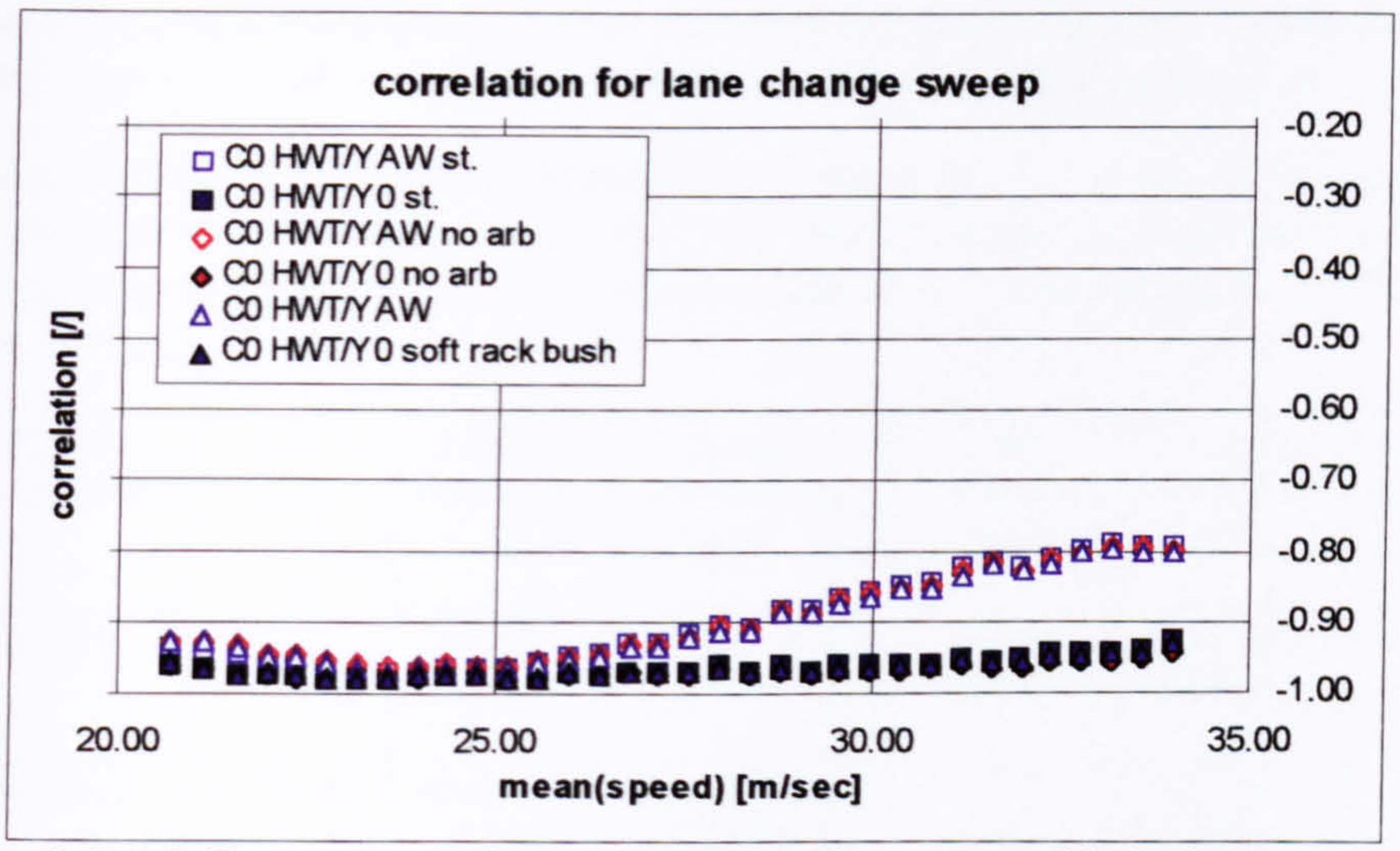

Fig. 9.3.1-9 Comparison of correlation coefficients established at zero time lag τ*=0 for the yaw rate and lateral acceleration responses with respect to the hand wheel torque input*

These results indicate that the lateral acceleration response is better matched to the hand wheel torque than to the hand wheel angle input. This applies especially for high severity manoeuvres. The hand wheel torque feedback seems to be a fast indicator of the manoeuvre severity.

In the following sections, results concerning the hand wheel torque characteristics are omitted. The parameter variations concerning suspension as well as tyre properties, which are discussed further on, had no significant influence on this characteristic.

summary

Although the proposed open loop 'lane change sweep' test failed to reproduce peak correlation coefficients decreasing with severity, as obtained from the proving ground data, it provided similar trends for other characteristics. The simulation results led to

lag times and correlation coefficients at zero time lag of comparable magnitudes to those calculated from test data. In contrast to the simulation based results, those derived from the proving ground data suggest that the vehicle with its anti-roll bar removed provides a slightly faster response than the standard set-up (fig. 7.3.4-3, 4) and maintains a higher correlation coefficient at zero time lag for the lateral acceleration response (fig. 7.3.4-5). However, the simulation results agree with the trend established by fig. 7.3.4-6, in that the limit handling of the more neutral vehicle deteriorates by a higher rate compared to the behaviour of the standard car.

The more neutral steering set-up proved to be less manoeuverable, and its response behaviour deteriorated at a higher rate than was the case for the other two set-ups. The more understeering vehicle achieved the same level of manoeuverability as the standard car, but approached the limit with a smaller rate of response loss.

9.3.2 Effects of first and second order suspension derivatives

An example of the effects of first order and second order suspension derivatives on the limit handling is given in this section. These properties control the rate of track and camber change with vertical wheel travel. In section 8.3 it was shown that these properties can be very influential in determining the steady state cornering performance of an axle. Their influence on the transient limit handling behaviour is analysed by comparing two alternative vehicle configurations to the standard set-up. The corresponding track change (scrub) and camber change characteristics are found in table 9.3.2-1. The scrub coefficients describe the track change as measured at ground level, as those given in tables 8.2-3 and 8.2-4.

For the first alternative configuration, second order properties were changed with respect to the standard set-up. The second order coefficients of the nominal front track and camber change were used for the rear suspension of 'vehicle B', while those of the nominal rear track and camber change were used for the front suspension.

The second vehicle alternative, denoted by 'vehicle C', involved exchanging the roll centre heights at the front and rear ends. The second order scrub properties and those for the camber are identical to those of the standard car. The variations are highlighted in table 9.3.2-1.

vehicle configuration	half track width [m]	1. scrub derivative [/]	2. scrub derivative [1/m]		static camber [rad]	1. camber derivative [1/m]	2. camber derivative [1/m**2]
standard	0.750 fr. 0.764 rr.	-0.1295 fr. -0.1934 rr.	-1.8550 fr. -1.4164 rr.		0.0 fr. 0.0 rr.	0.2751 fr. 0.6818 rr.	-7.0224 fr. -2.3912 rr.
vehicle B	0.750 fr. 0.764 rr.	-0.1295 fr. -0.1934 rr.	-1.4164 fr. -1.8550 rr.		0.0 fr. 0.0 rr.	0.2751 fr. 0.6818 rr.	-2.3912 fr. -7.0224 rr.
vehicle C	0.750 fr. 0.764 rr.	-0.1934 fr. -0.1295 rr.	-1.8550 fr. -1.4164 rr.		0.0 fr. 0.0 rr.	0.2751 fr. 0.6818 rr.	-7.0224 fr. -2.3912 rr.

Table 9.3.2-1 Suspension derivatives for the track and camber change characteristics

The graph given in fig. 9.3.2-1 indicates that comparable levels of manoeuvre severity were established for the three configurations. For each of the three vehicles, very similar peak magnitudes and standard deviations of the lateral acceleration were computed from the corresponding time histories.

As was the case for the results presented in the previous section, peak correlation coefficients remained at a high level near the ideal value of one. However, response delay times and consequently correlation coefficients established at zero time shift changed with severity, as shown in figures 9.3.2-2, 3.

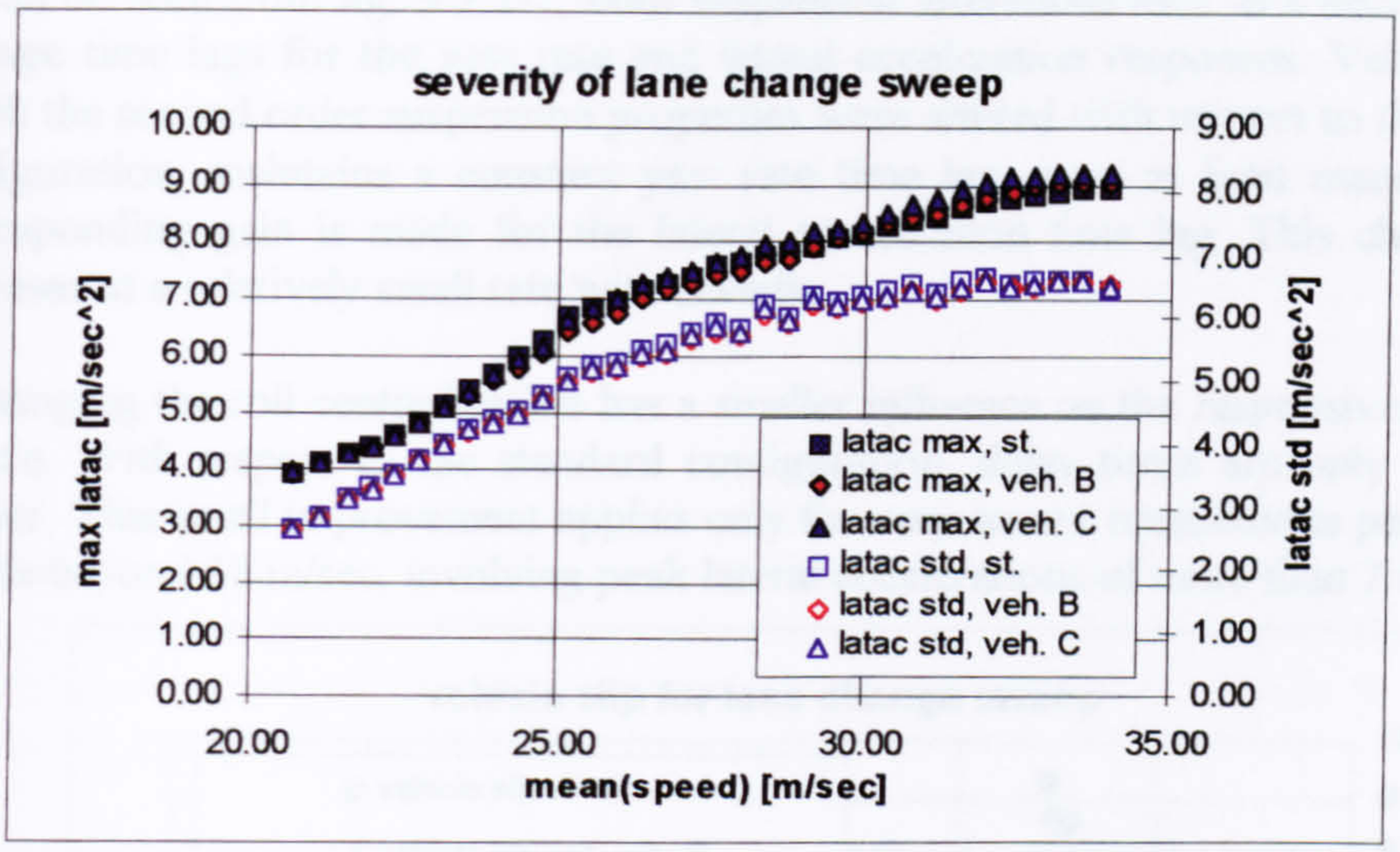

Fig. 9.3.2-1 Manoeuvre severity vs. vehicle speed

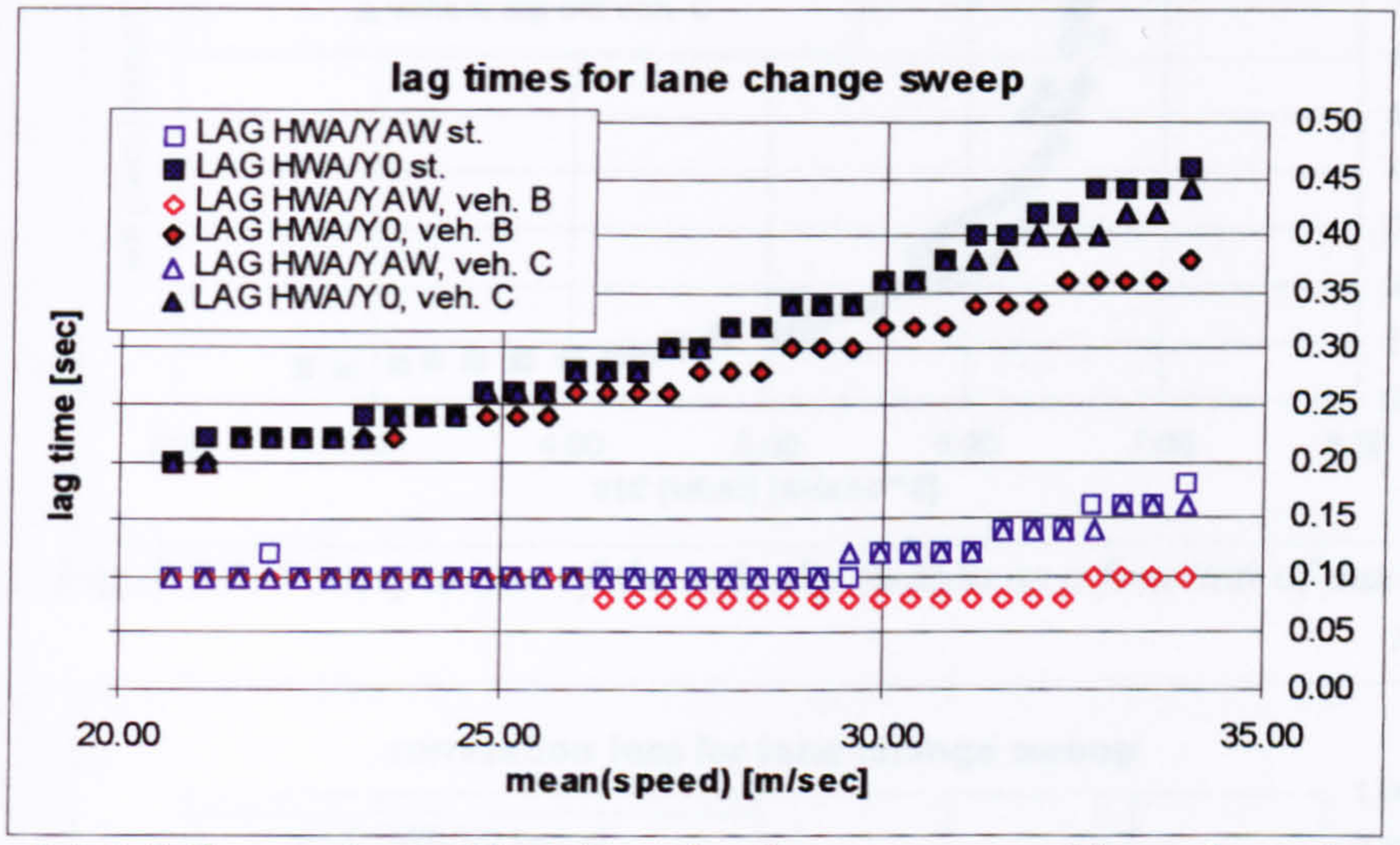

Fig. 9.3.2-2 Comparison of lag times for the yaw rate and lateral acceleration responses

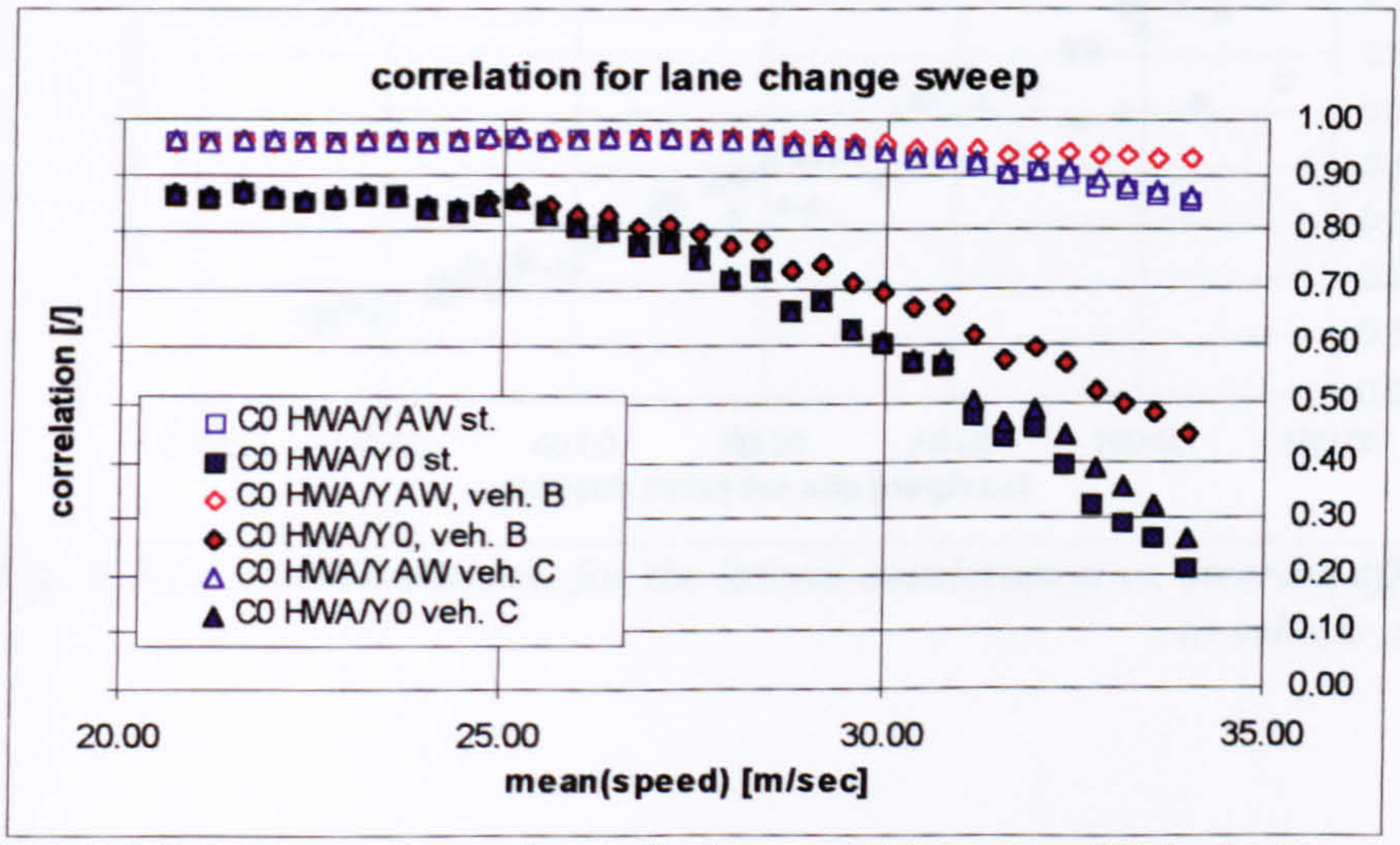

Fig. 9.3.2-3 Comparison of correlation coefficients established at zero time lag τ=0 for the yaw rate and lateral acceleration responses

As can be seen from fig. 9.3.2-2, both suspension alterations lead to a decrease in the average time lags for the yaw rate and lateral acceleration responses. Vehicle B, for which the second order suspension properties were altered with respect to the standard configuration, maintains a constant yaw rate time lag, even at limit manoeuvres. A corresponding gain is made for the lateral acceleration time lag. This characteristic increases at a relatively small rate with severity.

Exchanging the roll centre heights has a smaller influence on the responsiveness of the vehicle. With respect to the standard configuration, delay times are only marginally shorter. This small improvement applies only for very severe manoeuvres performed at speeds beyond 30 m/sec, involving peak lateral accelerations of more than 7 m/sec^2.

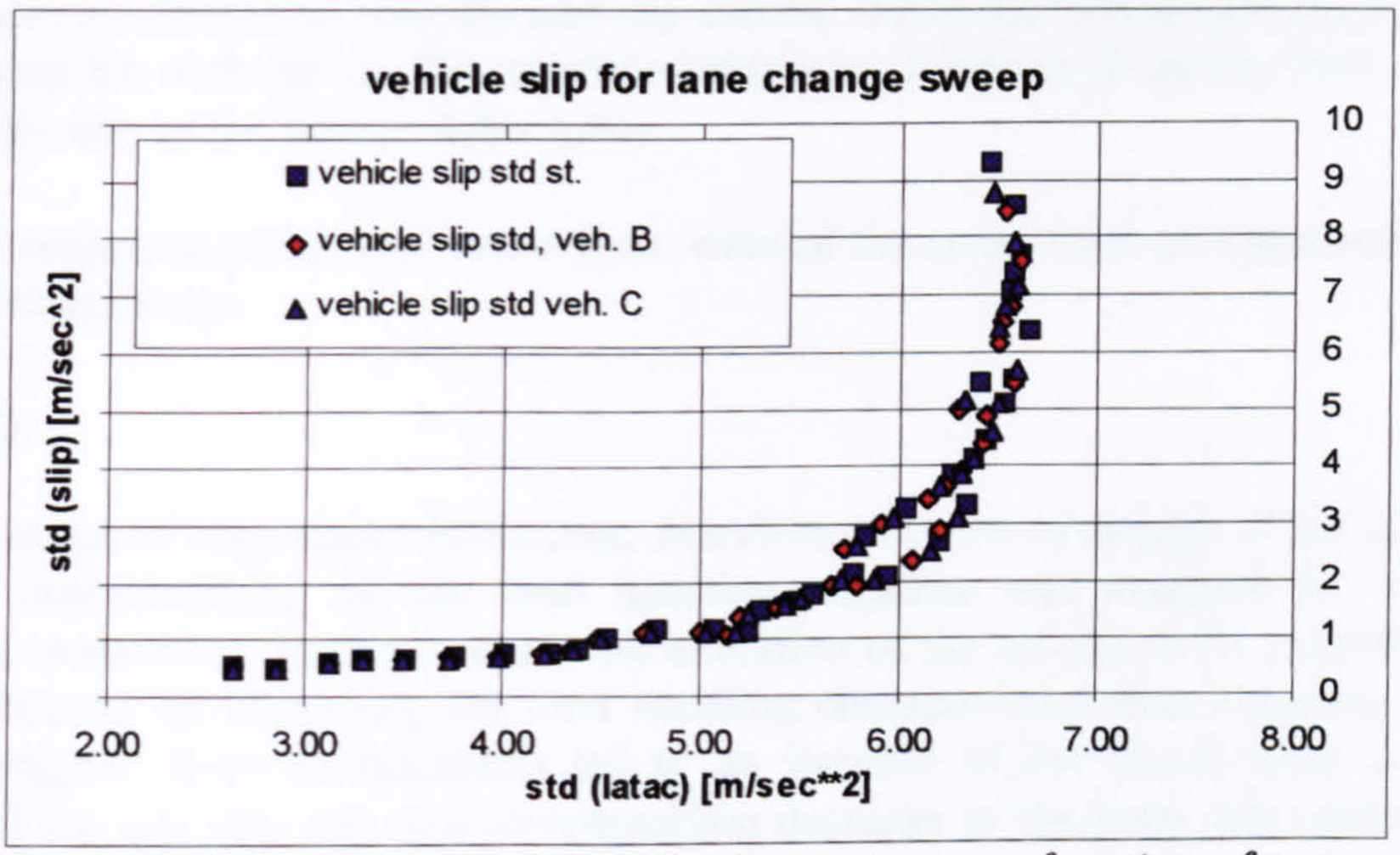

Fig. 9.3.2-4 Comparison of the side slip motion as a function of manoeuvre severity

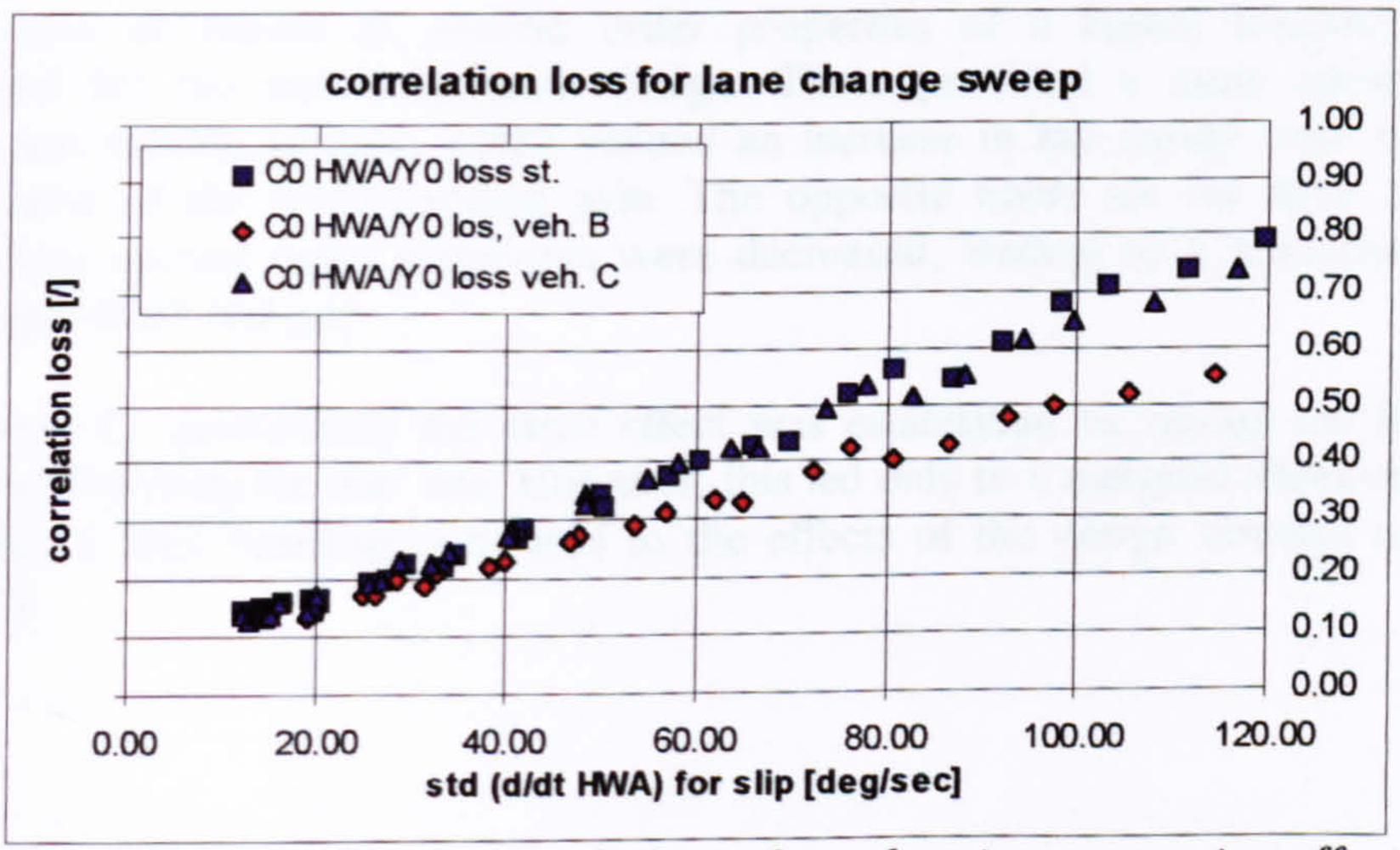

Fig. 9.3.2-5 Correlation loss for the lateral acceleration vs. steering effort due to vehicle side slip

The same trends, as established by the lag times, apply to the correlation coefficients obtained at zero time lag for the hand wheel angle/ yaw rate and hand wheel angle/ lateral acceleration pairs (fig. 9.3.2-3).

The side slip motion of the three configurations is illustrated by fig. 9.3.2-4. The side slip increases with severity for each design at the same progression rate. Furthermore, it can be established that the peak severity, or manoeuverability, is given by a value of 6.5 m/sec^2 for each specimen.

The sensitivity of the control quality to severity can be established from fig. 9.3.2-5, showing the correlation loss for the lateral acceleration plotted against the steering wheel activity associated with the side slip control. Since the vehicle side slip behaviour is the same for each set-up, the response behaviour of vehicle B proves least sensitive to severity due to the shorter delay times.

The roll angle variations, not shown here, were of the same order of magnitude for the three configurations.

<u>summary</u>

The influence of suspension derivatives, describing the rate of change of the scrub and camber characteristics, on the limit handling response was analysed for a severe transient manoeuvre. In this example the alteration of the second order properties was more effective for improving the limit handling characteristics than adjusting the roll centre heights. Both modifications led to an increase of the steady state cornering power of the rear axle and to a corresponding decrease of the front axle performance, as was demonstrated in section 8.8.

In the case of vehicle B, second order properties of a higher magnitude were introduced for the rear suspension design. These provided a more advantageous camber and jacking control, which yielded an increase in the steady state cornering performance of the corresponding axle. The opposite holds for the front axle, for which these second order properties were decreased, leading to a reduction of the steady state front end grip.

For vehicle C, qualitatively the same effect was established by raising the front roll centre and lowering the rear one. However, this led only to a marginal improvement of the vehicle's limit handling compared to the effects of the design changes made for vehicle B.

9.3.3 Combining McPherson type and double wishbone suspensions

A further example of the effects of suspension derivatives on the limit handling is given in this section. Simulations of two alternative vehicles were carried out. The first alternative vehicle, denoted by 'MP/DW', features a McPherson type suspension at the front end and a double wishbone design at the rear end. For the other vehicle the opposite set-up was chosen. The corresponding lateral scrub and camber change characteristics can be found in table 9.3.3-1.

In comparison to the standard car, the first alternative configuration features a lower roll centre at the front, but a more pronounced second order scrub characteristic. The roll angle compensation is smaller. The second order camber property is positive, which defines a decreasing roll angle compensation with increasing bump travel.

For the second vehicle alternative, denoted by 'DW/MP', the rear roll centre height was raised slightly. The McPherson strut assembly gives a more pronounced second order track change at the rear end, but provides less control of the camber changes compared to the double wishbone layout of the standard car.

vehicle configuration	half track width [m]	1. scrub derivative [/]	2. scrub derivative [1/m]		static camber [rad]	1. camber derivative [1/m]	2. camber derivative [1/m**2]
standard	0.750 fr. 0.764 rr.	-0.1295 fr. -0.1934 rr.	-1.8550 fr. -1.4164 rr.		0.0 fr. 0.0 rr.	0.2751 fr. 0.6818 rr.	-7.0224 fr. -2.3912 rr.
MP/DW	0.750 fr. 0.764 rr.	-0.0834 fr. -0.1934 rr.	-4.0564 fr. -1.4164 rr.		0.0 fr. 0.0 rr.	0.2119 fr. 0.6818 rr.	4.4906 fr. -2.3912 rr.
DW/MP	0.750 fr. 0.764 rr.	-0.1295 fr. -0.1713 rr.	-1.8550 fr. -4.0704 rr.		0.0 fr. 0.0 rr.	0.2751 fr. 0.3186 rr.	-7.0224 fr. 4.2310 rr.

Table 9.3.3-1 Suspension derivatives for the track and camber change characteristics

Comparable levels of manoeuvre severity were established for the three configurations, very similar to those shown in fig. 9.3.2-1. As can be seen from fig. 9.3.3-1, there is little difference between the delay times established for the standard car and those obtained for the vehicle with a McPherson type front suspension. The vehicle for which the double wishbone rear suspension was replaced with a McPherson strut design, denoted by 'DW/MP', seems to give an advantage in the speed range 27-33 m/sec, in which peak accelerations beyond 7 m/sec^2 are established. The delay times are slightly lower and even decrease slightly for the yaw rate response. For manoeuvres performed at even higher speeds and slightly higher severity levels, this advantage is lost however.

Fig. 9.3.3-2 shows the vehicle side slip measure $\sigma_{\dot{\beta}}$ plotted against manoeuvre severity. There is hardly any difference between the three set-ups. All three achieve the same peak standard deviation for the lateral acceleration.

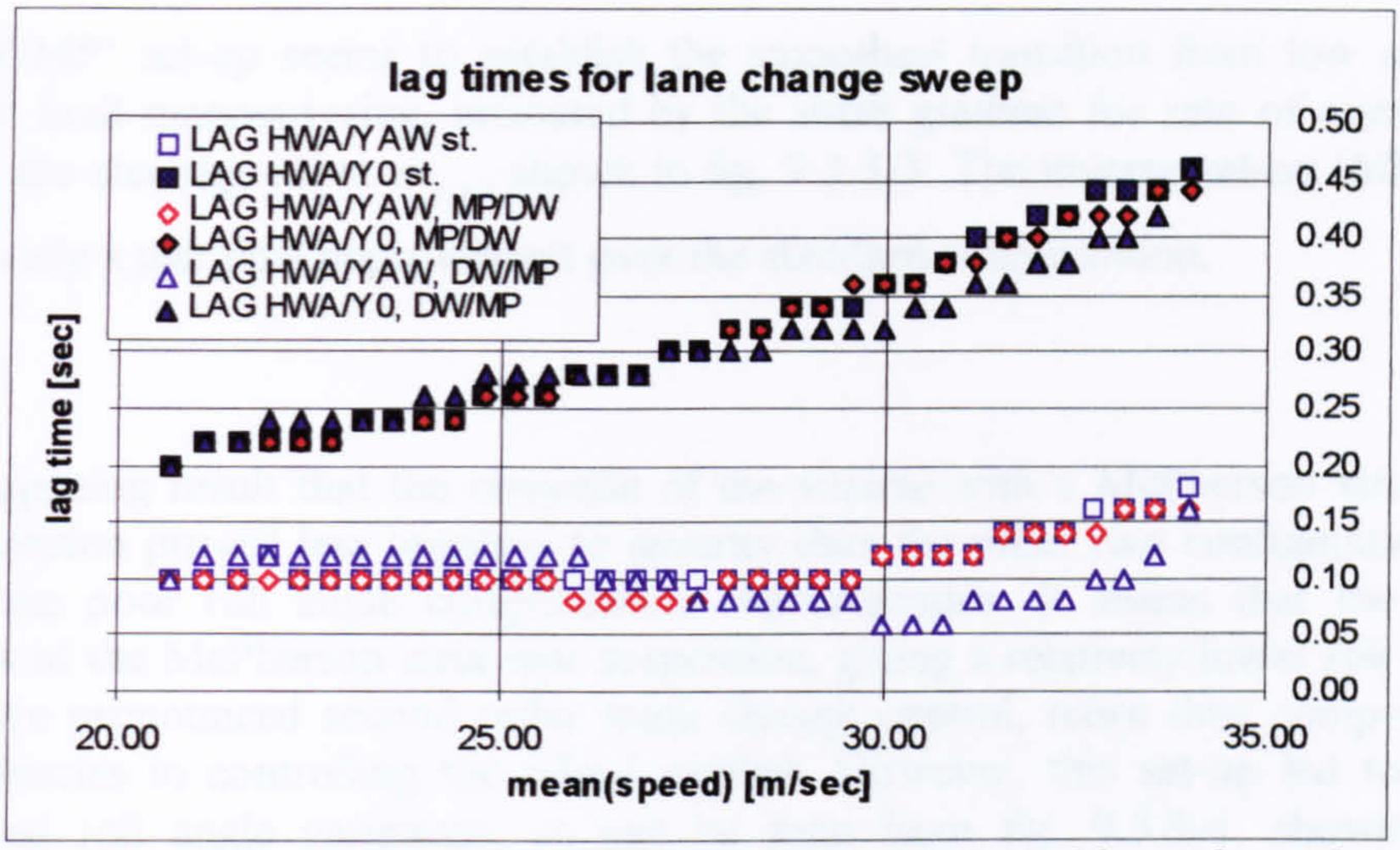

Fig. 9.3.3-1 Comparison of lag times for the yaw rate and lateral acceleration responses

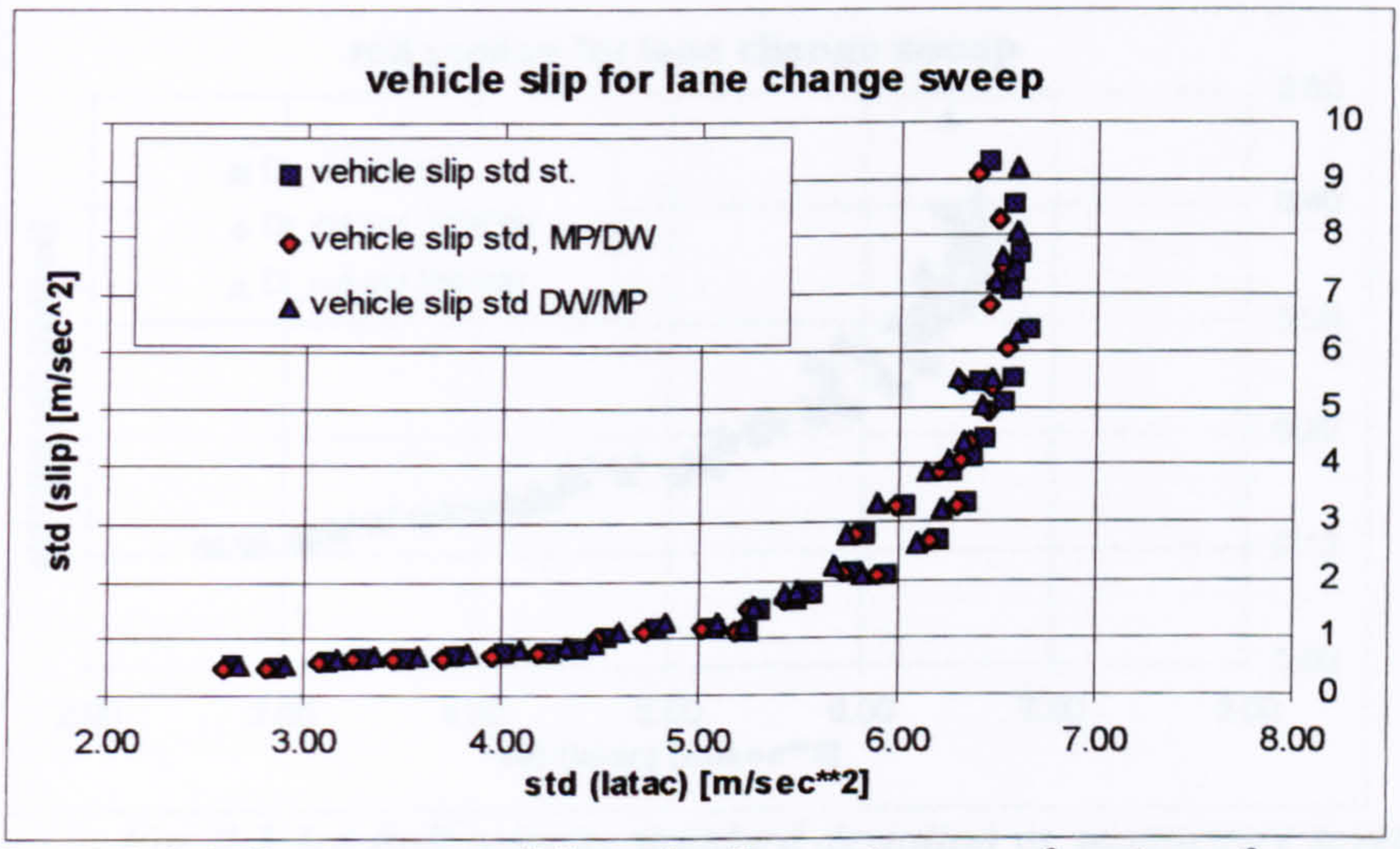

Fig. 9.3.3-2 Comparison of the side slip motion as a function of manoeuvre severity

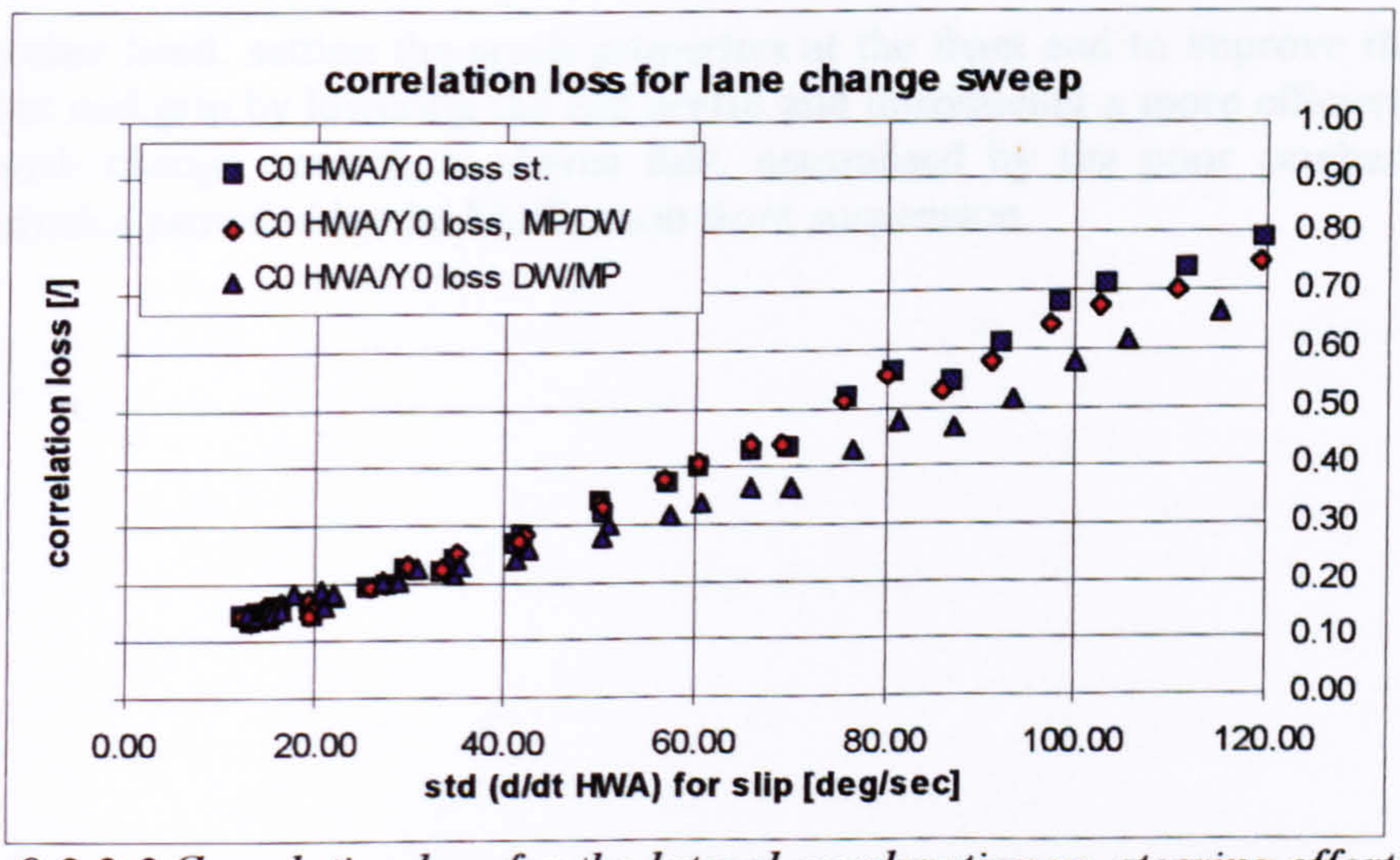

Fig. 9.3.3-3 Correlation loss for the lateral acceleration vs. steering effort due to vehicle side slip

The 'DW/MP' set-up seems to establish the smoothest transition from low severity driving to limit manoeuvering, indicated by the small gradient for rate of correlation loss with the steering effort $\sigma_{\dot{\delta},\beta}$, shown in fig. 9.3.3-3. The inverse set-up 'MP/DW' provides only a marginal improvement over the standard configuration.

summary

It is a surprising result that the response of the vehicle with a McPherson strut type rear suspension proved less sensitive to severity than the other two configurations, in spite of the poor roll angle compensation characteristics. It seems that the scrub properties of the McPherson strut rear suspension, giving a relatively lower roll centre and a more pronounced second order track change control, more than compensated the deficiencies in controlling the wheel camber. However, this set-up led to more pronounced roll angle variations, as can be seen from fig. 9.3.3-4, showing the standard deviation of the roll angle velocity against manoeuvre severity.

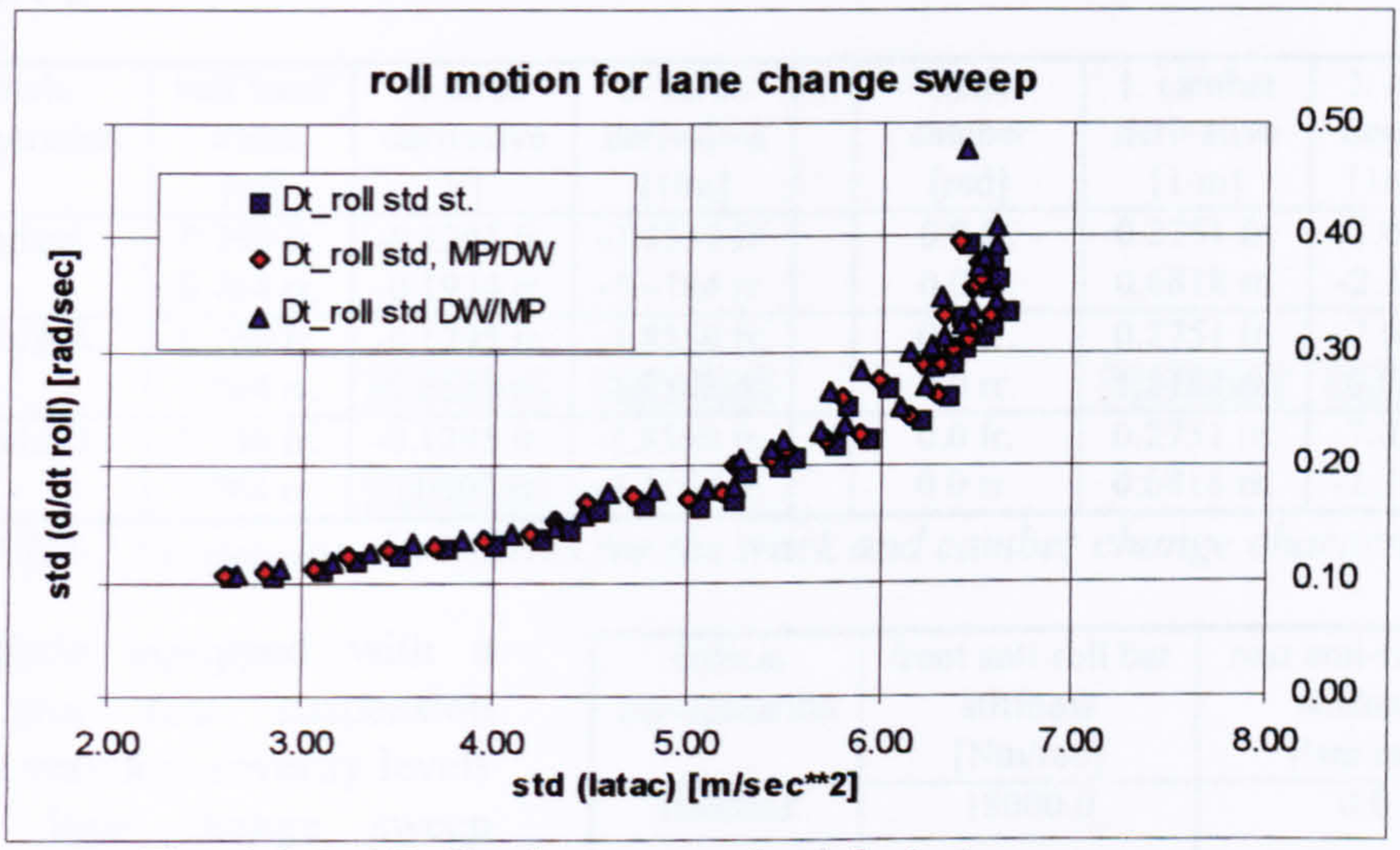

Fig. 9.3.3-4 Roll velocity standard deviation vs. manoeuvre severity represented by the standard deviation of the lateral acceleration

On the other hand, setting the scrub properties at the front end to improve the steady state front end grip by lowering the roll centre and introducing a more efficient second order track change control, is almost fully neutralised by the poor camber control characteristics provided by the McPherson front suspension.

9.3.4 Influence of modifications to the rear suspension

In this section results are discussed referring to the effects of alternative rear suspension designs on the limit handling behaviour. The double wishbone rear suspension of the standard vehicle was replaced by a swing axle suspension design with a radius arm of 0.55 m length. The swing axle layout provides a high roll centre by which the car's tendency to roll when cornering remains small in relation to the standard car so that a front anti-roll bar was not considered for this vehicle. This vehicle configuration is denoted by 'DW/SWA'.

Furthermore, the benchmark vehicle was simulated with a rear suspension giving a roll centre at ground level. In order to regain some of the roll stiffness lost by lowering the roll centre, a rear end anti-roll bar was introduced for this set-up, referenced by 'vehicle D'. The corresponding lateral scrub and camber change characteristics can be found in table 9.3.4-1, while the stiffness parameters for the anti-roll bars are given in table 9.3.4-2.

vehicle configuration	half track width [m]	1. scrub derivative [/]	2. scrub derivative [1/m]		static camber [rad]	1. camber derivative [1/m]	2. camber derivative [1/m**2]
standard	0.750 fr. 0.764 rr.	-0.1295 fr. -0.1934 rr.	-1.8550 fr. -1.4164 rr.		0.0 fr. 0.0 rr.	0.2751 fr. 0.6818 rr.	-7.0224 fr. -2.3912 rr.
DW/SWA	0.750 fr. 0.764 rr.	-0.1295 fr. -0.5555 rr.	-1.8550 fr. -1.8182 rr.		0.0 fr. 0.0 rr.	0.2751 fr. 1.8182 rr.	-7.0224 fr. 0.0000 rr.
vehicle D	0.750 fr. 0.764 rr.	-0.1295 fr. 0.0000 rr.	-1.8550 fr. -1.4164 rr.		0.0 fr. 0.0 rr.	0.2751 fr. 0.6818 rr.	-7.0224 fr. -2.3912 rr.

Table 9.3.4-1 Suspension derivatives for the track and camber change characteristics

vehicle configuration	front anti-roll bar stiffness [Nm/rad]	rear anti-roll bar stiffness [Nm/rad]
standard	18000.0	0.0
DW/SWA	0.0	0.0
vehicle D	18000.0	23410.0

Table 9.3.4-2 Anti-roll bar stiffness parameters

The vehicle equipped with a swing arm rear suspension achieved very low severity levels for the lane change sweep simulation, as shown in fig. 9.3.4-1. It neither achieves the peak lateral accelerations nor the standard deviations of the other two set-ups. Its manoeuverability seems far inferior to the other two vehicle configurations, which reach their limit at about 6.7 m/sec^2.

The response time lags as well as the correlation coefficients established at zero time shift are given in figures 9.3.4-2, and 9.3.4-3, respectively. These graphs illustrate the poor behaviour of the swing axle equipped vehicle. Its response times increase at a considerable rate beyond a severity level of 5 m/sec^2. For the high speed manoeuvres at speeds beyond 30 m/sec, the lag times remain fairly constant corresponding to almost constant severity levels. The correlation coefficients established at zero time lag

continue to decrease, which is due to the speed dependency of this characteristic as discussed in section 7.1.1.

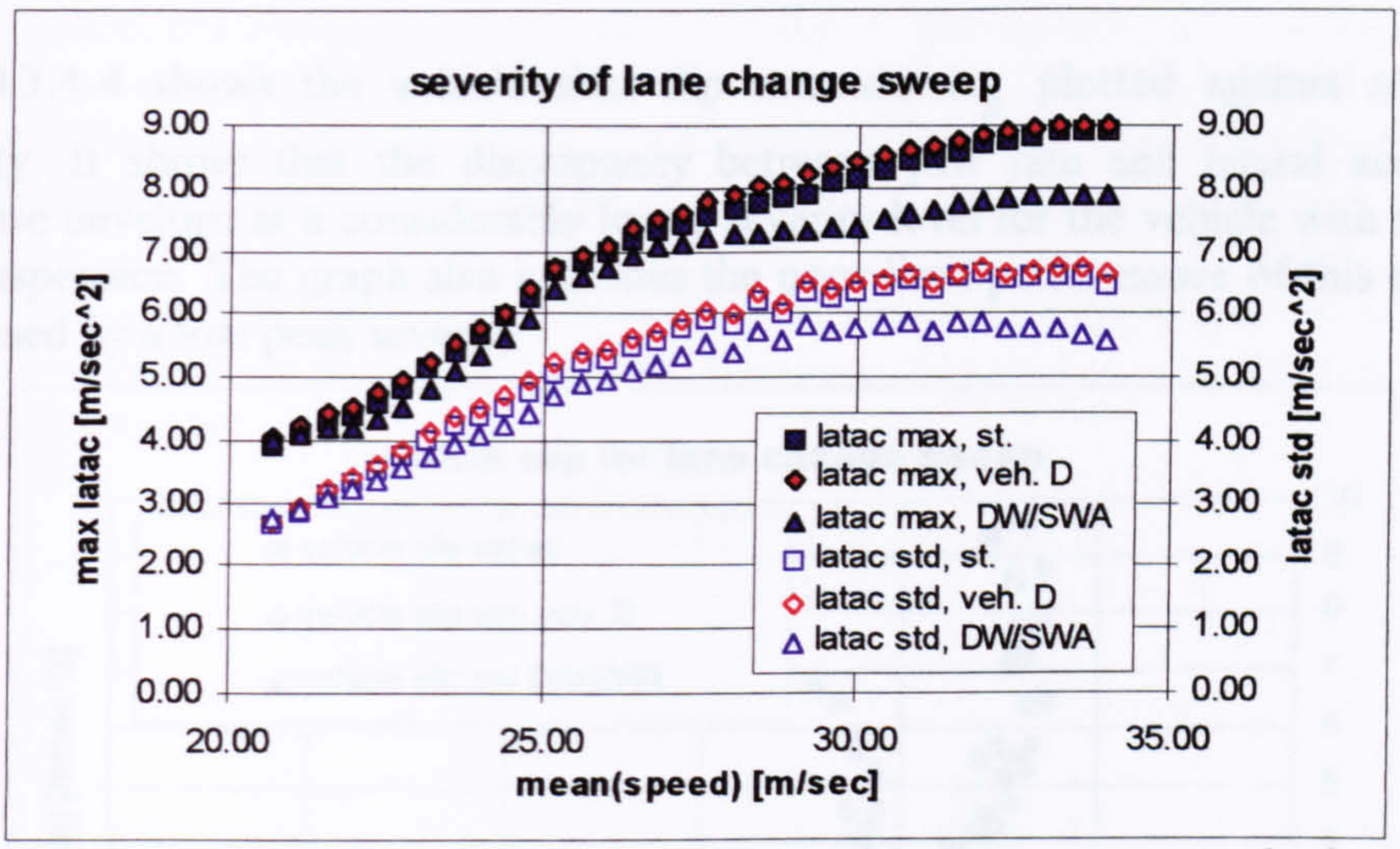

Fig. 9.3.4-1 Manoeuvre severity for a lane change sweep vs. vehicle speed

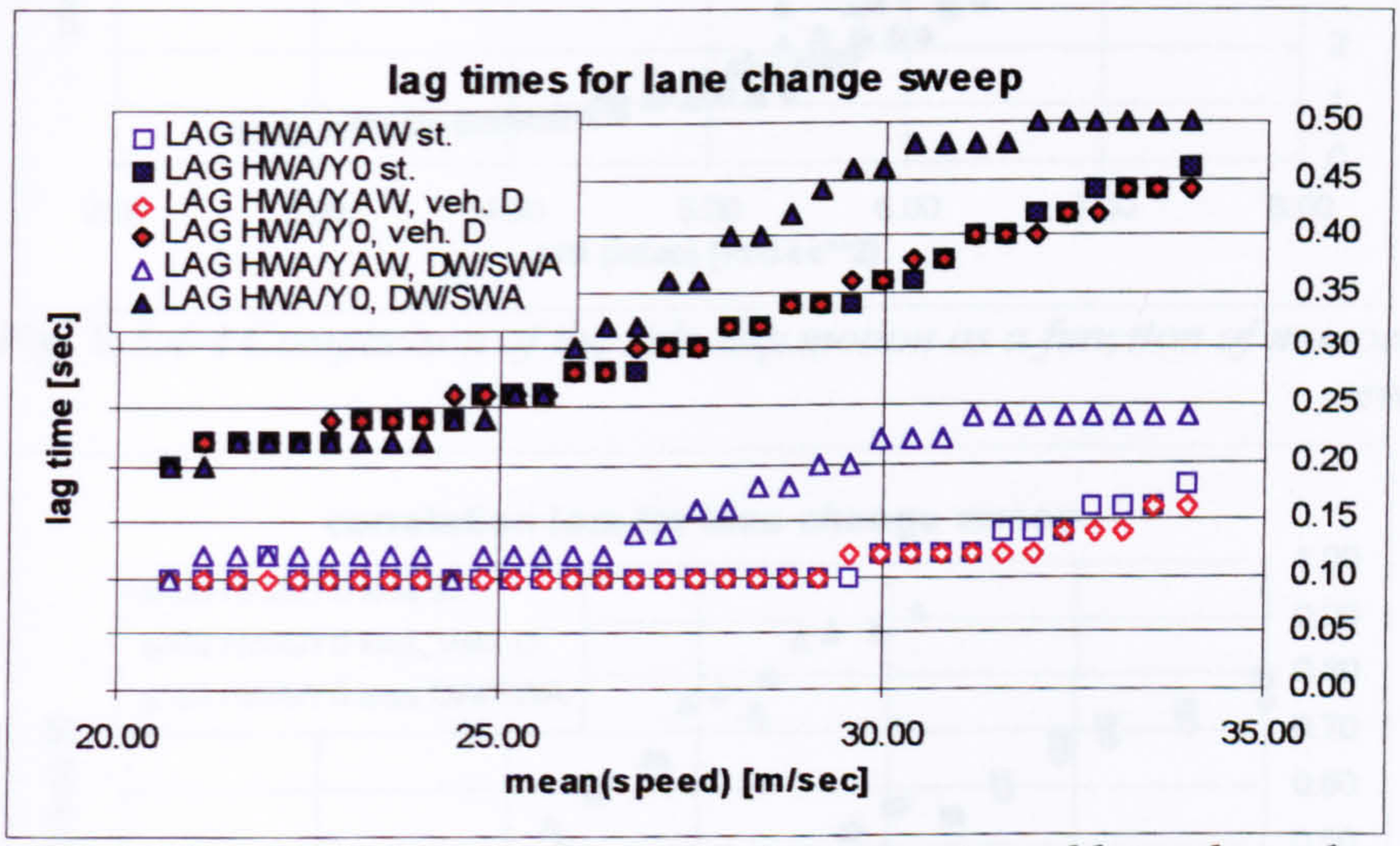

Fig. 9.3.4-2 Comparison of lag times for the yaw rate and lateral acceleration

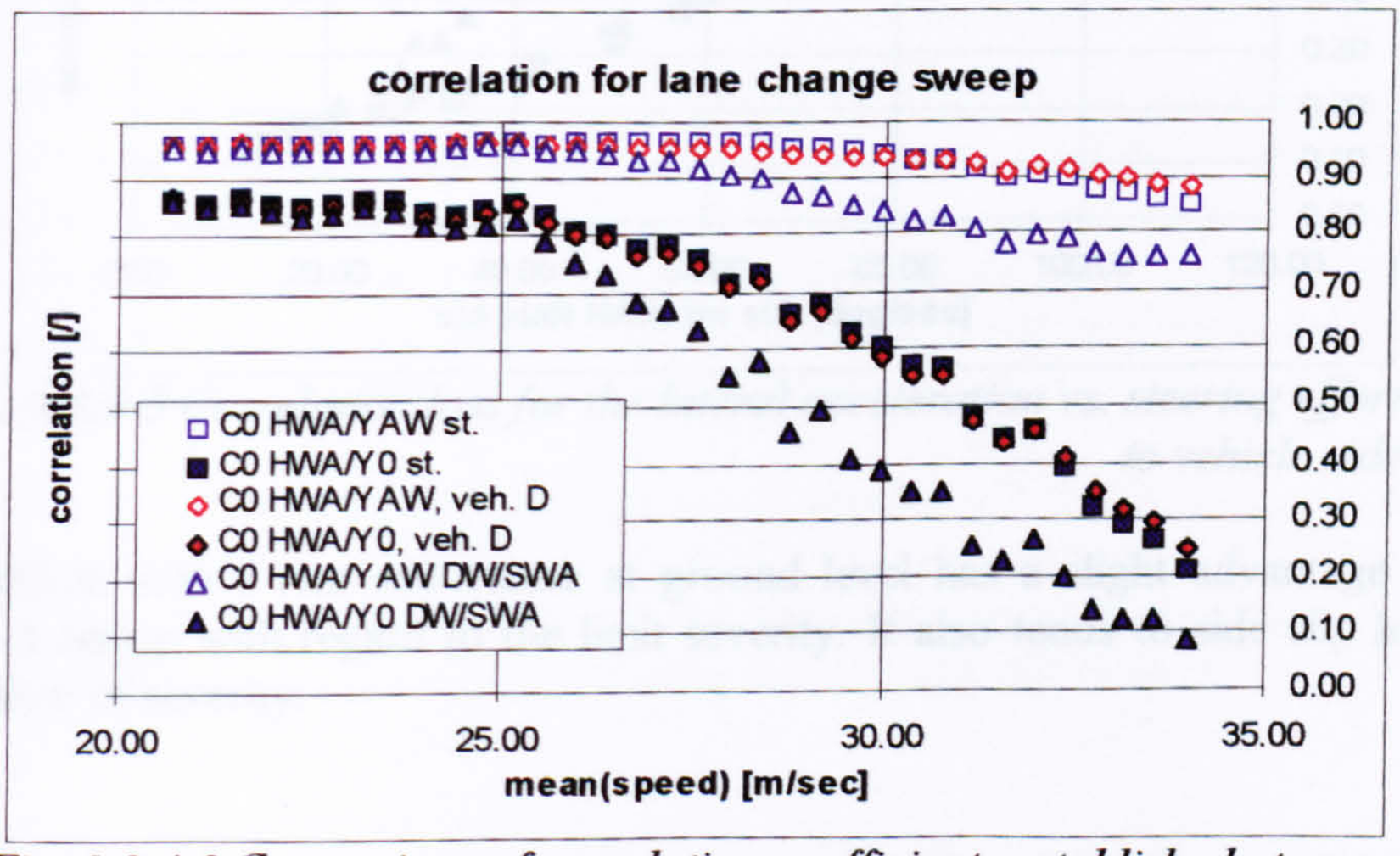

Fig. 9.3.4-3 Comparison of correlation coefficients established at zero time lag τ=0 for the yaw rate and lateral acceleration responses

Vehicle D seems to give little advantage compared to the standard car. Response lag times and the corresponding correlation coefficient are almost equal.

Fig. 9.3.4-4 shows the vehicle side slip measure $\sigma_{\dot{\beta}}$ plotted against manoeuvre severity. It shows that the discrepancy between yaw rate and lateral acceleration response develops at a considerably lower severity level for the vehicle with the swing arm suspension. The graph also indicates the poor limit performance of this design, as expressed by a low peak severity.

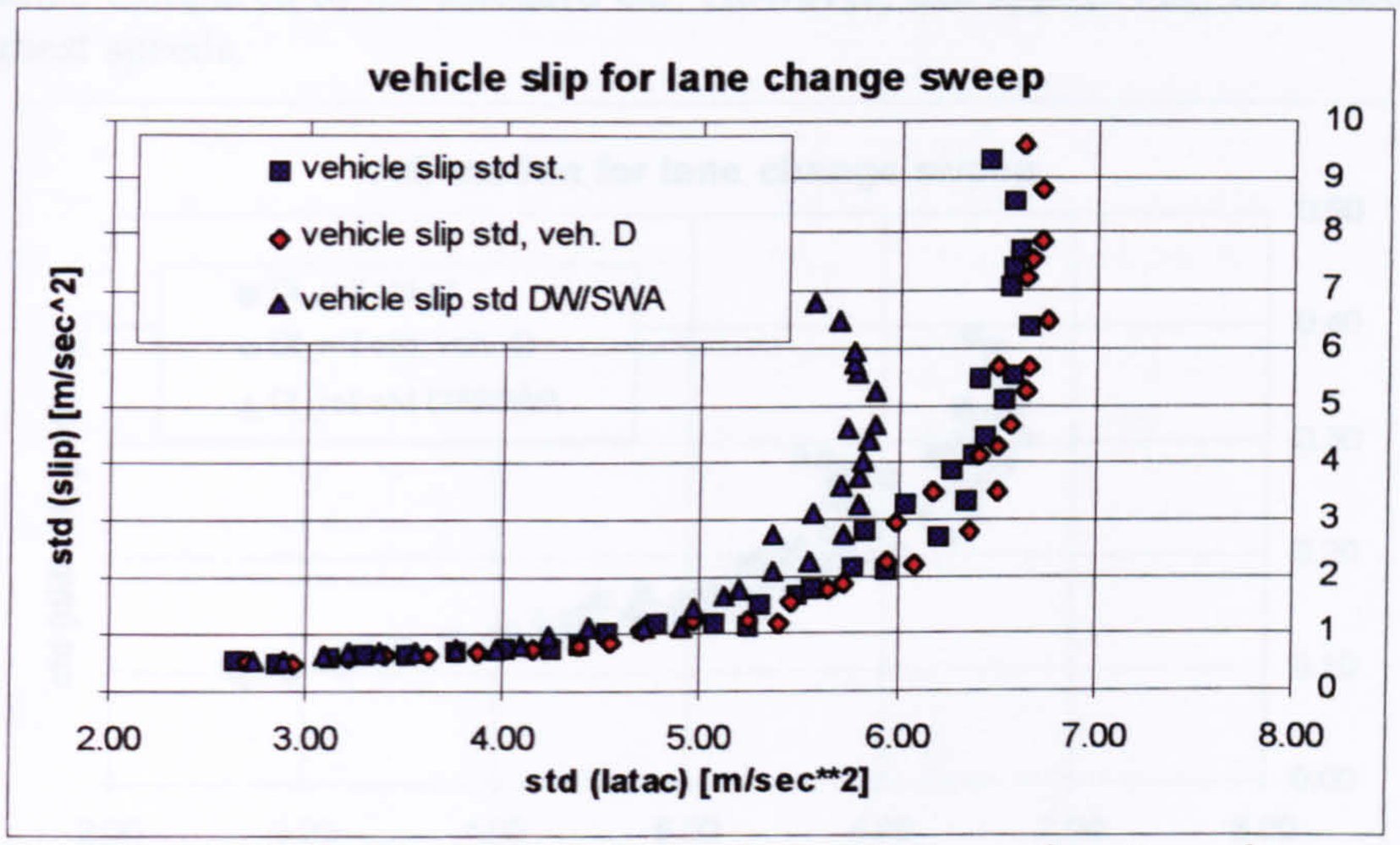

Fig. 9.3.4-4 Comparison of the side slip motion as a function of manoeuvre severity

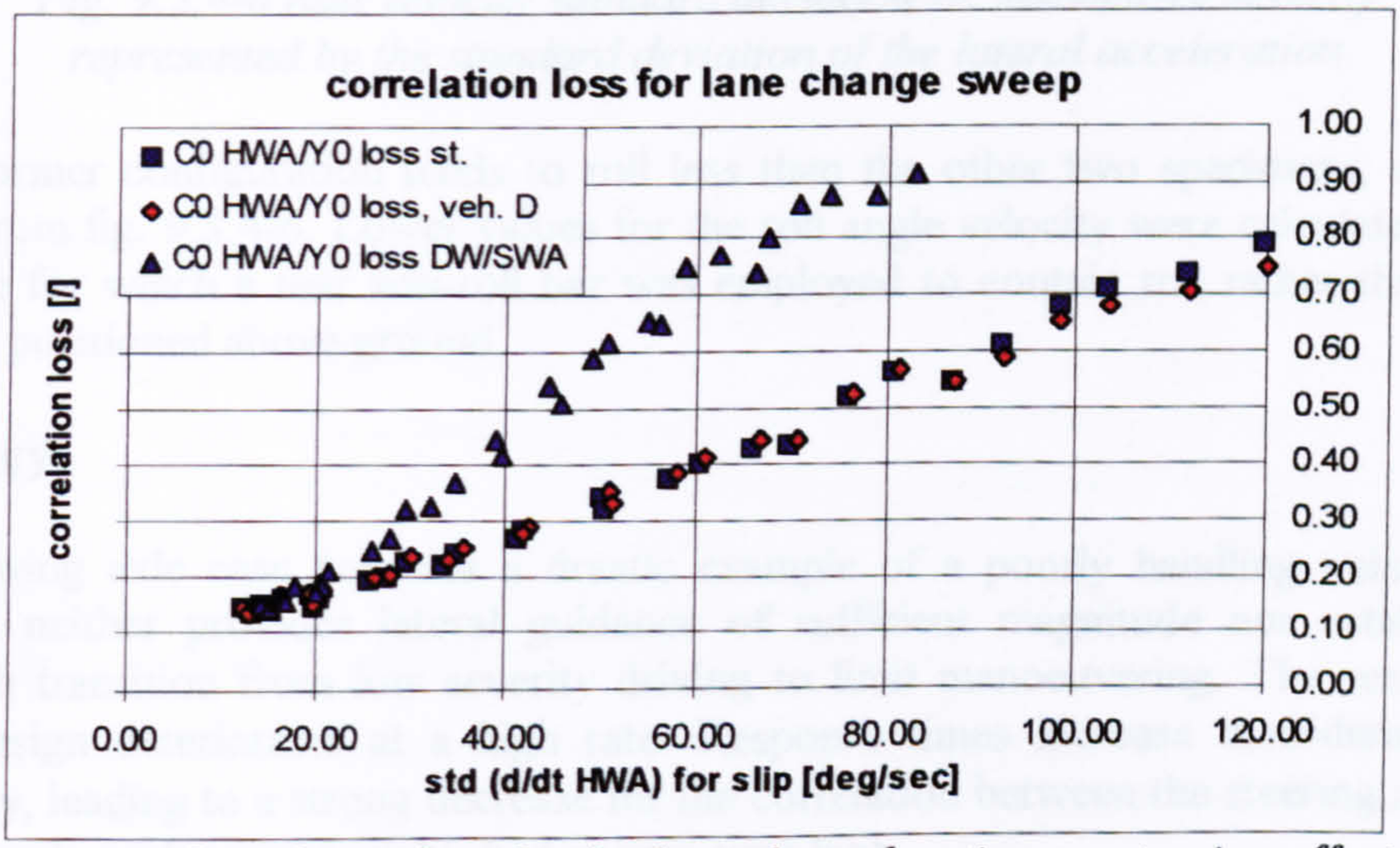

Fig. 9.3.4-5 Correlation loss for the lateral acceleration vs. steering effort due to vehicle side slip

The vehicle with a rear roll centre at ground level has a slight advantage over the standard set-up with regard to the limit severity. It also tends to side slip less at the same level of severity.

The poor limit handling behaviour of the swing axle equipped car and the slight advantage of vehicle D with respect to the standard car is further illustrated by fig. 9.3.4-5. The correlation between steering input and lateral acceleration response deteriorates at a high rate for the swing axle vehicle. The absolute values for the steering effort are lower for the limit manoeuvres, because of the comparatively low severity levels achieved by this design.

For the other alternative design, vehicle D, a slightly lower rate for the correlation loss is assumed compared to the standard car. However, this applies only for manoeuvres at the highest speeds.

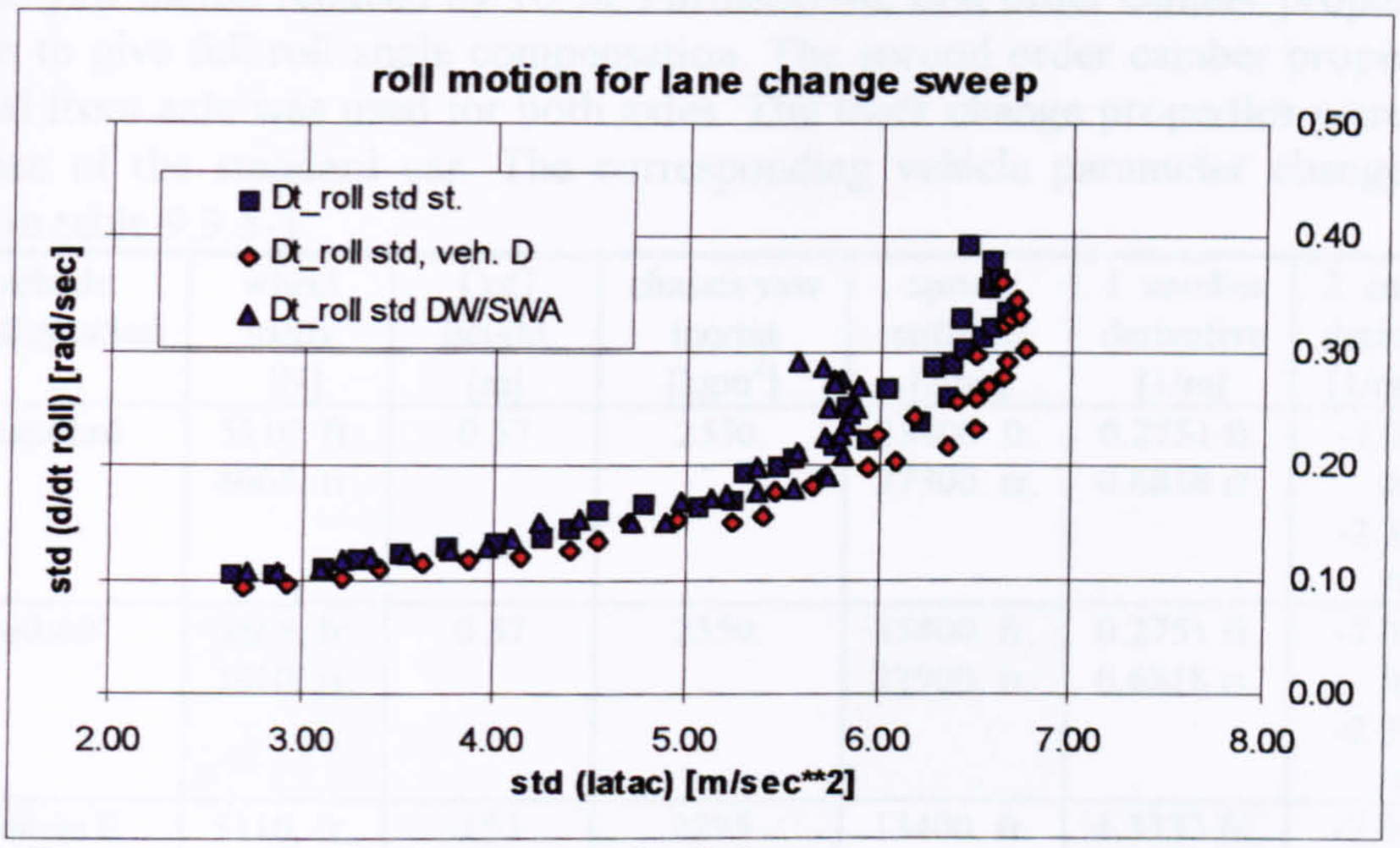

Fig. 9.3.4-6 Roll velocity standard deviation vs. manoeuvre severity represented by the standard deviation of the lateral acceleration

The former configuration tends to roll less than the other two specimens, as can be seen from fig. 9.3.4-6. Lower values for the roll angle velocity were calculated for the vehicle for which a rear anti-roll bar was employed to contain roll rather than a roll centre positioned above ground.

summary

The swing axle case provides a drastic example of a poorly handling vehicle. This design neither provides lateral guidance of sufficient magnitude nor establishes a smooth transition from low severity driving to limit manoeuvering. The response of this design deteriorates at a high rate. Response times increase considerably with severity, leading to a strong decrease for the correlation between the steering input and the lateral acceleration (established at zero time lag).

Using one of the design principles laid out in section 8.7 for improving the rear end grip, provided a small gain. The vehicle with a low rear end roll centre, maintained a similar behaviour to the standard car for the limit approach, but achieved slightly higher severity levels with relatively smaller side slip and roll motions.

9.3.5 Influence of vehicle mass distribution

Two further vehicle configurations were compared to the standard set-up. For the first alternative vehicle, a mass distribution of 60:40 towards the front was assumed compared to a 52:48 ratio for the standard car. The undamped ride eigenfrequency for each unsprung mass was maintained by changing the stiffness of the front and rear suspension springs accordingly. The suspension derivatives for the track and camber changes of the standard car were taken.

The second alternative design, denoted by 'vehicle E', had its centre of gravity height and the yaw inertia reduced by 10 %. Furthermore, first order camber properties were chosen to give full roll angle compensation. The second order camber property of the original front axle was used for both axles. The track change properties were identical to those of the standard car. The corresponding vehicle parameter changes can be found in table 9.3.5-1.

vehicle configuration	wheel loads [N]	CoG height [m]	chassis yaw inertia [kgm^2]	spring stiffness [N/m]	1. camber derivative [1/m]	2. camber derivative [1/m**2]
standard	5110. fr. 4665. rr.	0.57	2550.	13400. fr. 27300. rr.	0.2751 fr. 0.6818 rr.	-7.0224 fr. -2.3912 rr.
'60:40'	5865. fr. 3910. rr.	0.57	2550.	15400. fr. 22900. rr.	0.2751 fr. 0.6818 rr.	-7.0224 fr. -2.3912 rr.
vehicle E	5110. fr. 4665. rr.	0.51	2295.	13400. fr. 27300. rr.	1.3333 fr. 1.3089 rr.	-7.0224 fr. -7.0224 rr.

Table 9.3.5-1 Vehicle parameter variations

Vehicle E, having improved roll angle compensation and less inertia, achieves the highest severity levels, expressed by the peak value and standard deviation of the lateral acceleration, shown in fig. 9.3.5-1. The other two vehicles achieve similar performance levels. It is interesting to note that the 60:40 biased car achieves the same severity levels as the standard car, even though the coefficient of friction for the front tyres decreased due to the increased static load. Some of the 'static' friction loss is compensated by the more evenly distributed stiffness, giving relatively smaller dynamic wheel load variations in comparison to the standard car.

The response time lags and the correlation coefficients established at zero time shift are given in figures 9.3.5-2, and 9.3.5-3, respectively. In comparison to the standard car, vehicle E responds slightly faster and provides a higher correlation between the steering input and the lateral acceleration for the high speed tests, even though it manoeuvres at a higher severity for these speeds.

The vehicle with a 60:40 front end weight bias establishes the fastest response of the three specimens, throughout the speed range. The yaw rate response time remains at a very low level and the lateral acceleration response delay increases at a moderate level.

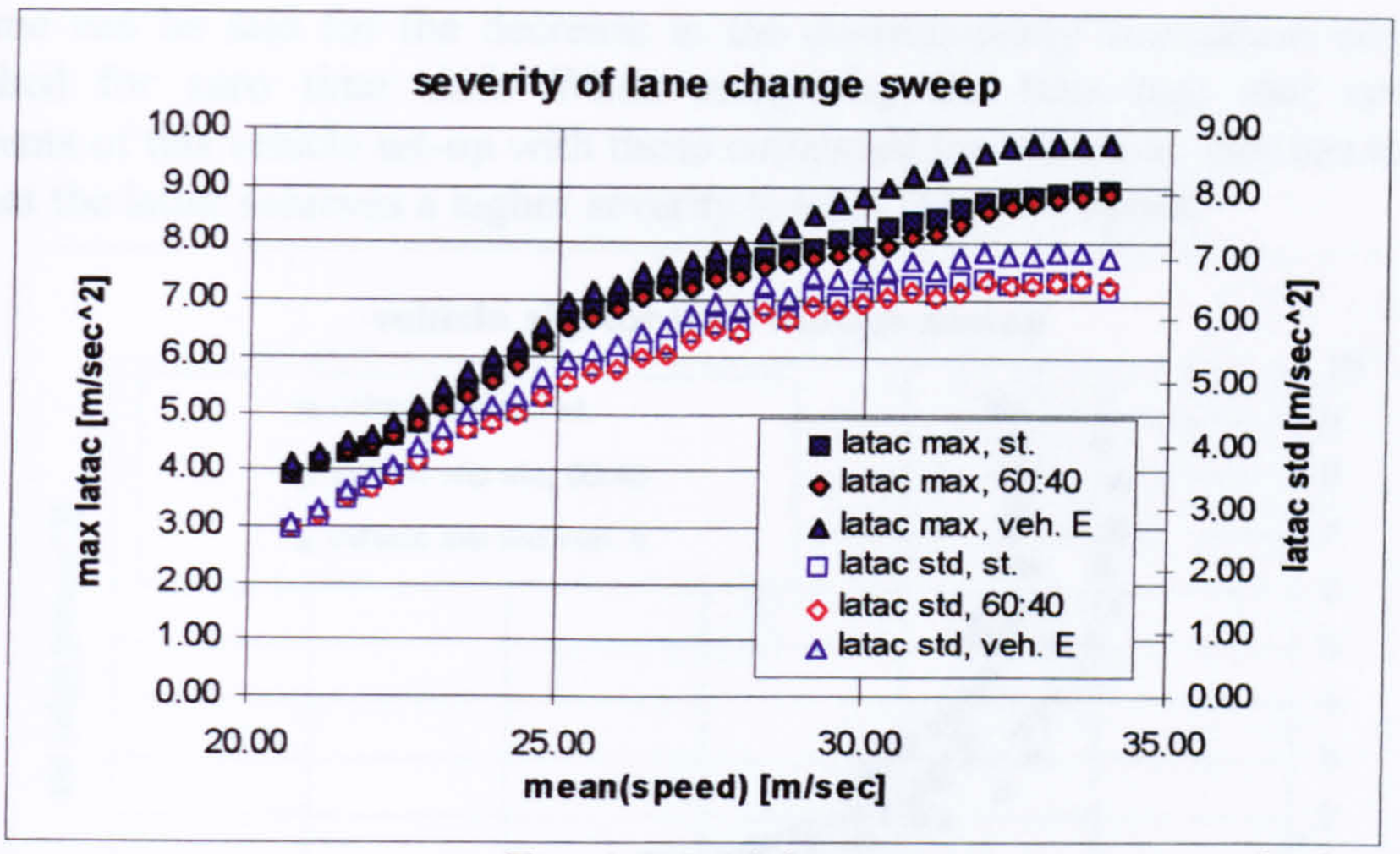

Fig. 9.3.5-1 Manoeuvre severity vs. vehicle speed

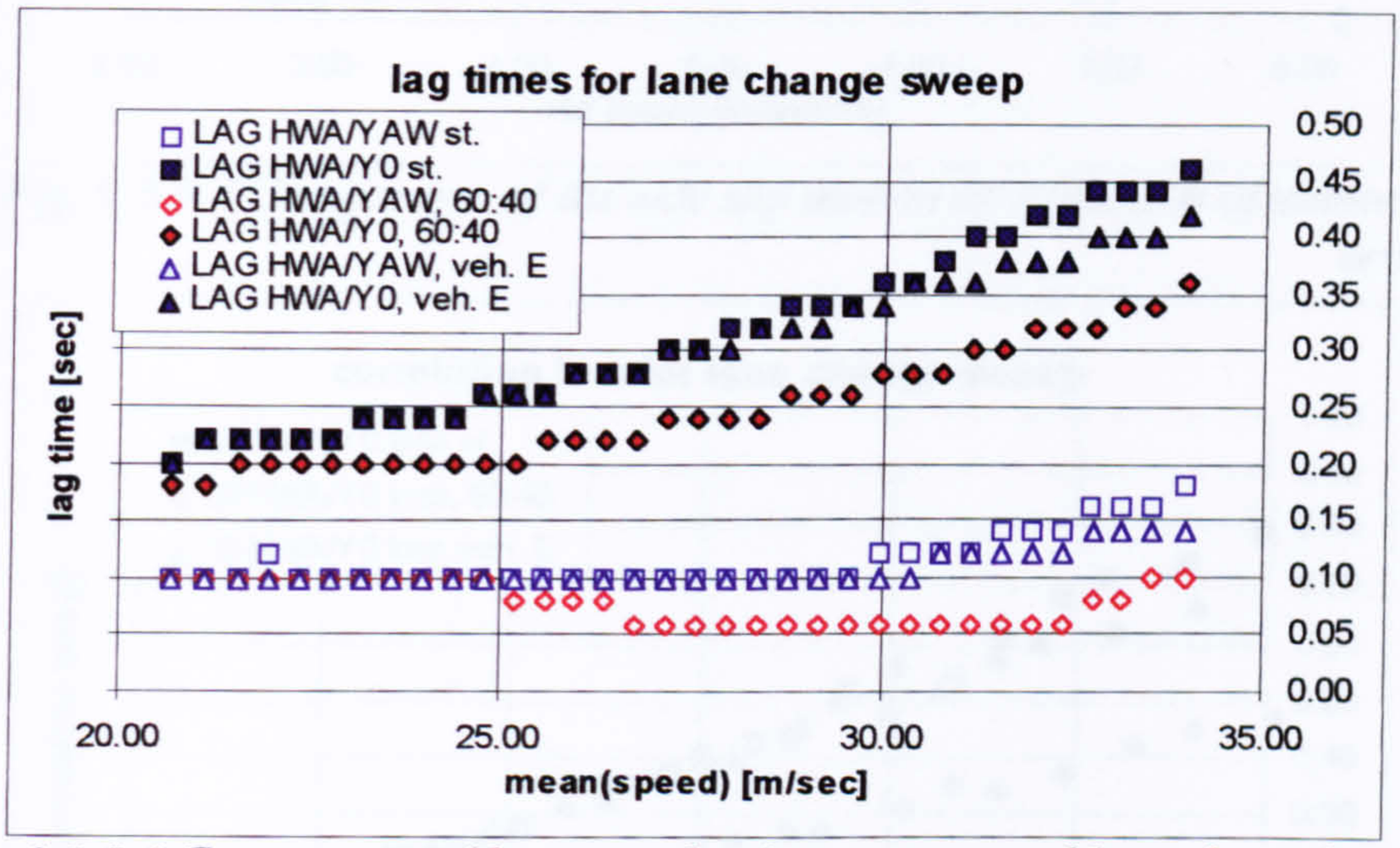

Fig. 9.3.5-2 Comparison of lag times for the yaw rate and lateral acceleration responses

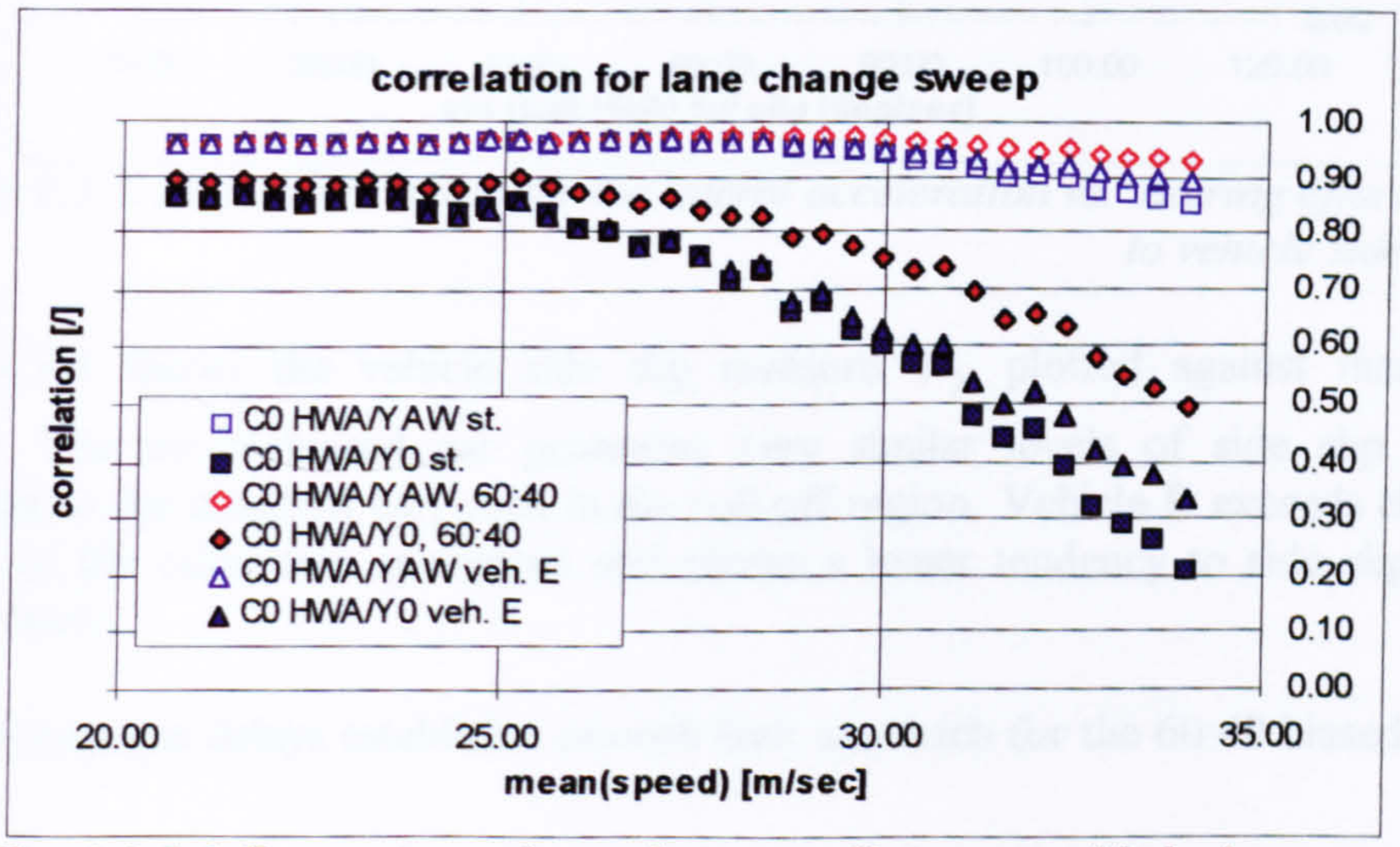

Fig. 9.3.5-3 Comparison of correlation coefficients established at zero time lag τ=0 for the yaw rate and lateral acceleration response

The same can be said for the decrease in the corresponding correlation coefficients established for zero time shift. When comparing the time lags and correlation coefficients of this vehicle set-up with those computed for vehicle E, one has to bear in mind that the latter achieves a higher severity level at the same speed.

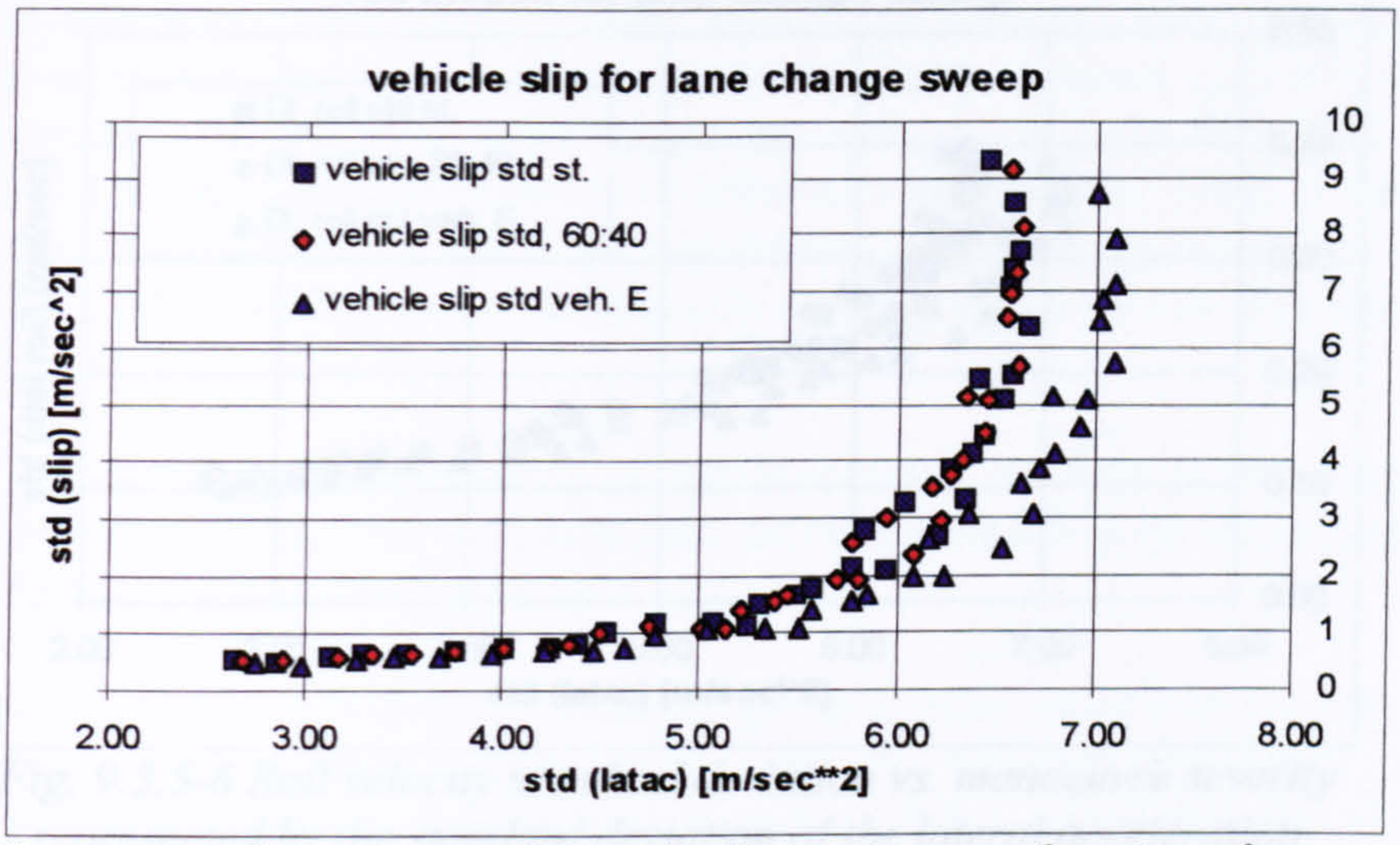

Fig. 9.3.5-4 Comparison of the side slip motion as a function of manoeuvre severity

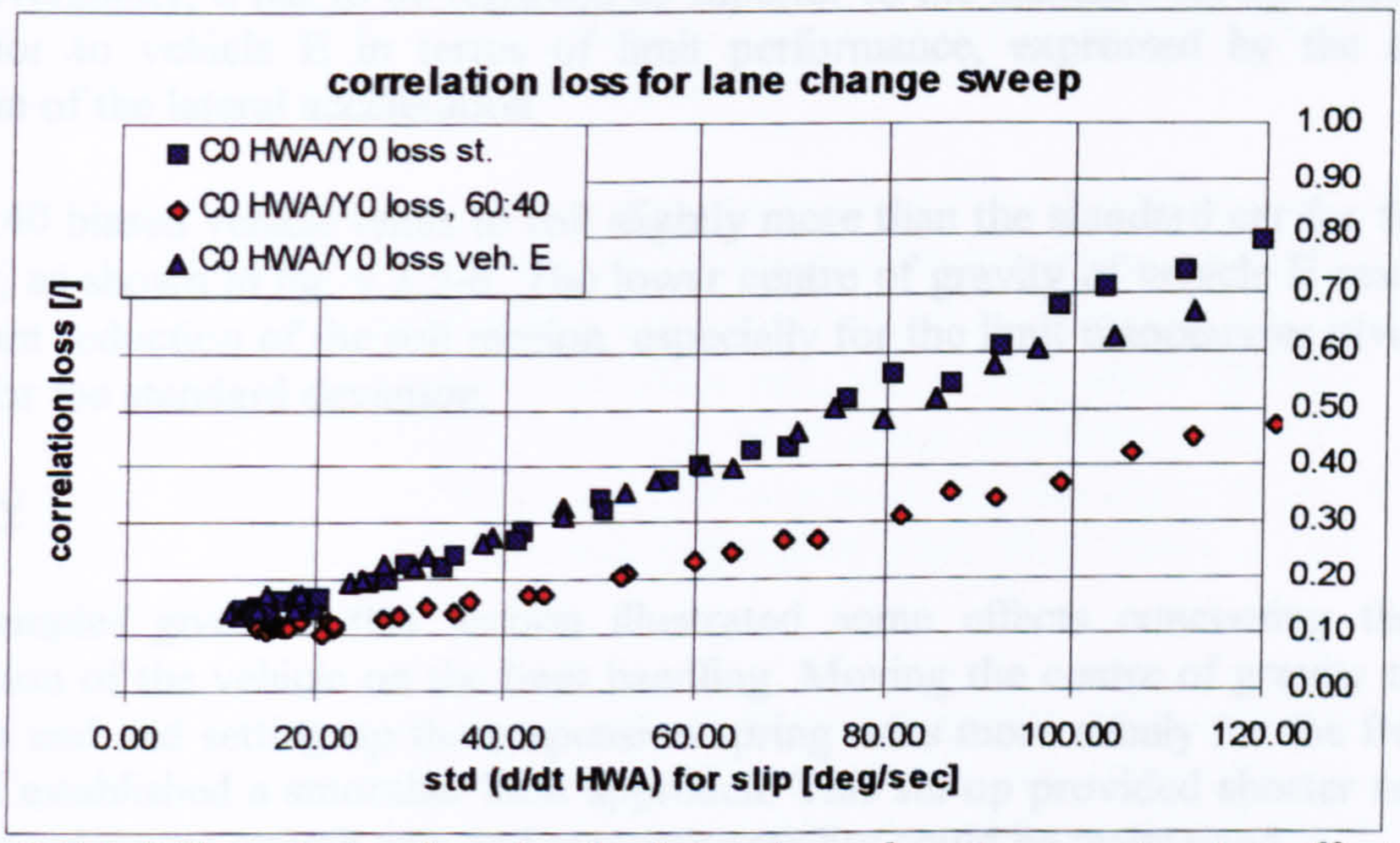

Fig. 9.3.5-5 Correlation loss for the lateral acceleration vs. steering effort due to vehicle side slip

Fig. 9.3.5-4 shows the vehicle side slip measure $\sigma_{\dot{\beta}}$ plotted against manoeuvre severity. The 60:40 biased car generates very similar levels of side slip motion compared to the standard car, even in the roll-off region. Vehicle E exceeds the peak severity of the other two specimens and shows a lesser tendency to side slip at the same severity.

The low response delays establish a smooth limit approach for the 60:40 biased car, as

can be seen from fig. 9.3.5-5. The correlation loss between the steering input and lateral acceleration response has a lower slope than established for the other two

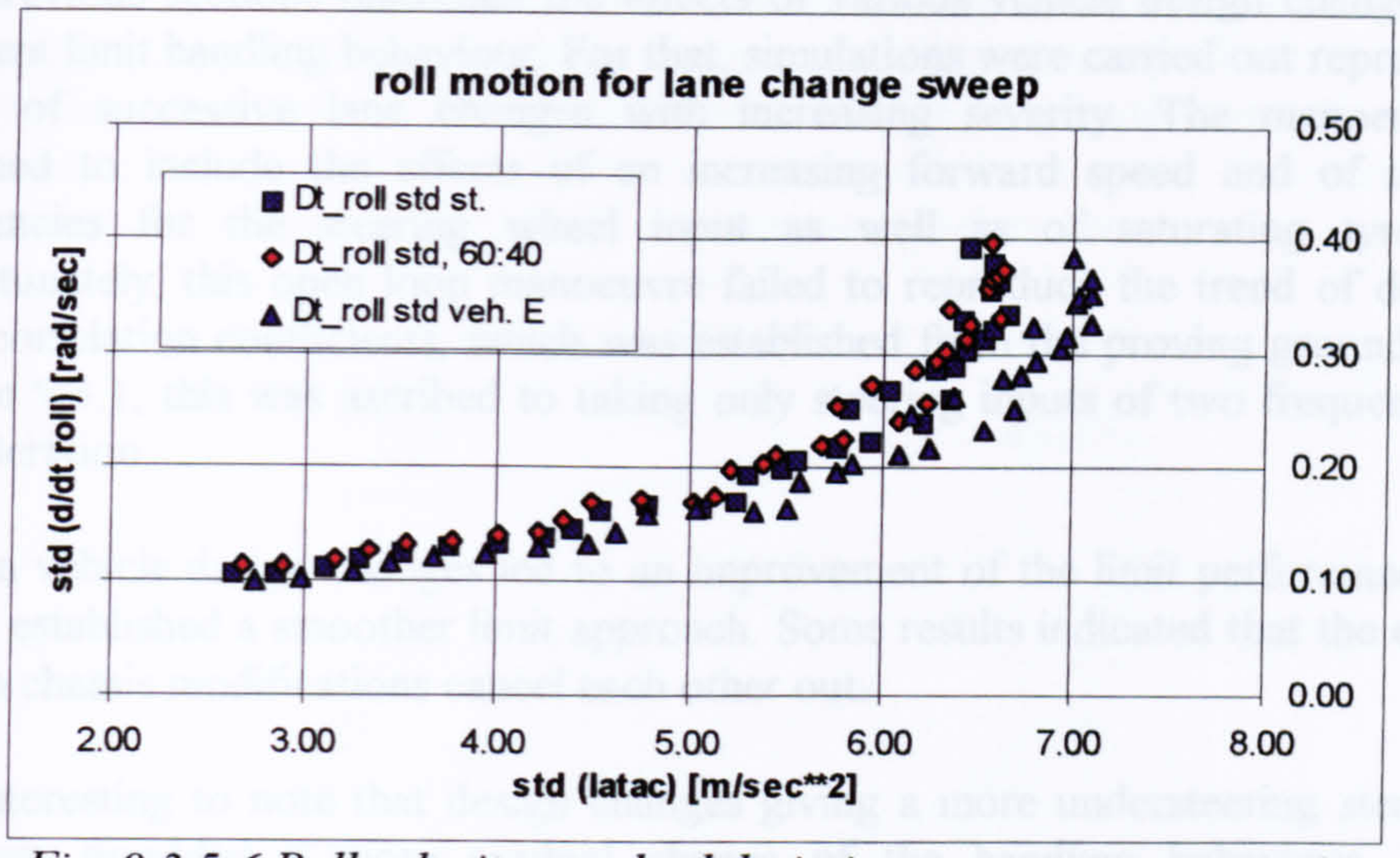

Fig. 9.3.5-6 Roll velocity standard deviation vs. manoeuvre severity represented by the standard deviation of the lateral acceleration

configurations. Considering that this set-up achieves the same level of manoeuverability, it has to be regarded as superior to the standard set-up. However, it is inferior to vehicle E in terms of limit performance, expressed by the standard deviation of the lateral acceleration.

The 60:40 biased vehicle tends to roll slightly more than the standard car for the same severity, as shown in fig. 9.3.5-6. The lower centre of gravity of vehicle E results in a significant reduction of the roll motion, especially for the limit manoeuvres giving high values for the standard deviation.

summary

The examples given in this section illustrated some effects concerning the mass distribution of the vehicle on the limit handling. Moving the centre of gravity towards the front end and setting up the suspension spring rates more evenly for the front and rear end established a smoother limit approach. This set-up provided shorter response time lags, while the overall grip and manoeuverability could be maintained.

The other alternative set-up provided a considerable gain in terms of limit performance. This was achieved by applying some of the design rules established in section 8.7. Full roll angle compensation was introduced for both axle designs. Furthermore, the centre of gravity and the yaw inertia of the chassis were reduced by 10 %. However, these design changes had little influence on the transitional behaviour. The rate of correlation loss with steering effort hardly differed from the gradient established for the standard set-up. It has to be considered though, that the decrease in correlation between the steering input and the lateral acceleration response occurs at higher severity levels in the case of vehicle E.

9.3.6 Conclusions

The previous sections discussed the effects of various vehicle design changes on the transient limit handling behaviour. For that, simulations were carried out representing a series of successive lane changes with increasing severity. The manoeuvre was designed to include the effects of an increasing forward speed and of increasing frequencies for the steering wheel input as well as of saturating tyre forces. Unfortunately, this open loop manoeuvre failed to reproduce the trend of decreasing peak correlation coefficients, which was established from the proving ground data. In section 9.3.1, this was ascribed to taking only steering inputs of two frequencies into consideration.

Certain vehicle design changes led to an improvement of the limit performance, while others established a smoother limit approach. Some results indicated that the effects of certain chassis modifications cancel each other out.

It is interesting to note that design changes giving a more understeering steady state handling, provided a more gradual change of the handling behaviour. A more compliant steering system, as discussed in section 9.3.1, improving the scrub and camber characteristics of the rear axle and accepting a degradation of those properties at the front end (vehicle B in 9.3.2) as well as shifting the centre of gravity towards the front end (9.3.5) were measures, leading to shorter response delays without having a detrimental effect on the peak manoeuverability.

The examples involving a McPherson strut suspension (9.3.3) showed that the effects of beneficial track change properties and detrimental camber change characteristics can cancel each other out. Using a McPherson strut at either front or rear end and keeping a double wishbone suspension for the other end, led to only small differences in the handling behaviour. The vehicle with a rear McPherson strut design proved to give a faster response, though. In section 9.3.3 it was argued that the improved track change properties of the McPherson strut rear suspension more than cancelled out its poor camber control characteristics.

The most drastic handling performances involved the vehicle with a swing axle rear suspension (9.3.4) and vehicle E (9.3.5). The latter was set up to achieve a higher steady state cornering performance by improving the camber control characteristics and by lowering the centre of gravity. Furthermore, the yaw inertia was lowered by 10 %. This design achieved the highest standard deviation for the lateral acceleration, which was regarded as a measure of the manoeuverability. However, the sensitivity of the response behaviour to increasing severity levels was similar to that of the standard vehicle. Improving the cornering performance of the front and rear axle by the same degree seems to give the same sensitivity at a higher performance level.

The vehicle with a swing axle rear suspension proved far inferior in terms of peak performance and in establishing a smooth transition of the response behaviour towards the limit. It achieved very low severity levels, and its response time delays deteriorated

at a high rate.

It seems that more emphasis has to be placed on improving the rear end design, i.e. by introducing proper track and camber change characteristics and relatively low wheel rates, than on the front end design, in order to achieve benefits in terms of a high peak performance and a gradual transition towards the limit. A more compliant steering system might be employed to 'detune' the front end performance.

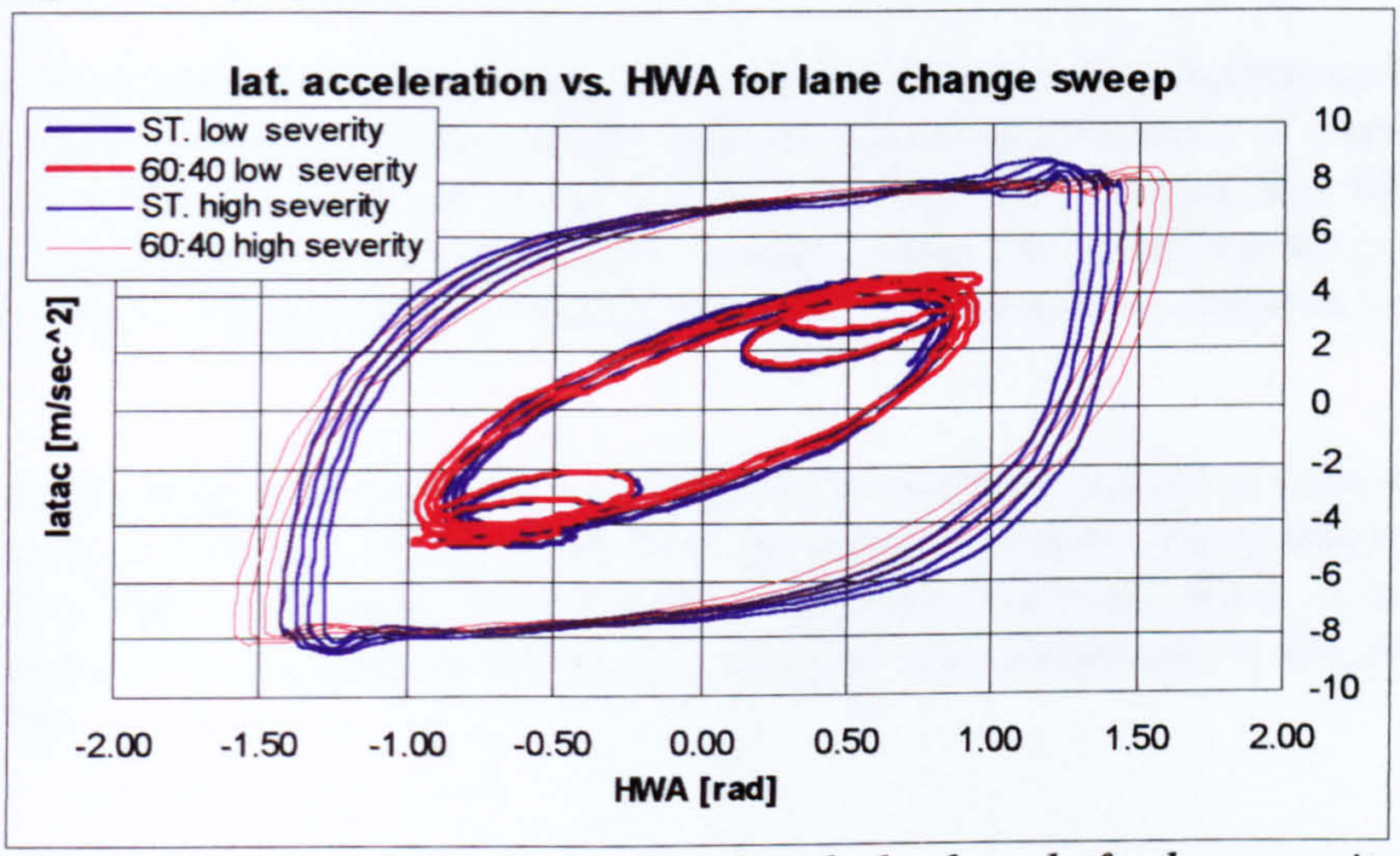

Fig. 9.3.6-1 Lateral acceleration vs. hand wheel angle for low severity and high severity lane changes; standard vs. '60:40' vehicle

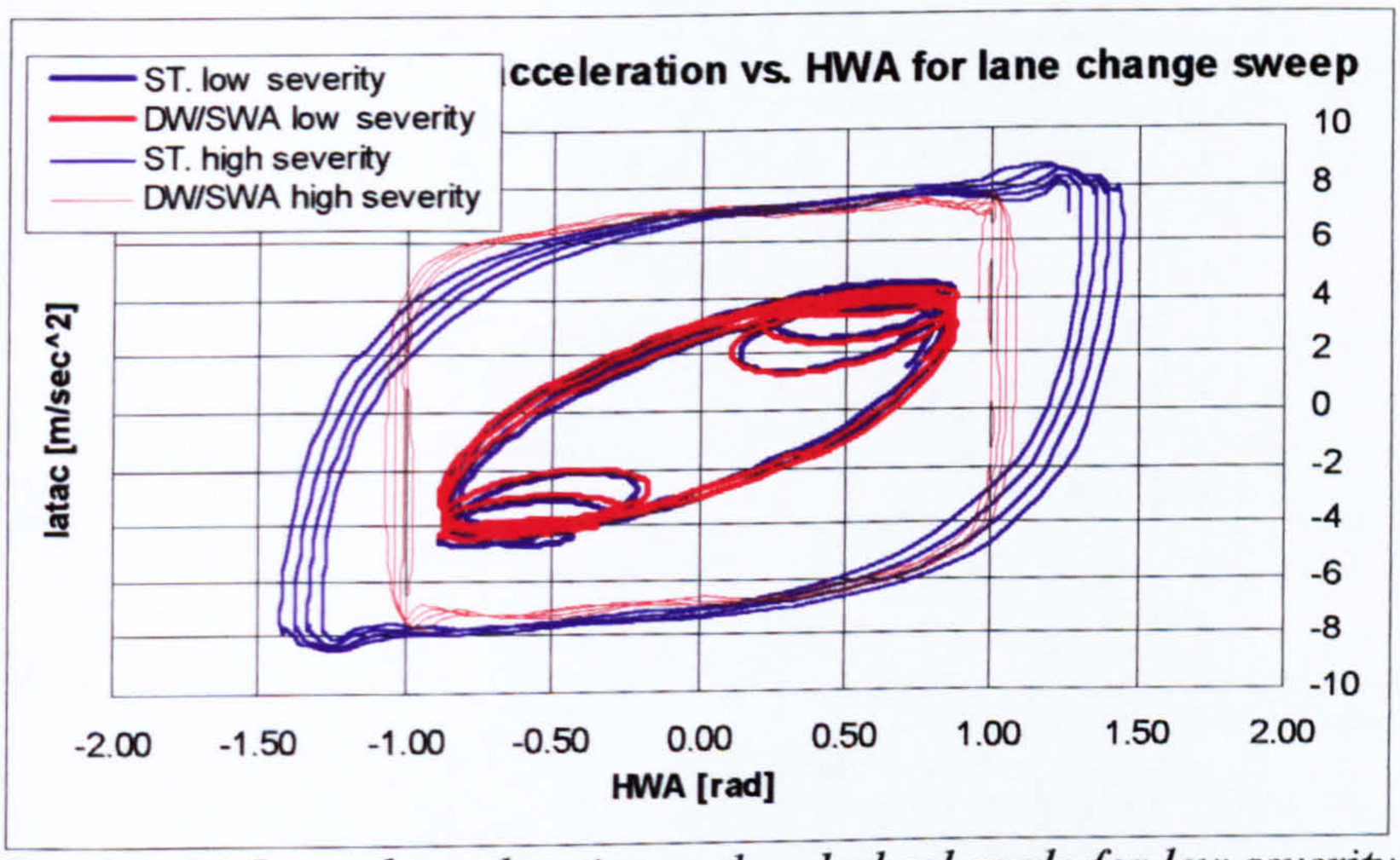

Fig. 9.3.6-2 Lateral acceleration vs. hand wheel angle for low severity and high severity lane changes; standard vs. 'DW/SWA' vehicle

Finally, some time domain results are used to illustrate the extreme cases. Fig.9.3.6-1 shows the cross-plots of the lateral acceleration and the hand wheel angle, obtained from 'lane change sweep' simulations of the standard vehicle and of the vehicle with a 60:40 weight distribution (9.3.5). The elliptic hysteresis loops in the centre of the

graph refer to low severity lane changes for speeds between 21 and 23 m/sec. The more lemon-shaped loops refer to high severity manoeuvres for speeds between 30 and 32 m/sec. The hysteresis loops for the low severity lane changes are narrow due to the low time delays. The width and the height of the loop increases with severity. The symmetrical shape is distorted into a lemon-shaped loop, reflecting the non-linear nature of the corresponding manoeuvre.

There is little difference in the width and height of the two outer hysteresis loops for the two vehicle set-ups. Both vehicles achieve lateral accelerations of more than 8 m/sec^2. However, the response of the vehicle with more front weight bias follows the steering wheel angle in a less progressive fashion, while the lateral acceleration of the standard vehicle changes with a strongly increasing gradient from negative to positive values.

The corresponding cross-plots for the swing axle equipped vehicle are shown in fig. 9.3.6-2 along with those already shown for the standard vehicle. The graph suggests a switch-like limit behaviour. The lateral acceleration remains fairly constant for increasing hand wheel angles until it changes sign and magnitude at the peak hand wheel angle.

9.4 Effects of tyre design

Section 9.4 gives a few examples illustrating the effect of certain tyre properties on the limit handling behaviour. Five alternative generic tyre designs were modelled by varying certain coefficients defining the 'Magic Formula' and subsequently used in 'lane change sweep' simulations. The simulations are based on the vehicle data of the Jaguar XJ6 and on tyre data obtained for a Dunlop SP2000 J of size 225/55 R16. This input data can be found in the appendix. Those 'Magic Formula' coefficients varied from the nominal values are given in this section. For this parameter study, only coefficients concerning the lateral force were altered. The parameter values defining the aligning torque remained identical to the nominal set.

9.4.1 Tyre parameter variations

The 'Magic Formula' coefficients of three alternative tyre designs are given in table 9.4.1-1. Values defining the parameters C, E and the cornering stiffness BCD were altered with respect to the nominal parameter set. For the fifth alternative tyre design, those coefficients describing the camber influence on the side force were decreased by 10 %. The parameters refer to the version of the 'Magic Formula' used in chapter 8. The peak friction was the same for each tyre.

parameter tyre design	C [/]	a_3 [N/rad]	a_4 [N]	a_6 [1/N]	a_7 [/]
standard	1.3	9.5E+04	1.6E+04	-0.9E-04	0.7
tyre 1	1.2	9.5E+04	1.6E+04	-0.1E-04	0.7
tyre 2	1.4	9.5E+04	1.6E+04	-1.7E-04	0.7
tyre 3	1.3	5.8E+04	7.5E+03	-0.9E-04	0.7
tyre 4	1.4	5.8E+04	7.5E+03	-1.7E-04	0.7

Table 9.4.1-1 'Magic Formula' coefficients defining C, E and BCD as used to simulate alternative tyre designs

The coefficients a_3 and a_4 define the cornering stiffness BCD, including the load dependency of this property. The coefficients a_6 and a_7 define parameter E, which in combination with parameter C defines the curvature by which the side force approaches its peak as a function of the side slip. The corresponding definitions of these parameters can be found in fig. 8.6-1.

For the tyre designs 'tyre 1' and 'tyre 2', the parameters C and E were altered with respect to their nominal values. Decreasing C and increasing E, as done for 'tyre 1', establishes a more compliant tyre for higher slip angles, as can be seen from fig. 9.4.1-1. The graph contains data for the lateral force at four different vertical loads. The opposite setting, denoted by 'tyre 2' in fig. 9.4.1-2, extends the linear tyre behaviour to higher slip angles.

For small slip angles, the differences in behaviour of these two designs are small, since the cornering stiffness BCD remained unchanged. Differences in behaviour are only apparent for high loads and large slip angles. The peak force of the 'tyre 1' design

coincides with a considerably higher slip angle, compared to the standard, and especially to the 'tyre 2' design. The lateral force increases with side slip gently towards the peak, while the lateral force of the 'tyre 2' design establishes a more distinct peak. The transition from the linear to the sliding dominated region of the side force-side slip curves assumes a much stronger curvature for the latter design.

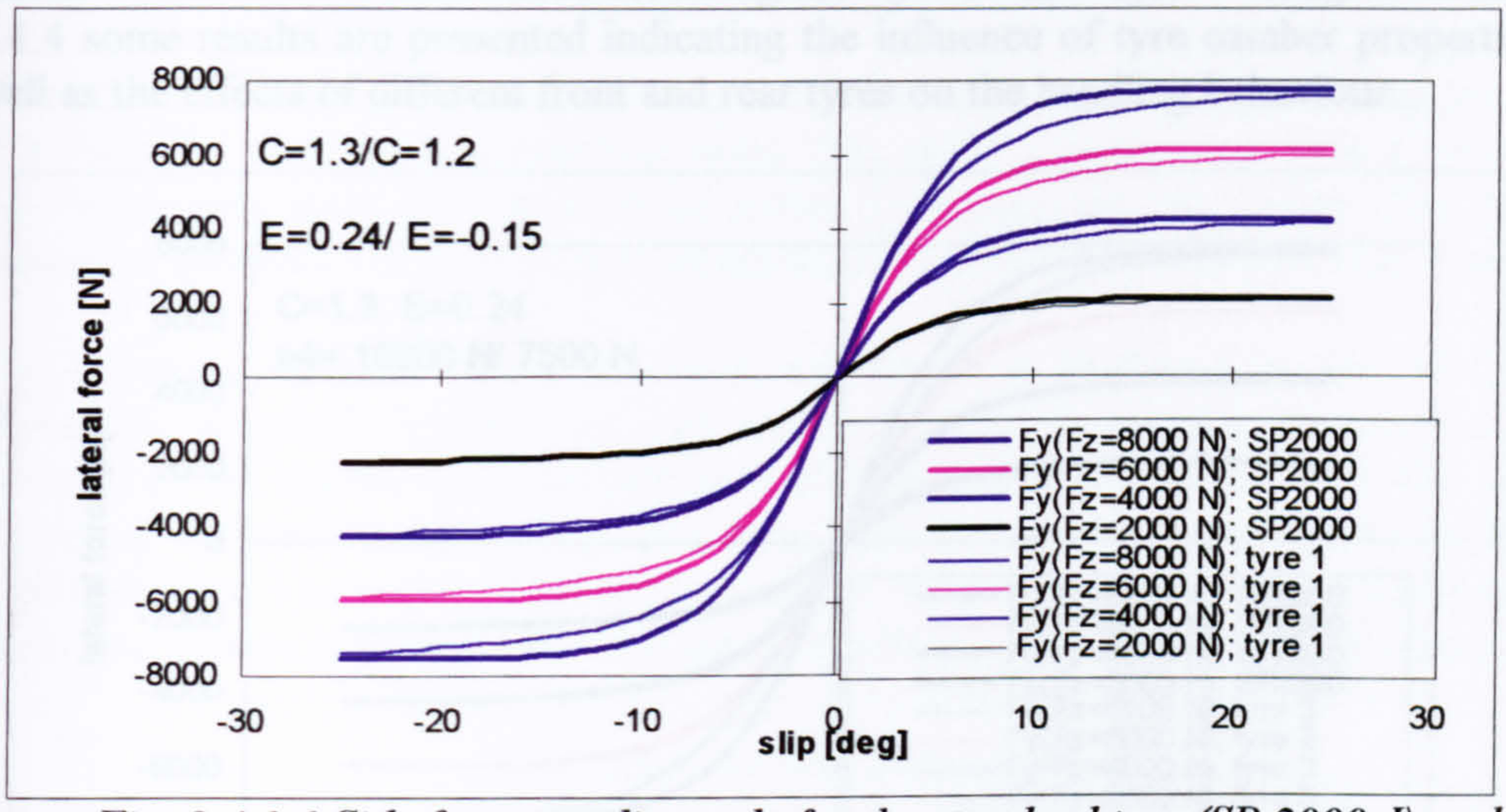

Fig. 9.4.1-1 Side force vs. slip angle for the standard tyre (SP 2000 J) and design alternative 'tyre 1'

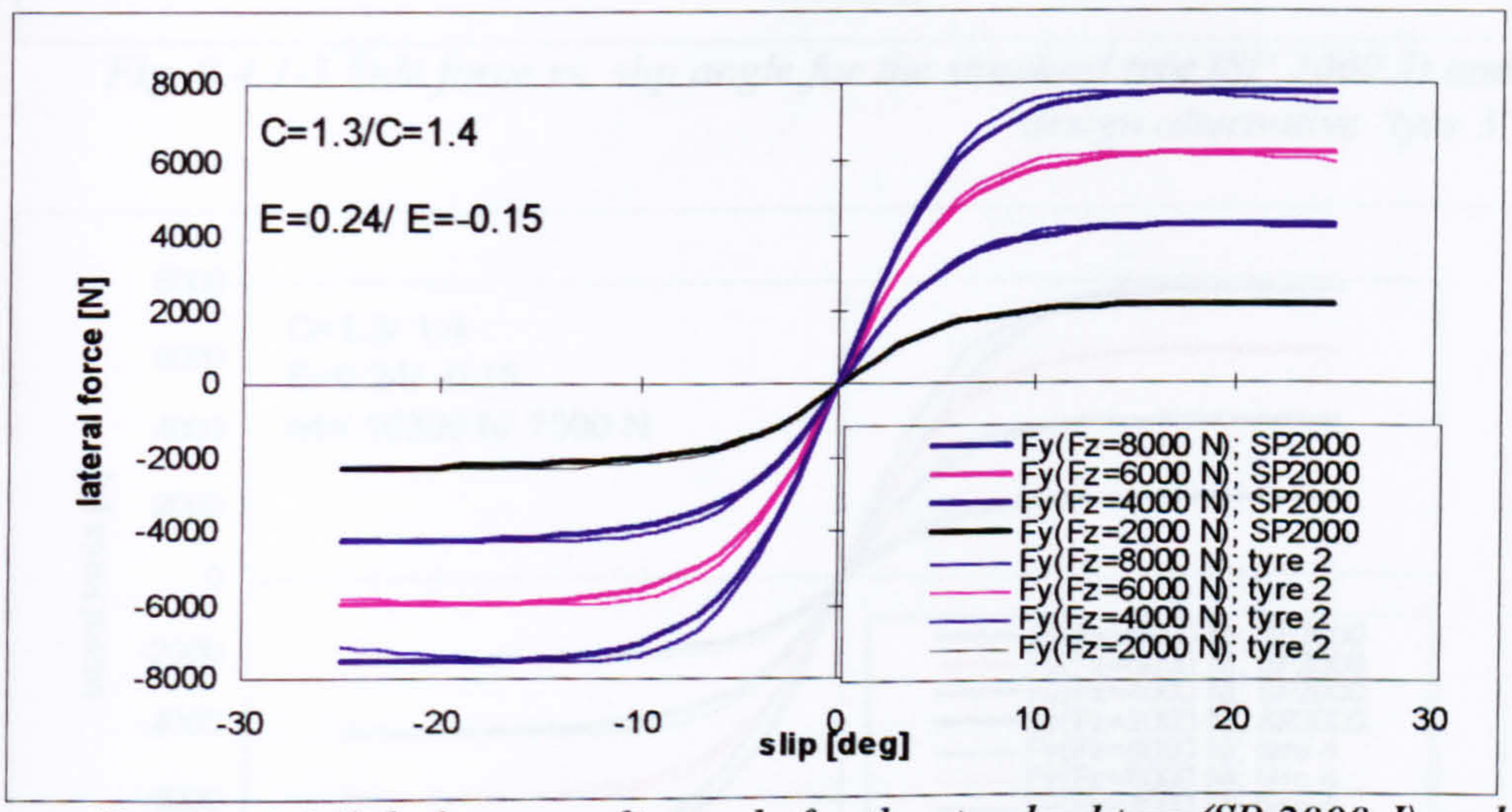

Fig. 9.4.1-2 Side force vs. slip angle for the standard tyre (SP 2000 J) and design alternative 'tyre 2'

For the other two alternative tyre designs, the coefficients a_3 and a_4 were altered. The designs 'tyre 3' and 'tyre 4' differ from the standard construction in that their peak cornering stiffness is established at a far lower load. This load is identical to the value of a_4. However, the coefficient a_3 was chosen to give the same cornering stiffness at the nominal front wheel load of 5000 N as the standard tyre. These two alternative designs differ from each other in how the side force approaches the peak performance for increasing side slip angles. As can be seen from fig. 9.4.1-3 and fig.

9.4.1-4, 'tyre 3' is more compliant at higher slip angles than 'tyre 4'. Both force characteristics differ only slightly from that of the standard tyre, except at high loads.

The effects of the first two alternative tyre designs on the limit handling of the standard vehicle are discussed in the following section, while section 9.4.3 summarises the results obtained from simulations involving the 'tyre 3' and 'tyre 4' designs. In section 9.4.4 some results are presented indicating the influence of tyre camber properties as well as the effects of different front and rear tyres on the handling behaviour.

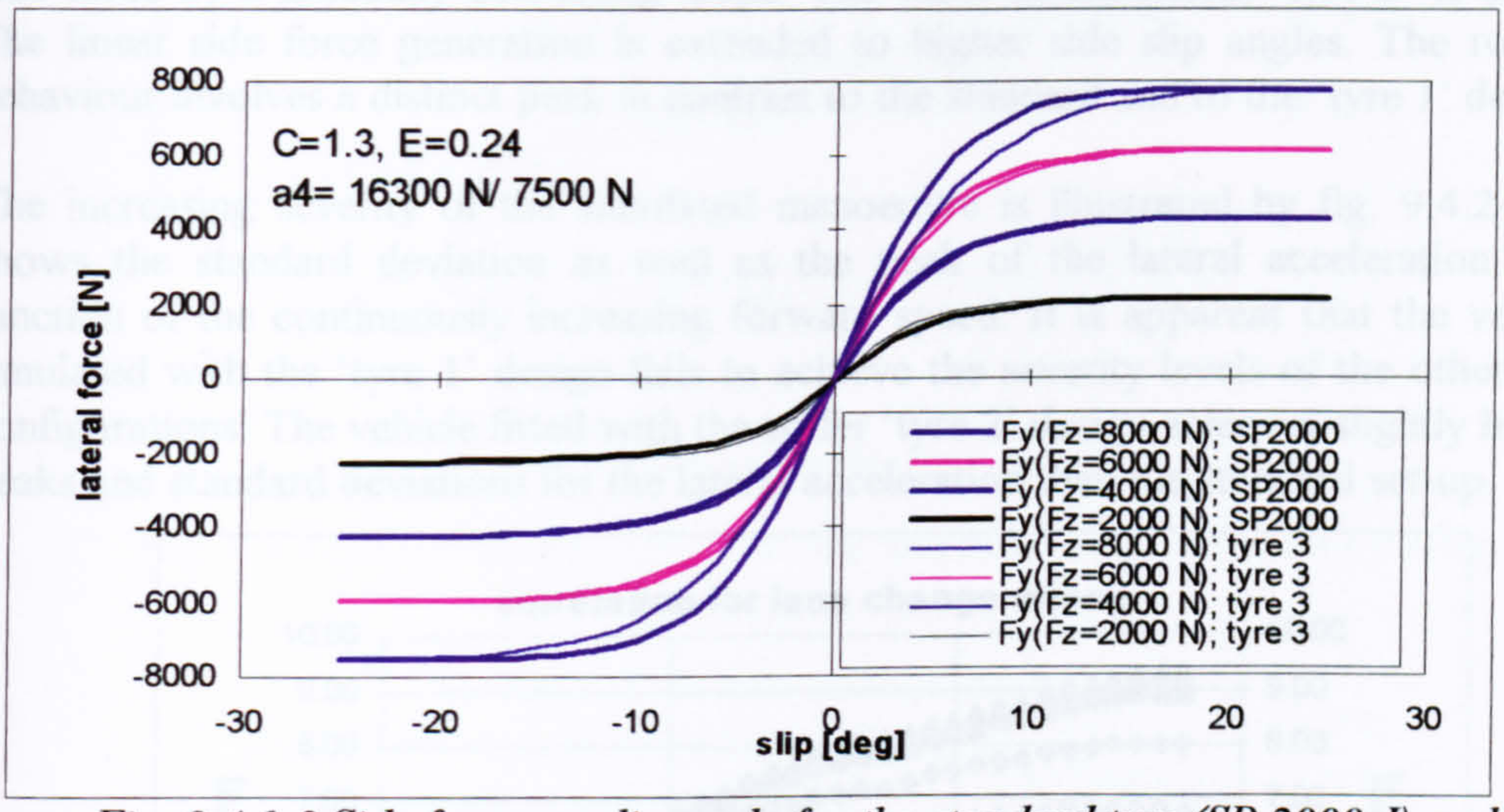

Fig. 9.4.1-3 Side force vs. slip angle for the standard tyre (SP 2000 J) and design alternative 'tyre 3'

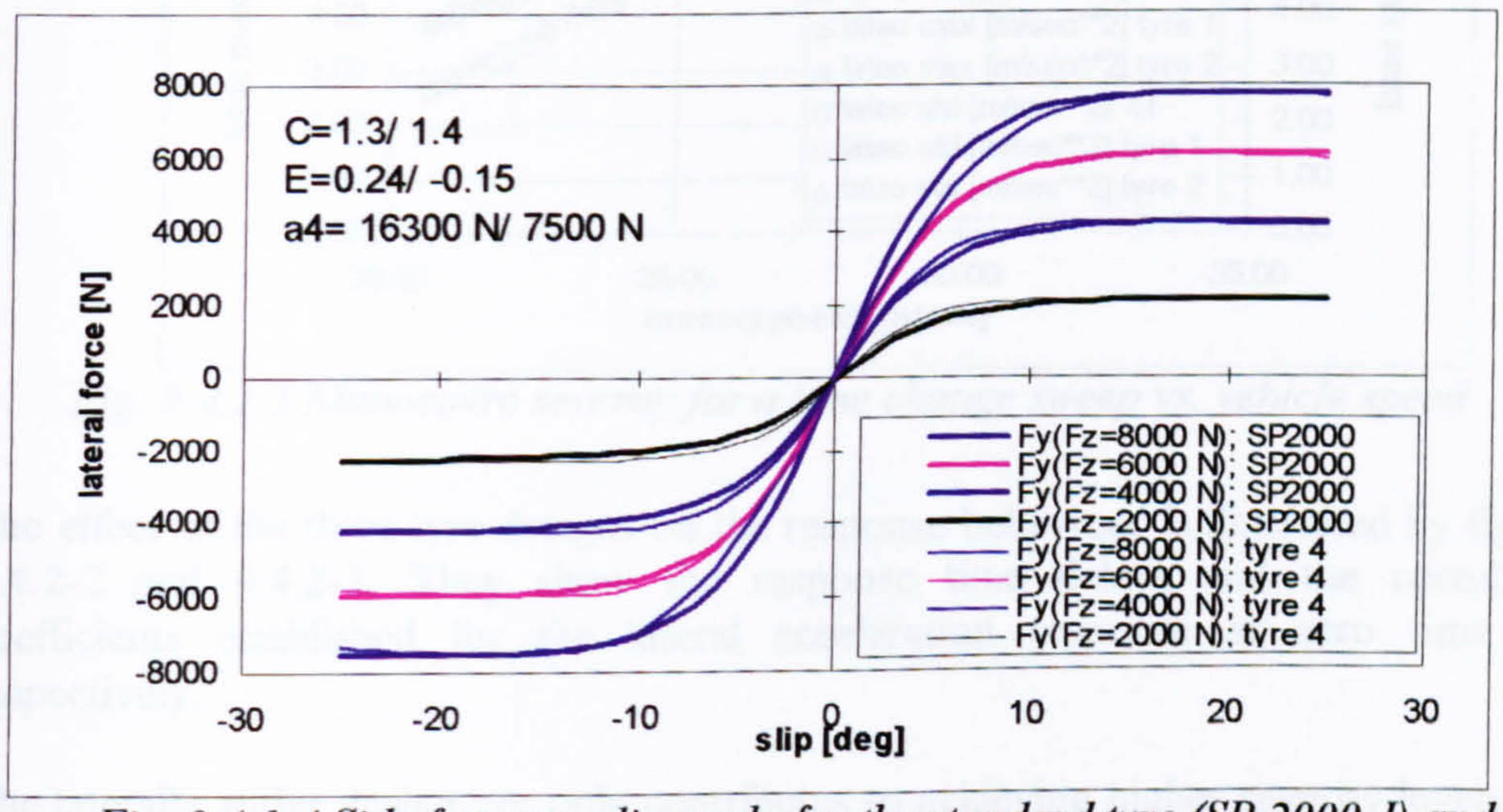

Fig. 9.4.1-4 Side force vs. slip angle for the standard tyre (SP 2000 J) and design alternative 'tyre 4'

9.4.2 Effects of the 'Magic Formula' parameters C and E on the limit handling

The effects of the 'Magic Formula' parameters C and E on the limit handling performance are illustrated in this section. Simulations of the 'lane change sweep' manoeuvre were carried out involving the alternative tyre designs 'tyre 1' and 'tyre 2'. Results are compared to those obtained for the standard tyres.

The 'tyre 1' design can be regarded as a more compliant tyre, approaching the peak side force by a gradually decreasing slope. The other construction, 'tyre 2' is stiffer. The linear side force generation is extended to higher side slip angles. The roll-off behaviour involves a distinct peak in contrast to the standard and to the 'tyre 1' design.

The increasing severity of the simulated manoeuvre is illustrated by fig. 9.4.2-1. It shows the standard deviation as well as the peak of the lateral acceleration as a function of the continuously increasing forward speed. It is apparent that the vehicle simulated with the 'tyre 1' design fails to achieve the severity levels of the other two configurations. The vehicle fitted with the stiffer 'tyre 2' design achieves slightly higher peaks and standard deviations for the lateral acceleration than the standard set-up.

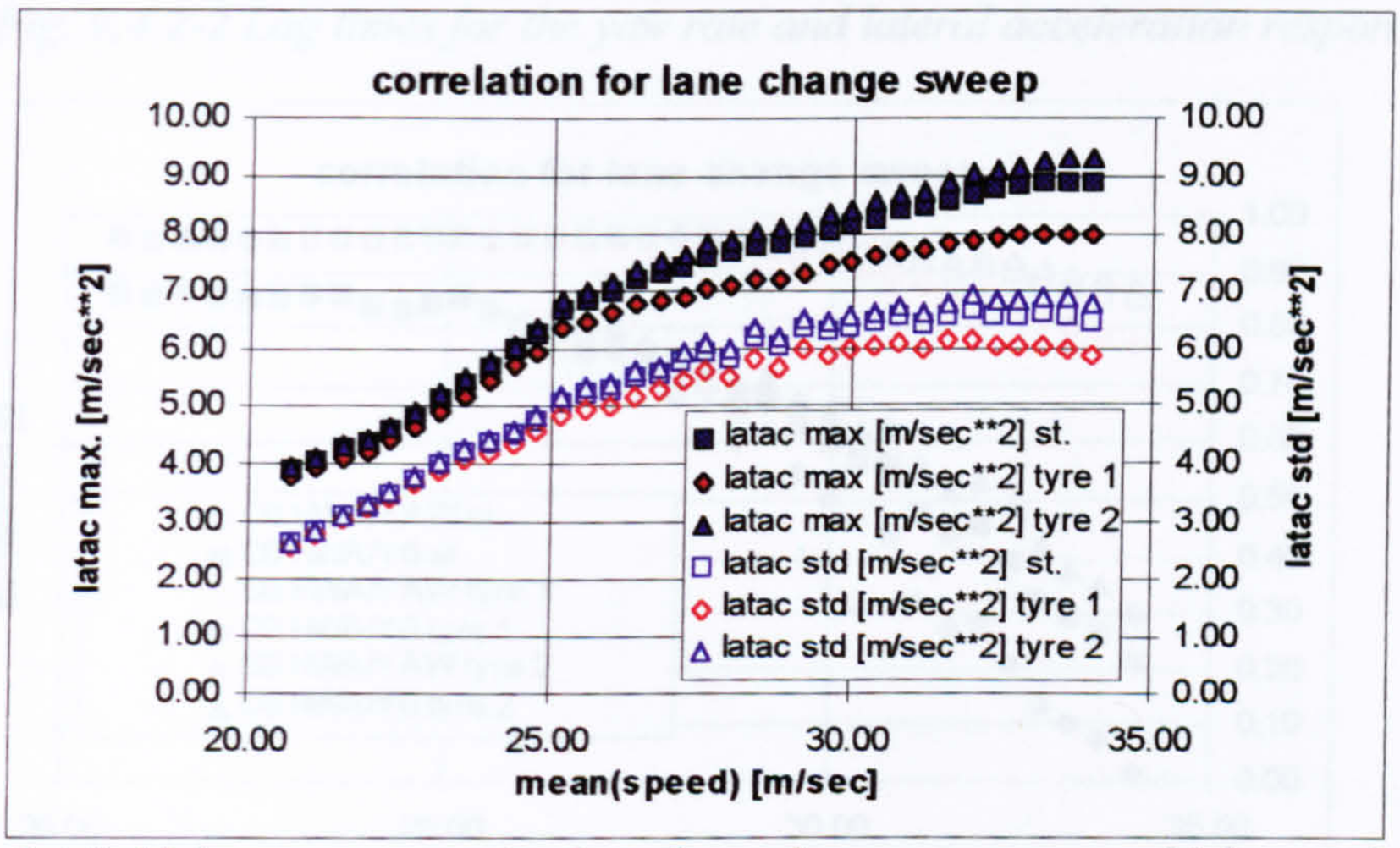

Fig. 9.4.2-1 Manoeuvre severity for a lane change sweep vs. vehicle speed

The effect of the three tyre designs on the response behaviour is illustrated by figures 9.4.2-2 and 9.4.2-3. They show the response time delays and the correlation coefficients established for the lateral acceleration response at zero time lag, respectively.

The laterally stiffer design not only contributes to achieving higher severity levels, but also provides a faster yaw rate and lateral acceleration response. Time delays increase and the correlation coefficients decrease at moderate rates compared to the other two configurations. The response characteristics of the vehicle, shod with the more compliant tyres, deteriorate at a considerable rate, although severity levels are comparatively low.

The disadvantages of the compliant tyre design are further illustrated by fig. 9.4.2-4, showing the values of the side slip variation $\sigma_{\dot{\beta}}$ as a function of vehicle speed. The vehicle equipped with these tyres cannot exceed a severity level of 6.2 m/sec^2. The

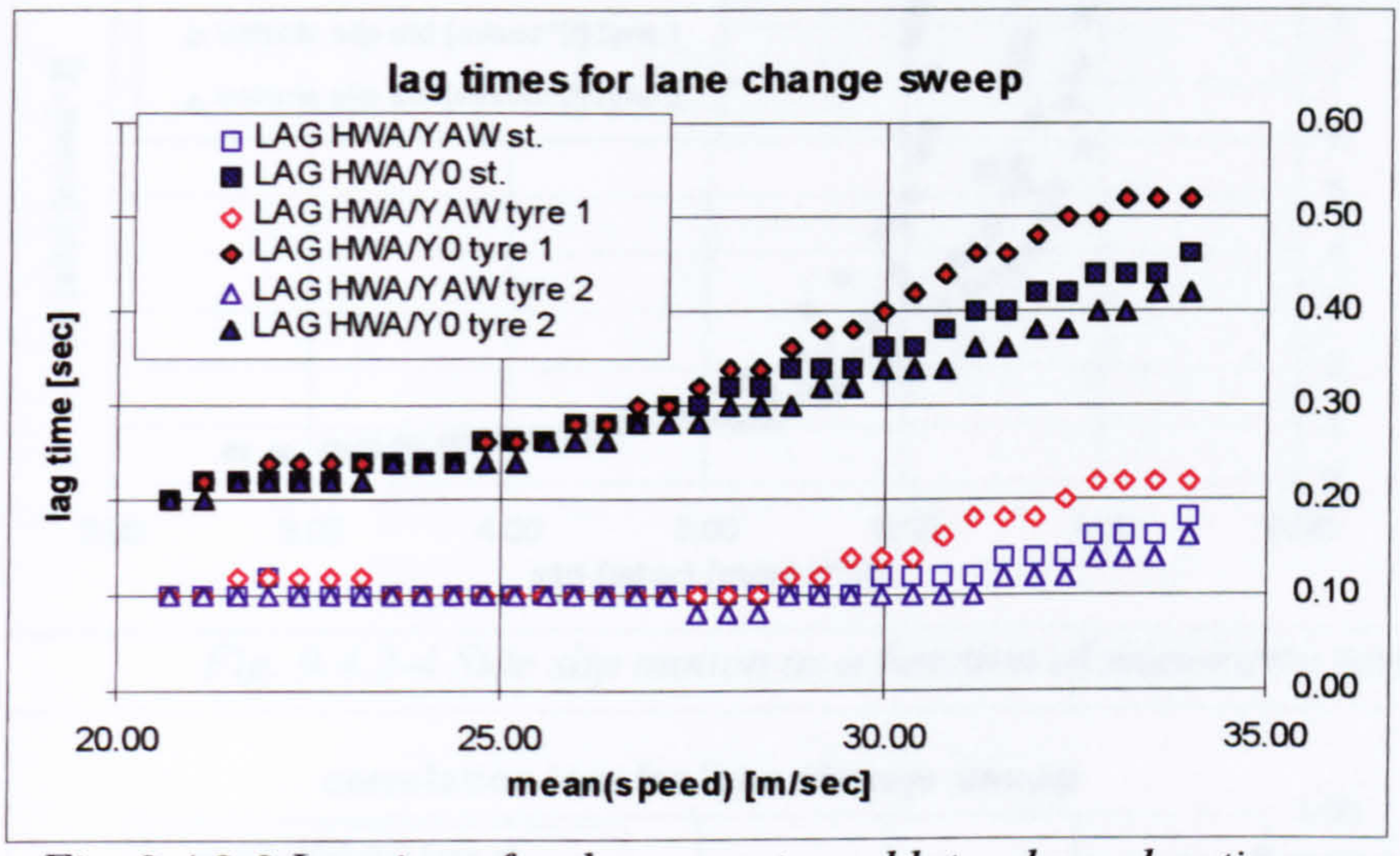

Fig. 9.4.2-2 Lag times for the yaw rate and lateral acceleration response

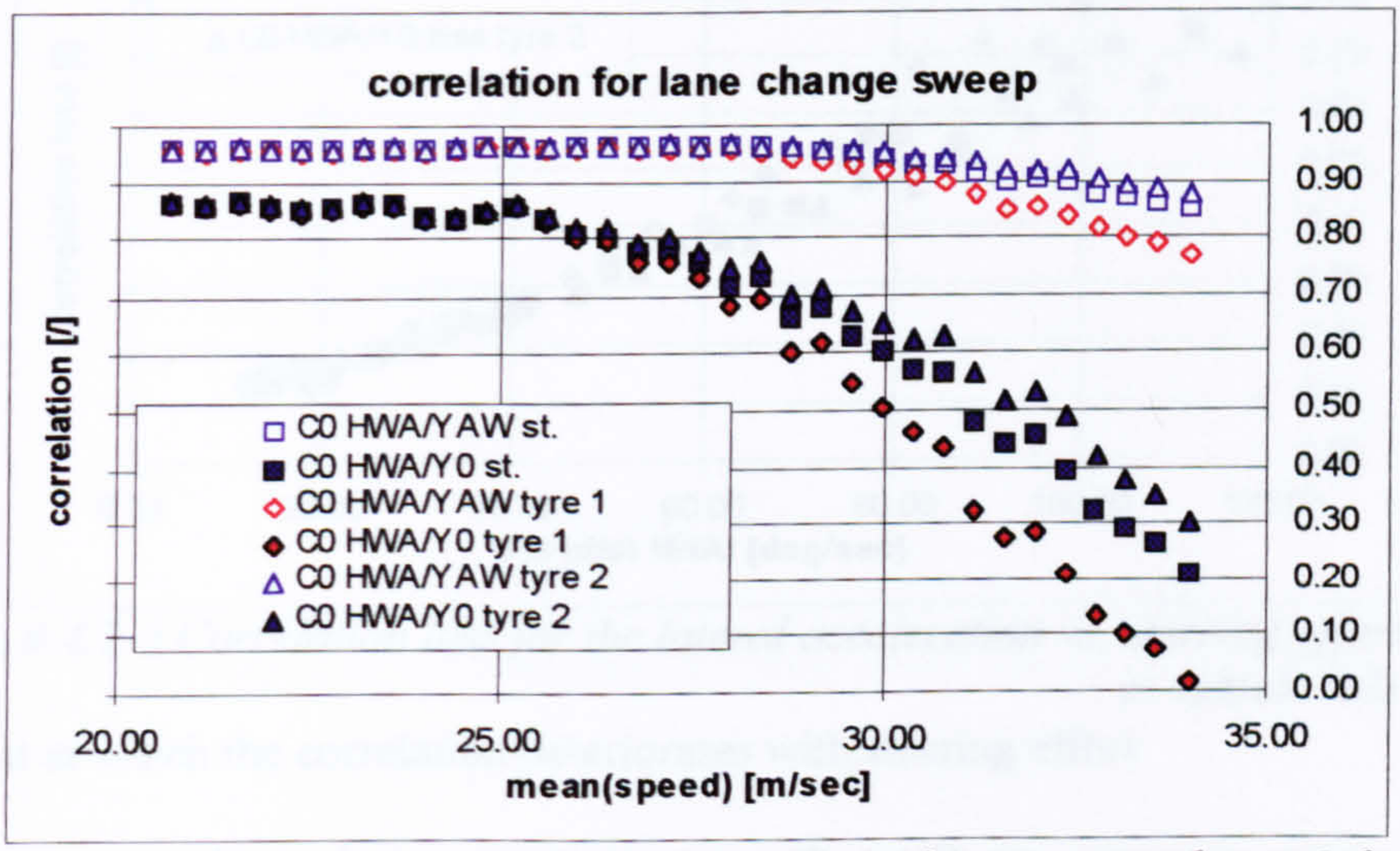

Fig. 9.4.2-3 Correlation coefficients established at zero time lag τ=0 *for the yaw rate and lateral acceleration responses*

discrepancy between the yaw rate and the lateral acceleration response starts to increase at a high rate near this limit severity. The other vehicles achieve a higher peak performance.

The sensitivity of the vehicle response to the limit approach can be established from fig. 9.4.2-5. The correlation loss is plotted against the steering effort parameter $\sigma_{\dot{\delta},\beta}$.

The graph shows that the stiffer tyre design 'tyre 2' also contributes to a more gradual limit approach, at least for the very severe manoeuvres, as can be seen from the lower

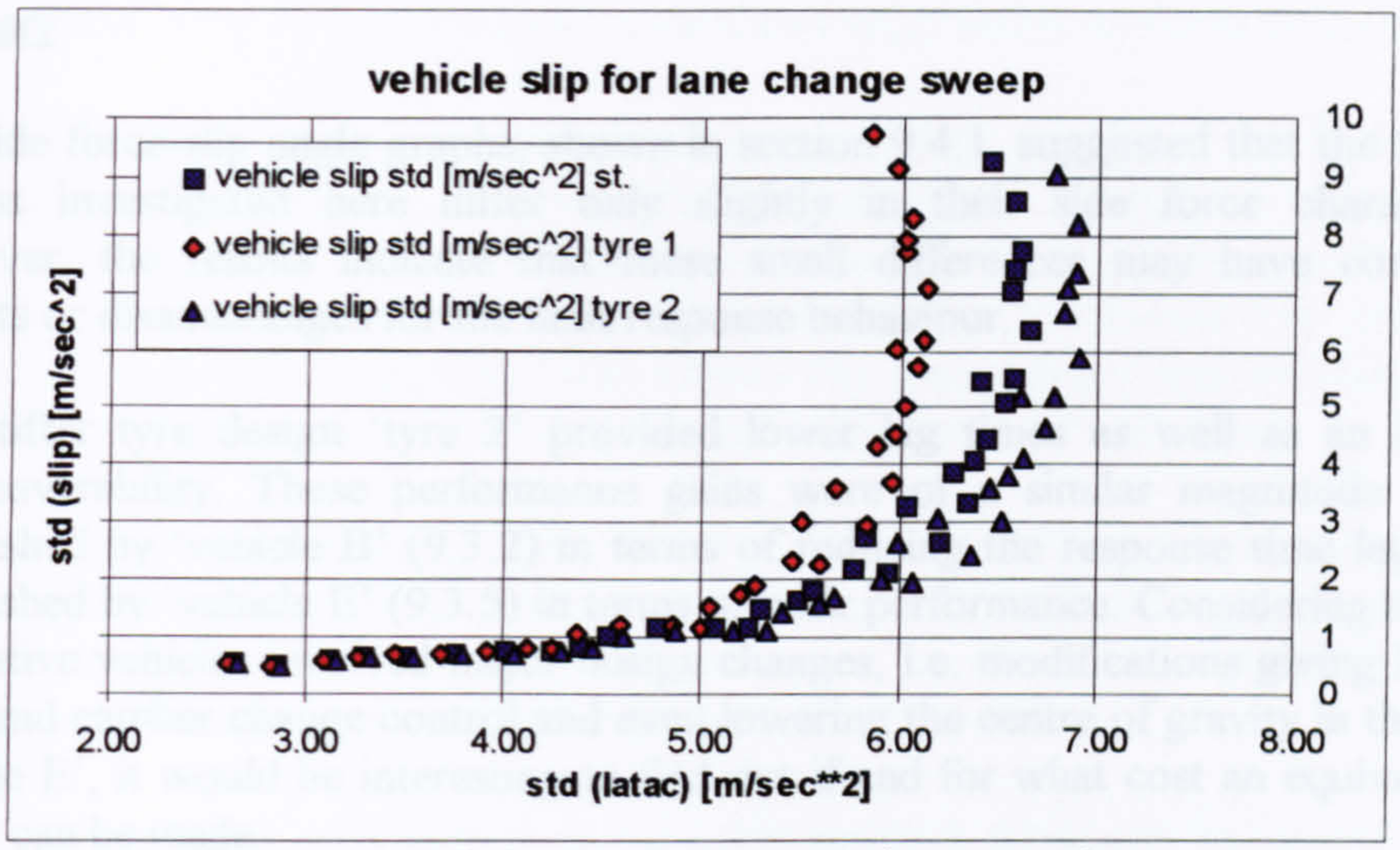

Fig. 9.4.2-4 Side slip motion as a function of manoeuvre severity

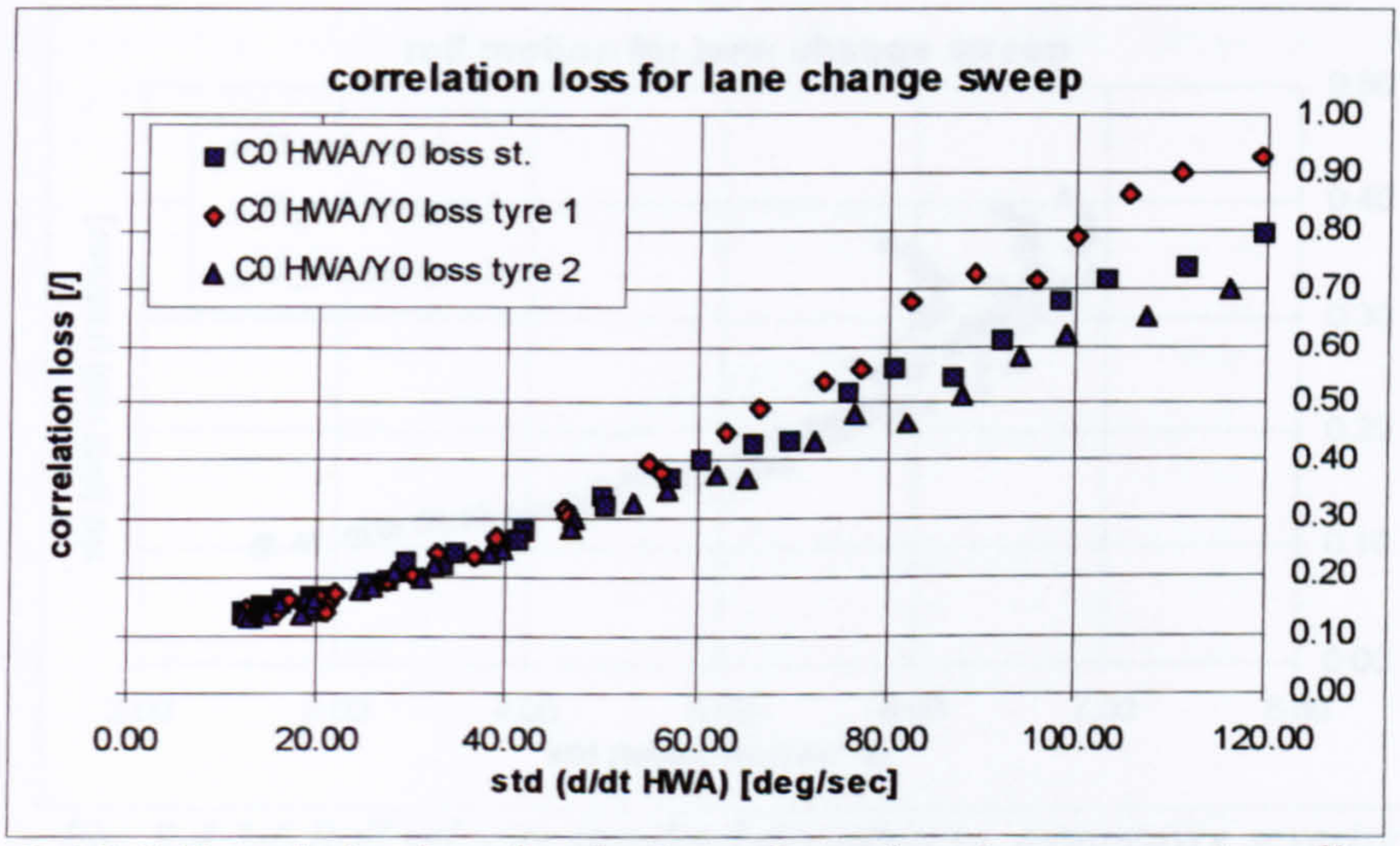

Fig. 9.4.2-5 Correlation loss for the lateral acceleration vs. steering effort due to vehicle side slip

gradient at which the correlation deteriorates with steering effort.

The more compliant design 'tyre 1' not only performs worse in terms of peak performance, but also increases the sensitivity of the vehicle response to manoeuvre severity.

As can be seen from fig. 9.4.2-6, this tyre-suspension combination also leads to slightly higher roll angle variations with respect to manoeuvre severity. The limit manoeuvres of the 'tyre 1' set-up involve larger standard deviations of the roll velocities compared to the other two configurations.

The 'tyre 2' shod vehicle tends to roll slightly less than the standard vehicle for the same level of severity.

summary

The side force-slip angle graphs, shown in section 9.4.1, suggested that the three tyre designs investigated here differ only slightly in their side force characteristics. However, the results indicate that these small differences may have considerable benefits or disadvantages for the limit response behaviour.

The stiffer tyre design 'tyre 2' provided lower lag times as well as an improved manoeuverability. These performance gains were of a similar magnitude to those established by 'vehicle B' (9.3.2) in terms of reducing the response time lags and as established by 'vehicle E' (9.3.5) in terms of peak performance. Considering that those alternative vehicles involved major design changes, i.e. modifications giving improved track and camber change control and even lowering the centre of gravity in the case of 'vehicle E', it would be interesting to find out if and for what cost an equivalent tyre design can be made.

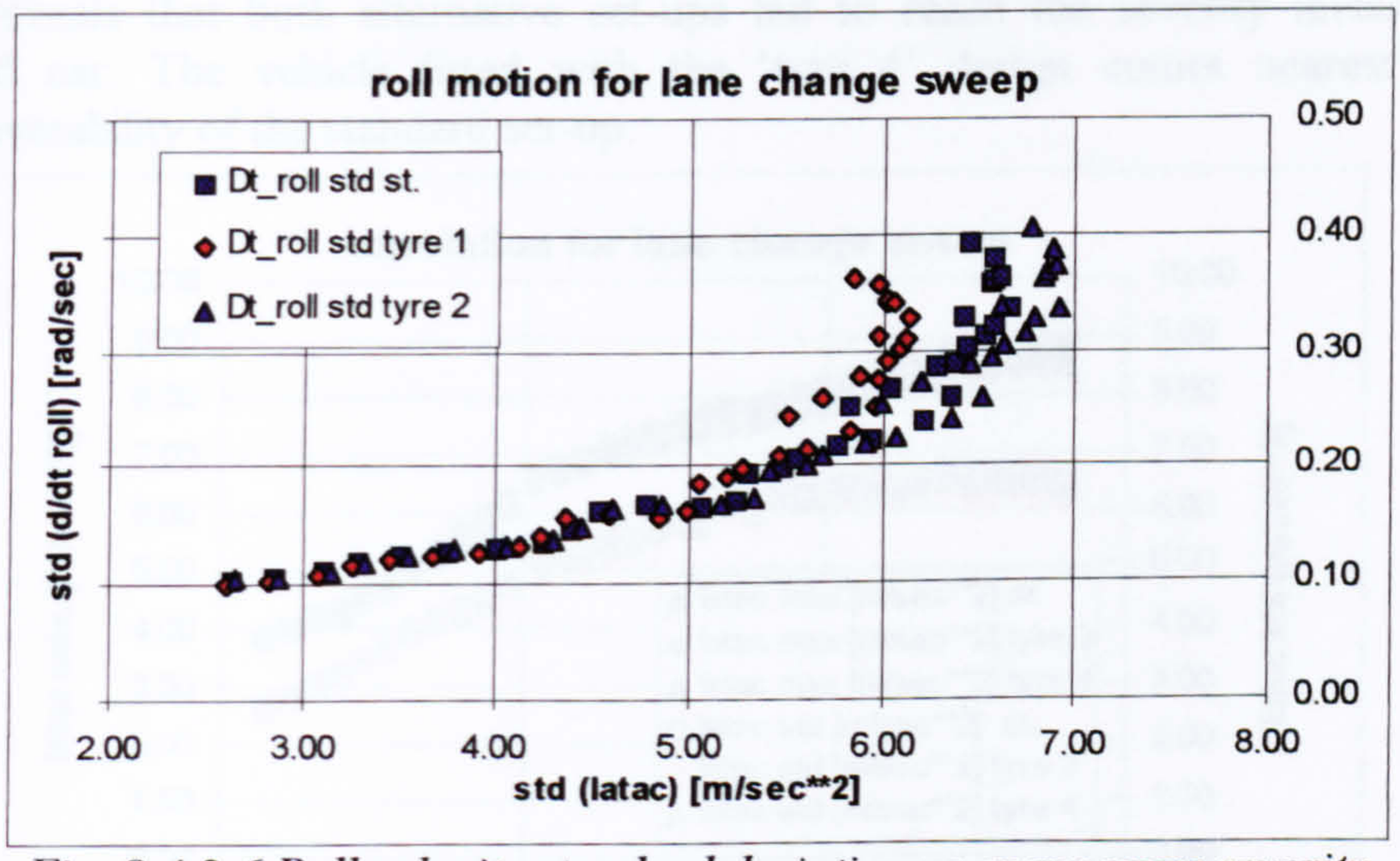

Fig. 9.4.2-6 Roll velocity standard deviation vs. manoeuvre severity represented by the standard deviation of the lateral acceleration

9.4.3 Effects of the 'Magic Formula' parameters BCD and E on the limit handling

The effects of the 'Magic Formula' parameters BCD and E on the limit handling performance are illustrated in this section. Although the nominal cornering stiffness BCD was not altered, its dependency on load was redefined for the 'tyre 3' and 'tyre 4' designs according to the values given in table 9.4.1-1. The former tyre design is the more compliant of the two, which was achieved by decreasing C and increasing E. The cornering stiffness and its dependency on load is the same for both tyres.

As can be seen from figures 9.4.1-3 and 9.4.1-4, the side force characteristics of the alternative designs are more sensitive to high vertical loads in comparison with the standard tyre. Their performances are compared to the results obtained from the simulation of the standard vehicle using standard tyres.

The severity of each 'lane change sweep' manoeuvre is illustrated by fig. 9.4.3-1. The graph reveals that both alternative set-ups fail to reach the severity levels of the standard car. The vehicle fitted with the 'tyre 4' design comes nearest to the manoeuverability of the standard set-up.

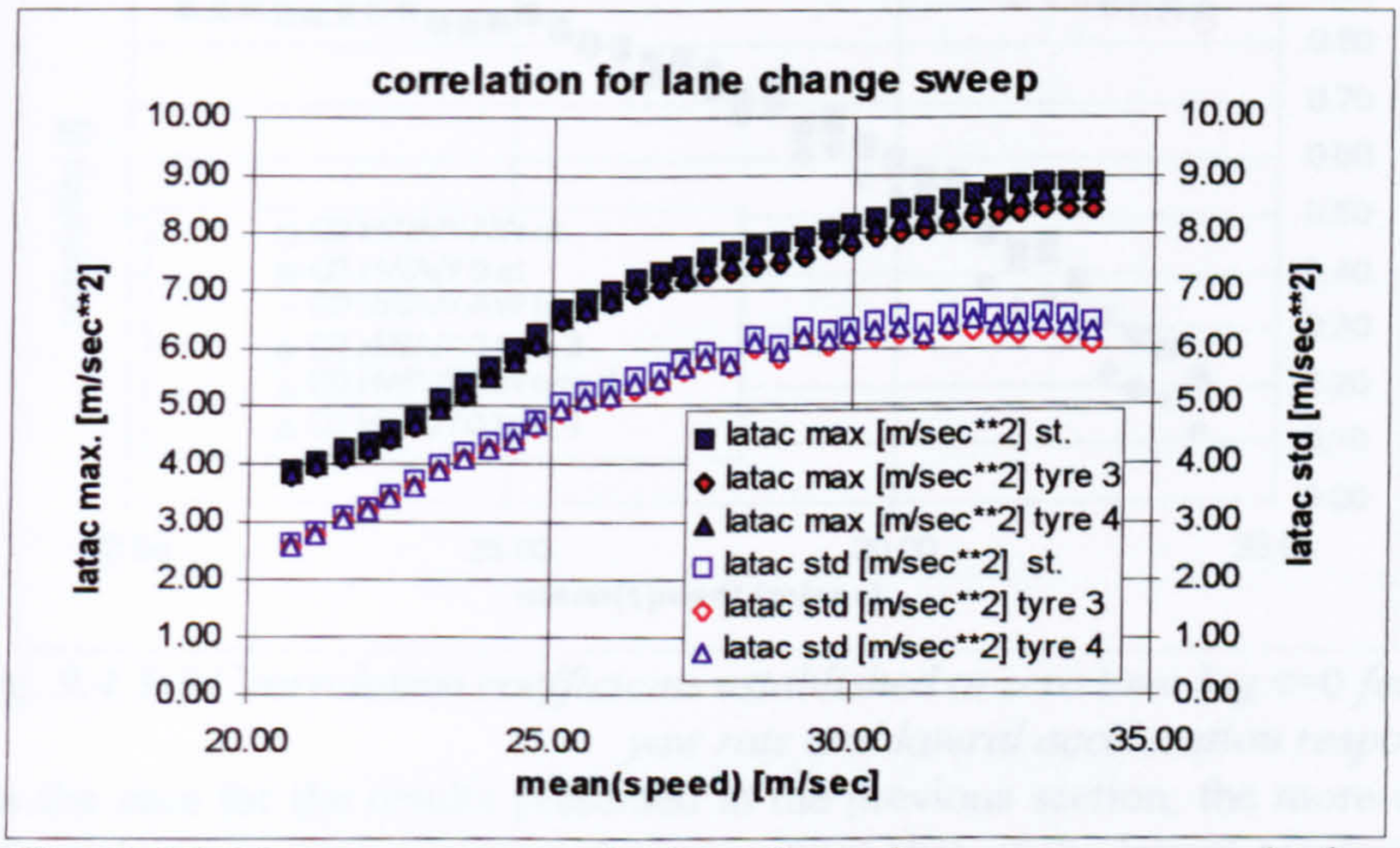

Fig. 9.4.3-1 Manoeuvre severity for a lane change sweep vs. vehicle speed

The effect of the two alternative tyre designs on the response behaviour is illustrated by figures 9.4.3-2 and 9.4.3-3. They show the response time delays and the correlation coefficients established for the lateral acceleration response at zero time lag.

The laterally stiffer design matches the response behaviour of the standard configuration. Lag times and correlation coefficients are almost identical. The 'tyre 3' set-up, however, yields longer lag times for the yaw rate and the lateral acceleration response as well as correspondingly decreasing correlation coefficients, beyond speeds of 27 m/sec.

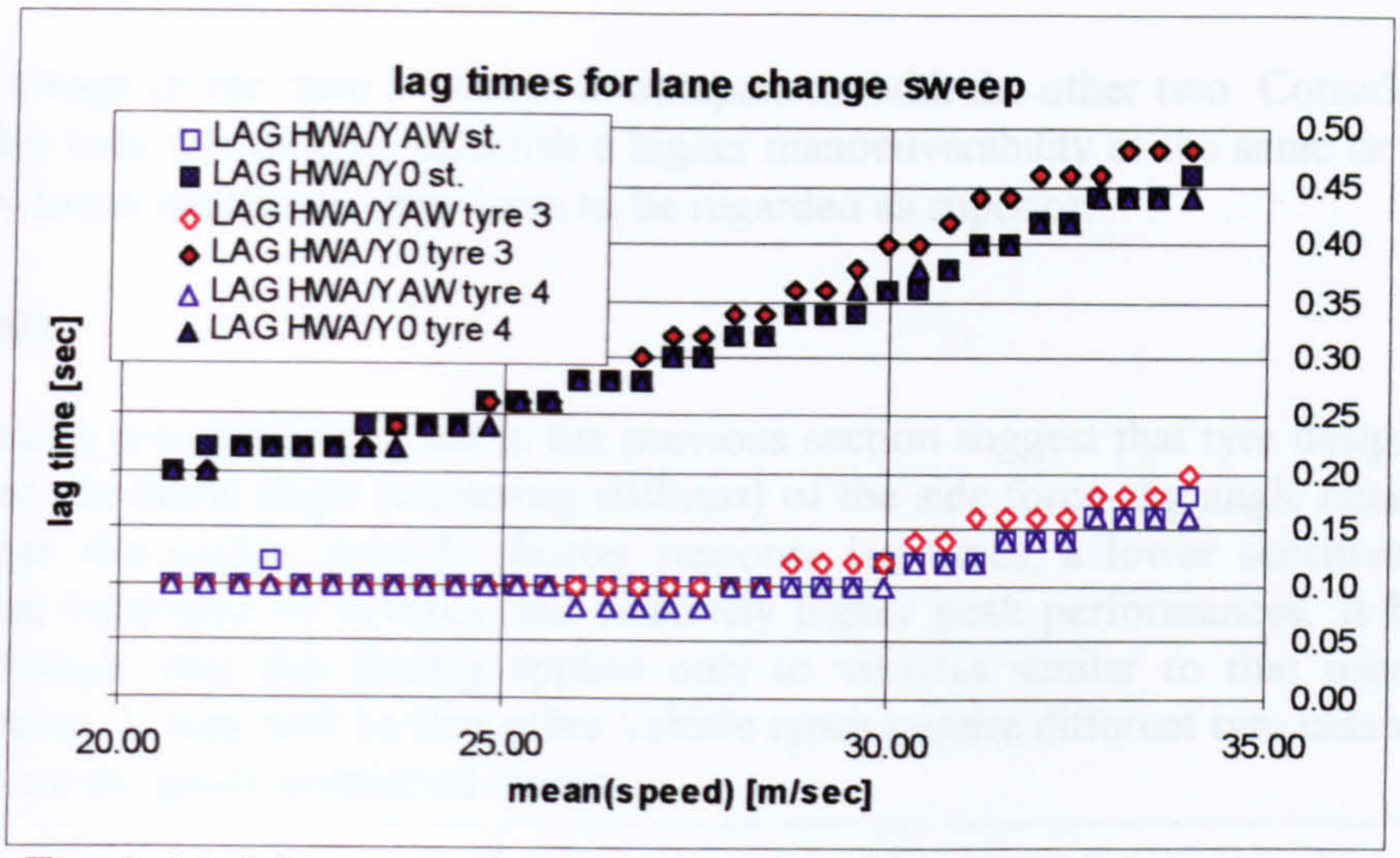

Fig. 9.4.3-2 Lag times for the yaw rate and lateral acceleration responses

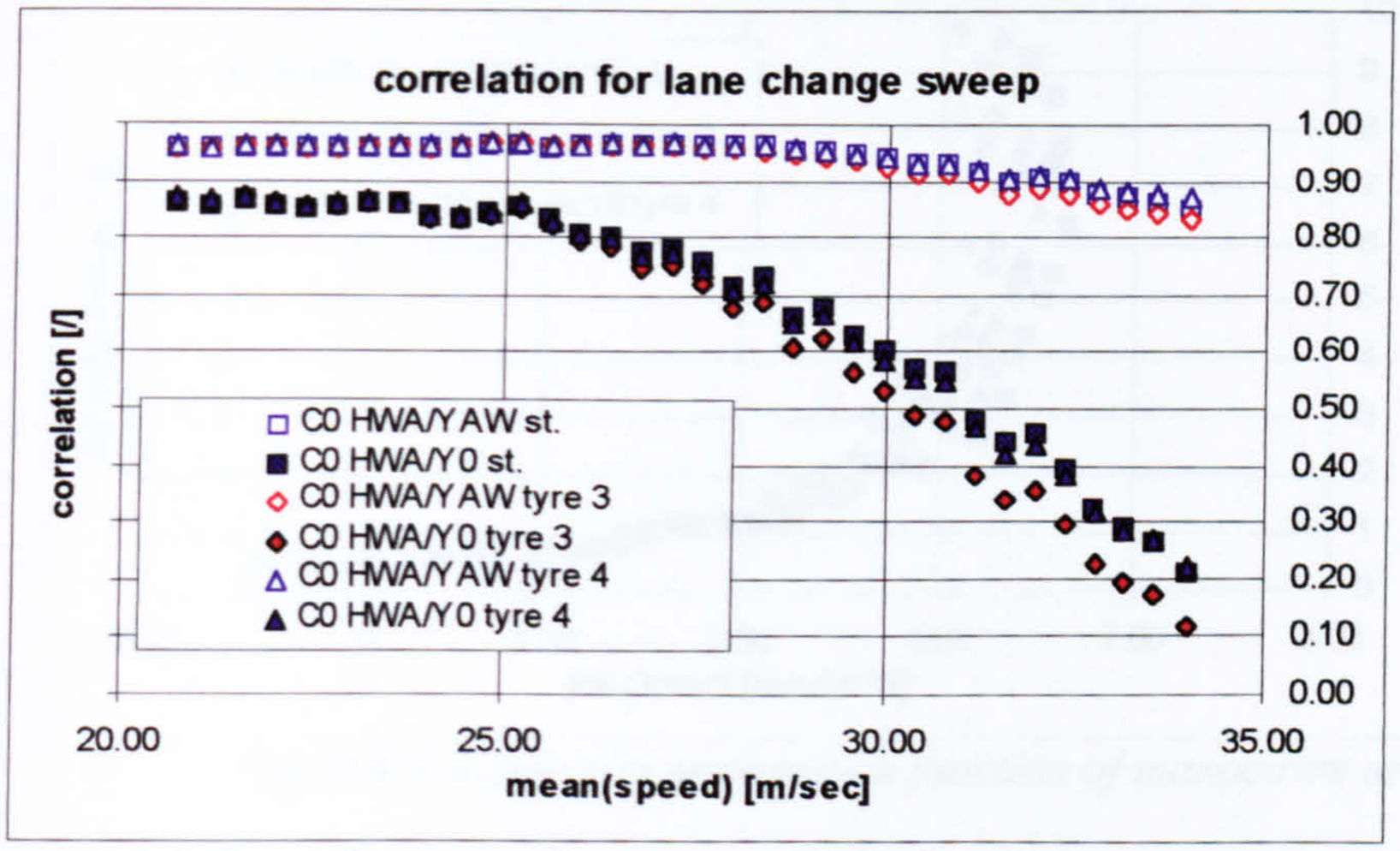

Fig. 9.4.3-3 Ccorrelation coefficients established at zero time lag τ=0 *for the yaw rate and lateral acceleration responses*

As was the case for the results presented in the previous section, the more compliant tyre provokes a yaw rate response diverging from that of the lateral acceleration at a lower severity. Beyond a severity level of 6 m/sec^2 the yaw rate response increases disproportionately in relation to the lateral acceleration response. This is established by fig. 9.4.3-4, showing the values of the side slip variation $\sigma_{\dot{\beta}}$ as a function of vehicle speed. The vehicles fitted with either of the other two tyre designs achieved a higher limit severity, before the lateral acceleration response saturated.

The sensitivity of the vehicle response to the limit approach can be established from fig. 9.4.3-5. The correlation loss is plotted against the steering effort parameter $\sigma_{\dot{\delta},\dot{\beta}}$.

Corresponding to the small differences in the side force characteristics, as illustrated by figures 9.4.1-3 and 9.4.1-4, all three vehicles established a rather similar sensitivity of their response behaviour to severity. Only the results for the high speed manoeuvres, yielding high correlation losses accompanied by large steering efforts, indicate a slight

disadvantage of the 'tyre 3' design in comparison with the other two. Considering that the other two tyre designs establish a higher manoeuverability at the same or even at a slightly lower sensitivity, they have to be regarded as superior.

summary

The results presented here and in the previous section suggest that tyre designs, which maintain the initial slope (cornering stiffness) of the side force-slip angle characteristic at higher slip angles, provide shorter response lag times, a lower sensitivity of the response behaviour to severity and relatively higher peak performances. It has to be said, though, that this finding applies only to vehicles similar to that used for the simulations. It may well be that other vehicle types require different tyre characteristics to achieve the goals mentioned above.

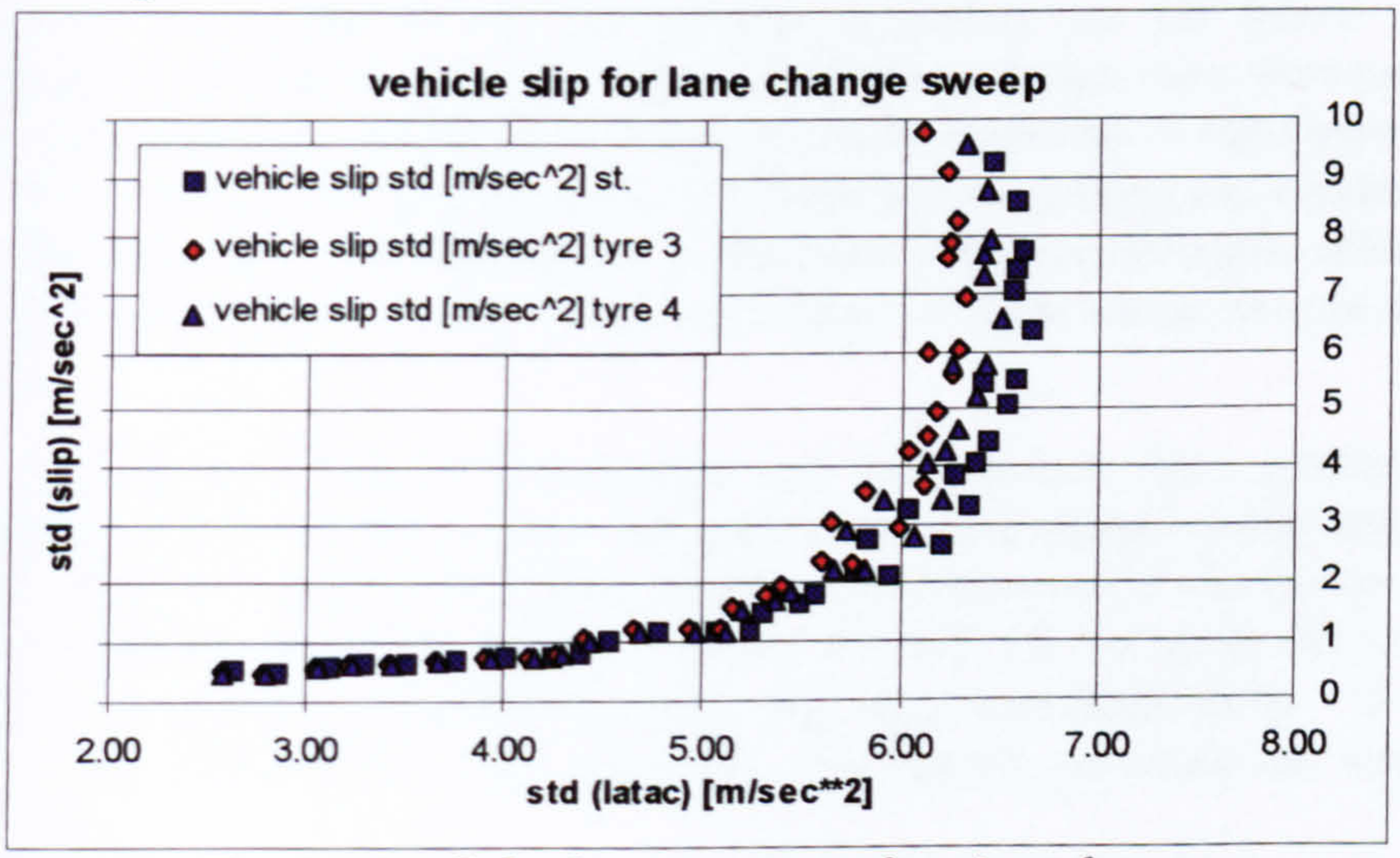

Fig. 9.4.3-4 Side slip motion as a function of manoeuvre severity

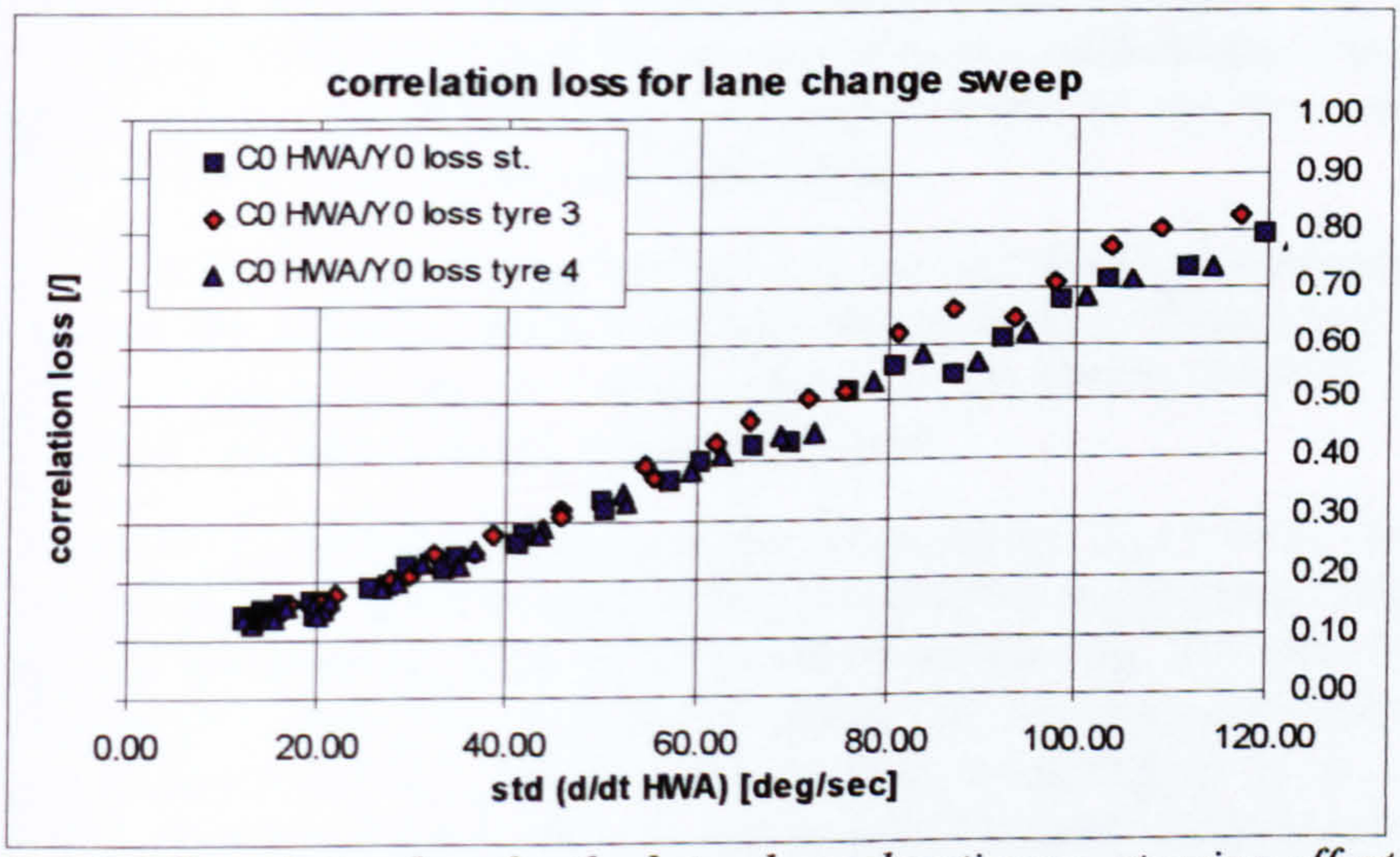

Fig. 9.4.3-5 Correlation loss for the lateral acceleration vs. steering effort due to vehicle side slip

9.4.4 Effects of tyre camber and of mixed front and rear tyres

This section gives an example of the influence of tyre camber properties on the limit handling performance. Some simulation results are presented, illustrating the effects of using different tyre designs for the front and rear axles.

In chapter 8 some results were shown indicating the effects of different suspension as well as tyre designs on the steady state limit performance. It was shown that, depending on the suspension geometry and the tyre design employed, the steady state limit behaviour could be changed drastically. It was concluded that the limit performance as well as the degree of limit under- or oversteer depend on how track and camber change characteristics of the suspension are matched to tyre properties.

Furthermore, the influence of tyre camber properties on the lateral adhesion performance of various axle designs was studied. Some design rules were established by which the peak side force of an axle design can be improved. It was shown that the interrelation between tyre camber on the one hand and the jacking and camber change control characteristics of a suspension on the other have a considerable effect on the effective lateral adhesion and on the roll-off behaviour of the lateral force at large side slip angles.

In this section the effect of tyre camber on the transient limit performance is illustrated by results obtained from a simulation of a 'lane change sweep' manoeuvre. For that, 'Magic Formula' coefficients, describing the influence of camber on the peak side force (D), the cornering stiffness (BCD), the roll- off curvature (E) and those defining the vertical and horizontal offsets (S_{vy}, S_{hy}) were reduced by 10 % with respect to the standard tyre. The simulation was carried out using the data of the standard car.

Additionally, the standard vehicle was simulated for a set of mixed tyre designs. The side force characteristics of the front tyres were described by the coefficients given for 'tyre 1' in section 9.4.1, while those for the rear tyres were identical to 'tyre 2'. The front tyres are fairly compliant for high slip angles, while the rear tyres maintain a linear side force - slip angle relation for higher slips.

As can be seen from figures 9.4.1-1 and 9.4.1-2, the side force characteristics of the alternative designs are more sensitive to high vertical loads in comparison with the standard tyre. Their performances are compared to the results obtained from the simulation of the standard vehicle using standard tyres.

The severity levels achieved by each set-up are given by fig. 9.4.4-1. The graph establishes that the less camber sensitive tyre hardly improves the manoeuverability, as expressed by the standard deviation of the lateral acceleration. The peak values are of equal magnitude. The vehicle with a set of mixed tyres did not achieve the severity levels of the other two configurations within the speed range of 25 up to 33 m/sec, although the peak steering wheel angle was increased. The peak lateral acceleration is lower. However, the magnitudes of the standard deviations are comparable.

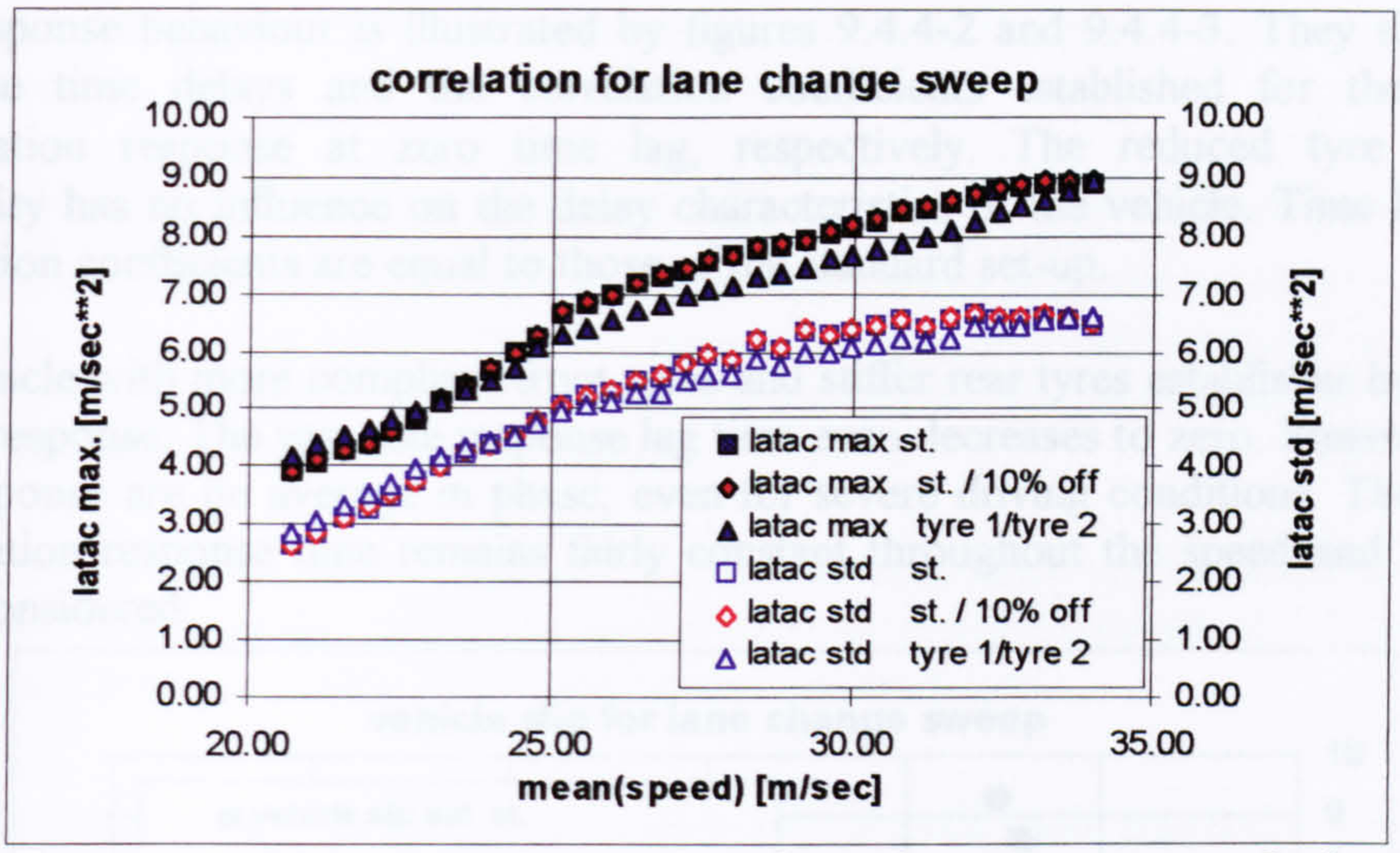

Fig. 9.4.4-1 Manoeuvre severity for a lane change sweep vs. vehicle speed

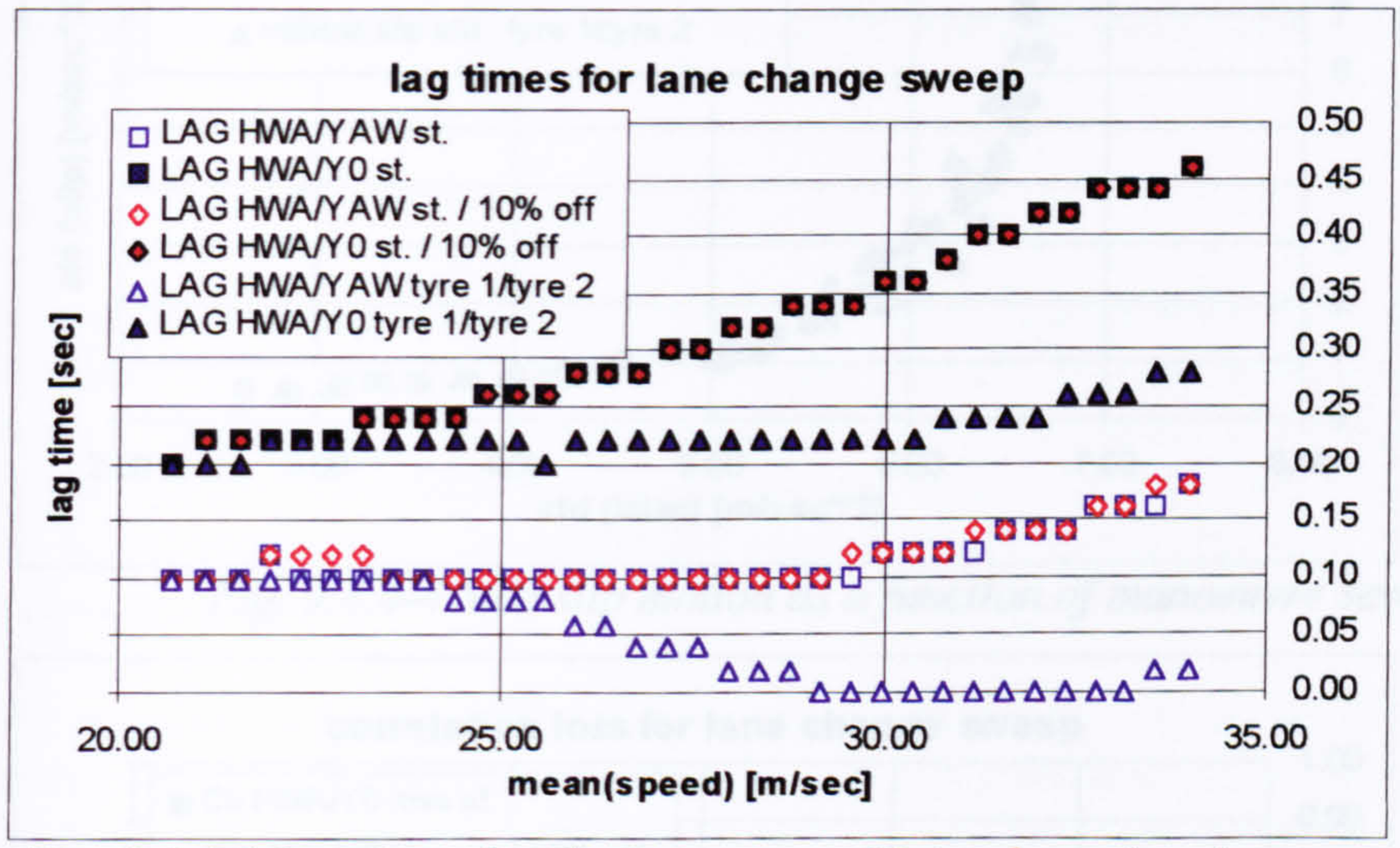

Fig. 9.4.4-2 Lag times for the yaw rate and lateral acceleration responses

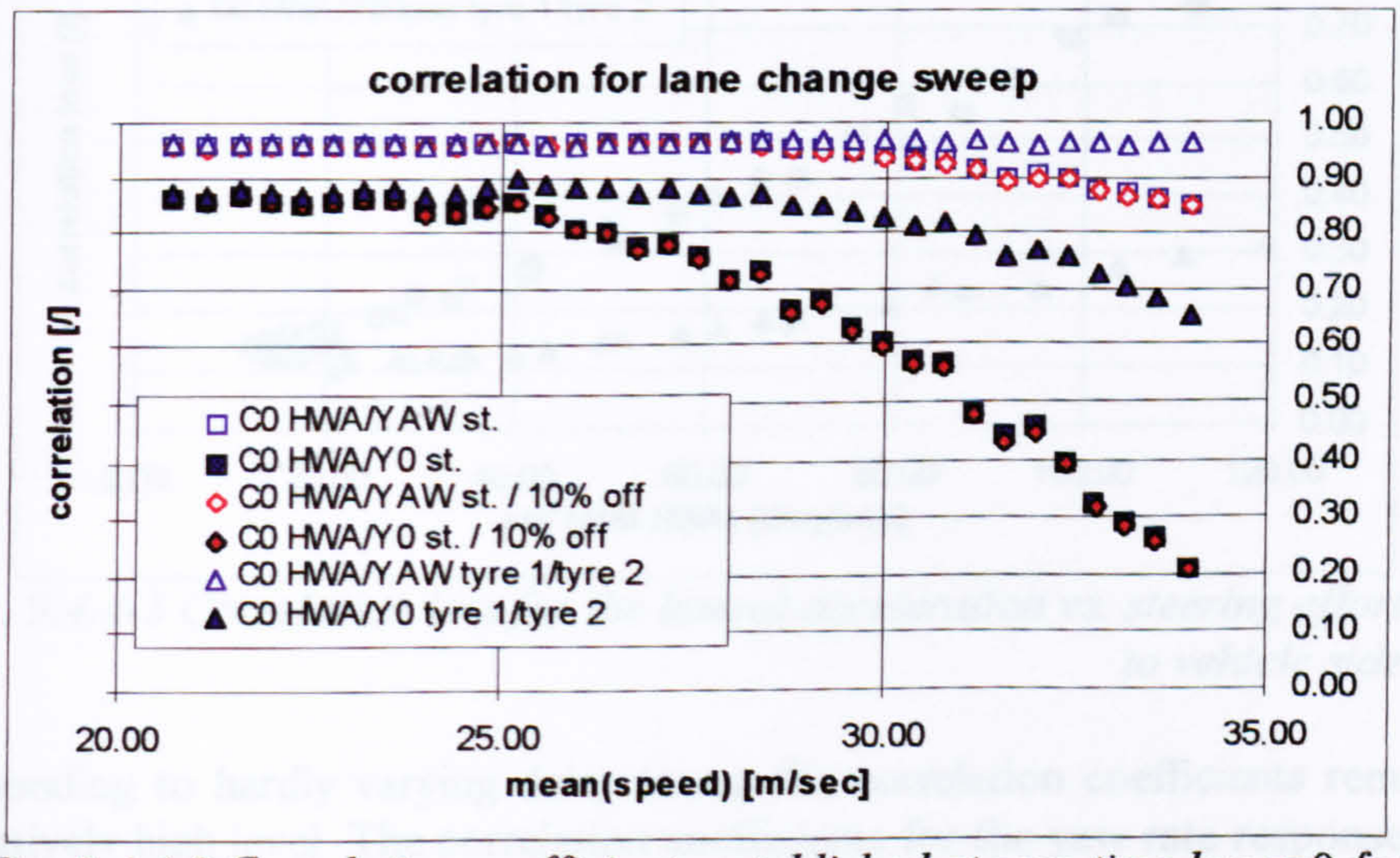

Fig. 9.4.4-3 Correlation coefficients established at zero time lag τ=0 for the yaw rate and lateral acceleration responses

The response behaviour is illustrated by figures 9.4.4-2 and 9.4.4-3. They show the response time delays and the correlation coefficients established for the lateral acceleration response at zero time lag, respectively. The reduced tyre camber sensitivity has no influence on the delay characteristics of the vehicle. Time lags and correlation coefficients are equal to those of the standard set-up.

The vehicle with more compliant front tyres and stiffer rear tyres establishes by far the fastest response. The yaw rate response lag time even decreases to zero. Steering input and response are on average in phase, even for severe driving conditions. The lateral acceleration response time remains fairly constant throughout the speed and severity range considered.

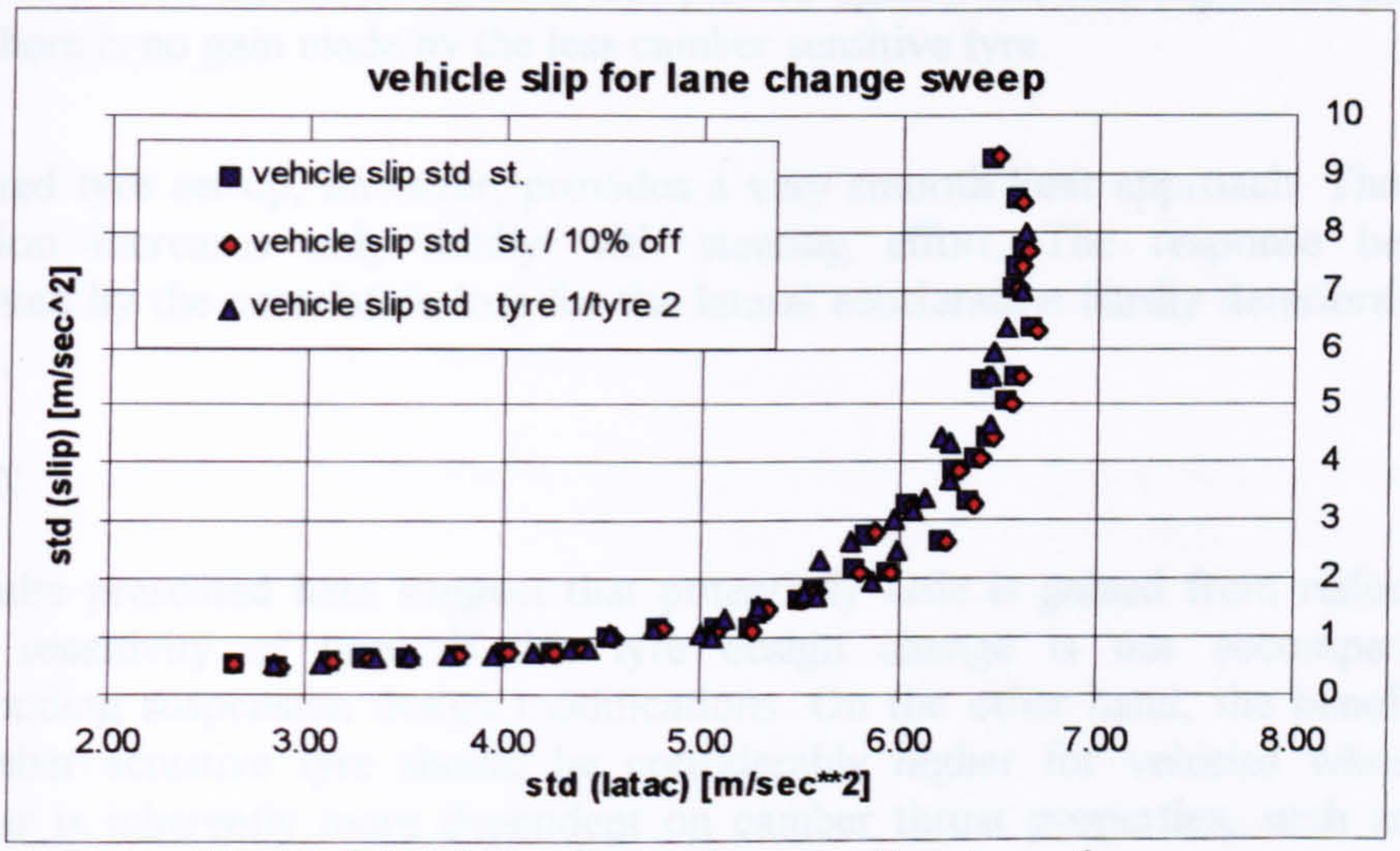

Fig. 9.4.4-4 Side slip motion as a function of manoeuvre severity

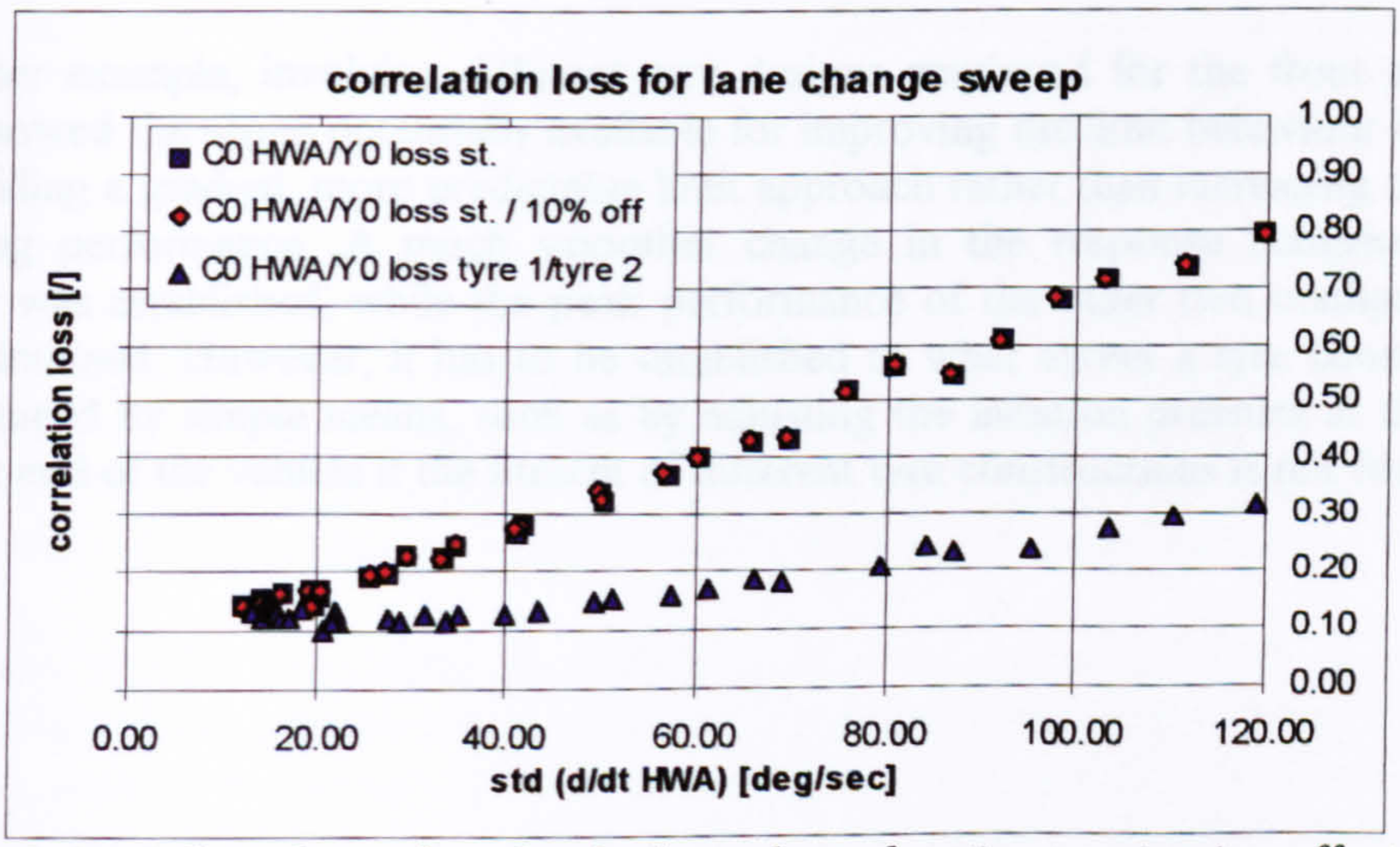

Fig. 9.4.4-5 Correlation loss for the lateral acceleration vs. steering effort due to vehicle side slip

Corresponding to hardly varying delay times, the correlation coefficients remain at a comparatively high level. The correlation coefficients for the yaw rate response remain

constant, while those referring to the lateral acceleration response decrease slightly with speed.

Fig. 9.4.4-4 shows the values of the side slip variation $\sigma_{\dot{\beta}}$ established for the three configurations. They are well matched. The less camber sensitive tyres give a slight advantage, in that they contain the discrepancy between yaw rate response and lateral acceleration slightly better than the other two set-ups for the same severity. The peak manoeuverability is also marginally higher.

The sensitivity of the vehicle response to the limit approach can be established from fig. 9.4.4-5, showing the correlation loss plotted against the steering effort parameter $\sigma_{\dot{\delta},\beta}$. There is no gain made by the less camber sensitive tyre.

The mixed tyre set-up, however, provides a very smooth limit approach. The loss of correlation increases only mildly with steering effort. The response behaviour represented by the correlation loss for the lateral acceleration hardly deteriorates with severity.

summary

The results presented here suggest that potentially little is gained from reducing the camber sensitivity of tyres if this tyre design change is not accompanied by corresponding suspension design modifications. On the other hand, the benefits of a less camber sensitive tyre should be considerably higher for vehicles whose limit behaviour is inherently more dependent on camber thrust properties, such as swing axle equipped vehicles.

The other example, involving different tyre designs employed for the front and rear ends, showed the scope potentially available for improving the limit behaviour in terms of providing a gradual, more predictable limit approach rather than increasing the peak cornering performance. A much smoother change in the response behaviour with severity was established, while the peak performance of the other two configurations was maintained. However, it has to be established to what extent a tyre construction can be tuned by simple means, such as by adjusting the inflation pressure at the front and rear end of the vehicle if the fitment of different tyre constructions is not feasible.

9.5 Summary and conclusions

Chapter 9 gave an overview of the simulation work carried out for investigating the transient limit handling performance. The vehicle model described in chapter 3 was validated against data recorded for a variety of proving ground test manoeuvres. Good agreement between model prediction and measurement was obtained for the lateral responses of the vehicle, even for severe driving conditions. The agreement between predicted and measured time histories of the lateral vehicle response was considerably less, though, for limit manoeuvres in which the test driver used the accelerator as an additional control input. This was ascribed to the fact that longitudinal traction forces were not included in the model. Inconclusive results were obtained for the hand wheel torque characteristics.

A simple driver model was used to establish whether the model could be validated for the closed loop case. The limitations of this model, however, meant that the agreement between predicted and measured steering input deteriorated considerably for manoeuvres involving higher severity levels.

The effects of several suspension design characteristics and tyre properties were studied using simulation results of a 'lane change sweep' manoeuvre, which involves the concurrent effects of increasing vehicle speeds and steering input frequencies as well as of tyres operating increasingly at larger slip angles.

The response behaviour of each design alternative was compared to the standard configuration with respect to criteria, representing the peak manoeuverability as well as the degree by which the response changes with severity. The peak manoeuverability was represented by the standard deviation of the lateral acceleration achieved for an open loop manoeuvre akin to a double lane change. Applying the concept of correlating the driver input to the vehicle responses, as was the case for the proving ground data analysis in chapter 7, changes of the response behaviour with severity were established. Similar trends as observed from the proving ground test results were reproduced. Response time lags as well as the discrepancy between the yaw rate and the lateral acceleration response increase with severity. The rate by which the correlation between steering input and lateral acceleration response deteriorates with increasing steering efforts was used as a criterion to establish whether the vehicle approaches its limit performance in a gradual fashion.

Simulation results concerning alternative chassis set-ups established that design modifications leading to an increased steady state understeer lead to lower response time lags, notably to a lower rate of increase with severity, without giving necessarily a lower manoeverability. The examples indicated potential benefits of improved second order track and camber control characteristics. Those involving a McPherson type suspension design showed that a poor roll angle compensation can be neutralised by improved track change characteristics.

The parameter study of certain tyre properties indicated to what extent response time lags as well as the sensitivity of the vehicle's response behaviour to manoeuvre severity can be reduced, by modifying the roll-off characteristics of the side force-slip angle relation. Tyres providing an extended linear region improved the limit handling. An example showed that a reduction of the tyre's camber sensitivity provides little gain for transient limit manoeuvres. It was concluded that such a tyre design feature has to be matched by suspension characteristics allowing the utilisation of the improved tyre performance.

Results obtained from a simulation for which different front and rear tyre characteristics were modelled, indicated the potential advantages of such a set-up. This configuration provided very low response time lags as well as a low rate of change in the response behaviour with severity, similar to the behaviour established for the subjectively highly rated tyre combinations 'M2/XY' and 'XY/XY', discussed in sections 7.3.2 and 7.3.3.

10 Conclusions

Some of the ground work for matching tyres to vehicles was completed. However, some important issues concerning the effects of tyre and chassis properties on the limit handling behaviour remain unresolved and require further work.

Proving ground and simulation results obtained for a variety of vehicle-tyre configurations suggest that response time lags and cross-correlation coefficients in combination with the steering effort parameter can be used as objective quality measures. The results quantified to what extent tyre and chassis modifications change the limit handling behaviour.

The transient limit behaviour was evaluated using test results obtained for lane change manoeuvres conducted according to the ISO standard and for avoidance manoeuvres performed while cornering at comparatively low speeds on a steering pad. The high speed ISO lane change test provided more conclusive results, distinguishing the handling quality of the different test configuration much better.

The analysis of the double lane change tests performed at increasing speeds suggested that controlling the yaw attitude of a vehicle, even in limit situations, should remain fairly straight forward. The yaw rate response remains well correlated with the steering wheel input and its delay remains almost constant at a low level. The lateral acceleration response, however, deteriorates with increasing manoeuvre severity. This is reflected by decreasing correlation coefficients and increasing time delays. The transition from a single input/ single output system, as is the case for low severity manoeuvres for which the lateral acceleration is almost proportional and in phase with the yaw rate response, to a single input/ dual output one was ascribed to the presence of increasing vehicle side slip. The steering effort required to control the side slip was used as a further measure of the handling quality.

Tests results of vehicle set-ups which were rated as 'poor' or 'inferior' by the test driver indicated a high rate of correlation loss accompanied by a high steering activity to control the side slip. Favourable subjective ratings corresponded to vehicles characterised by a low decrease in correlation with increasing steering wheel activity associated with the side slip control. The results of the various vehicle configurations tested suggested a trend in that modifications to the baseline set-up often associated with 'giving more understeer' improved the controllability.

Vehicle roll was identified as another important factor influencing the subjective appraisal. Some results suggested that the transient roll behaviour can be influenced significantly by the tyre design.

A realistic, 'Magic Formula' based tyre model was developed which interfaces with SP Tyres' in-house developed Tyre Property Prediction software (TPP) as well as with most of the vehicle dynamics software used by SP Tyres' customers.

A fairly detailed vehicle handling model was build-up allowing investigations of tyre and suspension design alterations on the handling behaviour. The model was validated against proving ground test data, which included data obtained for severe transient manoeuvres near the limit of adhesion.

Some basic rules for tyre and suspension design were derived and verified by simulations of steady state and transient driving manoeuvres. These rules describe how to control vehicle roll and jacking by a suitable suspension geometry that maintains acceptable wheel camber angles with respect to the ground. Furthermore, it was quantified to which extent tyre camber thrust influences the side force generation capability of different suspension types. The examples given show that these design rules can be used to improve the balance between front and rear side force generation.

The simulation of transient limit manoeuvres involving alternative chassis set-ups established that design modifications giving an increased steady state understeer lead to lower response time lags, notably to a lower rate of increase with severity. This conforms with the trend established by the proving ground results. Some of the simulation results also suggested that these modifications do not necessarily decrease the peak lateral acceleration performance for a lane change type manoeuvre.

Some examples indicated potential benefits of improved second order track and camber control characteristics. Those involving a McPherson type suspension design showed that adverse wheel camber due to poor roll angle compensation can be neutralised by improved track change characteristics.

The parameter study of certain tyre properties indicated to what extent response time lags as well as the sensitivity of the vehicle's response behaviour to manoeuvre severity can be reduced. Parameters BCD, C and E defining the 'Magic Formula' were varied to study the effect of different side force roll-off characteristics. Tyres providing an extended linear region improved the limit handling. The simulation for which different front and rear tyre characteristics were considered indicated potential advantages of such a particular set-up and, in more general terms, the benefits of matching tyre and suspension properties.

It has yet to be established, though, how generic tyre properties can be systematically modified by corresponding design or material alterations and which impact these tyre design modifications have on the handling performance of typical chassis designs. The former issue can be addressed by employing TPP for a parametric study, which may result in straight forward tyre design rules. Quantifying the effects of tyre design changes on the vehicle handling of typical vehicle designs may involve too many influential parameters preventing the derivation of general design principles. It seems more appropriate to evaluate the influence of generic, 'Magic Formula' type properties on the handling behaviour of a particular vehicle design. After target force and moment characteristics are found, the TPP program can be employed for establishing the design changes required to emulate the target properties.

During the research project some efforts were made to develop SPUK's Inertia Rig for obtaining reliable estimates of certain handling related vehicle parameters. Unfortunately, the development work was not brought to a satisfactory conclusion. However, it is believed that those test results obtained during the project indicating the limitations and problems of the rig and the test procedure as well as the suggestions made on analysing the test data may help completing the rig as a useful and straight forward to use means for estimating vehicle data essential for simulation purposes.

It is believed that the findings of the project and the analysis tools developed contribute to an earlier and more efficient collaboration between vehicle manufacturer and tyre supplier, improving product quality and safety as well as saving development costs.

References:

/1.0.1/ Kohn, H.J., Stephens, P., "Controllability of Road Vehicles at the Limit of Tyre Adhesion", CROVLA project report, 1997

/1.1.1/ Road Accidents in Great Britain: 1995, The Casualty Report, Department of Transport, HMSO, London, 1996

/1.2.1/ Shimada, K., Shibahata, Y., "Comparison of Three Active Chassis Control Methods for Stabilising Yaw Moments", SAE paper No. 940870

/1.2.2/ Lugner, P., Mittermayr, P., "Possibilities to improve the Vehicle Cornering Dynamics by the Control of the Tyre Forces", Proceedings of the 11th IAVSD Symposium, Swets & Zeitlinger, 1989, pp.377-390

/1.2.3/ Dreyer, A., Heitzer, H.-J., "Control Strategies for Active Chassis Systems with Respect to Road Friction", SAE paper No. 910660

/1.2.4/ Donges, E., "Supporting Drivers by Chassis Control Systems", Smart Vehicles: J.P. Pauwelussen, H.B.Pacejka (eds.), pp. 276-296

/1.2.5/ van Zanten, A.T., Erhardt, R., Pfaff, G., "VDC, The Vehicle Dynamics Control System of Bosch", SAE paper No. 950759

/1.2.6/ van Oosten, J.J.M., e.a., "TIME, Tire Measurements, Forces and Moments, proposal, Scientific and Technical Content, part A, TNO, Delft, 1995

/1.2.7/ van Oosten, J.J.M., Unrau, H.-J., Riedel, A., Bakker, E., "TYDEX Workshop: Standardisation of Data Exchange in Tyre Testing and Tyre Modelling", Proceedings of the 2nd International Colloquium on Tyre Models for Vehicle Dynamics Analysis, Vehicle System Dynamics Supplement 27, 1997, pp.272-288

/2.0.1/ Roberson, R.E., Schwertassek, H., "Dynamics of Multibody Systems", Berlin, Springer Verlag, 1988

/2.0.2/ Schiehlen, W., "Multibody Systems Handbook", Berlin, Springer Verlag, 1990

/2.0.3/ Chrstos, J.P., "A simplified method for the measurement of composite suspension parameters", SAE paper No. 910232, Vehicle Dynamics and Electronic Controlled Suspensions, 1991

/2.0.4/ Winkler, C.B, Campbell, K.L., Mink, C.E., "Variability in centre of gravity height measurement ", SAE paper No. 920050

/2.0.5/ Coffey, B.M., Fries, R.H., "Estimation of two-axle intermodal rail vehicle", 11th IAVSD Symposium on the Dynamics of Vehicles on Roads and Tracks, Swets & Zeitlinger, 1989, pp.137-147

/2.0.6/ Keresztes, A., Bokor, J., Varlaki, P., Michelberger, P., "Identification of partially known vibrating structures", 11th IAVSD Symposium on the Dynamics of Vehicles on Roads and Tracks, Swets & Zeitlinger, 1989, pp.310-321

/2.0.7/ Boehm, F., "Tire models for computational car dynamics in the frequency range up to 1000Hz", Tyre Models for Vehicle Dynamics Analysis, Swets & Zeitlinger, 1991, pp. 82-91

/2.0.8/ Springer, H., Ecker, H, Slibar, H., "A new analytical model to investigate transient conditions of a steel-belted tyre", 10th IAVSD Symposium on the Dynamics of Vehicles on Roads and Tracks, Prague, Swets & Zeitlinger, 1987, pp. 448-459

/2.0.9/ Lozia, Z., "A two dimensional model of the interaction between a pneumatic tyre and an even or uneven road surface", 10th IAVSD Symposium on the Dynamics of Vehicles on Roads and Tracks, Praque, Swets & Zeitlinger, 1987, pp. 227-238

/2.1.1/ Road Accidents in Great Britain: 1990, The Casualty Report, Department of Transport, HMSO, London, 1991, p. 61

/2.1.2/ Brinkman, C.P., Perchonok, K., "Hazardous Effects of Highway Features and Roadside Objects - Highlights", Public Roads, June 1979

/2.1.3/ Tignor, S.C., Brinkman, C.P. et. al., "Roadside Features" in "Synthesis of Safety Research related Traffic Control and Roadway Elements Vol.1", chapter 3, Report No. FHWA-TS-82-232, U.S. Department of Transport, Federal Highway Administration, December 1982

/2.1.4/ Salt, G.F., Szatkowski, W.S., "A guide to levels of skidding resistance for roads", TRRL Laboratory report 510, Department of Transport, 1973

/2.1.5/ Hosking, J.R., "Relationship between skidding resistance and accident frequency: estimates based on seasonal variation", TRRL Laboratory report 76, Department of Transport, 1986

/2.2.1/ Allen, R.W., Szostak, H.T., Rosenthal, T.J., "Characteristics influencing ground vehicle lateral/directional dynamic stability ", SAE paper No. 910234. pp.43-46

/2.2.2/ Sayers, M.W., Introductory Guide to AUTOSIM, UMTRI, The University of Michigan, Transport Research Institute, 1992

/2.2.3/ ADAMS Reference Manual, Version 6.1, Mechanical Dynamics, 1992

/2.3.1/ Linke, W., Richter, B., Schmidt, R., "Simulation and measurement of driver vehicle handling performance", SAE paper No. 730489

2.3.2/ Mitschke, M., "Dynamik der Kraftfahrzeuge", Bd. C, Fahrverhalten, Berlin, Springer Verlag, 1988, p. 25 et seq.

/2.3.3/ Road Vehicle - Lateral transient response test methods, ISO 7401, 1988

/2.3.4/ Sano, S., "Evaluation of motor vehicle handling", Int. J. of Vehicle Design, vol.3, no.2, pp.171-189

/2.3.5/ Bergmann, W., "Measurement and Subjective Evaluation of Vehicle Handling", SAE paper No. 730492

/2.3.6/ Jaksch, F.O., "Driver Vehicle Interaction with Respect to Steering Controllability", SAE paper No. 790740

/2.3.7/ Weir, D.H., DiMarco, R.J., "Correlation and Evaluation of Driver/Vehicle Directional Response", SAE paper No. 780010

/2.3.8/ Belsdorf, M.R., Rice, R.S., Bird, K.D., "Performance Tasks as Measures of Vehicle Handling Qualities at the Limit of Performance", SAE paper No. 710081

/2.3.9/ Ervin, R.D., Fancher, P.S., Segel, L., "Refinement and Application of Open-Loop Limit-Maneuver Response Methods", SAE paper No. 730491

/2.3.10/ Mitschke, M., "Dynamik der Kraftfahrzeuge", Bd. C, Fahrverhalten, Berlin, Springer Verlag, 1988, p. 83 et seq.

/2.3.11/ Crolla, D.A.,Whitehead, J.P., Chen, D.C., "Vehicle Handling Assessment Using a Combined Subjective-Objective Approach", SAE paper, 1998

/2.4.1/ Rimondi, G., "Basic car tyre development principles", Autotechnologies Proceedings, SAE paper No. 890103

/2.4.2/ Reimpell, J., Sponagel, P., "Fahrwerktechnik: Reifen und Raeder", Wuerzburg, Vogel Buch Verlag, 1986, p.198 et seq.

/2.4.3/ Pacejka, H.B., Sharp, R.S., "Shear force development by pneumatic tyres in steady state conditions: a review of modelling aspects", Vehicle System Dynamics, 1991, pp. 121-176

/2.4.4/ Mastinu, G., Gaiazzi, S., Montanaro, F., Pirola, D., "A Semi-Analytical Tyre Model for Steady- and Transient State Simulations", Proceedings of the 2nd International Colloquium on Tyre Models for Vehicle Dynamics Analysis, Vehicle System Dynamics Supplement 27, 1997, pp.2-21

/2.4.5/ Ammon, D., Gipser, M., Rauh, J., Wimmer, J.,"High Performance Systems Dynamics Simulation of the entire System Tire-Suspension-Steering-Vehicle", Vehicle System Dynamics, 27, 1997, pp. 435-455

/2.4.6/ Bakker, E., Pacejka, H.B., Lidner, L., "A new tire model with an application in vehicle dynamics studies", Autotechnologies Proceedings, SAE paper No. 890087

/2.4.7/ Pacejka, H.B., Bakker, E., "The magic formula tyre model", Tyre Models for Vehicle Dynamics Analysis, Swets & Zeitlinger, 1991, pp.1-18

/2.4.8/ Schuring, D.J., Pelz, W., Pottinger, M.G., "The BNPS Model-An Automated Implementation of the 'Magic Formula' Concept", IPC Conf. & Exposition, Arizona, 1993

/2.4.9/ van Oosten, J.J.M., Bakker, E., "Determination of magic tyre formula parameters", Tyre Models for Vehicle Dynamics Analysis, Swets & Zeitlinger, 1991, pp.19-29

/2.4.10/ Lidner, L., "Experience with the magic formula tyre model", Tyre Models for Vehicle Dynamics Analysis, Swets & Zeitlinger, 1991, pp.30-46

/2.4.11/ Takahashi, T., Pacejka, H.B., "Cornering on uneven roads", 10th IAVSD Symposium on the Dynamics of Vehicles on Roads and Tracks, Praque, Swets & Zeitlinger, 1987

/2.4.12/ Pacejka, H.B., Takahashi, T., "Pure slip characteristics of tyres on flat or undulated road surfaces", SAE paper No. 923064, AVEC 1992

/2.4.13/ Pacejka, H.B., Besselink, I.J.M., "Magic Formula Tyre Model with Transient Properties", Proceedings of the 2nd International Colloquium on Tyre Models for Vehicle Dynamics Analysis, Vehicle System Dynamics Supplement 27, 1997, pp.234-249

/2.4.14/ Bayle, P., Forissier, J.F., Lafon, S., "A new tyre model for vehicle dynamics simulations", Automotive Technology International '93, pp.193-198

/2.4.15/ Pacejka, H.B., "The tyre as a vehicle component", part 1A of the short course notes on "Active Chassis Control and the Role of the Tyre", Delft, 1995

/2.5.1/ Guo, K., Guan, H, "Modelling of Driver/Vehicle Directional Control Systems", Vehicle System Dynamics, vol. 22, 1993, pp. 141-184

/2.5.2/ Cho, Y.H., Kim, J., "Stability Analysis of the Human Controlled Vehicle Moving Along a Curved Path", Vehicle System Dynamics, vol. 25, 1996, pp. 51-69

/2.5.3/ Mitschke, M., "Dynamik der Kraftfahrzeuge", Bd. C, Fahrverhalten, Berlin, Springer Verlag, 1988, p. 115 et seq.

/2.5.4/ MacAdam, C.C., "Application of an Optimal Preview Control for Simulation of Closed-Loop Automobile Driving", IEEE Transactions on Systems, Man, and Cybernetics, Vol. SMC-11, No. 6, June 1981

/2.5.5/ Riedel, A., "IPG-Driver - Ein Modell des realen Fahrers für den Einsatz in Fahrdynamik-Simulationsmodellen", Automobil-Industrie 6/90

/2.5.6/ MacAdam, C.C., Johnson, G.E., "Application of Elementary Neural Networks and Preview Sensors for Representing Driver Steering Control Behaviour", Vehicle System Dynamics, vol. 25, 1996, pp. 3-30

/2.6.1/ Reed, D., "Passenger Car ABS", Automotive Engineering, July 1995

/2.6.2/ Leister, G., "New Procedures for Tyre Characteristic Measurement", Proceedings of the 2nd International Colloquium on Tyre Models for Vehicle Dynamics Analysis, Vehicle System Dynamics Supplement 27, 1997, pp.22-36

/2.6.3/ van der Jagt, P., Parsons, A.W., "Road Surface Correction of Tyre Test Data", Vehicle System Dynamics, vol. 25, 1996, pp. 147-165

/3.1.1/ Sharp, R.S., private communication

/3.1.2/ Mitschke, M., "Dynamik der Kraftfahrzeuge", Bd. C, Fahrverhalten, Berlin, Springer Verlag, 1988, p. 21 et seq.

/3.1.3/ Ellis, J.R., "Vehicle Dynamics", London, 1969, p. 60 et seq.

/4.1.1/ Barson, C.W., technical report No. TD1212, Fort Dunlop, Birmingham, 1980

/4.1.2/ Barson, C.W., technical report No. TD1181, Fort Dunlop, Birmingham, 1980

/4.1.3/ Barson, C.W., technical report No. TD1222, Fort Dunlop, Birmingham, 1981

/4.1.4/ Barson, C.W., technical report No. TD1356, Fort Dunlop, Birmingham, 1983

/4.1.5/ Barson, C.W., technical report No. TD1351, Fort Dunlop, Birmingham, 1983

/4.1.6/ SPMM- Suspension Parameter Measuring Machine, Anthony Best Dynamics Ltd, 1996

/4.1.7/ "Moment of inertia tests on a Jaguar XJ40 Vanden Plas saloon vehicle", Report to Jaguar Cars Ltd, Cranfield Institute of Technology, School of Mechanical Engineering, 1991

/4.1.8/ Curzon, A.M., Cooperrider, K., Limbert, D.A., "Light truck inertial properties", SAE paper No. 910122

/4.1.9/ Winkler, C.B, Campbell, K.L., Mink, C.E., "Variability in centre of gravity height measurement ", SAE paper No. 920050

/4.1.10/ Lin, Y., Kortüm, W., "Identification of system physical parameters for vehicle systems with nonlinear components", 12th IAVSD Symposium on the Dynamics of Vehicles on Roads and Tracks, Swets & Zeitlinger , Lyon 1991, pp. 354-365

/4.1.11/ Kallenbach, R.G., "Identification methods for vehicle system dynamics", Vehicle System Dynamics, 16 (1987), pp.107-127

/4.2.1/ Segel, L., "Theoretical Prediction and Experimental Substantiation of the Response of the Automobile to Steering Control", Proc. I. Mech. E. , 1956-7, No. 7

/4.2.2/ Ellis, J.R., "Vehicle Dynamics", London, 1969, p. 137 et seq.

/4.2.3/ Mitschke, M., "Dynamik der Kraftfahrzeuge", Bd. C, Fahrverhalten, Berlin, Springer Verlag, 1988, p. 5 et seq.

/4.2.4/ Rayner, J.D., "An investigation of vehicle parameter identification using the SP Tyres Vehicle Inertia Rig", MSc thesis, Cranfield University, School of Mechanical Engineering, 1995

/4.2.5/ DIA/DAGO Manual, GfS mbH, Aachen, 1994

/4.2.6/ MATLAB User's Guide, The Math Works Inc., 1992

/4.3.1/ Kohn, H.J., technical report No. TD 1739, Fort Dunlop, Birmingham, 1996

/7.0.1/ Mitschke, M., "Dynamik der Kraftfahrzeuge", Bd. C, Fahrverhalten, Berlin, Springer Verlag, 1988, pp. 83-86

/7.1.1/ Sharp, R.S., private communication

/7.1.2/ Bendat, J.S., Piersol, A.G., "Random Data: Analysis and Measurement Procedures", John Wiley & Sons, New York, 1971

/7.1.3/ Rill, G., "Steady State Cornering on Uneven Roadways", SAE paper No. 860575

/7.1.4/ Farrer, D.G., "An Objective Measurement Technique for the Quantification of On-Centre Handling Quality", SAE paper No. 930827

/8.2.1/ Automotive Engineer, Vol. 20, No. 2, April/ May 1995

/8.2.2/ Williams, R.A., Jaguar Cars, private communication

/8.2.3/ Reimpell, J., Sponagel, P., "Fahrwerktechnik: Reifen und Räder", Würzburg, Vogel Buch Verlag, 1986, p.212

/8.2.4/ Clark, S.K., (Edt.), "Mechanics of Pneumatic Tires", US Dept. of Transport, National Highway Traffic Safety Administration, Washington, 1981, p.693

/8.7.1/ Pina, D. et. al., "An active rear camber system to improve vehicle handling and safety", IMechE, 1993, C466/041

Appendix A1

3.1.11 Running the steady state cornering model

A simulation of a constant radius test requires the preparation of a few files, which contain vehicle and tyre data. These files are referenced in the batch control file 'sscorq15.bcf', which is read when the program is executed. The format and content of these files is given further on. After the input data is processed, the equations of equilibrium are solved by an Newton-Raphson procedure for an incrementally increasing lateral acceleration. When a further solution cannot be computed, execution continues to find alternative states for a decreasing lateral acceleration. These states describe the off-limit behaviour for either an under- or oversteering vehicle, characterised by further increasing steering angles and decreasing cornering performance for the understeering case, and by decreasing steering angles for the oversteering vehicle. Computation of these solutions is more demanding for the solver, and may be dependent on the tyre behaviour simulated.

3.1.12 Input files

Up to four files are necessary to run a simulation. The first one is the batch control file 'sscorq15.bcf', which is accessed by the program in order to identify the input files describing vehicle and tyre properties. It has the following format:

batch control file 'sscorq15.bcf'

```
!    B A T C H  COMMAND FILE FOR RUNNING SSCO15
!
!    VEHICLE DATA FILE:
!
TESTCAR.VDF
!
!    FRONT TYRE DATA FILE
!
!    CONTAINING DATA DESCRIBING FY-ALFA AND MZ-ALFA CHARACTERISTICS:
!
sp_D8_20.bnp
!
!    REAR TYRE DATA FILE
!
!    CONTAINING DATA DESCRIBING FY-ALFA IGNORING ANY FURTHER ENTRIES
!
sp_D8_20.bnp
!
!!!   OUTPUT FILE NAME
!
TESTCAR.OUT
!
!    TYPE OF SIMULATION / OUTPUT FORMAT SELECTION
!
!    1) STATIC CONST. RADIUS TEST LONG OUTPUT
!    2) STATIC CONST. RADIUS TEST SHORT OUTPUT
!    3) KINEMATIC ANALYSIS
!-->
2
!  <--
!!!!!!!!!!!!!!! END OF FILE
```

All lines beginning with an exclamation mark (!) are ignored. The first character string read by the program is the name of the vehicle data file containing suspension data, mass distribution etc. The next two strings give the names of the file in which the tyre model constants are stored. In this example, the same tyres are utilised front and rear. The forth string ('TESTCAR.OUT') defines the output file name. An integer determines the simulation type. Values of '1' or '2' invoke a constant radius test, whereas option '3' refers to suspension kinematics analysis. The later will be discussed later on.

Vehicle data as described in section 3.1.10 is provided by a separate file with a structure as given below. It must consist of 70 entries in the correct order. The first 19 parameter values refer to the front end of the vehicle and are discussed in more detail.

```
!       rover 8 series  INPUT DECK
!
! FRONT END DATA:
!
! 1  SPRUNG MASS FRONT: [KG]
876.
! 2  UNSPRUNG MASS FRONT: [KG]
35.0
! 3 ANTI ROLL BAR STIFFNESS FRONT: [Nm/RAD]
26010.0
! 4  COG HEIGHT FRONT: [M]
0.498
! 5  SPRING STIFFNESS RH SIDE: [N/M]
54200.0
! 6  SPRING STIFFNESS LH SIDE: [N/M]
54200.0
! 7  RADIAL TYRE STIFFNESS: [N/M]
200000.0
! 8  TRACK WIDTH FRONT: [M]
0.725
! 9  STATIC ROLLING RADIUS FRONT: [M]
0.305
! 10 STATIC CAMBER RH (GAMsf0): [RAD]
-0.0022
! 11 STATIC CAMBER LH (GAMpf0): [RAD]
0.0022
! 12 ZERO ORDER TRACK CHANGE COEFF.  (COF1f): [M]
0.0011
! 13 FIRST ORDER TRACK CHANGE COEFF. (COF2f): [M/M]
0.2221
! 14 SECOND ORDER TRACK CHANGE COEFF. (COF3f): [M/M**2]
-0.9795
! 15 ZERO   ORDER CAMBER CHANGE COEFF. (COF4f): [RAD]
0.0
! 16 FIRST  ORDER CAMBER CHANGE COEFF. (COF5f): [RAD/M]
-0.5263
! 17 SECOND ORDER CAMBER CHANGE COEFF. (COF6f): [RAD/M**2]
-1.8834
! 18 ZERO  ORDER SPRING LENGTH CHANGE COEFF. (COF7f): [M/M]
-0.704
! 19 FIRST ORDER SPRING LENGTH CHANGE COEFF. (COF8f): [M/M**2]
0.0
! ...
```

The first two entries give the values of sprung mass and unsprung mass at one side, which are easily calculated from measured wheel loads. Entry number 3 defines the additional roll stiffness due to a roll bar, while entries 5, 6, 18 and 19 determine the rates of the body springs, which contribute to both roll and vertical stiffness.

According to (3.1.36), wheel load and spring forces are related as follows: $F^z_{f,i} = F^S_{f,i} \frac{\partial \Delta l_{f,i}}{\partial z^W_{f,i}}$, if lateral forces are not considered. This equation can be used to adjust the spring parameters to a measured wheel rate represented by $F^z_{f,i}$. The spring force $F^S_{f,i}$ is proportional to the spring deflection $\Delta l_{f,i}$ according to (3.1.34) and constitutes a quadratic relationship between spring force and wheel travel. The spring definition allows modelling a progressive or regressive spring rate.

The entries 10, 11, 15, 16, 17 define the camber angle on the right hand side as a second order polynomial of the wheel travel, whereas the parameters 12, 13 and 14 give the coefficients for the track change. All of these polynomial coefficients refer to a wheel travel which is positive for a bump displacement on the right hand side (3.1.30-35). This means that for the right hand side, positive camber angles about the forward x-axis of the vehicle (fig. 3.1-6) are defined by positive coefficients given by entries 10, 15, 16 and 17. The camber angle for the nominal configuration on the right hand side is given by either entry 10 or 15. It is assumed that the corresponding anti symmetric relations for camber, spring deflection and track changes apply for the left hand side. However, a misalignment of the static camber may be introduced by declaring entry 10 and 11 appropriately.

```
! ...
!              ADDITIONAL DATA
!
! 39  CHASSIS TORSIONAL STIFFNESS: [Nm/RAD]
50000.0
! 40  WHEELBASE: [M]
2.5
! 41  FORWARD VELOCITY (NOW DUMMY VARIABLE /HJK): [M/SEC]
0.0
! 42  TURNING RADIUS: [M]
50.0
! note : if accmax < 0 then define negative radius roh
! 43  CHASSIS TORQUE ERROR: [Nm]
0.5
! 44  (CONFACT):
0.4
! 45  MAX. LATERAL ACCELERATION: [M/SEC**2]
10.00
! note : if accmax < 0 then define negative radius roh
!...
```

Some of the polynomial coefficients have a geometric meaning. For instance, the first order track change coefficient (entry 13) gives the negative ratio of roll centre height and half the track width. Therefore, a negative value would indicate that the roll centre lies below the ground. Together with the first order camber change coefficient, it also determines how the roll centre alters its location for increasing body roll.

Entries 20 to 38 deal accordingly with the data for the rear end of the vehicle and are not repeated here. The input file continues with some additional data, giving the wheelbase, chassis torsional stiffness and the turning radius the vehicle describes. Entry No. 41, the forward velocity is a dummy variable, since the simulation starts at zero lateral acceleration and finishes at a level beyond which a solution of the equations cannot be computed. Entries 43 ('CHASSIS TORQUE ERROR') and 44 ('CONFACT') are parameters controlling the convergence speed of the program, and may be accepted as defined in this example. Parameter 45 allows the user to restrict a simulation up to a certain level of lateral acceleration. The next section provides the description of the steering system.

Referring to the right hand side, we define positive steering angles as rotations about the vertical z-axis as shown in fig. 3.1-2. This means that a negative value for entry no. 46 had to be defined for a static toe in at the front. Entries 48 up to 55 correspond to the coefficients defined in (3.1.26-29), which relate the steering angles at each of the four wheels to the steering column rotation. A linear steering ratio is introduced for the front wheels by giving entry 48 and 50 equal values, while a linear rear steering ratio is defined by equal values of entry 52 and 55. A kind of Ackerman steering can be approximated by choosing the second order coefficients (49, 51, 53, 55) appropriately.

```
! ...
!              STEERING PARAMETERS
!
! 46  TOE RH FRONT : [RAD]
0.0000
! 47  TOE RH REAR  : [RAD]
0.00000
!
! 48  FIRST ORDER STEERING COEFF. FOR FRONT   RH    WHEEL
!                ( EQUALS STEERING RATIO ) : [RAD/RAD]
0.06
! 49  SECOND ORDER STEERING COEFF. FOR FRONT   RH   WHEEL: [RAD/RAD**2]
0.
! 50  FIRST ORDER STEERING COEFF.  FOR FRONT   LH   WHEEL
!                ( EQUALS STEERING RATIO ) : [RAD/RAD]
0.06
! 51  SECOND ORDER STEERING COEFF. FOR FRONT   LH   WHEEL: [RAD/RAD**2]
0.
!
! 52  FIRST ORDER STEERING COEFF.  FOR REAR    RH   WHEEL
!                ( EQUALS STEERING RATIO ) : [RAD/RAD]
0.
! 53  SECOND ORDER STEERING COEFF. FOR REAR    RH   WHEEL: [RAD/RAD**2]
0.
! 54  FIRST ORDER STEERING COEFF.  FOR REAR    LH   WHEEL
!                ( EQUALS STEERING RATIO ) : [RAD/RAD]
0.
! 55  SECOND ORDER STEERING COEFF. FOR REAR    LH   WHEEL: [RAD/RAD**2]
0.
! ...
```

Additionally to the steering angles due to the column rotation, roll steer effects on all four wheels are considered. The amount of roll steer prevalent at each wheel is assumed to relate to the wheel travel as given by (3.1.22-25). The values entered for the parameters 56, 57, 58 and 59 refer to the right hand side, giving additional toe out for a bump motion if positive.

The column stiffness (entry 60) reflects the compliance of the whole steering linkage, which leads to higher hand wheel angles compared to a rigid system. Steering compliance, the difference between hand wheel and column rotation, is proportional

```
! ...
!     BUMP / ROLL STEER
! 56  FIRST ORDER   FRONT RH  ROLL STEER COEFF.: [RAD/M]
0.3
!  GIVING TOE-OUT FOR BUMP AT R H SIDE
!
! 57  SECOND ORDER  FRONT RH  ROLL STEER COEFF.: [RAD/M**2]
0.
! 58  FIRST ORDER   REAR  RH  ROLL STEER COEFF.: [RAD/M]
-0.3
!   GIVING TOE-IN FOR BUMP AT R H SIDE
!
! 59  SECOND ORDER  REAR  RH  ROLL STEER COEFF.: [RAD/M**2]
0.
! 60  STEERING COLUMN STIFFNESS: [Nm/RAD]
200.
! 61  MECHANICAL TRAIL FRONT: [M]
!       NOTE: FOR A POS. SIDE FORCE AND A POS. MECHANICAL TRAIL
!                A NEG. ALIGNING MOMENT IS CALCULATED
0.01
! ...
```

to the aligning torques acting on the front wheels and the steering ratio as given by (3.1.39). The former can be pronounced by a positive mechanical trail provided by entry 61.

Entries 62 up 69 refer to the bump and rebound stop properties of the suspension. The first two define the threshold values for the wheel travel for which either the rebound (entry 62 and 64) or the bump stop (entry 63 and 65) and is engaged. The following two (entry 64 and 65) define the stiffness parameters controlling the sharpness of the force build-up associated with a rebound or bump engagement.

An integer referring to the maximal number of iterations for solving the steady state equations completes the vehicle data file.

```
! ...
!
! BUMP & REBOUND STOP PROPERTIES
!
! front:
! 62  MAX. WHEEL TRAVEL (>=0)
!    BEFORE REBOUND (DROOP) STOP IS ACTIVATED:
0.07
!
! 63  MAX. WHEEL TRAVEL (<=0)
!    BEFORE BUMP STOP IS ACTIVATED:
-0.07
!
! 64  STIFFNESS OF REBOUND STOP front:
!    NOTE THAT ADDITIONAL SPRING FORCE IS : K * (dL -dLo )**4
2.5277E+11
!
! 65  STIFFNESS OF BUMP STOP front:
!    NOTE THAT ADDITIONAL SPRING FORCE IS : K * (dL -dLo )**4
2.5277E+11
!
! ...
!
! 70  MAX. ITERATIONS (NTRIAL): [INTEGER]
100
!
! end of file
```

tyre data file

The tyre model used in the simulation is based on the 'Magic Formula' as presented in [?]. It describes the lateral force and the aligning torque as a functions of vertical load and slip angle. Camber effects are also considered. The 'Magic Formula' needs 18 parameters, ranging from A0-A17, for the side force representation and 21, ranging from C0-C20, for the aligning torque. Parameter values have to be given in an ascending order, beginning with A0. Users should refer to the appendix for a complete listing.

The program allows the simulation of rear tyres different from those at the front, provided that a filename corresponding to a second tyre data file is referenced in the batch control file. However, the aligning torque data of the rear tyre data file is not used in the simulation, even for the case of rear steered vehicle. We simply presume that the rear wheels would be actuated by a separate power source and that their aligning torques do not contribute to the steering compliance.

3.1.13 Output files

steady state cornering on constant radius simulation

Results of the steady state cornering simulation are written to a file in an ASCII format. For each value of lateral acceleration, from zero ascending to the maximum, a new row of results is written, leading to columns of output variables separated by commas. Output variables are vertical and lateral tyre forces, hand wheel angle and torque, tyre and vehicle slip angles, suspension characteristics etc. It can be opted for a short or long output file format, according to integer parameter given in the batch control file. A list of output parameters is added to the appendix. These data can be imported to standard spread sheet software (Excel) for analysis.

kinematics simulation

For the kinematics simulation an output file is created containing columns of suspension kinematics data referring to a simulated wheel travel going from rebound to bump. An example of output data for this type of simulation is discussed in the next section.

3.1.14 Kinematics simulation

Besides the steady state cornering simulation, the program allows analysing suspension kinematics to a certain extent. After the input is processed, the program determines the static equilibrium state at zero lateral acceleration, which may be slightly different from the nominal configuration given by the input. With respect to this state, the camber and track changes of the right hand front and rear suspensions are computed for 0.2m wheel travel, going from 0.1m rebound to 0.1m bump.

Based on the polynomial coefficients given for the track and camber change, a swing axle representation (fig. 3.1-8) of the modelled suspension is employed, in order to provide an alternative geometric description. It describes the suspension properties, originally given by 'generic' polynomials, by an equivalent inclined swing arm. For each vertical wheel displacement a swing arm length and its inclination from the horizontal is calculated, which may allow examination of the feasibility of the original data.

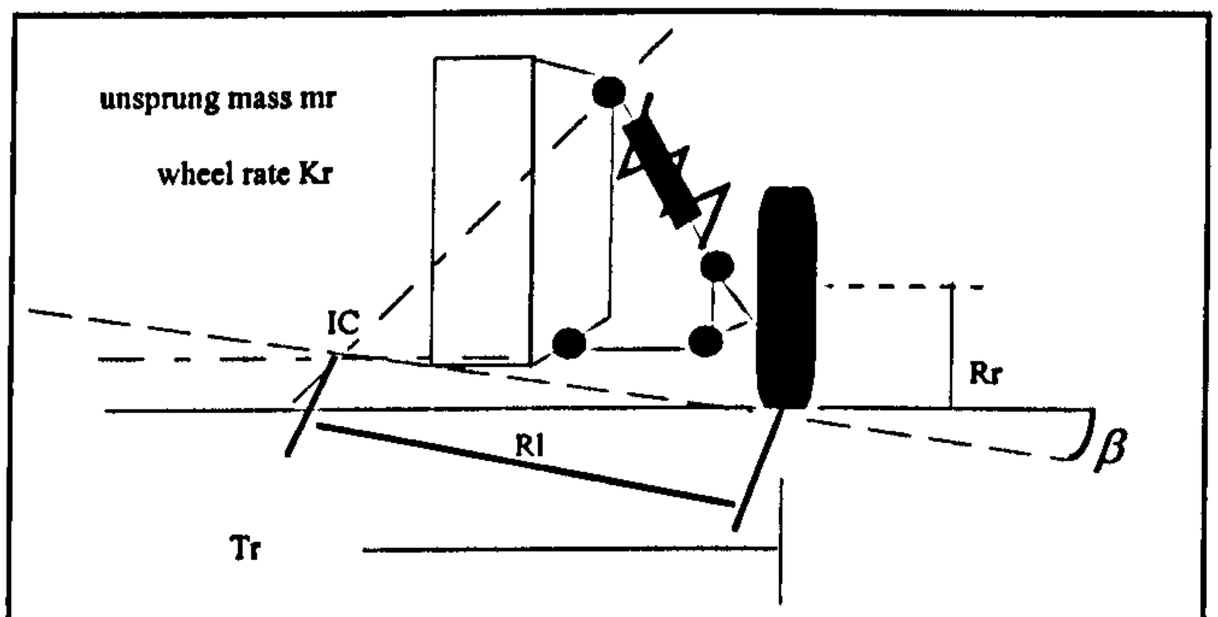

fig. 3.1-8 swing axle representation of McPherson strut suspension

Furthermore, the instantaneous centres of the wheels on the right hand side as well as the roll centres front and rear for pure roll conditions are calculated. These pure roll conditions are obtained for equal opposite wheel travel at the left and right hand side. Fig. 3.1-8 shows a swing arm representation of a McPherson suspension. The equivalent swing arm reaches from the instantaneous centre (IC) to the contact point of the wheel. Its length is indicated by Rl, and its inclination angle by β. For conventional designs, such as McPherson strut and double wishbone suspensions, the swing arm length Rl varies with the actual wheel travel from the datum position. For a parallel, equal length double wishbone layout it is infinitely long throughout the range of wheel displacement. For this case, the program gives a value of 1.E+06 [m] for the length Rl.

The output variables are calculated according to the formulas given below. The swing arm length is determined by:

$$Rl = \left(\frac{\partial y^{W}_{f,i}}{\partial z^{B}_{f,i}} \right)^{-1} \cdot \sqrt{1 + \left(\frac{\partial y^{W}_{f,i}}{\partial z^{B}_{f,i}} \right)^{2}}$$

and the inclination angle β by:

$$\tan\beta = -\frac{\partial y^{W}_{f,i}}{\partial z^{B}_{f,i}}$$

Furthermore, the coordinates $y_{0,f,i}$ and $z_{0,f,i}$ of the instantaneous centre of a wheel with respect to the wheel displacement, is given by:

$$y_{0,f,i} = y^{W}_{f,i} - \left(\frac{\partial y^{W}_{f,i}}{\partial z^{B}_{f,i}} \right) \text{ and}$$

$$z_{0,f,i} = z^{W}_{f,i} + \left(\frac{\partial y^{W}_{f,i}}{\partial z^{B}_{f,i}} \right) \cdot \left(\frac{\partial y^{W}_{f,i}}{\partial z^{B}_{f,i}} \right)^{-1}$$

and added to the output file. Plots given in fig. 3.1-9 are employed to show, how this data can be used. The plots shown were created based on the suspension data of a swing axle suspended vehicle. Both front and rear suspensions are equal. The swing arms on the left and right hand side are connected by a common hinge point on the centre line of the vehicle body. This means that the instantaneous centres of each wheel as well as the roll centres of the front and rear end remain in their nominal position, coinciding with the swing axle joints. The first plot in fig. 3.1-9 shows the vertical position of the instantaneous centre of the right hand front wheel and its wheel travel against the lateral position of the instantaneous centre. The plots suggest that the lateral position of both, the instantaneous centre and the roll centre, change according to wheel displacement, whereas the vertical positions remain constant. The

lateral changes in position, indicate the error magnitude due to the polynomial approximation of the suspension geometry. Since second order polynomials ($\sim z^2$) are employed, only the gradient and the second derivative of the camber and track change at zero wheel travel is described precisely.

The approximation of roll centre motions with wheel travel is obviously less efficient, since those depend on how good the derivatives of the functions, given for the camber and track change, agree to the design data. The plots shown may be helpful to analyse the feasibility of the suspension data used for the steady state cornering analysis. They also provide an additional geometric description to the purely analytical one given by polynomial functions.

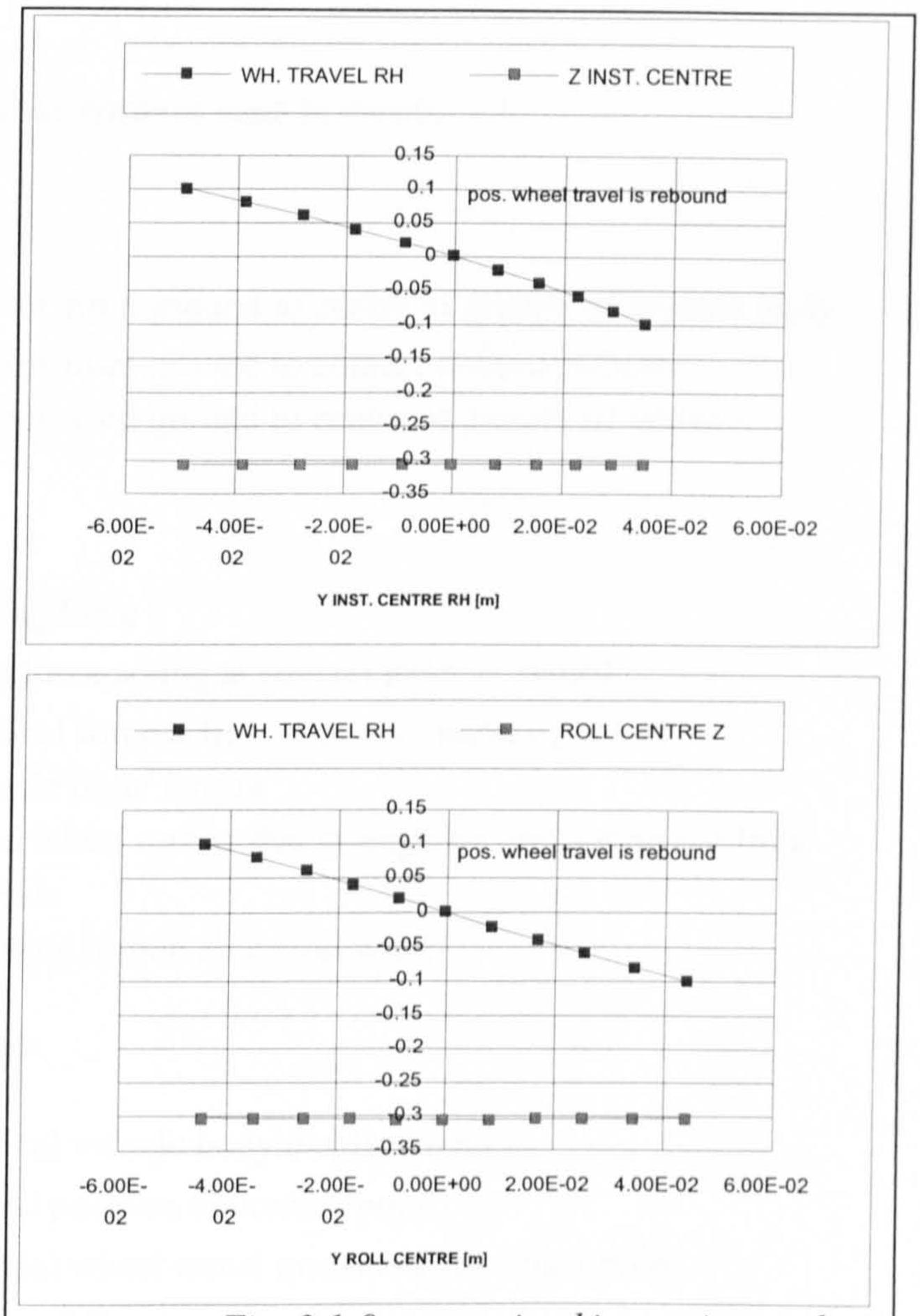

Fig. 3.1-9 suspension kinematics analysis

It has been demonstrated, that the approximation of the roll centre motion with wheel travel is limited, whereas good agreement for the camber and track change may be achieved. A listing of all output variables for this simulation can be found in the appendix.

Appendix A2

list of symbols used in section 3.1:

position vectors:

$\vec{r}_f^{\,CoG}$	: vector from ground to centre of gravity of vehicle body
$\vec{r}_i^{\,CP}$	: vector from ground to contact point of wheel i
$\vec{r}_i^{\,W}$	: vector from ground to centre of gravity of wheel i

forces and moments:

$F_{f,i}^{S}$	: spring force i
$F_{f,i}^{y}$	: side force acting at contact point of wheel i
$F_{f,i}^{z}$	: vertical force acting at contact point of wheel i
T	: vehicle body torque
M^{HW}	: hand wheel torque due to aligning torques on the front wheels
M_i^{AL}	: aligning torque acting on wheel i

coordinates and displacements:

z_f^B	: vertical vehicle body displacement
$y_{f,i}^{w}$	: lateral position of contact point
$z_{f,i}^{W}$	: vertical wheel travel measured at contact point
$\Delta l_{f,i}$	: spring deflection of spring i

angles:

φ_f	: roll angle front
$\gamma_{f,i}$	: camber angle of front wheel i
$\delta_{i\,r}$	: total steering angle at front wheel i
δ_i^{KP}	: steering angle at wheel i due to column rotation
$\Delta\delta_i$	: roll steer angle at wheel i
$\delta_{0,i}$	: static toe in
δ^{LC}	: angle at lower end of steering column
$\alpha_{i\,r}$	: slip angle at front wheel i
β	: vehicle slip angle

constants:

c_{φ}^{C}	: steering column torsional stiffness [Nm]
$c_{\varphi,f}^{RB}$	: anti roll bar torsional stiffness front [Nm]
H_f	: height of vehicle body centre of gravity [m]
m_f^B	: sprung mass front [kg]
$m_{f,i}^W$	: unsprung mass front [kg]
$R_{f,i}$	: static rolling radius of front tyre [m]
ρ	: turning radius [m]
v	: forward speed [m/s]

<u>list of output variables for constant radius cornering simulation</u>

Notes:

- all angles are given in radians [rad]
- forces measured in Newton [N]
- moments measured in Newton metres [Nm]
- all other variable units composed of [N], [m], [sec], [rad]
- sign convention according to fig. 3.1-2 and fig. 3.1-5

1) = ' LATAC ' : lateral acceleration
2) = ' FRONT : ' : [/]
3) = 'RHf SPRING GAIN : first derivative of spring deflection at front right hand side
4) = 'LHf SPRING GAIN' : first derivative of spring deflection at front left hand side
5) = 'RHf TRACK GAIN ' : first derivative of track change at front right hand side
6) = 'LHf TRACK GAIN ' : first derivative of track change at front left hand side
7) = 'RHf CAMBER GAIN' : first derivative of camber change at front right hand side
8) = 'LHf CAMBER GAIN' : first derivative of camber change at front left hand side
9) = ' RHf CAMBER ' : camber front right hand side
10) = ' LHf CAMBER ' : camber front left hand side
11) = 'RHf TR. CHANGE ' : track change right hand side
12) = 'LHf TR. CHANGE ' : track change left hand side
13) = 'RHf SIDE FORCE ' : side force acting on front right hand side
14) = 'LHf SIDE FORCE ' : side force acting on front left hand side
side forces positive for negative slip angles
15) = 'RHf VERT. FORCE' : vertical force acting on front right hand side
16) = 'LHf VERT. FORCE' : vertical force acting on front left hand side
vert. forces are positive
17) = 'RHf SIDE SLIP ' : slip angle front right hand side

18) = 'LHf SIDE SLIP ' : slip angle front left hand side
19) = 'FR. ROLL ANGLE ' : front roll angle
20) = 'FR. VERT. HEAVE' : vertical body heave (positive value is lift condition)
21) = 'RHf SPR. FORCE ' : spring force front right hand side
22) = 'LHf SPR. FORCE ' : spring force front left hand side
23) = ' REAR : ' : [/]
24) = 'RHr SPRING GAIN' : first derivative of spring deflection at rear right hand side
25) = 'LHr SPRING GAIN' : first derivative of spring deflection at rear left hand side
26) = 'RHr TRACK GAIN ' : first derivative of track change at rear right hand side
27) = 'LHr TRACK GAIN ' : first derivative of track change at rear left hand side
28) = 'RHr CAMBER GAIN': first derivative of camber change at rear right hand side
29) = 'LHr CAMBER GAIN': first derivative of camber change at rear left hand side
30) = ' RHr CAMBER ' : camber rear right hand side
31) = ' LHr CAMBER ' : camber rear left hand side
32) = 'RHr TR. CHANGE ' : track change right hand side
33) = 'LHr TR. CHANGE ' : track change left hand side
34) = 'RHr SIDE FORCE ' : side force acting on rear right hand side
35) = 'LHr SIDE FORCE ' : side force acting on rear left hand side
side forces positive for negative slip angles
36) = 'RHr VERT. FORCE' : vertical force acting on rear right hand side
37) = 'LHr VERT. FORCE' : vertical force acting on rear left hand side
vert. forces are positive
38) = 'RHr SIDE SLIP ' : slip angle rear right hand side
39) = 'LHr SIDE SLIP ' : slip angle rear left hand side
40) = 'RR. ROLL ANGLE ' : rear roll angle
41) = 'RR. VERT. HEAVE' : vertical body heave (positive value is lift condition)
42) = 'RHr SPR. FORCE ' : spring force rear right hand side
43) = 'LHr SPR. FORCE ' : spring force rear left hand side
44) = ' '
45) = 'TOTAL FR. ROLL ' : corrected front roll angle accounting for tyre compliance
46) = 'TOTAL RR. ROLL ' : corrected rear roll angle accounting for tyre compliance
47) = 'RHf ROLL ST ' : roll steer angle at front right hand wheel
48) = 'LHf ROLL ST ' : roll steer angle at front left hand wheel
49) = 'RHr ROLL ST ' : roll steer angle at rear right hand wheel
50) = 'LHr ROLL ST ' : roll steer angle at rear left hand wheel
51) = 'RHf STEER ' : steering angle at front right hand wheel due to toe in and column rotation
52) = 'LHf STEER ' : steering angle at front left hand wheel due to toe in and column rotation
53) = 'RHr STEER ' : steering angle at rear right hand wheel due to toe in and column rotation

54) = 'LHr STEER ' : steering angle at rear left hand wheel
due to toe in and column rotation
steering angles positive for right hand turn
55) = 'RHf SLIP ' : slip angle at front right hand wheel
due to vehicle slip angle β
56) = 'LHf SLIP ' : slip angle at front left hand wheel
due to vehicle slip angle β
57) = 'RHr SLIP ' : slip angle at rear right hand wheel
due to vehicle slip angle β
58) = 'LHr SLIP ' : slip angle at rear left hand wheel
due to vehicle slip angle β
59) = 'STEERING ANGLE ' : hand wheel angle
60) = 'S W TORQUE ' : hand wheel torque
steering torque positive for right hand turn
61) = 'RH ALIGN. TORQ ' : aligning torque at front right hand side
excluding mechanical trail contribution
62) = 'LH ALIGN. TORQ ' : aligning torque at front left hand side
excluding mechanical trail contribution
aligning torque positive for left hand turn or positive slip
63) = 'VEH. SLIP ANG. ' : vehicle slip angle β
64) = 'CHASSIS TORQUE ' : chassis torque
65) = ' TORQUE ERROR ' : torque difference between front and rear end of vehicle body

list of variables of the suspension kinematics simulation

1)= 'WH. TRAVEL RH ' : wheel travel of front right hand wheel
positive value indicates rebound condition
2)= 'CAMBER RH ' : camber angle of front right hand wheel
3)= 'TRACK CHANGE RH' : track change of front right hand wheel
4)= 'Y INST. CENTRE ' : lateral position of instantaneous centre of front right hand wheel
5)= 'Z INST. CENTRE ' : vertical position of instantaneous centre of front right hand wheel
positive value indicates position below ground
6)= 'INCLIN. ANGLE ' : inclination angle of equivalent swing arm
positive angle indicates rotation about longitudinal axis of vehicle
7)= 'RADIUS ARM LE. ' : length of equivalent swing arm
value of 1.E+06 indicates infinite length
8)= 'ROLL CENTRE Y ' : lateral roll centre position of vehicle front end
9)= 'ROLL CENTRE Z ' : vertical roll centre position of vehicle front end
positive value indicates position below ground
10)= 'WH. TRAVEL RH ' : wheel travel of rear right hand wheel
positive value indicates rebound condition
11)= 'CAMBER RH ' : camber angle of rear right hand wheel
12)= 'TRACK CHANGE RH' : track change of rear right hand wheel
13)= 'Y INST. CENTRE ' : lateral position of instantaneous centre of rear right hand wheel
14)= 'Z INST. CENTRE ' : vertical position of instantaneous centre of rear right hand wheel
positive value indicates position below ground
15)= 'INCLIN. ANGLE ' : inclination angle of equivalent swing arm
positive angle indicates rotation about longitudinal axis of vehicle
16)= 'RADIUS ARM LE. ' : length of equivalent swing arm
value of 1.E+06 indicates infinite length
17)= 'ROLL CENTRE Y ' : lateral roll centre position of vehicle rear end
18)= 'ROLL CENTRE Z ' : vertical roll centre position of vehicle rear end
positive value indicates position below ground

```
PARSFILE
* Echo file created by:
* Dynamic simulation of  full-vehicle model .
* Version created by AUTOSIM 2.0h on June 5, 1997.
* Copyright (c) The Regents of The University of Michigan, 1989 -
1995. All rights reserved.

TITLE Default values

* Input File:
* Run was made time & date not known
FORMAT text

INTOPT        0          , Type of integration (0=Adams, 1=Gear+PEDERV,
                           2=Gear diff., 3=RK2) (-)
IPRINT        2          , number of time steps between output printing
                           (counts)
EPSINT      .1000000000000E-01, Dimensionless integrator error
                          tolerance (-)
STARTT      .0000000000000    , simulation start time (s)
STEP        .1000000000000E-01, simulation time step (s)
STEP0       .1000000000000E-03, Initial integration step (s)
STEPMIN     .1000000000000E-05, Minimum allowable integration step(s)
STOPT        80.00000000      , simulation stop time (s)

* PARAMETER VALUES

A0HWA       0.500000000000    , HWA amplitude at beginning of
                               manoeuvre (rad) [9.3.3a]
A1HWA       1.720000000000    , max. HWA amplitude at end  of
manoeuvre (rad) [9.3.3a]
ACCX       -1.250000000000    , X coordinate of accelerometer
                               position (m)
ACCY       -0.250000000000    , Y coordinate of accelerometer position
(m)
ACCZ       -0.620000000000    , Z coordinate of accelerometer
                               position (m)
AREA        9.747E-04         , steering rack area (m**2)
                               [chapter 3.2.2]
*
* power assistence pressure (N/m**2)
* as a function of the scaled column twist angle (rad)
* the assisting torque is computed according to:
*                 torque = BOOST(twist*VSCALE) * AREA * DRDLC
* where VSCALE scales the column twist to an equivalent valve
                                                        opening
* where DRDLC, (m/rad), denotes ratio of rack displ. to road steer
                                                        angle (rad)
* find out more in 3.2.2
BOOST-CURVE boost curve for PAS
   -.0494565    ,   -60.0E+05    , point in table: (s, m)
   -.048913     ,   -50.0E+05    , point in table: (s, m)
   -.047826     ,   -45.0E+05    , point in table: (s, m)
   -.046739     ,   -40.0E+05    , point in table: (s, m)
   -.045652     ,   -35.0E+05    , point in table: (s, m)
   -.043478     ,   -30.0E+05    , point in table: (s, m)
   -.041304     ,   -25.0E+05    , point in table: (s, m)
   -.038044     ,   -20.0E+05    , point in table: (s, m)
   -.033696     ,   -15.0E+05    , point in table: (s, m)
   -.029348     ,   -10.0E+05    , point in table: (s, m)
   -.026630     ,   -8.00E+05    , point in table: (s, m)
   -.022826     ,   -5.00E+05    , point in table: (s, m)
```

```
-.017391     ,   -2.00E+05    , point in table: (s, m)
-.014130     ,    0.0000      , point in table: (s, m)
-.010870     ,    0.0000      , point in table: (s, m)
-.007609     ,    0.0000      , point in table: (s, m)
 .000000     ,    0.0000      , point in table: (s, m)
 .007609     ,    0.0000      , point in table: (s, m)
 .010870     ,    0.0000      , point in table: (s, m)
 .014130     ,    0.0000      , point in table: (s, m)
 .017391     ,    2.00E+05    , point in table: (s, m)
 .022826     ,    5.00E+05    , point in table: (s, m)
 .026630     ,    8.00E+05    , point in table: (s, m)
 .029348     ,    10.0E+05    , point in table: (s, m)
 .033696     ,    15.0E+05    , point in table: (s, m)
 .038044     ,    20.0E+05    , point in table: (s, m)
 .041304     ,    25.0E+05    , point in table: (s, m)
 .043478     ,    30.0E+05    , point in table: (s, m)
 .045652     ,    35.0E+05    , point in table: (s, m)
 .046739     ,    40.0E+05    , point in table: (s, m)
 .047826     ,    45.0E+05    , point in table: (s, m)
 .048913     ,    50.0E+05    , point in table: (s, m)
 .0494565    ,    60.0E+05    , point in table: (s, m)
ENDTABLE

BSCFR1    -0.009000000000    , 1.order bump steer coeff. fr. RH;
                                                    (rad/m)
* neg. value gives toe IN for rebound travel [3.1.22-23]
BSCFR2     0.000000000000    , 2.order bump steer coeff. fr. RH;
                                                    (rad/m2)
BSCFR3     0.000000000000    , 3.order bump steer coeff. fr. RH;
                                                    (rad/m3)
BSCRR1    -0.000700000000    , 1.order bump steer coeff. fr. RH;
(rad/m)
BSCRR2     0.000000000000    , 2.order bump steer coeff. fr. RH;
(rad/m2)
BSCRR3     0.000000000000    , 3.order bump steer coeff. fr. RH;
(rad/m3)
CASTER     0.086600000000    , (rad) castor angle; pos. value gives
bicycle castor
CBS_F      0.82E+08          , bump-stop rate fr.(N/m**4); [3.1.41]
CBS_R      0.000000000000    , bump-stop rate rr.(N/m**4); [3.1.41]
CCFRH0     0.000000000000    , static camber angle (rad)     fr. RH
CCFRH1     0.275100000000    , 1.order camber change (rad/m) fr. RH;
[3.1.30]
CCFRH2    -3.511200000000    , 2.order camber change (rad/m2)fr. RH
CCFRH3     0.000000000000    , 3.order camber change (rad/m3)fr. RH
CCRRH0     0.000000000000    , static camber angle (rad)     rr. RH
CCRRH1     0.681800000000    , 1.order camber change (rad/m) fr. RH;
[3.1.30]
CCRRH2    -1.195600000000    , 2.order camber change (rad/m2)fr. RH
CCRRH3     0.000000000000    , 3.order camber change (rad/m3)fr. RH
CRS_F      21.28E+10         , rebound-stop rate fr.(N/m**4);
[3.1.41]
CRS_R      779.21E+08        , rebound-stop rate rr.(N/m**4);
[3.1.41]
CSD_F      13400.00000000    , spring rate front RH (N/m)
[3.1.36]
CSD_R      27300.00000000    , spring rate rear  RH (N/m)
[3.1.36]
CTB_F      18000.00000000    , torsion bar stiffness fr.(Nm/rad)
CTB_R      0.000000000000    , torsion bar stiffness rr.(Nm/rad)
CZ_F       250000.0000000    , vert. tyre stiffness fr. (N/m)
CZ_R       250000.0000000    , vert. tyre stiffness rr. (N/m)
```

```
C_STCOL    25.00000000000    , composite column stiffness including
compliant rack (Nm/rad)
*                              [3.2.1]
*
* damper characteristics: spline gives damper force (N) vs. piston
speed
* important: damper unit is assumed to be aligned with suspension
spring
*            meaning that spring deflection = damper piston
displacement
*
DAMPER-CURVE-FRONT damper characteristics front
  -1.74530    ,-1129.500     , point in table: (s, m)
  -1.16360    , -729.000     , point in table: (s, m)
  -0.58180    , -481.500     , point in table: (s, m)
  -0.43630    , -423.000     , point in table: (s, m)
  -0.29090    , -355.500     , point in table: (s, m)
  -0.14540    , -270.000     , point in table: (s, m)
  -0.05820    , -139.500     , point in table: (s, m)
   .000000    ,  .000000     , point in table: (s, m)
   0.05820    ,  130.500     , point in table: (s, m)
   0.14540    ,  423.000     , point in table: (s, m)
   0.29090    ,  562.500     , point in table: (s, m)
   0.43630    ,  774.000     , point in table: (s, m)
   0.58180    ,  954.000     , point in table: (s, m)
   1.16360    , 1732.500     , point in table: (s, m)
   1.74530    , 2479.500     , point in table: (s, m)
ENDTABLE

DAMPER-CURVE-REAR damper characteristics rear
  -1.46257    , -948.700     , point in table: (s, m)
  -0.73128    , -608.600     , point in table: (s, m)
  -0.54846    , -508.400     , point in table: (s, m)
  -0.36564    , -390.200     , point in table: (s, m)
  -0.18282    , -243.400     , point in table: (s, m)
  -0.07313    , -103.800     , point in table: (s, m)
   .000000    ,  .000000     , point in table: (s, m)
   0.07313    ,  114.600     , point in table: (s, m)
   0.18282    ,  497.600     , point in table: (s, m)
   0.36564    , 1102.600     , point in table: (s, m)
   0.54846    , 1496.400     , point in table: (s, m)
   0.73128    , 1858.000     , point in table: (s, m)
   1.46257    , 4160.000     , point in table: (s, m)
ENDTABLE

DRDLC       8.0E-03           , ratio of rack travel and road steer
angle (m/rad)
DZ_F        300.0000000000    , tyre damping coefficient fr. (Nsec/m)
DZ_R        300.0000000000    , tyre damping coefficient rr. (Nsec/m)
D_STCOL     0.040000000000    , lower column damping (Nmsec/rad)
FHZ1         0.200000000000   , steering angle frequency of 1.
harmonic (Hz)
FHZ2         0.600000000000   , steering angle frequency of 2.
harmonic (Hz)
HTW_F        0.750000000000   , half front track width (m)
HTW_R        0.764000000000   , half front track width (m)
IB11         320.0000000000   , sprung mass moment of inertia  (kg-m2)
roll
IB12         .0000000000000   , sprung mass product of inertia (kg-m2)
IB13         .0000000000000   , sprung mass product of inertia (kg-m2)
IB22         2750.000000000   , sprung mass moment of inertia  (kg-m2)
pitch
```

```
IB23          .0000000000000    , sprung mass product of inertia (kg-m2)
IB33          2550.000000000    , sprung mass moment of inertia  (kg-m2)
yaw
IHW           0.020000000000    , moment of inertia of HAND WHEEL(kg-m2)
IMFR11        0.173000000000    , moment of inertia of unsprung mass fr.
RH (kg-m2) roll
IMFR22        0.345000000000    , moment of inertia of unsprung mass fr.
RH (kg-m2) spin
IMFR33        0.173000000000    , moment of inertia of unsprung mass fr.
RH (kg-m2) steer
IMRR11        0.173000000000    , moment of inertia of unsprung mass rr.
RH (kg-m2) roll
IMRR22        0.345000000000    , moment of inertia of unsprung mass rr.
RH (kg-m2) spin
IMRR33        0.173000000000    , moment of inertia of unsprung mass rr.
RH (kg-m2) steer
KPINC      -0.149900000000    , kingpin inclination (rad) fr. RH
* neg.angle cambers the lower tip of kingpin away from chassis
MFR           56.00000000000    , mass of unsprung mass fr. (kg)
MRR           68.00000000000    , mass of unsprung mass rr. (kg)
R0_F          0.326000000000    , fr. tyre radius (unladen) (m)
R0_R          0.325000000000    , rr. tyre radius (unladen) (m)
SCFLH1        0.060000000000    , 1. order steering ratio of road wheel
steer to column rotation (rad/rad)    fr. LH
SCFLH2        0.000000000000    , 2. order steering ratio of road wheel
steer to column rotation (rad/rad**2) fr. LH
SCFRH1        0.060000000000    , 1. order steering ratio of road wheel
steer to column rotation (rad/rad)    fr. RH
SCFRH2        0.000000000000    , 2. order steering ratio of road wheel
steer to column rotation (rad/rad**2) fr. RH
SL_F1         1.000000000000    , 1. order suspension spring deflection
[m/m]    fr. RH; if 1 than spring deflection=wheel travel
SL_F2         0.000000000000    , 2. order suspension spring deflection
[m/m^2] fr. RH;
SL_F3         0.000000000000    , 3. order suspension spring deflection
[m/m^3] fr. RH;
SL_R1         1.000000000000    , 1. order suspension spring deflection
[m/m]    rr. RH; if 1 than spring deflection=wheel travel
SL_R2         0.000000000000    , 2. order suspension spring deflection
[m/m^2] rr. RH;
SL_R3         0.000000000000    , 3. order suspension spring deflection
[m/m^3] rr. RH;
TOEFRH        0.000000000000    , toe fr. RH (rad)
TOERRH     -0.000000000000    , toe rr. RH (rad)
VSCALE        0.271740000000    , scaling factor for column twist
*                                 column twist * VSCALE = valve opening
VX-TIME forward speed vs. time
  .000000    ,  20.0000     , point in table: (s, m)
  .100000    ,  20.0000     , point in table: (s, m)
  .200000    ,  20.0000     , point in table: (s, m)
 5.0000      ,  21.0000     , point in table: (s, m)
10.00000     ,  22.0000     , point in table: (s, m)
15.00000     ,  23.0000     , point in table: (s, m)
20.00000     ,  24.0000     , point in table: (s, m)
25.00000     ,  25.0000     , point in table: (s, m)
30.00000     ,  26.0000     , point in table: (s, m)
35.00000     ,  27.0000     , point in table: (s, m)
40.00000     ,  28.0000     , point in table: (s, m)
45.00000     ,  29.0000     , point in table: (s, m)
50.00000     ,  30.0000     , point in table: (s, m)
55.00000     ,  31.0000     , point in table: (s, m)
60.00000     ,  32.0000     , point in table: (s, m)
```

```
 65.00000     ,   33.0000      , point in table: (s, m)
 70.00000     ,   34.0000      , point in table: (s, m)
 75.00000     ,   35.0000      , point in table: (s, m)
 80.00000     ,   35.0000      , point in table: (s, m)
 85.00000     ,   35.0000      , point in table: (s, m)
 100.0000     ,   35.0000      , point in table: (s, m)
 110.0000     ,   35.0000      , point in table: (s, m)
 120.0000     ,   35.0000      , point in table: (s, m)
ENDTABLE

VX0          20.00000000000    , forward vehicle speed at beginning of
manoeuvre (m/sec) [9.3.3]
VXM          35.00000000000    , vehicle speed at end of manoeuvre
(m/sec)                  [9.3.3]
WB           2.870000000000    , wheel base (m)
WL_FL        5110.000000000    , wheel load fr. LH (N)
WL_FR        5110.000000000    , wheel load fr. RH (N)
WL_RL        4665.000000000    , wheel load rr. LH (N)
WL_RR        4665.000000000    , wheel load rr. RH (N)
XGOFF        0.026450000000    , X coordinate of ground offset point RH
fr (m)
* long.distance between wheel contact point and intersection of
kinppin axis with ground
* positive value means intersection is ahead of fr. axle
YCFRH1     -0.045460000000     , 1.order lateral scrub of wheel CENTRE
fr. RH [m/m]
YCFRH2     -2.000000000000     , 2.order lateral scrub of wheel CENTRE
fr. RH [m/m^2]
YCFRH3      0.000000000000     , 3.order lateral scrub of wheel CENTRE
fr. RH [m/m^3]
YCRRH1      0.015000000000     , 1.order lateral scrub of wheel CENTRE
rr. RH [m/m]
YCRRH2     -1.074050000000     , 2.order lateral scrub of wheel CENTRE
rr. RH [m/m^2]
YCRRH3      0.000000000000     , 3.order lateral scrub of wheel CENTRE
rr. RH [m/m^3]
YGOFF      -0.054000000000     , Y coordinate of ground offset point RH
fr (m)
* lateral distance between wheel contact point and intersection of
kinppin axis with ground
* positive value means intersection is outside the track width
ZBMPF        0.02200000000     , wheel travel before bump stop fr. RH is
engaged (m) >0
ZBMPR        0.02000000000     , wheel travel before bump stop rr. RH is
engaged (m) >0
ZCG_MB     -0.26500000000      , CoG height of sprung mass (m) measured
from front axle centre line
ZRBDF        0.07000000000     , wheel travel before rebound stop fr. RH
is engaged (m) >0
ZRBDR        0.05200000000     , wheel travel before rebound stop rr. RH
is engaged (m) >0

* INITIAL CONDITIONS

Q(1)        -.3172556686908E-04, (comp.) Y trans. of HCFR0 rel. to
HCFRJ (m)
Q(2)        -.6091011269370E-05, (comp.) Z rot. of HCFRp rel. to MB
(rad)
Q(3)         .1844979533628E-03, (comp.) X rot. of HCFR rel. to HCFRp
(rad)
Q(4)        -.1579054518746E-02, (comp.) Z rot. of KPFR rel. to HCFR
(rad)
```

```
Q(5)          .2698496436007E-03, (comp.) Y trans. of HCFL0 rel. to
HCFLJ (m)
Q(6)          .4396310783297E-04, (comp.) Z rot. of HCFLp rel. to MB
(rad)
Q(7)         -.1259910627988E-02, (comp.) X rot. of HCFL rel. to HCFLp
(rad)
Q(8)         -.1579054518746E-02, (comp.) Z rot. of KPFL rel. to HCFL
(rad)
Q(9)         -.6742137259204E-04, (comp.) Y trans. of MRR0 rel. to MRRJ
(m)
Q(10)         .2504202377104E-05, (comp.) Z rot. of MRRp rel. to MB
(rad)
Q(11)        -.2454410212427E-02, (comp.) X rot. of MRR rel. to MRRp
(rad)
Q(12)        -.1035025715199E-04, (comp.) Y trans. of MRL0 rel. to MRLJ
(m)
Q(13)         .5097880002068E-06, (comp.) Z rot. of MRLp rel. to MB
(rad)
Q(14)        -.4958948071930E-03, (comp.) X rot. of MRL rel. to MRLp
(rad)
Q(15)         .0000000000000    , (comp.) X rot. of HW rel. to MB (rad)
Q(16)        0.000000000000     , X trans. of MB0 rel. to N0_REF (m)
Q(17)        -.0000000000000    , Y trans. of MB0 rel. to N0_REF (m)
Q(18)        -.2942513028445E-02, Z trans. of MB0 rel. to N0_REF (m)
Q(19)        -.1951554713571E-01, Abs. Z rot. of MBpp (rad)
Q(20)         .3228558657472E-02, X rot. of MBp rel. to MBpp (rad)
Q(21)         .1577417184967E-02, Y rot. of MB rel. to MBp (rad)
Q(22)         .6767790299300E-03, Z trans. of HCFR0 rel. to HCFRJ (m)
Q(23)         .4884789759219E-02, Z trans. of HCFL0 rel. to HCFLJ (m)
Q(24)        -.3577431967291E-02, Z trans. of MRR0 rel. to MRRJ (m)
Q(25)         .7282685717240E-03, Z trans. of MRL0 rel. to MRLJ (m)
Q(26)        -.2631757531243E-01, X rot. of LCOL rel. to MB (rad)
U(1)          .2525998400895E-02, Abs. Y trans. speed of MBCMC (m/s)
U(2)          .3147554447295E-01, Abs. Z trans. speed of MBCMC (m/s)
U(3)         -.1015144109169E-01, Abs. Z rot. speed of MB (rad/s)
U(4)          .2979965121266E-04, Abs. X rot. speed of MB (rad/s)
U(5)          .6339779240225E-03, Abs. Y rot. speed of MB (rad/s)
U(6)          .1218640420695E-02, Z trans. speed of HCFR0 rel. to MB
(m/s)
U(7)          .1234848444403E-02, Z trans. speed of HCFL0 rel. to MB
(m/s)
U(8)         -.5704948254079E-03, Z trans. speed of MRR0 rel. to MB
(m/s)
U(9)         -.5514340391392E-03, Z trans. speed of MRL0 rel. to MB
(m/s)
U(10)         .2298576540499E-03, X rot. speed of LCOL rel. to MB
(rad/s)

END
```

Appendix B2

'Magic Formula' tyre data used for AUTOSIM simulation /2.4.7/

```
! SP2000 225/55/ZR16 for X40 Jaguar
! NO camber coefficients given for aligning torque !!!
! A 0 =
.130000E+01
! A 1 =
-.258311E-04
! A 2 =
.116473E+01
! A 3 =
.951622E+05
! A 4 =
.162755E+05
! A 5 =
-.973548E-01
! A 6 =
-.914911E-04
! A 7 =
.697351E+00
! A 8 =
-.806307E-07
! A 9 =
-.121107E-02
! A10 =
-.161656E-01
! A11 =
.337472E-01
! A12 =
-.140511E+03
! A13 =
.198217E-04
! A14 =
.734082E+00
! A15 =
.394463E+00
! A16 =
-.971687E+01
! A17 =
.405124E+00
```

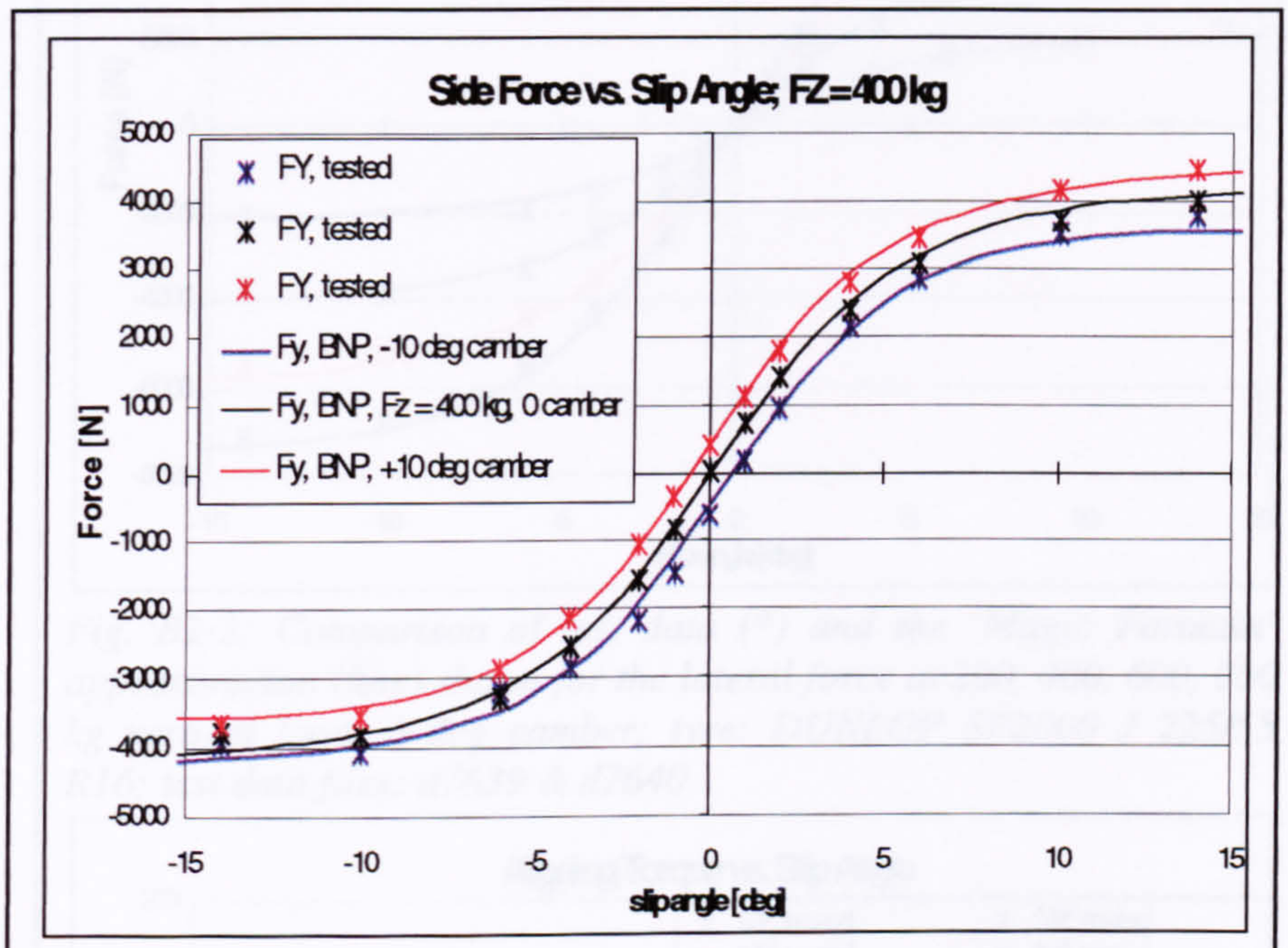

Fig. B2-1: Comparison of test data (*) and the 'Magic Formula' approximation (line) shown for the lateral force at 400 kg vertical load; 0, +/- 10 deg camber; tyre: DUNLOP SP2000 J 225/55 R16; test data files: d7639 & d7640, cs16r & cs17r

! C 0 =
.235000E+01
! C 1 =
.262186E-05
! C 2 =
.144855E-02
! C 3 =
-.184538E-03
! C 4 =
.164968E+00
! C 5 =
.126083E-03
! C 6 =
.000000E+00
! C 7 =
-.233803E-07
! C 8 =
.148982E-03
! C 9 =
-.435789E+00
! C10 =
.000000E+00
! C11 =
.203047E-06
! C12 =
.947272E-03
! C13 =
.000000E+00
! C14 =
-.222609E-02
! C15 =
.566762E+01
! C16 =
.000000E+00
! C17 =
.000000E+00
! C18 =
.000000E+00
! C19 =
.000000E+00
! C20 =
.000000E+00

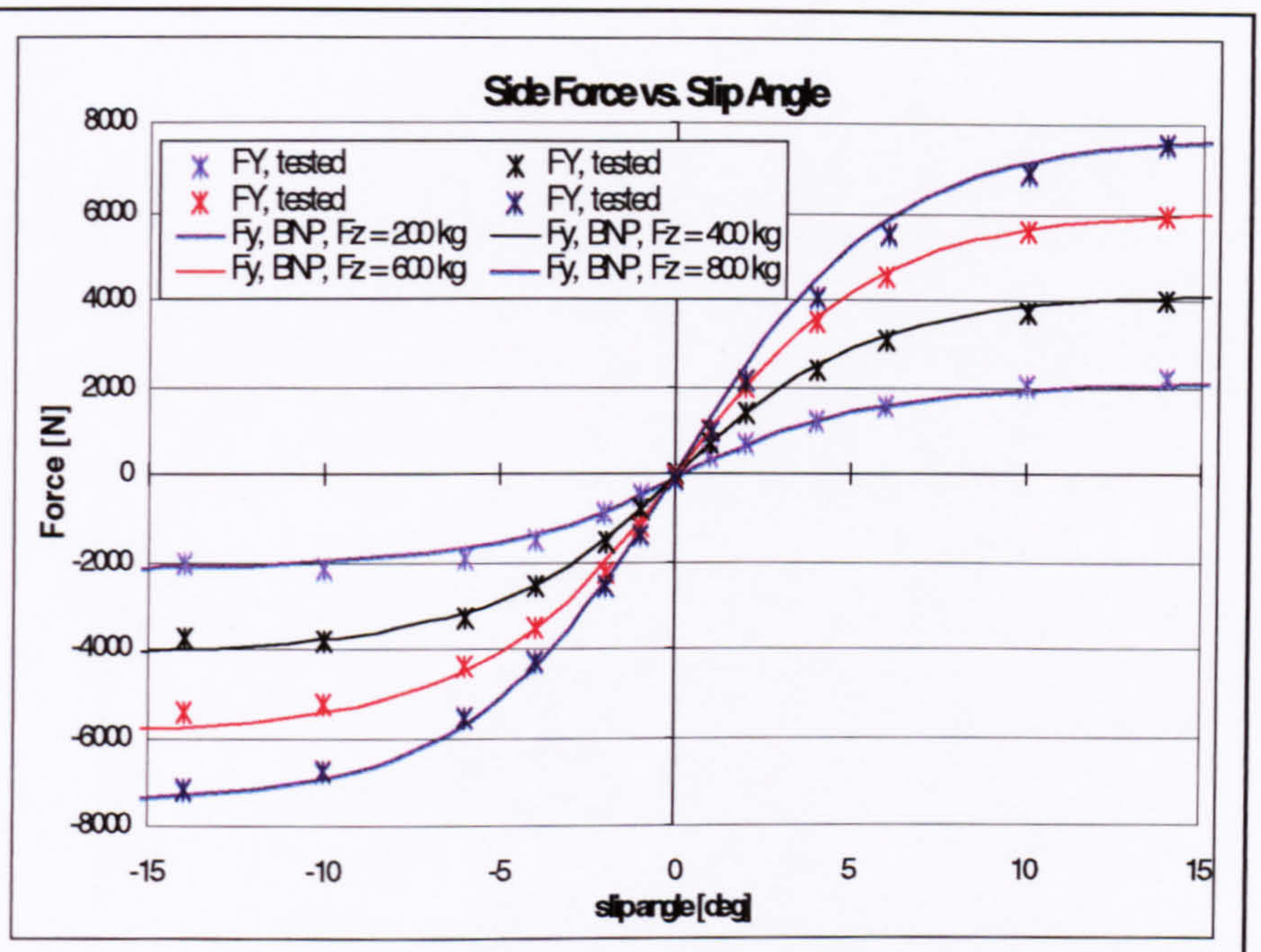

Fig. B2-2: Comparison of test data (*) and the 'Magic Formula' approximation (line) shown for the lateral force at 200, 400, 600, 800 kg vertical load, 0 deg camber; tyre: DUNLOP SP2000 J 225/55 R16; test data files: d7639 & d7640

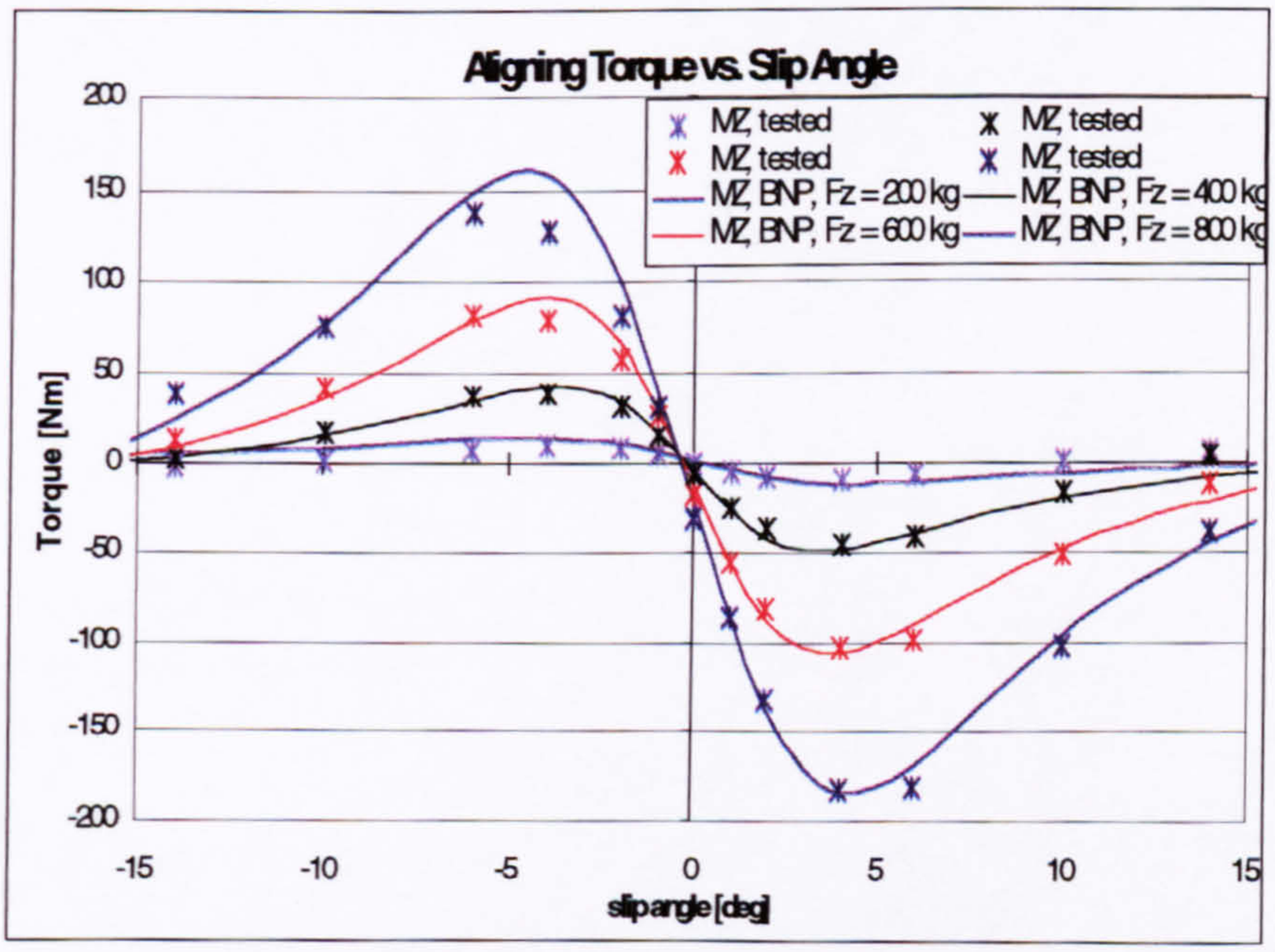

Fig. B2-3: Comparison of test data (*) and the 'Magic Formula' approximation shown for the aligning torque (line) *at 200, 400, 600, 800 kg vertical load, 0 deg camber; tyre:* DUNLOP SP2000 J 225/55 R16*; test data files: d7639 & d7640*